

**Mechanisms of radiation and
antibody-induced cell death in
lymphoma**

by

Andrejs Ivanovs

CRUK Paterson Institute for Cancer Research.

University of Manchester. School of Cancer and

Imaging Sciences

A thesis submitted to the University of Manchester for the degree of the

Doctor of Philosophy in the Faculty of Medical and Human Sciences

2008

ProQuest Number: U524998

All rights reserved

INFORMATION TO ALL USERS

The quality of this reproduction is dependent upon the quality of the copy submitted.

In the unlikely event that the author did not send a complete manuscript and there are missing pages, these will be noted. Also, if material had to be removed, a note will indicate the deletion.



ProQuest U524998

Published by ProQuest LLC (2019). Copyright of the Dissertation is held by the Author.

All rights reserved.

This work is protected against unauthorized copying under Title 17, United States Code
Microform Edition © ProQuest LLC.

ProQuest LLC.
789 East Eisenhower Parkway
P.O. Box 1346
Ann Arbor, MI 48106 – 1346

(Euq3j)

✕
Th32067/

THE
JOHN RYLANDS
UNIVERSITY
LIBRARY

Table of contents

Chapter 1. Introduction.....10

1-1. The modes of cell death induced by radiation and antibody therapy.....	10
Programmed cell death.....	14
1-1-1. Type 1 programmed cell death or apoptosis.....	14
1-1-2. Type 2 programmed cell death or autophagic cell death.....	19
1-1-3. Type 3 programmed cell death or paraptosis.....	22
1-1-4. Mitotic catastrophe.....	24
1-1-4-1. Polyploid giant cells – a hallmark of mitotic catastrophe.....	28
1-2. DNA repair.....	31
1-2-1. DNA single strand breaks.....	32
1-2-2. DNA double strand breaks.....	33
1-2-3. Homologous recombination.....	35
1-2-4. Non-homologous end joining.....	36
1-3. The use of monoclonal antibodies against cancer.....	39
1-4. Principles of radioimmunotherapy.....	40
Combining targeted radiation with antibody therapy	
1-5. CD20 antigen.....	44
1-6. Anti-CD20 antibody effector mechanisms.....	47
1-7. Radiation and antibody signalling cascades – Mitogen-activated protein kinase cascades.....	50
1-8. Death promoting role of ERK/MAPK cascade.....	53
1-9. Involvement of ERK/MAPK cascade in CD20 signalling.....	56
1-10. The aim of this investigation	57

Chapter 2. Materials and methods

2-1. Cell lines.....	72
2-2. Irradiation of cells.....	72
2-3. Therapeutic antibodies.....	72
2-4. Apoptosis detection and cell cycle analysis using propidium iodide flow cytometry.....	73
2-5. Cell death detection using Annexin V and PI flow cytometry.....	74
2-6. Two channel flow cytometry for cyclin B1 and DNA content.....	74
2-7. Two channel flow cytometry for Annexin V and DNA content.....	74
2-8. Immunofluorescent visualisation of Annexin V and Rad51-positive cells.....	75
2-9. DNA in situ image cytometry and image analysis.....	76
2-10. Single cell gel electrophoresis. Comet assay.....	76
2-11. Silencing of genes using siRNA.....	76
2-12. Western blotting.....	77
2-13. Measurement of DNA fragmentation: Fluorescence in situ end labeling (FISEL).....	78
2-14. Clonogenic survival assay.....	78
2-15. Reverse transcription polymerase chain reaction.....	79
2-16. XTT cell viability assay.....	79

2-17. Transmission electron microscopy.....	80
2-18. Fluorescence microscopy I.....	80
2-19. Fluorescence microscopy II. Digital pixel co-localization studies.....	81
2-20. Fluorescence recovery after photo bleaching (FRAP).....	82
2-21. Statistical analysis.....	83
 Chapter 3. Endopolyploid cells produced after severe genotoxic damage have the potential to repair DNA double strand breaks.....	84
 Chapter 4. Upregulation of meiosis-specific genes in lymphoma cell lines following genotoxic insult and induction of mitotic catastrophe.....	90
 Chapter 5. Segregation of genomes in polyploid tumour cells following mitotic catastrophe.....	91
 Chapter 6. Nuclear envelope-limited chromatin sheets are morphological expression of mitotic death.....	92
 Chapter 7. Image Analysis of DNA Repair and Apoptosis in Tumour Cells with Differing Sensitivity to DNA Damage.....	93
 Chapter 8. Endopolyploid cells resulting from irradiated p53 deficient tumours display long-lasting mitotic potential and active Aurora B- kinase.....	98
 Chapter 9. Mechanism of non-apoptotic cell death evoked by Type II anti-CD20 mAb (Tositumomab) and mAb to HLA-DR.....	99
 Chapter 10. Radiation therapy with Tositumomab (B1) anti-CD20 mAb initiates ERK/MAPK dependent cell death that overcomes resistance to apoptosis.....	100
 Chapter 11. General Discussion.....	101
 Appendix 1. The biology of CD20 and its potential as a target for mAb therapy.....	108
 Appendix 2. New insights into mechanisms of action of radioimmunotherapy.....	109
 Appendix 3. Curriculum Vitae.....	111

List of Figures

Figure 1-1. Morphological differences between cells undergoing apoptosis and necrosis.....	12
Figure 1-2. Morphology of early and late apoptosis.....	14
Figure 1-3. Overview of the two major apoptosis pathways.....	16
Figure 1-4. Formation of apoptosome and caspase-9 activation.....	18
Figure 1-5. Autophagic structures in neoplastic cells.....	20
Figure 1-6. Schematic representation of autophagy.....	21
Figure 1-7. Paraptosis-like programmed cell death in Raji cells.....	23
Figure 1-8. A summary of current concepts of mitotic catastrophe.....	28
Figure 1-9. Principal scheme of cell cycle regulation.....	27
Figure 1-10. Principal scheme of cell cycle checkpoint regulation.....	28
Figure 1-11. The involvement of DNA repair in cell metabolism.....	32
Figure 1-12. Schematic representation of cellular response to DNA DSB.....	34
Figure 1-13. DNA DSB repair via homologous recombination.....	36
Figure 1-14. Schematic representation of the pathway of DNA NHEJ.....	37
Figure 1-15. Model of the relative contributions of HR and NHEJ to the repair of radiation-induced DSB.....	38
Figure 1-16. The principal structure of anti-CD20 antibody Rituximab and Rituximab labelled with ⁹⁰ Y (Zevalin) used in radioimmunotherapy.....	40
Figure 1-17. Schematic diagram of the structure of CD20.....	44
Figure 1-18. The expression dynamics of CD20 antigen.....	46
Figure 1-19. Anti-CD20 antibody effector mechanisms.....	49
Figure 1-20. Mitogen-activated protein kinases.....	51
Figure 1-21. Schematic generic overview of the sequence of events leading to activation of MAP kinase pathways.....	52
Figure 2-1. The principle of FRAP.....	82
Figure 11-1. Hypothetical scheme of the involvement of ERK/MAPK cascade in radiation-induced mitotic catastrophe and antibody-induced non-apoptotic cell death.....	105

List of Tables

Table 1-1. Comparison of apoptosis, necrosis and paraptosis.....	13
Table 1-2. Summary of characteristics considered ideal in an antigen target for RIT	42
Table 1-3. Examples of ERK mediated cell death in different cell types and stimuli.....	55
Table 2-1. The list of therapeutic antibodies used in this study.....	72
Table 2-2. Sequences of primers used in the RT-PCR experiments.....	79

Abstract

Radiation and targeted antibody immunotherapy either used alone or combined in radioimmunotherapy are highly effective treatments for some haematological malignancies. However the underlying mechanisms of radiosensitivity and radioresistance in lymphoma and why radioimmunotherapy has such proven clinical efficacy in some patients with chemorefractory disease remain poorly understood.

In this work we have first demonstrated the mode of radiation-induced cell death in p53 mutated lymphoma cells. We have shown that endopolyploid cells produced after bypassing DNA damage-induced G2/M arrest have a transient survival advantage that may contribute to radioresistance of tumours undergoing radiation-induced mitotic catastrophe. These radiation-induced cell cycle deviations are associated with complex biochemical changes. We have shown that multiple genes (DMC1, STAG3, SYCP3, SYCP1 and MOS) are aberrantly activated during mitotic catastrophe in p53 mutated lymphoma cells after irradiation. Furthermore, we suggest that the coordinated expression of MOS and REC8 regulate the extent of arrested mitoses and polyploidy.

Previously, we demonstrated that Type II anti-CD20 mAb were able to evoke cell death and that this appeared linked with the induction of homotypic adhesion. In our next line of investigation we have shown that actin redistribution is critical for both adhesion and cell death induced by both Type II anti-CD20 mAb and HLA DR Class II mAb. Subsequent experiments revealed that actin dynamics are altered rapidly after mAb stimulation and that actin appears to influence the lysosomes which appear to swell and then disperse their contents into the cytoplasm, resulting in the loss of plasma membrane viability.

Important new insights into the cell death pathways that may underlie the impressive responses seen with radiolabelled anti-CD20 mAb in chemo-refractory patients in the clinic have been demonstrated combining radiation and anti-CD20 antibodies. Here we have investigated the downstream signalling events in a variety of human B-cell lymphomas treated with radiation treatment (RT) and anti-CD20 mAb. Increased cell death was observed with tositumomab and RT but this same additive cell death was not seen with rituximab and RT. This increased tumour cell death and loss of clonogenic survival could be reversed with the MEK inhibitors as well as siRNA targeting MEK1 or MEK 2. Interestingly although Bcl₂ over-expression resulted in decreased apoptosis after RT alone, it had no impact on the synergistic cytotoxicity of tositumomab plus RT which further suggests that apoptosis is unlikely to be the cause of increased cell death. Confirmation of a non-apoptotic form of cell death was made by ultrastructural analysis as well as the lack of TUNEL staining. These findings suggest that the ERK/MAPK pathway can be stimulated by some anti-CD20 mAb to function in a pro-death capacity.

In summary, our results show the importance of non-apoptotic forms of cell death in mediating therapeutic responses after radiation and anti-CD20 immuno- and radioimmuno-therapy.

Declaration

No portion of the work referred to in the thesis has been submitted in support of an application for another degree or qualification of this or any other university or other institute of learning.

Authorship statement

For first author articles the candidate designed and performed all the experiments, interpreted the data and wrote drafts of the manuscripts (chapters 3, 7, 9, 10 and appendix 2). Co-authors contributed by repeating experiments independently, providing critical advise and analysis of data, and by helping to write the manuscript. This is also true for all articles where K. Erenpreisa is listed as the first and corresponding author (chapter 6 and 8) as well as for articles with joint first authorship, where the candidate is listed as a second author (chapter 4). For other articles (chapter 5 and appendix 1) where the candidate is listed as a co-author, the candidate contributed by performing experiments and help in manuscript preparation.

Copyright statement

The author of this thesis (including any appendices and/or schedules to this thesis) owns any copyright in it (the "Copyright") and s/he has given The University of Manchester the right to use such Copyright for any administrative, promotional, educational and/or teaching purposes.

Copies of this thesis, either in full or in extracts, may be made only in accordance with the regulations of the John Rylands University Library of Manchester. Details of these regulations may be obtained from the Librarian. This page must form part of any such copies made.

The ownership of any patents, designs, trade marks and any and all other intellectual property rights except for the Copyright (the "Intellectual Property Rights") and any reproductions of copyright works, for example graphs and tables ("Reproductions"), which may be described in this thesis, may not be owned by the author and may be owned by third parties. Such Intellectual Property Rights and Reproductions cannot and must not be made available for use without the prior written permission of the owner(s) of the relevant Intellectual Property Rights and/or Reproductions.

Further information on the conditions under which disclosure, publication and exploitation of this thesis, the Copyright and any Intellectual Property Rights and/or Reproductions described in it may take place is available from the Head of School of Medicine.

**“Contraria non contradictoria, sed
complementaria sunt”**

Niels Henrik David Bohr

Chapter 1

Introduction¹

Radiation and anti-cancer antibodies are known to result in a wide range of cellular effects including cell death, cell signalling, DNA damage, and activation of immune effector cells. Through overlapping mechanisms, these effects make a complex pattern of cellular response that, in turn, might result in non-linear effects, substantially different from a simple sum of treatment responses. In introduction, these mechanisms will be reviewed separately, however, some integration will be presented as well. First we will consider the different modes of cell death that may be evoked by radiation or antibody therapy.

1-1 The modes of cell death by radiation and antibody therapy. Programmed cell death.

Programmed cell death (PCD) plays an essential role in the physiology and development of living organisms. Its deregulation features in developmental, neoplastic, neurodegenerative, infectious, traumatic, ischaemic and metabolic disorders. It has been 100 years since the first description of developmental cell death (Studnicka FK. Die Parietal organe. In: Oppel A. Ed 1905). In 1964, Lockshin and colleagues introduced the term programmed cell death to describe an apparently endogenous pathway or set of

¹ Partly published as Ivanov A, Swann R, Illidge T. New insights into mechanisms of action of radioimmunotherapy. *J Pharm Pharmacol*. In press. 2008 and Cragg MS, Walshe CA, Ivanov AO, Glennie MJ. The biology of CD20 and its potential as a target for mAb therapy. *Curr Dir Autoimmun*. 2005;8:140-74 (See appendix).

pathways used by cells to commit suicide during insect development (Lockshin and Williams, 1964). The fact that this process requires active protein synthesis was demonstrated in 1966 by the Nobel Prize winner Rita Levi-Montalcini (Levi-Montalcini, 1966). The term apoptosis was introduced by Kerr et al., (1972) to describe the characteristic set of morphological stages which occur during cell death in many different situations (Kerr et al., 1972). Since then, apoptosis has been studied extensively, with over 150,000 scientific articles published in this research area up to May 2008.

For a long time PCD has often been equated with apoptosis. However, along with research on apoptosis, it was becoming increasingly clear that other, non-apoptotic forms of PCD do exist. For example, certain developmental cell death patterns like “autophagy” (Lokshin and Williams, 1964; Clarke, 1990; Schwartz, 1991; Schweichel, 1972; Schweichel, 1973) and “cytoplasmic” cell death (Clarke, 1990; Cunningham, 1982; Oppenheim, 1985; Pilar and Landmesser, 1976) do not morphologically resemble apoptosis. Furthermore, certain neurodegenerative diseases such as Huntington’s disease and amyotrophic lateral sclerosis display cell death that is does not fulfil the morphological criteria of apoptosis (Dal Canto and Gurney, 1994; Turmaine et al., 2000), Ischemia-induced cell death also displays non-apoptotic morphology, referred to as oncosis (Majno and Joris, 1995).

In keeping with our increasing knowledge about the complexity of PCD a number of classifications have been proposed based on morphology. At the current time, the data required for *mechanistic* classification of PCD are far from complete and thus will without doubt be revisited over time. Morphologically, cell death can be divided into

two broad categories: PCD where the cell plays an active role in its elimination; and necrotic or passive cell death (Figure 1-1).

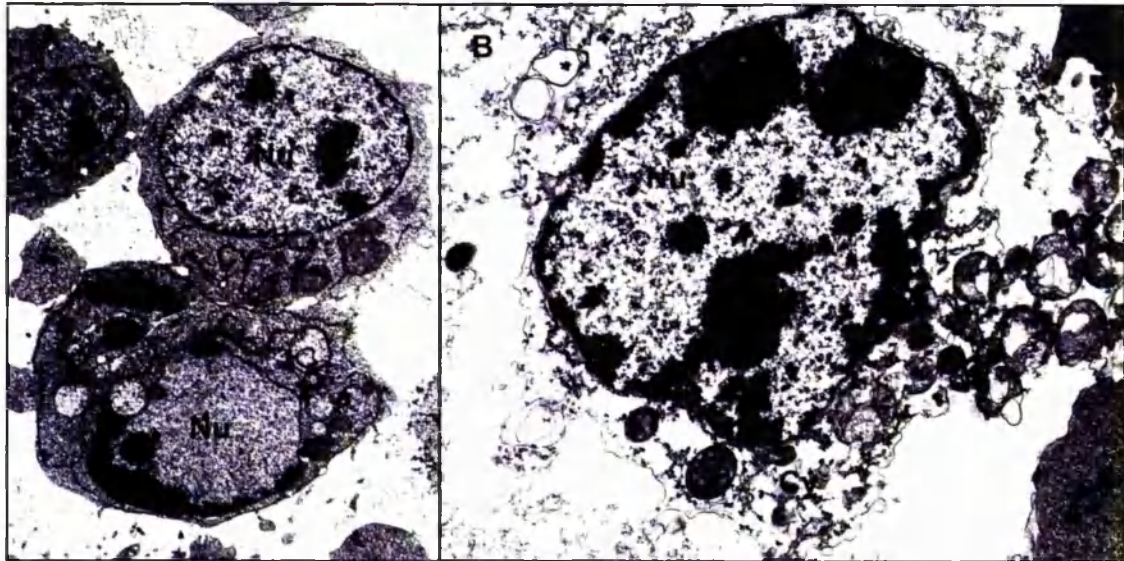
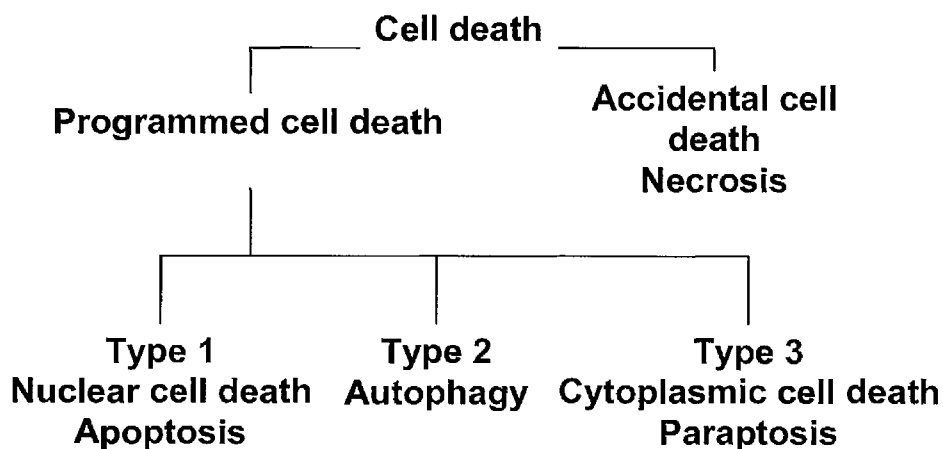


Figure 1- 1. Morphological differences between cells undergoing apoptosis and necrosis. (A) In comparison to normal cell (top), compaction of the nucleus (Nu) is occurring in the apoptotic cell (bottom). For a considerable amount of time, the cytoplasm (Cy) remains intact in these cells. (B) The primary effect in necrotic cells occurs within the cytoplasm (Cy) that is decomposing before nuclear (Nu) changes can be observed

Developmental studies revealed three different morphologies of programmed cell death: type I (nuclear or apoptotic); type II (autophagic); and type III (cytoplasmic) (Clarke, 1990). Broadly speaking, cell death can be morphologically classified as follows:



The major morphological and biochemical differences between various types of cell death are summarised in Table 1.

Table 1-1. Comparison of apoptosis, necrosis and paraptosis (taken from Sperandio et al., 2000)

	Apoptosis	Necrosis	Paraptosis
Morphology			
Nuclear fragmentation	+	—	—
Chromatin condensation	+	—	±
Apoptotic bodies	+	—	—
Cytoplasmic vacuolation	—	+	+
Mitochondrial swelling	Sometimes	+	Late
Genomic effect			
TUNEL	+	Usually —	—
Internucleosomal DNA fragmentation	+	—	—
Caspase activity			
DEVD-cleaving activity	+	—	—
Caspase-3 processing	+	—	—
PARP cleavage	+ (85-kDa fragment)	+ (50- to 62-kDa fragments)	—
Inhibition by:			
zVAD.fmk	+	—	—
BAF	+	—	—
p35	+	—	—
Xiap CAPS	+	—	—
Bcl-x _L	+	Usually —	—
Actinomycin D	Sometimes	—	+
Cycloheximide	Sometimes	—	+

DEVD, Asp-Glu-Val-Asp; PARP, poly(ADP-ribose) polymerase.

1-1-1. Type 1 programmed cell death or apoptosis

Apoptosis (Greek, for the "dropping off" of petals or leaves from plants or trees) is the best characterised form of PCD where the primary morphological affect occurs within the nucleus. At the beginning of this process, condensation of peripheral heterochromatin occurs, later comprising the entire nucleus. Subsequently, the nucleus condenses and fragments together with the cytoplasm and cellular portions (apoptotic bodies) bud off (Figure 1-2).

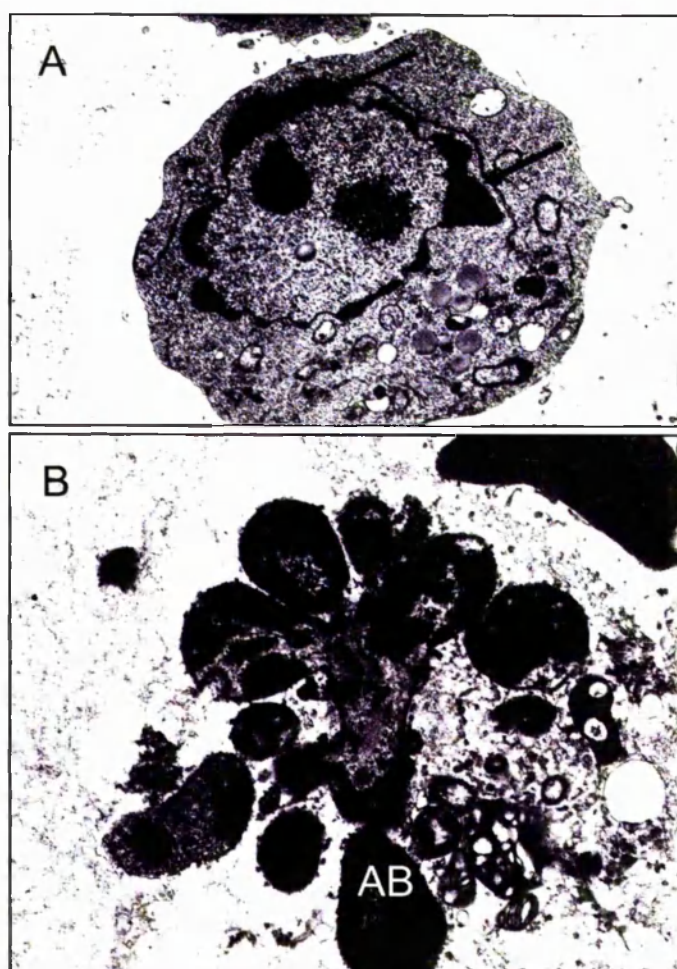


Figure 1- 2. Morphology of early (A) and late (B) apoptosis. (A) Condensation of peripheral chromatin (arrows), starting from the periphery of the cell nucleus is a morphological hallmark of early apoptosis. (B) At later stages of apoptosis, both the nucleus and cytoplasm fragment and collapse, forming apoptotic bodies (AB).

The morphological changes occurring during apoptosis are to a major extent the result of activation of caspases, a set of apoptosis-specific cysteine proteases (Thornberry and Lezebnik, 1998; Yuan et al., 1993).

The activation of apoptosis is shown to occur via two general pathways (Figure 1-3): (i) the intrinsic pathway that is triggered by the release of cytochrome c and associated activation of caspase 9; and (ii) extrinsic pathway, originating from cell surface death receptors and resulting from activation of caspases 8 or 10 (Salvesen and Dixit, 1997). Endoplasmic reticulum stress, regarded as occurring through the intrinsic apoptosis pathway, is attributable to unfolded or misfolded proteins, for example occurring during ischemia (Tajiri et al., 2004; Rao et al., 2001; Rao et al., 2002). In addition, such organelles as nucleus and Golgi complex also have damage sensors linked to apoptosis (Green and Kroemer, 2005).

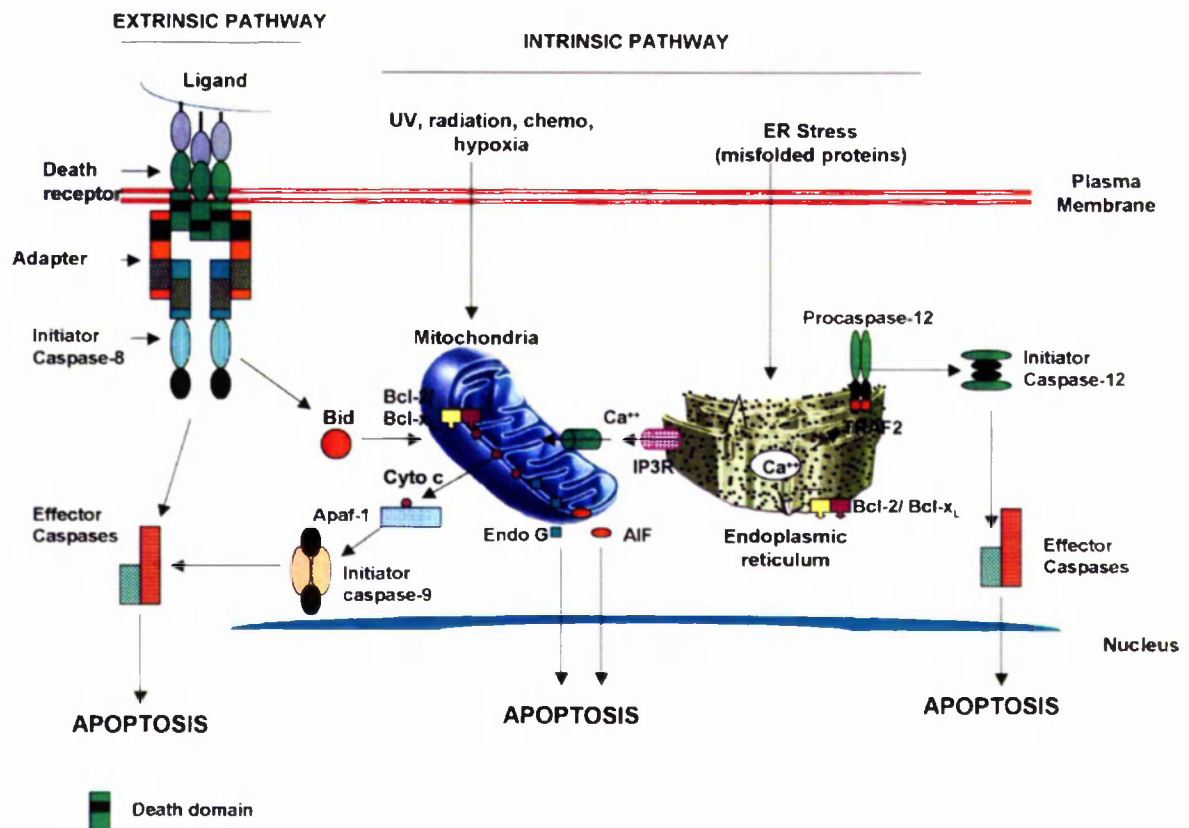


Figure 1- 3. Overview of the two major apoptosis pathways (taken from Gupta *et al.* 2006)

It is now well accepted that the induction of apoptosis plays a key role in many successful anti-cancer treatments and that proteins of the Bcl-2 protein family are key regulators of apoptosis, particularly in lymphoid cells. Members of the Bcl-2 protein family regulate the so-called mitochondrial or intrinsic apoptosis pathway (reviewed in Huang and Strasser 2000) and they can be separated into three distinct groups; the effector pro-apoptotic Bax/Bak-like proteins, the pro-apoptotic BH3-only proteins and the pro-survival Bcl-2-like proteins. Although the exact details of how apoptosis is regulated by these proteins is still the subject of intense scrutiny, the current data indicate that when Bax and/or Bak become activated, these proteins perturb the mitochondrial outer membrane, resulting in release of cytochrome c, formation of the (Apaf-1/caspase-9)

apoptosome, effector caspase activation and cellular destruction. To prevent inappropriate cell death, Bax and Bak are tightly regulated, bound and inhibited by the pro-survival Bcl-2 family members. In response to apoptotic stimuli, such as DNA damage, BH3-only proteins are induced and/or activated and they are then able to antagonise the pro-survival Bcl-2-like proteins allowing de-repression and activation of Bax and Bak, resulting in the process of cell death detailed above (Figure 1-3). To date, eight BH3-only proteins have been identified in mammals and shown to be induced after different and specific cellular insults. As such, two BH3-only proteins, Puma and Noxa, have been shown to be involved in DNA damage-induced cell death, whilst Bim is pivotal for negative selection of autoreactive T and B cells (reviewed in Strasser, 2005). Importantly, deletion of the genes encoding Bim or Noxa have been reported for a number of lymphomas, illustrating their likely importance in lymphomagenesis (Mestre-Escorihuela et al. 2006 and references therein).

Triggers of the intrinsic pathway shift the biochemical machinery towards apoptosis by increasing the ratio of pro-apoptotic members: pro-survival members. This mechanism allows the release of intermembrane mediators of apoptosis, such as cytochrome c, Smac/Diablo, AIF, and endonuclease G. The other pro-apoptotic mechanism is mediated by Nur77/TR3 that binds Bcl-2 and exposes its pro-apoptotic BH3 domain (Li et al., 2000). The anti-apoptotic proteins Bcl-2 and Bcl-XL interact with pro-apoptotic members and prevent the permeabilisation of the outer mitochondrial membrane. Thus, the anti-apoptotic members prevent the release of cytochrome c and other proapoptotic proteins from the mitochondrial interstitial space (Kluk et al., 1997).

Released from mitochondria, cytochrome c interacts with a cytosolic protein Apaf-1 which, in turn, undergoes conformational change resulting in heptamerisation. The

resulting exposure of the Apaf-1 CARD (caspase activation and recruitment domain) recruits procaspase-9 into the so-called apoptosomal complex (Figure 1-4) leading to their activation (Boatright et al., 2003). Activation of the apical caspase-9 leads to a cascade of caspase activation, including effector caspases 3 and 7.

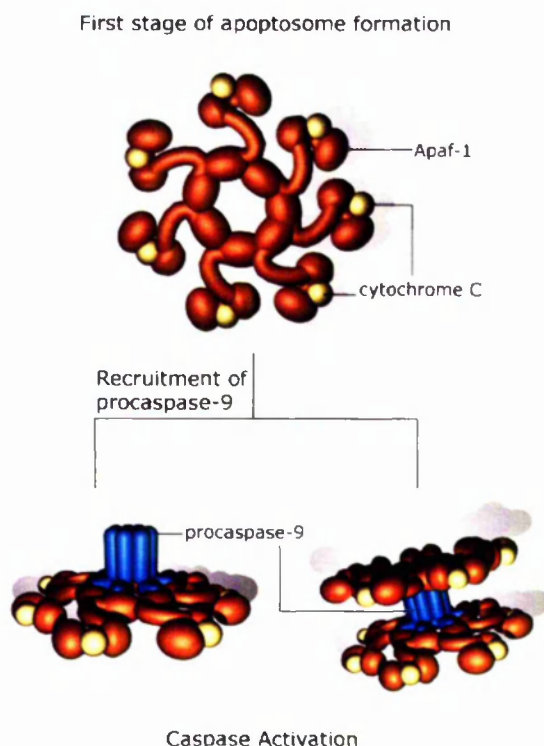


Figure 1- 4. Formation of the apoptosome and caspase-9 activation (Author – Philip Dash, with permission).

Contrary to the intrinsic apoptosis pathway, the extrinsic apoptosis pathway features caspase-8 or caspase-10 as its apical caspases. The best characterised example of the extrinsic apoptosis pathway is Fas induced apoptosis. Fas is bound by Fas ligand that, in turn, results in recruitment of FADD (Fas-associated death domain) through its death domain and then caspase-8 through the DED (death effector domain) of FADD (Muzio et al., 1996). As in the case of caspase-9 and intrinsic pathway, the induced proximity of the apical caspase leads to further activation of effector caspases. In summary, both intrinsic and extrinsic pathways of apoptosis induce the activation of effector caspases.

In addition to intrinsic and extrinsic pathways of apoptosis, endoplasmic reticulum stress may also induce caspase activation. Misfolded protein and other activators of ER stress trigger an alternative intrinsic pathway that also leads to caspase-9 activation via caspase 12 and includes both Apaf-1 dependent and independent activation of PCD (Rao et al., 2001).

1-1-2 Type 2 programmed cell death or autophagic cell death

Autophagy (Greek, “self eating”) is a lysosomal pathway of degradation of cellular organelles, proteins and protein aggregates. Targets of degradation are engulfed by an autophagosome, which then fuses with a lysosome, resulting in the degradation of the contents of the autophagosome (Figures 1-5 and 1-6).

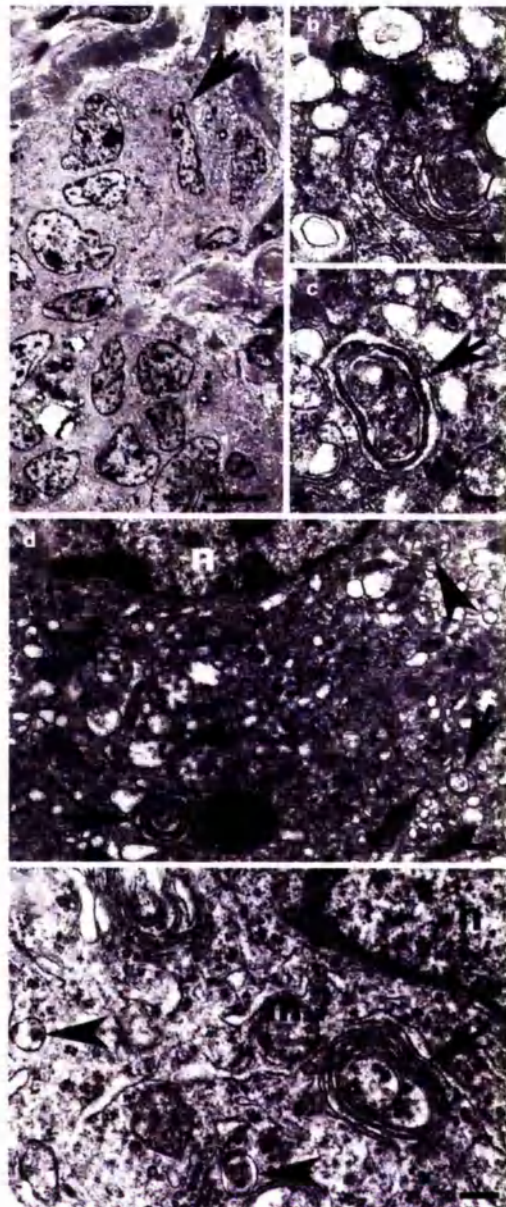


Figure 1- 5. Autophagic structures are present in neoplastic cells of multiple types of tumours. (a) Cells of a pancreatic islet cell tumour that display autophagic features and lack the hallmarks of apoptosis (arrow). (b, c) Neoplastic pancreatic islet cell tumours contain early-stage multilamellate (arrows) and single membrane-bound (arrowhead) autophagic structures. (d) Adenocarcinoma of the lung contains several multilamellate (arrows) and single membrane-bound (arrowhead) autophagic structures, while the nucleus (n) appears normal. (e) A ganglioneuroma cell with a normal nucleus (n) and mitochondria (m) contains multilamellate (arrows) and single membrane-bound (arrowhead) autophagic structures. Scale bars=10 M (a), 0.3 M (b–e). (taken from Alva et al., 2004.)

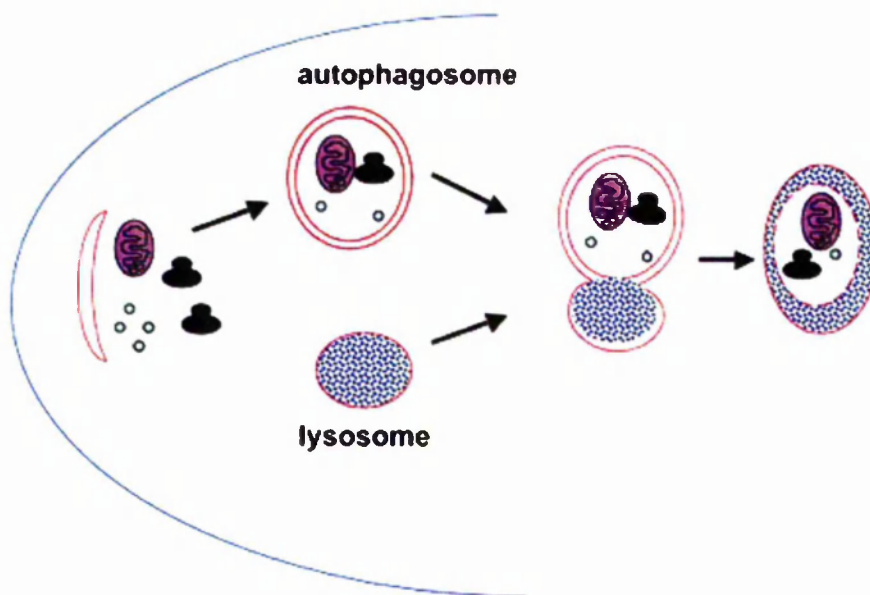


Figure 1- 6. Schematic representation of autophagy - a membrane trafficking process leading to lysosomal degradation (taken from Jin, 2007).

Three forms of autophagy have been identified: chaperone-mediated autophagy, microautophagy and macroautophagy (reviewed by Levine and Kroemer, 2008). Macroautophagy that is generally referred to as autophagy, is the major catabolic mechanism that cells use to degrade proteins and organelles. The degradation of molecules and organelles by autophagy results in energy and amino acids for protein synthesis. Normally, it is a cellular protective pathway that, being active constitutively at low level, can be upregulated by nutrient starvation. The withdrawal of nutrients inactivates mTOR (mammalian Target of Rapamycin), activating a complex of Atg proteins (Levine and Kroemer, 2008).

Although the role of autophagy in protein and organelle degradation is well accepted, the role of autophagy in cell death is still controversial (Levine and Yuan, 2005; Shimizu et al., 2004). This is because the term “autophagic cell death” has been applied to two distinct observations: cell death *associated* with autophagy and cell death *requiring* autophagy. Increasing evidence suggests that the process of autophagy is indeed required for at least some of what has been reported as autophagic cell death. Thus, mouse

embryo fibroblasts that lack both Bak and Bax, the key pro-apoptotic genes responsible for intrinsic mitochondrial death, undergo autophagic PCD after treatment with the apoptosis inducers staurosporine and etoposide. This death is dependent on the autophagy genes Atg5 and Beclin-1, and inhibited by the autophagy/classIII PI3 kinase inhibitor 3-methyladenine (Lum et al., 2005). Also, caspase inhibition by zVAD.fmk in L929 cells results in autophagy-dependent PCD (Yu et al., 2006).

Although it is presently unclear whether cell survival/cell death effects are relevant to the tumour suppressor role of autophagy (Kroemer and Jaattela, 2005), such effects are likely to be important in cancer therapeutics. A large series of clinically approved and experimental anti-cancer therapies induce the accumulation of autophagosomes in tumour cells in vitro (Maiuri et al., 2007). For many years, it was thought that these therapies kill cells through autophagy ("autophagic cell death"). However, specific inhibition of autophagy with siRNAs targeted against ATG genes usually accelerates, rather than prevents cell death in these settings (Maiuri et al., 2007), indicating that autophagy activation represents a cellular attempt to cope with stress induced by cytotoxic agents.

1-1-3. Type 3 programmed cell death or paraptosis

In comparison to apoptosis, relatively little data are available on autophagic PCD. Even less is known about other non-apoptotic forms of cell death. The vast majority of what is known about other forms of PCD is based on morphological observations. Cytoplasmic or type 3 programmed cell death, recently dubbed paraptosis, is not accompanied by caspase activation, it cannot be inhibited by caspase inhibitors (p35, zVAD.fmk, xiap, Boc-aspartyl.fmk) or mitochondrial antiapoptotic factors such as Bcl-xL and requires

new gene transcription and translation (Sperandio et al., 2000). Morphologically, paraptosis features progressive swelling of mitochondria and the endoplasmic reticulum (Figure 1-7).

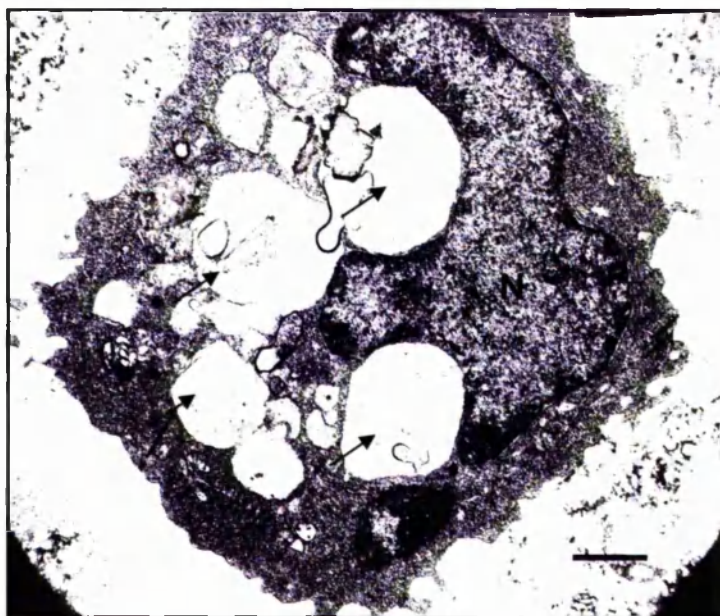


Figure 1-7. Paraptosis-like programmed cell death in Raji cells treated with anti-CD20 antibody Tositumomab. Gross vacuolisation of cytoplasm (arrows) and relatively intact nucleus (N) is the hallmark of this form of programmed cell death.

The molecular activation of type 3 programmed cell death is to a major extent unknown. Based on observations in gliocytes, ERK has been linked to the promotion of type 3 programmed cell death (Subramaniam et al., 2004; Castro-Obregon et al., 2004). Insulin-like growth factor I has also been shown to induce paraptosis, mediated by MAPK and JNK cascades in 293T cells (Sperandio et al., 2004). Also, paraptosis is reported to be triggered by cytoplasmic Ca^{2+} overload through the VR1 Ca^{2+} channel (Jambrina et al., 2003), TAJ/TROY, a member of TNF factor receptor superfamily, and PDCD-5, ubiquitously expressed cell death promoting protein with unknown function (Wang et al., 2003). Recently, the first specific endogenous inhibitor of paraptosis, AIP-1/Alix, has been described (Sperandio et al., 2004).

1-1-4. Mitotic catastrophe

Mitotic catastrophe is a mode of cell death that results from premature entry of cells into mitosis and can be caused by several pathological or physiological stresses. Initially, it was described as the main form of cell death induced by ionizing radiation. Today, it is known to be triggered also by treatment with agents influencing the stability of microtubules, various anti-cancer drugs and defective cell cycle checkpoints. Although various descriptions of mitotic catastrophe exist, there is still no general accepted definition of this phenomenon (Figure 1-8). The major feature of mitotic catastrophe is death after entry into at least the first mitosis after genotoxic insult, whereas the ultimate cell death mechanism may differ and the final outcome of mitotic catastrophe largely depends on the molecular profile of the cell.

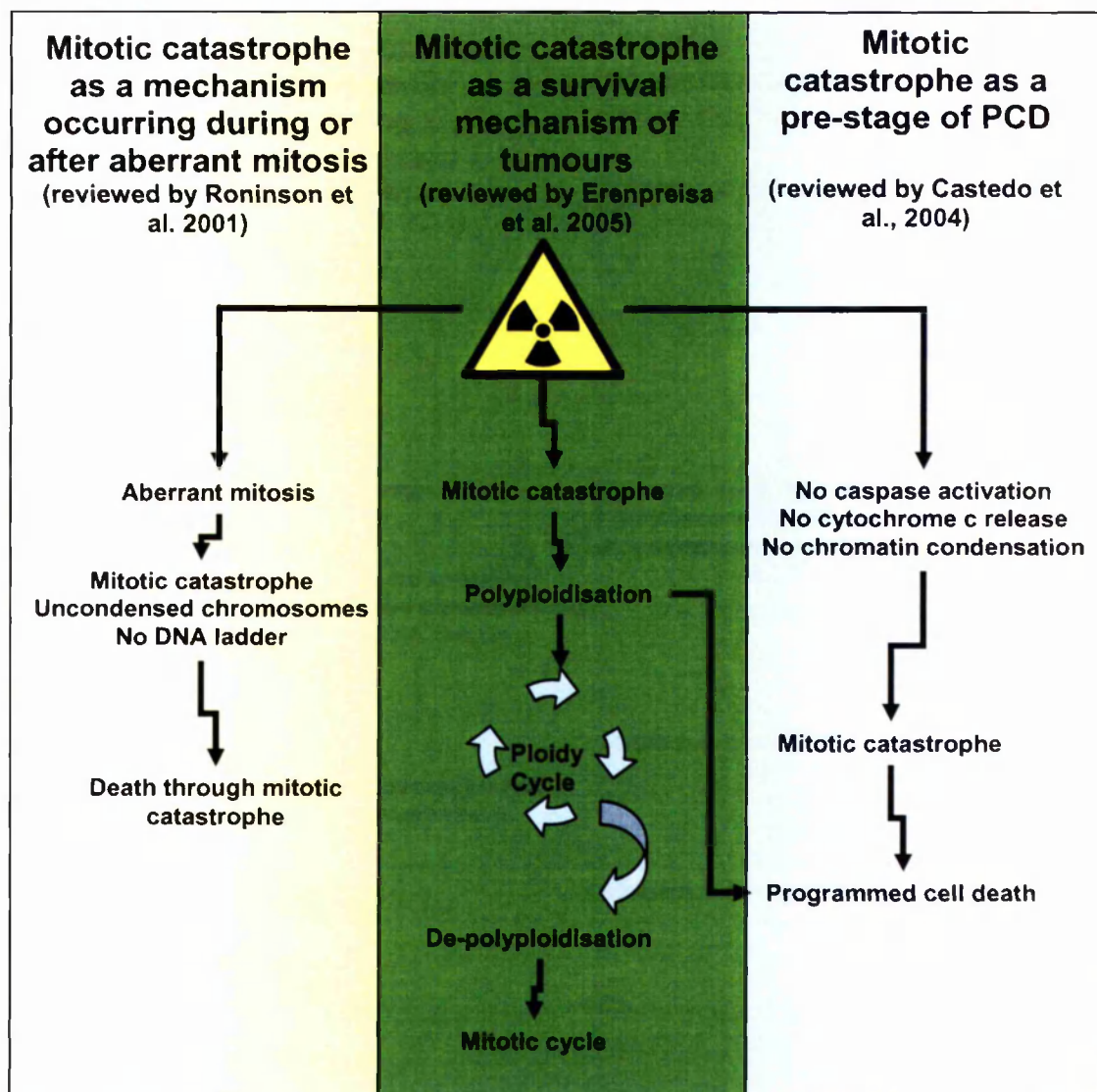


Figure 1- 8. A summary of current concepts of mitotic catastrophe.

Mitotic catastrophe has been described as an aberrant form of mitosis associated with various morphological and biochemical changes. The final step of mitotic catastrophe is almost always associated with the formation of nuclear envelopes around individual clusters of chromosomes. It is well established that tumours differ in their sensitivity to treatment. Cells sensitive to cytotoxic treatment usually die in interphase via apoptotic or other forms of PCD. Cells that do not undergo immediate apoptosis in interphase become arrested in G1 and/or G2.

If injury is not repaired within these cell cycle compartments (Figure 1-9), DNA damage can lead the cell to different death associated consequences.

Cell cycle checkpoint regulations have evolved to coordinate the response to DNA damage (Nyberg et al., 2002) (Figure 1-10) and are mediated through the activation of two different protein kinase pathways: regulated by ATM (ataxia-teleangiectasia-mutated) and ATR (ataxia teleangiectasia Rad3-related), respectively. The alert signal is modulated through the action of the so-called checkpoint adaptors (e.g. BRCA1) and further transduced through phosphorylation of effector kinases Chk1 and Chk2 (Bartek and Lucas, 2003). Furthermore, each of the cell cycle compartments requires different downstream substrates to facilitate DNA replication and mitosis. The p53/MDM2-p21 axis is dominant in G1/S arrest where the DNA damage is repaired before chromosome replication. In contrast, the G2/M checkpoint reversibly halts cell cycle progression into mitosis, preventing the segregation of damaged chromosomes (Nyberg et al., 2002). Induced expression of cell cycle inhibitors, such as the Cdk inhibitors p21 and the 14-3-3 σ protein, by p53 and checkpoint mediator BRCA1, probably affects the duration of the G2/M arrest (Xiong et al., 1993).

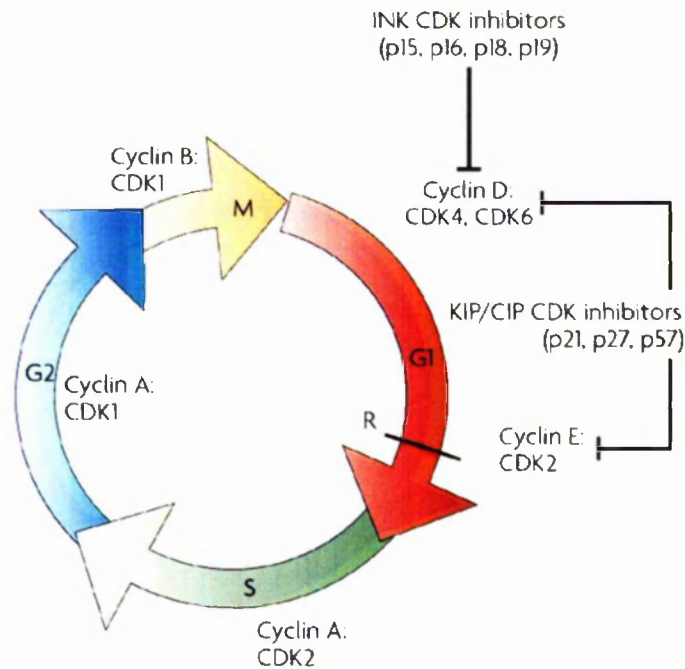


Figure 1- 9. Principal scheme of cell cycle regulation (adapted from Dehay and Kennedy, 2007)

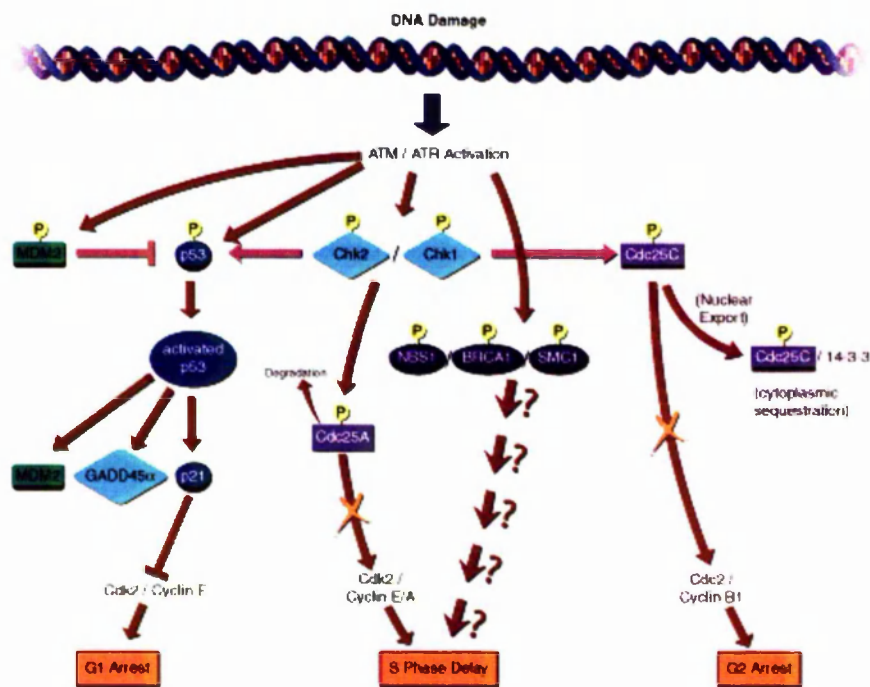


Figure 1- 10. Principal scheme of cell cycle checkpoint regulation (adapted from RnB systems webpage)

Cells with impaired or lost checkpoint functions are unable to maintain this arrest and enter mitosis prematurely before DNA damage is repaired (Radford and Murphy, 1994; Bunz et al., 1998).

1-1-4-1 Polyploid giant cells – a hallmark of mitotic catastrophe

Formation of polyploid giant cells is a hallmark of mitotic catastrophe that was first observed in colonies of X-ray irradiated cells (Tolmach and Marcus, 1960). Following irradiation, the size of some cells continually increased finally becoming 200 times bigger than normal cells (Tolmach and Marcus, 1960). The formation of giant cells was initially explained by several mechanisms: either by fusion of daughter cells after cell division or by abnormal cell division, or by a combination of both. Recently, it was shown that the formation of giant cells is generally not a consequence of daughter cell fusion but is a result of (i) fusion between mitotic cells and cells in S or G2 phase or (ii) the lack of fission of the mitotic cell (Castedo et al., 2004). The second assumption is based on the suggestion that irradiated cells can go through a sequence of S phase repetitions *in status nascendi* (endoreplication) before they enter mitosis in a polyploid state (Yu and Sinclair, 1964).

Although endopolyploidy may be the main mechanism for the formation of giant cells, it seems that uncoupling of DNA synthesis from cell division (endocycling) is the primary cause of the formation of polyploid cells (reviewed by Erenpreisa et al., 2005). Endocycling has been observed in many tumour cells and specifically in those lacking p53 (Illidge et al., 2000; Castedo et al., 2004).

The ability of these polyploid cells to participate in the restitution process of tumour cells after genotoxic damage is still controversial. Previously, we have shown that the endopolyploid cells produced as a result of mitotic arrest induced by genotoxic stress have the capacity to repair DNA double strand breaks (DSB) by homologous recombination, which may provide a survival advantage for cells that undergo mitotic catastrophe in response to severe genotoxic treatment (Ivanov et al., 2003). These findings are in keeping with other emerging reports linking the survival of acute myeloid leukemia cells after treatment with daunorubicin with delayed apoptosis and the formation of large endopolyploid cells (Come et al., 1999). The formation of endopolyploid cells as a response to genotoxic insult is clearly a common phenomenon of tumour cells in vitro and there are many reports linking the presence of endopolyploid tumour cells with poor response to therapy (for reviews, see Levine, 1999; Evans and Podratz, 1996). Furthermore, disease outcome prognosis, or indeed p53 status and multiploidy, but not aneuploidy, appear to be adverse prognostic factors for stage II colorectal cancers (Buglioni et al., 2001).

Several possible scenarios for the fate of giant cells have been suggested. According to one of them, their death is a direct cause of mitotic catastrophe and it is distinct from apoptosis (Roninson et al., 2001). This conclusion was based on dissimilarities in morphology between cells undergoing mitotic catastrophe, illustrated by the formation of nuclear envelopes around individual clusters of missegregated, uncondensed chromosomes (Erenpreisa et al., 2002), and apoptotic cells, which are recognized by a reduced volume, condensed chromatin, nuclear fragmentation, membrane blebbing and formation of apoptotic bodies (Kerr et al., 1972). Despite their distinct morphology, some authors have suggested that both processes share several biochemical hallmarks. For example, inhibition of Chk2 in syncytia generated by the fusion of asynchronous

HeLa cells, resulting in metaphase-associated mitotic catastrophe was accompanied by sequential caspase-2 activation, mitochondrial release of pro-apoptotic proteins, activation of caspase-3, DNA fragmentation and chromatin condensation (Castedo et al., 2004). However, it was also reported that dying giant cells are characterized by uncondensed chromatin and the absence of DNA ladder formation (Roninson et al., 2001). It seems that the presence or absence of chromatin condensation during mitotic catastrophe depends on differing events that includes the stage when mitotic arrest takes place. Indeed, caspases are essential for the termination of mitotic catastrophe, suggesting that mitotic catastrophe related morphological changes are followed by activation of the apoptotic machinery (Erenpreisa et al., 2005). Thus, mitotic catastrophe it appears is not an ultimate manifestation of cell death but rather a process leading to apoptosis. Indeed, it was shown that irradiation of various tumours of lymphoid origin induced mitotic arrest and accumulation of giant cells, which seemed to die due to apoptosis (Erenpreisa et al., 2000; Illidge et al., 2000). It is of note that, apart from giant cells, other cell populations, such as micronucleated cells, might result from mitotic catastrophe and, finally, die due to apoptosis.

Mitotic arrest is strongly associated with apoptosis, but the exact molecular mechanism of this association remains to be elucidated (Woods et al., 1995; DeLuca et al., 2002). Premature mitosis leading to an arrest during the metaphase–anaphase transition is a p53-independent event and readily occurs in p53 mutated tumours (Illidge et al., 2001; Ivanov et al., 2003). Apoptosis in metaphase has also been suggested to occur independently from p53 but as a consequence of caspase-2 activation (Castedo et al., 2004). Apoptosis, however, is not always required for mitotic catastrophe-associated cell death lethality, as some giant cells can undergo death in a necrosis-like manner. This conclusion is based on some similarities between morphological changes during mitotic

catastrophe and necrosis (the loss of nuclear and plasma membrane integrities) (Eom et al., 2005; Schimming et al., 1999). Necrosis-like cell death following mitotic catastrophe could be an effect of genetic instability caused by aneuploidy and/or polyploidy (Rajagopalan et al., 2003). Taken together, it is important to note that cells that are facing a mitotic-linked cell death can in fact die by two separate mechanisms, by either apoptosis or necrosis.

In addition to metaphase arrest-induced apoptosis, tetraploid cells that are generated through catastrophic mitosis followed by mitotic slippage also undergo apoptosis. An immediate induction of p21 after mitotic slippage is an indicator of a p53-dependent checkpoint response in G1, which would act as a second 'fail-system' after an aberrant mitosis (Vogel et al., 2004). However, as there are some examples when cells do not halt in response to the G1 checkpoint even in the presence of a functional p53, it is not clear whether activation of this arrest has any role in cell death initiation. Despite this knowledge, it is obvious that tetraploid cells require activation of p53 and its target genes for induction of the mitochondrial apoptotic pathway (Vitalc et al., 2005).

1-2. DNA repair

DNA repair is the process by which cells detect and correct the damage to the DNA molecule. During normal homeostasis, both metabolic activities and environmental factors can cause DNA damage, resulting in as many as 500,000 individual molecular lesions per cell per day (Lodish et al., 2004). The rate of DNA repair is dependent on several factors, including the cell type, age, and the extracellular environment. A cell that has accumulated a large amount of DNA damage, or one that no longer effectively repairs damage incurred to its DNA, can enter one of three possible states: (i) cell

senescence, (ii) cell death, (iii) unregulated cell division that might ultimately lead to neoplasia (Figure 1-11).

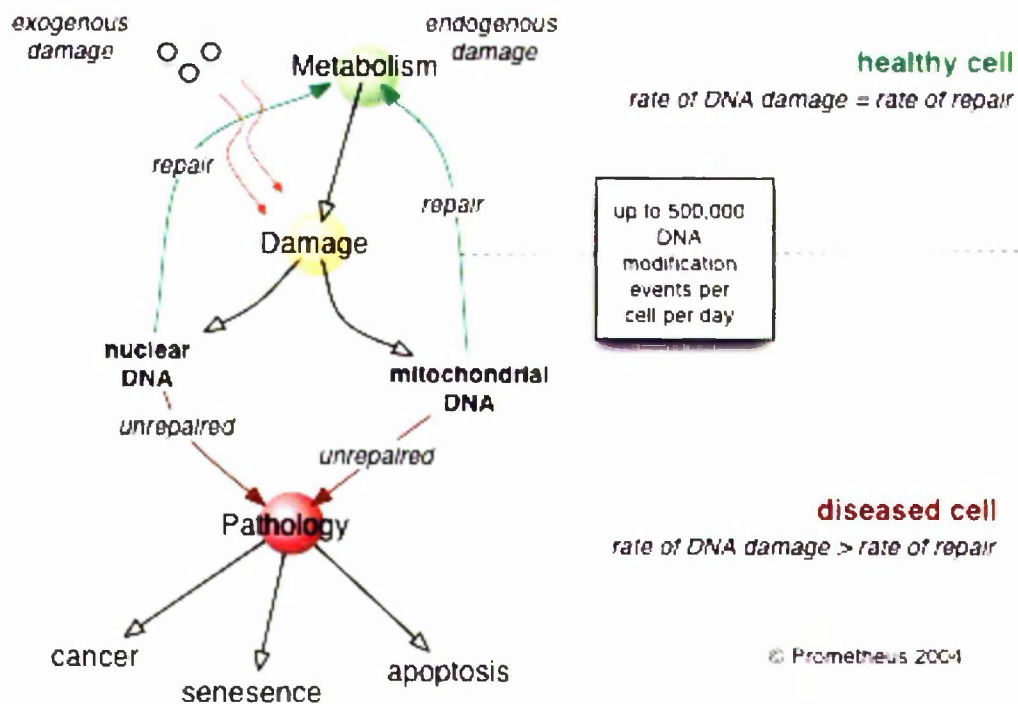


Figure 1- 11. The involvement of DNA repair in cell metabolism. Author - Harold Brenner (with permission).

1-2-1. DNA single strand breaks

When only one of the two strands of a double helix has a defect, the other strand can be used as a template to correct the damaged strand. In order to repair damage to one of the two paired molecules of DNA, a number of excision repair mechanisms exist that remove the damaged nucleotide and replace it with an undamaged nucleotide complementary to that found in the undamaged DNA strand (Watson et al., 2004). Examples of these mechanisms are detailed below:

1. **Base excision repair (BER)**, which repairs damage to a single nucleotide caused by oxidation, alkylation, hydrolysis, or deamination. The base is removed by a glycosylase and ultimately replaced by repair synthesis with DNA ligase.

2. **Nucleotide excision repair (NER)**, which repairs damage affecting longer strands of 2–30 bases. This process recognizes bulky, helix-distorting changes such as thymine dimers as well as single-strand breaks (repaired with enzymes such as UvrABC endonuclease). A specialized form of NER known as Transcription-Coupled Repair (TCR) deploys high-priority NER repair enzymes to genes that are being actively transcribed.

3. **Mismatch repair (MMR)**, which corrects errors of DNA replication and recombination that result in mispaired (but normal, that is non-damaged) nucleotides following DNA replication.

1-2-2. DNA double strand breaks (DSB)

The DNA DSB is the principle cytotoxic lesion resulting from ionizing radiation and radio-mimetic chemicals but can also be caused by mechanical stress on chromosomes or when a replicative DNA polymerase encounters a DNA single-strand break or other type of DNA lesion. Inaccurate repair or lack of repair of a DSB can lead to mutations or to larger-scale genomic instability through the generation of dicentric or acentric chromosomal fragments. Such genome changes may have tumourigenic potential. In other instances, DSB can be sufficient to induce apoptosis.

As shown in Figure 1-12, cells respond to DNA DSB through the systems that detect the DNA lesion and then trigger various downstream events. At least in some cases, these systems can be viewed as classical signal-transduction cascades in which a 'signal' (DNA damage) is detected by a 'sensor' (DNA-damage binding protein) that then triggers the activation of a 'transducer' system (protein kinase cascade), which amplifies and diversifies the signal by targeting a series of downstream 'effectors' of the DNA-damage response. Clearly, such systems need to be exquisitely sensitive and selective, as they must be triggered rapidly and efficiently by low numbers of, and maybe just one, chromosomal DNA DSB, yet must remain inactive under other conditions, such as during normal replication.

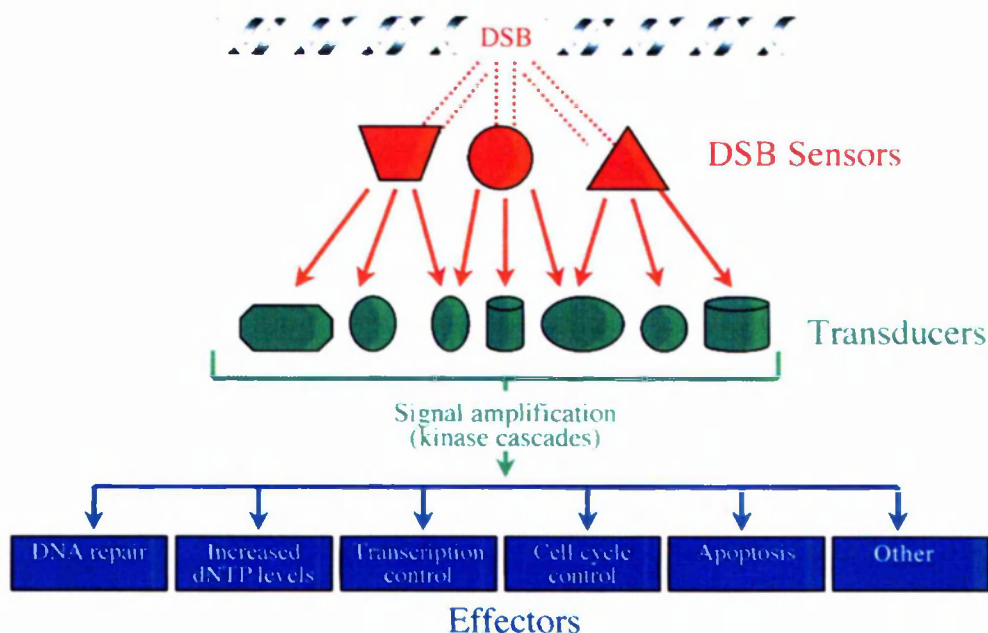


Figure 1- 12. Schematic representation of cellular response to DNA DSB. Multiple sensor proteins are shown that physically recognize DNA damage. Multiple transducer proteins then amplify and diversify the DNA-damage signal, and a range of downstream effectors regulate various aspects of cellular function (adapted from Jackson, 2002).

DNA DSB are repaired through either of two distinct biochemical pathways, homologous recombination (HR) or non-homologous end joining (NHEJ). Defects in

either of these pathways can impact at different developmental stages and in different tissues. A distinguishing feature between the DNA DSB pathways is the requirement of HR for a sister chromatid to be present in the S/G2 phase of replicating cells, implying that the repair of DSB in non-replicating cells occurs via NHEJ.

1-2-3. Homologous recombination (HR)

HR (Figure 1-13) is an error-free process that uses a sister chromatid as template DNA to achieve precise repair (Thacker and Zdzienicka, 2003; West, 2003; Helleday et al., 2007). Homology-directed repair initially involves an Mre11–Rad50–Nbs1 (MRN)-mediated 5'-3' resection followed by Rad51-mediated homology search and strand invasion. The Rad51 recombinase functions in concert with a series of other factors including the Rad51 paralogs (Xrcc2, Xrcc3, RAD51L1, RAD51L2, RAD51L3), Rad52 and Rad54 proteins to promote strand invasion and subsequent recombination (West, 2003; Thacker and Zdzienicka, 2004; Wyman et al., 2004; Helleday et al., 2007). Strand invasion and migration involves formation of a structure termed a Holliday Junction, resolution of which via Rad54, Mus81/Emc1 and Rad51C/Xrcc3 occurs following synthesis by DNA polymerase to complete the repair process.

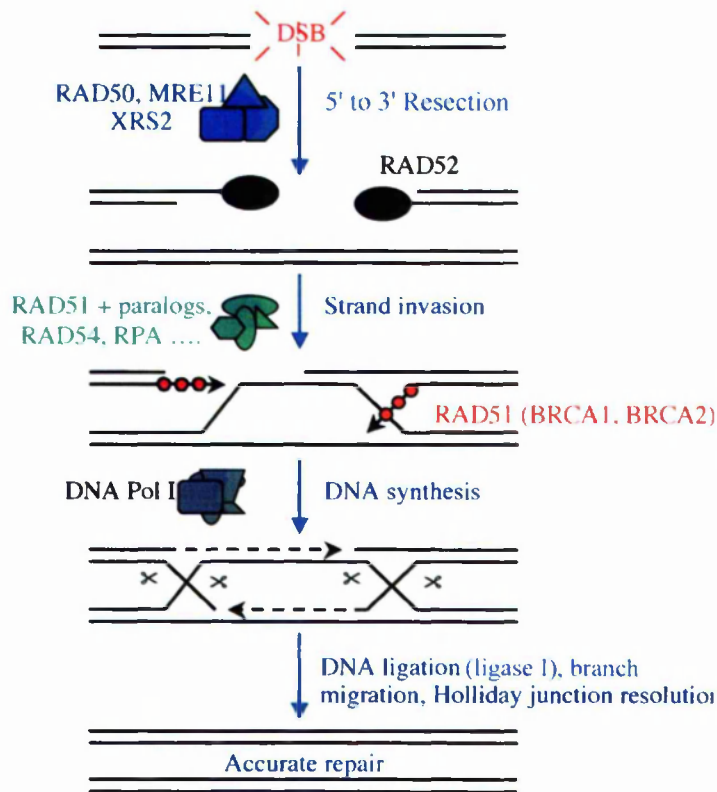


Figure 1- 13. DNA DSB repair via homologous recombination. Homologous recombination is a type of genetic recombination whereby physical rearrangement occurs between two strands of DNA. Homologous recombination involves the alignment of similar sequences, a cross-over between the aligned DNA strands, and breaking and repair of the DNA to produce an exchange of material between the strands (adapted from Jackson, 2002).

1-2-4. Non-homologous end joining

In contrast to HR, NHEJ is an error-prone DSB repair mechanism (Figure 1-14), that involves the DNA-dependent protein kinase (DNA-PK) and the DNA ligase IV (Lig4) complex, which together facilitate re-joining of broken non-compatible DNA ends (Lieber et al., 2003).

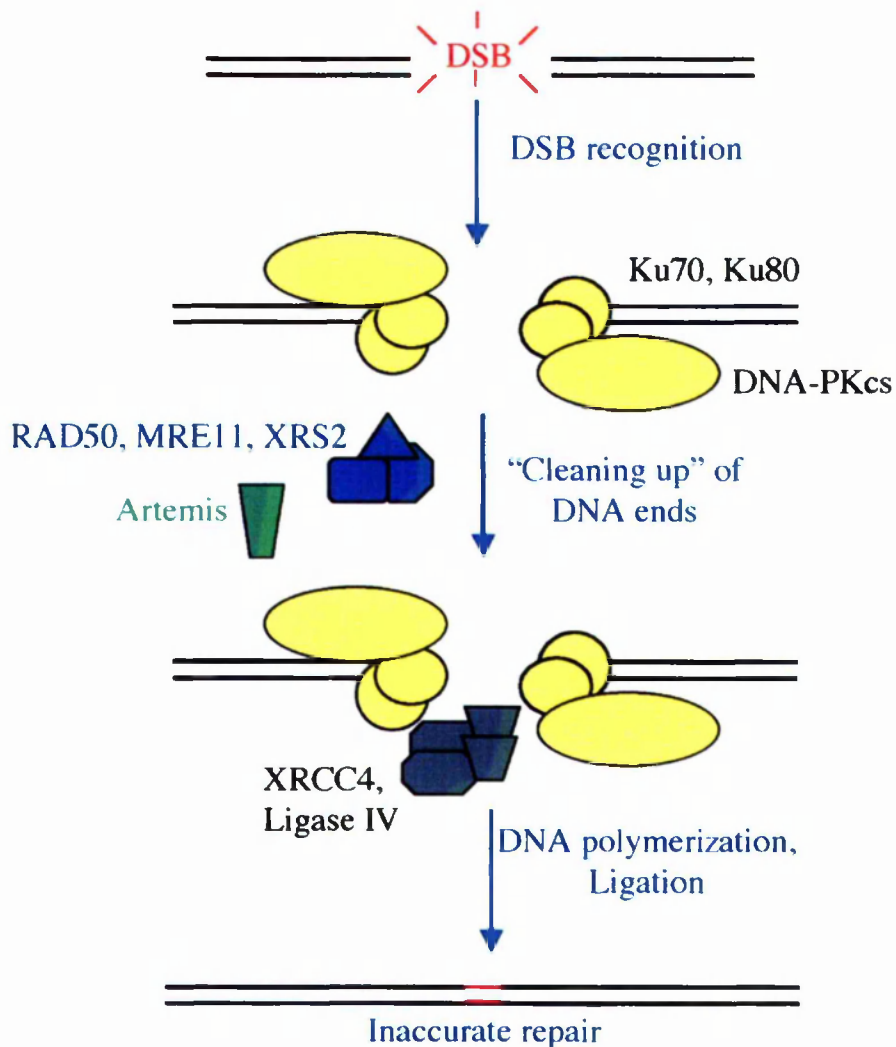


Figure 1- 14. Schematic representation of DNA NHEJ, indicating the known players in this pathway in vertebrates. NHEJ rejoins the two broken ends directly and generally leads to small deletions of DNA sequence. It requires Ku70/80, which binds to free ends and recruits DNA-PKcs. Ku then recruits XRCC4 along with DNA ligase IV, and DNA-PKcs-mediated phosphorylation of XRCC4 may influence its activity. Ligase IV then brings about the physical religation of the DNA ends. The MRE11–RAD50–NBS1 complex, which contains exo- and endo-nuclease and helicase activities, may also function in NHEJ, particularly if the DNA ends require processing before ligation. However, it is possible that other nucleases are involved in addition to or instead of the MRE11 complex, and candidates for such a nuclease include mammalian Artemis (shown) and *S.cerevisiae* Rad27p. In many cases, NHEJ may also require the actions of a DNA polymerase(s) (adapted from Jackson, 2002).

The DNA-PK complex contains Ku70 and Ku80 proteins, which recognize the break and mediate recruitment of the DNA-PK catalytic subunit, a protein kinase required for

efficient NHEJ (Lees-Miller and Meek, 2003; Bassing and Alt, 2004). Ligation of the DNA ends occurs via Lig4 in conjunction with its binding partner Xrcc4. An additional factor, Cernunnos/XLF, has been identified as a binding partner of the Lig4-Xrcc4 complex and appears to be necessary for efficient ligation via NHEJ (Ahnesorg et al., 2006). Subsets of NHEJ may involve other factors such as Artemis (Moshous et al., 2001; Jeggo and O'Neill, 2002). The extent to which Artemis is required during canonical NHEJ (independent of V(D)J recombination) remains uncertain, as conflicting data on its requirement for end joining have been reported (Rooney et al., 2003; Riballo et al., 2004).

Overall, while HR is available for repair during late S/G₂, NHEJ is most prominently activated in G₁, G₀ and early S phase of the cell cycle (Rothkamm et al., 2003) (Figure 1-15).

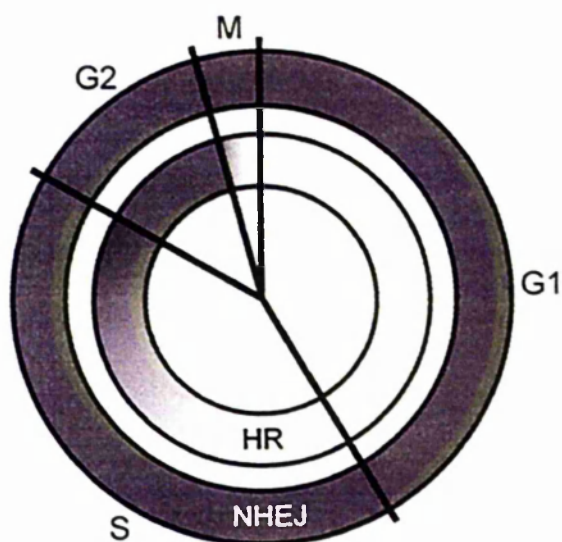


Figure 1- 15. Model of the relative contributions of HR and NHEJ to the repair of radiation-induced DSB in different cell cycle phases, based on mutant phenotypes. Whereas NHEJ predominates in G₁/early S, both HR and NHEJ contribute substantially to DSB repair during late S/G₂ (taken from Rothkamm et al., 2003)

1-3. The use of monoclonal antibodies against cancer

The use of monoclonal antibodies (mAb) as anti-cancer therapies has been explored since their initial development by Kohler and Milstein (Kohler and Milstein, 1975). Given their high specificity, unlike chemotherapy, antibodies have the potential to preferentially bind to tumour cells over normal tissues. This specificity may allow targeted killing of malignant cells and relative sparing of unbound normal tissues. Many investigators have explored immunotoxins or radioimmunoconjugates as methods to deliver a toxic compound or radioactivity to tumour cells (Park and Press, 2007). Unlabelled mAb may employ a number of mechanisms to cause direct anti-cancer effects or induce a secondary immune response against tumour cells through complement dependent cytotoxicity (CDC) or antibody dependent cytotoxicity (ADCC). The relatively prominent vascularity of most lymphomas, as well as their general responsiveness to immune system manipulation, chemotherapy and radiotherapy, suggest that they may have a favourable setting for this treatment modality. In fact, the first successful use of mAb as treatments for cancer was demonstrated in lymphoma, and these agents have now been employed to benefit thousands of patients with NHL. The chimeric anti-CD20 antibody rituximab was the first food and drug administration approved therapeutic antibody to use in human malignancy and displayed impressive clinical responses (Maloney et al., 1997). The clear activity of mAb as single agents has subsequently led to further evaluation of combinations with chemotherapy and other biologics.

1-4. Principles of radioimmunotherapy. Combining targeted radiation with antibody therapy

The exquisite sensitivity of haematological malignancies to targeted radiation (Park and Press, 2007) alongside the impressive results achieved by the pioneers in this field suggests that radioimmunotherapy is likely to be a productive area for future clinical research. Recent experimental work has demonstrated that the combination of targeted radiation and antibody effector mechanisms are critical to long term clearance of tumour (Du et al., 2004).

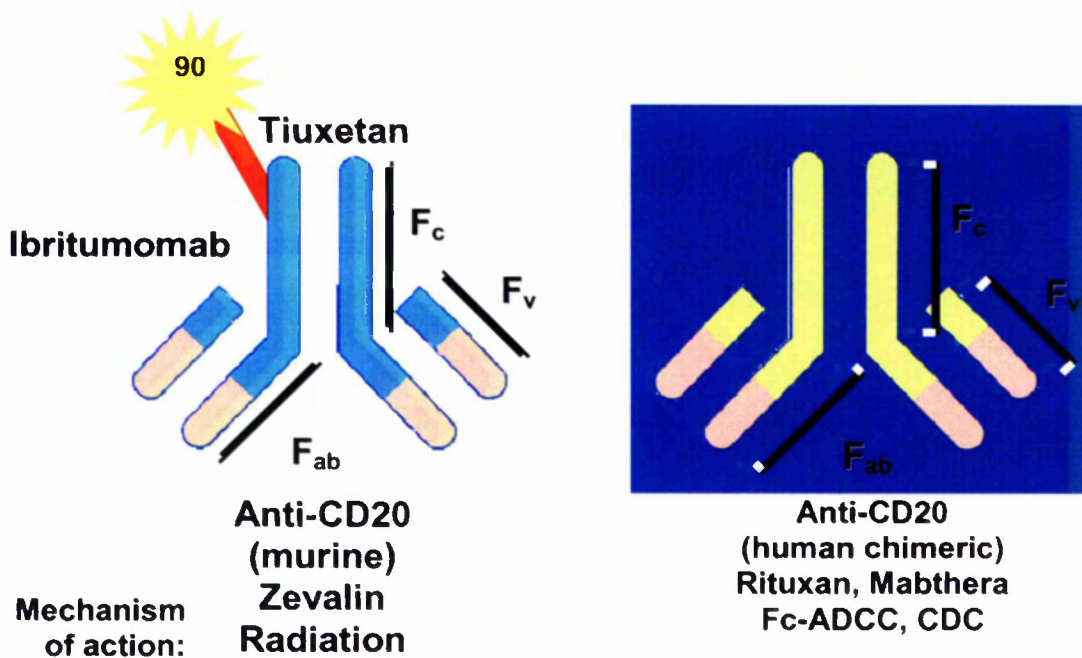


Figure 1- 16. The principal structure of anti-CD20 antibody Rituximab and Rituximab labelled with 90Y (Zevalin) used in radioimmunotherapy.

The use of mAb (Figure 1-16) in routine clinical practice is now well established and has led to impressive improvements in outcome for patients with a range of human cancers (Adams and Weiner, 2005; Robak, 2004). Although the single agent activity of

most mAb has been modest, when used in combination with both chemotherapy and radiotherapy highly impressive increases in clinical responses and improvement in survival have been seen (Coiffier et al., 2002; Robak, 2004). In this context, mAb were initially regarded simply as direct carriers for the radioisotope which deliver systemically targeted cytotoxic radiation to areas of disease, with relative sparing of normal tissue. It is however becoming clearer that the mAb effector mechanisms may also play an important additional role in killing lymphoma cells. The nature of RIT determines that its efficacy depends on a number of factors, including the properties of the **targeted antigen** (tumour-specificity, density, signalling activity, availability, shedding and heterogeneity of expression), the **tumour** (degree of vascularisation, blood flow and permeability), the **mAb** (immunoreactivity, stability, isotype and affinity) and the properties of the chosen **radioisotope** (emission characteristics, half-life and bioavailability) (Knox and Meredith, 2000).

A wide variety of different mAb, delivery schedules, radioisotopes, and doses of radioactivity have been used in RIT and have resulted in impressive, durable, partial and complete responses (PRs and CRs) in the treatment of non-Hodgkin's lymphoma (NHL) (Park and Press, 2007).

The use of radiotherapy in the treatment of haematological malignancies is well established and for localised disease it is a highly effective treatment modality, given the exquisite sensitivity of lymphomas and leukaemias to radiation induced cell death (Adams and Weiner, 2005). The systemic nature of the majority of lymphomas and leukaemias however makes localized irradiation inappropriate for most patients. Therefore the systemic delivery of targeted radiation in the form of RIT, is a logical

strategy given for disseminated tumours, especially those known to be so radiosensitive. The effective delivery of RIT requires the selection of a suitable tumour antigen target.

Tumour specific antigens would be the ideal targets for RIT, but such a degree of specificity is unusual. In practice tumour associated antigens, expressed abundantly on tumour cells as well as on a restricted subset of normal tissues represent the majority of potential targets. As most NHL are of B-cell origin the predominantly B-cell specific antigens such as Human Leukocyte Antigen DR (HLA-DR), CD19, CD20, CD22, and CD37 have been extensively evaluated as targets for RIT (Adams and Weiner, 2005; Robak, 2004; Kaminski et al., 2001; DeNardo et al., 1998; Illidge et al., 1999, Press et al., 1989). Table 1 shows the antigen characteristics that are considered ideal for RIT.

Table 1-2 Summary of characteristics considered ideal in an antigen target for RIT (Taken from Ivanov et al., 2008)

The characteristics of an ideal target antigen
Tumour cell specific
Highly expressed on tumour cells
No tendency to mutation
Not secreted or shed
Not rapidly modulated on antibody binding
Critical for target cell survival
Not expressed on critical or non renewable host cells
Delivers death/CCA signals to the target cell (eg. anti-Id)

From these initial investigations, the CD20 antigen emerged as having many of the characteristics thought to be important for a good tumour target. Targeting this antigen has thus dominated clinical RIT of lymphoma (Grossbard et al., 1992).

Although RIT has emerged as an effective treatment for lymphoma, the relative contributions of antibody effector mechanisms and targeted radiation to tumour cell death remain poorly understood. By using different syngeneic murine B cell lymphoma models the relative contributions of mAb and targeted radiation to the clearance of tumour *in vivo* been investigated (Du et al., 2004). There is now substantial evidence that mAb form an important active component of RIT and that mAb effector mechanisms may be important in the clearance of tumour *in vivo* (see chapter 1-6).

I^{131} has been the radionuclide used most often for RIT because it is relatively cheap, easily conjugated and can be used for both imaging and therapy, and has demonstrated marked clinical efficacy in treating malignancies such as thyroid cancer and, more recently, B cell lymphomas (Press and Rasey, 2000). However, I^{131} -conjugates are rapidly degraded after endocytosis into tumour cells, and the resultant small molecular weight I^{131} -metabolites are rapidly released into the bloodstream (Press and Rasey, 2000). In addition, the rays emitted by I^{131} present a potential radiation hazard for family members and health care providers, thereby necessitating hospitalization for radiation isolation if very large doses are employed.

Y^{90} is the second most commonly used radionuclide. It emits β particles that are five times more energetic than those from I^{131} , emits very few rays, has a favourable half-life (2.5 days), is easily employed on an outpatient basis, and is stably retained by tumour cells even after endocytosis (Press and Rasey, 2000). However, the absence of

emissions means that Y-90 cannot be used for scintigraphy by conventional methods. However, Indium⁻¹¹¹ is very similar to Y-90 in its radiochemistry and its bio-distribution behaviour, rendering it suitable for use as a surrogate radioisotope for imaging purposes. Y-90 is generally more expensive and more difficult to obtain than I-131, though the cost differential may be offset by fewer hospitalizations. Y-90 has a tendency to accumulate non-specifically in the liver and bones, though this is less of a problem with newer, more stable chelation methods. Other β -emitting isotopes such as Copper-67 also appear very promising and may be superior to I-131 but their accessibility is currently limited.

1-5. CD20 antigen

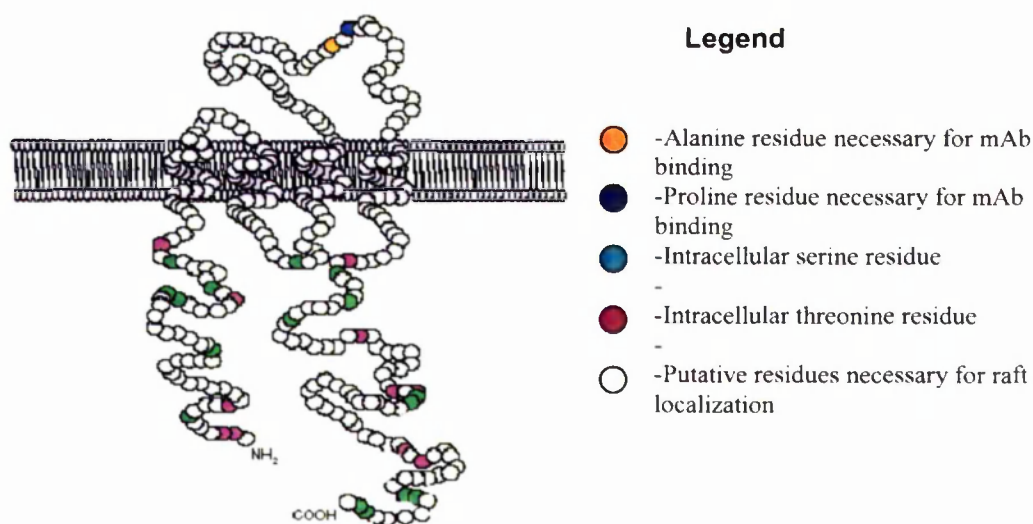


Figure 1- 17. “Schematic diagram of the structure of CD20. CD20 spans the membrane 4 times and possesses intracellular C- and N-termini. Two regions of CD20 are extracellular, forming a small and large loop, although only the large loop which contains an Ala - Pro motif appears vital for mAb binding. Also shown are the potential sites for Ser/Thr phosphorylation and region of human CD20 thought to be important for localisation to membrane rafts. Proposed signalling mechanism of anti-CD20 mAb: In resting cells, (stage 1) CD20 multimers (probably at least tetramers) are found in small pre-formed mini-raft domains associated with PAG. PAG is constitutively phosphorylated, resulting in its association with Csk via a phosphotyrosine at residue 317. Csk inhibits Src kinases such as Lyn through phosphorylation of an inhibitory tyrosine in the C-terminus. Together, these three proteins establish a steady state of kinase activity. When anti-CD20 mAb bind, they cause clustering of CD20 multimers

(stage 2). This may cause a change in the steady-state interaction of Lyn, Csk and PAG, possibly resulting in a reduction in the phosphorylation of PAG at residue 317, leading to the release of Csk. Once Lyn is released from Csk-mediated inhibition (stage 3), it will become dephosphorylated on the C-terminal inhibitory tyrosine and adopt a more open conformation with a corresponding increase in kinase activity. Potentially, Lyn will then phosphorylate the stimulatory tyrosine residue present in the active site of an adjoining Lyn molecule, causing a further increase in protein tyrosine kinase activity, resulting in the phosphorylation of other cellular substrates" (Taken from Cragg et al., 2005).

CD20 is a B lymphocyte-specific cell-surface molecule involved in the regulation of transmembrane Ca^{2+} conductance and cell-cycle progression during human B cell activation (Tedder and Engel, 1994). The CD20 cDNAs encode a membrane-embedded protein with hydrophobic regions of sufficient lengths to pass through the membrane 4 times (Tedder and Schlossman., 1988; Einfeld et al., 1988). The cytoplasmic domains are serine and threonine rich with multiple consensus sequences for phosphorylation. Human CD20 is not glycosylated, but three isoforms (33, 35 and 37,000 M_r) result from the differential phosphorylation of a single protein on different serine and threonine residues (Valentine et al., 1989).

The precise role of CD20 remains poorly defined but it appears to play a role in the regulation of human B cell activation, proliferation and Ca^{2+} transport (Bubien et al., 1993). Antibody ligation of CD20 can generate transmembrane signals that result in enhanced CD20 phosphorylation (Tedder and Schlossmann, 1988), induction of *c-myc* and *B-myb* oncogene expression (Smeland et al., 1987), induced serine/threonine and tyrosine phosphorylation of cellular proteins (Deans et al., 1993), increased CD18, CD58 and MHC class II molecule expression (White et al., 1991), and protein tyrosine kinase activation that induces B cell adhesion (Kansas and Tedder, 1991). CD20 ligation promotes transmembrane Ca^{2+} transport (Bubien et al., 1993), but does not usually lead to increased intracellular calcium ($[\text{Ca}^{2+}]_i$)³ levels (Bubien et al., 1993; Tedder et al., 1986; Golay et al., 1985), except after extensive cross-linking (Deans et al., 1993).

Antibody binding to CD20 inhibits B cell progression from the G₁ phase into the S/G₂ + M stages of the cell cycle following mitogen stimulation, and inhibits mitogen-induced B cell differentiation and antibody secretion (Tedder et al., 1986; Golay et al., 1985). Extensive CD20 cross-linking can also influence apoptosis (Holder et al., 1995; Shan et al., 1998). These divergent observations may be explained in part by the finding that CD20 is a component of an oligomeric complex that forms a membrane transporter or Ca²⁺ ion channel that is activated during cell-cycle progression (Kanzaki et al., 1995). Despite this, B cell development and function in a line of CD20-deficient (CD20^{-/-}) mice is reported to be normal (O'Keefe et al., 1998).

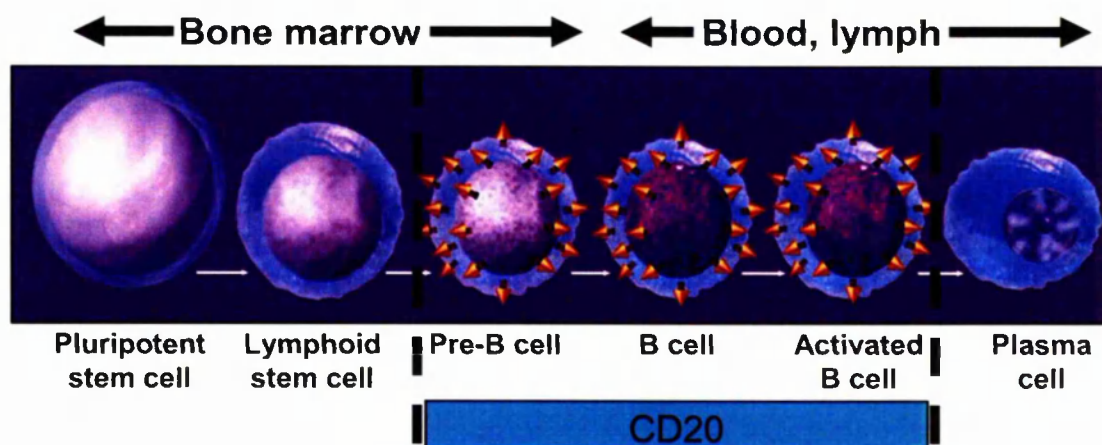


Figure 1- 18. The expression of CD20 antigen throughout development (taken from Press, 1999).

Human CD20 expression commences at the early pre-B cell stage just before the expression of the cytoplasmic IgM (μ) heavy chain and is lost during terminal plasma cell differentiation (Figure 1-18) (Tedder and Engel, 1994). This tight control of CD20 expression coincides with important stages of B cell development and may be due to PU.1/Pip binding to the proximal end of the CD20 promoter at position - 160 (Himmelman et al., 1997). PU.1 and Pi are members of the Ets family and important

regulators of μ E3-specific transcription factors such as TFE3 and USF that are found expressed in most cell types.

Another regulatory region in the CD20 promoter contains a binding site for the B cell-specific activator protein (BSAP). This protein is encoded by the Pax5 gene which itself is a highly regulated and required for B cell commitment (Nutt et al., 2001). BSAP is involved in the regulation of CD19 and Blk amongst other B cell-specific genes.

The majority of human B cell-lineage malignancies express CD20 (Tedder and Engel, 1984). Although selection of CD20-negative tumour variants has been reported, this appears to occur very rarely with CD20 antibodies, occurring in less than 1 in 300 cases. Because of this, anti-CD20 mAb have become an effective therapy for NHL (reviewed by Emmanouilides, 2007). Whether CD20 function or its membrane-embedded structure contributes most to its effectiveness as a therapeutic target remains an open issue since studies assessing *in vivo* B cell function and therapeutic mechanisms are difficult in humans.

1-6. Anti-CD20 antibody effector mechanisms.

The first anti-CD20 antibody (B1) has been characterised over 20 years ago and since then a large panel of anti-CD20 antibodies have been generated. It has long been known that the biological response after ligation of CD20 antigen by antibodies is dependent on the antibody itself. This example is perhaps best illustrated when observing the actions of B1 (tositumomab) and rituximab on B cells. Cragg et al. (2003) have previously shown that anti-CD20 mAb may be sub-divided as either rituximab-like (Type I) or B1-like (Type II) according to their linked activity in a number of *in vitro* assays. For

example, rituximab and other Type I mAb redistribute CD20 into Triton X-100 insoluble membrane rafts, correlating with their ability to engage complement effectively and cause target cell lysis (Cragg et al., 2003). In contrast Type II mAb such as B1 do not redistribute CD20 membrane rafts, but are generally potent at inducing cell death in target cells (Chan et al., 2003). Importantly, these differences appear to translate to the *in vivo* mechanisms employed by these mAb, at least in xenograft tumour models. In this context, Cragg and Glennie (2004) have shown that directed to the same target antigen, and in the case of 1F5 (Type I) and B1 (Type II) anti-CD20 antibodies with the same immunoglobulin isotype, can achieve *in vivo* clearance of tumour cells by different mechanisms (Figure 1-19). Thus, Type I anti-CD20 antibodies 1F5 and rituximab, which redistribute CD20 into membrane rafts, are bound efficiently by C1q, deposit C3b, and result in CDC. This activity is important *in vivo*, because complement depletion using cobra venom factor (CVF) markedly reduced the efficacy of rituximab and 1F5 in two lymphoma xenograft models (Cragg and Glennie, 2004). On the contrary, complement depletion had no effect on the potent therapeutic activity of B1 (tositumomab), a mAb that does not redistribute CD20 into membrane rafts, binds C1q, or cause efficient CDC. Also, F(ab')₂ fragments of B1 but not 1F5 were able to provide substantial immunotherapy, indicating that non-Fc-dependent mechanisms are involved with Type II anti-CD20 antibody B1. Thus, although complement is important for the action of rituximab and 1F5, this is not so for B1, which more likely functions through its ability to signal cell death.

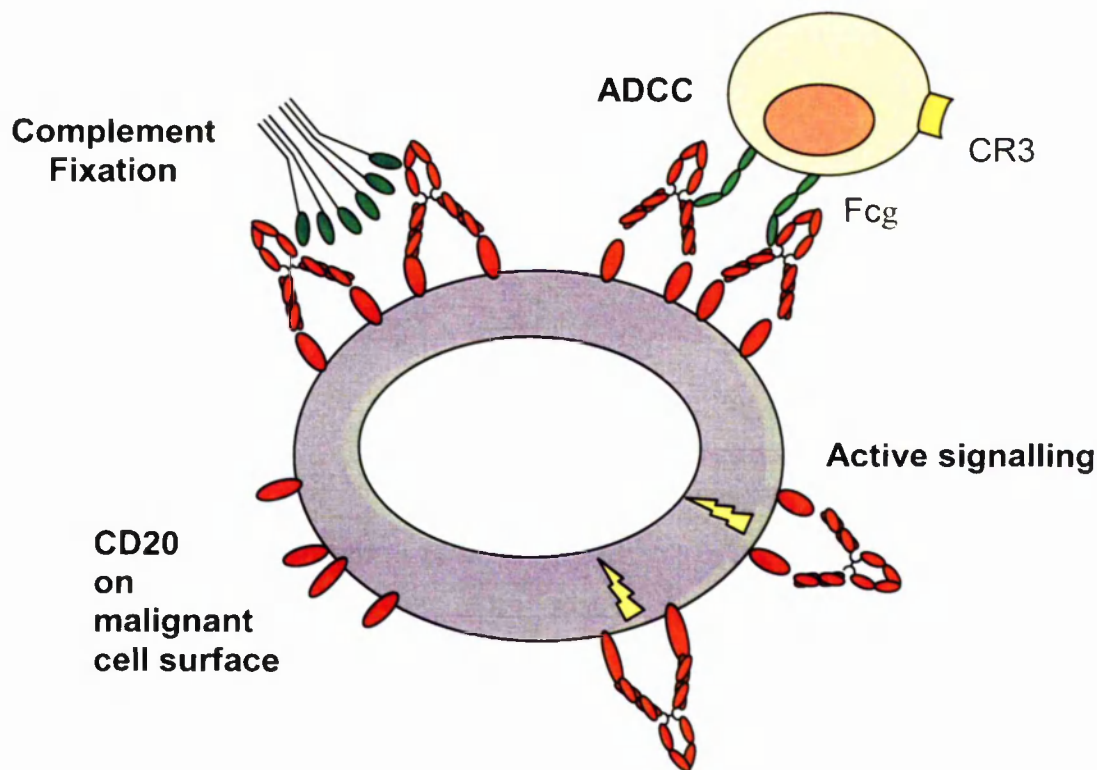


Figure 1- 19. Multiple anti-CD20 mAb effector mechanisms Four potential effector mechanisms are available to mAb in regulating tumour cells: (1) complement dependent cytotoxicity (CDC), (2) antibody dependent cellular cytotoxicity (ADCC) via the recruitment of immune effector cells, (3) direct induction of growth inhibition and/or cell death and (4) stimulation of host-adaptive immunity (Cragg et al., 2005).

There is now significant experimental data to support the first three mechanisms (as in Figure1-19) in anti-CD20 mAb immunotherapy, although robust evidence for the latter is currently lacking. In particular, several lines of evidence indicate that rituximab operates through conventional effector mechanisms involving complement and immune effector cells (Johnson and Glennie, 2003). The most conclusive initial evidence for the role of immune effector cell recruitment by antibody Fc receptors comes from primate experiments where an IgG4 variant of rituximab (which does not engage FcR or activate complement) was shown to be unable to deplete normal B cells (Anderson et al., 1997). More recently, data has emerged demonstrating that type I anti-CD20 mAb such as rituximab and 1F5 require their Fc domains for optimal therapeutic activity in human lymphoma xenograft models (Cragg and Glennie, 2004).

1-7. Radiation and antibody signalling - Mitogen-activated protein kinase cascades

One of the most exciting developments in molecular and cell biology has been the step-by-step construction of signalling cascades that trace the path of the effects of an extracellular stimulus all the way from the external membrane to the cell nucleus.

Mitogen activated protein kinases (MAPK) are Ser/Thr specific protein kinases that respond to extracellular stimuli and regulate various cellular activities, such as gene expression, mitosis, differentiation, and cell survival/death (Pearson et al., 2001). MAPKs are activated by protein kinase cascades (Figure 1-20) consisting of three or more protein kinases in series: MAPK kinase kinases (MAP3Ks) activate MAPK kinases (MAP2Ks) by dual phosphorylation on S/T residues; MAP2Ks then activate MAPKs by dual phosphorylation on Y and T residues. MAPKs then phosphorylate target substrates on select Ser/Thr residues.

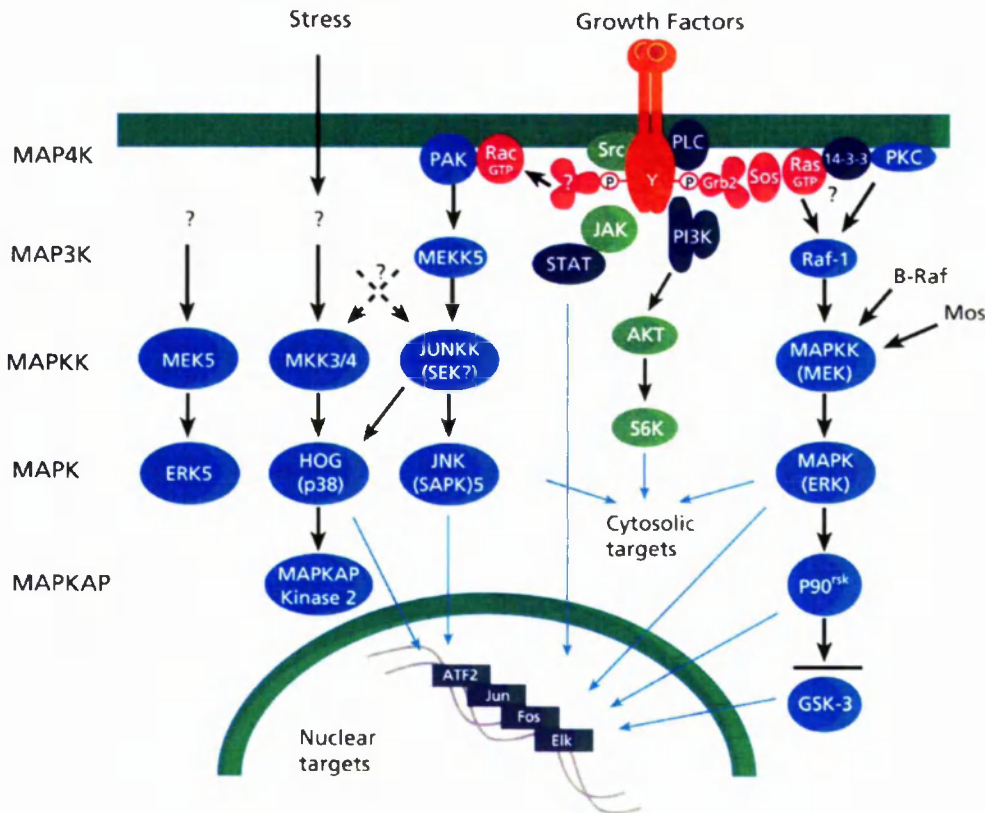


Figure 1- 20. Mitogen-activated protein kinases. Several MAPK cascades have been identified in mammalian cells, including the extracellular signal-related kinase pathways (ERK1/2, ERK5) and the stress activated kinase pathways (JNK/SAPK, p38 MAPK). These pathways are linked to many G protein-linked cell surface receptors and receptor tyrosine kinases. Thus, most cytokines, growth factors, hormones, and neurotransmitters can selectively activate these cascades via receptor activation of intracellular second messengers. All MAPK pathways operate through sequential phosphorylation events to phosphorylate transcription factors and regulate gene expression. They can also phosphorylate cytosolic targets to regulate intracellular events. These cascades are implicated in the regulation of cellular proliferation, differentiation, development, cell cycle, and transmission of oncogenic signals (adapted from Sigma-Aldrich web page – address with permission).

In the ERK1/2 cascade the MAP3K is usually a member of the Raf family. Many diverse MAP3Ks reside upstream of the p38 and the c-Jun N-terminal kinase/stress-activated protein kinase (JNK/SAPK) MAPK groups, which have generally been associated with responses to cellular stress. Downstream of the activating stimuli, the kinase cascades may themselves be stimulated by combinations of small G proteins, MAP4Ks, scaffolds,

or oligmerisation of the MAP3K in a pathway. In the ERK1/2 pathway, Ras family members usually bind to Raf proteins leading to their activation (Figure 1-21) (Lewis et al., 1998; Raman et al., 2007; Johnson et al., 2002).

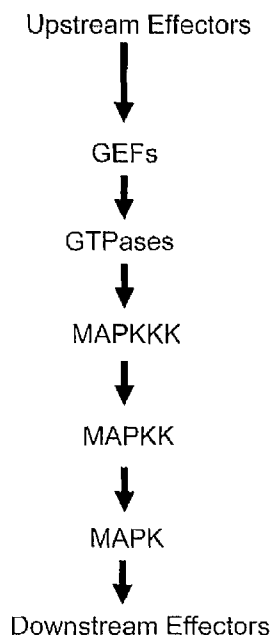


Figure 1- 21. Schematic generic overview of the sequence of events leading to activation of Map kinase pathways. (adapted from Platanias, 2003)

Through these cascades, the MAPKs process signals from a variety of stimuli such as most ligands and changes in cell state, thus, affecting large numbers of cellular pathways and responses. Signalling by MAPKs affects specific events such as the activity or localization of individual proteins, transcription of genes, increased cell cycle entry and promote changes that orchestrate complex processes such as embryogenesis and differentiation. These enzymes mediate acute responses to hormones such as changes in membrane permeability, cell motility, and transcription of immediate early genes; homeostatic responses of intermediate duration such as stimulus-induced long term potentiation in neurons; and sequenced programs required for animal development (Gille et al., 1995; Khoo et al., 2004; Maekawa et al., 2005). In fact, ERK2 is an essential gene.

Animals that lack it, die early in embryonic development (Saba-El-Leil et al., 2003). Furthermore, germline mutations in the ERK1/2 cascade are associated with serious developmental abnormalities such as cardio-facio-cutaneous syndrome (Rodriguez-Viciano et al., 2006).

The biologic activities of different MAPK signalling cascade branches vary with the specific family of MAPK activated and the distinct stimulus inducing such activation. In general, the stress-activated p38 and JNK kinase pathways mediate pro-death and growth inhibitory signals (Chang et al, 2001). However, activation of the p38 pathway may also induce anti-apoptotic, proliferative, and cell survival signals under certain conditions, depending on the tissue and specific isoform involved (Davis, 2000). On the other hand, the Ras/Erk pathway mediates primarily cell growth and survival signals, but under certain circumstances also promotes induction of cell differentiation (reviewed by Chang et al, 2001).

1-8. Death promoting role of ERK/MAPK cascade

There is increasing evidence suggesting that the activation of ERK1/2 also contributes to cell death in some cell types and organs under certain conditions. In this manner, Bhat and Zhang (1999) first reported that inhibition of ERK using the MEK1 inhibitor PD98059 rescues oligodendrocytes from H₂O₂-induced cell death, and this observation was also confirmed in HeLa cells (Wang et al., 2000), cortical neurons (Lesuisse and Martin, 2002), and primary beta-cells (Pavlovic et al., 2000). In renal cell lines and primary cultures of renal proximal tubular cells, inhibition of ERK improved cell survival after cisplatin exposure (Ishikawa and Kitamura, 2000; Nowak, 2002). However, the pro-cell death role of ERK in renal epithelial cells is not limited to

cisplatin exposure. ERK activation is also associated with cell death induced by reactive oxygen species (ROS) (Tikoo et al., 2001; Ramachandiran et al., 2002), *Escherichia coli* toxins (Chen et al., 2004), zinc (Matsunaga et al., 2005), and cephaloridine (Kohda et al., 2003). ERK activation has also been implicated in cell death induced by deprivation of survival factors. For example, withdrawal of survival factors from mouse kidney proximal tubular epithelial cells led to a progressive increase in ERK1/2 activity, and inhibition of ERK1/2 maintained cell survival (Sinha et al., 2004). ERK1/2 activation is involved in doxorubicin-induced apoptosis in human hepatoma cell lines (HepG2 and Huh-7) (Alexia et al., 2004), amyloid-induced neurotoxicity in primary hippocampal neurons (Medina et al., 2005), and CD40-mediated apoptosis in cholangiocytes (Ahmed-Choudhury et al., 2006). Finally, ERK activation has been reported to mediate cell death induced in immature B cells after ligation of their surface IgM (Gauld et al., 2002).

Most of the above-mentioned studies addressed the role of ERK in apoptosis using the MEK inhibitors PD98059 or U0126 (Alessi et al., 1995; Favata et al., 1998). Kim et al. (2005) used molecular approaches to examine the role of the ERK pathway in cell death of renal epithelial cells. They found that transient transfection of constitutively active MEK1 increased H₂O₂-induced cell death, whereas the dominant-negative mutant of MEK1 led to an inhibition of H₂O₂-mediated cell death. Likewise, Goillot et al. (1997) demonstrated that interference with the ERK pathway by expression of dominant-negative MEK1 resulted in inhibition of Fas-mediated apoptosis. Finally, Joo et al., (2007) demonstrated that fernesol-induced cell death is coupled to endoplasmic reticulum stress and that activation of MEK1/2 is an early upstream event in the endoplasmic reticulum stress signalling cascade. These *in vitro* studies support a significant role for ERK in mediating cell death.

Table 1-3. Examples of ERK mediated cell death in different cell types and stimuli.

Cell Types	Inducers	Reference
Burkitt's lymphoma	Tositumomab/irradiation	Ivanov et al., Clin Cancer Res. 2008
Lung carcinoma cells	Fernesol	Joo et al., Cancer Res 2007
Fibroblasts	Basic fibroblast growth factor	Ma et al., J Biol Chem 2008
Renal epithelium	Ischemia/Reperfusion	Alderliesten et al., Am J Pathol 2007
Keratinocytes	H ₂ O ₂	Rygiel et al., J Cell Sci 2008
Immature B cells	Anti-IgM antibody	Gauld et al., J Immunol 2002
Oligodendrocyte	H ₂ O ₂	Bhat and Zhang, J Neurochem 1999
Hippocampal neurons	Amyloid	Medina et al., EMBO J 2005
Glial cells	Glutathione depletion	de Bernardo et al., J Neurochem 2004
CGN (cerebellar granule neurons)	Low potassium	Subramaniam et al., J Biol Chem 2003 ; J Cell Biol 2004.
	Steroid hormone	Wong et al., J Neurosci 2003
Pyramidal cells	Okadaic acid	Runden et al., J Neurosci 1998
Renal proximal tubular cells	Cisplatin	Nowak, J Biol Chem 2002; Arany et al., Am J Physiol 2004
Hepatoma cell line (HepG2)	Doxorubicin	Alexia et al., Biochem Pharmacol 2004
HeLa (cervical carcinoma cells)	Cisplatin	Wang et al., J Biol Chem 2000
Renal epithelial cells	Growth factors depletion	Sinha et al., J Biol Chem 2004
Renal epithelial cells	<i>Escherichia coli</i> toxin	Chen et al., J Infect Dis 2004
Renal epithelial cells	ROS	Tikoo et al., Mol Pharmacol 2001; Ramachandiran et al., Chem Res Toxicol 2002
Osteoblastic cells	H ₂ O ₂	Park et al., Toxicology 2005
Pancreatic β -cells	Interleukin-1 β	Pavlovic et al., Eur Cytokine Netw 2000
TM4 cells (Sertoli cell line)	CD95L	Ulissee et al., Cell Death Differ 2000
Lens epithelial cells	Calcium	Li et al., Mol Cell Biol 2005
Bone marrow stromal cells	Leptin	Kim et al., J Biol Chem 2003
B65 cell line (dopamine neuron)	6-Hydroxydopamine	Kulich and Chu, J Neurochem 2001
SH-SY5Y (neuroblastoma cell line)	1-Methyl-4-phenylpyridinium	Gomez-Santos et al., Brain Res 2002

1-9. Involvement of ERK/MAPK cascade in CD20 signalling

Binding of anti-CD20 mAb to lymphoma cells *in vitro* has been shown to induce modest levels of cell death presumably via signalling through the CD20 molecule (Shan et al., 1998). A range of signalling events may be induced following ligation of CD20 (reviewed by Cragg et al., 2005), including activation of the MAPK cascade (Mathas et al., 2000). Although commonly thought of as a component of proliferation and survival pathways, ERK1/2 signalling has been associated with apoptotic signalling in immature B cell lymphoma (Lee and Koretzky, 1998) and diffuse large B cell lymphoma cells (Hollmann et al., 2006). Similarly, it has been suggested that the overall balance of MAPK activity may determine B cell fate depending on the kinetics of activation and maturation state of the cell (Sutherland et al., 1996; Gauld et al., 2002).

Intriguingly, the MAPK cascade is also triggered by radiation and other DNA damaging agents (Hagan et al., 2000; Lyng et al., 2006) where it may be necessary for DNA double strand break repair by homologous recombination (Golding et al., 2007).

1-10. Thesis aims

Cell death has historically been subdivided into regulated and unregulated mechanisms. Apoptosis, a form of regulated cell death, reflects a cell's decision to die in response to environmental cues and is executed by intrinsic cellular machinery. Unregulated cell death (necrosis) is caused by overwhelming stress that is incompatible with cell survival. Based on this assumption, many investigators desperately searched for 'DNA ladders' during the 1980s and 1990s to characterise programmed cell death induced by various anti-tumour agents. Recent data point to the existence of multiple non-apoptotic, but still regulated cell death mechanisms, some of which overlap or are mutually exclusive with apoptosis. There are also numerous examples in which cell death demonstrates mixed features, for instance with morphological signs of both apoptosis and necrosis. In addition, a number of studies have shown that non-apoptotic cell death is not just an artifact of *in vitro* experimentation - it makes important contributions to pathological regulation *in vivo*. Despite this successful experimental development of the concept of non-apoptotic cell death in other, non-clinically relevant systems, very little is known about the involvement of these forms of cell death in tumour cell kill by radiation and immunotherapy.

The ever-increasing relativism of the concept of programmed cell death provides us a rationale for a broader look at the antibody and radiation-induced lymphoma cell death not focusing on apoptosis as the only way to kill tumour cells.

The aims of this thesis were to examine what kind of cell death pathways are involved in lymphoma cell death induced by radiation, antibody therapy and the combination of these. Further, to examine the relationship between cell death and activation of DNA

repair and cell survival pathways in p53 mutated lymphoma cells. We believe that investigating non-apoptotic forms of cell death in one system will contribute significantly to the understanding of the mechanism of action of many other anti-tumour agents, e.g. chemotherapy, potentially leading to successful clinical trials, based on tumour cell death profile.

References

- Adams, G. P., Weiner, L. M. Monoclonal antibody therapy of cancer. *Nat. Biotechnol.* 2005 **23**:1147–1157.
- Ahmed-Choudhury J, Williams KT, Young LS, Adams DH, and Afford SC CD40 mediated human cholangiocyte apoptosis requires JAK2 dependent activation of STAT3 in addition to activation of JNK1/2 and ERK1/2. *Cell Signal.* 2006 **18**:456–468.
- Alderliesten M, de Graauw M, Oldenampsen J, Qin Y, Pont C, van Buren L, van de Water B. Extracellular signal-regulated kinase activation during renal ischemia/reperfusion mediates focal adhesion dissolution and renal injury. *Am J Pathol.* 2007 **171**:452–462.
- Alessi DR, Cuenda A, Cohen P, Dudley DT, and Saltiel AR. PD 098059 is a specific inhibitor of the activation of mitogen-activated protein kinase kinase in vitro and in vivo. *J Biol Chem* 1995 **270**:27489–27494.
- Alexia C, Fallot G, Lasfer M, Schweizer-Groyer G, Groyer A An evaluation of the role of insulin-like growth factors (IGF) and of type-I IGF receptor signalling in hepatocarcinogenesis and in the resistance of hepatocarcinoma cells against drug-induced apoptosis. *Biochem Pharmacol* 2004 **68**:1003–1015.
- Alva AS, Gultekin SH, Baehrecke EH. Autophagy in human tumours: cell survival or death? *Cell Death Differ.* 2004 **11**:1046–8.
- Anderson DR, Grillo-López A, Varns C, Chambers KS, Hanna N. Targeted anti-cancer therapy using rituximab, a chimaeric anti-CD20 antibody (IDEC-C2B8) in the treatment of non-Hodgkin's B-cell lymphoma. *Biochem Soc Trans.* 1997 **25**:705–8.
- Arany I, Megyesi JK, Kaneto H, Price PM, and Safirstein RL Cisplatin-induced cell death is EGFR/src/ERK signalling dependent in mouse proximal tubule cells. *Am J Physiol* 2004 **287**:543–549.
- Bartek J, Lukas J. DNA damage checkpoints: from initiation to recovery or adaptation. *Curr Opin Cell Biol* 2007 **19**:238–245.
- Bassing CH, Alt FW. The cellular response to general and programmed DNA double strand breaks. *DNA Repair (Amst)* 2004 **3**:781–96.
- Bhat NR and Zhang P Hydrogen peroxide activation of multiple mitogen-activated protein kinases in an oligodendrocyte cell line: role of extracellular signal-regulated kinase in hydrogen peroxide-induced cell death. *J Neurochem* 1999 **72**:112–119.
- Boatright KM, Renatus M, Scott FL, Sperandio S, Shin H, Pedersen IM, Ricci JE, Edris WA, Sutherlin DP, Green DR, Salvesen GS. A unified model for apical caspase activation. *Mol Cell* 2003 **11**:529–541.

Bubien JK, Zhou LJ, Bell PD, Frizzell RA, Tedder TF. Transfection of the CD20 cell surface molecule into ectopic cell types generates a Ca^{2+} conductance found constitutively in B lymphocytes. *J Cell Biol* 1993 **121**:1121-1132.

Buglioni S, D'Agnano I, Vasselli S, Perrone Donnorso R, D'Angelo C, Brenna A, Benevolo M, Cosimelli M, Zupi G, Mottotese M. p53 nuclear accumulation and multiploidy are adverse prognostic factors in surgically resected stage II colorectal cancers independent of fluorouracil-based adjuvant therapy. *Am J Clin Pathol* 2001 **116**:360-368.

Bunz F, Dutriaux A, Lengauer C, Waldman T, Zhou S, Brown JP et al. Requirement for p53 and p21 to sustain G2 arrest after DNA damage. *Science* 1998 **282**:1497-1501.

Castedo M, Perfettini JL, Roumier T, Andreau K, Medema R, Kroemer G. Cell death by mitotic catastrophe: a molecular definition. *Oncogene* 2004 **23**:2825-37.

Castro-Obregón S, Rao RV, del Rio G, Chen SF, Poksay KS, Rabizadeh S, Vesce S, Zhang XK, Swanson RA, Bredesen DE. Alternative, nonapoptotic programmed cell death: mediation by arrestin 2, ERK2, and Nur77. *J Biol Chem* 2004 **279**:17543-17553.

Chan HT, Hughes D, French RR, Tutt AL, Walshe CA, Teeling JL, Glennie MJ, Cragg MS. CD20-induced lymphoma cell death is independent of both caspases and its redistribution into triton X-100 insoluble membrane rafts. *Cancer Res* 2003 **63**: 5480-5489.

Chang L, Karin M. Mammalian MAP kinase signalling cascades. *Nature* 2001 **410**:37-40.

Chen M, Bao W, Aizman R, Huang P, Aspevall O, Gustafsson LE, Ceccatelli S, and Celsi G Activation of extracellular signal-regulated kinase mediates apoptosis induced by uropathogenic *Escherichia coli* toxins via nitric oxide synthase: protective role of heme oxygenase-1. *J Infect Dis* 2004 **190**:127-135.

Clarke PG. Developmental cell death: morphological diversity and multiple mechanisms. *Anat Embryol* 1990 **181**:195-213.

Coiffier B. Monoclonal antibodies combined to chemotherapy for the treatment of patients with lymphoma. *Blood Rev* 2003 **17**: 25-31.

Coiffier, B., Lepage, E., Briere, J., Herbrecht, R., Tilly, H., Bouabdallah, R., Morel, P., Van Den Neste, E., Salles, G., Gaulard, P., Reyes, F., Lederlin, P., Gisselbrecht C. CHOP chemotherapy plus rituximab compared with CHOP alone in elderly patients with diffuse large-B-cell lymphoma. *N Engl J Med* 2002 **346**:235-242.

Côme MG, Skladanowski A, Larsen AK, Laurent G. Dual mechanism of daunorubicin-induced cell death in both sensitive and MDR-resistant HL-60 cells. *Br J Cancer* 1999 **79**:1090-1097.

Cragg MS, Glennie MJ. Antibody specificity controls in vivo effector mechanisms of anti-CD20 reagents. *Blood* 2004 **103**:2738-2743.

Cragg MS, Morgan SM, Chan HT, Morgan BP, Filatov AV, Johnson PW, French RR, Glennie MJ. Complement-mediated lysis by anti-CD20 mAb correlates with segregation into lipid rafts. *Blood* 2003 **101**:1045-1052.

Cragg, M. S., Walshe, C. A., Ivanov, A. O., Glennie, M. J. The biology of CD20 and its potential as a target for mAb therapy. *Curr Dir Autoimmun* 2005 **8**:140-174.

Cunningham TJ. Naturally occurring neuron death and its regulation by developing neural pathways. *Int Rev Cytol* 1982 **74**:163-186.

Dal Canto MC, Gurney ME. Development of central nervous system pathology in a murine transgenic model of human amyotrophic lateral sclerosis. *Am J Pathol* 1994 **145**:1271-1279.

Davis RJ. Signal transduction by the JNK group of MAP kinases. *Cell*. 2000 **103**:239-252.

de Bernardo S, Canals S, Casarejos MJ, Solano RM, Menendez J, and Mena MA. Role of extracellular signal-regulated protein kinase in neuronal cell death induced by glutathione depletion in neuron/glia mesencephalic cultures. *J Neurochem* 2004 **91**: 667-682.

Deans JP, Schieven GL, Shu GL, Valentine MA, Gilliland LA, Aruffo A, Clark EA, Ledbetter JA. Association of tyrosine and serine kinases with the B cell surface antigen CD20. Induction via CD20 of tyrosine phosphorylation and activation of phospholipase C-gamma 1 and PLC phospholipase C-gamma 2. *J Immunol* 1993 **151**:4494-504.

Dehay C, Kennedy H. Cell-cycle control and cortical development. *Nat Rev Neurosci* 2007 **8**:438-50.

DeLuca JG, Moree B, Hickey JM, Kilmartin JV, Salmon ED. hNuf2 inhibition blocks stable kinetochore-microtubule attachment and induces mitotic cell death in HeLa cells. *J Cell Biol* 2002 **159**:549-555.

DeNardo, G. L., DeNardo, S. J., Goldstein, D. S., Kroger, L. A., Lamborn, K. R., Levy, N. B., McGahan, J. P., Salako, Q., Shen, S., Lewis, J. P. Maximum-tolerated dose, toxicity, and efficacy of (131)I-Lym-1 antibody for fractionated radioimmunotherapy of non-Hodgkin's lymphoma. *J Clin Oncol* 1998 **16**:3246-3256.

Einfeld DA, Brown JP, Valentine MA, Clark EA, Ledbetter JA. Molecular cloning of the human B cell CD20 receptor predicts a hydrophobic protein with multiple transmembrane domains. *EMBO J* 1988 **7**:711-717.

Emmanouilides C. Radioimmunotherapy for non-hodgkin lymphoma : historical perspective and current status. *J Clin Exp Hematop* 2007 **47**:43-60.

Eom YW, Kim MA, Park SS, Goo MJ, Kwon HJ, Sohn S et al. Two distinct modes of cell death induced by doxorubicin: apoptosis and cell death through mitotic catastrophe accompanied by senescence-like phenotype. *Oncogene* 2005 **24**:4765-4777.

Erenpreisa J, Ivanov A, Cragg M, Selivanova G, Illidge T. Nuclear envelope-limited chromatin sheets are part of mitotic death. *Histochem Cell Biol* 2002 **117**:243-55.

Erenpreisa J, Kalejs M, Cragg MS. Mitotic catastrophe and endomitosis in tumour cells: an evolutionary key to a molecular solution. *Cell Biol Int* 2005 **29**:1012-1018.

Evans MP, Podratz KC. Endometrial neoplasia: prognostic significance of ploidy status. *Clin Obstet Gynecol* 1996 **39**:696-706.

Favata MF, Horiuchi KY, Manos EJ, Daulerio AJ, Stradley DA, Feeser WS, Van Dyk DE, Pitts WJ, Earl RA, Hobbs F, et al. Identification of a novel inhibitor of mitogen-activated protein kinase kinase. *J Biol Chem* 1998 **273**:18623-18632.

Gauld SB, Blair D, Moss CA, Reid SD, Harnett MM. Differential roles for extracellularly regulated kinase-mitogen-activated protein kinase in B cell antigen receptor-induced apoptosis and CD40-mediated rescue of WEHI-231 immature B cells. *J Immunol* 2002 **168**:3855-3864.

Gille H, Kortenjann M, Thomae O, Moomaw C, Slaughter C, Cobb MH, Shaw PE. ERK phosphorylation potentiates Elk-1-mediated ternary complex formation and transactivation. *EMBO J* 1995 **14**:951-962.

Glennie MJ, McBride HM, Worth AT, Stevenson GT. Preparation and performance of bispecific F(ab' gamma)2 antibody containing thioether-linked Fab' gamma fragments. *J Immunol*. 1987 **139**:2367-2375.

Goillot E, Raingeaud J, Ranger A, Tepper RI, Davis RJ, Harlow E, and Sanchez I. Mitogen-activated protein kinase-mediated Fas apoptotic signalling pathway. *Proc Natl Acad Sci USA* 1997 **94**:3302-3307.

Golay JT, Clark EA, Beverley PC. The CD20 (Bp35) antigen is involved in activation of B cells from the G0 to the G1 phase of the cell cycle. *J Immunol* 1985 **135**:3795-3801.

Golding SE, Rosenberg E, Neill S, Dent P, Povirk LF, Valerie K. Extracellular signal-related kinase positively regulates ataxia telangiectasia mutated, homologous recombination repair, and the DNA damage response. *Cancer Res* 2007 **67**:1046-1053.

Gomez-Santos C, Ferrer I, Reiriz J, Vinals F, Barrachina M, and Ambrosio S. MPP+ increases alpha-synuclein expression and ERK/MAP-kinase phosphorylation in human neuroblastoma SH-SY5Y cells. *Brain Res* 2002 **935**:32-39.

Green DR, Kroemer G. Pharmacological manipulation of cell death: clinical applications in sight? *J Clin Invest* 2005 **115**:2610-2617.

Grossbard, M. L., Press, O. W., Appelbaum, F. R., Bernstein, I. D., Nadler, L. M. Monoclonal antibody-based therapies of leukemia and lymphoma. *Blood* 1992 **80**: 863-878.

Gupta S, Agrawal A, Agrawal S, Su H, Gollapudi S. A paradox of immunodeficiency and inflammation in human aging: lessons learned from apoptosis. *Immun Ageing*. 2006 **3**:5.

Hagan M, Wang L, Hanley JR, Park JS, Dent P. Ionizing radiation-induced mitogen-activated protein (MAP) kinase activation in DU145 prostate carcinoma cells: MAP

- kinase inhibition enhances radiation-induced cell killing and G2/M-phase arrest. *Radiat Res* 2000 **153**:371-383.
- Helleday T, Lo J, van Gent DC, Engelward BP. DNA double-strand break repair: from mechanistic understanding to cancer treatment. *DNA Repair (Amst)* 2007 **6**:923-35.
- Himmelfmann A, Riva A, Wilson GL, Lucas BP, Thevenin C, Kehrl JH: PU.1/Pip and basic helix loop helix zipper transcription factors interact with binding sites in the CD20 promoter to help confer lineage- and stage-specific expression of CD20 in B lymphocytes. *Blood* 1997 **90**:3984-3995.
- Holder M, Grafton G, MacDonald I, Finney M, Gordon J. Engagement of CD20 suppresses apoptosis in germinal center B cells. *Eur J Immunol* 1995 **25**:3160-3164.
- Hollmann CA, Owens T, Nalbantoglu J, Hudson TJ, Sladek R. Constitutive activation of extracellular signal-regulated kinase predisposes diffuse large B-cell lymphoma cell lines to CD40-mediated cell death. *Cancer Res* 2006 **66**:3550-7.
- Illidge TM, Cragg MS, Fringes B, Olive P, Erenpreisa JA. Polyploid giant cells provide a survival mechanism for p53 mutant cells after DNA damage. *Cell Biol Int* 2000 **24**:621-633.
- Illidge TM, Cragg MS, Fringes B, Olive P, Erenpreisa JA. Polyploid giant cells provide a survival mechanism for p53 mutant cells after DNA damage. *Cell Biol Int* 2000 **24**:621-33.
- Illidge, T. M., Cragg, M. S., McBride, H. M., French, R. R., Glennie, M. J. The importance of antibody-specificity in determining successful radioimmunotherapy of B-cell lymphoma. *Blood* 1999 **94**:233-243.
- Ishikawa Y and Kitamura M Anti-apoptotic effect of quercetin: intervention in the JNK- and ERK-mediated apoptotic pathways. *Kidney Int* 2000 **58**:1078-1087.
- Ivanov A, Cragg MS, Erenpreisa J, Emzinsh D, Lukman H, Illidge TM. Endopolyploid cells produced after severe genotoxic damage have the potential to repair DNA double strand breaks. *J Cell Sci* 2003 **116**:4095-106.
- Jackson SP. Sensing and repairing DNA double-strand breaks. *Carcinogenesis* 2002 **23**:687-96.
- Jambrina E, Alonso R, Alcalde M, del Carmen Rodríguez M, Serrano A, Martínez-A C, García-Sancho J, Izquierdo M. Calcium influx through receptor-operated channel induces mitochondria-triggered paraptotic cell death. *J Biol Chem* 2003 **278**:14134-14145.
- Jeggo P, O'Neill P. The Greek Goddess, Artemis, reveals the secrets of her cleavage. *DNA Repair (Amst)* 2002 **1**:771-777.
- Jin, SV. Autophagy in cancer and aging. *UMDNJ Research*. Spring 2007.
- Johnson GL, Lapadat R. Mitogen-activated protein kinase pathways mediated by ERK, JNK, and p38 protein kinases. *Science* 2002 **298**:1911-1912.

Johnson P, Glennie M. The mechanisms of action of rituximab in the elimination of tumour cells. *Semin Oncol* 2003 **30**:3-8.

Joo JH, Liao G, Collins JB, Grissom SF, Jetten AM. Farnesol-induced apoptosis in human lung carcinoma cells is coupled to the endoplasmic reticulum stress response. *Cancer Res.* 2007 **67**:7929-7936.

Kaminski M, S., Zelenetz, A. D., Press, O. W., Saleh, M., Leonard, J., Fehrenbacher, L., Lister, T. A., Stagg, R. J., Tidmarsh, G. F., Kroll, S., Wahl, R. L., Knox, S. J., Vose, J. M. Pivotal study of iodine I 131 tositumomab for chemotherapy-refractory low-grade or transformed low-grade B-cell non-Hodgkin's lymphomas. *J. Clin. Oncol.* 2001 **9**:3918-3928.

Kansas GS, Tedder TF. Transmembrane signals generated through MHC class II, CD19, CD20, CD39, and CD40 antigens induce LFA-1-dependent and independent adhesion in human B cells through a tyrosine kinase-dependent pathway. *J Immunol* 1991 **147**:4094-4102.

Kanzaki M, Shibata H, Mogami H, Kojima I: Expression of calcium-permeable cation channel CD20 accelerates progression through the G1 phase in Balb/c 3T3 cells. *J Biol Chem* 1995 **270**:13099-13104.

Kerr JF, Wyllie AH, Currie AR. Apoptosis: a basic biological phenomenon with wide-ranging implications in tissue kinetics. *Br J Cancer* 1972 **26**:239-257.

Khoo S, Griffen SC, Xia Y, Baer R, German MS, Cobb MH. Regulation of insulin gene transcription by extracellular-signal regulated protein kinases (ERK) 1 and 2 in pancreatic beta cells. *J Biol Chem* 2003 **278**:32969-32977.

Kim GS, Hong JS, Kim SW, Koh JM, An CS, Choi JY, and Cheng SL. Leptin induces apoptosis via ERK/cPLA2/cytochrome c pathway in human bone marrow stromal cells. *J Biol Chem* 2003 **278**:21920-21929.

Kluck RM, Bossy-Wetzel E, Green DR, Newmeyer DD. The release of cytochrome c from mitochondria: a primary site for Bcl-2 regulation of apoptosis. *Science* 1997 **275**:1132-1136.

Knox, S. J., Meredith, R. F. Clinical radioimmunotherapy. *Semin Radiat Oncol* 2000 **10**:73-93.

Kohda Y, Hiramatsu J, Gemba M. Involvement of MEK/ERK pathway in cephaloridine-induced injury in rat renal cortical slices. *Toxicol Lett* 2003 **143**:185-194.

Kolch W. Coordinating ERK/MAPK signalling through scaffolds and inhibitors. *Cancer Res* 2000 **60**:7170-7176.

Kroemer G, Jäättelä M. Lysosomes and autophagy in cell death control. *Nat Rev Cancer* 2005 **5**:886-897.

Kulich SM and Chu CT. Sustained extracellular signal-regulated kinase activation by 6-hydroxydopamine: implications for Parkinson's disease. *J Neurochem* 2001 **77**: 1058–1066.

Kuwana T, Bouchier-Hayes L, Chipuk JE, Bonzon C, Sullivan BA, Green DR, Newmeyer DD. Bcl-2 domains of Bcl-2-only proteins differentially regulate Bax-mediated mitochondrial membrane permeabilization both directly and indirectly. *Mol Cell* 2005 **17**:525–535.

Kuwana T, Mackey MR, Perkins G, Ellisman MH, Latterich M, Schneider R, Green DR, Newmeyer DD. Bcl-2, Bax, and lipids cooperate to form supramolecular openings in the outer mitochondrial membrane. *Cell* 2002 **111**:331–342.

Lee JR, Koretzky GA. Extracellular signal-regulated kinase-2, but not c-Jun NH2-terminal kinase, activation correlates with surface IgM-mediated apoptosis in the WEHI 231 B cell line. *J Immunol* 1998 **161**:1637–1644.

Lees-Miller SP, Meek K. Repair of DNA double strand breaks by non-homologous end joining. *Biochimie* 2003 **85**:1161–1173.

Lesuisse C and Martin LJ. Immature and mature cortical neurons engage different apoptotic mechanisms involving caspase-3 and the mitogen-activated protein kinase pathway. *J Cereb Blood Flow Metab* 2002 **22**:935–950.

Levi-Montalcini R. The nerve growth factor: its mode of action on sensory and sympathetic nerve cells. *Harvey Lect* 1966 **60**:217–259.

Levine B, Kroemer G. Autophagy in the pathogenesis of disease. *Cell* 2008 **132**:27–42.

Levine B, Yuan J. Autophagy in cell death: an innocent convict? *J Clin Invest* 2005 **115**:2679–2688.

Levine EA. Prognostic factors in soft tissue sarcoma. *Semin Surg Oncol* 1999 **17**:23–32.

Lewis TS, Shapiro PS, Ahn NG. Signal transduction through MAP kinase cascades. *Adv Cancer Res* 1998 **74**:49–139.

Li DW, Liu JP, Mao YW, Xiang H, Wang J, Ma WY, Dong Z, Pike HM, Brown RE, and Reed JC. Calcium-activated RAF/MEK/ERK signalling pathway mediates p53-dependent apoptosis and is abrogated by alpha B-crystallin through inhibition of RAS activation. *Mol Biol Cell* 2005 **16**:4437–4453.

Li H, Kolluri SK, Gu J, Dawson MI, Cao X, Hobbs PD, Lin B, Chen G, Lu J, Lin F, Xie Z, Fontana JA, Reed JC, Zhang X. Cytochrome c release and apoptosis induced by mitochondrial targeting of nuclear orphan receptor tr3. *Science* 2000 **289**:1159–1164.

Lieber MR, Ma Y, Pannicke U, Schwarz K. Mechanism and regulation of human non-homologous DNA end-joining. *Nat Rev Mol Cell Biol* 2003 **4**:712–20.

Lockshin RA, Williams CM. Programmed cell death. II. Endocrine potentiation of the breakdown of the intersegmental muscles of silkworms. *J Insect Physiol* 1964 **10**:643–649.

Lodish H, Berk A, Matsudaira P, Kaiser CA, Krieger M, Scott MP, Zipursky SL, Darnell J. *Molecular Biology of the Cell*, p963. WH Freeman: New York, NY. 2004 5th ed.

Lum JJ, Bauer DE, Kong M, Harris MH, Li C, Lindsten T, Thompson CB. Growth factor regulation of autophagy and cell survival in the absence of apoptosis. *Cell* 2005 **120**:237–248.

Lyng FM, Maguire P, McClean B, Seymour C, Mothersill C. The involvement of calcium and MAP kinase signalling pathways in the production of radiation-induced bystander effects. *Radiat Res* 2006 **165**:400-409.

Ma C, Bower KA, Chen G, Shi X, Ke ZJ, Luo J. Interaction between ERK and GSK3 β mediates basic fibroblast growth factor-induced apoptosis in SK-N-MC neuroblastoma cells. *J Biol Chem*. 2008 **283**:9248-9256.

Maekawa M, Yamamoto T, Tanoue T, Yuasa Y, Chisaka O, Nishida E. Requirement of the MAP kinase signalling pathways for mouse preimplantation development. *Development* 2005 **132**:1773–1783.

Maiuri MC, Zalckvar E, Kimchi A, Kroemer G. Self-eating and self-killing: crosstalk between autophagy and apoptosis. *Nat Rev Mol Cell Biol*. 2007 Sep;**8**(9):741-52.

Majno G, Joris I. Apoptosis, oncosis, and necrosis: an overview of cell death. *Am J Pathol* 1995 **146**:3–15.

Mathas S, Rickers A, Bommert K, Dörken B, Mapara MY. Anti-CD20- and B-cell receptor-mediated apoptosis: evidence for shared intracellular signalling pathways. *Cancer Res* 2000 **60**:7170-7176.

Matsunaga Y, Kawai Y, Kohda Y, and Gamba M Involvement of activation of NADPH oxidase and extracellular signal-regulated kinase (ERK) in renal cell injury induced by zinc. *J Toxicol Sci* 2005 **30**:135–144.

Medina MG, Ledesma MD, Dominguez JE, Medina M, Zafra D, Alameda F, Dotti CG, and Navarro P Tissue plasminogen activator mediates amyloid-induced neurotoxicity via Erk1/2 activation. *EMBO J* 2005 **24**:1706–1716.

Moshous D, Callebaut I, de Chasseval R, Corneo B, Cavazzana-Calvo M, Le Deist F, Tezcan I, Sanal O, Bertrand Y, Philippe N, Fischer A, de Villartay JP. Artemis, a novel DNA double-strand break repair/V(D)J recombination protein, is mutated in human severe combined immune deficiency. *Cell* 2001 **105**:177-186.

Muzio M, Chinnaiyan AM, Kischkel FC, O'Rourke K, Shevchenko A, Ni J, Scaffidi C, Bretz JD, Zhang M, Gentz R, Mann M, Krammer PH, Peter ME, Dixit VM. Flice, a novel Fadd-homologous ice/ced-3-like protease, is recruited to the cd95 (fas/apo-1) death-inducing signalling complex. *Cell* 1996 **85**:817– 827.

Nowak G. Protein kinase C- α and ERK1/2 mediate mitochondrial dys-function, decreases in active Na⁺ transport, and cisplatin-induced apoptosis in renal cells. *J Biol Chem* 2002 **277**:43377–43388.

Nutt SL, Eberhard D, Horcher M, Rolink AG, Busslinger M: Pax5 determines the identity of B-cells from the beginning to the end of B-lymphopoiesis. *Int Rev Immunol* 2001 **20**:65–82.

Nyberg KA, Michelson RJ, Putnam CW, Weinert TA. Toward maintaining the genome: DNA damage and replication checkpoints. *Annu Rev Genet* 2002 **36**:617–656.

O'Keefe TL, Williams GT, Davies SL, Neuberger MS. Mice carrying a CD20 gene disruption. *Immunogenetics*. 1998 **48**:125-132.

Oppenheim RW. Naturally occurring cell death during neural development. *Trends Neurosci*. 1985 **17**:487– 493.

Park BG, Yoo CI, Kim HT, Kwon CH, and Kim YK. Role of mitogen-activated protein kinases in hydrogen peroxide-induced cell death in osteoblastic cells. *Toxicology* 2005 **215**:115–125.

Park, S. I., Press, O. W. Radioimmunotherapy for treatment of B-cell lymphomas and other hematologic malignancies. *Curr Opin Hematol* 2007 **14**:632–638.

Pavlovic D, Andersen NA, Mandrup-Poulsen T, and Eizirik DL Activation of extracellular signal-regulated kinase (ERK)1/2 contributes to cytokine-induced apoptosis in purified rat pancreatic beta-cells. *Eur Cytokine Netw* 2000 **11**:267–274.

Pilar G, Landmesser L. Ultrastructural differences during embryonic cell death in normal and peripherally deprived ciliary ganglia. *J Cell Biol* 1976 **68**:339 –356.

Platanias LC. Map kinase signalling pathways and hematologic malignancies. *Blood* 2003 **101**:4667-79.

Press OW. Radiolabeled antibody therapy of B-cell lymphomas. *Semin Oncol*. 1999 **26**:58-65.

Press, O. W., Farr, A. G., Borroz, K. I., Anderson, S. K., Martin, P. J. Endocytosis and degradation of monoclonal antibodies targeting human B-cell malignancies. *Cancer Res* 1989 **49**:4906–4912.

Press, O. W., Rasey, J. Principles of radioimmunotherapy for hematologists and oncologists. *Semin Oncol*. 2000 **27**:62–73.

Puig PE, Guilly MN, Bouchot A, Droin N, Cathelin D, Bouyer F, Favier L, Ghiringhelli F, Kroemer G, Solary E, Martin F, Chauffert B. Tumor cells can escape DNA-damaging cisplatin through DNA endoreduplication and reversible polyploidy. *Cell Biol Int*. 2008 May 2. [Epub ahead of print].

Radford IR, Murphy TK. Radiation response of mouse lymphoid and myeloid cell lines. Part III. Different signals can lead to apoptosis and may influence sensitivity to killing by DNA double-strand breakage. *Int J Radiat Biol* 1994 **65**:229–239.

Rajagopalan H, Nowak MA, Vogelstein B, Lengauer C. The significance of unstable chromosomes in colorectal cancer. *Nat Rev Cancer* 2003 **3**:695–701.

- Rajaraman R, Guernsey DL, Rajaraman MM, Rajaraman SR. Stem cells, senescence, neosis and self-renewal in cancer. *Cancer Cell Int* 2006 **6**:25.
- Ramachandiran S, Huang Q, Dong J, Lau SS, and Monks TJ. Mitogen-activated protein kinases contribute to reactive oxygen species-induced cell death in renal proximal tubule epithelial cells. *Chem Res Toxicol* 2002 **15**:1635–1642.
- Raman M, Chen W, Cobb MH. Differential regulation of MAPKs. *Oncogene* 2007 **26**:3100–3112.
- Rao RV, Castro-Obregon S, Frankowski H, Schuler M, Stoka V, Del Rio G, Bredesen DE, Ellerby HM. Coupling endoplasmic reticulum stress to the cell death program: an apaf-1-independent intrinsic pathway. *J Biol Chem*. 2002 **277**:21836 –21842.
- Rao RV, Hermel E, Castro-Obregon S, del Rio G, Ellerby LM, Ellerby HM, Bredesen DE. Coupling endoplasmic reticulum stress to the cell death program: mechanism of caspase activation. *J Biol Chem* 2001 **276**:33869 –33874.
- Riballo E, Kühne M, Rief N, Doherty A, Smith GC, Recio MJ, Reis C, Dahm K, Fricke A, Krempler A, Parker AR, Jackson SP, Gennery A, Jeggo PA, Löbrich M. A pathway of double-strand break rejoining dependent upon ATM, Artemis, and proteins locating to gamma-H2AX foci. *Mol Cell* 2004 **16**:715-24.
- Robak, T. Monoclonal antibodies in the treatment of chronic lymphoid leukemias. *Leuk. Lymphoma* 2004 **45**:205–219.
- Rodriguez-Viciana P, Tetsu O, Tidyman WE, et al. Germline mutations in genes within the MAPK pathway cause cardio-facio-cutaneous syndrome. *Science* 2006 **311**:1287–1290.
- Roninson IB, Broude EV, Chang BD. If not apoptosis, then what? Treatment-induced senescence and mitotic catastrophe in tumour cells. *Drug Resist Updat* 2001 **4**:303-13.
- Rooney S, Alt FW, Lombard D, Whitlow S, Eckersdorff M, Fleming J, Fugmann S, Ferguson DO, Schatz DG, Sekiguchi J. Defective DNA repair and increased genomic instability in Artemis-deficient murine cells. *J Exp Med*. 2003 **197**:553-65.
- Rothkamm K, Krüger I, Thompson LH, Löbrich M. Pathways of DNA double-strand break repair during the mammalian cell cycle. *Mol Cell Biol* 2003 **23**:5706-5715.
- Runden E, Seglen PO, Haug FM, Ottersen OP, Wieloch T, Shamloo M, and Laake JH. Regional selective neuronal degeneration after protein phosphatase inhibition in hippocampal slice cultures: evidence for a MAP kinase-dependent mechanism. *J Neurosci* 1998 **18**:7296–7305.
- Rygiel TP, Mertens AE, Strumane K, van der Kammen R, Collard JG. The Rac activator Tiam1 prevents keratinocyte apoptosis by controlling ROS-mediated ERK phosphorylation. *J Cell Sci* 2008 **121**:1183-92.
- Saba-El-Leil MK, Vella FD, Vernay B, et al. An essential function of the mitogen-activated protein kinase Erk2 in mouse trophoblast development. *EMBO Rep* 2003 **4**:964–968.

Salvesen GS, Dixit VM. Caspases: intracellular signalling by proteolysis. *Cell* 1997 **91**:443–446.

Schimming R, Mason KA, Hunter N, Weil M, Kishi K, Milas L. Lack of correlation between mitotic arrest or apoptosis and antitumour effect of docetaxel. *Cancer Chemother Pharmacol* 1999 **43**:165–172.

Schwartz LM. The role of cell death genes during development. *Bioessays* 1991 **13**:389–395.

Schweichel JU, Merker HJ. The morphology of various types of cell death in prenatal tissues. *Teratology* 1973 **7**:253–266.

Schweichel JU. [electron microscopic studies on the degradation of the apical ridge during the development of limbs in rat embryos]. *Z Anat Entwicklungsgesch.* 1972 **136**:192–203.

Shan D, Ledbetter JA, Press OW. Signalling events involved in anti-CD20-induced apoptosis of malignant human B cells. *Cancer Immunol Immunother* 2000 **48**:673–683.

Shimizu S, Kanaseki T, Mizushima N, Mizuta T, Arakawa-Kobayashi S, Thompson CB, Tsujimoto Y. Role of bcl-2 family proteins in a nonapoptotic programmed cell death dependent on autophagy genes. *Nat Cell Biol* 2004 **6**:1221–1228.

Sinha D, Bannerjee S, Schwartz JH, Lieberthal W, and Levine JS Inhibition of ligand-independent ERK1/2 activity in kidney proximal tubular cells deprived of soluble survival factors up-regulates Akt and prevents apoptosis. *J Biol Chem* 2004 **279**:10962–10972.

Smeland EB, Beiske K, Ek B, Watt R, Pfeifer-Ohlsson S, Blomhoff HK, Godal T, Ohlsson R. Regulation of c-myc transcription and protein expression during activation of normal human B cells. *Exp Cell Res* 1987 **172**:101–109.

Sperandio S, de Belle I, Bredesen DE. An alternative, non-apoptotic form of programmed cell death. *Proc Natl Acad Sci U S A* 2000 **97**:14376–14381.

Sperandio S, Poksay K, de Belle I, et al. Paraptosis: mediation by MAP kinases and inhibition by AIP-1/Alix. *Cell Death Differ* 2004 **11**:1066–1075.

Studnicka FK. Die parietalorgane. In: Oppel A, ed. *Lehrbuch der vergleichende mikroskopischen anatomie der wirbeltiere*. Jena: S.G. Fischer Verlag; 1905.

Subramaniam S, Strelau J, and Unsicker K. Growth differentiation factor-15 prevents low potassium-induced cell death of cerebellar granule neurons by differential regulation of Akt and ERK pathways. *J Biol Chem* 2003 **278**:8904–8912.

Subramaniam S, Unsicker K. Extracellular signal-regulated kinase as an inducer of non-apoptotic neuronal death. *Neuroscience* 2006 **138**:1055–1065.

Subramaniam S, Zirrgiebel U, von Bohlen Und Halbach O, Strelau J, Laliberte C, Kaplan DR, and Unsicker K. ERK activation promotes neuronal degeneration

predominantly through plasma membrane damage and independently of caspase-3. *J Cell Biol* 2004 **165**:357–369.

Sundaram M, Guernsey DL, Rajaraman MM, Rajaraman R. Neosis: a novel type of cell division in cancer. *Cancer Biol Ther*. 2004 **3**:207-218.

Sutherland CL, Heath AW, Pelech SL, Young PR, Gold MR. Differential activation of the ERK, JNK, and p38 mitogen-activated protein kinases by CD40 and the B cell antigen receptor. *J Immunol* 1996 **157**:3381-3390.

Tajiri S, Oyadomari S, Yano S, Morioka M, Gotoh T, Hamada JI, UshioY, Mori M. Ischemia-induced neuronal cell death is mediated by the endoplasmic reticulum stress pathway involving chop. *Cell Death Differ*. 2004 **11**:403– 415.

Tedder TF, Forsgren A, Boyd AW, Nadler LM, Schlossman SF: Antibodies reactive with the B1 molecule inhibit cell cycle progression but not activation of human B lymphocytes. *Eur J Immunol* 1986 **16**:881–887.

Tedder TF, Schlossman SF. Phosphorylation of the B1 (CD20) molecule by normal and malignant human B lymphocytes. *J Biol Chem* 1988 **263**:10009–10015.

Tedder, T. F., Engel, P. CD20: a regulator of cell-cycle progression of B lymphocytes. *Immunol Today* 1994 **15**:450–454.

Thacker J, Zdzienicka MZ. The mammalian XRCC genes: their roles in DNA repair and genetic stability. *DNA Repair (Amst)* 2003 **2**:655-72.

Thornberry NA, Lazebnik Y. Caspases: enemies within. *Science* 1998 **281**:1312–1316.

Tikoo K, Lau SS, and Monks TJ. Histone H3 phosphorylation is coupled to poly-(ADP-ribosylation) during reactive oxygen species-induced cell death in renal proximal tubular epithelial cells. *Mol Pharmacol* 2001 **60**:394–402.

Tolmach LJ, Marcus PI. Development of x-ray induced giant HeLa cells. *Exp Cell Res* 1960 **20**:350–360.

Turmaine M, Raza A, Mahal A, Mangiarini L, Bates GP, Davies SW. Nonapoptotic neurodegeneration in a transgenic mouse model of Huntington's disease. *Proc Natl Acad Sci U S A*. 2000 **97**:8093– 8097.

Ulissee S, Cinque B, Silvano G, Rucci N, Biordi L, Cifone MG, and D'Armiento M Erk-dependent cytosolic phospholipase A2 activity is induced by CD95 ligand cross-linking in the mouse derived Sertoli cell line TM4 and is required to trigger apoptosis in CD95 bearing cells. *Cell Death Differ* 2000 **7**:916–924.

Valentine MA, Meier KE, Rossie S, Clark EA. Phosphorylation of the CD20 phosphoprotein in resting B lymphocytes. Regulation by protein kinase C. *J Biol Chem* 1989 **264**:11282–11287.

Vitale I, Galluzzi L, Vivet S, Nanty L, Dessen P, Senovilla L, Olaussen KA, Lazar V, Prudhomme M, Golsteyn RM, Castedo M, Kroemer G. Inhibition of Chk1 kills tetraploid tumour cells through a p53-dependent pathway. *PLoS ONE* 2007 **2**:e1337.

Vogel C, Kienitz A, Hofmann I, Muller R, Bastians H. Crosstalk of the mitotic spindle assembly checkpoint with p53 to prevent polyploidy. *Oncogene* 2004 **23**: 6845–6853.

Wang X, Martindale JL, and Holbrook NJ Requirement for ERK activation in cisplatin-induced apoptosis. *J Biol Chem* 2000 **275**:39435–39443.

Wang Y, Li X, Wang L, Ding P, Zhang Y, Han W, Ma D. An alternative form of paraptosis-like cell death, triggered by TAJ/TROY and enhanced by PDCD5 overexpression. *J Cell Sci* 2004 **117**:1525-32.

Watson JD, Baker TA, Bell SP, Gann A, Levine M, Losick R. (2004). *Molecular Biology of the Gene*, ch. 9 and 10. Peason Benjamin Cummings; CSHL Press. 5th ed. West SC. Molecular views of recombination proteins and their control. *Nat Rev Mol Cell Biol* 2003 **4**:435-45.

White MW, McConnell F, Shu GL, Morris DR, Clark EA. Activation of dense human tonsillar B cells. Induction of c-myc gene expression via two distinct signal transduction pathways. *J Immunol* 1991 **146**:846-53.

Wong JK, Le HH, Zsarnovszky A, and Belcher SM. Estrogens and ICI182,780 (Faslodex) modulate mitosis and cell death in immature cerebellar neurons via rapid activation of p44/p42 mitogen-activated protein kinase. *J Neurosci* 2003 **23**:4984–4995.

Woods CM, Zhu J, McQuency PA, Bollag D, Lazarides E. Taxol-induced mitotic block triggers rapid onset of a p53-independent apoptotic pathway. *Mol Med* 1995 **1**: 506–526.

Wyman C, Ristic D, Kanaar R. Homologous recombination-mediated double-strand break repair. *DNA Repair (Amst)* 2004 **3**:827-33.

Xiong Y, Hannon GJ, Zhang H, Casso D, Kobayashi R, Beach D. p21 is a universal inhibitor of cyclin kinases. *Nature* 1993 **366**:701-704.

Yu CK, Sinclair WK. Polyploidy induced by X-rays in Chinese hamster cells in vitro. *Science* 1964 **145**:508–510.

Yu L, Alva A, Su H, Dutt P, Freundt E, Welsh S, Baehrecke EH, Lenardo MJ. Regulation of an atg7-beclin 1 program of autophagic cell death by caspase-8. *Science* 2004 **304**:1500 –1502.

Yuan J, Shaham S, Ledoux S, Ellis HM, Horvitz HR. The *C. elegans* cell death gene *ced-3* encodes a protein similar to mammalian interleukin-1 beta-converting enzyme. *Cell* 1993 **75**:641– 652.

Chapter 2.

Materials and methods

2-1. Cell lines

All cell lines were maintained in the culture medium described below at 37°C in a 5% CO₂ humidified incubator. Cells used for experimental studies were maintained in log phase of growth for at least 24 hours prior to experiment. All cell lines were cultured in RPMI 1640 medium (Gibco; Paisley, UK), supplemented with 10% foetal calf serum (FCS; Gibco, Paisley, UK).

2-2. Irradiation of cells

Cell lines were irradiated using a Gulmay D3 225 X-ray source using a dose rate of 0.77 Gy/minutes.

2-3. Therapeutic antibodies

Therapeutic anti B cell antibodies have been added to cells at concentration of 5 or 10 µg/ml. The stock solution of antibodies has been prepared in PBS at concentration 500 µg/ml.

Antibody	Target antigen	Source
Tositumomab	CD20	Corixa
Rituximab	CD20	Roche
M15/8	BCR	Tenovus laboratory, Southampton
L243	HLA-DR	American Type Tissue Collection, Rockville, MD
OKT3	CD3	Tenovus laboratory, Southampton

Table 2-1. The list of therapeutic antibodies used in this study.

2-4. Apoptosis detection and cell cycle analysis using propidium iodide flow cytometry.

Samples were analysed essentially as detailed previously (Cragg et al., 1999). Briefly, samples of cells were taken at relevant time points, resuspended in hypotonic fluorochrome solution (50 µg/ml propidium iodide (PI), 0.1% (w/v) sodium citrate, 0.1% (v/v) Triton X-100) and stored at room temperature in the dark for 4 hours. Analysis of samples was performed on a FACScan flow cytometer (BD Pharmingen) equipped with 488 nm argon laser. Samples were represented as DNA histograms using CellQuest software (BD Pharmingen) and the distribution of cells in the G1, S, G2/M and polyploid phases of the cell cycle calculated. Apoptosis was quantified by measuring the proportion of cells with sub-G1 levels of DNA and confirmed by microscopy.

2-5. Cell death detection using Annexin V and PI flow cytometry

Cells (1×10^5) were washed and re-suspended in binding buffer [10 mM HEPES (pH 7.4), 140 mM NaCl, and 2.5 mM CaCl_2], containing 1 µg/ml FITC-annexin V (BD Biosciences; Oxford, UK). Propidium iodide (10 µg/ml) was added to the samples to distinguish between early cell death and secondary necrosis. Subsequently, cells were assessed by flow cytometry on a FACScan or FACScalibur (BD Biosciences).

2-6. Two channel flow cytometry for cyclin B1 and DNA content

Cells were harvested, washed in cold PBS, and fixed in cold (-20°C) 70% ethanol for 30 minutes. After two washes in PBS, cells were permeabilized with PBS, 0.5% BSA, 0.5% saponin for 10 minutes at room temperature and incubated with 5 µg/ml solution of mouse monoclonal anti-cyclin B1 antibody (Santa Cruz Biotech; SC-245; Wembley, UK) in PBS, 0.5% BSA, 0.5% saponin for 45 minutes at room temperature. Following

two washes in PBS, cells were incubated in the solution of anti-mouse Fab2-FITC (Dako) conjugate, 1:30 in PBS/0.5% BSA/0.5% saponin for 30 minutes in the dark, then stained with 10 µg/ml PI solution in PBS, containing 200 µg/ml RNase (Sigma, Dorset, UK). The cells were then assessed by FACS (BD Pharmingen) using CellQuest software (BD Pharmingen).

2-7. Two channel flow cytometry for Annexin V and DNA content

For detection of apoptosis and DNA content 1 µl of Annexin V (BD Pharmingen) was added to 100 µl of cells for 15 minutes at 37°C. After washing in Annexin V binding buffer (0.01 M Hepes, pH 7.4; 0.14 M NaCl; 2.5 mM CaCl₂), cells were fixed in cold 70% ethanol, washed in PBS and stained with 10 µg/ml PI solution in PBS, containing 200 µg/ml RNase (Sigma, Dorset, UK). Then cells were assessed by FACS (BD Pharmingen) using CellQuest software (BD Pharmingen).

2-8. Immunofluorescent visualisation of Annexin V and Rad51-positive cells

Fluorescein-conjugated Annexin V-FITC (BD Pharmingen) was added to the cell culture medium at a final concentration of 1.5 µg/ml for 15 minutes. Harvested cells were washed twice with fresh culture medium to remove excess Annexin V, washed in 10 mM Hepes/NaOH, pH 7.4, 140 mM NaCl and 5 mM CaCl₂, resuspended in FCS at a density of approximately 100000 cells/ml and centrifuged onto glass slides. After fixation in methanol for 30 minutes, the preparations were incubated with mouse anti-Rad51 monoclonal antibodies (NeoMarkers; 51RAD01; LabVision (UK) Ltd. UK), biotin-conjugated goat anti-mouse antibodies (Vector Laboratories Ltd., UK), and finally in streptavidin-Alexa fluor 633 solution (Molecular Probes; Cambridge BioScience, UK).

2-9. DNA in situ image cytometry and image analysis

For DNA in situ cytometry, cells on cytopins were fixed in ethanol/acetone (1:1) for 30 minutes at room temperature. Cells were then stained with modified Feulgen reaction using depurinising acid hydrolysis, 2, 4-dinitrophenylhydrazine treatment and Toluidine Blue counterstaining as detailed previously (Erenpreisa et al., 2000). Images were taken using a Leitz Ergolux L03-10 microscope equipped with a Sony DXC 390P color videocamera. DNA content was measured as the integral optical density of the green channel using Image Pro Plus 4.1 software (Media Cybernetics; REO 2001, Riga, Latvia). The stoichiometry of DNA staining was verified using the values obtained for metaphases compared to anaphases or telophases (ratio 2 ± 0.03). The variation coefficient for DNA content was also assessed in normal human lymphocytes where it was determined as 2% and the device error estimated as 0.5%.

2-10. Single cell gel electrophoresis. Comet assay

For the single cell gel electrophoresis (comet) assay, 110 μ l of normal melting point agarose (0.5% in PBS) was added to a poly-L-lysine-coated microscope slide, covered with a coverslip and placed at 4°C for 10-15 minutes to allow the agarose to solidify. The coverslip was then gently removed and 10 μ l of cell suspension (10,000 cells/10 μ l of PBS) was mixed with 65 μ l of low melting point agarose (at 37°C) and placed on the top of the previous layer of agarose, re-covered and returned to 4°C until solid. After removing the coverslip, 75 μ l of normal melting point agarose was added, the coverslip replaced, and the slide returned to 4°C. Coverslips were subsequently removed and slides placed in chilled lysis solution (2.5 M NaCl, 100 mM EDTA, 10 mM Tris (pH 10.0), 1% Triton X-100) at 4°C overnight. Slides were then incubated in electrophoresis buffer (1 mM EDTA, 300 mM NaOH, pH 12.1), for 30 minutes to allow DNA to

unwind before electrophoresis at 25 V for 20 minutes in the dark. After electrophoresis slides were neutralised by slow washing with neutralisation buffer (0.4 M Tris, pH 7.5), stained with 30 μ l of ethidium bromide solution in PBS (1 μ g/ml) and coverslips applied. At least 100 consecutive cells were evaluated per slide (2 slides per sample) using a 40x objective and a Zeiss epifluorescence microscope supplemented with a Zeiss AxioCam digital camera. The comet tail moment was measured using Scion Image software and a comet assay macro described previously (Helma and Uhl, 2000).

2-11. Silencing of genes using siRNA

Silencer™ validated siRNA against MEK1 and MEK2 (or scrambled control siRNA) were obtained from Ambion (Europe Ltd. Huntingdon, UK) and used at 100 nM. siRNA was delivered to cells using the Amaxa nucleofection device, nucleofection, kit T and programme G-016 according to manufacturers protocol. The nucleofection efficiency was assessed using the pmaxGFP control vector (supplied with nucleofection kit) and was 86-93% for Raji and 55-60 % for SU-DHL4 cells at the 24 h time point.

2-12. Western blotting

Whole cell lysates were prepared from 5×10^6 cells in lysis solution containing 1% Triton X-100, 150 mM NaCl, 10 mM Tris (tris(hydroxymethyl)aminomethane) HCl, 2.5 mM ethylenediaminetetraacetic acid (EDTA), 1 mM phenylmethylsulfonyl fluoride (PMSF), 2.5 mM iodoacetic acid, and 1 mg/ml aprotinin. Insoluble material was removed by centrifugation at 13,000 g in a Kendro microcentrifuge for 15 minutes at 4°C. Samples were then diluted 1:2 in sample buffer and heated at 100°C for 3 minutes prior to loading and then separated using SDS-PAGE electrophoresis. For western blotting, proteins were transferred immediately onto nitrocellulose membrane (Hybond; Amersham Pharmacia Biotech, UK) using a semi-dry transfer system (TE 22 system;

Hoeffer, Amersham Pharmacia Biotech, UK). The blot was blocked overnight with 5% non-fat dried milk or 5% BSA for the detection of phosphorylated epitopes, then incubated with the appropriately diluted primary antibodies for 1 hour, washed and then incubated with horseradish peroxidase-conjugated anti-mouse or anti-rabbit IgG (Sigma-Aldrich, UK) for 1 hour and washed again. Antibody binding was visualised by enhanced chemiluminescence (ECL) reagents (Amersham Pharmacia Biotech, United Kingdom) before exposure to light-sensitive film (Hyperfilm ECL, Amersham Pharmacia Biotech, UK).

Alternatively, cell lysates were prepared in PhoshoSafe lysis solution (MERCK biosciences LTD, Nottingham, UK), containing protease inhibitors and then proteins were separated by SDS-PAGE as above.

2-13. Measurement of DNA fragmentation: Fluorescence in situ end labeling (FISEL)

The fluorescence variant of Terminal dUTP N-end labeling (TUNEL) was been performed essentially as described previously (24). The reaction mix (100 μ l) contained 1 μ l (25 units) terminal transferase (Promega, Southampton, UK), 20 μ l 5 \times cacodylate buffer (supplied with the enzyme), 1 μ l 0.5 mM biotin-16-dUTP (Roche), 3 μ l 0.5 mM dTTP, and 75 μ l H₂O. Preparations were incubated at 37°C for 1 h with this reaction mix and the reaction terminated by washing. The incorporated biotin-dUTP was detected with fluorescein isothiocyanate-conjugated avidin (Vector Laboratories, Peterborough, UK). The proportion of FISEL positive cells was determined using a fluorescence microscope (Zeiss AxioScope). At least 300 cells in at least 5 viewing fields were observed.

2-14. Clonogenic survival assay

To measure clonogenic survival, a serial dilution assay was performed, using a method similar to that published previously (Illidge et al., 2001). Briefly, each sample was treated with a range of doses of irradiation and seeded into individual wells of a 96-well plate over a range of cell densities (12 wells per cell density, eight cell densities per dose) in 20% conditioned medium. After 14 days the fraction of wells containing no surviving cells was determined using a light microscope. The cell number that resulted in 30% empty wells was calculated and used to generate a clonogenic survival curve that was normalized according to plating efficiency.

2-15. Reverse transcription polymerase chain reaction

Reverse transcription polymerase chain reaction (RT-PCR) was performed in thin walled PCR tubes with 100 ng of cDNA, 100 ng of 5' and 3' primers, 1 unit (U) of DNA polymerase in the presence of dNTPs, 1 × reaction buffer and Taq polymerase (Promega, Southampton, UK). DNA was denatured at 95°C for 1 min, followed by 30 amplification cycles, using an annealing temperature of 56°C and extension at 72°C. The sequences of primers used are listed in Table 2-2. PCR products were analysed by electrophoresis in 1–2 % agarose gels and visualized under UV light after staining with ethidium bromide.

Table 2-2. Sequences of primers used in the RT-PCR experiments.

Gene	Forward	Reverse Primer
<i>MOS</i>	5'-CGGTGTTTCCTGTGGCCATAA	5'-GCAGGCCGTTTACAAACATC
<i>REC8</i>	5'-TGAGGGTGAATGTGGTGAAA	5'-CTGGGATTGCAGCCTCTAAG
<i>SYCP3</i>	5'-TGCAGAAAGCTGAGGAACAA	5'-TGCTGCTGAGTTTCCATCAT
<i>SYCP1</i>	5'-TGGCGATGTGATGGAATTTA	5'-TGTTTTCCCCATTTTTGGAG
<i>SPO11</i>	5'-AGGAAGATGGCACCAAAGTG	5'-GGTCCCTTTTTGTGTCAGTGGA
<i>STAG3</i>	5'-GGATGCAAAGCTACAGCA	5'-CATCCGGTCCTTGAAGC
<i>DMC1</i>	5'-AGCAGCAAAGTTCCATGAAG	5'-TGAGCTCTCCTCTTCCCTTT

2-16. XTT cell viability assay

The assay is based on the cleavage of the tetrazolium salt XTT in the presence of an electron-coupling reagent, producing a soluble formazan salt. This conversion only occurs in viable cells. After this incubation period, the formazan dye formed is quantitated using a scanning multi-well spectrophotometer (ELISA reader). The absorbance revealed directly correlates to the cell number.

Colorimetric XTT cell viability assays were performed using the Cell Proliferation Kit II (XTT) (Roche Diagnostics Ltd. Burgess Hill, UK) according to the manufacturer's instructions. Cells were treated in 96 well plates and 72h later XTT reagent was added. After 4 hours of incubation, absorbance was measured with the GENios Multi-Detection Microplate Reader (Tecan UK Ltd., Reading, UK) using 485 nm detection and 680 nm reference filters.

2-17. Transmission electron microscopy

Cells were spun down and resuspended in 2.5% glutaraldehyde in 0.1M sodium cacodylate buffer at 4°C, for a minimum of 4 hours. After washing in 0.1M buffer for 1 hour twice, cells were post fixed in osmium tetroxide in 0.2M buffer for 1 hour and then rinsed twice in 0.2M buffer for 5 mins. Following this step, cells were dehydrated in

series of increasing concentrations alcohol for 10 min in each solution. Then, cells were incubated for 10 min twice with propylene oxide followed by 1 hour incubation with propylene oxide/epoxy resin mixture (50/50). After that, cell were embedded in epoxy resin and incubated at 60 °C for 48 hours to allow polymerisation of resin.

Samples were sectioned using a diamond knife, with the ultramicrotome set to cut at around 100nm using heat advance.

The sections are picked up onto 300 mesh (300 squares), thin-bar, copper grids and then stained in 1% solution of uranyl acetate in distilled water. After that, samples were air dried and observed under the E.M.

2-17. Fluorescence microscopy I

For immunofluorescent staining, harvested cells were cytospun onto clean poly-L-lysine-coated microscope slides. Samples were fixed in absolute methanol at -20°C for 30 minutes and rinsed in ice-cold acetone for a few seconds. Slides were washed three times for 10 minutes, and then incubated with appropriate dilution of primary antibodies for 60 minutes at room temperature. All primary antibodies were diluted in PBS/0.1% BSA. Subsequently, slides were washed in PBS (3x10 minutes) and incubated in appropriately diluted FITC-conjugated or Texas Red-conjugated secondary antibodies for 40 minutes. After three washes in PBS/0.1% Tween 20, cells were counterstained with propidium iodide (5 µg/ml), DAPI (1 µg/ml) or 7-aminoactinomycin (7-AAD) solution (1 µg/ml) for 5 minutes before mounting in mowiol, containing 0.1% citifluor or ProLong Gold antifade reagent (Invitrogen). For quantitative analysis, at least 300 cells were analysed for each sample. Qualitative images were taken with a Leica SP2 confocal laser-scanning microscope or Leica DM LS2 fluorescent microscope. Sequential scanning was performed in triple colour studies. Image analysis was performed using Leica Confocal or Image Pro Plus 4.1 software.

2-18. Fluorescence microscopy II. Digital pixel co-localization studies

Colocalization, in a biological manifestation, is defined by the presence of two or more different molecules residing at the same physical location in a specimen. Within the context of a tissue section, individual cell, or sub-cellular organelle viewed in the microscope, colocalization may indicate that the molecules are attached to the same receptor, while in the context of digital imaging; the term refers to colours emitted by fluorescent molecules sharing the same pixel in the image.

For immunofluorescent staining, harvested cells were cytospun onto clean poly-L-lysine-coated microscope slides. Samples were fixed in absolute methanol at -20°C for 30 minutes and rinsed in ice-cold acetone for a few seconds. Slides were washed three times for 10 minutes, and then incubated with primary antibodies for 60 minutes at room temperature. Subsequently, slides were washed in TBS (3x10 minutes) and stained using anti-rabbit Alexa fluor 488 SFX kit (Invitrogen Ltd. Paisley, UK) according to the manufacturer's protocol. After three washes in TBS/0.05% Tween 20, DNA was counterstained with 7-aminoactinomycin D before mounting in ProLong Gold antifade reagent (Invitrogen Ltd. Paisley, UK). Images were obtained using an epifluorescence microscope (Olympus BX51, equipped with a ColorView 12 camera. The amount of pERK1/2 colocalized with DNA was determined using the colocalization module in Image-Pro Plus 6.0 software (MediaCybernetics), using algorithms (Manders et al., 1993) to generate colocalization coefficients (Cgr). Cgr represents the fraction of green pixels that have a red component and is determined by the equation $Cgr = \Sigma Gi (coloc) / \Sigma Gi$ where Gi = green intensity. At least 50 cells in at least three viewing fields were analyzed per sample.

2-19. Fluorescence recovery after photo bleaching (FRAP)

Samples for FRAP experiments (Figure 2-1) were prepared by placing a droplet of GFP-Actin labelled Raji cells into IWAKI glass-bottom Petri dishes. The optical plane was set to be approximately in the middle of the sample. Before bleaching, a stack of ten images was scanned using Olympus BX71 microscope to record the pre-bleach situation. Bleach was carried out to the region of interest of a 1 μm circle within the cytoplasm at a wavelength of 488 nm for 1 s with the Argon laser.

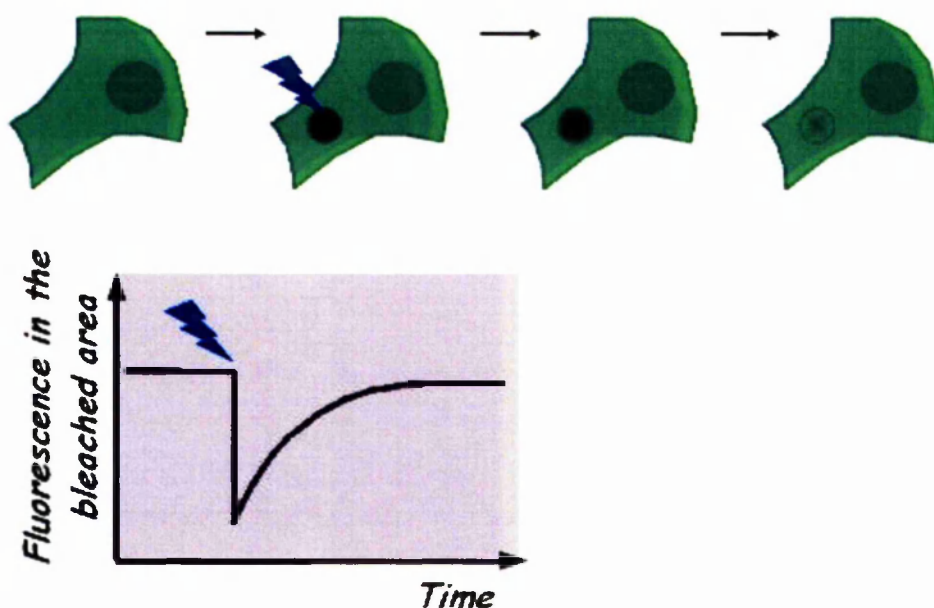


Figure 2- 1. The principle of FRAP (Presented according to Free Software Foundation GNU Free Documentation License).

2-20. Statistical analysis

To compare differences between the experimental groups, a two-tailed *t*-test was performed using Microsoft Excel or SPSS 13 software (SPSS Inc, Chicago, IL).

Chapter 3

Endopolyploid cells produced after severe genotoxic damage have the potential to repair DNA double strand breaks.

Reprinted from Ivanov et al., J Cell Sci. 2003 Oct 15;116(Pt 20):4095-106.

Endopolyploid cells produced after severe genotoxic damage have the potential to repair DNA double strand breaks

Andrei Ivanov^{1,3,*}, Mark S. Cragg^{2,*}, Jekaterina Erenpreisa³, Dzintars Emzinsh⁴, Henny Lukman¹ and Timothy M. Illidge^{1,‡}

¹Cancer Research UK, Wessex Oncology Unit, Cancer Sciences Division, School of Medicine, Southampton University Hospital, Southampton SO16 6YD, UK

²Tenovus Research Laboratory, Cancer Sciences Division, School of Medicine, Southampton University Hospital, Southampton SO16 6YD, UK

³Biomedical Research and Study Center, Latvian University, Ratsupites 1, Riga, LV-1067, Latvia

⁴Oncology Center of Latvia, Riga, Latvia

*These authors contributed equally to this work

‡Author for correspondence (e-mail: t.m.illidge@soton.ac.uk)

Accepted 4 July 2003

Journal of Cell Science 116, 4095–4106 © 2003 The Company of Biologists Ltd
doi:10.1242/jcs.00740

Summary

p53 mutant tumour cells respond to genotoxic insults by bypassing G1 arrest and halting in G2. Following release from G2 arrest they undergo mitotic catastrophe, whereby mitotic cycling is suppressed, delayed apoptosis begins and endopolyploid cells are produced. The ability of these endopolyploid cells to participate in the restitution process is controversial. To facilitate recovery, these endopolyploid cells must repair the extensive DNA damage induced. DNA damage and its resolution were studied by observing the kinetics of γ -H2AX foci formation and by comet assay analysis. Subsequently, the kinetics and distribution of Rad51 foci were studied as a measure of homologous recombination. Here we present evidence of the resolution of DNA damage in endopolyploid cells through a decrease of tail moment by comet assay and in the number of cells

expressing γ -H2AX foci. Rad51 foci expression reached a maximum in endopolyploid cells on days 5–6 after irradiation, when delayed apoptosis was maximal, indicating that cells were being selected for survival at this time. Furthermore, the proportion of Annexin-V-positive polyploid cells decreased as they continued ongoing rounds of DNA replication, suggesting endoreduplication is involved in selecting cells resistant to apoptosis. Our findings suggest that after severe genotoxic insult endopolyploid cells have a transient survival advantage that may contribute to radioresistance of tumours that undergo mitotic catastrophe.

Key words: polyploidy, DNA repair, γ -H2AX protein, Rad51 protein, Mitotic catastrophe

Introduction

Cell cycle progression after DNA damage is regulated by checkpoint controls, which prevent continued transit through the cycle until the damage has been repaired, hence protecting the integrity of the genome. Arrest in G1 permits repair prior to replication, whereas arrest in G2 allows repair prior to mitotic chromosome segregation. The p53 tumour suppressor gene, which is mutated in roughly half of human tumours, has been shown to be integral to both G1 and G2 damage checkpoint machinery (for a review, see Taylor and Stark, 2001).

The response of p53 mutated radioresistant tumours to genotoxic damage is hallmarked by a failure to arrest at G1 and the induction of mitotic catastrophe. Mitotic catastrophe, which involves micronucleation, delayed apoptosis and the formation of endopolyploid cells (reviewed by Erenpreisa and Cragg, 2001), appears to be triggered by the presence of secondary chromosome lesions produced by errors in primary DNA damage detection and repair (Scott et al., 1974; Radford and Murphy, 1994; Chadwick and Leenhouts, 1998; Bryant, 1998; Ianzini and Mackey, 1998).

Secondary chromatid breaks may also be produced as a result

of incomplete recombinational exchange (Rogers-Bald et al., 2000). Chromosome abnormalities are detected at the spindle checkpoint and there are conflicting reports concerning the state of adaptation and importance of this checkpoint in p53 mutated tumours (Sablina et al., 1999; Lanni and Jacks, 1998). If the DNA is incompletely repaired during G2 and the spindle checkpoint is adapted, either aneuploid cells are produced or the endocycle is initiated with the subsequent formation of endopolyploid cells. Endopolyploid cells are generally accepted as reproductively dead (Hall et al., 1996; Dini et al., 1996; Waldman et al., 1996; Bunz et al., 1998), although we and others have provided data suggesting that endopolyploid cells produced after severe genotoxic damage may facilitate an alternative pathway of cell survival (De la Hoz and Baroja, 1993; Erenpreisa et al., 2000a; Illidge et al., 2000; Baroja et al., 1996; Baroja et al., 1998). If endopolyploid cells can provide an alternative pathway of cell survival and therefore contribute to genotoxic resistance, then a critical initial step in this survival pathway would depend on the ability of such cells to repair DNA damage.

The two major mechanisms of DNA double strand break (DSB) repair that have been described in mammalian cells are

homologous recombination (HR) and non homologous end joining (NHEJ). HR may play a dominant role in the repair of DNA DSBs (Liang et al., 1998; Johnson and Jasin, 2000), however this role depends both on cell type and the cell cycle phase. Thus, NHEJ was shown to be the dominant DNA DSB repair pathway in G1 and early S phase, whilst HR appears to play a major role in late S and G2, with these two pathways being complementary (Takata et al., 1998). One of the first responses of eukaryotic cells to the introduction of DNA DSB is the phosphorylation of histone H2AX (Rogakou et al., 1998), and this is known to play a critical role in recruitment of DNA repair factors, such as BRCA1, Rad50 and Rad51 (Paull et al., 2000), and Nbs1 and 53bp (Celeste et al., 2002) to the site of damage. Importantly, a one-to-one correlation between the number of γ -H2AX foci and radiation-induced DSBs has been observed (Rothkamm and Löbrich, 2003). Therefore, given that other types of DNA damage induced by irradiation do not significantly contribute to γ -H2AX formation, the detection of phosphorylated H2AX (γ -H2AX) allows for the direct and specific investigation of the induction and resolution of DNA DSB.

Rad51 is a recombinase that forms nucleoprotein complexes with single stranded DNA (ssDNA), mediating homologous pairing and strand exchange between ssDNA and homologous double-stranded DNA (dsDNA) (Sung, 1994; Baumann et al., 1996; Gupta et al., 1997). Rad51 plays an essential role in homologous recombination in mammalian cells, with the knockout being embryonic lethal in the mouse and arrest and death after the G2/M checkpoint being observed in DT40 cells lacking Rad51 (Sonoda et al., 1998). The percentage of cells containing nuclear Rad51 foci has been shown to increase after DNA damage (Haaf et al., 1995) and such foci are known to form at sites of ssDNA (Raderschall et al., 1999). It is believed that Rad51 foci induced by DNA damage represent complexes of Rad51 and other proteins that are essential for DNA repair by homologous recombination.

In vertebrate somatic cells normal DNA replication is known to generate DSBs that are efficiently repaired through homologous recombination (HR) between sister chromatids (Sonoda et al., 1998; Haber, 1999; Sonoda et al., 2001). We therefore hypothesised that the additional rounds of DNA replication performed during the formation of endopolyploid cells may provide additional DSB repair capacity and afford a mechanism by which endopolyploid cells may contribute to radioresistance. To address this question, we investigated the kinetics of apoptosis, DNA damage and repair of endopolyploid cells produced following irradiation of p53 mutant tumour cells. Here we describe the kinetics of γ -H2AX formation and its resolution as well as the simultaneous kinetics of Rad51 foci formation in these endopolyploid cells. We believe that the novel pattern of the Rad51 foci formation linked to endoreduplication, and the subsequent protection from apoptosis of these endopolyploid cells is indicative of their potential for DNA repair, that could provide an additional mechanism for tumour cell survival.

Materials and Methods

Cell lines

The Burkitt's lymphoma cell line Namalwa was obtained from the American Type Culture Collection (ATCC) and has an established p53

mutant allele (O'Connor et al., 1993) (our own unpublished observations). TK6 and WI-L2-NS human B-lymphoblast cell lines were derived from the same WI-L2 isolate, are near diploid and have stable and indistinguishable karyotypes. TK6 are p53 wild-type and WI-L2-NS p53 mutated and have been described previously (Amundson et al., 1993) (our own unpublished observations). All cell lines were maintained in the culture medium described below at 37°C in a 5% CO₂ humidified incubator. Cells used for experimental studies were maintained in log phase of growth for at least 24 hours prior to irradiation. All cell lines were cultured in RPMI 1640 medium (Gibco; Paisley, UK), supplemented with antibiotics and 10% foetal calf serum (FCS; Gibco, Paisley, UK). The recovery of the diploid cell line after irradiation was determined as the time post-irradiation when the amount of G1 cells reached at least 25% of cell population but the amount of apoptotic cells was 10% or less.

Irradiation of cells

Cell lines were irradiated using a Gulmay D3 225 X-ray source using a dose rate of 0.77 Gy/minutes.

Apoptosis detection and cell cycle analysis using flow cytometry

Samples were analysed essentially as detailed previously (Cragg et al., 1999). Briefly, samples of cells were taken at relevant time points, resuspended in hypotonic fluorochrome solution (50 μ g/ml propidium iodide (PI), 0.1% (w/v) sodium citrate, 0.1% (v/v) Triton X-100) and stored at room temperature in the dark for 4 hours. Analysis of samples was performed on a FACScan flow cytometer (BD Pharmingen) equipped with 488 nm argon laser. Samples were represented as DNA histograms using CellQuest software (BD Pharmingen) and the distribution of cells in the G1, S, G2/M and polyploid phases of the cell cycle calculated. Apoptosis was quantified by measuring the proportion of cells with sub-G1 levels of DNA and confirmed by microscopy as described below.

Two channel flow cytometry for cyclin B1 and DNA content

Cells were harvested, washed in cold PBS, and fixed in cold (-20°C) 70% ethanol for 30 minutes. After two washes in PBS, cells were permeabilized with PBS, 0.5% BSA, 0.5% saponin for 10 minutes at room temperature and incubated with 5 μ g/ml solution of mouse monoclonal anti-cyclin B1 antibody (Santa Cruz Biotech; SC-245; Wembley, UK) in PBS, 0.5% BSA, 0.5% saponin for 45 minutes at room temperature. Following two washes in PBS, cells were incubated in the solution of anti-mouse Fab2-FITC (Dako) conjugate, 1:30 in PBS/0.5% BSA/0.5% saponin for 30 minutes in the dark, then stained with 10 μ g/ml PI solution in PBS, containing 200 μ g/ml RNase (Sigma, Dorset, UK). The cells were then assessed by FACS (BD Pharmingen) using CellQuest software (BD Pharmingen).

Two channel flow cytometry for Annexin V and DNA content

For detection of apoptosis and DNA content 1 μ l of Annexin V (BD Pharmingen) was added to 100 μ l of cells for 15 minutes at 37°C. After washing in Annexin V binding buffer (0.01 M Hepes, pH 7.4; 0.14 M NaCl; 2.5 mM CaCl₂), cells were fixed in cold 70% ethanol, washed in PBS and stained with 10 μ g/ml PI solution in PBS, containing 200 μ g/ml RNase (Sigma, Dorset, UK). Then cells were assessed by FACS (BD Pharmingen) using CellQuest software (BD Pharmingen).

Immunofluorescent visualisation of Annexin V and Rad51-positive cells

Fluorescein-conjugated Annexin V-FITC (BD Pharmingen) was

added to the cell culture medium at a final concentration of 1.5 µg/ml for 15 minutes. Harvested cells were washed twice with fresh culture medium to remove excess Annexin V, washed in 10 mM Hepes/NaOH, pH 7.4, 140 mM NaCl and 5 mM CaCl₂, resuspended in FCS at a density of approximately 10⁵ cells/ml and centrifuged onto glass slides. After fixation in methanol for 30 minutes, the preparations were incubated with mouse anti-Rad51 monoclonal antibodies (NeoMarkers; 51RAD01; LabVision (UK) Ltd. UK), biotin-conjugated goat anti-mouse antibodies (Vector Laboratories Ltd., UK), and finally in streptavidin-Alexa fluor 633 solution (Molecular Probes; Cambridge BioScience, UK).

Light microscopy

For light microscopy, cytopins were prepared as detailed previously (Erenpreisa et al., 2000b). Briefly, cells were fixed with ethanol/acetone, air-dried, treated with 0.1 M HCl at 4°C for 5 minutes, washed and stained with 0.05% Toluidine Blue (Gurr, Poole, UK) pH 5.0. Slides were then rinsed, blotted, dehydrated in butanol, passed through HistoClear (R. A. Lamb; Eastbourne, UK) and embedded into DPX (R. A. Lamb; Eastbourne, UK). These preparations were used for cytological studies and counts of apoptotic, mitotic, segmenting and micronucleating cells, scoring 1000-1500 cells in each sample.

DNA image cytometry and image analysis

For DNA in situ cytometry, cells on cytopins were fixed in ethanol/acetone (1:1) for 30 minutes at room temperature. Cells were then stained with modified Feulgen reaction using depurinating acid hydrolysis, 2, 4-dinitrophenylhydrazine treatment and Toluidine Blue counterstaining as detailed previously (Erenpreisa et al., 2000b). Images were taken using a Leitz Ergolux L03-10 microscope equipped with a Sony DXC 390P color videocamera. DNA content was measured as the integral optical density of the green channel using Image Pro Plus 4.1 software (Media Cybernetics; REO 2001, Riga, Latvia). The stoichiometry of DNA staining was verified using the values obtained for metaphases compared to anaphases or telophases (ratio 2±0.03). The variation coefficient for DNA content was also assessed in normal human lymphocytes where it was determined as 2% and the device error estimated as 0.5%.

Western blotting

Whole cell lysates were prepared from 5×10⁶ cells in lysis solution containing 1% Triton X-100, 150 mM NaCl, 10 mM Tris (tris(hydroxymethyl)aminomethane) HCl, 2.5 mM ethylenediaminetetraacetic acid (EDTA), 1 mM phenylmethylsulfonyl fluoride (PMSF), 2.5 mM iodoacetic acid, and 1 mg/ml aprotinin. Insoluble material was removed by centrifugation at 13,000 *g* in a Kendro microcentrifuge for 15 minutes at 4°C. Samples were then diluted 1:2 in sample buffer and heated at 100°C for 3 minutes prior to loading. For western blotting, proteins were transferred immediately onto nitrocellulose membrane (Hybond; Amersham Pharmacia Biotech, UK) using a semi-dry transfer system (TE 22 system; Hoefer, Amersham Pharmacia Biotech, UK). The blot was blocked overnight with 5% non-fat dried milk or 5% BSA for the detection of phosphorylated epitopes, then incubated with the appropriately diluted primary antibodies for 1 hour, washed and then incubated with horseradish peroxidase-conjugated anti-mouse or anti-rabbit IgG (Sigma-Aldrich, UK) for 1 hour and washed again. Antibody binding was visualised by enhanced chemiluminescence (ECL) reagents (Amersham Pharmacia Biotech, United Kingdom) before exposure to light-sensitive film (Hyperfilm ECL, Amersham Pharmacia Biotech, UK).

Immunofluorescent staining

For immunofluorescent staining, harvested cells were cytopun onto

clean poly-L-lysine-coated microscope slides. Samples were fixed in absolute methanol at -20°C for 30 minutes and rinsed in ice-cold acetone for a few seconds. Slides were washed three times for 10 minutes, and then incubated with primary antibodies for 60 minutes at room temperature. The dilutions of primary antibody were 1:100 for mouse monoclonal anti-Rad51 (NeoMarkers; 51RAD01; LabVision (UK) Ltd. UK) and anti-cyclin B1 antibodies (SC-245; Santa Cruz Biotech; Wembley, UK), 1:70 for rabbit polyclonal anti-γ-H2AX (Trevigen; AMS Biotechnology, UK), all diluted in

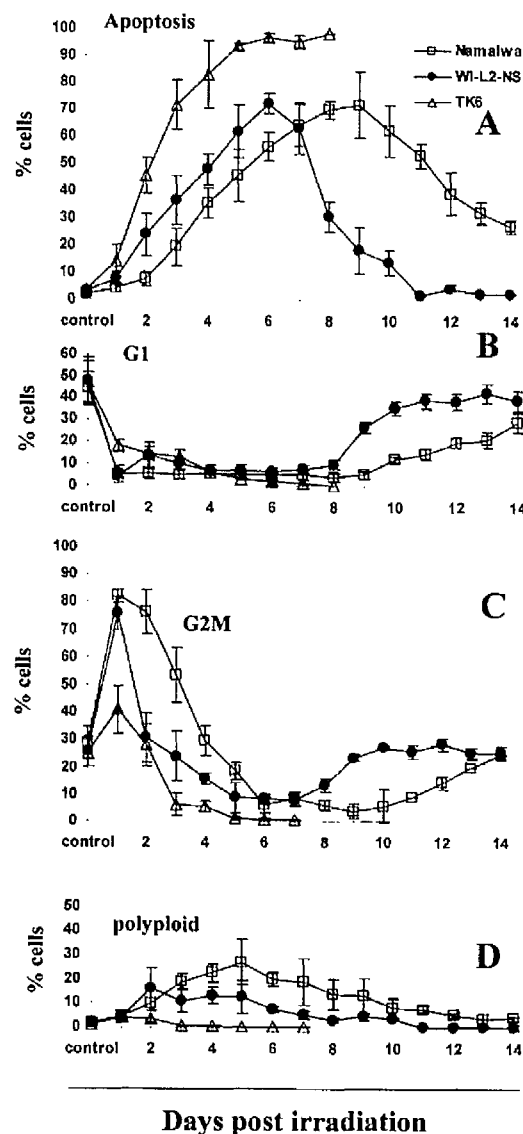


Fig. 1. Typical changes in the levels of apoptosis (A), G1 (B), G2/M (C) and polyploidy (D) observed in Namalwa (open square), WI-L2-NS (black circle) and TK6 (open triangle) cells after 10 Gy irradiation. Cells were irradiated and then samples taken regularly throughout a 14-day time course and assessed by DNA flow cytometry to determine the proportion of cells in each phase of the cell cycle. The data represent mean values with associated standard deviations taken from 6-10 experiments.

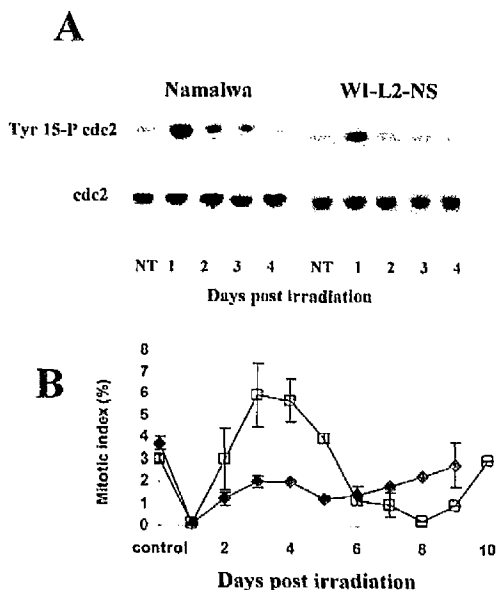


Fig. 2. Mitoses observed over the time course after irradiation in two p53 mutated cell lines. (A) After 10 Gy irradiation, cell samples were taken for 4 days and assessed by western blotting for the presence of p34^{cdc2} and Tyr15-phosphorylated p34^{cdc2}. The delay in G2 for Namalwa and W1-L2-NS cells shown in Fig. 1 was associated with prominent Tyr15 phosphorylation of p34^{cdc2} thus indicating a decrease in p34^{cdc2} activity. The control level of p34^{cdc2} activity was restored by day 3 (W1-L2-NS) or 4 (Namalwa) after irradiation. (B) The number of cells undergoing mitosis was assessed every day for 10 days by light microscopy, compared with untreated control cells and expressed as the mitotic index. These data show that adaptation of G2 arrest was followed by accumulation of W1-L2-NS (black diamonds) and Namalwa (open square) cells in mitosis. The drop in mitosis in the Namalwa cell line after 10 Gy, following the initial accumulation, is a result of mitotic failure. These data represent averages from three experiments and bars represent standard deviations.

PBS/0.1% BSA. Subsequently, slides were washed in PBS (3×10 minutes) and incubated in appropriately diluted FITC-conjugated anti-mouse IgG or Texas Red-conjugated anti-rabbit IgG (Vector Laboratories Ltd., UK) antibodies for 40 minutes. After three washes in PBS/0.1% Tween 20, cells were counterstained with propidium iodide (5 µg/ml), DAPI (1 µg/ml) or 7-aminoactinomycin (7-AAD) solution (1 µg/ml) for 5 minutes before mounting in mowiol, containing 0.1% citifluor. The number of positive cells as well as the number of foci per nucleus were counted in a blind manner using a 100× objective and Zeiss epifluorescence microscope. At least 300 cells were analysed for each sample. Qualitative images were taken with a Leica SP2 confocal laser-scanning microscope. Sequential scanning was performed in triple colour studies. Image analysis was performed using Leica Confocal or Image Pro Plus 4.1 software.

Comet assay

For the single cell gel electrophoresis (comet) assay, 110 µl of normal melting point agarose (0.5% in PBS) was added to a poly-L-lysine-coated microscope slide, covered with a coverslip and placed at 4°C for 10–15 minutes to allow the agarose to solidify. The coverslip was then gently removed and 10 µl of cell suspension (10,000 cells/10 µl

of PBS) was mixed with 65 µl of low melting point agarose (at 37°C) and placed on the top of the previous layer of agarose, re-covered and returned to 4°C until solid. After removing the coverslip, 75 µl of normal melting point agarose was added, the coverslip replaced, and the slide returned to 4°C. Coverslips were subsequently removed and slides placed in chilled lysis solution (2.5 M NaCl, 100 mM EDTA, 10 mM Tris (pH 10.0), 1% Triton X-100) at 4°C overnight. Slides were then incubated in electrophoresis buffer (1 mM EDTA, 300 mM NaOH, pH 12.1), for 30 minutes to allow DNA to unwind before electrophoresis at 25 V for 20 minutes in the dark. After electrophoresis slides were neutralised by slow washing with neutralisation buffer (0.4 M Tris, pH 7.5), stained with 30 µl of ethidium bromide solution in PBS (1 µg/ml) and coverslips applied. At least 100 consecutive cells were evaluated per slide (2 slides per sample) using a 40× objective and a Zeiss epifluorescence microscope supplemented with a Zeiss AxioCam digital camera. The comet tail moment was measured using Scion Image software and a comet assay macro described previously (Helma and Uhl, 2000).

Time-lapse video microscopy

For time-lapse studies, cells were irradiated and cultured for 6 days as usual prior to seeding at 2×10⁴ cells/well in a 24-well plate with 50% conditioned medium in the presence of 50–100 mM Hepes (pH 7.6). The plate was then placed under an encapsulated inverted microscope with regulated CO₂ and temperature and filmed for 16 hours taking images every 20 minutes.

Results

Mitotic catastrophe and subsequent endopolyploid cell formation after irradiation of p53 mutant tumour cells

Following irradiation with 10 Gy, the cell cycle changes observed in Namalwa and W1-L2-NS (both p53 mutant) and TK6 cells (p53 wild type) was assessed. These data show the percentage of cells in G1, G2, polyploid (>4N) and having undergone apoptosis over a 2 week time course (Fig. 1). In TK6 cells, large amounts of early apoptosis were seen with no discernible polyploid cell response and these cells failed to recover (Fig. 1). However, in both p53 mutated cell lines, although the G1 diploid fraction was strongly depressed throughout the restitution period, recovery was observed by day 15 (range 14–18 days) for Namalwa (Fig. 1A), and by day 9 (range 8–10 days) for W1-L2-NS. Profound and prolonged G2 arrest was observed in both Namalwa and W1-L2-NS cells (Fig. 1C). Importantly, the suppression in G1 for over 7 days in both cell lines exceeds the time spent in G2 arrest, suggesting that normal mitotic cycling is severely repressed during this time. In contrast, endocycling cells were clearly apparent during this time in both cell lines (Fig. 1D). Following the failure of mitosis, endopolyploid cells transiently became the dominating fraction in the culture from day 5 onwards, until the time when the mitotic fraction reappeared.

To investigate the cell cycle progression for cells after they had traversed the G2/M checkpoint we determined the activity of cdc2 for 4 days and the mitotic index over the whole 2- to 3-week period post irradiation. After irradiation, Namalwa cells showed an increase in p34^{cdc2} phosphorylation compared to untreated cells from day 1 to 3 post-irradiation that coincided precisely with the pronounced and prolonged G2/M arrest detailed above. Phosphorylation of p34^{cdc2} was decreased to control levels by day 4, facilitating the abrogation

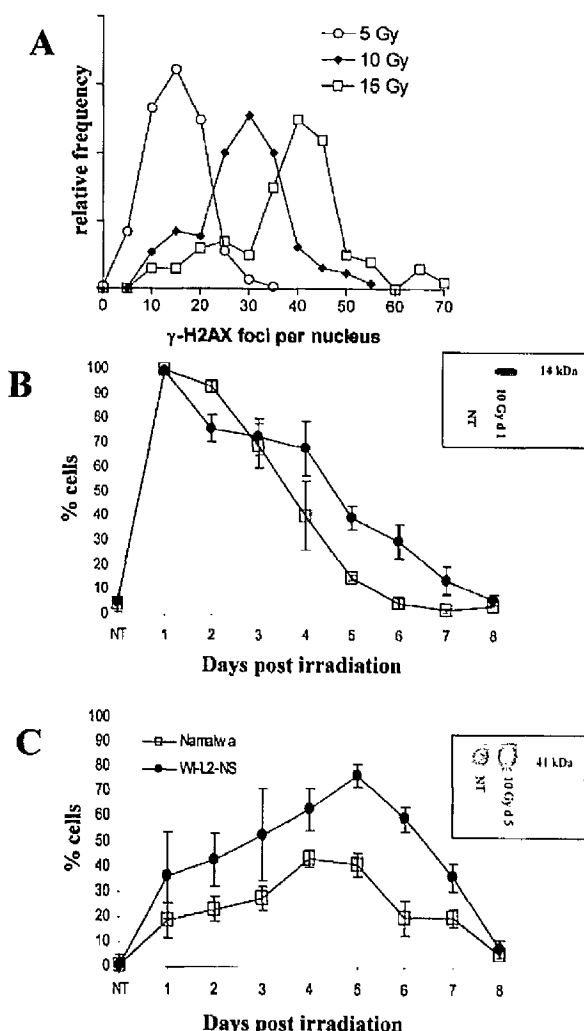


Fig. 3. Kinetics of γ -H2AX and Rad51 foci formation in Namalwa and WI-L2-NS cells after irradiation. (A,B) Starting from 3 minutes after 10 Gy irradiation, cell samples were taken, cytopun, fixed and stained for γ -H2AX and the amount of cells expressing γ -H2AX foci scored by immunofluorescent microscopy. (A) A histogram representing the relative frequencies of γ -H2AX foci per Namalwa cell, 24 hours after irradiation. The number of γ -H2AX foci per nucleus appeared to be dose dependent with a median number of foci of 14, 30 and 42 for 5, 10 and 15 Gy, respectively. (B) The proportion of the γ -H2AX foci-containing cells 24 hours post-irradiation was ~100% and remained high for 2 days for Namalwa (open square) and 4 days for WI-L2-NS (black circle) cells. Then it consequently decreased reaching nearly zero for Namalwa on day 7 and 6.5% for WI-L2-NS cells on day 8. Inset: immunoblotting analysis of Namalwa whole cell lysates of γ -H2AX, 24 hours after irradiation. (C) The abundance of Namalwa (open square) and WI-L2-NS (black circle) cells with Rad51 foci was detected on days 2 to 6-7 after 10 Gy irradiation. Cell samples were taken, cytopun, fixed and stained for Rad51 and the amount of cells expressing Rad51 foci scored by immunofluorescent microscopy. Inset: immunoblotting for Rad51 expression level. No difference in the overall level of Rad51 protein was found between untreated and irradiated cells. Data represent averages from at least three experiments \pm s.e.m.

of G2 arrest and progression of Namalwa cells into mitosis (Fig. 2A). Similar results were observed with WI-L2-NS cells, with dephosphorylation of p34^{cdc2} coinciding with the release from G2 arrest, approximately 1 day earlier than in Namalwa cells.

The mitotic index of the WI-L2-NS cell line increased transiently after a near total absence on day 1 but subsequently remained below the level of the control samples. In Namalwa cells the same decrease in mitotic index was observed on day 1 after irradiation, but this was followed by a 2- to 2.5-fold increase over control levels, peaking on days 3-4. After the mitotic index had reached a maximum it then dropped to below the level of the control until the final late recovery was observed (Fig. 2B). Importantly, in both cases very few anaphase accompanied the mitoses indicating extensive suppression of the mitotic cycle (data not shown).

Kinetics of γ -H2AX foci formation

In order to investigate the DNA damage and repair response we examined the kinetics of γ -H2AX foci formation and removal over the same time course as that detailed above (Fig. 3A,B). As expected, the number of γ -H2AX-positive cells increased rapidly after irradiation in a dose-dependent manner (Fig. 3A) and immunofluorescence studies revealed the formation of γ -H2AX foci in 100% of cells within the first hour (data not shown). This elevated level of expression was maintained for up to 24 hours after DNA damage in both p53 mutated cell lines as determined both by immunofluorescence and western blotting (Fig. 3B). The number of γ -H2AX-positive, non-apoptotic, cells subsequently decreased from day 1 onwards, although remained high during the first 5 days after irradiation of Namalwa cells and for the whole of the first week for WI-L2-NS cells (Fig. 3B). This suggests that DNA DSB repair was incomplete within the initial 48 hours post-irradiation when the cells were arrested in the G2 compartment and that subsequent repair occurred outside of the G2 compartment.

Late formation of Rad51 foci linked to endoreduplication after irradiation

We next investigated the quantity of cells containing Rad51 foci over the 10 days after irradiation. For both of the cell lines studied, less than 1% of the control cells displayed Rad51 foci (Fig. 3C). However, the number of cells with microscopically detectable Rad51 foci increased to 6.8 and 19.5% within 4 hours after irradiation.

Subsequently a delayed and prolonged increase in Rad51 foci formation was evident from day 2 onwards, which coincided with a decrease in the number γ -H2AX-positive cells (Fig. 3B). The number of Rad51 foci-positive cells increased up to day 5 post-irradiation and then fell sharply to approximately 10% on day 7 for Namalwa cells (Fig. 3C). The maximum number of Rad51-positive cells appeared to coincide with the peak number of endopolyploid cells (Fig. 3B and Fig. 1D) and also with the maximal suppression of the diploid fraction (Fig. 1B), which occurred on approximately days 5-6. Importantly, on day 5 post-irradiation, we found no increase in Rad51 protein synthesis (Fig. 3B, insertion) in agreement with the work of Chen et al., (Chen et al., 1997) and Vispe et al.

(Vispe et al., 1998), indicating that intracellular redistribution and not de novo synthesis, of Rad51 accounts for the extensive foci formation.

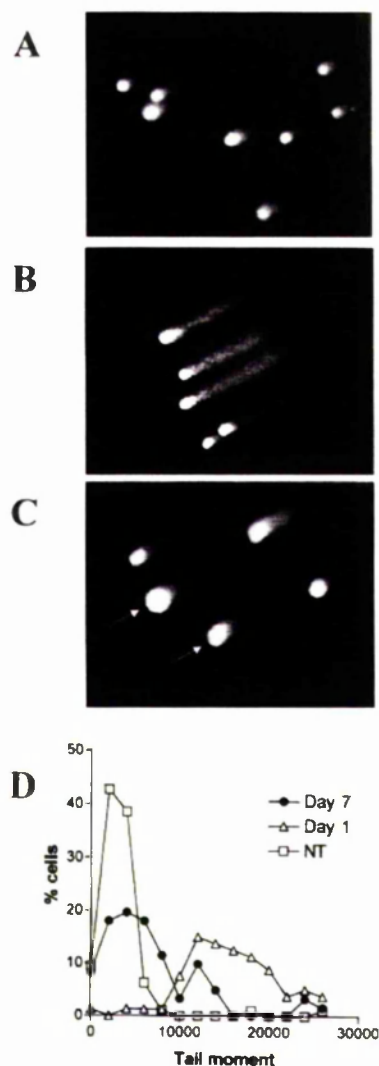


Fig. 4. Detection of DNA strand breaks by comet assay in Namalwa cells, 1 or 7 days after irradiation. After treatment and incubation for the desired time, cells were embedded in agarose and subjected to electrophoresis at pH 12.1. This alkaline electrophoresis allows the detection of single and double DNA strand breaks. The tail moment (% of migrated DNA \times tail length) was measured using Scion image software and a comet assay macro. (A) 96% of non-irradiated Namalwa cells had a tail moment of between 2000 and 8000. (B) On day 1 after 10 Gy irradiation, nearly all of the cells had a tail moment greater than 10,000, providing evidence that DNA strand breaks were not repaired within 24 hours. (C) The vast majority of Namalwa polyploid cells (arrows) on day 7 post irradiation displayed tail moments similar to non-irradiated control cells. Overall, 75.2% of non-apoptotic cells on day 7 had tail moment values equal to those observed in controls. (D) Frequency histograms representing the distribution of tail moments in non-irradiated control Namalwa cells and cells on days 1 and 7 after 10 Gy irradiation.

Induction and delayed resolution of DNA strand breaks revealed by comet assay

To verify that the cytological markers detailed above were truly reflecting the appearance and resolution of DNA strand breaks, the alkaline comet assay was performed during the time course after irradiation with 10 Gy. The median tail moment detected for non-irradiated control cells (Fig. 4A) was 2806.54 ± 324 (median \pm s.e.m.; range between 240.7 and 26,010). On day 1 after irradiation nearly all cells had tail moments $>10,000$ ($16,312 \pm 912.9$; Fig. 4B), indicating that DNA strand breaks were induced by irradiation and not repaired within the first 24 hours. Interestingly, the majority of polyploid cells present on day 7 after 10 Gy irradiation displayed DNA migration properties similar to control cells (Fig. 4C). In fact, the overall tail moment redistribution for this treatment group, presented on Fig. 4D, revealed a biphasic histogram pattern, with 75.2% of non-apoptotic cells displaying a tail moment similar to non-treated control cells and the remainder possessing tail moments indicative of persistent DNA strand breaks. This proportion (24.8%) of cells determined as having DNA breaks by the comet assay is higher than the proportion of cells expressing γ -H2AX foci at this time (Fig. 3B). The reason for this difference is not certain but may reflect a higher sensitivity of the comet assay or could be due to the fact that the alkaline comet assay also detects DNA single strand breaks.

Co-localisation and redistribution of Rad51 and γ -H2AX

Subsequently, we assessed the co-localisation of γ -H2AX and Rad51 foci staining in 300 cells that expressed both foci, over the extended time period after irradiation. 12 hours after irradiation, 41% of Rad51 foci co-localised with the γ -H2AX label for Namalwa cells, as detected by confocal microscopy and digital pixel co-localisation studies. However, subsequently the percentage of co-localisation decreased over time to 18.6% on day 5 in Namalwa cells.

Interestingly, we noted that there were clear differences in the expression patterns of γ -H2AX foci appearing within the first 8 hours (Fig. 5A) and those appearing 24 hours after irradiation. Discrete, bright γ -H2AX foci were seen in the first 8 hours (Fig. 5A – left panel), however larger, presumably fused γ -H2AX foci appear within 24 hours post-irradiation and beyond (Fig. 5B,C). These larger clustered foci appeared to be located in cell nuclei of approximately 20 μ m in size, corresponding to 4C cells (Fig. 5B) compatible with the idea that they represent the G2/M-arrested cells seen by DNA flow cytometry (Fig. 1A,B). Substantial amounts of DNA DSB clearly remain in these G2/M-arrested cells at this time. Conversely, the expression of γ -H2AX was diminished in the large, endopolyploid cells on days 3–6, indicating that these cells had repaired the DNA DSB. In the first 3 days after irradiation, the Rad51 foci that were observed were small and discrete (Fig. 5A), whilst large coalescent foci were scarce (Fig. 5B,C). After this time, we observed clustering and coalescence of Rad51 foci into higher order structures (Fig. 5C). Interestingly, Rad51 and γ -H2AX were rarely seen in the same cell on days 3–6 post-irradiation (Fig. 5B,C).

An interesting and consistent feature during this time period (days 3–7) was the presence of two adjacent or contiguous but distinct Rad51 foci in interphase nuclei of endopolyploid cells (Fig. 5C, insertion). In order to verify these paired foci

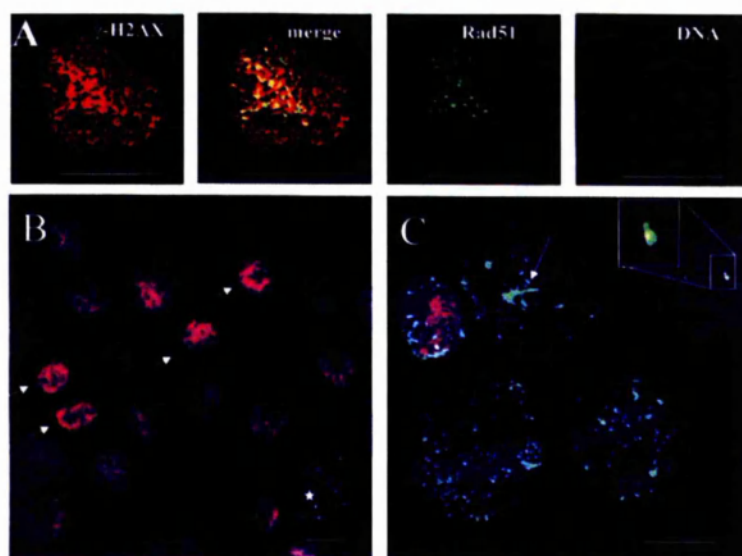


Fig. 5. Double labelling to show concurrent γ -H2AX and Rad51 immunofluorescence after irradiation. Following irradiation of Namalwa cells, cell samples were taken, cytopun, fixed and stained for γ -H2AX and Rad51 and assessed by confocal immunofluorescent microscopy. (A) γ -H2AX and Rad51 foci in a Namalwa cell 4 hours after 10 Gy irradiation; red channel represents Texas Red-labelled γ -H2AX, green channel represents FITC-labelled Rad51 foci in the same cell. (B) Namalwa cells 3 days post irradiation. The γ -H2AX labelling pattern (red) has changed to confluent higher order γ -H2AX structures. Note the increased γ -H2AX immunoreactivity in smaller, presumably 4C cells (arrows) and low/absent γ -H2AX signal in the large Rad51-positive Namalwa endopolyploid cell (asterisks). (C) Namalwa cells, day 4 post-irradiation. The amount of Rad51 foci (green)-positive cells has increased in comparison with day 1. Clustering of the label and formation of higher-order Rad51 structures (arrow) are observed during this time period. Two adjacent or contiguous Rad51 foci was a consistent feature of endopolyploid cells (insertion). DNA was counterstained with 7-AAD. Scale bars: 20 μ m.

statistically, we performed image analysis to measure the centre-to-centre distance between all of the fluorescent foci within the nuclei of 50 Namalwa cells on day 5 after irradiation. The modal distance between all Rad51 foci was 453 nm (range 280 to 30,535 nm). This figure coincided with the measured centre-to-centre distance between double Rad51 foci of 453 ± 110 nm. Often, one of the two foci was brighter than its partner (Fig. 5E).

To address whether these kinetics of DNA repair pathways were specific for B cell lines, or for cells undergoing mitotic catastrophe, we performed the same analysis in the p53-negative, cervical cancer cell line C33A. Following irradiation with 10 Gy, these cells undergo G2 arrest leading to mitotic catastrophe, polyploidization and delayed apoptosis, before eventual recovery, similar to Namalwa and WI-L2-NS cells (H.L., unpublished results). Following irradiation, the extent and kinetics of γ -H2AX and Rad51 foci formation in C33A was similar to that observed in the Namalwa and WI-L2-NS cells. As such, 100% of cells expressed γ -H2AX foci after irradiation on day 1, decreasing gradually to approximately 5% on day 6, whilst the number of cells with Rad51 foci increased from day 2 and reached its maximum on day 6 when Rad51 was visible in 77.3% of cells (data not shown). These data suggest that the delayed formation of Rad51 foci is a general phenomenon of tumour cells that undergo mitotic catastrophe.

Pre-mitotic arrest and proliferative potential of endopolyploid cells after irradiation

We next used two-channel flow cytometry to determine the presence and distribution of cyclin B1 in relation to cell ploidy in the time course after irradiation. We found that on day 1 after irradiation, 65–80% of 4C Namalwa cells were cyclin B1 positive, which reduced to 30% of 4C cells, 3 days later (Fig. 6A). Therefore, in agreement with the data shown in Fig. 1, cells are overcoming G2 arrest and 70% of these cells have entered the endocycle. Up to 41% of the endopolyploid Namalwa cells, mostly of 8C DNA content were cyclin-B1

positive on day 4 after irradiation as shown by flow cytometry and confirmed by immunofluorescent studies (Fig. 6A). Cyclin B1 was predominantly localised in the cytoplasm in these ~40 μ m cells suggesting that these cells were tetraploid in a G2 state. A substantial proportion of these cells did not contain γ -H2AX foci, indicating that they have undergone DSB repair (Fig. 6B).

The ability of tetra and octaploid Namalwa and WI-L2-NS cells to proceed through mitosis was subsequently assessed by quantifying the DNA content in anaphase observed in the first 5 days after irradiation using in situ DNA cytometry. Although mitotic division of polyploid cells was rare in the first 5 days after irradiation, bi-polar mitoses with tetraploid anaphase DNA content and tetrapolar mitoses with diploid content of DNA in anaphase were occasionally observed (Fig. 6C). Time-lapse video-microscopy was also performed and the division of a presumably tetraploid Namalwa cell can be seen in Fig. 6D (arrow) on day 7 after irradiation. Neither aneuploid anaphases and telophases, nor anaphases and telophases with a DNA content higher than 8C, were seen in either of the lymphoma cell lines studied. Taken together, these data indicate that tetraploid cells have a limited ability to undergo mitotic cycling during the first 5 days after irradiation and that this cycling is prohibited for aneuploid cells.

Endopolyploid cells are protected from apoptosis

Next, we hypothesised that if endopolyploid cells repair their DNA damage, the death signals associated with the damage should have gone and these cells would therefore be less likely to undergo apoptosis. Annexin V binding is now well established for characterising early apoptotic cells (Van Engeland et al., 1996; Aubry et al., 1999) and therefore we used this in combination with PI to detect DNA content (cell ploidy) to determine whether endoreduplication was linked to rescue from apoptosis.

In both cell lines, we assessed Annexin V-positive cells over the first 4 days after irradiation and separated the diploid (2C-

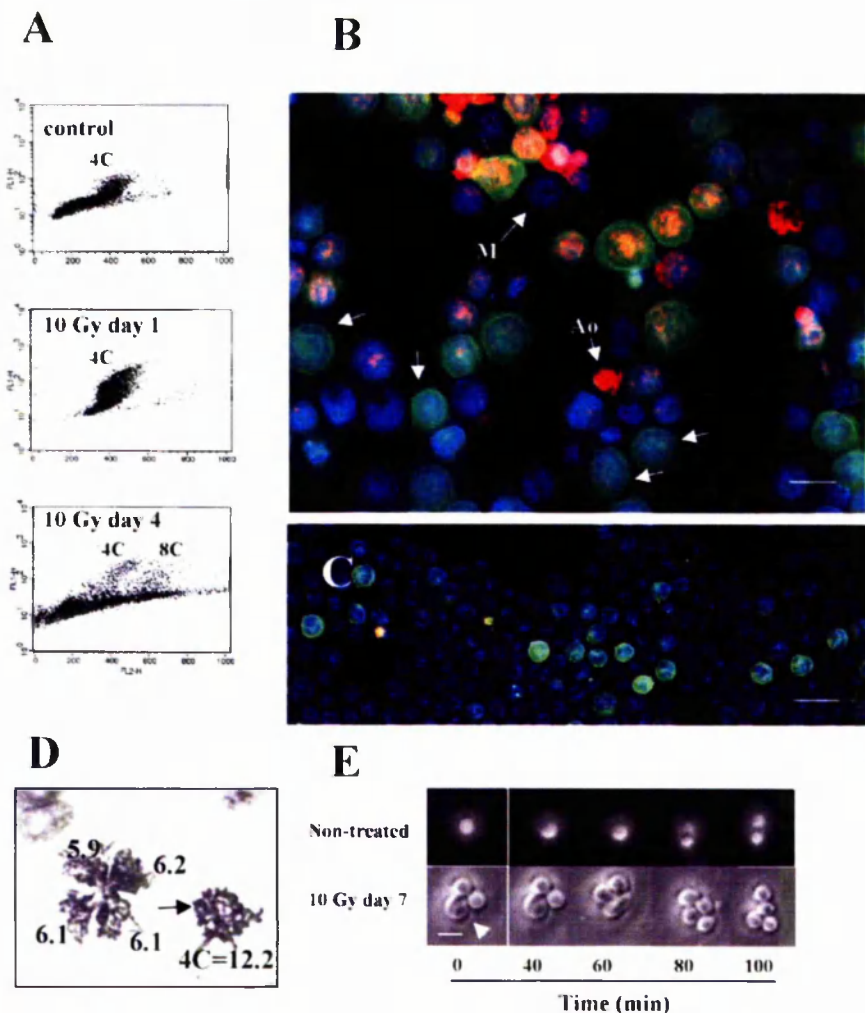


Fig. 6. Proliferative potential of Namalwa endopolyploid cells after irradiation. (A) Two channel cyclin B1-FITC/PI flow cytometry was performed on Namalwa cells for the first 4 days after irradiation. These data revealed an accumulation of cyclin B1 in G2 arrested 4C cells on day 1 after irradiation. However, on day 4 the amount of cyclin B1-positive cells decreased to below the control values for the 4C fraction, but comprised 41% of the 8C fraction. (B) Cyclin B1 and γ -H2AX double staining was performed on fixed Namalwa cells 3 days post-irradiation and assessed by immunofluorescent microscopy. These studies revealed the localisation of cyclin B1 (green) in the cytoplasm of large polyploid cell nuclei, indicating that many of these cells are maintained in a G2-like state. γ -H2AX (red) was excluded from a proportion of these cells (arrows). Rare polyploid cells undergoing mitosis (M) were γ -H2AX negative. Ao indicates an apoptotic cell with aggregated γ -H2AX label. DNA was counterstained with DAPI (blue). (C) Identical cyclin B1 and γ -H2AX double staining was performed on untreated Namalwa cells. (D) DNA image cytometry for multipolar anaphase on day 4 after 10 Gy irradiation. Cytospun cells were fixed, processed and the DNA stained with Toluidine Blue to allow stoichiometric measurement of DNA content by light microscopy and image analysis. Integral optical density (IOD) values, presented for each pole, are relevant to 2C DNA content in control G1 cells. Metaphases (arrow) had double IOD values corresponding to 4C. (E) A frame from

a time-lapse video showing the division of a tetraploid Namalwa cell (arrow) on day 7 after irradiation (bottom); division of a diploid untreated 4C cell in culture was taken as a control (top). Scale bars: 40 μ m.

4C) and polyploid (>4C) fractions. These data, shown in Fig. 6A,B, reveal that, during the first 4 days after irradiation, the proportion of endopolyploid cells that were Annexin V-positive was significantly less than the proportion of diploid cells (Namalwa $P<0.01$; W1-L2 NS $P<0.02$, Student's t -test). This difference increased with time after irradiation, for both cell lines. Finally, we determined the distribution of Annexin V-positive cells in relation to actual cell ploidy on day 4 after irradiation, to assess whether increasing ploidy was associated with protection from apoptosis. These data, shown in Fig. 7D, reveal that the amount of Annexin V-positive cells decreases with increasing ploidy (Fig. 7D). Furthermore, simultaneous staining of irradiated Namalwa cells for Annexin V and Rad51 revealed that Rad51 foci were predominantly absent from Annexin V-positive cells at this time and that Rad51-positive cells were conversely Annexin V negative (Fig. 7E). Taken together, these data suggest that a proportion of endopolyploid cells are protected from apoptotic cell death during

endoreduplication and this protection is associated with the formation of Rad51 foci.

Discussion

The longstanding radiobiological explanation for the survival of cells after DNA damage is that cells repair both potentially lethal damage and sublethal damage within the mitotic cycle (Curtis, 1986). Accordingly, after adaptation of G2 arrest, cells enter mitosis where primary DNA DSB may be transformed into chromosome aberrations that in turn are detected by the spindle checkpoint. At this point, normal mitotic recovery cannot ensue.

In both of the p53 mutated cell lines studied here, G1/S and S phase checkpoints have been adapted and therefore these cells undergo little or no repair within the G1/S compartment after irradiation and pass into the G2 compartment where attempts to repair DSBs by HR are performed. However, the

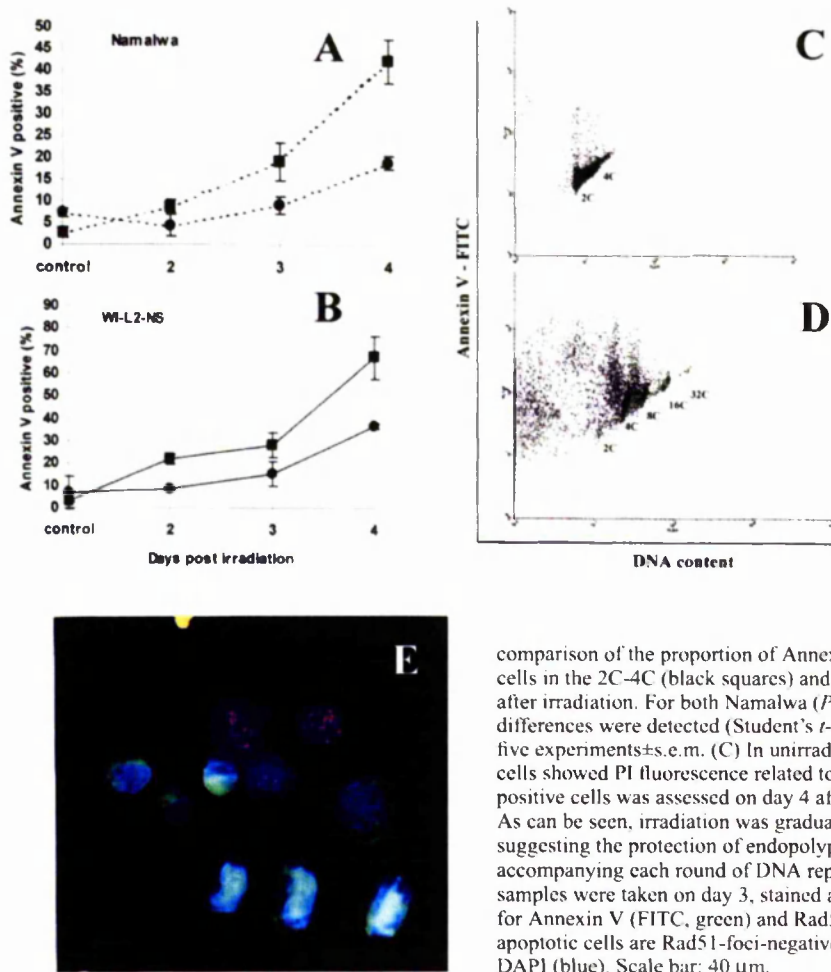


Fig. 7. Protection of polyploid cells from apoptosis. After irradiation, cell samples were taken and assessed by two-channel FACS analysis for Annexin V and PI. Subsequently, cells were characterised according to their DNA content and the percentage of Annexin V-positive cells in each fraction compared. (A) The

comparison of the proportion of Annexin V-positive Namalwa (A) and WI-L2-NS (B) cells in the 2C-4C (black squares) and >4C (black circles) ploidy fractions on days 2-4 after irradiation. For both Namalwa ($P < 0.01$) and WI-L2-NS ($P < 0.02$) cells, significant differences were detected (Student's *t*-test). Data represent mean values from three to five experiments \pm s.e.m. (C) In unirradiated control cells, 85% of Annexin V-positive cells showed PI fluorescence related to 2C-4C cells. (D) The proportion of Annexin V-positive cells was assessed on day 4 after 10 Gy in relation to the actual ploidy value. As can be seen, irradiation was gradually decreasing with each step of ploidy increase, suggesting the protection of endopolyploid cells or their positive selection by apoptosis, accompanying each round of DNA replication. (E) After irradiation, Namalwa cell samples were taken on day 3, stained and assessed by immunofluorescent microscopy for Annexin V (FITC, green) and Rad51 (Alexa Fluor 633; red). Annexin-V-positive apoptotic cells are Rad51-foci-negative and vice versa. DNA is counterstained with DAPI (blue). Scale bar: 40 μ m.

lack of early apoptosis and the near total absence of G1 cells after adaptation of G2 arrest suggest that these radioresistant cell lines do not readily re-enter the mitotic cycle and that attempts at DNA repair in the G2 compartment are to a large extent unsuccessful. Instead, a large population of endopolyploid cells emerges that is present for over 7 days, up until restitution. We suggest that this endoreduplication pathway, initiated after metaphase arrest in these cells, may provide a survival advantage for these cells by preventing the completion of aberrant mitoses that would fix and propagate non-repairable DNA lesions, ultimately leading to cell death. In contrast, for TK6 cells, the p53 wild-type analogue of WI-L2-NS, both G1/S arrest and early apoptosis are apparent after irradiation, endopolyploid cells are not produced and there is no recovery of the cell line after 10 Gy.

We have shown that a HR protein, Rad51, is localised into foci in these endopolyploid cells for a prolonged period of time during which DNA DSBs are repaired, as judged by a decrease in γ -H2AX foci and DNA migration during single cell electrophoresis. Rad51 plays an essential role in homologous recombination in mammalian cells and the percentage of cells containing nuclear Rad51 foci has been shown to increase after

DNA damage (Haaf et al., 1995). These foci form at sites of ssDNA (Raderschall et al., 1999) and recent data has suggested that cells over-expressing Rad51 and containing Rad51 foci are arrested during the cell cycle and are protected from apoptosis (Raderschall et al., 2002). However, Rad51 foci remain enigmatic structures and their true function remains to be elucidated. It is believed that Rad51 foci induced by DNA-damage represent complexes of Rad51 and other proteins that are essential for DNA repair by homologous recombination (Raderschall et al., 2002). It has also been postulated that Rad51 foci appear at sites where the DNA repair machinery has difficulty repairing the breaks that are present.

The early formation of Rad51 foci co-localising with γ -H2AX and the subsequent prolonged maintenance of γ -H2AX and Rad51 over several days, is very suggestive of ongoing DNA repair and misrepair in our cells. However, an unexpected finding was the poor co-localisation of γ -H2AX and Rad51 foci on day 5 after irradiation. One possible explanation for this phenomenon may be that Rad51 protein exits and clusters away from sites where DNA repair has been performed and the process of successful repair is not visible cytologically. Alternatively, the formation of Rad51 foci may represent

stalled intermediates in the homologous recombination reaction that will never be resolved. These sites should contain regions of DNA-DNA cross-linking. Therefore, in an attempt to address this issue, we have estimated the proportion of cells with DNA-DNA cross-links using a modified comet assay. In preliminary experiments we have found that, in comparison to non-irradiated control cells, there is no apparent increase in the proportion of cells containing DNA-DNA cross-links during the first week after 10 Gy irradiation (data not shown), whilst 20-50% of cells have Rad51 foci during this time. This observation, together with the fact that the G1 and G2 cell fractions are substantially suppressed at this time, suggests that the majority of stalled intermediates are resolved in polyploid cells on day 7 after 10 Gy irradiation. From these data, it is reasonable to suggest that the presence of Rad51 foci corresponds to ongoing repair of DNA DSBs during the S phase of the endoreduplication cycle. In agreement with this hypothesis, Rad51 protein expression level in tissues has been shown to correlate with the number of cycling cells (Shinohara et al., 1993; Yamamoto et al., 1996), and various experiments have demonstrated the association of Rad51 foci with post-replicative chromatin during S phase (Tashiro et al., 2000). Finally, taking into account a recent report by Celeste et al., (Celeste et al., 2002) showing that the recruitment of Rad51 into foci is not impaired in *H2AX*^{-/-} mice embryonic fibroblasts, the possibility remains that phosphorylation of H2AX and the formation of Rad51 foci may be independent events or events separated in time. In relation to this DNA DSB repair, we would speculate that the increased amount of homologous sequences in endopolyploid cells after replication may provide additional templates for homologous recombination, facilitating effective repair.

An interesting feature of these endopolyploid cells was the presence of doublets of Rad51 foci. Double Rad51 foci were first identified by Haaf et al. (Haaf et al., 1995) who, referring to the work of Selig et al. (Selig et al., 1992), linked their appearance with reparative DNA synthesis. More recently, double Rad51 foci have been described by Franklin et al. (Franklin et al., 2001) for paired chromosomes during the zygotene stage of meiotic prophase in *Zea mays*. Based on their association with paired chromosomes, these authors suggested that paired Rad51 foci are the sites at which chromosome homology is being compared. The modal centre-to-centre distance between foci was reported to be 460 ± 130 nm on average in that model. Interestingly this figure is extremely close to that found by us for endopolyploid cells (453 ± 110 nm) and perhaps also reflects the sites where homologous chromosome regions are being compared. This latter fact indicates that the distance between paired chromosomes undergoing homologous recombination reported to be occurring in the meiotic bouquet structure may have a more general impact also for lymphoma endopolyploid cells after severe genotoxic treatment.

Although the molecular nature of this Rad51 double foci structure is currently unknown, there are several possibilities. First, the Rad51 double foci structure may represent an antibody staining phenomenon, whereby part of the Rad51 is rendered inaccessible to staining antibody by the secondary structure of the complex (Franklin et al., 2001). Alternatively, the doublet could represent a double Holliday junction (Schwacha and Kleckner, 1995), which would account for the

two adjacent foci of the doublet. This hypothesis embraces the observation that Rad51 foci would co-localise with ssDNA as a consequence of strand invasion and the formation of double Holliday junctions in endopolyploid cells after irradiation. Finally, double Rad51 foci could be attributed to tandems of ssDNA/Rad51 complexes within paired homologous chromosomes.

Our data also indicate that after severe genotoxic treatment some endopolyploid cells, although having limited proliferative potential, perform attempts to enter and complete mitosis. The appearance of bipolar tetraploid and multipolar diploid anaphases suggests the route through which endopolyploid cells return to the mitotic cycle that has been previously documented for mammalian cells (Brodsky and Uryvayeva, 1985; de la Hoz and Baroja, 1993) and was confirmed here for tetraploid cells by time-lapse videomicroscopy. Although in this work we have not provided direct evidence that endopolyploid cells provide clonogenic survivors, we have shown that these cells are not quiescent, but have an active and potentially productive life cycle compared with their mitotic counterparts. In agreement with this suggestion, we have also shown that the higher ploidy fraction (8C-32C) is relatively protected from apoptosis compared with the 2-4C fraction, providing a survival advantage for the higher ploidy cells after severe genotoxic treatment. Furthermore, the decrease in the proportion of Annexin-V-positive cells with increasing DNA content indicates that a process of positive selection by apoptosis occurs preceding or accompanying each round of DNA replication.

In conclusion, we have shown that the endopolyploid cells produced as a result of mitotic arrest induced by genotoxic stress have the capacity to repair DNA DSBs, which may provide a survival advantage for cells that undergo mitotic catastrophe in response to severe genotoxic treatment. These findings are in keeping with other emerging reports linking the survival of acute myeloid leukemia cells after treatment with daunorubicin with delayed apoptosis and the formation of large endopolyploid cells (Come et al., 1999). The formation of endopolyploid cells as a response to genotoxic insult is clearly a common phenomenon of tumour cells *in vitro* and there are many reports linking the presence of endopolyploid tumour cells with poor response to therapy (for reviews, see Levine, 1999; Evans and Podratz, 1996). Furthermore, disease outcome prognosis, or indeed p53 status and multiploidy, but not aneuploidy, appear to be adverse prognostic factors for stage II colorectal cancers (Buglioni et al., 2001). We believe that our data strongly suggest that homologous recombination linked to endoreduplication may be an important factor contributing to genotoxic resistance of tumours that form endopolyploid cells after DNA damage.

The authors would like to acknowledge the help and support of the whole Biomedical imaging Unit, Southampton General Hospital, in particular Mr Roger Alston. We also gratefully acknowledge helpful discussions and comments from colleagues within the Cancer Sciences Division at Southampton University.

References

- Amundson, S. A., Xia, F., Wolfson, K. and Liber, H. L. (1993). Different cytotoxic and mutagenic responses induced by X-rays in two human lymphoblastoid cell lines derived from a single donor. *Mutat. Res.* **286**, 233-241.

- Aubry, J. P., Blaecke, A., Lecoanet-Henchoz, S., Jeannin, P., Herbaud, N., Caron, G., Moine, V. and Bonnefoy, J. Y. (1999). Annexin V used for measuring apoptosis in the early events of cellular cytotoxicity. *Cytometry* 37, 197-204.
- Baroja, A., de la Hoz, C., Alvarez, A., Ispizua, A., Bilbao, J., and de Gandarias, J. M. (1996). Genesis and evolution of high-ploidy tumour cells evaluated by means of the proliferation markers p34 (cdc2), cyclin B1, PCNA and 3[H]-thymidine. *Cell Prolif.* 29, 89-100.
- Baroja, A., de la Hoz, C., Alvarez, A., Vielba, A., Sarra, R., Arechaga, R. J. and de Gandarias, J. M. (1998). Polyploidization and exit from cell cycle as mechanisms of cultured melanoma cell resistance to methotrexate. *Life Sci.* 62, 2275-2282.
- Baumann, P., Benson, F. E. and West, S. C. (1996). Human Rad51 protein promotes ATP-dependent homologous pairing and strand transfer reactions in vitro. *Cell* 87, 757-766.
- Brodsky, V. Y. and Uryayeva, I. V. (1985). *Genome Multiplication in Growth and Development*. Cambridge: Cambridge University Press.
- Bryant, P. E. (1998). The Signal Model, a possible explanation for the conversion of DNA double-strand breaks into chromatid breaks. *Int. J. Radiat. Biol.* 73, 243-251.
- Buglioni, S., D'Agnano, L., Vasselli, S., Perrone Donnorso, R., D'Angelo, C., Brenna, A., Benevolio, M., Cosimelli, M., Zupi, G. and Mottolese, M. (2001). p53 nuclear accumulation and multiploidy are adverse prognostic factors in surgically resected stage II colorectal cancers independent of fluorouracil-based adjuvant therapy. *Am. J. Clin. Pathol.* 116, 360-368.
- Bunz, F., Dutraux, A., Lengauer, C., Waldman, T., Zhou, S., Brown, J. P., Sedivy, J. M., Kinzler, K. W. and Vogelstein, B. (1998). Requirement for p53 and p21 to sustain G2 arrest after DNA damage. *Science* 282, 1497-1500.
- Celeste, A., Petersen, S., Romanienko, P. J., Fernandez-Capetillo, O., Chen, H. T., Sedelnikova, O. A., Reina-San-Martin, B., Coppola, V., Meffre, E., Difilippantonio, M. J., Redon, C., Pilch, D. R., Olaru, A., Eckhaus, M., Camerini-Otero, R. D., Tessarollo, L., Livak, F., Manova, K., Bonner, W. M., Nussenzweig, M. C. and Nussenzweig, A. (2002). Genomic instability in mice lacking histone H2AX. *Science* 296, 922-927.
- Chadwick, K. H. and Leenhouts, H. P. (1998). Radiation induced chromosome aberrations, some biophysical considerations. *Mutat. Res.* 404, 113-117.
- Chen, F., Nastasi, A., Shen, Z., Brennenman, M., Crissman, H. and Chen, D. J. (1997). Cell cycle-dependent protein expression of mammalian homologs of yeast DNA double-strand break repair genes Rad51 and Rad52. *Mutat. Res.* 384, 205-211.
- Come, M. G., Skladanowsky, A., Larsen, A. K. and Laurent, G. (1999). Dual mechanism of daunorubicin-induced cell death in both sensitive and MDR-resistant HL-60 cells. *Br. J. Cancer* 79, 1090-1097.
- O'Connor, P. M., Jackman, J., Jondle, D., Bhatia, K. and Magrath, I. (1993). Role of the p53 tumour suppressor gene in cell cycle arrest and radiosensitivity of Burkitt's Lymphoma cell lines. *Cancer Res.* 53, 4776-4780.
- Cragg, M. S., Zhang, L., French, R. R. and Glennie, M. J. (1999). Analysis of the interaction of monoclonal antibodies with surface IgM on neoplastic B-cells. *Br. J. Cancer* 79, 850-857.
- Curtis, S. B. (1986). Lethal and potentially lethal lesions induced by radiation - a unified repair model. *Radiat. Res.* 106, 252-270.
- De la Hoz, C. and Baroja, A. (1993). Proliferative behaviour of high-ploidy cells in two murine tumour lines. *J. Cell Sci.* 104, 31-36.
- Dini, L., Coppola, S., Ruzittu, M. T. and Ghibelli, L. (1996). Multiple Pathways for Apoptotic Nuclear Fragmentation. *Exp. Cell Res.* 223, 340-347.
- van Engeland, M., Ramaekers, F. C., Schutte, B. and Reutelingsperger, C. P. (1996). A novel assay to measure loss of plasma membrane asymmetry during apoptosis of adherent cells in culture. *Cytometry* 24, 131-139.
- Erenpreisa, J. A., Cragg, M. S., Fringes, B., Sharakhov, I. and Illidge, T. M. (2000a). Release of mitotic descendants by giant cells from irradiated Burkitt's lymphoma cell line. *Cell Biol. Int.* 24, 635-648.
- Erenpreisa, J., Ivanov, A., Dekena, G., Vitina, A., Krampe, R., Freivalds, T., Selivanova, G. and Roach, H. I. (2000b). Arrest in metaphase and anatomy of mitotic catastrophe, mild heat shock in two human osteosarcoma cell lines. *Cell Biol. Int.* 24, 61-70.
- Erenpreisa, J. and Cragg, M. S. (2001). Mitotic death, a mechanism of survival? A review. *Cancer Cell Int.* 1, 1.
- Evans, M. P. and Podratz, K. C. (1996). Endometrial neoplasia, prognostic significance of ploidy status. *Clin. Obstet. Gynecol.* 39, 696-706.
- Franklin, A. E., McElver, J., Sunjevaric, I., Rothstein, R., Bowen, B. and Cande, W. Z. (2001). Three-dimensional microscopy of the Rad51 recombination protein during meiotic prophase. *Plant Cell* 11, 809-824.
- Gupta, R. C., Bazemore, L. R., Golub, E. I. and Radding, C. M. (1997). Activities of human recombination protein Rad51. *Proc. Natl. Acad. Sci. USA* 94, 463-468.
- Haber, J. E. (1999). DNA recombination, the replication connection. *Trends Biochem. Sci.* 24, 271-275.
- Haaf, T., Golub, E. I., Reddy, G., Radding, C. M. and Ward, D. C. (1995). Nuclear foci of mammalian Rad51 recombination protein in somatic cells after DNA damage and its localization in synaptonemal complexes. *Proc. Natl. Acad. Sci. USA* 92, 2298-2302.
- Hall, L. L., Th'ng, J. P., Guo, X. W., Teplitz, R. L. and Bradbury, E. M. (1996). A brief staurosporine treatment of mitotic cells triggers premature exit from mitosis and polyploid cell formation. *Cancer Res.* 56, 3551-3559.
- Helma, C. and Uhl, M. (2000). A public domain image-analysis program for the single-cell-gel-electrophoresis comet assay. *Mutat. Res.* 466, 9-15.
- Ianzini, F. and Mackey, M. A. (1998). Delayed DNA damage associated with mitotic catastrophe following X-irradiation of HeLa S3 cells. *Mutagenesis* 13, 337-344.
- Illidge, T. M., Cragg, M. S., Fringes, B., Olive, P. and Erenpreisa, J. A. (2000). Polyploid giant cells provide a survival mechanism for p53 mutant cells after DNA damage. *Cell Biol. Int.* 24, 621-633.
- Johnson, R. D. and Jasin, M. (2000). Sister chromatid gene conversion is a prominent double-strand break repair pathway in mammalian cells. *EMBO J.* 19, 3398-3407.
- Lanni, J. S. and Jacks, T. (1998). Characterization of the p53-dependant postmitotic checkpoint following spindle disruption. *Mol. Cell. Biol.* 18, 1055-1064.
- Levine, E. A. (1999). Prognostic factors in soft tissue sarcoma. *Semin. Surg. Oncol.* 17, 23-32.
- Liang, F., Han, M., Romanienko, P. J. and Jasin, M. (1998). Homology-directed repair is a major double-strand break repair pathway in mammalian cells. *Proc. Natl. Acad. Sci. USA* 95, 5172-5177.
- Pauli, T. T., Rogakou, E. P., Yamazaki, V., Kirchgessner, C. U., Gellert, M. and Bonner, W. M. (2000). A critical role for histone H2AX in recruitment of repair factors to nuclear foci after DNA damage. *Curr. Biol.* 10, 886-895.
- Raderschall, E., Golub, E. I. and Haaf, T. (1999). Nuclear foci of mammalian recombination proteins are located at the single-stranded DNA regions formed after DNA damage. *Proc. Natl. Acad. Sci. USA* 96, 1921-1926.
- Raderschall, E., Bazarov, A., Cao, J., Lurz, R., Smith, A., Mann, W., Ropers, H.-H., Sedivy, J. M., Golub, E. I., Fritz, E. and Haaf, T. (2002). Formation of higher-order nuclear Rad51 structures is functionally linked to p51 expression and protection from DNA damage-induced apoptosis. *J. Cell Sci.* 115, 153-164.
- Rogakou, E. P., Pilch, D. R., Orr, A. H., Ivanova, V. S. and Bonner, W. M. (1998). DNA double-stranded breaks induce histone H2AX phosphorylation on serine 139. *J. Biol. Chem.* 273, 5858-5868.
- Radford, I. R. and Murphy, T. K. (1994). Radiation response of mouse lymphoid and myeloid cell lines. Part III. Different signals can lead to apoptosis and may influence sensitivity to killing by DNA double-strand breakage. *Int. J. Radiat. Biol.* 65, 229-239.
- Rogers-Bald, M., Sargent, R. G. and Bryant, P. E. (2000). Production of chromatid breaks by single dsb. Evidence supporting the signal model. *Int. J. Radiat. Biol.* 76, 23-29.
- Rothkamm, K. and Lühlich, M. (2003). Evidence for a lack of DNA double-strand break repair in human cells exposed to very low X-ray doses. *Proc. Natl. Acad. Sci. USA* 100, 5057-5062.
- Sablina, A. A., Agapova, L. S., Chumakov, P. M. and Kopnin, B. P. (1999). p53 does not control the spindle assembly cell cycle checkpoint but mediates G1 arrest in response to disruption of microtubule system. *Cell Biol. Int.* 23, 323-334.
- Schwacha, A. and Kleckner, N. (1995). Identification of double Holliday junctions as intermediates in meiotic recombination. *Cell* 83, 783-791.
- Scott, D., Fox, M. and Fox, B. W. (1974). The relationship between chromosomal aberrations, survival and DNA repair in tumour cell lines of differential sensitivity to X-rays and sulphur mustard. *Mutat. Res.* 22, 207-221.
- Selig, S., Okumura, K., Ward, D. C. and Cedar, H. (1992). Delineation of DNA replication time zones by fluorescence in situ hybridization. *EMBO J.* 11, 1217-1225.
- Shinohara, A., Ogawa, H., Matsuda, Y., Ushio, N., Ikeo, K. and Ogawa, T. (1993). Cloning of human, mouse and fission yeast recombination genes homologous to RAD51 and RecA. *Nat. Genet.* 4, 239-243.

- Sonoda, E., Takata, M., Yamashita, Y. M., Morrison, C. and Takeda, S. (2001) Homologous DNA recombination in vertebrate cells. *Proc. Natl. Acad. Sci. USA* **98**, 8388-8394.
- Sonoda, E., Sasaki, M. S., Buerstedde, J. M., Bezzubova, O., Shinohara, A., Ogawa, H., Takata, M., Yamaguchi-Iwai, Y. and Takeda, S. (1998). Rad51-deficient vertebrate cells accumulate chromosomal breaks prior to cell death. *EMBO J.* **17**, 598-608.
- Sung, P. (1994). Catalysis of ATP-dependant homologous DNA pairing and strand exchange by yeast rad51 protein. *Science* **265**, 1241-1243.
- Tashiro, S., Walter, J., Shinohara, A., Kamada, N. and Cremer, T. (2000). Rad51 accumulation at sites of DNA damage and in postreplicative chromatin. *J. Cell Biol.* **150**, 283-291.
- Takata, M., Sasaki, M. S., Sonoda, E., Morrison, C., Hashimoto, M., Utsunomiya, H., Yamaguchi-Iwai, Y., Shinohara, A. and Takeda, S. (1998). Homologous recombination and non-homologous end-joining pathways of DNA double-strand break repair have overlapping roles in the maintenance of chromosomal integrity in vertebrate cells. *EMBO J.* **17**, 5497-5508.
- Taylor, W. R. and Stark, G. R. (2001). Regulation of the G2/M transition by p53. *Oncogene* **20**, 1803-1815.
- Vispe, S., Cazaux, C., Lesca, C. and Defais, M. (1998). Overexpression of Rad51 protein stimulates homologous recombination and increases resistance of mammalian cells to ionizing radiation. *Nucleic Acids Res.* **26**, 2859-2864.
- Waldman, T., Lengauer, C., Kinzler, K. W. and Vogelstein, B. (1996). Uncoupling of S phase and mitosis induced by anticancer agents in cells lacking p21. *Nature* **381**, 713-716.
- Yamamoto, A., Taki, T., Yagi, H., Habu, T., Yoshida, K., Yoshimura, Y., Yamamoto, K., Matsushiro, A., Nishimune, Y. and Morita, T. (1996). Cell cycle dependent expression of the mouse Rad51 gene in proliferating cells. *Mol. Gen. Genet.* **251**, 1-12.

Appendix

ERK/MAPK activation promotes resolution of DNA double strand breaks and radiation-induced mitotic catastrophe in lymphoma cells

Introduction

In this appendix we have assessed the impact of ERK/MAPK inhibition on cell cycle progression and mitotic catastrophe in the Burkitt's lymphoma cell line, Namalwa, following severe genotoxic insult. Namalwa cells were irradiated with 10 Gy external beam irradiation with or without 10 nM U0126. Then, cell cycle redistribution was assessed by FACS after staining cells with hypotonic propidium iodide. Apoptosis was detected as the hypo-diploid fraction on DNA ploidy histograms and activation of ERK/MAPK assessed by Western blotting. DNA double strand breaks were visualised by immunocytochemistry for γ -H2AX foci within the cell nuclei.

Results

Prominent mitotic catastrophe, accompanied by segmentation and micronucleation of cell nuclei as well as production of polyploid giant cells, occurred starting from day 3 following 10 Gy irradiation (Figure 1A). The mitotic index (MI) increased starting from day 2 after 10 Gy irradiation highlighting the bypass of G2/M checkpoint in irradiated cells. However, cells pre-treated with the MEK1/2 specific inhibitor U0126 maintained radiation induced G2 arrest up to day 7 post irradiation and no significant increase in MI and cell death occurred in these samples (Figure 1A, B). Figure 1C demonstrates that the

adaptation of G2/M was accompanied by activation of ERK/MAPK that reached its maximum on days 2 and 3 after irradiation preceding and then coinciding with the peak of MI.

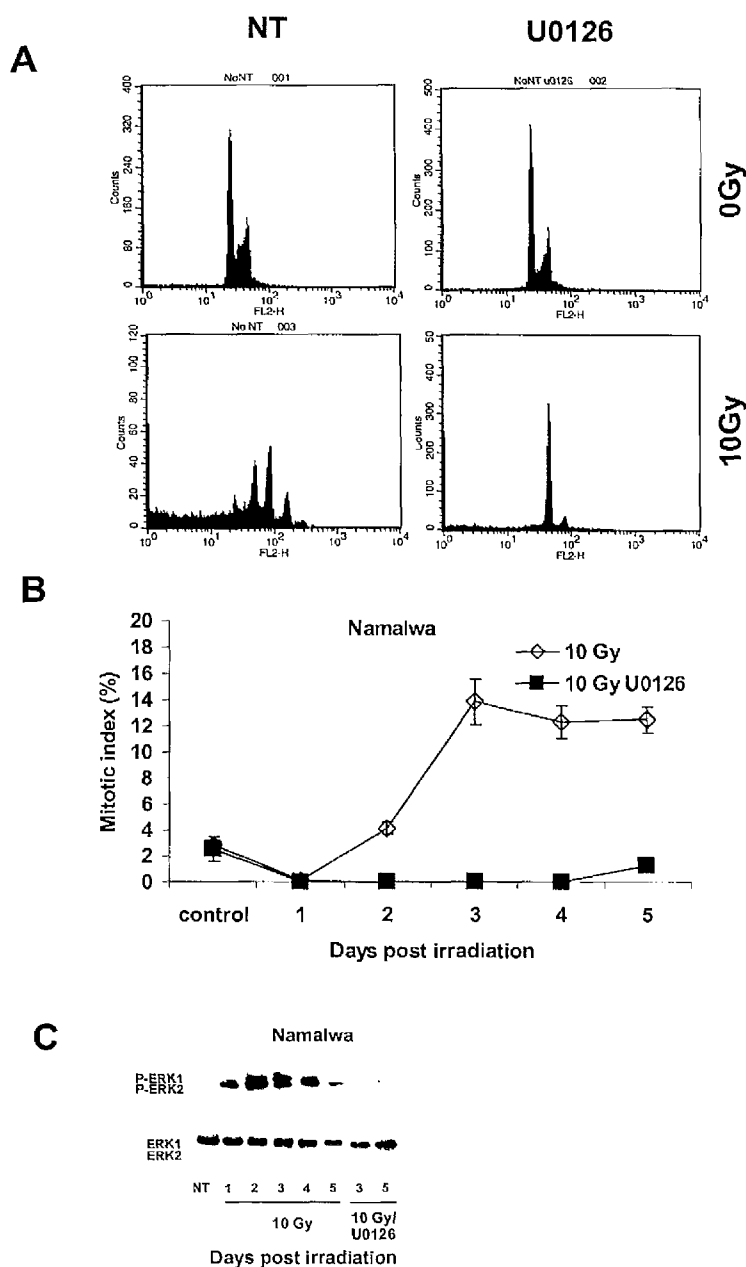


Figure 1. Activation of MAPK and mitotic catastrophe in Namalwa cells following 10 Gy irradiation. A) Upper panel: non-irradiated control cells on day 5 of restitution. Lower panel: cells were irradiated with a 10 Gy dose with or without U0126 and DNA ploidy assessed on day 5 after treatment. B) Kinetics of mitotic index following 10 Gy irradiation, with or without U0126. Irradiated cells were cytopspun onto poly-L-lysine coated microscope slides, stained with DAPI and the proportion of nuclei undergoing mitosis assessed under luminescence microscope. At least 300 cells in at least 5 viewing field were registered. Results represent average of two independent experiments \pm SEM. C) Activation of ERK/MAPK in Namalwa cells following 10 Gy irradiation. Non-treated or irradiated cells were harvested and assessed by Western blotting for phosphorylated ERK1/2. Total amount of ERK protein was detected as a loading control.

Next, we assessed the impact of MEK inhibition on repair of DNA double strand breaks following irradiation. Figure 2A demonstrates that the majority of DNA strand breaks have been repaired by day 5 after irradiation. However, repair of DNA double strand breaks was accompanied by gross alteration of nuclear shape, blebbing, micronucleation and production of multipolar and aberrant mitoses – a hallmark of mitotic catastrophe. Contrary to irradiated samples, samples pre-treated with U0126 displayed an abundance of cells expressing γ -H2AX signal in their nuclei (Figure 2A and B) but virtually no signs of mitotic catastrophe.

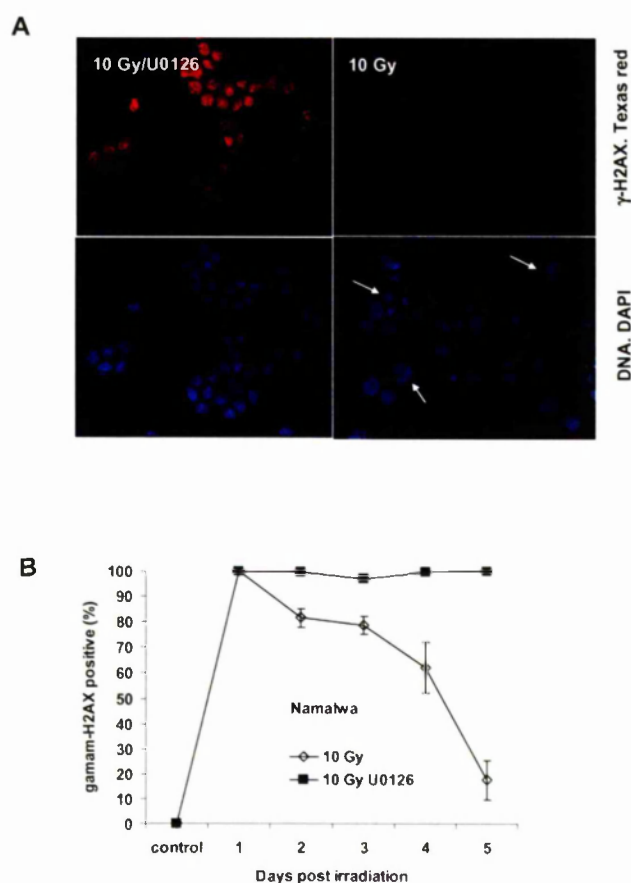


Figure 2. Resolution of DNA double strand breaks on day 5 after 10 Gy irradiation. Cells were irradiated in the presence or absence of U0126 and the proportion of cells expressing gamma-H2AX foci determined by fluorescence microscopy. A) Upper panel: gamma-H2AX foci in cells irradiated with (left) or without (right) U0126. Lower panel: cell nuclei counterstained with DAPI. Arrows: micronucleation of irradiated cells on day 5 after treatment. B) The proportion of cells expressing gamma-H2AX foci during 5 days restitution process. At least 300 cells in at least 5 viewing fields were analysed. Results represent average of two independent experiments \pm SEM

Discussion

Here we show that radiation-induced activation of the ERK/MAPK cascade triggers cell cycle progression and mitotic catastrophe after severe genotoxic damage. Interestingly, it also promoted the resolution of radiation induced DNA double strand breaks as pre-treatment of cells with the MEK1/2 specific inhibitor U0126 completely blocked disappearance of γ -H2AX foci during the 6 day restitution process. Moreover, U0126 completely blocked formation of polyploid cells and micronucleation, hallmarks of mitotic catastrophe. Combining these two phenomena together, it is reasonable to suggest that activation of the ERK/MAPK cascade after severe genotoxic insult, promoting adaptation of G2/M arrest even if DNA double strand breaks are not repaired, facilitates conversion of primary DNA double strand breaks into chromosome aberrations, ultimately leading to mitotic catastrophe and loss of cell viability (Figure 3).

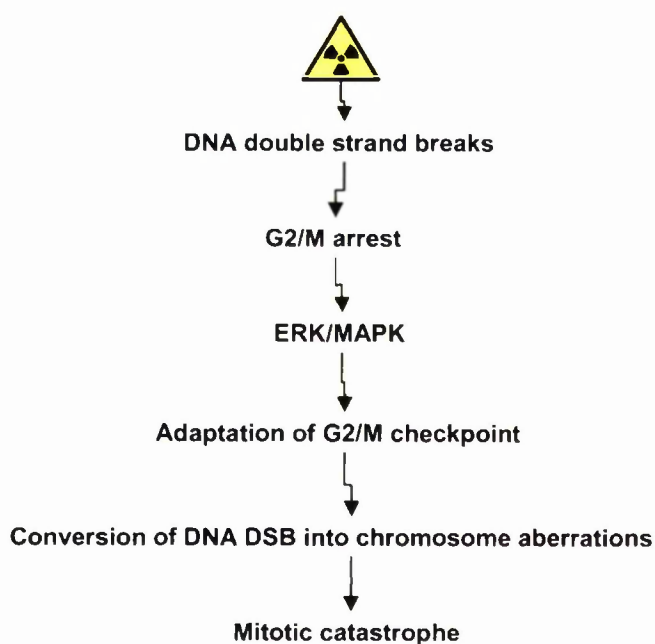


Figure 3. Hypothetical scheme of the involvement of ERK/MAPK cascade in radiation-induced mitotic catastrophe.

Chapter 4

Upregulation of meiosis-specific genes in lymphoma cell lines following genotoxic insult and induction of mitotic catastrophe.

Reprinted from Kalejs M*, Ivanov A*, Plakhins G, Cragg MS, Emzinsh D, Illidge TM, Erenpreisa J. BMC Cancer. 2006 Jan 9;6:6.

* joint first authorship

Research article

Open Access

Upregulation of meiosis-specific genes in lymphoma cell lines following genotoxic insult and induction of mitotic catastrophe

Martins Kalejs^{*†1}, Andrey Ivanov^{†1,2}, Gregory Plakhins¹, Mark S Cragg^{3,4}, Dzintars Emzinsh⁵, Timothy M Illidge² and Jekaterina Erenpreisa¹

Address: ¹Biomedical Research and Study Centre, Latvian University, Ratsupites 1, Riga, LV-1067, Latvia, ²Paterson Institute Cancer Research, Christie Hospital, Cancer Sciences Division University of Manchester, Manchester, Wilmslow Road, M20 4BX, UK, ³Tenovus Research Laboratory, Cancer Sciences Division, School of Medicine, Southampton University Hospital, Southampton SO16 6YD, UK, ⁴Walter and Eliza Hall Institute of Medical Research, 1G Royal Parade, Parkville, Victoria 3050, Australia and ⁵Oncology Center of Latvia, Hipokrata 4, Riga, LV-1079, Latvia

Email: Martins Kalejs^{*} - m.kalejs@no.lv; Andrey Ivanov - aivanov@PICR.man.ac.uk; Gregory Plakhins - gregplakhin@yahoo.com; Mark S Cragg - cragg@wehi.EDU.AU; Dzintars Emzinsh - dzintars@onkoc.mt.lv; Timothy M Illidge - tmi@manchester.ac.uk; Jekaterina Erenpreisa - katrina@biomed.lv.lv

^{*} Corresponding author [†]Equal contributors

Published: 09 January 2006

Received: 30 September 2005

BMC Cancer 2006, 6:6 doi:10.1186/1471-2407-6-6

Accepted: 09 January 2006

This article is available from: <http://www.biomedcentral.com/1471-2407/6/6>

© 2006 Kalejs et al; licensee BioMed Central Ltd.

This is an Open Access article distributed under the terms of the Creative Commons Attribution License (<http://creativecommons.org/licenses/by/2.0>), which permits unrestricted use, distribution, and reproduction in any medium, provided the original work is properly cited.

Abstract

Background: We have previously reported that p53 mutated radioresistant lymphoma cell lines undergo mitotic catastrophe after irradiation, resulting in metaphase arrest and the generation of endopolyploid cells. A proportion of these endopolyploid cells then undergo a process of depolyploidisation, stages of which are partially reminiscent of meiotic prophase. Furthermore, expression of meiosis-specific proteins of the cancer/testis antigens group of genes has previously been reported in tumours. We therefore investigated whether expression of meiosis-specific genes was associated with the polyploidy response in our tumour model.

Methods: Three lymphoma cell lines, Namalwa, WI-L2-NS and TK6, of varying p53 status were exposed to a single 10 Gy dose of gamma radiation and their responses assessed over an extended time course. DNA flow cytometry and mitotic counts were used to assess the kinetics and extent of polyploidisation and mitotic progression. Expression of meiotic genes was analysed using RT-PCR and western blotting. In addition, localisation of the meiotic cohesin REC8 and its relation to centromeres was analysed by immunofluorescence.

Results: The principal meiotic regulator *MOS* was found to be significantly post-transcriptionally up-regulated after irradiation in p53 mutated but not p53 wild-type lymphoma cells. The maximum expression of *MOS* coincided with the maximal fraction of metaphase arrested cells and was directly proportional to both the extent of the arrest and the number of endopolyploid cells that subsequently emerged. The meiotic cohesin REC8 was also found to be up-regulated after irradiation, linking sister chromatid centromeres in the metaphase-arrested and subsequent giant cells. Finally, RT-PCR revealed expression of the meiosis-prophase genes, *DMC1*, *STAG3*, *SYCP3* and *SYCP1*.

Conclusion: We conclude that multiple meiotic genes are aberrantly activated during mitotic catastrophe in p53 mutated lymphoma cells after irradiation. Furthermore, we suggest that the coordinated expression of *MOS* and REC8 regulate the extent of arrested mitoses and polyploidy.

Background

DNA damage induces a G2 phase cell-cycle arrest in most tumour cell lines that lack functional p53 protein. Following abrogation of the G2 checkpoint, these cells arrest in mitosis and can subsequently form polyploid cells. This response is thought to represent an alternative to immediate death through apoptosis. This abnormal arrest in mitosis and the subsequent formation of mono- and multi-nucleated endopolyploid giant cells is incorporated under the collective term 'mitotic catastrophe' [1]. The mechanisms underlying such responses remain unclear [1-4]. Our group has previously described the morphological features of these endopolyploid cells and observed that certain stages of the cytological rearrangements that lead to their de-polyploidisation, and return to mitosis are partly reminiscent of meiotic prophase [5,6]. Interestingly, ectopic expression of meiotic proteins of the so-called cancer/testis antigens group, namely SCP1 and SPO11, has been reported in the literature as a feature of progressing tumours [7-9] and it has been suggested that this phenomenon could represent a link between the malignant behaviour of tumours and a gametogenesis-like processes [10-12].

One of the central signalling pathways involved in switching cells from mitosis to meiosis is regulated by the MOS kinase. During meiosis, MOS is translationally up-regulated, where it first stimulates the first reduction division of the cell and then further acts as a cytostatic factor to maintain the oocyte in metaphase arrest at meiosis II until fertilization occurs [13]. These separate functions are attributed to two different downstream targets of the MOS/MAPK pathway, cdk1 and Rsk90, respectively. In addition, MOS directly interacts with kinetochores thereby interrupting mitosis [14].

Meiosis functions to generate cells with a reduced number of chromosome sets. There are two obligate and interdependent requirements for this reduction division: (1) Sister chromatid cohesion and homologous chromosome pairing to facilitate the correct segregation and reduction of maternal and paternal chromosomes; (2) recombination between homologous chromosomes [15,16]. Pivotal to these processes is the meiotic cohesin REC8 [17,18]

which sustains the cohesion between sister chromatids and particularly centromeres preventing separation until anaphase II [19]. Rec8 functions to ensure that both homolog pairing and reduction division occurs during meiosis. Recently, Rec8 dominant negative mutants have been shown to prevent synapse formation of homologs in mammalian cells [20], whilst in yeast mutants over-expressing REC8 fail to produce sister chromatid separation [21].

During pre-meiotic replication REC8 associates with an axial structure on the meiotic chromosomes which later forms the lateral element of the synaptonemal complex (SC) [22]. REC8 has been found to form complexes with the meiosis-specific recombinase DMC1 [23]. This enzyme is necessary for the Rad51-mediated stable DNA strand invasion and homology search which occurs during the homologous recombination stages of meiosis [24]. Other important proteins of the SC are SCP3 and SCP2 which form the lateral elements of the SC. A third protein, SCP1 forms the central element of the SC, providing a bridge to hold the two homologous chromosomes together, assisted by recombination chiasma between the homologs [25-27]. REC8 colocalizes with another meiosis specific cohesin, STAG3. STAG3 stabilizes cohesion between sister chromatids during meiosis I and together with REC8 marks the lateral element of the SC [28].

Thus, REC8 and MOS, together with a number of specific cohesins and recombinases are important in the regulation and execution of meiosis, combining to achieve homologous recombination and chromosome separation/reduction. Although the molecular machinery for meiotic reduction divisions is largely understood, little is known regarding the regulation of reduction division in somatic polyploid cells which is thought to be a rare event [29]. We hypothesised that polyploid cells may have the same common regulators involved in reduction division as meiosis on the basis that meiosis has probably evolved as a means of reducing the chromosome number in asexual polyploid protists [10,30]. Therefore, we sought to address whether the transformations observed in the endopolyploid tumour cells were linked with the ectopic expression of these genes. In this study we demonstrate

Table 1: Sequences of primers used in the RT-PCR experiments.

Gene	Forward	Reverse Primer
MOS	5'-CGGTGTTCTGTGGCCATAA	5'-GCAGGCCGTTCCACAACATC
REC8	5'-TGAGGGTGAATGTGGTGAAA	5'-CTGGGATTGCAGCCTCTAAG
SYCP3	5'-TGCAGAAAGCTGAGGAACAA	5'-TGCTGCTGAGTTTCCATCAT
SYCP1	5'-TGGCGATGTGATGGAATTTA	5'-TGTTTCCCCATTTTGGAG
SPO11	5'-AGGAAGATGGCACCAAGTG	5'-GGTCCCTTTTGTCACTGGA
STAG3	5'-GGATGCAAAGCTACAGCA	5'-CATCCGGTCCTTGAAGC
DMC1	5'-AGCAGCAAAGTTCCATGAAG	5'-TGAGCTCTCTCTTCCCTTT

Table 2: Antibody source and usage

Primary antibodies	Secondary antibodies
Polyclonal goat anti-human REC8 (E-18); sc-15152 (Santa Cruz)	Rabbit anti-goat-Cy3 (Sigma)
Polyclonal rabbit anti-mouse REC8 antibody (602; kindly donated by Dr. C. Heyting, Wageningen, NL [23])	Goat anti-rabbit IgG-Texas red (Vector Laboratories Ltd., UK),
CREST serum against human kinetochore proteins (Acris Antibodies, Hiddenhausen, Germany)	Mouse anti-human IgG-FITC (Dr. MS Cragg)
Polyclonal rabbit anti-MOS (C237: sc-86; Santa Cruz Biotech; Wembley, UK)	Mouse anti-rabbit IgG-FITC (Sigma, Dorset, UK)
Polyclonal rabbit anti-SCP3 antiserum (kindly donated by Dr. C. Heyting, Wageningen, NL [46])	Goat anti-rabbit IgG-FITC (Vector Laboratories Ltd., UK),

the expression of several key meiotic prophase genes including *MOS*, *SYCP1*, *REC8*, *DMC1*, *STAG3* and *SYCP3* in tumour cells.

Methods

Cell lines and irradiation of cells

The Burkitt's lymphoma cell line Namalwa was obtained from the American Type Culture Collection (ATCC) and carries mutated p53 [31]. The TK6 and WI-L2-NS human lymphoblastoid cell lines were derived from the same WI-L2 isolate and were obtained from Dr. P. Olive (Vancouver, Canada). TK6 cells are p53 wild type and WI-L2-NS p53-mutated [32]. The p53 mutation status of all three cell lines was confirmed by sequencing analysis. Cells were grown in RPMI 1640 medium, 10 % Foetal Calf Serum (FCS; Gibco, Paisley, UK) at 37°C in a 5 % CO₂ humidified incubator. Cells were maintained in log phase of growth for at least 24 hours prior to irradiation which was at a density of 5×10^5 cells/ml using a Gulmay D3 225 X-ray source at a dose rate of 0.77 Gy/min. Cell culture medium was replenished every 48–72 hours.

Mitotic counts and DNA flow cytometry

Mitotic counts were measured from cytopspins stained for DNA. Metaphases, anaphases and telophases were counted per 1000 cells, in at least three independent experiments. DNA flow cytometry for detection of polyploid cells (>4C) was performed as described previously [32].

Isolation of mRNA and conversion into cDNA

mRNA was isolated using the microquickprep mRNA kit (Amersham Pharmacia Biotech UK Ltd, Little Chalfont, UK) and converted to cDNA using the first strand cDNA synthesis kit (Amersham Pharmacia Biotech UK Ltd) according to the manufacturer's instructions.

RT-PCR

Reverse transcription polymerase chain reaction (RT-PCR) was performed in thin walled PCR tubes with 100 ng of cDNA, 100 ng of 5' and 3' primers, 1 unit (U) of DNA polymerase in the presence of dNTPs, 1 × reaction buffer

and Taq polymerase (Promega, Southampton, UK). DNA was denatured at 95°C for 1 min, followed by 30 amplification cycles, using an annealing temperature of 56°C and extension at 72°C. The sequences of primers used are listed in Table 1. PCR products were analysed by electrophoresis in 1–2 % agarose gels and visualized under UV light after staining with ethidium bromide.

Sequencing

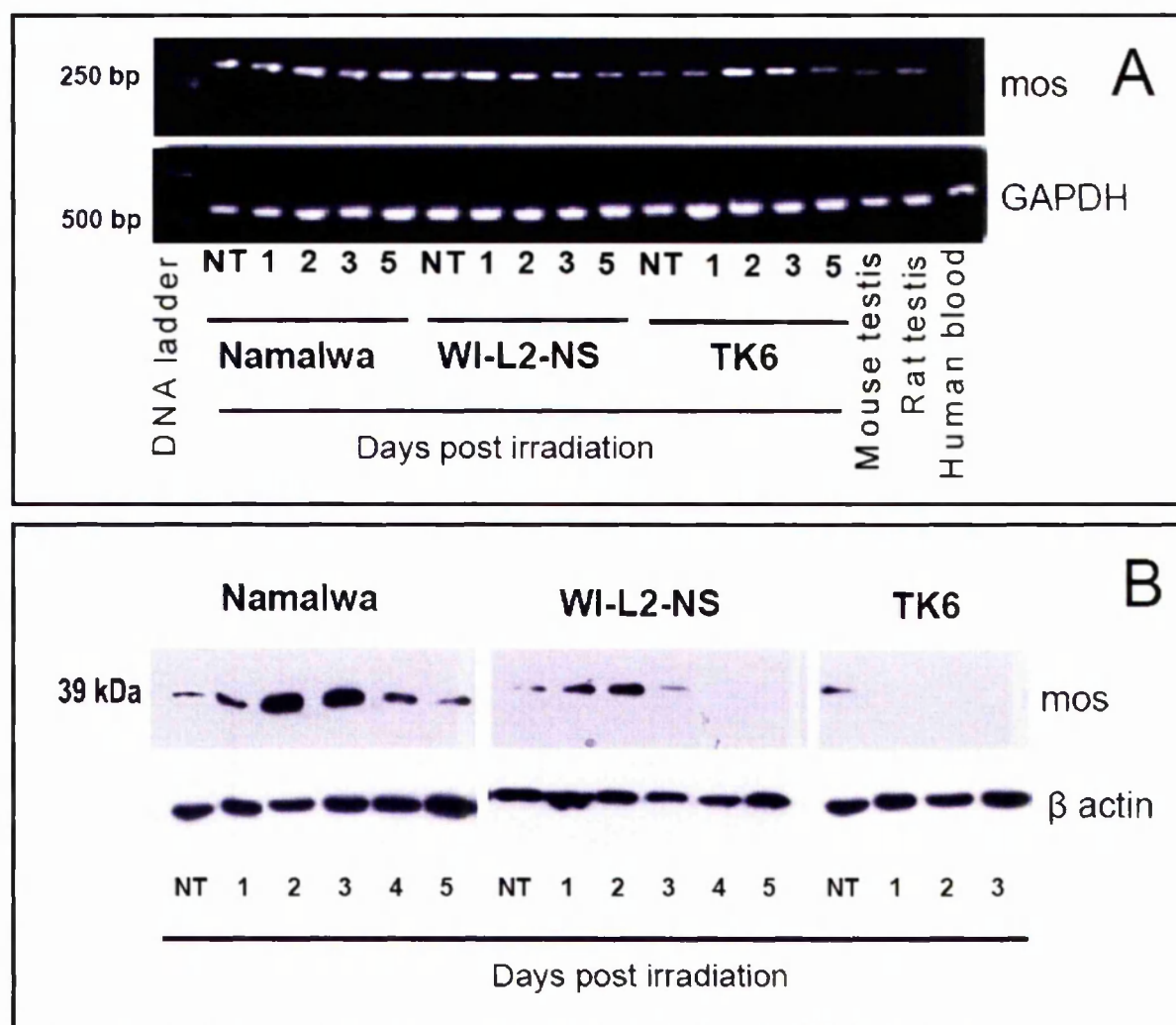
To verify the sequence of the RT-PCR products, additional PCR experiments were performed with Pfu polymerase rather than Taq. These products were gel purified and cloned into PCR-Blunt II- TOPO vector (Invitrogen Life Technologies, UK). Sequencing was performed with T7 and sp6 primers along with standard PCR dye based dideoxy chain termination technology and analyzed on an AB Prism 377 sequencer (Perkin-Elmer Applied Biosystems, Warrington, UK). The MOS nucleotide sequence was submitted to GenBank (accession number AY279177).

Western blotting

Western blotting was performed on cytoplasmic cell lysates to detect MOS and β -actin proteins accordingly to the methods as previously described [33]. The anti-nuclear REC8 antibody (Santa Cruz Biotech.) was used to detect REC8. For MOS detection, 2×10^6 cells were lysed in 100 μ l of 2× PSB, sonicated for 30 seconds, heated at 96°C for 5 minutes, resolved via 10% SDS-PAGE and transferred to PVDF membranes. After incubation with appropriately diluted primary antibodies (see Table 2), membranes were incubated with horseradish peroxidase-conjugated anti-mouse or anti-rabbit IgG (Sigma; Dorset, UK) for 1 hour at room temperature and washed. Antibody binding was visualized by SuperSignal West Pico Chemiluminescent Substrate (Pierce Biotechnology, Perbio Science UK Ltd., UK) before exposure to light-sensitive film (Hyperfilm ECL, Amersham Pharmacia Biotech, UK).

Immunofluorescent (IF) staining

For immunofluorescent staining, harvested cells were suspended in FCS, cytopun onto poly-L-lysine coated micro-

**Figure 1**

Post transcriptional accumulation of p39mos protein in response to 10 Gy irradiation. (A) Transcription of MOS from Namalwa, WI-L2-NS or TK6 cells on different days after irradiation. Messenger RNA was first isolated from samples and then reverse transcribed to yield cDNA for semi-quantitative PCR. Primers for GAPDH were used to verify integrity and quantity of cDNA. Mos expression was observed in all 3 cell lines with minor differences seen during the five days after irradiation; (B) upper panel: in comparison to non-treated control (NT), accumulation of p39mos was detected by Western blotting on days 1 to 4 after irradiation, with maximum expression observed on days 2–3 in Namalwa, and days 1 and 2 for WI-L2-NS cells. In TK6 cells, p39mos was not detectable after irradiation. Lower panel: for loading control PVDF membranes were re-blotted with mouse monoclonal anti-β-actin antibodies.

scope slides, fixed in absolute methanol for 10–20 minutes at -20°C. Slides were then rinsed in ice-cold acetone, semi-dried and washed in PBS. Detection of various proteins was performed with the respective antibodies

according to [34]. The pairs of antibodies used and their source are presented in Table 2. Samples were counterstained with DAPI (0.5 µg/ml) (Molecular Probes, Cambridge, UK). Slides were mounted in mowiol (Harlow

Chemical Company Ltd, UK), containing 0.1% citifluor (Agar Scientific, Stansted, UK). Images were taken with a Leica DM LS2 fluorescent microscope.

Results

Translation of MOS is enhanced by irradiation in p53 mutated lymphoma cell lines

MOS was transcriptionally expressed in all three lymphoma cell lines, and no significant changes were detected following irradiation (Fig. 1A). However, when protein expression was assessed by Western blotting, a particularly pronounced accumulation of p39mos was observed in Namalwa cells after irradiation (Fig. 1B) with the peak levels of expression coinciding with the maximal metaphase arrest on day 3 (Fig. 2A and 2B). The p39mos expression was also elevated in WI-L2-NS cells after irradiation, which again coincided with the maximum mitotic arrest (in this case on day 2), albeit less pronounced (both the expression of p39mos and cell arrest) than that observed in the Namalwa cells. In contrast, p39mos protein was expressed at a very low level in p53 wild-type TK6 cells and its expression was not enhanced following irradiation. The expression level of p39mos also correlated with the amount of polyploid cells produced (Fig. 2C). These data suggest that the post-translational events responsible for the induction of MOS only occur in p53 mutated irradiated lymphoma cells following irradiation. Next we sought to examine the expression of the meiotic cohesin REC8.

Expression of REC8 is enhanced after irradiation

Although transcribed at a low level in untreated cells, REC8 was substantially up-regulated following irradiation in all five independent experiments performed with the Namalwa cell-line (Figure 3A). Up-regulation was observed from day 3 until day 7–9 post-irradiation over the period during which the largest number of polyploid cells are present in the culture (Fig. 2C). REC8 was also expressed in WI-L2-NS cells and elevated following irradiation, albeit with different kinetics than that seen in Namalwa cells where a prominent increase in transcription was seen only from day 5. In contrast, in TK6 cells, REC8 was transcribed prior to irradiation but its expression fell afterwards. Due to almost all of the TK6 cells undergoing apoptosis by day 3, it was impossible to analyze expression levels on subsequent days. Western blot analysis performed for REC8 protein in Namalwa cells further confirmed the translation of this meiotic cohesion protein over this protracted period post-irradiation with a peak in protein expression on day 3 (Fig. 3B).

Distribution of REC8 in endopolyploid cells

Given the pronounced upregulation of REC8 following irradiation, we next assessed the localisation of REC8 in cells at various times after irradiation. As a positive control

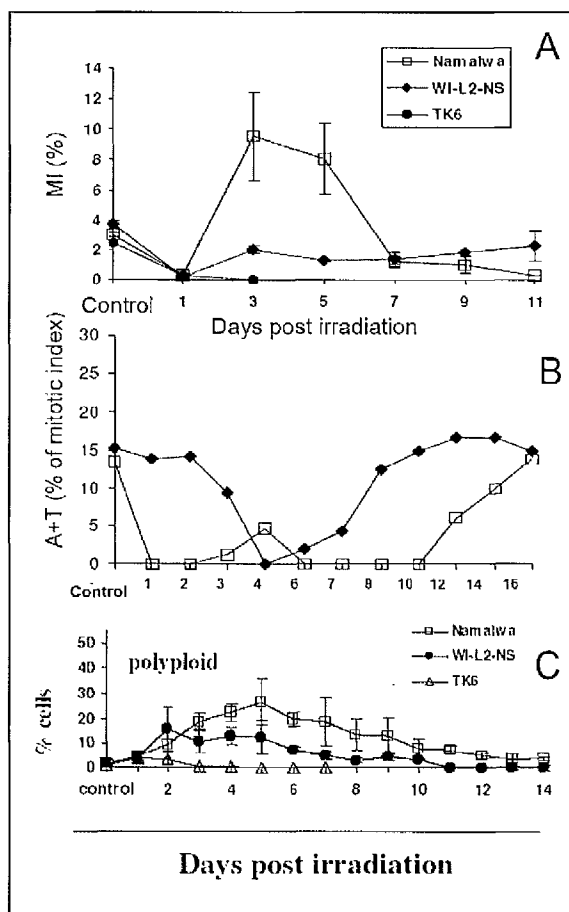
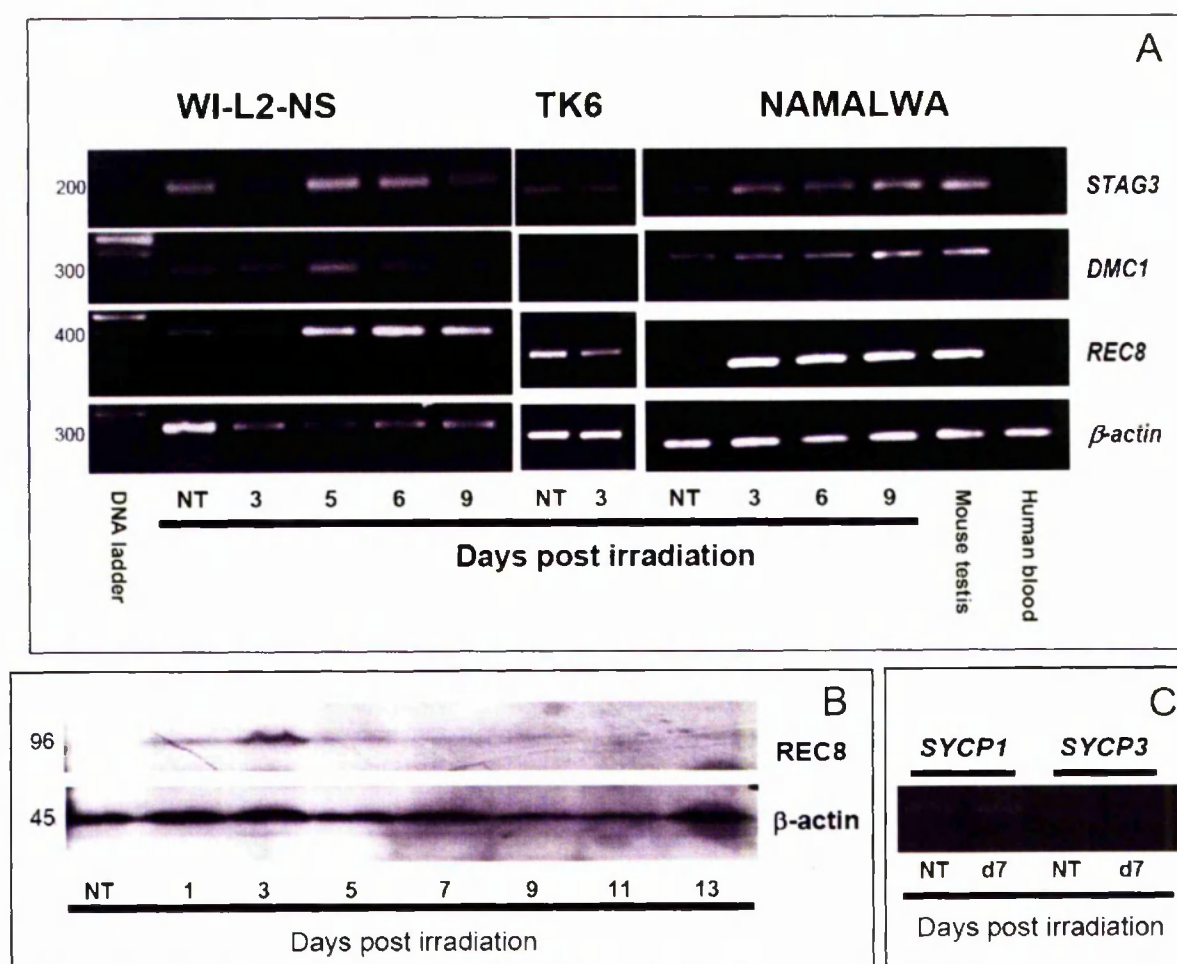


Figure 2

Metaphase arrest and levels of polyplody in lymphoma cell lines after 10 Gy irradiation. p53 mutated Namalwa cells show a pronounced arrest in metaphase as seen by the high mitotic index on day 3 to day 5 (A) and near absence of anaphases and telophases (B) for a period of almost 10 days. Metaphase arrest is smaller and shorter in WI-L2-NS; (C) typical changes in the levels of polyplody observed by DNA flow cytometry in Namalwa, WI-L2-NS and TK6 cells. (C) Reprinted from Ivanov et al., 2003. Both mitotic and endocycling are abrogated in wt p53 TK6 cells, which do not survive this irradiation insult.

for REC8 staining we first assessed two different antibodies directed to REC8 on rat testes tissue and, as expected, we observed strongly positive staining in the primary spermatocytes (Fig. 4A insert). Using the same antibodies, we then assessed the expression of REC8 in the lymphoma cells. Untreated Namalwa cells in interphase or undergoing mitosis were negative for REC8. Interestingly, however, a few bright, large, REC8-positive foci were observed

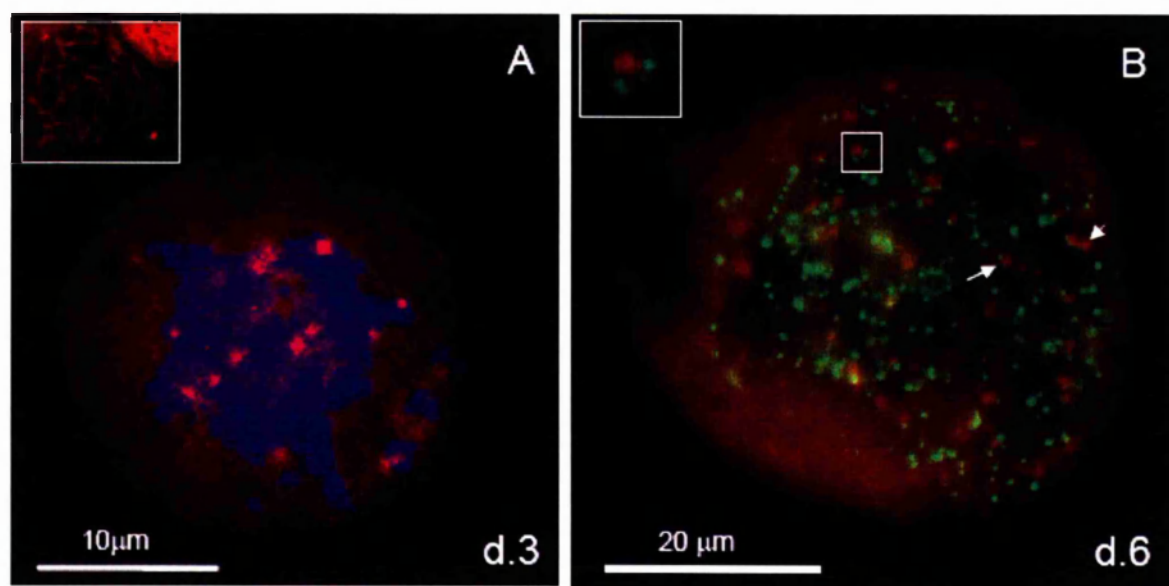
**Figure 3**

The expression of meiosis-specific genes DMC1, REC8, STAG3, SYCP1 and SYCP3 in irradiated lymphoma cells in the time-course post-irradiation: (A) Transcription of REC8, STAG3 and DMC1, shown by RT-PCR of mRNA isolated from WI-L2-NS, TK6 or Namalwa cells on different days post irradiation and from non-treated control cells (NT). Primers for actin were used to verify integrity and quantity of cDNA; (B) Expression of REC8 protein in Namalwa cells, detected by Western blotting (antibody from Santa Cruz). The highest level of transcription was detected on day 3. Lower panel: for loading control PVDF membranes were re-blotted with mouse monoclonal anti- β -actin antibodies. (C) Transcription of SYCP1 and SYCP3 shown by RT-PCR of mRNA isolated from non treated Namalwa cells or on day 7 post irradiation showing very weak background expression. **NB:** In this experiment three times as much cDNA was used for the WI-L2-NS non treated samples as was used for the WI-L2-NS samples post irradiation. This was done in order to verify the increase in transcription after irradiation treatment. Although the amount of cDNA taken for PCR with the REC8 primers is much smaller on day 5 post irradiation (as judged by beta actin level) it still shows obviously higher level of REC8 expression.

in the chromatin of rare mitotic cells undergoing arrest in metaphase (data not shown).

Following irradiation of Namalwa cells, bright REC8-positive foci appeared in about 10–15% of the cells on day 3.

These data are in accordance with the western blot REC8 protein expression coincident with the peak of mitotic arrest. REC8 was localised within the arrested aberrant metaphases characterised by the swollen and adhered chromosomes (Fig 4A), evidently undergoing restitution

**Figure 4**

In situ localisation of REC8 post-mitotic catastrophe in endopolyploid Namalwa cells: (A) REC8 (red) appears on day 3 in the metaphase-arrested cells which, as judged by the adhered swollen chromosomes, undergo restitution into endopolyploid cells. DNA counterstained by DAPI (blue) (insert- rat testis control for Rec8); (B) IF double-staining for kinetochores/centromeres by CREST antibody (FITC, green) and REC8 (red) in a polyploid interphasic cell, where interaction of REC8 foci with kinetochores/centromeres is shown; arrow and arrowhead indicate the insertion of several REC8 foci in CREST-positive arrayed structures; the image insert shows a higher magnification of a centromere doublet cohesed with a focus of REC8.

into interphase. After day 3, the amount of REC8 staining increased in the nuclei of subsequent endopolyploid interphase cells. During this period (day 3–6), DNA endoreduplication and repair by homologous recombination were observed as documented by us previously [5,35,36].

Subsequently, we assessed if REC8 was associated with centromeres by combining immunostaining with REC8 and a CREST antibody known to detect kinetochore proteins associated with centromeres. This staining revealed REC8- and CREST-positive foci to be associated and juxtaposed from day 5 to day 9–11, although somewhat irregularly. REC8 foci were seen inserted between doublets or chains of CREST-positive foci (Fig. 4B).

Expression of other meiosis-specific genes

Next, we assessed whether other meiosis specific proteins were expressed in the lymphoma cells. The *DMC1* gene encodes for a meiosis specific recombinase from the RecA family and appears to act in cooperation with REC8 [23] and Rad51 [37]. We found by RT-PCR that *DMC1* was also expressed, both in irradiated and non-treated samples of all three cell lines, with a prominent decrease after

irradiation in the p53 wild-type TK6 cells (Fig. 3A). We also found that *STAG3*, a meiosis-specific cohesin, is transcribed in all three cell lines, although with no apparent change in transcription after irradiation. The translational expression of Rad51 in endopolyploid cells, a recombinase engaged in DNA repair, has previously been shown by us to occur following irradiation in these same p53 mutated cell lines [33]. Studies of the genes involved in the formation of the synaptonemal complex, *SYCP1* and *SYCP3* revealed some weak background expression in Namalwa cells. Although only weakly transcribed, the identity of these PCR products was confirmed by sequencing. The transcriptional expression of these genes was not elevated by irradiation (Fig. 3C).

On day 6 post-irradiation, approximately 8% of irradiated Namalwa cell nuclei displayed atypical weak SCP3 staining by IF in the perinuclear region (not shown).

Discussion

In this study we have investigated the expression of several meiotic genes in p53 wild-type and p53 mutated lymphoma cells both before and after an irradiation insult that induces mitotic catastrophe. This study reveals that a

group of previously well defined meiosis-specific proteins are clearly upregulated in the p53 mutated cells after DNA damage with irradiation. In particular, the meiosis-regulatory protein, MOS, was strongly post-transcriptionally up-regulated in the Namalwa and WIL2NS cells after irradiation. This up-regulation was only apparent in p53 mutated cells and was lacking from the wild-type TK6 cells, implying that up-regulation of MOS by DNA damage is inhibited by wild type p53 function. Interestingly, this elevation in MOS protein was a post-translational event as transcription remained constant after irradiation. Therefore increases in MOS may arise from either increased translation from the mRNA or increased protein stability. For example, post-translational modification of the MOS protein by (auto)phosphorylation on Ser-3 could lead to its increased stability and decreased proteasome-mediated degradation [14].

This observation of mos upregulation in p53 mutated cells, is in line with data of Fukasawa and Vande Woude [38] who demonstrated that only p53^{-/-} somatic cells can tolerate high levels of MOS and the subsequent downstream elevation of MAPK activity. It should also be noted that up-regulation of MOS protein has been previously shown in human ovarian cancer cells arrested at the spindle checkpoint by microtubule-damaging agents [39]. Hence, the quantitative and temporal relationship between MOS up-regulation and the arrest in the spindle checkpoint were also found in that system, although a different type of tumour cell was used and a different metaphase arrest strategy employed. These data strengthen the notion that MOS expression may be directly involved in the metaphase arrest in mitotic catastrophe.

During the homologous recombination processes of meiosis, Rad51 is known to cooperate with the meiotic cohesin Rec8 and meiotic recombinase DMC1 [37]. It is striking that in the irradiated p53 mutant lymphoid tumours shown here, we observed the expression of a major meiotic cohesin REC8 and the meiotic recombinase DMC1. In addition to its potential role in DNA recombination and repair, the chromatid-cohesing function of REC8 may also provide for the induction of polyploidising ('catastrophic') mitosis. Whether it represents an adaptive response which favours escape from mitotic cell death, providing an option for the formation of giant cells, additional DNA repair and their segregation by somatic reduction still remains to be elucidated.

An interesting and unexpected finding was that a number of other meiotic prophase-specific genes are also expressed in the lymphoma cell lines. Importantly, the induced activation of these meiotic genes seen in the p53 mutated cell lines was not observed in the wild-type p53 TK6 cells. In accord, TK6 cells produce a very small poly-

ploid cell fraction after irradiation, approximately 6 to 10 times less than WI-L2-NS or Namalwa cells and do not survive the 10 Gy irradiation dose (see Fig. 1).

It is noteworthy that the meiosis-specific genes that were observed by us to be aberrantly expressed in the p53 mutated lymphoma cells (*MOS*, *REC8*, *DMC1*, *STAG3*, *SYCP1*, and *SYCP3*) can all be classified as cancer/testis antigens as defined by Simpson et al. [12]. Many of the cancer/testis gene products belong to a broad and ever expanding group of tumour antigens [7,10] and some have been used, with various success rates, as targets for vaccine therapy in clinical trials [40].

To our knowledge, four of these meiotic prophase-associated genes (*REC8*, *DMC1*, *STAG3* and *SYCP3*) are reported to be expressed in malignant tissue for the first time. Interestingly, at least a proportion of these meiosis specific genes appear to be associated with the induction of mitotic catastrophe and the generation of endopolyploid tumour cells.

Finally, recent advances in long-term video-microscopy have found that the endopolyploid cells resulting from mitotic catastrophe appear to have some reproductive potential [4,41-45]. Given these observations and the potential importance of the meiosis-specific genes in the response of p53 mutated tumour cells to genotoxic treatment, further study of these meiotic genes in tumours may reveal novel therapeutic strategies.

List of abbreviations used

IF- immunofluorescence

SC- synaptonemal complex

Competing interests

The author(s) declare that they have no competing interests.

Authors' contributions

MK carried out the RT-PCR studies together with GP, performed the IF experiments, participated in REC8 western analysis and did most of the manuscript preparation. Al carried out RT-PCR and western for *MOS* and *REC8* as well as the counts of mitotic plates. GP carried out part of the RT-PCR studies of cohesins including primer design. MSC carried out flow cytometry studies, contributed substantially to the data analysis and editing of the manuscript. DzE did the calculations for and designed the irradiation procedure and participated in data analysis. TMI participated in data analysis and critical editing of the manuscript. JeE is the principal investigator, proposed working hypotheses, coordinated research, together with MK carried out IF studies, and edited the manuscript.

All authors participated in the design of the study, read and approved the final manuscript.

Acknowledgements

We wish to acknowledge Dr. Bodo Liebe (Max-Planck-Inst. for Molecular Genetics, Berlin) and Dr. Harry Scherthan (Inst. of Radiation Biology, Munich) for their help with SCP3 staining and for the helpful discussions. Many thanks go to Mrs. Galina Boka from the Latvian Oncology Centre for her help with cell irradiation. This work was performed with financial assistance from grant No 02. 040 of the Latvian Scientific Council and a grant from the Royal Society of London for the Joint Research Project 'The role of giant cells in mechanisms of tumour resistance and survival after genotoxic insult' (2002–2003) enabling exchange visits between Southampton and Riga.

References

- Hartwell LH, Kastan MB: **Cell cycle control and cancer.** *Science* 1994, **266**(5192):1821-1828.
- Roninson IB, Broude EV, Chang BD: **If not apoptosis, then what? Treatment-induced senescence and mitotic catastrophe in tumor cells.** *Drug Resist Updat* 2001, **4**(5):303.
- Erenpreisa J, Cragg MS: **Mitotic death: a mechanism of survival? A review.** *Cancer Cell Int* 2001, **1**(1):1.
- Ianzini F, Mackey MA: **Development of the large scale digital cell analysis system.** *RadiatProtDosemetry* 2002, **99**(1-4):289.
- Erenpreisa JA, Cragg MS, Fringes B, Sharakhov I, Illidge TM: **Release of mitotic descendants by giant cells from irradiated Burkitt's lymphoma cell line.** *Cell Biol Int* 2000, **24**(9):635.
- Erenpreisa J, Kalejs M, Ianzini F, Kosmacek EA, Mackey MA, Emzins D, Cragg MS, Ivanov A, Illidge TM: **Segregation of genomes in polyploid tumour cells following mitotic catastrophe.** *Cell Biol Int* 2005:1005-1011.
- Scanlan MJ, Simpson AJ, Old LJ: **The cancer/testis genes: review, standardization, and commentary.** *Cancer Immun* 2004, **4**:1.
- Tureci O, Sahin U, Zwick C, Koslowski M, Seitz G, Pfreundschuh M: **Identification of a meiosis-specific protein as a member of the class of cancer/testis antigens.** *Proc Natl Acad Sci USA* 1998, **95**(9):5211.
- Koslowski M, Tureci O, Bell C, Krause P, Lehr HA, Brunner J, Seitz G, Nestle FO, Huber C, Sahin U: **Multiple splice variants of lactate dehydrogenase C selectively expressed in human cancer.** *Cancer Res* 2002, **62**(22):6750.
- Kalejs M, Erenpreisa J: **Cancer/testis antigens and gametogenesis: a review and "brain-storming" session.** *Cancer Cell Int* 2005, **5**(4):4.
- Old LJ: **Cancer/testis (CT) antigens - a new link between gametogenesis and cancer.** *Cancer Immun* 2001, **1**:1.
- Simpson AJ, Caballero OL, Jungbluth A, Chen YT, Old LJ: **Cancer/testis antigens, gametogenesis and cancer.** *Nat Rev Cancer* 2005, **5**(8):615-625.
- Tachibana K, Tanaka D, Isobe T, Kishimoto T: **c-Mos forces the mitotic cell cycle to undergo meiosis II to produce haploid gametes.** *Proc Natl Acad Sci USA* 2000, **97**(26):14301.
- Sagata N: **What does Mos do in oocytes and somatic cells?** *Bioessays* 1997, **19**(1):13.
- Walker MY, Hawley RS: **Hanging on to your homolog: the roles of pairing, synapsis and recombination in the maintenance of homolog adhesion.** *Chromosoma* 2000, **109**(1-2):3.
- Bishop DK, Zickler D: **Early decision; meiotic crossover interference prior to stable strand exchange and synapsis.** *Cell* 2004, **117**(1):9.
- Klein F, Mahr P, Galova M, Buonomo SB, Michaelis C, Nairz K, Nasmyth K: **A central role for cohesins in sister chromatid cohesion, formation of axial elements, and recombination during yeast meiosis.** *Cell* 1999, **98**(1):91.
- Parisi S, McKay MJ, Molnar M, Thompson MA, van der Spek PJ, Drunen-Schoenmaker E, Kanaar R, Lehmann E, Hoeijmakers JH, Kohli J: **Rec8p, a meiotic recombination and sister chromatid cohesion phosphoprotein of the Rad21p family conserved from fission yeast to humans.** *Mol Cell Biol* 1999, **19**(5):3515.
- Watanabe Y, Nurse P: **Cohesin Rec8 is required for reductional chromosome segregation at meiosis.** *Nature* 1999, **400**:461.
- Xu H, Beasley MD, Warren WD, van der Horst GT, McKay MJ: **Absence of mouse REC8 cohesin promotes synapsis of sister chromatids in meiosis.** *Dev Cell* 2005, **8**(6):949-961.
- Kitajima T, Kawashima S, Watanabe Y: **The conserved kinetochore protein shugoshin protects centromeric cohesion during meiosis.** *Nature* 2003, **427**:510.
- van Heemst D, Heyting C: **Sister chromatid cohesion and recombination in meiosis.** *Chromosoma* 2000, **109**(1-2):10.
- Eijpe M, Offenberger H, Jessberger R, Revenkova E, Heyting C: **Meiotic cohesin REC8 marks the axial elements of rat synaptonemal complexes before cohesins SMC1 beta and SMC3.** *J Cell Biol* 2003, **160**(5):657.
- Shinohara A, Shinohara M: **Roles of RecA homologues Rad51 and Dmcl during meiotic recombination.** *Cytogenet Genome Res* 2004, **107**(3-4):201.
- Yuan L, Liu JG, Hoja MR, Lightfoot DA, Hoog C: **The checkpoint monitoring chromosomal pairing in male meiotic cells is p53-independent.** *Cell Death Differ* 2001, **8**(3):316.
- Colaiacovo MP, MacQueen AJ, Martinez-Perez E, McDonald K, Adamo A, La Volpe A, Villeneuve AM: **Synaptonemal complex assembly in C. elegans is dispensable for loading strand-exchange proteins but critical for proper completion of recombination.** *Dev Cell* 2003, **5**(3):463.
- Liebe B, Alshelmer M, Hoog C, Benavente R, Scherthan H: **Telomere attachment, meiotic chromosome condensation, pairing, and bouquet stage duration are modified in spermatocytes lacking axial elements.** *Mol Biol Cell* 2004, **15**(2):827.
- Prieto I, Tease C, Pezzi N, Buesa JM, Ortega S, Kremer L, Martinez A, Martinez AC, Hulten MA, Barbero JL: **Cohesin component dynamics during meiotic prophase I in mammalian oocytes.** *Chromosome Res* 2004, **12**(3):197-213.
- Storchova Z, Pellman D: **From polyploidy to aneuploidy, genome instability and cancer.** *Nat Rev Mol Cell Biol* 2004, **5**(1):45.
- Erenpreisa J, Kalejs M, Cragg MS: **Mitotic catastrophe and endomitosis in tumour cells: An evolutionary key to a molecular solution.** *Cell Biol Int* 2005, **29**:1012-1018.
- O'Connor PM, Jackman J, Jondle D, Bhatia K, Magrath I, Kohn KW: **Role of the p53 tumor suppressor gene in cell cycle arrest and radiosensitivity of Burkitt's lymphoma cell lines.** *Cancer Res* 1993, **53**(20):4776-4780.
- Amundson SA, Xia F, Wolfson K, Liber HL: **Different cytotoxic and mutagenic responses induced by X-rays in two human lymphoblastoid cell lines derived from a single donor.** *Mutat Res* 1993, **286**(2):233-241.
- Ivanov A, Cragg MS, Erenpreisa J, Emzins D, Lukman H, Illidge TM: **Endopolyploid cells produced after severe genotoxic damage have the potential to repair DNA double strand breaks.** *J Cell Sci* 2003, **116**(Pt 20):4095.
- Scherthan H, Jerratsch M, Li B, Smith S, Hulten M, Lock T, de Lange T: **Mammalian meiotic telomeres: protein composition and redistribution in relation to nuclear pores.** *Mol Biol Cell* 2000, **11**(12):4189.
- Illidge TM, Cragg MS, Fringes B, Olive P, Erenpreisa JA: **Polyploid giant cells provide a survival mechanism for p53 mutant cells after DNA damage.** *Cell Biol Int* 2000, **24**(9):621.
- Erenpreisa J, Ivanov A, Cragg M, Selivanova G, Illidge T: **Nuclear envelope-limited chromatin sheets are part of mitotic death.** *Histochem Cell Biol* 2002, **117**(3):243.
- Gerton JL, Hawley RS: **Homologous chromosome interactions in meiosis: diversity amidst conservation.** *Nat Rev Genet* 2005, **6**(6):477-487.
- Fukasawa K, Vande Woude GF: **Synergy between the Mos/mitogen-activated protein kinase pathway and loss of p53 function in transformation and chromosome instability.** *Mol Cell Biol* 1997, **17**(1):506.
- Ling YH, Yang Y, Tornos C, Singh B, Perez-Soler R: **Paclitaxel-induced apoptosis is associated with expression and activation of c-Mos gene product in human ovarian carcinoma SKOV3 cells.** *Cancer Res* 1998, **58**(16):3633.
- Stevanovic S: **Identification of tumour-associated T-cell epitopes for vaccine development.** *Nat Rev Cancer* 2002, **2**(7):514.
- Ianzini F, Mackey MA: **Mitotic Catastrophe.** In *Apoptosis and Senescence in Cancer Chemotherapy and Radiotherapy* Edited by: Gewirtz, Holt, Grant. Humana Press; 2005.

42. Prieur-Carrillo G, Chu K, Lindqvist J, Dewey WC: **Computerized video time-lapse (CVTL) analysis of the fate of giant cells produced by X-irradiating EJ30 human bladder carcinoma cells.** *Radiat Res* 2003, **159**(6):705-712.
43. Sundaram M, Guernsey DL, Rajaraman MM, Rajaraman R: **Neosis: a novel type of cell division in cancer.** *Cancer Biol Ther* 2004, **3**(2):207.
44. Mackey MA, Anderson KR, Bresnahan LE, Domann FE, Gallardo G, Ianzini F, Kosmacek EA, Li Y, Sonka M, Spitz DR, Sun Y, Wang L, Yang F: **The Large Scale Digital Cell Analysis System: A Unique Tool for the Study of Molecular and Cellular Phenomena in Living Cell Populations.** *Molecular Imaging* 2003, **2**:226.
45. Ianzini F, Bresnahan L, Wang L, Anderson K, Mackey MA: **The Large Scale Digital Cell Analysis System and its Use in the Quantitative Analysis of Cell Populations.** In *The Second Annual International IEEE-EMBS Special Topic Conference on Microtechnologies in Medicine and Biology* Edited by: Dittmar A, Beebe E. Piscataway, NJ, IEEE Press; 2002:470-475.
46. Lammers JH, Offenberg HH, van Aalderen M, Vink AC, Dietrich AJ, Heyting C: **The gene encoding a major component of the lateral elements of synaptonemal complexes of the rat is related to X-linked lymphocyte-regulated genes.** *Mol Cell Biol* 1994, **14**(2):1137-1146.

Pre-publication history

The pre-publication history for this paper can be accessed here:

<http://www.biomedcentral.com/1471-2407/6/6/prepub>

Publish with **BioMed Central** and every scientist can read your work free of charge

"BioMed Central will be the most significant development for disseminating the results of biomedical research in our lifetime."

Sir Paul Nurse, Cancer Research UK

Your research papers will be:

- available free of charge to the entire biomedical community
- peer reviewed and published immediately upon acceptance
- cited in PubMed and archived on PubMed Central
- yours — you keep the copyright

Submit your manuscript here:
http://www.biomedcentral.com/info/publishing_adv.asp



BioMed Central

Chapter 5

Segregation of genomes in polyploid tumour cells following mitotic catastrophe.

Reprinted from Erenpreisa J, Kalejs M, Ianzini F, Kosmacek EA, Mackey MA,
Emzinsh D, Cragg MS, Ivanov A, Illidge TM. Cell Biol Int. 29(12):1005-11.

Short communication

Segregation of genomes in polyploid tumour cells following mitotic catastrophe

Jekaterina Erenpreisa^{a,*}, M. Kalejs^a, F. Ianzini^{b,c,d}, E.A. Kosmacek^c, M.A. Mackey^{b,c},
D. Emzinsh^c, M.S. Cragg^{f,g}, A. Ivanov^{a,h}, T.M. Illidge^h

^a Biomedicine Centre of the Latvia University, Ratsupites 1, Riga LV-1067, Latvia

^b Department Pathology, University of Iowa, Iowa City, IA, USA

^c Department Biomedical Engineering, University of Iowa, Iowa City, IA, USA

^d Department of Radiation Oncology, University of Iowa, Iowa City, IA, USA

^e Oncology Centre of Latvia, Riga, Latvia

^f University of Southampton, Southampton, UK

^g WEHI, Melbourne, Australia

^h Paterson Cancer Research Institute, Manchester, UK

Abstract

Following irradiation p53-function-deficient tumour cells undergo mitotic catastrophe and form endopolyploid cells. A small proportion of these segregates nuclei, and give rise to viable descendants. Here we studied this process in five tumour cell lines. After mitotic failure, tumour cells enter the endocycle and form mono-nucleated or multi-nucleated giant cells (MOGC and MNGC). MNGC arise from arrested anaphases. MOGC, from arrested metaphases. In both cases the individual genomes establish a radial pattern by links to a single microtubule organizing centre. Segregation of genomes is also ordered. MNGC present features of mitosis being resumed from late anaphase. In MOGC the sub-nuclei retain arrangement of stacked metaphase plates and are separated by folds of the nuclear envelope. Mitosis then resumes in sub-nuclei directly from metaphase. The data presented indicate that endopolyploid tumour cells preserve the integrity of individual genomes and can potentially re-initiate mitosis from the point at which it was interrupted.

© 2005 International Federation for Cell Biology. Published by Elsevier Ltd. All rights reserved.

Keywords: Radial arrangement of genomes; Link to microtubule-organising centre; De-polyploidisation; Resuming of mitosis; Mitotic catastrophe

1. Introduction

The possibility that endopolyploid tumour cells have a survival potential has been suggested by us previously (Illidge et al., 2000; Erenpreisa et al., 2000; Erenpreisa and Cragg, 2001; Ivanov et al., 2003). Recently, it has been shown that endopolyploid cells can emerge from various sources of human cells including p53-mutant and p53 non-functional human tumour cells exposed to genotoxic insult, human embryonic cells infected with the SV-40 virus (the infection inactivates p53), and from senescent cell cultures. More

importantly, using digital video-microscopy systems it has been shown that these endopolyploid cells can, albeit at relatively low frequency, successfully segregate their genomes to produce descendants which survive at least several generations post-treatment (Walen, 2002, 2004; Ianzini and Mackey, 2002, 2005; Ianzini et al., 2002, 2005; Mackey et al., 2003; Prieur-Carrillo et al., 2003; Sundaram et al., 2004).

The term 'segregation of genomes' or de-polyploidisation, was first introduced by Grell (1953) to describe the separation of the polyploid nucleus of the ciliate *Aulocantha*. In turn, studies of E. and T. Zybina revealed that whole genome segregation also occurs in the giant nuclei of the mammalian trophoblast, suggesting that genome segregation has been preserved throughout evolution (Zybina et al., 1979; Zybina and Zybina, 1996, 2005). Therefore, it is conceivable that

* Corresponding author. Tel.: +371 7 808 220; fax: +371 7 442 407.

E-mail address: katrina@biomed.lu.lv (J. Erenpreisa).

a mechanism allowing for whole genome segregation from multigenomic polyploid nuclei should also exist in higher organisms. Interestingly, somatic reduction in higher organisms is considered a rare event (Nagl, 1978; Storchova and Pellman, 2004). However, this might not be the case in tumour cells where a highly unstable genome is present, in particular in the absence of p53 function. Potentially, then this additional pathway of cellular division may provide a unique pathway through which tumour cells survive genotoxic stress. Understanding the central tenets of this mechanism of cell division may provide us with unique opportunities for cancer treatment. The present study was carried out to gain a greater understanding of the processes involved in tumour genomes segregation. To determine if these processes are common to tumour cells, a range of lymphoid and epithelial tumour cells were examined.

2. Materials and methods

2.1. Cell lines and irradiation

The present studies were performed using TP53 mutant lymphoid and TP53 non-functional epithelial cell lines irradiated with a single dose of 10 Gy of either γ - or X-rays. The lymphoid cells were the B-lymphoid Ramos, Namalwa (ATCC) and WI-L2-NS cell lines (kindly donated by Dr. P. Olive, Terry Fox Cancer Centre, British Columbia, Vancouver, Canada), and the T-lymphoid Jurkat cell line (Bcl-transfected) (kindly donated by Dr. S. Scott, Stanford University, USA). The epithelial cells were the HeLa S3 (ATCC) cell line. The lymphoid cells were grown as suspension cultures in RPMI 1640 medium, 10% Fetal Calf Serum (FCS; Gibco, Paisley, UK) at 37 °C in a 5% CO₂ humidified incubator. HeLa S3 cells were grown in suspension culture in Joklik's MEM media containing 10% heat-inactivated calf serum (Hyclone) and antibiotics. Cells were maintained in log phase of growth for at least 24 h prior to irradiation. Lymphoid cells were further cultivated by replenishing culture medium every 48–72 h, and HeLa S3 by replenishing culture media every 24 h, and studied over a period of three weeks.

2.2. Immunofluorescence

For immunofluorescence (IF) staining, harvested cells were suspended in 100% FCS, cytospun onto poly-L-lysine coated microscope slides, and fixed in absolute methanol for 10–20 min at 20 °C. Slides were then rinsed in ice-cold acetone, dried 30 s and washed in PBS 3 times for 10 min. Detection of beta-tubulin was performed using mouse monoclonal anti- β -tubulin antibody (1:50) (Ab-3 DM1B; NeoMarkers; LabVision Ltd., UK) followed by goat anti-mouse IgG-biotin antibody (1:100) (Vector Labs, UK) and by streptavidin-FITC antibody (1:150) (Vector Labs, UK) at room temperature. Gamma-tubulin was revealed using mouse monoclonal anti- β -tubulin antibody (1:100) (Sigma-Aldrich) followed by goat anti-mouse IgG-FITC antibody (1:200) (Vector Labs Ltd.) at room temperature. Kinetochores were revealed using CREST serum against human kinetochore proteins (Acris Antibodies, Hiddenhausen, Germany) (1:25), at 37 °C for 1 h followed by incubation with mouse anti-human IgG-FITC antibody (Dr. MS Cragg) (1:50), at 37 °C for 30 min. Immunostaining was preceded by blocking procedure in 1%BSA/PBS/0.05% Tween-20 for 15 min. IF samples were counterstained with Propidium Iodide (5 μ g/ml) or DAPI (0.5 μ g/ml) for 1–5 min. IF slides were mounted in mowiol media (Harlow Chemical Company Ltd, UK), containing 0.1% citifluor (Agar Scientific, Stansted, UK).

2.3. Telomere FISH

For telomere FISH, to preserve cell 3D structure, cells were attached onto polylysine slides and fixed wet in 1% paraformaldehyde in PBS. Telomere

FISH was performed using a Cy3 or FITC-conjugated PNA FISH Kit (DAKO, UK Ltd.) according to slightly modified manufacturer's recommendations: 1) samples were hybridized overnight at 37 °C in a moist chamber. 2) DNA was counterstained with DAPI before embedding in Vectashield. Preparations were embedded in antifade (Vector Laboratories) containing 0.5 μ g/ml DAPI as DNA counterstain.

2.4. DNA image cytometry

For DNA in situ cytometry, cells on cytopins were fixed in ethanol/acetone (1:1, v:v) for 30 min at room temperature. Cells were then stained with modified Feulgen reaction using Toluidine blue. Images were taken using a Leitz Ergolux L03-10 microscope equipped with a calibrated Sony DXC 390P colour video-camera. DNA content was measured as the integral optical density in the green channel or in the red channel using the interference filter 289 nm using Image Pro Plus 4.1 software (Media Cybernetics; REO 2001, Riga, Latvia). The stoichiometry of DNA staining was verified using the values obtained for metaphases compared to anaphases and telophases (ratio 2.03); diploid DNA values were averaged from measuring 50 anaphases in non-treated tumour cells. The variation coefficient for DNA content was also assessed in normal human lymphocytes where it was determined as to be in the range 2–5% while the device error was estimated as to be equal to 0.5%.

Fluorescent images were taken using either a Leica DM LS2 fluorescent microscope or a Leica SP2 confocal laser-scanning microscope.

2.5. Electron Microscopy (EM) and morphology

EM analysis and staining of cytospin preparations for morphology analysis were carried out as described elsewhere (Erenpreisa et al., 2000).

3. Results

In the last decade, many studies on the response to irradiation in Ramos, Namalwa, WI-L2-NS, Jurkat and HeLa cell lines have been conducted by our groups (Swanson et al., 1995; Ianzini and Mackey, 1997, 1998; Mackey and Ianzini, 2000; Ianzini et al., 1999; Illidge et al., 2000; Erenpreisa et al., 2002; Ivanov et al., 2003). In this communication we briefly focus on cytological mechanisms of polyploidisation and de-polyploidisation occurring following irradiation treatment. As a consequence of irradiation, all the five cell lines mentioned above enter G2-arrest and then undergo mitotic catastrophe (MC) and form mono-nucleated and multi-nucleated giant cells (MONGC and MNGC, respectively). Pertinent cytological observations show that MONGC form from restitution of mitosis aborted in metaphase, while MNGC, from mitosis aborted in late anaphase ('bridged'), more often in the second multi-polar division.

In MNGC the sub-nuclei have nearly conventional nuclear structure (Fig. 1a). Kinetochore/centromeres label revealed with CREST immunofluorescence (Fig. 2c, thick arrow) and telomeres revealed by PNA FISH probe (not shown) are evenly distributed, similarly to patterns present in the nuclei of non-treated cells. The sub-nuclei converge in a radial arrangement upon a central region of concentrated DNA ('DNA button' or 'DNA-circle'), while micronuclei often lack this connection (Fig. 1a). Sub-nuclei are also united through microtubules which radically emerge and embrace them from a single microtubule organizing centre (MTOC) (Figs. 1b,c). Thick microtubule tracks reach individual nucleoli (Fig. 1b). FISH analysis (for the peri-centromeric sequences of

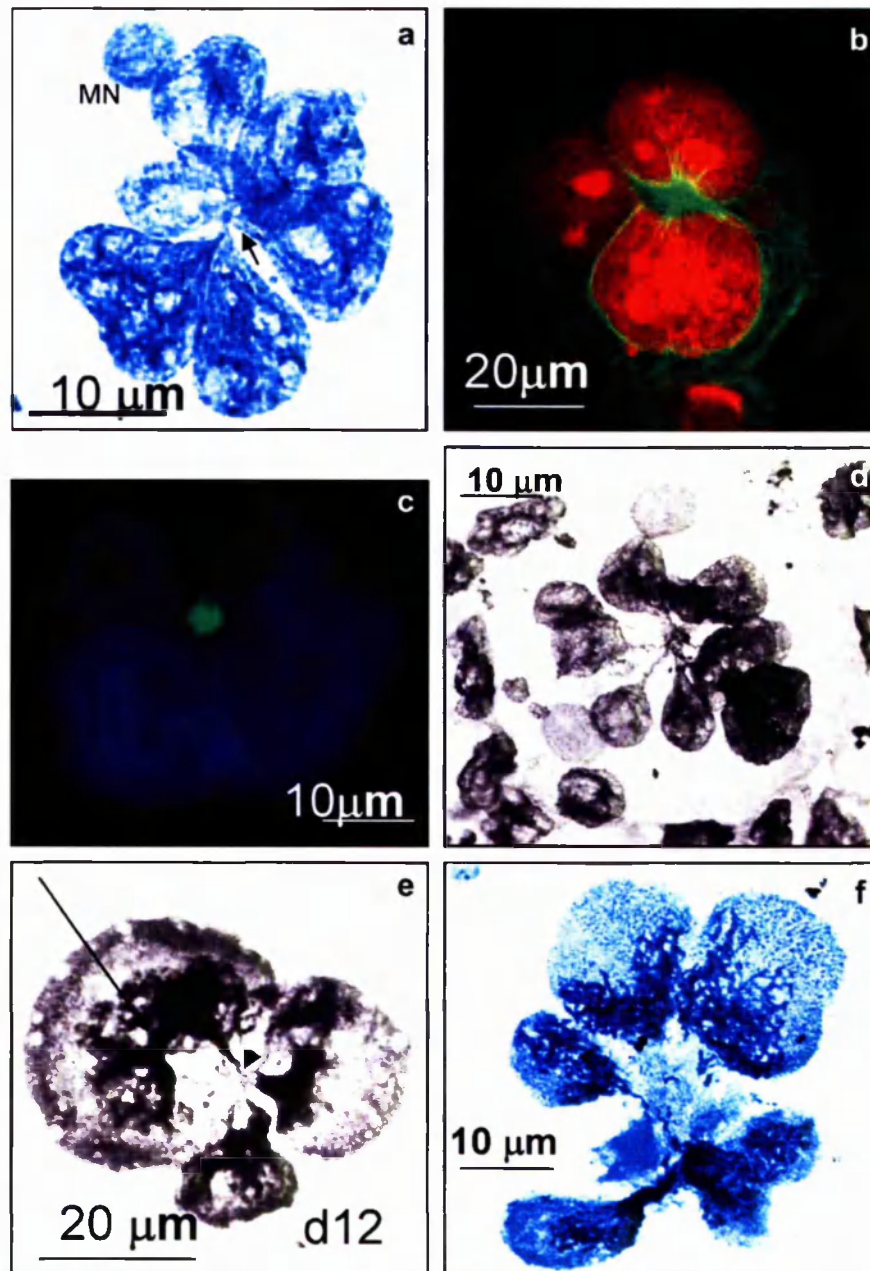


Fig. 1. Arrangement and radial segregation of sub-nuclei in MNGC: (a) Sub-nuclei possess conventional chromatin structure and are arranged radially, united by the DNA-containing central 'button'. Micronucleus (MN) lacks this connection. Feulgen-type DNA staining. 4 days post-irradiation. (b) Sub-nuclei are united around single MTOC. Beta-tubulin IF (FITC), DNA counterstained by Propidium iodide. 6 days post-irradiation. (c) Composed nature of a centrosome in a MNGC as seen by one-patch IF staining for gamma-tubulin (FITC). DNA counterstained with DAPI. 6 days post-irradiation. (d) Radial arrangement of sub-nuclei converging by 'tails' to a central small circular structure. Morphological staining (toluidine blue pH 5.0 after partial extraction of RNA). 12 days post-irradiation. (e) Radial division of MNGC. Chromatin in sub-nuclei is condensed, cytotomy is occurring releasing unequal sub-cells. Small circular structure (arrowhead) and 'tails' of sub-nuclei converging to it are seen. Nuclear bridge in the larger secondary cell (thin arrow) is apparently preventing equal segregation of genomes. The same staining as in (d). 3 days post-irradiation. (f) Unequal radial division of MNGC. Cytotomy has occurred and repulsion of sub-cells shearing connecting nuclear 'tails' is very apparent. Chromatin is semi-condensed; the two larger sub-nuclei are bi-lobed. The same staining as in (d). 5 days post-irradiation. a,d,e,f – HeLa S3 cells; b,c – Namalwa cells.

chromosomes 1, 3 and 9) show that during polyploidisation, most sub-nuclei are disomic, with a lower proportion tetrasomic, and less monosomic (Erenpreisa et al., 2000). DNA image cytometry shows that the majority of MNGC possess

four sub-nuclei, with para-2C and 4C DNA contents, aneuploid and 1C fragments can also be found (data not shown).

In turn, MONGC are partially polytenised as shown by the 'thready' chromatin structure in DNA staining (Fig. 2a),

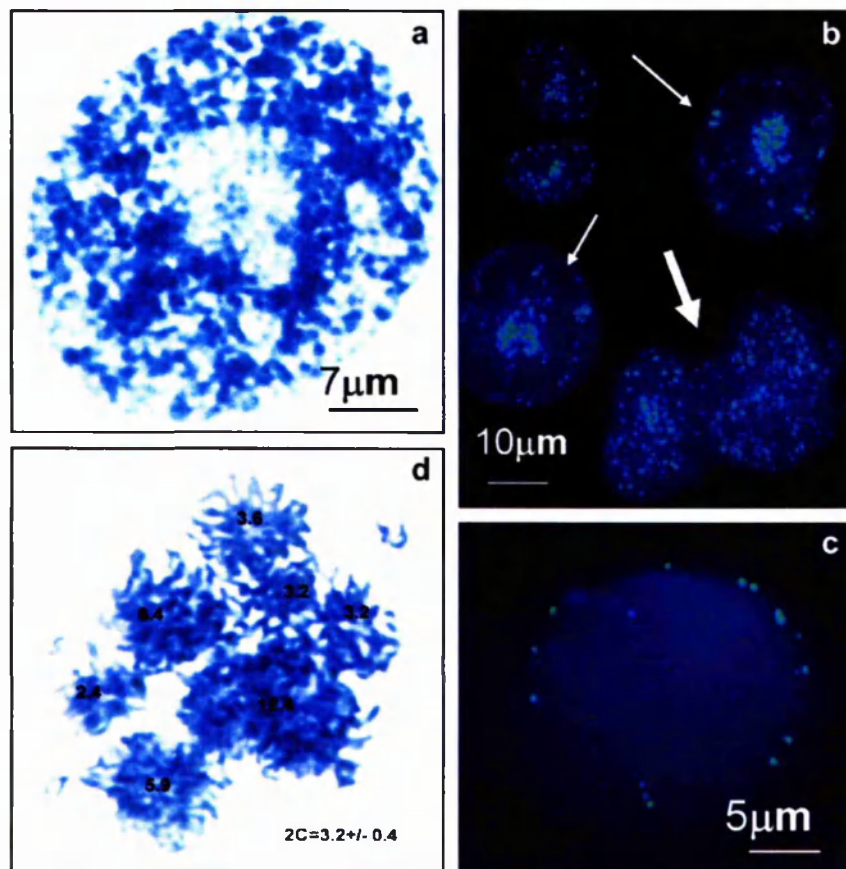


Fig. 2. Metaphasic arrangement and segregation of genomes in MOGC: (a) DNA staining showing large central nucleolus and non-conventional 'thready' chromatin structure (partial polyteny). Ramos cell, 4 days post-irradiation. (b) Localisation of kinetochores/centromeres revealed by IF with CREST-serum against human kinetochores proteins (FITC) showing preferential clustering of centromeres around 1–2 central nucleoli in a proportion of MOGCs (thin arrows). In MNGC (thick arrow) the label is random. DNA counterstained with DAPI. HeLa S3, 6 days post-irradiation. (c) Telomeres localisation on the nuclear envelope in a proportion of MOGC. 6 days post-irradiation. FISH with PNA telomere probe (FITC). DNA counterstained by DAPI. (d) Reduction divisions as seen by a set of anaphases halving DNA contents in one giant cell, 24C. It is composed of one 8C nucleus, two 4C plates, and four 2C plates (one of them, with the smallest DNA content was damaged on preparation). DNA stoichiometric staining, image cytometry. Namalwa cell, 12 days post-irradiation.

electron microscopy (EM), and the relationships between centromeres and telomeres. The kinetochores/centromeres of MOGC form chains and clusters in some cells (data not shown) and heavily precipitate upon one-two central nucleoli, in other cells (Fig. 2b). In about 10% of MONGC telomeres are located on the nuclear envelope (Fig. 2c, confirmed by 3D confocal microscopy), however associations of telomeres is a rare event. Therefore, as formed by mitosis abortion in metaphase, the chromatin in these cells seems to retain metaphasic arrangement of the polytenic chromosomes cohesed by centromeres. MONGC also possess one microtubule organizing centre MTOC which is often located in the deep invagination of the nuclear envelope (NE) (Fig. 3a). Usually, the 1–2 large nucleoli are juxtaposed with a single MTOC, from the nuclear side. EM data show that MTOC of the monopolar spindle in both MNGC and MONGC is multi-centriolar (data not shown).

Up to the first 4–5 days after irradiation, all the examined cells undergo extensive endoreplication and increase their DNA contents up to 8–16C, and up to 32–64C (documented

by DNA flow cytometry and reported elsewhere by Illidge et al., 2000). In this period, MOGC often enter cycles of endomitotic condensation of chromosomes within intact nuclear envelope. Endomitosis might play an important role in the development of MOGC. More details of this process are described in another paper of this issue (Erenpreisa et al., 2005). By the end of the first week post-irradiation, most of giant cells (predominantly MNGC) die by 'apoptotic crisis' as described by Illidge et al. (2000). In the following period, 7–9 days post-irradiation and later, the polyploid cells that have escaped crisis halt their DNA synthesis and initiate the de-polyploidisation process. This process follows different route in MNGC and MOGC.

MNGC attempts cell radial division (often repeated), as it is evidenced by the partial nuclear condensation, the intensive radial repulsion of sub-nuclei, and the radial cytotomy (Figs. 1d–f). Attempts at cell radial division are very intensive in HeLa cells (and begin after a short pause, from dd.3–4) as compared to Jurkat and WI-L2-NS cells, where this process is more postponed in time. This phenomenon is rarer in Ramos

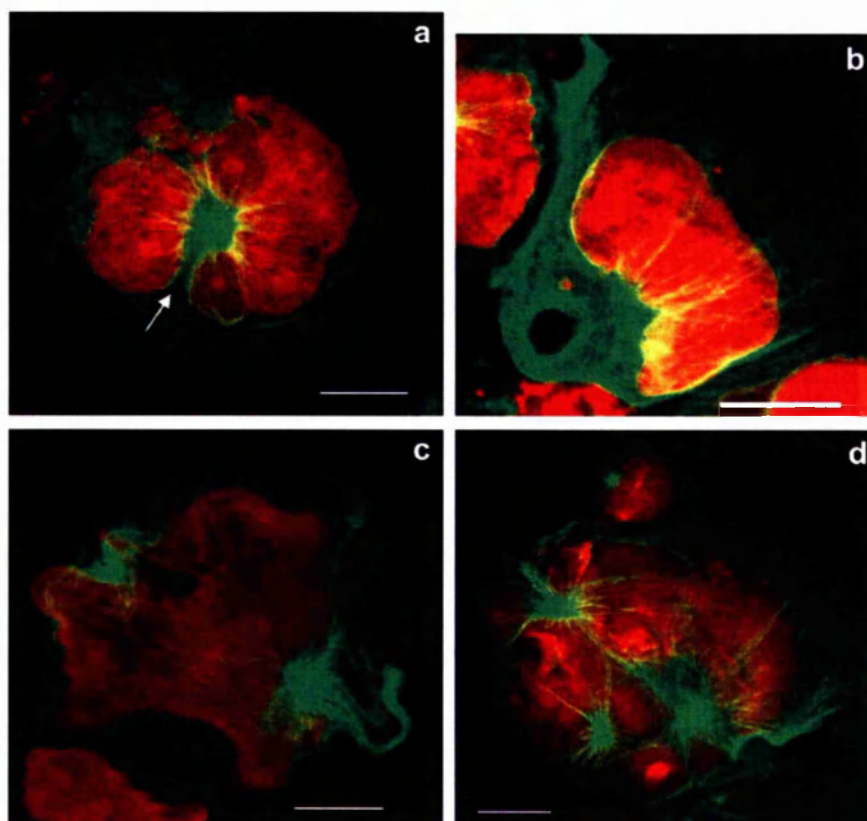


Fig. 3. Behaviour of the microtubular apparatus in MOCs as studied on Namalwa, 6–7 days post 10 Gy irradiation. Bars = 10 μ m. (a) A MOC with a composed single MTOC in the invagination of the nuclear envelope (arrow). Here and further, IF for beta-tubulin (FITC), counterstained with propidium iodide, 3D confocal microscopy. (b) Polar displacement of a single MTOC of the monopolar spindle. A cell assumes characteristic pear-like form. (c) A two-polar spindle. Flagella appeared from a single pole before this stage. (d) Several secondary beta-tubulin-positive stars (FITC) have segregated from composed MTOC favouring segregation of the MOC into secondary genomes and organising individual microtubular network for secondary cells. The chromatin remains non-condensed.

and Namalwa cells. Correspondingly, in HeLa MNGC comprise about 80% and MOC about 20%; in Jurkat and WI-L2-NS this ratio is about 60/40, and in Ramos and Namalwa cells these proportions are inverted being MNGC 20% and MOC 80%.

Centripetal DNA 'tails' joining sub-nuclei are extended by radial repulsion of sub-nuclei and torn if a sub-cell is released (Figs. 1e,f). These 'tails' appear in EM preparations as extravagations of the NE enclosing chromatin sheets (ELCS). ELCS have been described in detail by us (Erenpreisa et al., 2002) as correlating in number with the extent of nuclear segmentation occurring in the giant tumour cells in MC. Association of ELCS with nucleoli have also been reported.

De-polyploidisation of MOC has been mostly described by us previously, in Ramos and Namalwa cell lines (Erenpreisa et al., 2000). We have shown that on dd.6–7 the giant cells and nuclei polarly extend and that sub-nuclei are further split by folds of the nuclear envelope from the wider nuclear pole disclosing a DNA convergence point of sub-nuclei on an opposite narrow pole of a giant nucleus (reminding a 'bouquet'). In this study we describe that these events are initiated by polar displacement of a single MTOC (Fig. 3b), while further activation of a bi-polar mitotic spindle and migration from

it of secondary stars accompanies segregation of sub-nuclei (Figs. 3c,d). Peculiarly, however, they retain the NE and de-condensed chromatin.

Following this period, metaphases and anaphases are evidenced in secondary nuclei, usually before the cytoplasmic body of the mother cell has been segregated into secondary cells. In these and other cell lines, we noted that when mitosis resumes within non-disintegrated giant cells, prophase is not observed. DNA image cytometry revealed that these mitoses can reduce the DNA contents from 8C to 2C in anaphases in subsequent reduction divisions, which evidently omit S-phase (Fig. 2e). Endomitotic nuclei sometimes dissipate into stacks of multiples or a few separate metaphase plates (Erenpreisa et al., 2005), in most cases, this seems to be a degenerative pathway.

4. Discussion

The results presented in this paper demonstrate that the response to radiation of different tumour cell lines shows intriguing similarities. These data support the intriguing hypothesis that there exist conserved mechanisms of genomes ordered assembly and disassembly in multi-genomic endopolyploid tumour cells.

These common features are as follows:

(1) The ordered radial arrangement of individual sub-nuclei (genomes or their oligomeres) during the polyploidisation stage. Both mono-nuclear and multi-nuclear giant cells have radial arrangement of genomes. This appears to predetermine the subsequent segregation of secondary cells through 'budding' (Walen, 2002; Sundaram et al., 2004). A constriction point of this radial arrangement is represented by some unknown structural DNA associated with the MTOC (possibly through the lamin of NE) of the monopolar spindle. This chromatin is possibly derived from ELCS, related both to the nucleoli and NE. To our present knowledge this unique structure upon which the sub-nuclei converge has not previously been reported. However, subsequent analysis reveals that these connections have in fact been seen previously but (f.ex., Kroh and Cervos-Navarro, 1988) misinterpreted as nuclear bridges. Although not yet proven, our observations indirectly suggest a permanent association between a genome set and its centriole pair in the composed MTOC which facilitates the persistence of each individual genome. A similar hypothesis was proposed by Raikov (1982) describing the segregation of polygenomic nuclei of Protozoans.

(2) Features reminiscent of mitosis. In MNGC, it appears as mitosis completion starting from anaphase B, although unbalanced, as cytotomy begins before the chromatin is de-condensed. In MONGC, endomitosis and the ability to condense chromatin precede separation of sub-nuclei by NE and by activation of the mitotic spindle. Afterwards mitoses restart directly from metaphase.

Although preliminary, these results suggest that a 'mitotic clock' in tumour cells can be halted by MC and the initiation of the endocycles and then re-started with the resumption of mitotic signaling from the point where it was interrupted. Furthermore, it appears that the subsequent sequence of events observed in the various types of giant cell is pre-determined by the existing arrangement of the chromatin in these cells, which itself is pre-determined by the point at which mitosis was halted.

To form MNGC, cells adapt spindle checkpoint and then restart from anaphase B; while to form MONGC, cells are halted in a spindle checkpoint and then restart mitosis from that point. The kinetic reason for this difference can be explained from the molecular data regarding the two extremes in our panel of cell lines: HeLa S3 and Namalwa cells. HeLa cells (producing mostly MNGC) are overriding spindle checkpoint, evidently due to exaggerated constitutive cyclin B1 activity (Ianzini and Mackey, 1997, 1998; Mackey and Ianzini, 2000), while Namalwa cells (producing mostly MONGC) are enhancing spindle checkpoint, evidently due to ectopic expression of several regulators of meiotic pathway (Erenpreisa et al., 2005; Kalejs and Erenpreisa, 2005).

Clearly these additional pathways of cell division and survival require much greater study. One intriguing fact is that these pathways are rarely observed in normal mammalian tissues and appear to be specific of mutant and/or non-functional TP53 tumour cells. Elucidation of the regulators involved in these pathways of survival could provide a novel set of

molecular targets for specifically destroying tumour cells potentially avoiding the deleterious side-effects of current treatments.

Acknowledgments

We are indebted to Mr Roger Alston, Mrs Sue Cox, Mr Nick Barnett and Dr. Anton Page (Southampton University Imaging Unit) for their many years of assistance in the Southampton University. We are similarly indebted to Mr. Vladislav Zelchs (Biomedicine Centre of the Latvian University) for assistance in electron microscopy; to Drs. Bodo Liebe (Max-Planck-Inst. for Molecular Genetics, Berlin) and Harry Scherthan (Inst. of Radiation Biology, Munich) for their help with FISH, and the latter, in addition, for the helpful discussion of our results. Thanks also go to Dr. D. Emzinsh and Mrs. Galina Boka (Latvian Oncology Centre) for their help in cell irradiation. This work was partly supported by the Latvian Scientific Council, a Grant from the Royal Society of London and a Latvian-USA Governmental Grant enabling exchange visits between Riga and Southampton and Riga and Iowa City, and by the National Institutes of Health Grants CA74899, CA58648, and CA/GM94801, and by the Whitaker Foundation Special Opportunity Award.

References

- Erenpreisa J, Cragg MS. Mitotic death: a mechanism of survival? A review. *Cancer Cell Int* 2001;1:1.
- Erenpreisa JA, Cragg MS, Fringes B, Sharakhov I, Illidge TM. Release of mitotic descendants by giant cells from irradiated Burkitt's lymphoma cell line. *Cell Biol Int* 2000;24:635–48.
- Erenpreisa J, Ivanov A, Cragg M, Selivanova G, Illidge T. Nuclear envelope-limited chromatin sheets are part of mitotic death. *Histochem Cell Biol* 2002;117:243–55.
- Erenpreisa J, Kalejs M, Cragg MS. Mitotic catastrophe and endomitosis in tumour cells: an evolutionary key to a molecular solution. *Cell Biology International* 2005;29:1012–8.
- Grell KG. Die Chromosomen von *Aulacantha scolymantha* Haeckel. *Arch Protistenkunde* 1953;99:1–54.
- Ianzini F, Mackey MA. Spontaneous premature chromosome condensation and mitotic catastrophe following irradiation of HeLa S3 cells. *Int J Radiat Biol* 1997;72:409–21.
- Ianzini F, Mackey MA. Delayed DNA damage associated with mitotic catastrophe following X-irradiation of HeLa S3 cells. *Mutagenesis* 1998;13:337–44.
- Ianzini F, Mackey MA. Development of the large scale digital cell analysis system. *Radiat Prot Dosimetry* 2002;99:289–93.
- Ianzini F, Mackey MA. Mitotic catastrophe. In: Gewirtz DA, Holt SE, Grant S, editors. *Apoptosis and Senescence in Cancer Chemotherapy and Radiotherapy*. Humana Press; 2005.
- Ianzini F, Cherubini R, Mackey MA. Mitotic catastrophe induced by exposure of V79 Chinese hamster cells to low-energy protons. *Int J Radiat Biol* 1999;75:717–23.
- Ianzini F, Bresnahan L, Wang L, Anderson K, Mackey MA. The large scale digital cell analysis system and its use in the quantitative analysis of cell populations. In: Dittmar A, Beebe E, editors. *The Second Annual International IEEE-EMBS Special Topic Conference on Microtechnologies in Medicine and Biology*. Piscataway, NJ: IEEE Press; 2002. p. 470–5.
- Ianzini F, Keller BA, Davis PJ, Mackey MA. 13-P2. Cells that Undergo Radiation-Induced Mitotic Catastrophe Have the Potential to Survive for Many Generations Post-Treatment: A LSDCAS Study. 24. 2005. Riga: Riga Meeting on Comprehensive Cell Biology, 2005.

- Illidge TM, Cragg MS, Fringes B, Olive P, Erenpreisa JA. Polyploid giant cells provide a survival mechanism for p53 mutant cells after DNA damage. *Cell Biol Int* 2000;24:621–33.
- Ivanov A, Cragg MS, Erenpreisa J, Emzish D, Lukman H, Illidge TM. Endopolyploid cells produced after severe genotoxic damage have the potential to repair DNA double strand breaks. *J Cell Sci* 2003;116:4095–106.
- Kalejs M, Erenpreisa J. Cancer/testis antigens and gametogenesis: a review and “brain-storming” session. *Cancer Cell Int* 2005;5:4.
- Kroh H, Cervos-Navarro J. Back to the nuclear bridges. *Acta Neuropathol (Berl)* 1988;76:539–40.
- Mackey MA, Ianzini F. Enhancement of radiation-induced mitotic catastrophe by moderate hyperthermia. *Int J Radiat Biol* 2000;76:273–80.
- Mackey MA, Anderson KR, Bresnahan LE, Domann FE, Gallardo G, Ianzini F, et al. The large scale digital cell analysis system: a unique tool for the study of molecular and cellular phenomena in living cell populations. *Mol Imaging* 2003;2:226.
- Nagl W. Endopolyploidy and Polyteny in Differentiation and Evolution. Amsterdam-New York-Oxford: North-Holland Pub; 1978.
- Prieur-Carrillo G, Chu K, Lindqvist J, Dewey WC. Computerized video time-lapse (CVTL) analysis of the fate of giant cells produced by X-irradiating EJ30 human bladder carcinoma cells. *Radiat Res* 2003;159:705–12.
- Raikov IB. The Protozoan Nucleus, Morphology and Evolution. Wien-New York: Springer Verlag; 1982.
- Storchova Z, Pellman D. From polyploidy to aneuploidy, genome instability and cancer. *Nat Rev Mol Cell Biol* 2004;5:45–54.
- Sundaram M, Guernsey DL, Rajaraman MM, Rajaraman R. Neosis: a novel type of cell division in cancer. *Cancer Biol Ther* 2004;3:207–18.
- Swanson PE, Carroll SB, Zhang XF, Mackey MA. Spontaneous premature chromosome condensation, micronucleus formation, and non-apoptotic cell death in heated HeLa S3 cells. Ultrastructural observations. *Am J Pathol* 1995;146:963–71.
- Walen KH. The origin of transformed cells. Studies of spontaneous and induced cell transformation in cell cultures from marsupials, a snail, and human amniocytes. *Cancer Genet Cytogenet* 2002;133:45–54.
- Walen KH. Spontaneous cell transformation: karyoplasts derived from multinucleated cells produce new cell growth in senescent human epithelial cell cultures. *In Vitro Cell Dev Biol Anim* 2004;40:150–8.
- Zybina EV, Kudryavtseva MV, Kudryavtsev BN. The distribution of chromosome material during giant nuclei division by fragmentation in the trophoblast of rodents. Morphological and cytophotometrical study. *Tsitologiya* 1979;21:12–20.
- Zybina EV, Zybina TG. Polytene chromosomes in mammalian cells. *Int Rev Cytol* 1996;165:53–119.
- Zybina TG, Zybina EV. Whole-genome chromosome distribution in the course of nuclear fragmentation of giant trophoblast cells of *Microtus rossiaemeridionalis* studied with the use of gonosomal chromatin arrangement. *Cell Biology International* 2005;29:1066–70.

Chapter 6

**Nuclear envelope-limited chromatin sheets are
morphological expression of mitotic death.**

Reprinted from Erenpreisa J, Ivanov A, Cragg M, Selivanova G, Illidge T.

Histochem Cell Biol. 2002 117(3):243-55.

Jekaterina Erenpreisa · Andrey Ivanov · Mark Cragg
Galina Selivanova · Timothy Illidge

Nuclear envelope-limited chromatin sheets are part of mitotic death

Accepted: 8 January 2002 / Published online: 8 February 2002
© Springer-Verlag 2002

Abstract Nuclear envelope-limited chromatin sheets (ELCS) are enigmatic membranous structures of uncertain function. This study describes the induction of ELCS in p53 mutated Burkitt's lymphoma cell lines after treatment with irradiation or the microtubule inhibitor, SK&F 96365. Both treatments evoked similar mitotic death, involving metaphase arrest followed by extensive endopolyploidisation and delayed apoptosis, although the kinetics were different. We found that induction of ELCS and nuclear segmentation correlated with the amount and kinetics of M-phase arrest, mitosis restitution and delayed apoptosis of endopolyploid cells. In metaphases undergoing restitution, ELCS are seen participating in the restoration of the nuclear envelope, mediating the attachment of peripheral chromatin to it. In interphase cells, ELCS join nuclear segments, ectopically linking and fusing with heterochromatin regions. In cells with segmented nuclei, continued DNA replication was observed, along with activation and redistribution of Ku70, suggestive of non-homologous DNA end-joining. Induction of ELCS also parallels the induction of cytoplasmic stacked membrane structures, such as confronting cisternae and annulate lamellae, which participate in the turnover and degeneration of ELCS. The results suggest that arrest at a spindle checkpoint and the uncoupling of mitosis from DNA replication lead to the emergence of ELCS in the resulting endopolyploid cells.

Keywords Nuclear envelope-limited chromatin sheets · Irradiation · Microtubule inhibitors · Mitotic arrest · Endopolyploidy

Introduction

Nuclear envelope-limited chromatin sheets (ELCS) were initially described by Davies (1968) and are structures of enigmatic function. They represent flat folds of the inner nuclear envelope which project into the perinuclear cistern and sometimes cytoplasm, encompassing a chromatin band, before fusing with the nuclear envelope again, enclosing the embraced material in a nuclear pocket (NP). The chromatin band is delineated by the inner and outer nuclear membranes on both sides and has been shown to consist of DNA and to be associated with lamin B (Olins et al. 1998). This association indicates the intimate connection between the chromatin and the inner nuclear membrane.

An abundance of NPs is pathognomonic and virtually diagnostic for lymphoma and leukaemia (Ghadially 1988a). However, ELCS are also found in other tumours and some normal cells, such as human spermatogonia (Chemes et al. 1978), fetal thymus (Sebuwufu 1966), monocytes, lymphocytes and neutrophils (Huhn 1967; Smith and Ohara 1967). In addition, ELCS are observed in neutrophils of neonatal mouse bone marrow before apoptotic death (Sasaki et al. 1995) and in HL60 cells during neutrophilic differentiation induced by retinoic acid (Olins et al. 1998). The number of ELCS-like abnormalities in leukaemia and other tumours is found to correlate with chromosome abnormalities, DNA damage and aneuploidy, whilst successful anticancer therapy promotes their reduction (Ahearn et al. 1974). Clausen and Von Haam (1969) have suggested that NPs are a morphological expression of chromatin dislocation, whereas Gisselsson et al. (2001) have associated these abnormalities with chromosome fusion.

Other poorly understood membranous structures include annulate lamellae (AL) and confronting cisternae (CC). AL have also been observed in a variety of

J. Erenpreisa (✉) · A. Ivanov
Laboratory of Tumour Cell Biology,
Biomedicine Centre of the Latvian University, Ratsupites str. 1,
Riga, 1067, Latvia
e-mail: cancer@latnet.lv
Tel.: +371-7808220, Fax: +371-7442407

M. Cragg
TENOVUS Cancer Research Laboratory,
Southampton General Hospital, Southampton SO16 6YD, UK

G. Selivanova
Institute of Cytology, Russian Academy of Science,
Tichoretsky pr. 4, St. Petersburg, Russia

T. Illidge
CRC Wessex Medical Oncology Unit, Southampton University,
Southampton SO16 6YD, UK

tumours, germ-line, embryonic and virus-infected cells, as well as after treatment with microtubule inhibitors (Ghadially 1988b; Kessel 1992). Similarly, CC of the rough endoplasmic reticulum (RER) have often been observed in cells arrested in metaphase and are sometimes continuous with the nuclear envelope (Ghadially 1988c, d; Wheatley 1991).

Many p53 mutated tumours are known to respond to genotoxic damage through a complex series of cellular events. These are characterised by initial G2 arrest followed by aberrant and lethal mitoses, uncoupling of mitosis from replication with the formation of polyploid giant cells, and delayed apoptosis (Lock and Ross 1990; Bernhard et al. 1996; Waldman et al. 1996). The hallmark of the process appears to be mitotic death (Erenpreisa and Cragg 2001), which is thought to occur due to the presence of secondary chromosome aberrations caused by genomic instability, aneuploidy and DNA mis/non-repair (Scott et al. 1974; Radford and Murphy 1994; Rogers-Bald et al. 2000).

In the present study, we have investigated the effect of irradiation and the microtubule inhibitor SK&F 96365 (SK&F) on two p53 mutated, radioresistant Burkitt's lymphoma cell lines, Ramos and Namalwa. Treatment with a single high dose of irradiation will induce extensive DNA damage, whilst SK&F is known to depolymerise microtubules and therefore cause cells to accumulate in mitosis (Nordstrom et al. 1992; Mitsui-Saito et al. 2000). Interestingly, irradiation and SK&F treatment, causing DNA or microtubule damage, respectively, resulted in a similar response, which included mitotic death. Here we present data on the induction of ELCS in cells undergoing mitotic death and reveal some novel ultrastructural features and details regarding their degeneration.

Materials and methods

Cell lines, culture materials and cytotoxic treatments

The Burkitt's lymphoma cell lines Ramos and Namalwa were obtained from the American Tissue Type Culture collection and have established p53 mutant alleles (O'Connor et al. 1993). All cell lines were maintained in RPMI 1640 (Gibco) culture medium supplemented with antibiotics and 10% FCS (Myoclonal; Gibco) at 37°C in humidified conditions and 5% CO₂. Cell lines were irradiated in a logarithmic phase of growth using a Gulmay D3 225 kV X-ray source at a dose rate of 1.15 Gy/min with a single exposure of 10 Gy. SK&F (Calbiochem) was added to the cells at a final concentration of 10 mM.

Cell cycle analysis using flow cytometry

Samples were analysed essentially as detailed previously (Cragg et al. 1999). Briefly, samples of cells were taken at relevant time points, resuspended in hypotonic fluorochrome solution [50 mg/ml propidium iodide (PI), 0.1% (w/v) sodium citrate, 0.1% (v/v) Triton X-100] and stored at room temperature in the dark for 4 h. Analysis of samples was performed on a FACScan flow cytometer (Becton Dickinson). Samples were represented as DNA histograms using Cellquest software (Becton Dickinson) and the distribution of cells in the G1, S, G2 M and polyploid phases of the cell cycle calculated. Apoptosis was quantified by measuring the proportion of cells with sub-G1 levels of DNA. Apoptosis was

also confirmed by microscopy as described below and by TUNEL staining as described by Erenpreisa et al. (1997).

DNA in situ cytometry

DNA in situ cytometry was performed on cytospin samples, after fixation in ethanol/acetone (1:1) for 30 min at 40°C. Samples were then stained with the modified Feulgen reaction using depurinating acid hydrolysis, 2,4-dinitrophenylhydrazine treatment and toluidine blue counterstaining as detailed previously (Erenpreisa et al. 2000a). DNA cytometry was carried out at 590 nm with a two wave length cytophotometer (MCFU-1; LOMO). The stoichiometry of staining was verified with rat di- and tetraploid hepatocyte nuclei, as well as Ramos cell metaphases and telophases (ratio 2±0.02). The variation coefficient for human lymphocytes was determined as 2% (n=35) and the device error estimated as 1%. The ploidy unit was determined from tumour telophases and the G0/G1 fraction, with both yielding the same value.

Light and electron microscopy

For morphological examination, cytospins were fixed in ethanol/acetone (1:1) for 30 min at 4°C, hydrolysed with 0.1 N HCl at 4°C for 5 min, washed and then stained with 0.05% toluidine blue in 50% MacIlvain buffer pH 5. After a brief rinse in distilled water, slides were dehydrated in warm tertiary butanol, cleared in Histoclear and embedded in DPX. These and Feulgen-stained samples were used for scoring cells with segmented (including micronucleated and budding) nuclei. For each sample, 500–1,000 cells were counted (hyperchromic, shrunk and apoptotic cells were omitted from these counts).

For chromosome visualisation of irradiated samples, Nocodazole (Sigma) was added at 40 ng/ml to the cells for the last 6 h of culture and the cells pelleted by centrifugation. Cell pellets were then treated with 0.075 M KCl solution for 30 min, fixed in methanol/acetic acid (3:1) overnight at 4°C, dropped in fresh fixative onto ice-cold clean slides and then dried and stained with 5% Giemsa solution (Merck) in Soerensen buffer, pH 6.8. Metaphase spreads from SK&F-treated cells were prepared similarly but with Nocodazole pretreatment omitted.

For electron microscopy (EM), cells were fixed in 3% glutaraldehyde in 0.1 M cacodylate buffer, pH 7.2, containing 1 mM CaCl₂, washed in this buffer with 0.23 M sucrose, postfixed in 2% osmium tetroxide in cacodylate buffer and 2% uranyl acetate in distilled water, dehydrated and embedded in Spurr resin. Ultrathin sections were contrasted with lead citrate. Cells displaying ELCS were scored in random sections, cut at several layers, with 300 cells counted per sample.

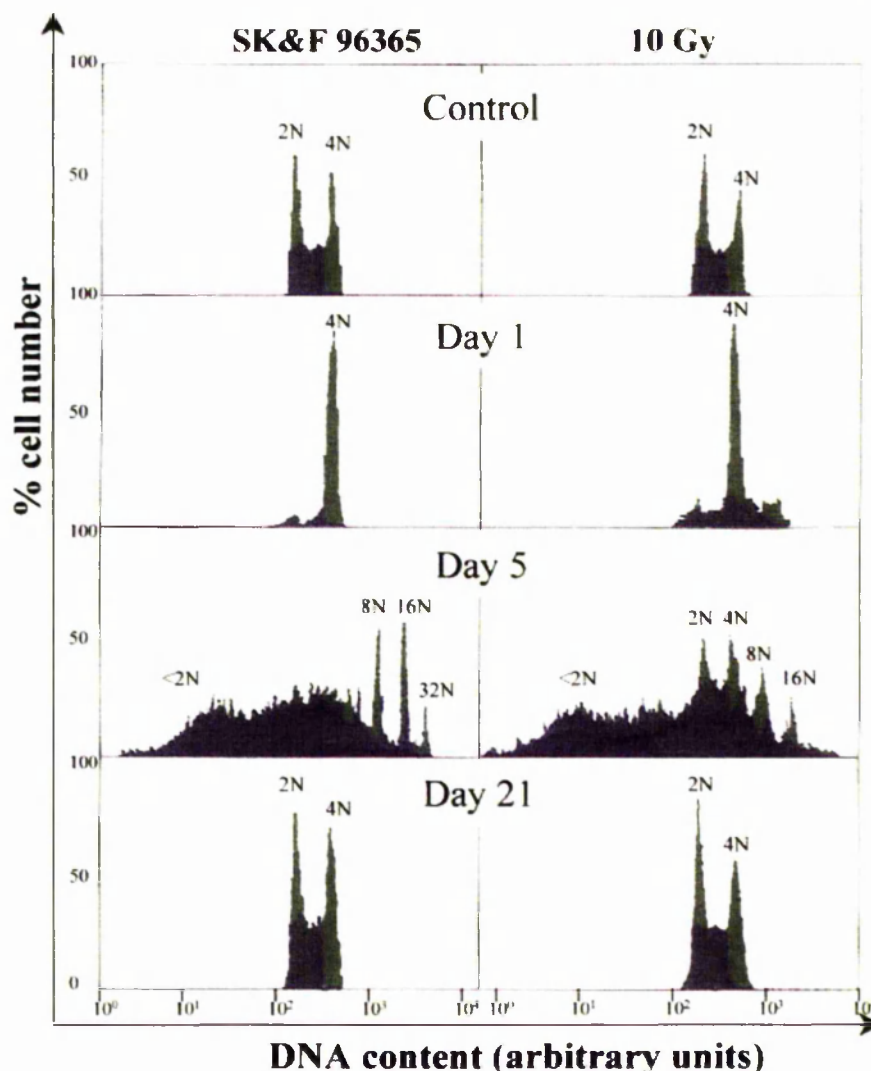
Immunocytochemistry

Immunolocalisation of Ku70 protein was performed on cytospin cells fixed at –20°C for 6 min in methanol. Fixation was followed by air drying and blocking in blocking solution (2% bovine serum albumin, 0.1% Triton X-100 in PBS) at room temperature (RT) for 15 min. Polyclonal goat anti-Ku70 antibody (M-19; Santa Cruz; a kind gift from Dr. Carl Smythe) was then added at a 1:100 dilution for 60 min at RT, before washing off the unbound material. Bound antibody was detected with FITC-conjugated anti-goat secondary antibody (Miles Yeda) at a 1:2,000 dilution for 30 min at RT, before washing and counterstaining with PI (Molecular Probes).

Immunostaining of β -tubulin was performed on cytospin cells following methanol/acetone fixation (1:1) at –20°C for 10 min. Anti- β -tubulin antibody (clone DM 1B; Ncomarkers) was added to fixed cells at a dilution of 1:100 for 1 h at RT. Unbound antibody was then removed by washing in PBS and bound antibody detected by incubation with biotinylated anti-mouse IgG (Vector Laboratories) at a dilution of 1:100 for 1 h, followed by washing and incubation with FITC-conjugated streptavidin (Vector Laboratories) at a dilution of 1:200 for 30 min. Cells were counterstained with PI.

Statistical analysis was performed using Student's *t*-test.

Fig. 1 DNA flow cytometry histograms of Namalwa cells, treated with either SK&F (10 mM) or irradiation (10 Gy). Similar cell cycle events can be seen, with G2 M arrest on day 1, polyploidy and delayed apoptosis on day 5, and recovery by day 21. The DNA content is presented on a logarithmic scale to fully encompass the extent of polyploidy



Results

Cell cycle response after irradiation or treatment with SK&F

DNA flow cytometry analysis revealed that both irradiation and SK&F treatments resulted in a similar cell cycle response (Fig. 1). The cells entered G2 M arrest on the first day after treatment, followed by delayed apoptosis and polyploid cell formation, which reached a maximum in the first week after treatment. Polyploid giant cells of apparently very large ploidy were also seen by light microscopy in the second week post-treatment. The diploid cell line recovered by the third week post-treatment, although clonogenic assays performed on the Namalwa cell line revealed that only 0.05–0.1% cells ultimately recover after 10 Gy irradiation (data not shown).

Mitotic response of SK&F-treated cells

A very large proportion of the cells arrested in G2 M, 24 h after SK&F treatment were actually arrested in metaphase (Fig. 2a). As expected, the mitotic spindle in these arrested metaphases was disrupted, as shown using β -tubulin in situ immunostaining (Fig. 2b). Indeed, these SK&F-treated cells had a tenfold higher mitotic index (MI) compared to control cells after 24 h. Furthermore, most of these mitoses were still retained 24 h later, only being slowly released on day 3 and thereafter as revealed by the decrease in MI (Fig. 3a). Samples taken 24 h after SK&F treatment, displayed typical colchicine-like mitotic plates with disseminated chromosomes. However, on day 2 after SK&F treatment, more than half of the mitoses displayed chromosomes sticking in chains and groups. Electron microscopy revealed that a proportion of mitoses at this time were undergoing chromosome fusions, formation and reunion of micronuclei, and reas-

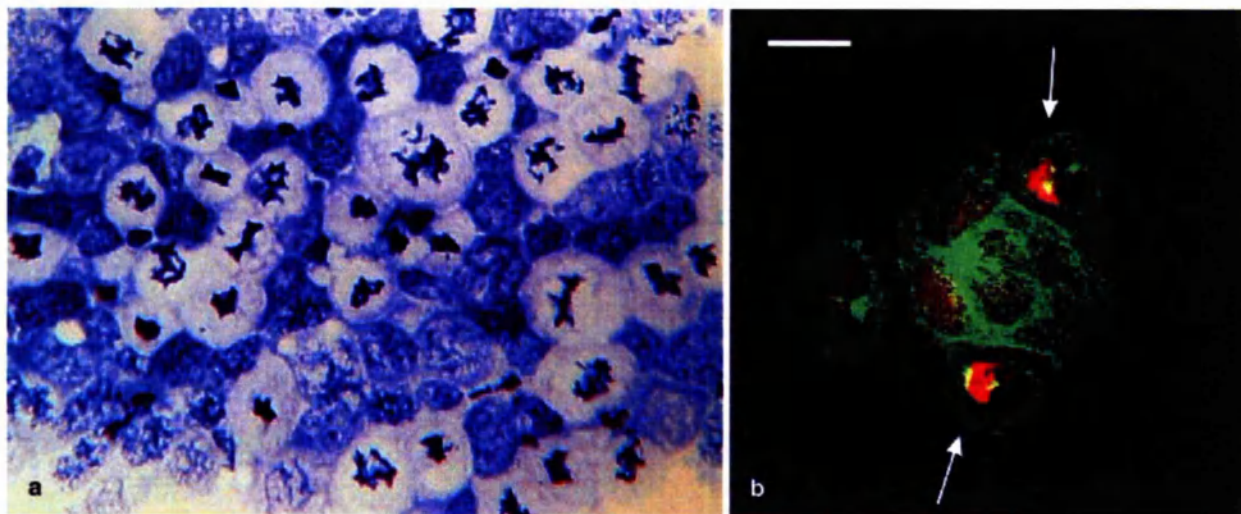


Fig. 2a, b Arrest in metaphase and the appearance of polyploidy in Namalwa cells after SK&F treatment. **a** Toluidine blue staining, 24 h post-treatment. $\times 2,000$. **b** In situ detection of β -tubulin (FITC) and counterstaining with propidium iodide (PI), 48 h post-treatment. Confocal three-dimensional (3-D) picture. Note the disruption of the mitotic spindle in the metaphase-arrested cells (arrows). A large polyploid cell with one centrosome is observed in the centre of the group. Bar 20 μ m

sembly of the nuclear envelope, indicating the reset of interphase (data not shown).

Mitotic response and DNA replication of irradiated cells

We have previously reported (Illidge et al. 2000) that, after irradiation, cells enter prolonged G2 arrest which, once released, is followed by a few rounds of highly aberrant mitoses. These mitoses display chromosome bridges, laggards, disordered metaphase plates, di- and tracentrics, and fragmented chromosomes (data not shown). Metaphase arrest followed mostly after the second or third round of mitoses after irradiation, demonstrated as a sharp increase in MI (Fig. 3b). Many of the arrested metaphases collapsed and underwent apoptosis as documented by us earlier (Illidge et al. 2000) and as shown by the abrupt decrease in MI (Fig. 3b), which remained depressed over the second week post-irradiation (not shown). However, a small proportion of cells arrested in metaphase displayed signs of interphase restitution on metaphase plates (data not shown), which was also confirmed in EM preparations (see Fig. 7c).

Using ^3H -thymidine pulse labelling, we revealed that the endopolyploid cells which recovered from the process of restitution began unscheduled DNA synthesis. This was found by incorporation of label into chromosomes when not fully decondensed and subsequently into the multilobulated nuclei (Fig. 3c). Endopolyploidisation resulted in DNA contents of 32 N and more (Fig. 1), and this intensive DNA replication was observed in many segmenting endopolyploid cells over

several days. In some endopolyploid cells, asynchronous DNA replication occurred in subnuclei, micronuclei and nuclear buds (Fig. 3d), as also published before (Erenpresia et al. 2000b). Approximately 0.5–1% of endopolyploid cells underwent further abortive mitoses, most of which collapsed or restituted again. In metaphase spreads of such cells, double-minutes (DM), which were sometimes multiple, were observed, indicative of gene amplification (Fig. 3e).

Induction of ELCS and nuclear segmentation

ELCS were encountered in 11–12% of non-treated Ramos and Namalwa cells in random thin EM sections. After irradiation, the number of cells bearing ELCS increased approximately fourfold (Fig. 4a, b). By EM, ELCS were observed most frequently in large cells with lobulating, segmenting, budding and micronucleating nuclei. After recovery of the diploid stem-line the number of ELCS-bearing cells decreased again back to normal levels. The kinetics of ELCS induction was similar to that of nuclear segmentation and polyploidisation (Fig. 4a, b). The steep increase in ELCS and nuclear segmentation frequency coincided with the release of metaphase arrest (compare Fig. 3b with Fig. 4a, b). In turn, the extent of polyploidy correlated with the appearance of delayed apoptosis (Fig. 4a, b) indicating that these cells destruct via apoptosis and have a short lifespan. In accordance with this observation, the vast majority of endopolyploid cells underwent apoptosis, as judged by TUNEL positivity, by the end of the first week after irradiation in what we have previously termed 'apoptotic crisis' (Illidge et al. 2000).

ELCS were also induced after SK&F treatment (Fig. 4c). They were again predominantly encountered in polyploid segmenting cells, although initially the NPs were usually smaller in size. ELCS were more rapidly induced, much more numerous and more frequently observed in cells after SK&F treatment than after irradiation.

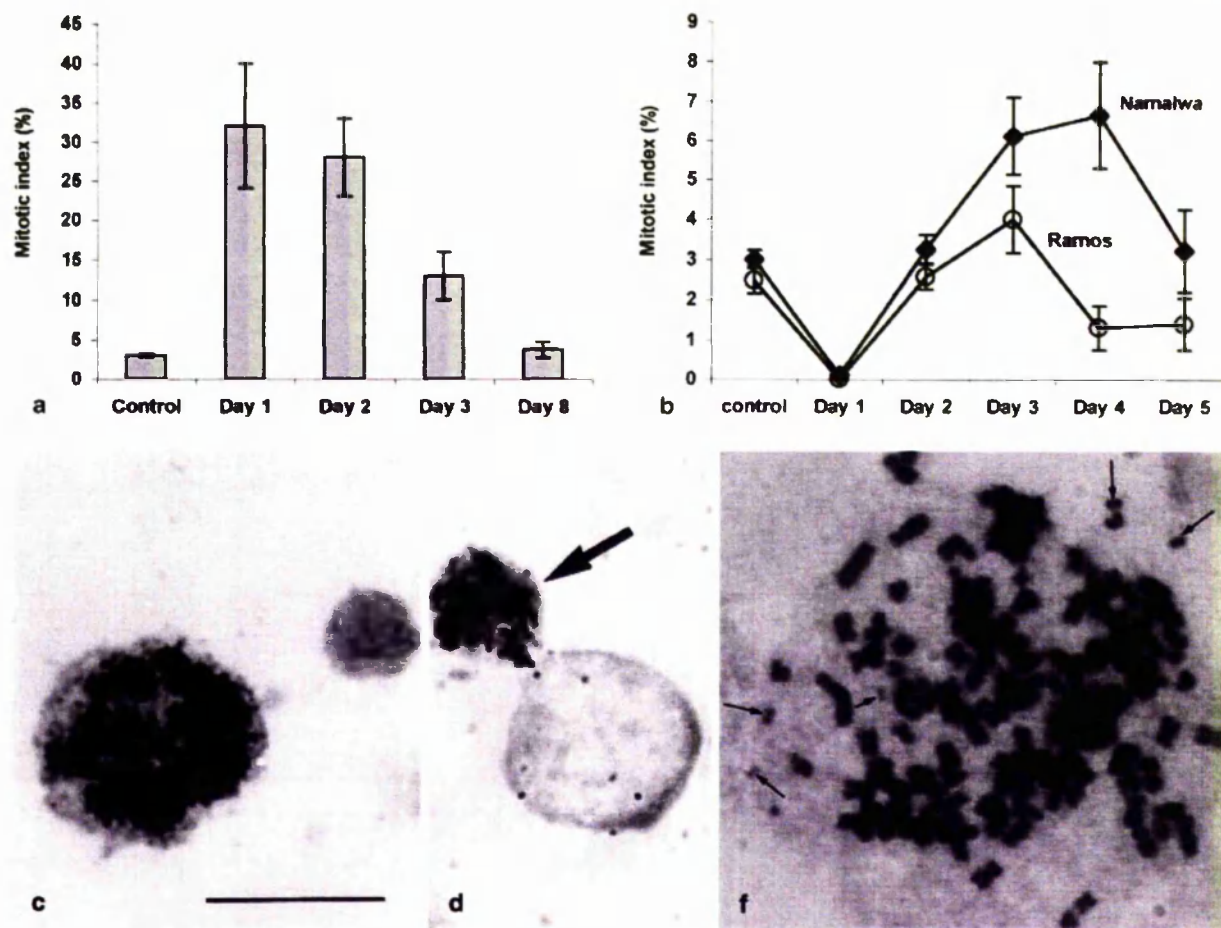


Fig. 3a–e Mitotic arrest and unscheduled DNA synthesis after treatment with SK&F or irradiation. **a** Extensive early arrest in mitosis and its slow release, after SK&F treatment in the Namalwa cell line. Bars represent the mean of two independent experiments with the standard error of the mean (SEM) shown. **b** Delayed arrest in mitosis after irradiation of Namalwa and Ramos cell lines. Bars represent the mean from six independent experiments with the standard deviation (SD) shown. **c, d** Autoradiographs of Ramos cells, 3 days after irradiation, pulse-labelled with ^3H -thymidine, showing incorporation of label all over the lobulated nucleus of a giant cell (**c**) and in the nuclear bud specifically (**d**, arrow). Bar 20 μm . **e** Metaphase of a polyploid Namalwa cell induced 5 days after irradiation and spread following 6 h of Nocodazole treatment. The metaphase spread shows a degree of chromosome sticking and double-minutes (small arrows). $\times 3,000$

Aneuploidy and DNA repair of giant cells

Uncoupling of mitosis from replication is known to cause aneuploidy (Grafí 1998). Having observed such uncoupling in segmenting giant cells, we wished to determine the DNA content of these cells and also the DNA content of their individual subnuclei. Using selective in situ DNA cytometry we determined that giant cells produced after irradiation possess varying amounts of DNA, most frequently between 2N multiples, indicating aneuploidy and extensive DNA synthesis (Fig. 5a). Their nuclear segments were also highly aneuploid (Fig. 5b).

Aneuploidy is often due to, or accompanied by, genome instability and ectopic chromosome fusions. As chromosome fusions leading to aneuploidy are known to arise from illegitimate non-homologous end-joining (NHEJ), in which Ku proteins are the principal participants (Takata et al. 1998; Price 1999), we sought to check the activity of NHEJ in the segmenting giant cells by studying the localisation of Ku70. Using immunocytochemistry, in line with literature reports (Mimori et al. 1986; Cai et al. 1994), we determined that Ku70 was present preferentially in the nucleoplasm of interphase nuclei and in the cytoplasm of normal mitotic cells

tion. The much higher frequency of ELCS and nuclear segmentation observed after SK&F treatment was thought to correspond to the higher numbers of arrested mitoses, higher frequency of mitosis restitution and higher proportion of polyploid cells, seen as early as day 2 post-SK&F (Figs. 2b, 4c). The number of large segmenting cells displaying ELCS slowly reduced in the second week after SK&F treatment, reflecting the slower depolyploidisation or breakdown of these compared to irradiated cells (Fig. 4c).

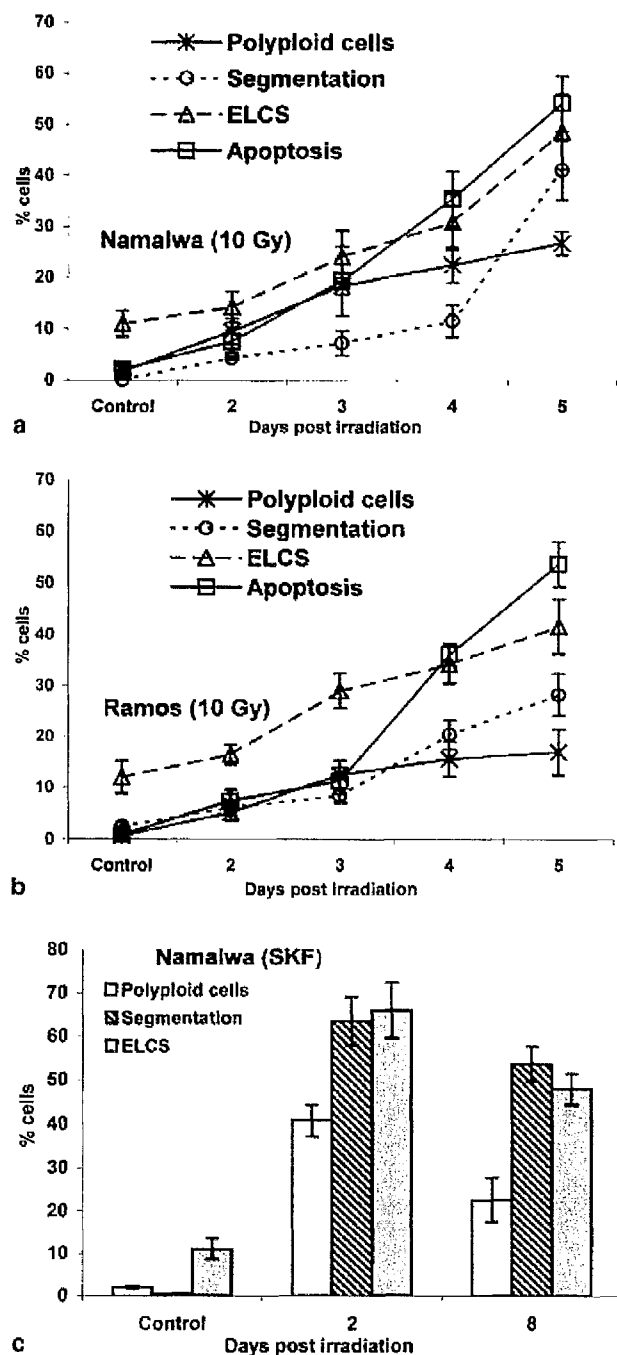


Fig. 4a–c Kinetics of the induction of endopolyploidy, nuclear segmentation, envelope-limited chromatin sheets (ELCS) and delayed apoptosis in irradiated or SK&F-treated cells. Namalwa (a, c) or Ramos cells (b) were treated with irradiation (a, b) or SK&F (c) and the extent of polyploidy, nuclear segmentation, ELCS and delayed apoptosis assessed by flow cytometry or microscopic examination. Values represent means from four to six experiments \pm SD (a, b) or means from two experiments \pm SEM (c). Segmentation and ELCS indexes were scored only among viable cells

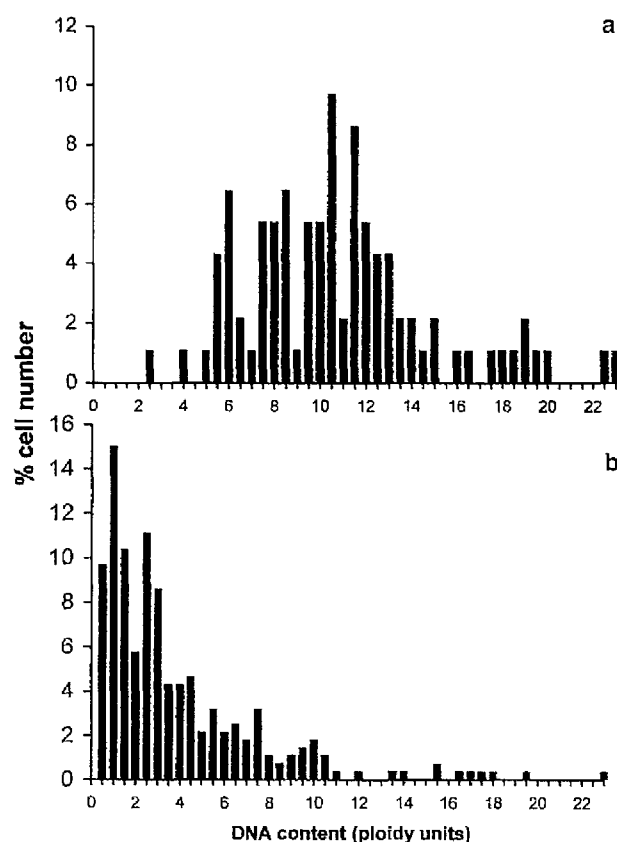
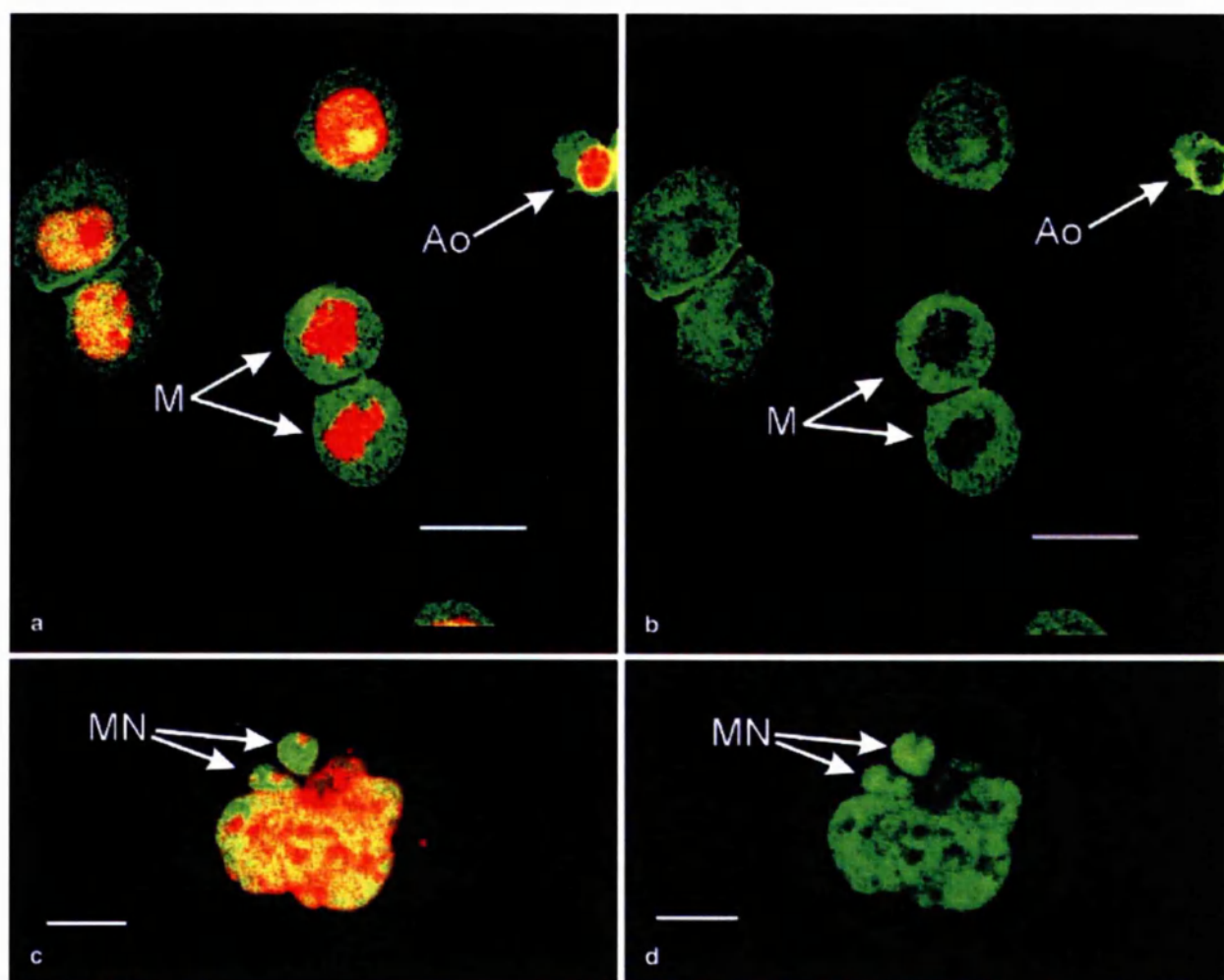


Fig. 5a, b DNA in situ cytometry of irradiated Ramos cells or their nuclear segments. Following irradiation, samples were taken on day 7, and 60 Ramos cells with segmented nuclei (a) and the individual segments of these cells (b) were assessed for their DNA content using interactive DNA cytometry. The DNA content is presented on a linear scale. Both show clear aneuploidy

(Fig. 6a, b), with weak perichromosomal staining observed. Conversely, in giant cells induced after irradiation, intrachromatin localisation of Ku70 was greatly enhanced, particularly in the micronuclei (Fig. 6c, d). In stark contrast, Ku70 was entirely absent from the nuclei of apoptotic cells (Fig. 6a, b).

Ultrastructural details of ELCS

The ultrastructure of ELCS in non-treated controls and induced after irradiation or SK&F treatment was essentially the same as described by others (Ghadially 1988a; Olins et al. 1998). Thus, two types of ELCS were observed: firstly, those where the loop of the inner nuclear membrane with the enclosed chromatin band reached only into the perinuclear space (Figs. 7b, 9c) and secondly where the loop also extended into the cytoplasm (Figs. 7d, 9a, b). ELCS loops starting from different points of the nuclear envelope and aligned in parallel in the perinuclear space were encountered more often in larger giant cells at later time points after both treatments (Figs. 7b, 9c).



Features relating to chromatin linking

ELCS were often found to join nuclear segments and attach micronuclei to the main nucleus (Figs. 7a, 8a). In addition, both types of ELCS, either running through the cytoplasm or intruding only into the perinuclear cistern, had a tendency to fuse again with the nuclear envelope and underlying chromatin (Figs. 7b, 9c). The chromatin band representing a single 35- to 40-nm row of dense granules was often observed to form at the ELCS origin by fusing the two separate layers of granular chromatin underlying the inner nuclear membrane, from both sides of the nuclear envelope extension. Here we observed the chromatin layers coming together 'granule to granule', with subsequent fusion into a single one-granule chain (Fig. 7a). At the terminus of the ELCS the reverse was observed, as the single chromatin band dissociated into two. A layer of chromatin was also observed on each side in the frequent splits of ELCS (Fig. 9a). The sites where the loop originated/fused with the nuclear envelope were usually marked by a patch of underlying heterochromatin. In approximately 50% of cases, ELCS were seen in the vicinity of, or physically con-

Fig. 6a-d In situ localisation of Ku70 in Namalwa cells 6 days after irradiation. Following staining with goat anti-Ku70 antibody and indirect immunofluorescent detection by FITC-conjugated anti-goat antibody, and counterstaining with PI, 3-D confocal images were captured. Control untreated cells (a, b) and cells 6 days post-irradiation (c, d) were assessed. In a and c both FITC and PI staining is shown; in b and d only the FITC-channel for Ku70 staining is shown. Note the predominant cytoplasmic localisation of Ku70 in the mitotic (M) and apoptotic (Ao) cells. By contrast, note the high concentration of Ku70 in the nucleus and micronuclei (MN) of the giant cell, and relatively weak staining of the cytoplasm. Bars 20 μ m

Fig. 7a-d The chromatin connecting feature of ELCS. Following various treatments, cells were processed for electron microscopy and the ELCS examined. In a, two sheets of peripheral chromatin are fusing into a single chromatin band 'granule to granule' (arrows). $\times 135,000$. b Two parallel arrays of ELCS in the perinuclear cistern of a giant Ramos cell, starting from (or fusing to) different sites in the peripheral chromatin (arrows), 15 days post-irradiation. Note also the confronting cisternae (CC) in the cytoplasm (blank arrow). $\times 20,000$. c ELCS linking decondensing chromosomes through the nuclear envelope vesicles (arrows) in an aberrant metaphase reconstituting into a multinucleated giant cell. MN Degenerating micronucleus. Picture taken from a Namalwa cell, 3 days post-irradiation. $\times 30,000$. d ELCS loop originating from the nucleolus-associated chromatin (arrow) in a Namalwa cell, 2 days post-SK&F treatment. $\times 22,500$

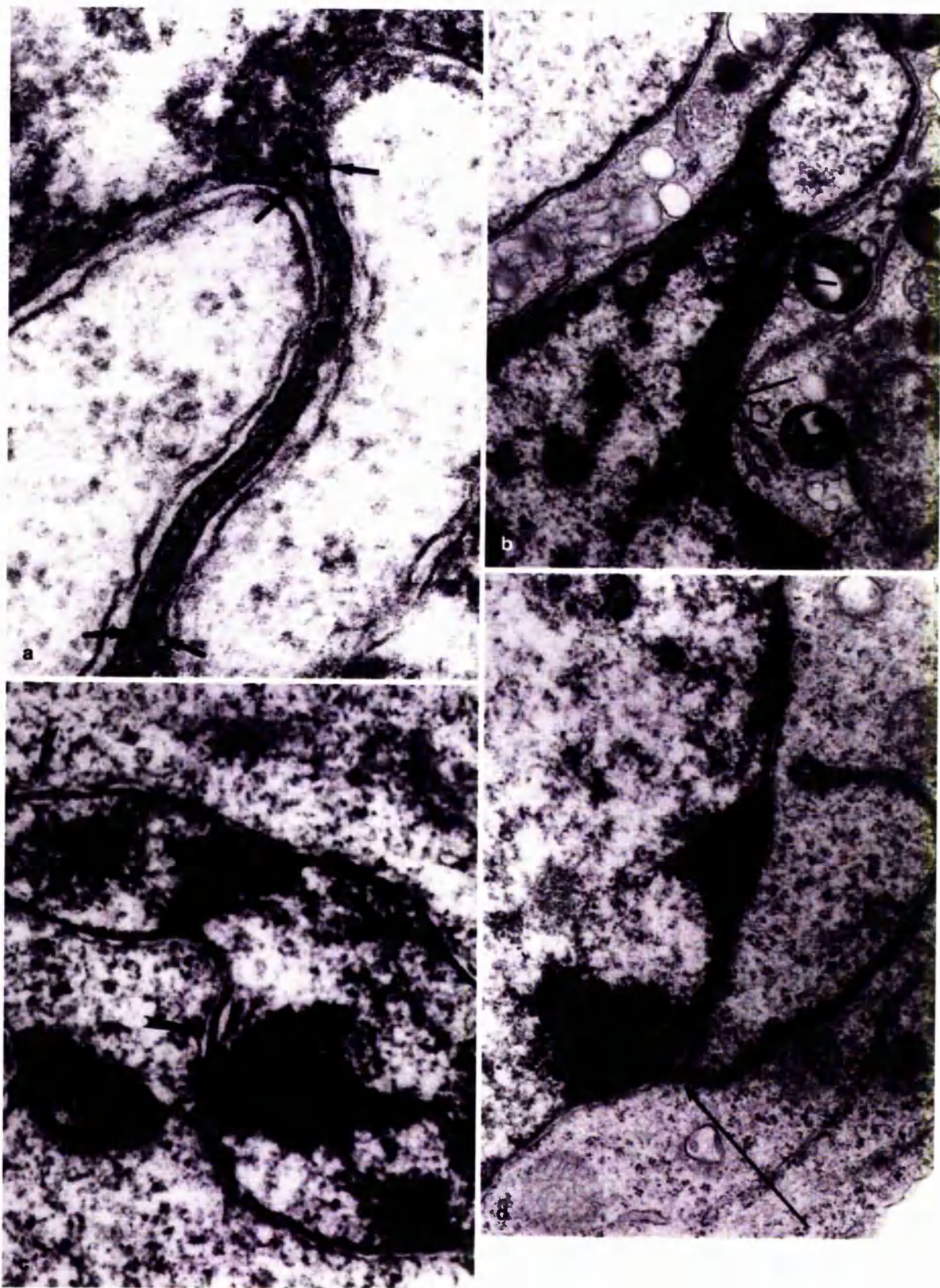


Fig. 7a-d Legend see page 249

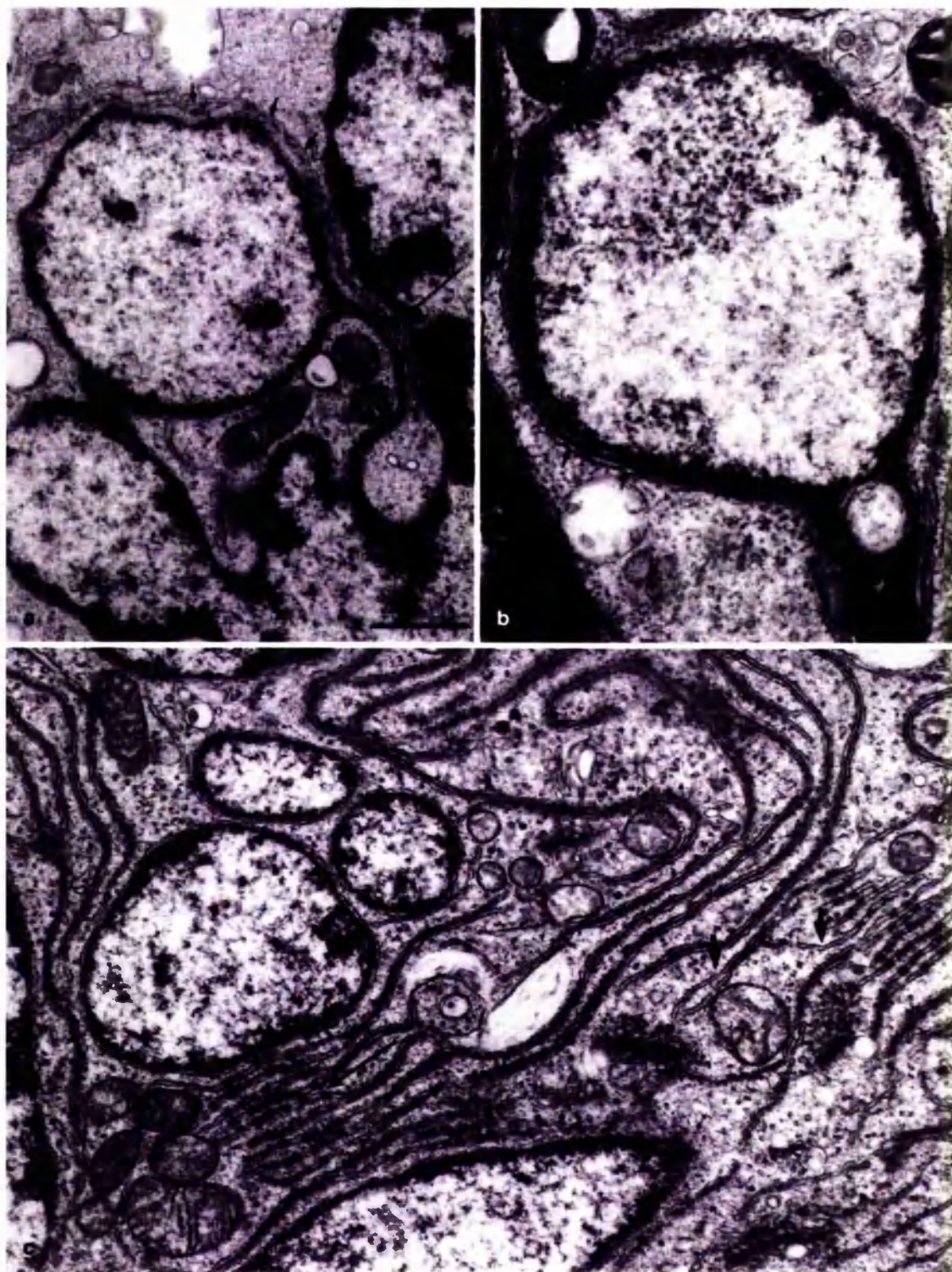


Fig. 8a-c Association of ELCS with other aligned membranes. Cells were processed as in Fig. 7. In **a**, a micronucleus is connected with the main nucleus by ELCS (*arrow*). Note also a single annulate lamella (AL), seemingly derived from the nuclear envelope and sequestering cytoplasm around the micronucleus (*small arrows*). $\times 22,500$. Bar 1 μm . In **b**, CC are observed in the

perinuclear space of the nuclear segment (*small arrows*). $\times 30,000$. **a, b** Namalwa cell nuclei day 14 post-irradiation. **c** Namalwa giant multinuclear cell showing multiple stacked AL and CC in continuity with each other (*long arrow*) and with rough endoplasmic reticulum (RER; *short arrows*). Day 7 post-SK&F treatment. $\times 16,000$

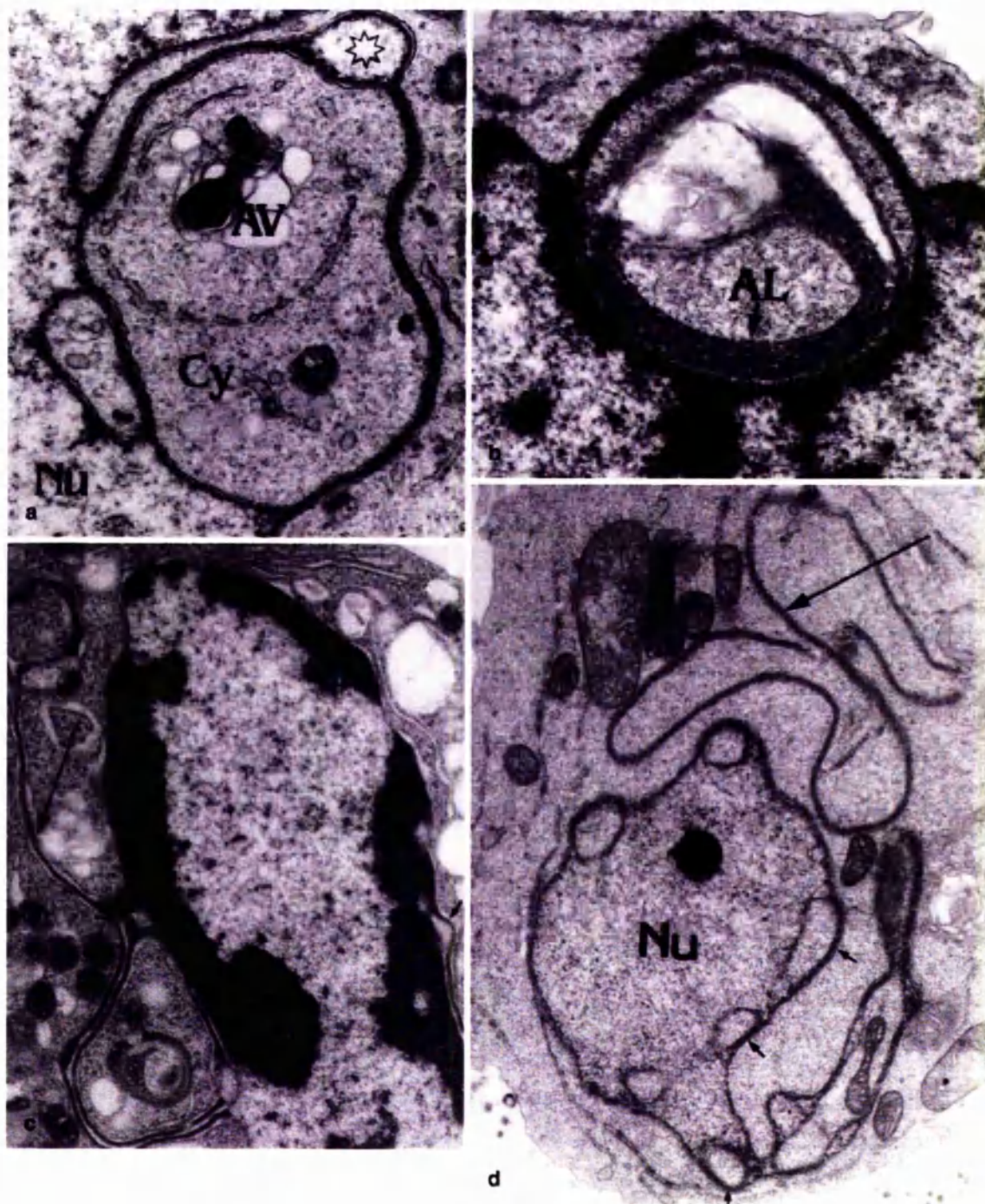


Fig. 9a-d Isolated degeneration of ELCS and death of ELCS bearing cells. **a** Initiation of isolated degeneration in Namalwa cells 4 days after SK&F treatment. Note the appearance of the autophagic vacuole (AV) constrained by RER in the nuclear pocket. The split of the ELCS showing dissociation of a single chromatin band is indicated by a *star*. Nu Nucleus, Cy cytoplasm. $\times 15,000$. **b** ELCS degeneration by whirling in a nuclear pocket, seemingly converting into AL (arrow), which undergo autodigestion in Namalwa cells 7 days post-irradiation. $\times 18,000$. **c** A cell undergoing early apoptosis, as judged by margination of destruc-

tured, hypercompacted chromatin and loss of the nuclear membrane. Similar changes occur within the ELCS in the cytoplasm (arrow) and where the ELCS runs into the perinuclear space (small arrow). Seven days after SK&F in a Namalwa cell. $\times 18,000$. **d** The nucleus (Nu) 'flopping' into a CC 'tail' (long arrow). Note that CC are intermittent with ELCS containing the chromatin band (small arrows). A small patch of condensed chromatin within the nucleus and active mitochondria indicate some features reminiscent of apoptosis. A Ramos cell, 12 days post-irradiation. $\times 10,000$

nected with, the nucleolus-associated heterochromatin (Fig. 7d).

ELCS were often found in cells exhibiting advanced restituting metaphases, either after irradiation or SK&F treatments or in untreated cells. In these cases, ELCS were seen to connect patches of decondensing chromosomes and micronuclei through the assembling vesicles of the nuclear membrane. Subsequently, by the end of restitution, the chromatin band establishing connections with the peripheral chromatin, enclosed the whole perimeter of the reset interphase nucleus (Fig. 7c). As such, the chromatin band was seen to establish connections between the peripheral chromatin and the restituted nuclear envelope.

Connections between ELCS and other structures

In addition to the connection with chromatin detailed above, ELCS can also form attachments with arrays of microtubules, after both treatments and in non-treated cells (not shown). Large, apparently activated or even hyperactive mitochondria are also frequent neighbours of ELCS (Figs. 7b, 8a, b). Similarly, single AL with relatively scarce annuli were seen in close vicinity to ELCS where they were observed sequestering cytoplasm around micronuclei, nuclear segments and buds (Fig. 8a). Occasionally, short stacks of AL were found in the cytoplasm of irradiated cells (not shown). On rare occasions, CC were found in the cytoplasm (Fig. 7b) or in the perinuclear space of giant cells and their micronuclei (Fig. 8b). Contrary to their scarcity in post-irradiated giant cells, CC and AL were abundant in the cytoplasm of SK&F-treated giant cells, where a clear continuity between the stacks of both membranous structures and the RER was observed (Fig. 8c).

Importantly, all of the features described above correspond to large cells (≥ 20 μ m in diameter), which were judged to be metabolically active by EM criteria.

ELCS degeneration and relationship to cell death

We have observed the degeneration of isolated ELCS in apparently metabolically active, viable cells. In these cases, the ELCS were rolled into the NPs and the concentric rolls of ELCS often had a somewhat 'fuzzy' structure, indicating that "whirling" was associated with their degeneration. Sometimes, concentric rolls of ELCS continued as concentric rings of AL. Such NPs, initially sequestered from the rest of the cytoplasm by RER, converted into autophagic vacuoles (Fig. 9a, b). This isolated degeneration was only rarely seen in irradiated samples (from day 6 post-treatment onwards), but was more frequently observed and at early time points in SK&F-treated cells (from day 2 onwards).

ELCS were often observed in the nuclei when endopolyploid cells underwent delayed apoptosis. In such cases, chromatin hypercondensation and degradation was

seen to be accompanied by disappearance of the nuclear envelope, both in the main nucleus and in the ELCS extensions (Fig. 9c).

Other rare types of cell death were observed. These were typified by cells with atrophic nuclei, devoid of any peripherally condensed chromatin and confined by nuclear CC intermittent with short segments of ELCS. These nuclei 'flopped', demonstrating that the continuity between ELCS and CC extended into the cytoplasm as a long meandering CC 'tail' (Fig. 9d). Apoptotic-like death was indicated by the presence of small patches of condensed chromatin and large mitochondria.

Discussion

In this study we have explored the generation of ELCS after severe DNA damage or disruption of the mitotic spindle. The common central event of these treatments was the induction of mitotic death. In both cases, this was displayed as arrest in M-phase, mitotic failure, uncoupling of DNA replication from mitosis and formation of giant cells, which themselves exhibited ELCS and later underwent delayed apoptosis.

An important finding to emerge from this work is that, although ELCS appear in cells where mitosis has failed, these cells do not undergo immediate cell death. Indeed, these ELCS-bearing cells undergo DNA replication and apparently repair. Although most of these cells will ultimately die, their death occurs via an extremely protracted and delayed apoptosis as detailed using TUNEL, EM and flow cytometric analysis. All of these observations suggest that induction of ELCS precedes the irreversible effector stage of apoptosis.

Although the majority of workers consider the spindle checkpoint to be independent of p53 function, p53 is important to prevent re-replication of DNA and formation of giant cells if the cells are arrested in metaphase (Lanni and Jacks 1998). In turn, arrest in mitosis and endoreduplication can lead to aneuploidy in p53 mutant cells (Satya-Prakash et al. 1984; Nagl 1990; Lilly and Spradling 1996). The association of ELCS with aneuploidy was confirmed in this work and is in agreement with previous reports (Ahearn et al. 1974).

Detailed analysis of the kinetics of mitotic arrest resulting from SK&F or irradiation treatment reveals notable differences. Whereas mitotic arrest was observed rapidly and abundantly after SK&F treatment, it was delayed and less extensive after irradiation. The kinetics and amounts of ELCS induced appeared to correlate with these differences. In addition, in Ramos cells a more modest post-irradiation M-arrest and polyploidisation was seen compared with Namalwa cells and this also correlated with a smaller induction of ELCS. Taken together, with the observation that ELCS have been visualised in restituting mitosis, these data allow us to come to the novel conclusion that arrest at the spindle checkpoint and uncoupling of mitosis from DNA replication lead to the emergence of ELCS in the resulting endopolyploid cells.

We have microscopically observed chromosome fusion events and noted the participation of ELCS during and after restitution cycles in these events, in irradiated and SK&F-treated cells. We have also observed DNA synthesis that is uncoupled from mitosis in these giant cells, including signs of gene amplification, through identification of DMs. Shimitzu et al. (1998) noted selective entrapment of amplified DNA in nuclear buds and micronuclei during S-phase. In parallel, we have observed an increase in concentration and intrachromatin localisation of the Ku70 protein in segmenting giant cells, particularly enhanced in micronuclei. It is known that the Ku70/80 heterodimer, together with Sir 2, 3 and 4 silencing proteins, participate in both telomere stabilisation and illegitimate double-strand break (DSB) repair by NHEJ (Price et al. 1999). It is also known that NHEJ requires active DNA synthesis. In addition to extra-DNA replication by amplification, under-replication of DNA in late S-phase is a well-described facet of endopolyploid cells (Nagl 1990; Lilly and Spradling 1996). It seems probable then, that extra- and under-replication of DNA, as well as the micronucleation of acentric chromosome fragments in failed mitoses, would be sensed by the proteins of the Ku group as DSB and targeted for ectopic NHEJ. Similar sequestration of Rad51-recombination protein into micronuclei of irradiated cells found by Haaf et al. (1999) and the absence of Ku70 from the interior of normal mitotic chromosomes and apoptotic cell nuclei would appear to validate this hypothesis.

Tsukamoto et al. (1997) have suggested that Ku and silencing family proteins when redistributed to DNA strand-breaks are able to protect the chromatin from degradation by nucleases. This hypothesis may offer a potential explanation for the postponement of apoptosis in giant cells.

In accordance with our observations, Gisselsson and co-workers (2001) have shown in a number of irradiated and untreated non-lymphoid tumours that the vast majority of nuclear envelope abnormalities (which include ELCS using our terminology) correlate with chromosome fusion events. In turn, incorrect arrangement of chromosomes in restituted interphase nuclei might alter the establishment of normal interactions between chromatin and the nuclear envelope. In HL60 cells, where nuclear segmentation and ELCS are induced by addition of retinoic acid (Olins et al. 2001), the cells display a several-fold excess of lamin B receptors (LBR). LBR play a critical role in targeting nuclear membranes to chromatin during mitosis (Gant and Wilson 1997). These data, in conjunction with ours, detailing the extensive ectopic chromosome fusion events accompanied by ELCS in giant cells, indirectly support the concept that there is an excess of nuclear envelope docking sites in relation to specific chromatin regions with affinity for them in these cells. This disproportion and attempted docking, may result in the induction of nuclear segmentation and ELCS in endopolyploid cells.

Besides ELCS, we have also observed the emergence of other aligned membranous structures during mitotic

death. These include AL and CC, which were observed to be continuous with the nuclear envelope and ELCS, and the RER, respectively. These associations demonstrate the dynamic relationship between the nuclear envelope and the RER. Our observations also indicate that these three structures are interlinked and are capable of interconversion. In particular, AL and CC appear related to the destruction of ELCS.

In explanation of the fact that ELCS are observed in various normal cells, it is noteworthy that the heterologous expression of LBR leads to the induction of stacked cytoplasmic membranes, in close vicinity and in connection with the nuclear envelope (Smith and Blobel 1994). By analogy, the ELCS and AL in spermatocytes and stacked AL in oocytes and early blastomeres, as well as the ELCS seen in rare leukocytes may represent similar disproportions in the number of the membrane-associated chromatin docking sites and availability of the chromatin for them. The physiological disproportions in oocytes and early embryo may be brought about through amplifying stacked membranes with chromatin docking sites in preparation for future rapid divisions.

Acknowledgements The authors acknowledge the excellent technical assistance of Sue Cox, Nick Barnett and Anton Page of the Image Processing Unit, Southampton University, and the assistance of Vladislavs Zelchs in the Electron Microscopy Unit of the University of Latvia. We are grateful for helpful discussions with Ada Olins, Donald Olins and Carl Smythe. We would like to acknowledge the financial support of the Royal Society of London for enabling the exchange visits between Riga, Latvia, and Southampton, UK.

References

- Ahearn MJ, Trujillo JM, Cork A, Fowler A, Hart JS (1974) The association of nuclear blebs with aneuploidy in human acute leukemia. *Cancer Res* 34:2887-2896
- Bernhard EJ, Muschel RJ, Bakanauskas VJ, McKenna W (1996) Reducing the radiation-induced G2 delay causes HeLa cells to undergo apoptosis instead of mitotic death. *Int J Radiat Biol* 69:575-584
- Cai QQ, Plet A, Imbert J, Lafage-Pochitaloff M, Cerdan C, Blanchard JM (1994) Chromosomal location and expression of the genes coding for Ku p70 and p80 in human cell lines and normal tissues. *Cytogenet Cell Genet* 65:221-227
- Chemes HE, Fawcett DW, Dym M (1978) Unusual features of the nuclear envelope in human spermatogenic cells. *Anat Rec* 192:495-512
- Clausen KP, Von Haam E (1969) Fine structure of malignancy-associated changes (MAC) in peripheral human leukocytes. *Acta Cytol* 13:435-442
- Cragg MS, Zhang L, French RR, Glennie MJ (1999) Analysis of the interaction of monoclonal antibodies with surface IgM on neoplastic B-cells. *Br J Cancer* 79:850-857
- Davies HG (1968) Electron-microscopical observations on the organisation of heterochromatin in certain cells. *J Cell Sci* 3:129-150
- Erenpreisa J, Freivalds T, Roach H, Alston R (1997) Apoptotic cell nuclei favour aggregation and fluorescence quenching of DNA dyes. *Histochem Cell Biol* 108:67-75
- Erenpreisa J, Ivanov A, Dekena G, Vitina A, Krampe R, Freivalds T, Selivanova G, Roach HI (2000a) Arrest in metaphase and anatomy of mitotic catastrophe: mild heat shock in two human osteosarcoma cell lines. *Cell Biol Int* 24:61-70

- Erenpreisa JA, Cragg MS (2001) Mitotic death: a mechanism of survival? A review. *Cancer Cell Int* 1:1 (<http://www.canceri.com>)
- Erenpreisa JA, Cragg MS, Fringes B, Sharakhov I, Illidge TM (2000b) Release of mitotic descendants by giant cells from irradiated Burkitt's lymphoma cell lines. *Cell Biol Int* 24: 635-648
- Gant TM, Wilson KL (1997) Nuclear assembly. *Annu Rev Cell Dev Biol* 13:669-695
- Ghadially FN (1988a) Nuclear projections, pockets, loops, satellites and clefts. In: Ghadially FN (ed) *Ultrastructural pathology of cell and matrix*, 3rd edn, vol 1. Butterworths, London, pp 140-180
- Ghadially FN (1988b) Annulate lamellae. In: Ghadially FN (ed) *Ultrastructural pathology of cell and matrix*, 3rd edn, vol 1. Butterworths, London, pp 573-587
- Ghadially FN (1988c) Confronting cisternae. In: Ghadially FN (ed) *Ultrastructural pathology of cell and matrix*, 3rd edn, vol 1. Butterworths, London, pp 462-465
- Ghadially FN (1988d) Thickenings, proliferation and reduplication of nuclear envelope. In: Ghadially FN (ed) *Ultrastructural pathology of cell and matrix*, 3rd edn, vol 1. Butterworths, London, pp 42-47
- Gisselsson D, Bjork J, Hoglund M, Mertens F, Dal Cin P, Akerman M, Mandahl N (2001) Abnormal nuclear shape in solid tumours reflects mitotic instability. *Am J Pathol* 158:199-206
- Grafi G (1998) Cell cycle regulation of DNA replication. The endoreduplication perspective (minireview). *Exp Cell Res* 244:372-378
- Haaf T, Raderschall E, Reddy G, Ward DC, Radding CM (1999) Sequestration of mammalian Rad51-recombination protein into micronuclei. *J Cell Biol* 144:11-20
- Hulin D (1967) Nuclear pockets in normal monocytes. *Nature* 216:1240
- Illidge TM, Cragg MS, Fringes B, Olive P, Erenpreisa JA (2000) Polyploid giant cells provide a survival mechanism for p53 mutant cells after DNA damage. *Cell Biol Int* 24:621-633
- Kessel RG (1992) Annulate lamellae: a last frontier in cellular organelles. *Int Rev Cytol* 133:43-120
- Lanni JS, Jacks T (1998) Characterization of the p53-dependent postmitotic checkpoint following spindle disruption. *Mol Cell Biol* 18:1055-1064
- Lilly MA, Spradling AC (1996) The *Drosophila* endocycle is controlled by cyclin E and lacks a checkpoint ensuring S-phase completion. *Genes Dev* 10:2514-2526
- Lock RB, Ross WI (1990) Possible role for the p34cdc2 kinase in etoposide-induced cell death of Chinese hamster ovary cells. *Cancer Res* 50:3767-3771
- Mimori ET, Hardin JA, Steitz JA (1986) Characterization of the DNA-binding protein antigen Ku recognized by antibodies from patients with rheumatic disorders. *J Biol Chem* 261: 2274-2278
- Mitsui-Saito M, Nakahata N, Ohizumi Y (2000) Inhibition of microtubule polymerization by SK&F 96365, a blocker of receptor-linked Ca^{2+} entry. *Jpn J Pharmacol* 82:269-271
- Nagl W (1990) Polyploidy in differentiation and evolution. *Int J Cell Clon* 8:216-223
- Nordstrom T, Nevanlinna HA, Andersson LC (1992) Mitosis-arresting effect of the calcium channel inhibitor SK&F 96365 on human leukemia cells. *Exp Cell Res* 202:487-494
- O'Connor PM, Jackman J, Jondle D, Bhatia K, Magrath I (1993) Role of the p53 tumor suppressor gene in cell cycle arrest and radiosensitivity of Burkitt's lymphoma cell lines. *Cancer Res* 53:4776-4780
- Olins A, Buendia B, Herrmann H, Lichter P, Olins D (1998) Retinoic acid induction of nuclear envelope-limited chromatin sheets in HL-60. *Exp Cell Res* 245:91-104
- Olins AL, Herrmann H, Lichter P, Kratzmeier M, Doenecke D, Olins DE (2001) Nuclear envelope and chromatin compositional differences comparing undifferentiated and retinoid acid- and phorbol ester-treated HL-60 cells. *Exp Cell Res* 268:115-127
- Price CM (1999) Telomeres and telomerase: broad effects on cell growth. *Curr Opin Genet Dev* 9:218-224
- Radford R, Murphy TK (1994) Radiation response of mouse lymphoid and myeloid cell lines. Part III. Different signals can lead to apoptosis and may influence sensitivity to killing by DNA double-strand breakage. *Int J Radiat Biol* 65:229-239
- Rogers-Bald M, Sargent RG, Bryant PE (2000) Production of chromatid breaks by single dsb: evidence supporting the signal model. *Int J Radiat Biol* 76:23-29
- Sasaki K, Iwatsuki H, Suda M, Itano C (1995) Accumulation and massive cell death of polymorphonuclear neutrophils in the developing bone marrow of the mouse: a histological study. *Acta Anat (Basel)* 153:111-118
- Satya-Prakash KL, Hsu TC, Wheeler WJ (1984) Metaphase arrest, anaphase recovery and aneuploidy induction in cultured Chinese hamster cells following exposure to mitotic arrestants. *Anticancer Res* 4:351-356
- Scott D, Fox M, Fox BW (1974) The relationship between chromosomal aberrations, survival and DNA repair in tumour cell lines of differential sensitivity to X-rays and sulphur mustard. *Mutat Res* 22:207-221
- Sebuwufu PH (1966) Nuclear blebs in the human foetal thymus. *Nature* 212:1382-1383
- Shimitzu N, Itoh N, Utiyama H, Wahi GM (1998) selective entrapment of extrachromosomally amplified DNA by nuclear budding and micronucleation during S-phase. *J Cell Biol* 140:1307-1320
- Smith S, Blobel G (1994) Colocalization of vertebrate lamin B and lamin B receptor (LBR) in nuclear envelopes and in LBR-induced membrane stacks of the yeast *Saccharomyces cerevisiae*. *Proc Natl Acad Sci U S A* 91:10124-10128
- Smith GF, O'Hara PT (1967) Nuclear pockets in normal leukocytes. *Nature* 215:773
- Takata M, Sasaki MS, Sonoda E, Morrison C, Hashimoto M, Utsumi H, Yamaguchi-Iwai Y, Shinohara A, Takeda S (1998) Homologous recombination and non-homologous end-joining pathways of DNA double-strand break repair have overlapping roles in the maintenance of chromosomal integrity in vertebrate cells. *EMBO J* 17:5497-5508
- Tsukamoto Y, Kato J-I, Ikeda H (1997) Silencing factors participate in DNA repair and recombination in *Saccharomyces cerevisiae*. *Nature* 388:900-903
- Waldman T, Lengauer C, Kinzler KW, Vogelstein B (1996) Uncoupling of S phase and mitosis induced by anticancer agents in cells lacking p21. *Nature* 381:713-716
- Wheatley DN (1991) Confronting cisternae in cultured mammalian cells: development and prevalence in arrested metaphases. *J Submicrosc Pathol* 23:559-568

Chapter 7

Image Analysis of DNA Repair and Apoptosis in Tumour Cells with Differing Sensitivity to DNA Damage

Reprinted from A. Ivanov, M. Ivanova, Je. Erenpreisa, S.V. Gloushen, T. Freivalds
and M.S. Cragg. Proc Int Fed Med Biol Eng, Elsevier, 2008.

Image Analysis of DNA Repair and Apoptosis in Tumor Cells with Differing Sensitivity to DNA Damage

A. Ivanov¹, M. Ivanova¹, J. Erenpreisa³, S.V. Gloushen², T. Freivalds⁴ and M.S. Cragg⁵

¹Paterson Institute of Cancer Research, Manchester, UK;

²Belarusian State University, Minsk, Belarusia;

³Latvian Biomedicine Centre, Riga, Latvia;

⁴Latvian Institute of Experimental and Clinical Medicine, Riga, Latvia;

⁵Tenovus Research Laboratory, Southampton University School of Medicine, Southampton, UK

Abstract — Homologous recombination of DNA double strand breaks was previously found to be protective against apoptosis in tumor cells lacking p53 function. Here, we studied the spatial and temporal relationship between the two processes in a pair of lymphoblastoid cell lines with wild-type or mutant p53 status. Clonogenic assays revealed that p53 mutant WI-L2-NS cells were ~ ten-fold more resistant to X-ray damage than p53 wild type TK6 cells and displayed 2-3 times lower levels of apoptosis 24 h after irradiation. The kinetics of DNA damage and repair after irradiation (5 Gy) were assessed by immunofluorescent staining for g-H2AX and Rad51, and DNA stained with DAPI. Using image analysis in the three (red/green/blue) fluorescence channels we found that repair foci were more prevalent in the p53 mutant radioresistant WI-L2-NS cells at many time points: 2.2 versus 1 per nucleus at 5 min, 3.2 versus 1.6 at 6 h, and 6.1 versus 3.6 at 72 h post-irradiation although the number of repair foci were equal at 24 h (8.8). Furthermore, the average size of foci in TK6 cells was smaller at all times post-irradiation ($p < 0.001$). In contrast to the functional repair foci which were characterised by the co-localisation and high concentration of g-H2AX and Rad51, in pre-apoptotic cell nuclei, foci with greater quantities of g-H2AX relative to Rad51 were prevalent. The g-H2AX-predominant foci colocalized with little or no Rad51 and fused in a pattern typical of apoptotic chromatin. This pattern was seen more often in TK6 cells, where at 6 h the sum area occupied by g-H2AX was seven-fold higher than that of the Rad51 label. In contrast, WI-L2-NS cells displayed approximately equal areas of both components. These data suggest that formation of stable functional repair foci topologically protects the chromatin from relaxation and initiation of apoptotic fragmentation.

Keywords — tumors, DNA repair, apoptosis, image analysis.

I. INTRODUCTION

Tumor cells lacking p53 function are selected during tumor progression and are resistant to therapy with DNA damaging agents. Homologous recombination (HR) of DNA double strand breaks (DSB) was previously found to be abnormally enhanced in p53 mutated tumor cells resulting in a reduction in tumor cell death through apoptosis [1,2]. Although it is

generally accepted that failed DNA repair leads to apoptosis, the spatial relationship between the two processes and its dependence on p53 status is unknown. In mammalian cells, the signaling cascade downstream of DNA damage phosphorylates histone H2AX (termed g-H2AX) at sites of DSB. In turn, g-H2AX plays a critical role in the organization of DNA repair foci by helping to recruit DNA repair factors involved in HR, such as the recombinase Rad51 [3]. g-H2AX forms at sites on the chromatin where DSB are present, including those sites where extensive apoptotic DNA fragmentation is occurring. Therefore, we applied immunofluorescent staining of g-H2AX and Rad51 and used image analysis to study the topological and kinetic relationships between HR and apoptosis, in a pair of linked human lymphoblastoid cell lines with wild-type (wt) or mutant (mut) p53 status.

II. MATERIALS AND METHODS

Human lymphoblastoid cells lines TK6 and WI-L2-NS were obtained from the ATCC and grown in suspension in RPMI medium with 10% fetal calf serum. WI-L2-NS is a p53 mutated cell-line derived from the same source as the p53 wt TK6. Cells were irradiated using a Gulmay D3 225 X-ray source with a dose rate of 0.77 Gy/minute. Samples were analysed by flow cytometry and immunofluorescent staining for g-H2AX/ Rad51/DNA as detailed previously (Ivanov et al., 2003). Images were obtained by AxioCam (1300x1030) equipped with a calibrated Sony DXC 390P colour video camera. Image analysis was performed using Image Pro Plus 4.1 software (Media Cybernetics; REO 2001, Riga, Latvia). To discriminate DNA repair foci, the image was segmented using 180-255 empirically chosen intensity levels. Student's t- and non-parametric sign-test were used for statistical analysis of measurement results.

III. RESULTS

Clonogenic assay: Clonogenic assays from three independent experiments showed that the p53 mut WI-L2-NS cells are approximately ten-fold more resistant to X-ray radiation than the related p53 wt TK6 cells.

Kinetics of the cell cycle: DNA flow cytometry revealed that 60% of irradiated TK6 cells and about 75% of WI-L2-NS cells have passed the first S-phase and arrived in the G2 arrest compartment at 24 h post 5 Gy irradiation (in control, G2-fraction comprised 22-26%, in the both tumours). Mitotic cycling restarted then, albeit at a low level, and returned to the normal level between day 5 to 7. Between d.2 to d.5, WI-L2-NS formed about 20% of polyploid cells ($\geq 4C$), while TK6 produced almost none.

Apoptosis: The amount of apoptosis determined as the sub-G1 fraction by DNA flow cytometry at 24 h comprises 7% for WI-L2-NS and 15% for TK6. However later the difference increases further: at 72 h 65% of TK6 cells are in apoptosis, while only 25% of WI-L2-NS cells are apoptotic.

Topological analysis of the DNA repair by HR: Repair foci were observed in both cell-lines within 5 min post-damage. Notably, they were first assembled from diffuse forms of g-H2AX and Rad51 at the interface between the condensed chromatin and the interchromatin (nuclear matrix) space. Larger areas of g-H2AX and Rad51 were observed in WI-L2-NS 5 min after damage and the average number of repair foci per cell was 2.2 as compared with 1.0 for TK6 cells (Table 1).

Table 1. Kinetic analysis of g-H2AX and Rad51 components after irradiation determined by immunofluorescent staining and image analysis. Only foci containing both g-H2AX and Rad51 components were scored as repair foci.

Time after irradiation	5 min		6 h		24h		72h	
Cell line	TK6	WI-L2-NS	TK6	WI-L2-NS	TK6	WI-L2-NS	TK6	WI-L2-NS
Number of repair foci/cell	1.0	2.2	1.5	3.2	8.8	8.8	3.6	6.1
Average area of Rad51 foci (pxl)	38.4	45.1	51.0	56.8	52	53.6	43.9	49.3
Area occupied by Rad51/cell	37.6	98.8	78.9	182.7	456	471	160	301
Area occupied by g-H2AX/cell	14.0	54.6	58.4	319.0	663	513	196	328

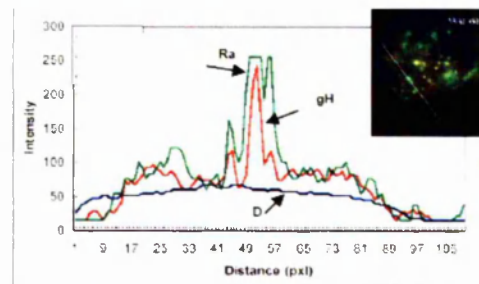


Fig. 1. Segmentation of g-H2AX repair foci saturated with Rad51 in a WI-L2-NS cell, 6 h post-irradiation

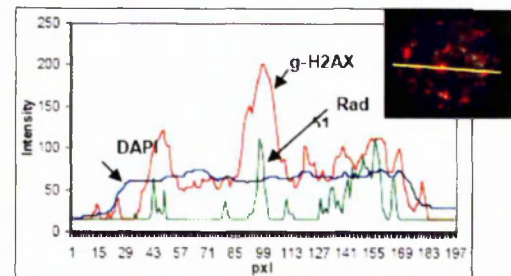


Fig. 2. Segmentation through g-H2AX foci binding negligible amounts of Rad51 in a TK6 cell, 6 h post-irradiation

More effective formation of repair foci in WI-L2-NS was also observed at 6 h post-damage (3.2 versus 1.5 per nucleus) and notably, at this term the sum area occupied by g-H2AX in TK6 was seven-fold higher than the sum area of the Rad51 label, while this difference in WI-L2-NS cells was only 1.7 (Table 1).

The difference was also seen by one-line, three-colour (red, green, blue) scanning through the repair foci. In WI-L2-NS the highly colocalized concentration of g-H2AX/Rad51 sharply defined the functional repair foci (Fig. 1).

In contrast, Rad51 was much less prevalent in the centre of large g-H2AX foci in many irradiated TK6 cells (Fig. 2).

The g-H2AX-labelled foci, which were free of Rad51, tended to cluster and fuse forming the chromatin pattern typical of early apoptotic cells (Fig. 3).

The discrepancy between the cell lines was diminished at 24 h, when similar amounts of cells were arrested in the G2 cell cycle compartment. At this time, both cell-lines showed similar levels of g-H2AX and Rad51 staining and the highest average number of repair foci per nucleus (8.8)

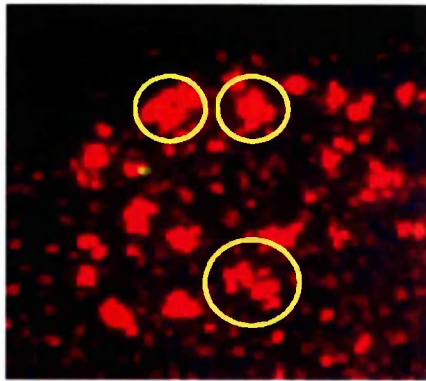


Fig. 3. Clustering and fusion of multiple g-H2AX foci in a pre-apoptotic TK6 cell nucleus.

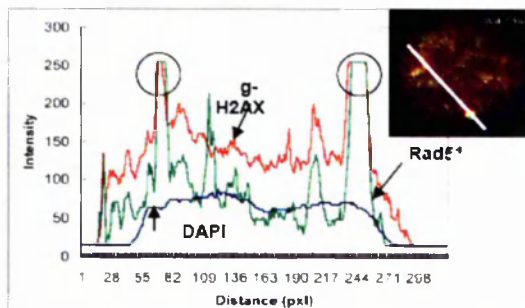


Fig. 4. Giant repair foci segmented in a polyloid WI-L2-NS cell nucleus, 72 h post irradiation.

was apparent (Table 1). Some cell nuclei in both cell lines became free of both components (presumably having repaired the DSB). However, at 72 h, the difference in HR foci again showed the higher repair potential of the WI-L2-NS cells (6.1 versus 3.6 foci in TK6 cells). The average size of Rad51 foci in TK6 cells between 6–72 h was determined to be statistically smaller by the non-parametrical sign test ($p=0.001$). At 72 h, some of WI-L2-NS polyloid cells displayed giant repair foci of heterogeneous size, with high concentration of the both components and increased local DAPI binding (Fig. 4).

IV. DISCUSSION

Here we analysed the DNA damage response in two different lymphoblastoid cell lines derived from the same source which differ in their p53 status. After ionising irradiation, both cell lines formed HR repair foci containing

colocalized g-H2AX and Rad51. However, the p53 competent TK6 cells had a reduced ability to target Rad51 to g-H2AX-signaling foci coincident with the timing of the first (6h) and further (72h) S phases. Recombination in S-phase is assumed to be illegitimate as it favours mutation. Mutations arising as a result of enhanced recombination repair were found previously in WI-L2-NS cells as compared with TK6 [4]. More recently, a specific helicase Srs2 has been discovered which normally prevents uploading of Rad51 to the DNA replication processivity clamp [5]. Our data indirectly suggest that this mechanism may be p53-dependent, while phosphorylation of H2AX in the damage-signalling cascade may be independent of p53. The topological consequence of the restricted association of Rad51 with the g-H2AX foci was evidenced by their structural deterioration, multiplication of g-H2AX domains and decrease in DAPI binding. In contrast, the unrestricted binding of Rad51 to g-H2AX repair sites in p53 mutant polyloid WI-L2-NS cells leads to the formation of enormous, well-shaped foci and notably – to the local increase of DAPI binding. DAPI is a DNA intercalating dye whose binding is dependent on both its DNA content and double-strandedness. DAPI does not bind single-stranded DNA. Therefore, our observations suggest that Rad51 may prevent relaxation of the DNA in the HR repair foci. Possibly, Rad51 filaments may penetrate into the sites of damage, locating single strand breaks (SSB) searching for the homology to 'plug' the breaks, thus favouring staining with DAPI. The relaxation of chromatin in the Rad51-depleted g-H2AX-foci was observed by us as the initiating step switching the chromatin from attempts of HR towards the initiation of apoptosis in the p53-competent TK6 cells. Excessive g-H2AX formation was shown to appear during apoptosis concurrently with the initial appearance of high molecular weight DNA fragments [6]. These high molecular weight DNA fragments observed during apoptosis are produced by topoisomerase II (Topo II). Paradoxically, Topo II has also recently been linked with preventing mutagenic DNA repair by illegitimate non-homologous recombination [7]. Therefore, currently the temporal regulation of this process is unclear – i.e. whether initial apoptosis started by Topo II is then interrupted by binding of Rad51 to SSB (shifting Topo II activity from DNA cleavage to religation) or whether the DNA repair by HR fails, releasing Rad51 and thus allowing apoptosis to initiate (via Topo II). Regardless, it seems clear that protection from apoptosis by HR in p53-deficient tumor cells occurs in the chromatin providing these cells with genotoxic resistance and increased mutagenicity, thus promoting tumor progression.

V. CONCLUSION

A restriction in binding of Rad51 recombinase to γ -H2AX HR repair foci was observed in S-phase in p53 wt TK6 lymphoma cells, compared to the p53 mutated counterpart WI-L2-NS. The inability to stably bind Rad51 leads to a visible relaxation of the DNA resulting in the multiplication and fusion of γ -H2AX domains in early apoptotic chromatin. These data indicate that prevention of apoptosis in p53-deficient tumor cells occurs through HR at the level of the chromatin.

VI. ACKNOWLEDGMENT

Grant 05.1634 and 05.1634.1 of the Latvian Scientific Council supported this research in Riga, the exchange visit grant of the Royal Society of London and Cancer Research Foundation, in Southampton and Manchester, UK.

VII. REFERENCES

1. Raderschall E, Bazarov A, Cao J et al (2002) Formation of higher-order nuclear Rad51 structures is functionally linked to p21 expression and protection from DNA damage-induced apoptosis. *J Cell Sci* 115:153-164
2. Ivanov A, Cragg MS, Erenpreisa J et al (2003) Endopolyploid cells produced after severe genotoxic damage have the potential to repair DNA double strand breaks. *J Cell Sci* 116: 4095-4106
3. Paull T, Rogakou EP, Yamazaki V, Kirchgessner CU et al (2000) A critical role for histone H2AX in recruitment of repair factors to nuclear foci after DNA damage. *Curr Biol* 10 886-893
4. Xia F, Amundson SA, Nickoloff JA et al (1994) Different capacities for recombination in closely related human lymphoblastoid cell lines with different mutational responses to X-irradiation. *Mol Cell Biol* 14:5850-5857
5. Pfander B, Moldovan GL, Sacher M et al (2005) SUMO-modified PCNA recruits Srs2 to prevent recombination during S phase. *Nature* 436:428-433
6. Rogakou EP, Nieves-Neira W, Boon C et al (2000) Initiation of DNA fragmentation during apoptosis induces phosphorylation of H2AX histone at serine 139. *J Biol Chem* 275:9390-9395
7. Umanskaya ON, Lebedeva SS, Gavrilov AA et al (2006) Inhibition of DNA topoisomerase II may trigger illegitimate recombination in living cells: experiments with a model system. *J Cell Biochem* 99:598-608

Author: Jekaterina Erenpreisa
Institute: Latvian Biomedicine Centre
Street: Ratsupites 1
City: Riga
Country: Latvia
Email: katrina@biomed.lu.lv

Chapter 8

**Endopolyploid cells resulting from irradiated p53
deficient tumours display long-lasting mitotic
potential and active Aurora B - kinase.**

**Erenpreisa J, Ivanov A, Wheatley SP, Kosmacek EA, Ianzini F, Anisimov AP,
Mackey M, Davis P, Plakhins G, Illidge TM.**

Cell Biol Int. In press.

Endopolyploidy in irradiated p53-deficient tumour cell lines: Persistence of cell division activity in giant cells expressing Aurora-B kinase

Jekaterina Erenpreisa^{a,*}, Andrei Ivanov^b, Sally P. Wheatley^c, Elizabeth A. Kosmacek^d,
Fiorenza Ianzini^d, Alim P. Anisimov^c, Michael Mackey^d, Paul J. Davis^d,
Grigorijs Plakhins^a, Timothy M. Illidge^b

^a Latvia Biomedicine Research and Study Centre, Riga, Latvia

^b Paterson Institute for Cancer Research, Manchester, UK

^c Genome Damage and Stability Centre, Sussex University, Brighton, UK

^d University of Iowa, Iowa City, IA, USA

^e Far-East State University, Vladivostok, Russian Federation

Accepted 3 June 2008

Abstract

Recent findings including computerised live imaging suggest that polyploidy cells transiently emerging after severe genotoxic stress (and named 'endopolyploid cells') may have a role in tumour regrowth after anti-cancer treatment. Until now, mostly the factors enabling metaphase were studied in them. Here we investigate the mitotic activities and the role of Aurora-B, in view of potential depolyploidisation of these cells, because Aurora-B kinase is responsible for coordination and completion of mitosis. We observed that endopolyploid giant cells are formed via different means in irradiated p53 tumours, by: (1) division/fusion of daughter cells creating early multi-nucleated cells; (2) asynchronous division/fusion of sub-nuclei of these multi-nucleated cells; (3) a series of polyploidising mitoses reverting replicative interphase from aborted metaphase and forming giant cells with a single nucleus; (4) micronucleation of arrested metaphases enclosing genomic fragments; or (5) incomplete division in the multi-polar mitoses forming late multi-nucleated giant cells. We also observed that these activities can release para-diploid cells, although infrequently. While apoptosis typically occurs after a substantial delay in these cells, we also found that ~2% of the endopolyploid cells evade apoptosis and senescence arrest and continue some form of mitotic activity. We describe here that catalytically active Aurora-B kinase is expressed in the nuclei of many endopolyploid cells in interphase, as well as being present at the centromeres, mitotic spindle and cleavage furrow during their attempted mitoses. The totally micronucleated giant cells (containing sub-genomic fragments in multiple micronuclei) represented only the minor fraction which failed to undergo mitosis, and Aurora-B was absent from it. These observations suggest that most endopolyploid tumour cells are not reproductively inert and that Aurora-B may contribute to the establishment of resistant tumours post-irradiation.

© 2008 International Federation for Cell Biology. Published by Elsevier Ltd. All rights reserved.

Keywords: Mitotic catastrophe; Tumours; Polyploidy; Aurora-B kinase

1. Introduction

The application of genotoxic insults including irradiation is an established method of treatment of malignant tumours. Tumours lacking functional p53 are defective in many cell cycle

checkpoints and often respond to genotoxic stress by undergoing mitotic catastrophe (MC). Although MC is defined as "cell death occurring during or shortly after a failed mitosis" (Kroemer et al., 2005; Galluzzi et al., 2007), p53-deficient tumours undergoing MC are resistant to genotoxic treatments. As a result of mitotic failure, cells alternatively reset interphase becoming tetraploid (Castedo et al., 2004a,b). Therefore, MC has also been defined as mitotic events that produce tetraploid progeny cells in the first post-damage

* Corresponding author.

E-mail address: katrina@biomed.lu.lv (J. Erenpreisa).

generation (Andreassen et al., 2001). p53 mutant tumour cells that have incurred genotoxic stress and become tetraploid can continue endoreplication and achieve DNA content from 8C to 64C (Illidge et al., 2000; Chu et al., 2004). Association of genotoxic resistance with the induced endopolyploidy was found in rodent and human tumours (Baroja et al., 1998; Come et al., 1999). Our earlier observations revealed that transient endopolyploid p53-Burkitt lymphoma cells were able to facilitate DNA repair and release para-diploid mitotic progeny post-irradiation (Erenpreisa et al., 2000; Illidge et al., 2000; Ivanov et al., 2003). These observations led us to hypothesise that transient endopolyploid cells, which are capable of depolyploidisation, may in fact constitute an alternative survival pathway (Erenpreisa and Cragg, 2001, 2007). Similarly, de la Hoz and Baroja (1993) and Baroja et al. (1996, 1998) reported that rodent tumour cells of high ploidy are capable of proliferating, despite certain peculiarities in their cell cycle. Using computerised live imaging, Ianzini and Mackey (2002) have demonstrated that a small proportion of endopolyploid cells formed *in vitro* post-mitotic catastrophe successfully undergo polyploidy reduction and form viable clones. Priour-Carrillo et al. (2003) found that ~2% of human bladder carcinoma giant cells formed after irradiation release potentially clonogenic 2N progeny. Stewenius et al. (2005) showed that events of mitotic catastrophe in colorectal cancer are compatible with survival, and underlined the role of anaphase bridged mitoses in clonogenic growth. Furthermore, the striking live-imaging studies of Chu et al. (2004) on CDKN1A-deficient cells (CDKN1A is up-regulated by the tumour suppressor p53 controlling G1/S checkpoint) have clearly shown the viability of the endopolyploid cells produced by multiple mitotic catastrophe events. These authors concluded that MC is not directly responsible for individual cell death. Similar observations were made and reviewed by Rajaraman et al. (2006).

These intriguing reports underscore the importance to study further the division potential of endopolyploid cells in p53-deficient tumours. Although the presence of high ploidy cells in malignant tumours has long been documented (Baroja et al., 1998), their biological significance is not well understood, with much controversy persisting over their proliferative potential. However, if as a result of genotoxic treatment, genetically unstable giant cells can give rise even to a few selected clones, these might be genetically changed, promoting resistant regrowth and further tumour progression. Therefore detailed study of the mechanisms of the reproductive/apoptotic behaviour of giant cells is important.

We have investigated the reproductive activities of endopolyploid cells post-irradiation in p53 defective human cell lines through the involvement of Aurora-B kinase, the essential regulator of mitosis (Carmena and Earnshaw, 2003; Vagnarelli and Earnshaw, 2004). Aurora-B belongs to the group of mitosis regulators called “chromosome passengers”. Within this group, Aurora-B kinase provides for fidelity and procession of mitosis by coordinating chromosome alignment onto metaphase spindle with anaphase and cytotomy (Ditchfield et al., 2003). The easily recognisable immunocytochemical markers of its presence are the attachment of Aurora-B to

centromeres in metaphase plate, to microtubules of the central mitotic spindle during anaphase B and participation in the formation of the mid-body in ana-telophase. The mid-body is marked by the two bands of Aurora-B and two lateral bands of tubulin. In immunofluorescent staining for the two proteins, these two-coloured bands and a central split in the mature mid-body (the place of the centriolin ring) assign the whole structure its unique appearance. While the main events of mitosis occur within 1 h, the mid-body, which is responsible for cytotomy completion, persists in the cytoplasmic bridge between daughter cells for 2+ hours longer (Gromley et al., 2005). Thus the mid-body represents a characteristic marker of the process of mitosis. Our data reveal that catalytically active Aurora-B kinase is intimately associated with the formation, division, and extended survival of endopolyploid cells resulting from MC in functionally p53-deficient tumour cell lines.

2. Methods

2.1. Cell lines

Namalwa Burkitt's lymphoma cells (ATCC) were grown as suspension cultures in RPMI 1640 medium, 10% foetal calf serum (Gibco or Sigma) at 37 °C in a 5% CO₂ in air humidified incubator. HeLa S3 cells (ATCC) were grown either in suspension culture or as adherent clone 3. Suspension HeLa culture was grown under constant rotation in Joklik's MEM media containing 10% heat-inactivated calf serum (Hyclone) and antibiotics. Suspension cultures were maintained in log phase of growth for at least 24 h prior to irradiation. Namalwa cells were further cultivated by replenishing culture medium every 48–72 h, and HeLa S3 every 24 h.

HeLa adherent clone 3 cells were grown as monolayer in F-10 medium (Hyclone) containing 10% heat-inactivated foetal calf serum (Sigma or Hyclone) and antibiotics (100× penicillin–streptomycin, Sigma P4333) in a 37 °C incubator supplied with 5% CO₂ in air, either on 13 mm polylysine-coated coverglasses in 24× wells, for immunocytochemistry and DNA cytometry or in a T-25 tissue culture flasks for live-imaging.

To determine the cells in S-phase, BrdU was added at 10 µg/ml to the cell culture for 60 min prior to cell fixation on slides with methanol. DNA denaturation was performed by 2 N HCl, 37 °C for 20 min. After washes in PBS, the primary and secondary antibodies were applied (Table 1). In some experiments, proteasome inhibitors (Sigma) Mg-132 (5 µg/ml), inhibitor of calpain (25 µg/ml), and lactocystin (10 µg/ml) were added for 2 h prior to cell harvest. Autophagic vacuoles were detected by monodansylcadaverin (MDC) and by Sa-β-galactosidase. For MDC (Sigma) staining the cultures were incubated with 0.05 mM MDC at 37 °C for 60 min followed by fixation in 4% paraformaldehyde, washing twice in PBS. The slides were mounted into Perm Mount and immediately scored in the DAPI channel. For Sa-β-galactosidase detection, the instruction of the Sigma kit (Code CS0030) was followed (staining was extended overnight).

Table 1
Antibodies: Source and usage

Primary antibodies against:	Secondary antibodies
Aurora-B-kinase polyclonal in a rabbit (Abcam, ab2254), 1:300	Goat a-rabbit-IgG-Alexa Fluor 480 or 594 (Invitrogen) 1:400
α -tubulin mouse monoclonal (Sigma, B-512) 1:2,000	Goat a-mouse IgG-Alexa Fluor 480 or 594 (Invitrogen) 1:400
β -tubulin mouse monoclonal (Neomarkers; clone DM1B) 1:100	Goat a-mouse IgG-Alexa Fluor 480 (Invitrogen) 1:400
Cyclin B mouse monoclonal (SC-245; Santa Cruz Biotech) 1:50	Goat a-mouse IgG-Alexa Fluor 480 or 594 (Invitrogen) 1:400
Human-anti-centromere/kinetochore (Antibodies Inc: 15–234), 1:100	Sheep a-h-IgG-FITC (Dr. M.S. Cragg) 1:50
Lamin B, goat polyclonal (Santa Cruz Biotech), 1:50	Donkey a-goat IgG-Alexa Fluor 594 (Invitrogen) 1:400
Active caspase-3 rabbit polyclonal (Promega, G7481) 1:50	Goat a-rabbit- IgG-Alexa Fluor 594 (Invitrogen) 1:400
phospho-H3 ^{ser10} rabbit polyclonal (Santa Cruz Biotech.) 1:300	Goat a-rabbit- IgG-Alexa Fluor 480 or 594 (Invitrogen) 1:400
Bromodeoxyuridine (BdU) mouse monoclonal (Invitrogen) 1:200	Goat a-mouse IgG-Alexa Fluor 480 (Invitrogen) 1:400

2.2. Irradiation

Irradiation for live imaging at the University of Iowa was delivered at room temperature using a PANTAK Bipolar 2HF320 irradiator (200 kV, 0.35 Cu/1.5 Al filter). Dosimetry was performed using a Victoreen electroscope at a dose rate of 1.27 Gy/min. *In vitro* cell culture irradiation was applied using a Gulmay D3 225 X-ray source at a dose rate of 0.77 Gy/min. A single dose of 10 Gy was delivered in all experiments.

2.3. LSDCAS imaging analysis

Large-Scale Digital Cell Analysis System (LSDCAS), a live imaging and analysis system that includes quantitative cell analysis software, is amenable to determine the kinetics of various cellular mechanisms on a cell-by-cell basis (Janzini and Mackey, 2002; Davis et al., 2007). For live imaging, HeLa adherent clone 3 cells were maintained for irradiation by the scheme described above. Two days prior to irradiation, 1×10^5 cells were plated as a cell suspension and placed into the CO₂ incubator. After irradiation, the cells were re-incubated for 2 h, at which time an equal volume of fresh, complete and warmed media was added prior to the flask being positioned on to the LSDCAS stage for imaging acquisition for 72 h. One hundred random fields were manually chosen. Division-related events were categorised as follows: normal, normal followed by cleavage regression (sister cells fusion), and unrelated cell fusion (non-sister cell fusion). The number of cells alive at the end of the experiment was also counted.

2.4. Immunofluorescent (IF) staining

Suspension cells were pelleted, resuspended in FCS and cytospun on to polylysine-coated slides. Cultures on cover-glasses were rinsed before fixation in PBS and FCS. Cells were allowed to dry for 1 min (drying was not done when tubulins were being detected) and were fixed at -20°C in methanol followed by 5–10 short rinses in cold acetone or methanol/acetone (1:1) at -20°C . A 1 min rinse in 70% methanol and several in PBS followed, after which blocking in 1% bovine serum albumin in PBS (for some stains adding 0.01–0.05% Tween-20) was performed for 15 min. Application of the primary antibody and further manipulations were done in

the usual routine manner (antibodies listed in Table 1). Post-staining was performed with propidium iodide (5 $\mu\text{g}/\text{ml}$), DAPI (1 $\mu\text{g}/\text{ml}$) or 1 $\mu\text{g}/\text{ml}$ of amino actinomycin (7-AAD). Cells were finally embedded in Prolong Gold (Invitrogen).

2.5. DNA image cytometry

For DNA in situ cytometry, cells were fixed in ethanol/acetone (1:1, v/v) for 30 min at room temperature and stained with by modified Feulgen reaction using toluidine blue. Images were taken with a Leitz Ergolux L03-10 microscope equipped with a calibrated Sony DXC 390P colour video camera. DNA content was measured as the integral optical density in the green channel or in the red channel with interference filter 289 nm, using Image Pro Plus 4.1 software (Media Cybernetics; REO 2001, Riga, Latvia). The stoichiometry of DNA staining was verified using the values obtained for metaphases compared to anaphases and telophases (ratio 2.0); arbitrary diploid (2C) DNA values were averaged from measuring 50 anaphases in non-treated tumour cells. The device error was estimated at 0.5%. The variation coefficient for DNA content was also assessed in normal human lymphocytes where it was determined as being in the range 2–5%, while for HeLa mitotic cells it reached 20%.

2.6. Fluorescent in situ hybridisation (FISH)

HeLa cells were harvested, treated with 75 mM KCl at room temperature for 10 min and fixed with five changes of methanol/glacial acetic acid (3:1). The suspension was dropped onto slides and allowed to dry. Satellite probes for chromosomes 10 and X were used in the kits provided by Molecular Cytogenetics (Q-BIOgene) by the applied instruction. These chromosomes were chosen as containing three normal copies and not participating in clonal markers (Macville et al., 1999). The number of labels per individual nuclei was counted. The results were grouped as normal (three labels) and abnormal (all other counts) and compared in pairs by Fisher's Exact Test (<http://www.matforsk.no/ola/fisher.htm>).

2.7. Fluorescent, bright field, and confocal microscopy

For these images, a Leica confocal laser microscope DM 600 and a Leitz Ergolux L03-10 microscope were used.

3. Results

3.1. Irradiation causes anaphase bridging and bi-nucleation

Irradiation (10 Gy dose) induces a G2 arrest that persists for 8–10 h in HeLa cells. Cells then enter mitosis displaying elevated mitotic indices of 10–11% at 24 h and 15% at 48 h. About 25% of metaphases in HeLa become arrested and many of them reconstitute interphase as micronucleated (many small nuclear vesicles enclosing separate chromosomes or their groups) or mono-nucleated polyploidy cells. However, the majority of irradiated HeLa cells proceed through anaphase. About 70% of all HeLa cells in the first mitosis at 19–24 h and 96% of cells in the second mitosis at 42–48 h display anaphase bridges due to dicentric chromosomes (checked by CREST-immunoserum staining for centromere proteins), compared to 2–5% in controls. As a result, 40% of cells become bi-nucleate on day 1 post-irradiation. Live-imaging confirmed that mitotic cleavage furrow regression between nuclei-bridged daughter cells was responsible for the initiation of bi-nuclearity in these cells, as 82.2% of daughter cells fused ($n = 107$), of which 96.7% were still alive at the end of the 3-day filming session (Fig. 1 and Table 2). The nuclei of the bridged post-mitotic daughter cells often display irregular contours and/or contain in addition a few micronuclei;

Table 2

Results of computed live imaging

Analysed cells that divide normally in 72 h	16.6% (107/645)
Analysed cells that divide normally and then fuse	82.2% (88/107)
Cells that divide, then fuse and live to the end of the movie	96.7% (85/88)
Non-sister cell fusions in 72 h	3% (20/645)

however, as judged by DNA image cytometry, segregation was mostly equal (Fig. 2a–c.e.f). FISH studies using pericentromeric probes for chromosomes X and 10, which do not participate in HeLa clonal markers, showed that a small proportion of nuclei (5%) aneusomic by these chromosomes was present in the control population, which increased to 15% after the first cell cycles in irradiated samples (Table 3). A second smaller wave of bridged anaphases appeared 3 days post-irradiation, with increased bi-nucleation following 24 h later.

Irradiated Namalwa cells arrest in G2 for 24 h, start aberrant mitoses from day 2, which are mostly arrested in metaphase, giving an increased mitotic index on days 3–4 (Ivanov et al., 2003). Contrary to HeLa cells, which mostly pass anaphase and form bi- and multi-nucleated giant cells (MNGC), the later contain three or more nuclei. The majority of Namalwa cells reconstitute the arrested metaphases as mononucleated giant cells (MONGC).

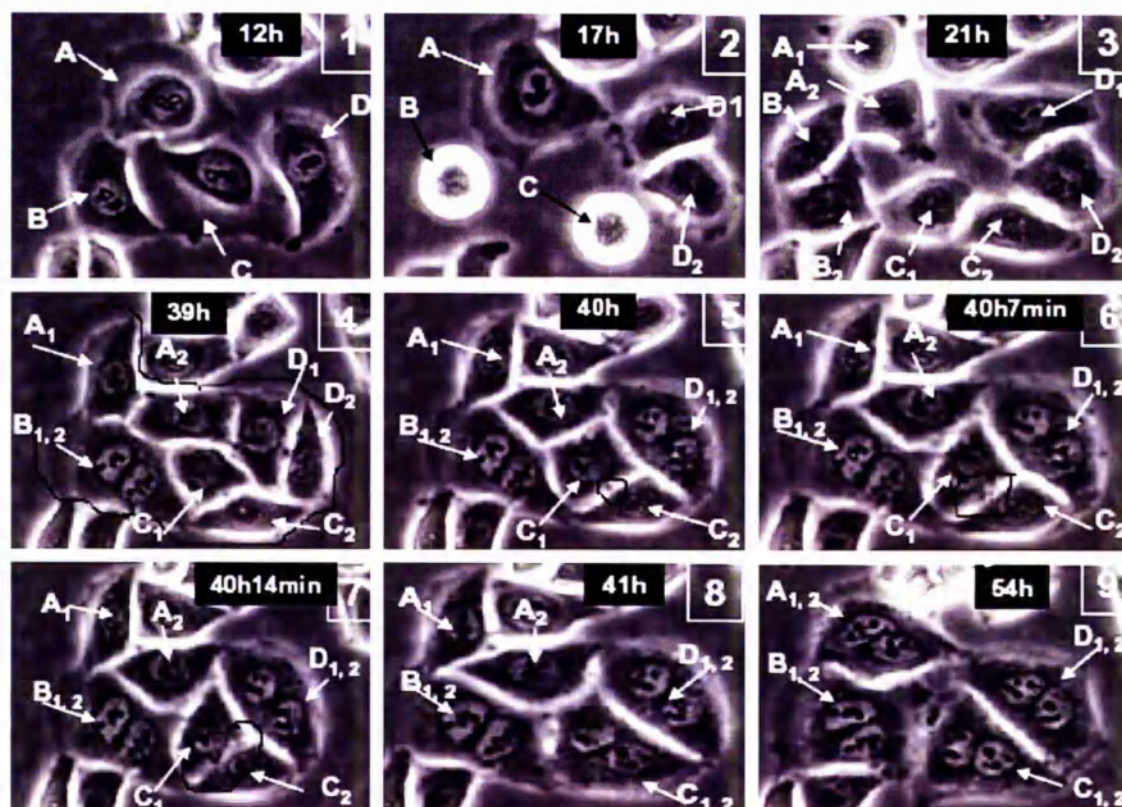


Fig. 1. A series of images of irradiated HeLa cells in LINDCAS system starting live-imaging 12 h post-irradiation. Four cells (A–D) divide remaining connected by nuclear bridges and then each daughter pair regresses a cleavage furrow forming a bi-nucleate cell.

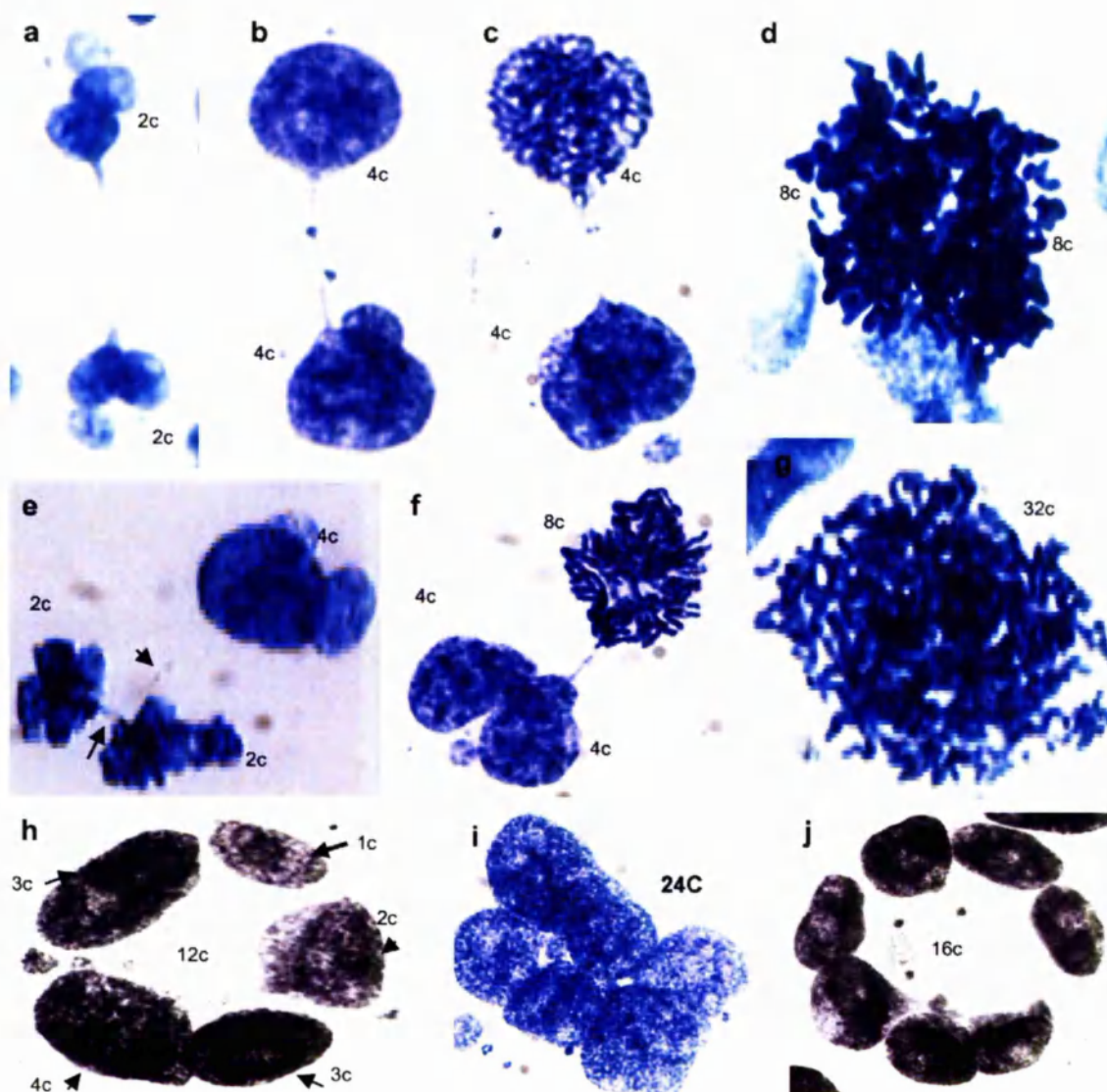


Fig. 2. Characteristic patterns of the DNA cytometry images of HeLa cells. (a–c,e,f) DNA bridges arising from bipolar mitoses in the first three days post-irradiation. (d) Synchronous divisions of two sub-nuclei in bi-nucleate cells. (h–j) Late multi-nuclear cells on days 6–9 with circularly arranged sub-nuclei. “2c” DNA content is an arbitrary value which corresponds to average of 50 anaphase halves in the control non-irradiated cells.

3.2. Aurora-B localises normally in cells during the first division events post-irradiation

During mitosis in untreated tumour cells, Aurora-B kinase localises sequentially to the centromeres, spindle mid-zone

and equatorial cortex, and the mid-body (Fig. 3a and c). Despite the clear presence of bridged chromosomes in irradiated cells (Fig. 2a and b), Aurora-B kinase localised normally and the microtubules forming the mitotic spindle, the anaphase mid-zone, and the mid-body, were organised correctly (Fig. 3b and c). However, some of these cells showed additional diffuse staining in the cytoplasm (Fig. 3b).

3.3. Polyploidy doubles with a periodicity of one generation time

After the second round of mitosis (day 2) the frequency of bi-nucleate cells (4C) fell in HeLa cells from 40% to 20%. However, the incidence of MNGC increased from 10% to ~70%, with most multi-nucleated cells containing eight chromosome

Table 3

Statistical results of studies of aneusomy by FISH reaction for pericentromeric probes of chromosomes X and 10 in HeLa cell nuclei, in control and 48 h after irradiation

Samples	Chr #X		Chr #10	
	Control	48 h	Control	48 h
Number of normal nuclei (3 labels)	577	450	637	667
Number of abnormal nuclei	28	69	35	101
% Abnormal (aneusomic) nuclei	4.85	15	5.5	15
Fisher Exact Test, <i>p</i> -value	<i>p</i> < 0.001		<i>p</i> < 0.001	

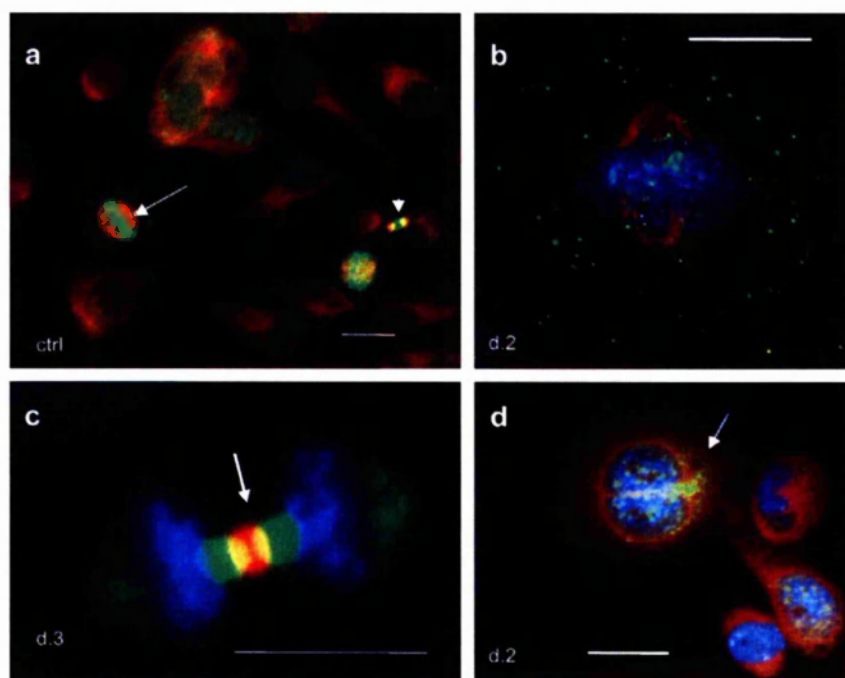


Fig. 3. Aur B/ α -tubulin/DNA cellular localisation in the first mitotic activities of HeLa cells. (a) Non-treated control: in metaphase Aur B is equatorially attached to centrosomes (arrow); a mid-body connecting post-telophasic sister cells is indicated by arrowhead. (b–d) After irradiation: (b) in metaphase; (c) a proper mid-body in late anaphase; (d) formation of a bi-nuclear cell enclosing mid-body in its cytoplasm (arrow)—a witness of post-anaphasic or post-mitotic re-union of sister nuclei/cells. For a,b,d: Aurora-B green, α -tubulin red, DAPI blue; for c: Aurora-B red, α -tubulin green, DAPI blue. Bars = 20 nm.

sets. Polyploidy increased each day post-damage. By day 4, HeLa cells typically displayed DNA contents of 8C, 16C and 32C corresponding to completion of four polyploidising cycles-phases over the 4-day period (Fig. 4). The proportion of polyploid cells reached 50–60%. Consistent with our previously published results, the same polyploidy limit (32C, occasionally 64C) was exhibited in irradiated Namalwa cells, which also increased in ploidy by a daily doubling (Erenpreisa et al., 2000).

3.4. Asynchronous mitosis occurs in multi-nucleated cells

At 2–4 days post-irradiation, ~30% of HeLa cells were paired with long DNA bridges (Fig. 5a–g) surrounded by

the nuclear envelope and thin layer of cytoplasm, as judged by staining for lamin B and tubulin (Fig. 5f). Frequently the two daughter cells comprising the DNA-bridged pair exhibited a loss in synchrony during their second or third division, such that one daughter nucleus/cell was in mitosis, while the other was in interphase (Fig. 2c,e,f). About 5% of MNGC exhibited asynchronous division of only one of sub-nucleus (Fig. 5a,d,e). The same phenomenon, although at a smaller scale and at later terms, was found in Namalwa (Fig. 5h). These divisions had normal or nearly normal Aurora-B positive mid-bodies, suggesting that elements of mitosis were retained during this event (Fig. 5a–c,g,h). Similar quantities of DNA appeared to be segregating by this asynchronous division, as judged by voxel intensity of the DAPI signal (see Fig. 5d and e). These secondary divisions were also often DNA- and nuclear envelope-bridged (Fig. 5d and f). These apparently symmetric “daughter nuclei” on either side of the bridge suggest that early bi- and multi-nucleated cells have mostly originated from successful previous mitosis followed by fusion of daughter nuclei or cells. This process continued later on a smaller scale, where both asynchronous bipolar mitosis and cytoplasmic mid-bodies were found in multi-nucleate cells (Fig. 5h,i). Synchronous divisions of two sub-nuclei in bi-nucleate cells were rarely observed (Fig. 2d). Totally micronucleate cells, which represented a minority, were Aurora-B-negative (Fig. 6a, arrow); they never entered mitosis and often died (by necrosis). However, some of them, as seen from inclusion of BrdU and increasing size, grew indefinitely solely by endoreplication (data not shown).

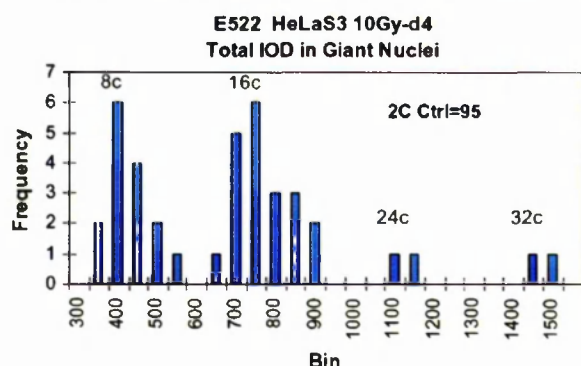


Fig. 4. A histogram of the DNA content in giant HeLa cells on day 4 after irradiation ($n = 110$). It is seen that 8C and 16C cells are in the cell cycle, while 24C and 32C apparently represent the end-point of polyploidisation.

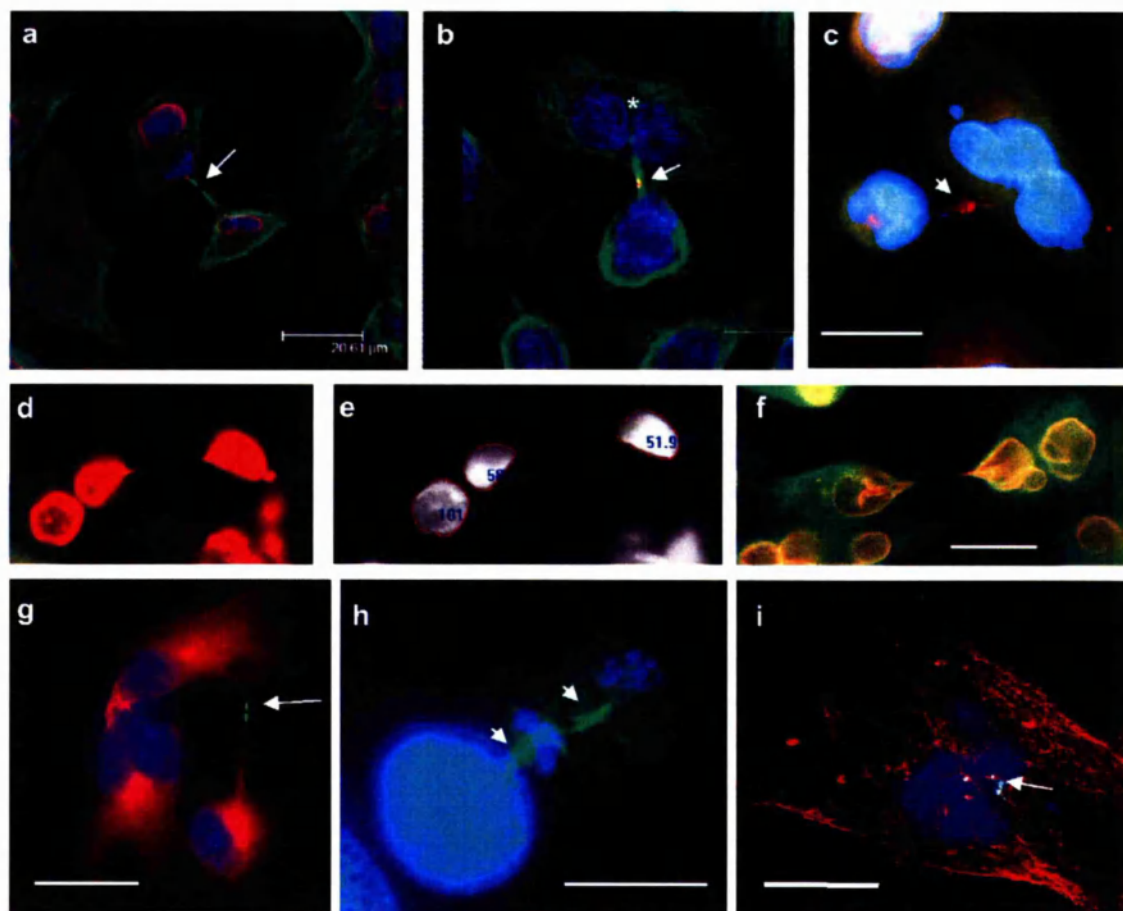


Fig. 5. Asymmetric bipolar divisions of sub-nuclei in multi-nucleated HeLa and Namalwa cells after irradiation: (a–f) Day 2; (g–i) days 4–7. (a,b,f) Lamin B (red)/ α -tubulin (green)/DAPI; (b,c) Aur B (red)/ α -tubulin (green)/DAPI; (g–i) Aur B (green)/ α -tubulin (red)/DAPI; (E) DAPI only, fluorescence intensity measured. The presence of mid-bodies (arrowed) indicates the mitotic character of these divisions. In (a) telophase chromatin figures are outlined by lamin B; (b) after mitotic division of a presumably tetraploid HeLa cell, one of the daughter cell nuclei (asterisk) has further divided amitotically; (c) a multi-lobulated HeLa giant cell is joined with a smaller one by a tubulin bridge with remnant mid-body; (d,e) illustrates an equal division of one of the nuclei in a bi-nuclear cell; (g) a low ploidy HeLa cell is still connected to the high ploidy multi-nuclear cell by a tubulin bridge with a mid-body. This well-shaped mid-body displays a clear central split—the place of the centriolin ring, necessary for the completion of cytokinesis. (h) A sample was collected after 2 h treatment with lactocystin, proteasome inhibitor. In (h) two subsequent asymmetric reduction bipolar divisions of a giant Namalwa cell are seen displaying two persisting mid-bodies. These divisions result in a small ana-telophase. Persistence of the two subsequent mid-bodies and small final mitotic figures suggest that the second division rapidly followed the first, most probably without intermittent S-phase. (i) A mid-body within a multi-nucleate cell—a probable result of the failed cytotomy and reverse of asymmetric mitotic division in a HeLa cell. Bars = 20 μ m.

In summary, the majority of early multi-nucleated HeLa cells (days 1–3) resulted from a series of bipolar mitosis/sister fusion events, with a ~ 10 -fold smaller amount occurring by non-sister fusion of stressed cells, and a minor population by micronucleation of the failed mitosis. The majority of endopolyploid cells ($\sim 70\%$) from irradiated Namalwa were mononucleate.

3.5. Aurora-B kinase is present in MONC and MNGC nuclei but is targeted for degradation

Control cells undergoing mitosis stain positively for Aurora-B. Aurora-B is also present in the nuclei of G2

cells and rare giant cells, albeit far less abundantly than in mitotic cells (Fig. 3a). About 60% of giant cells on days 3–4 post-irradiation display enhanced nuclear positivity for Aurora-B. However, Aurora-B-negative MONG and MNGC cells lacking signs of degradation are also present in the population (Fig. 6b). On day 5 the positive giant cells comprise about 40%, on day 7 only 10%. MONGC sometimes have a very strong karyoplasmic reaction for Aurora-B (Fig. 6a). Expression of Aurora-B in the interphase nuclei of giant cells was much more prevalent after treatment with the proteasome inhibitors, lactocystin, MG132 or inhibitor of calpain (2 h), suggesting that Aurora-B is normally targeted for proteasome-mediated degradation when present in the nucleus (Fig. 6d and e).

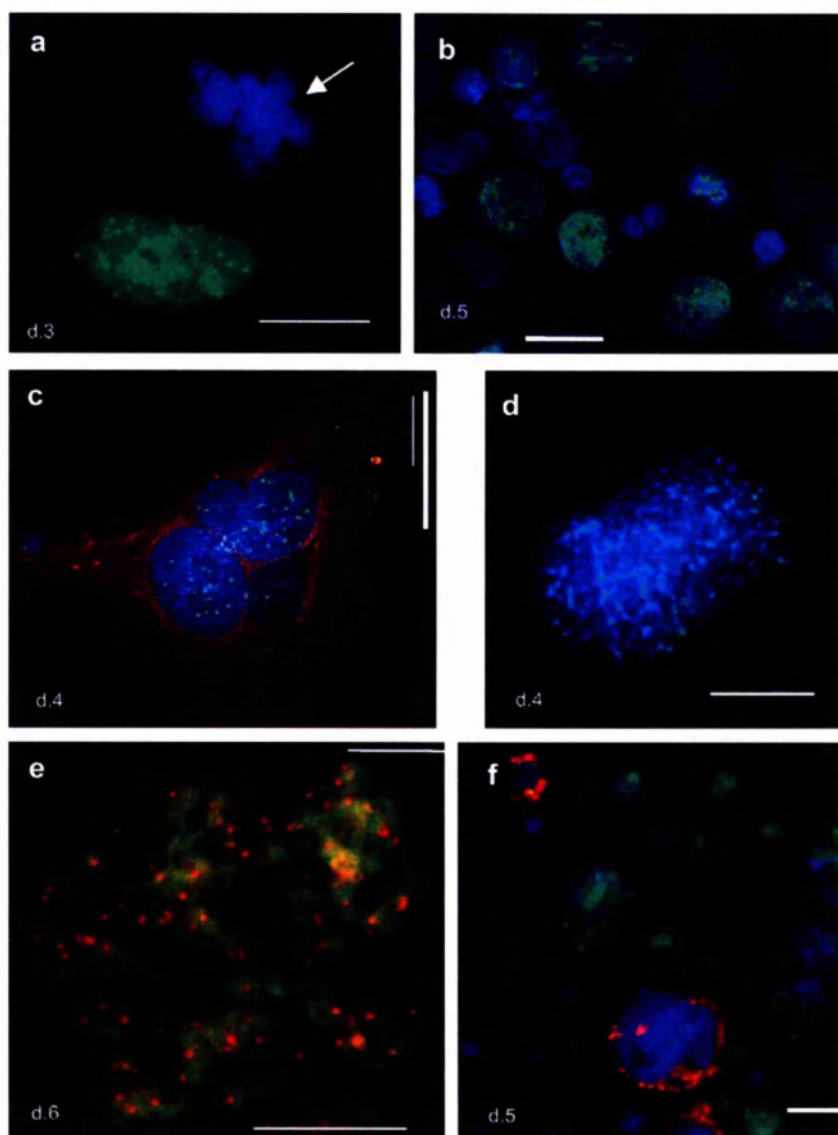


Fig. 6. Distribution of Aurora-B kinase in and among irradiated cells. (a) Strongly positive MONGC; however, always negative micronucleated HeLa cells (arrow). (b) A proportion of cells with Aurora-B-positive nuclei in Namalwa. (c) A positive MNGC of HeLa (green for Aurora, counterstained with red for α -tubulin). (d) Thin dotted arrays of Aurora-B (green) in the chromatin of the nucleus reconstituting from the arrested polyploid metaphase: fixed 2 h after application of Mg-132. (e) A rare finding: clear Aurora-B dots over minimally condensed preprophasic chromosomes; red for Aurora-B, green a false colour for overexposed DAPI. (f) Annexin-positive dying cells (red) are negative for Aurora-B kinase (Namalwa cells). Bars = 20 μ m.

We also noted that Aurora-B was absent from annexin V-positive apoptotic cells (Fig. 6f), but again its expression could be rescued by the application of proteasome inhibitors (not shown).

Since Aurora-B is generally considered a mitotic kinase, and its activity is stimulated primarily by its mitotic partner protein, inner centromere protein INCENP (Adams et al., 2001), we studied the co-localisation of Aurora-B with centromere proteins by CREST immunoserum (Fig. 7a–c). In metaphase plates of control cells Aurora-B co-localises with individual centromeres (Fig. 7a). After irradiation, the majority of Aurora-B-rich nuclei of giant cells contain one large central nucleolus and clustered centromeres. Aurora-

B-positive nuclear foci in giant interphase cells rarely co-localise fully with individual centromeres (Fig. 7b), but rather are found as larger patches in centromere clusters, mostly in the perinucleolar heterochromatin, in chromocentres, and at the nuclear envelope in some cells (Fig. 7c,d). To test whether Aurora-B present in giant interphase nuclei was active, we used the immunoprobe for phospho-H3^{ser10}, a specific substrate of Aurora-B kinase. Some giant cell nuclei contained speckles of phosphorylated histone H3, mostly around their nucleoli (Fig. 7e). However, giant aberrant metaphases were extensively positive for phosphorylated histone H3, indicating a high level of Aurora-B kinase activity (Fig. 7f).

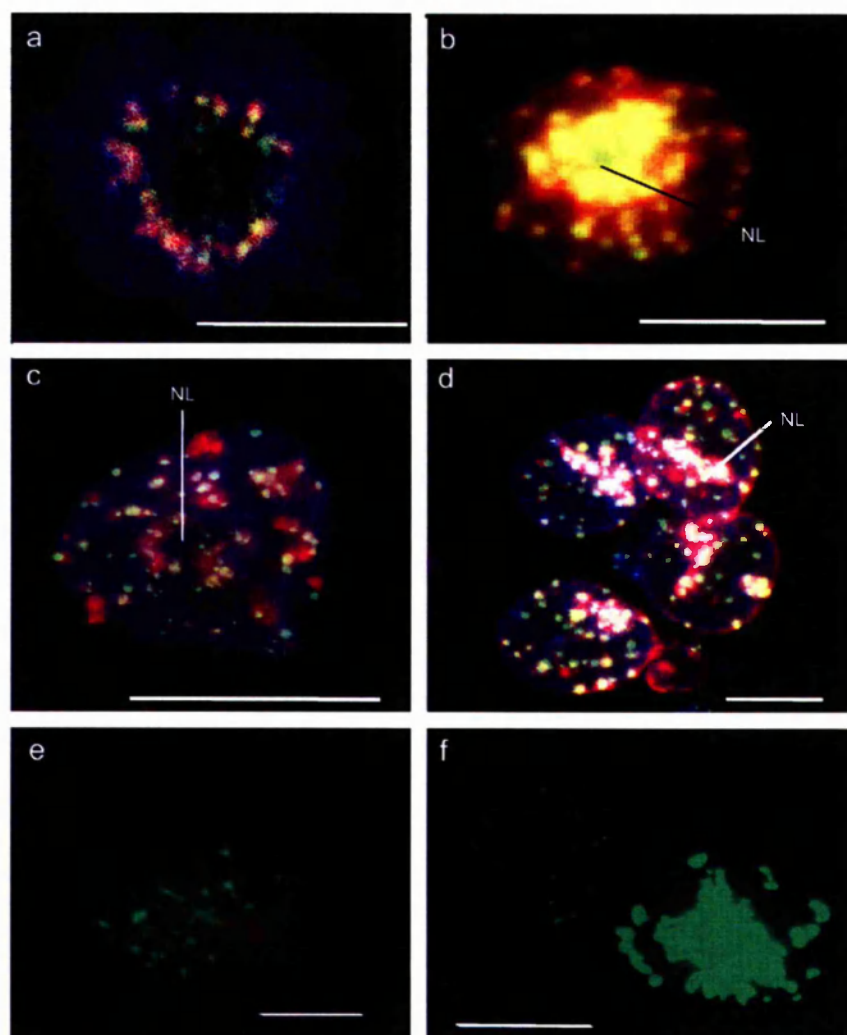


Fig. 7. Specific activities of Aurora-B kinase in polyloid tumour cells after irradiation. (a) In control, foci of Aurora-B (Alexa, red) co-localise with kinetochores (FITC, green) in the metaphase plate (DAPI); (b–f) After irradiation. (b) nearly full co-localisation of Aurora-B and kinetochores, especially heavy around central nucleolus (NL) in the interphase cell, presumably G2; DAPI channel is not overlaid; (c) large patches of Aurora-B at centromere clusters and chains in a late giant cell; (d) heavy precipitation of Aurora-B onto the centromeres around nucleoli (NL), tendency of co-localisation at the nuclear envelope; however, absence of co-localisation in most centromeres inside the nuclei; (e,f) IF for substrate of Aurora-B phosphorylation phospho-H3^{ser10} (green) in interphase and mitotic giant cells shows catalytical activity of kinase. This activity is very high in the numerous polyloid aberrant mitoses arrested at this stage (on day 4 post-irradiation) in metaphase; one of them is seen in (f). (a–d) Sequential scanning by confocal microscope in 3-colour channels. Bars = 20 μ m.

3.6. Multi-polar mitoses and formation of late multi-nucleated cells

A small proportion of HeLa cells undergo tripolar mitoses in the first days post-irradiation, which show Aurora-B kinase-positive mid-body with three spindle twigs (Fig. 8a). These cells often complete division into three daughters (not shown). However, the majority of multi-polar mitoses in giant cells which they attempt before day 5 become arrested in metaphase showing clumped, poorly condensed, often partially polytenised chromosomes (Fig. 8b). In metaphase arrested cells, Aurora-B-kinase is often found both on the chromosomes and in the cytoplasm. Massive apoptosis observed around days 5–6 closely follows this period in both cell lines, as determined

by cell morphology and caspase 3 activity (not shown), involving ~30% of giant HeLa cells and up to 80–90% of giant Namalwa cells, as reported previously (Illidge et al., 2000; Ivanov et al., 2003). In the survivors, occasionally from day 5–6 and then more frequently from day 10 post-irradiation, MNGC and MOGC underwent true endomitosis (as initially defined by Geitler (1937)). In these cells, individual chromosomes were condensed, but the nuclear envelope and nucleoli remained intact. Despite the absence of nuclear envelope breakdown, Aurora-B strongly accumulated at these endomitotic chromosomes (Fig. 8c). At the same late period, Aurora-B was concentrated on metaphase centromeres of well condensed chromosomes in a number of multi-polar mitoses (Fig. 8d) and on the central spindles

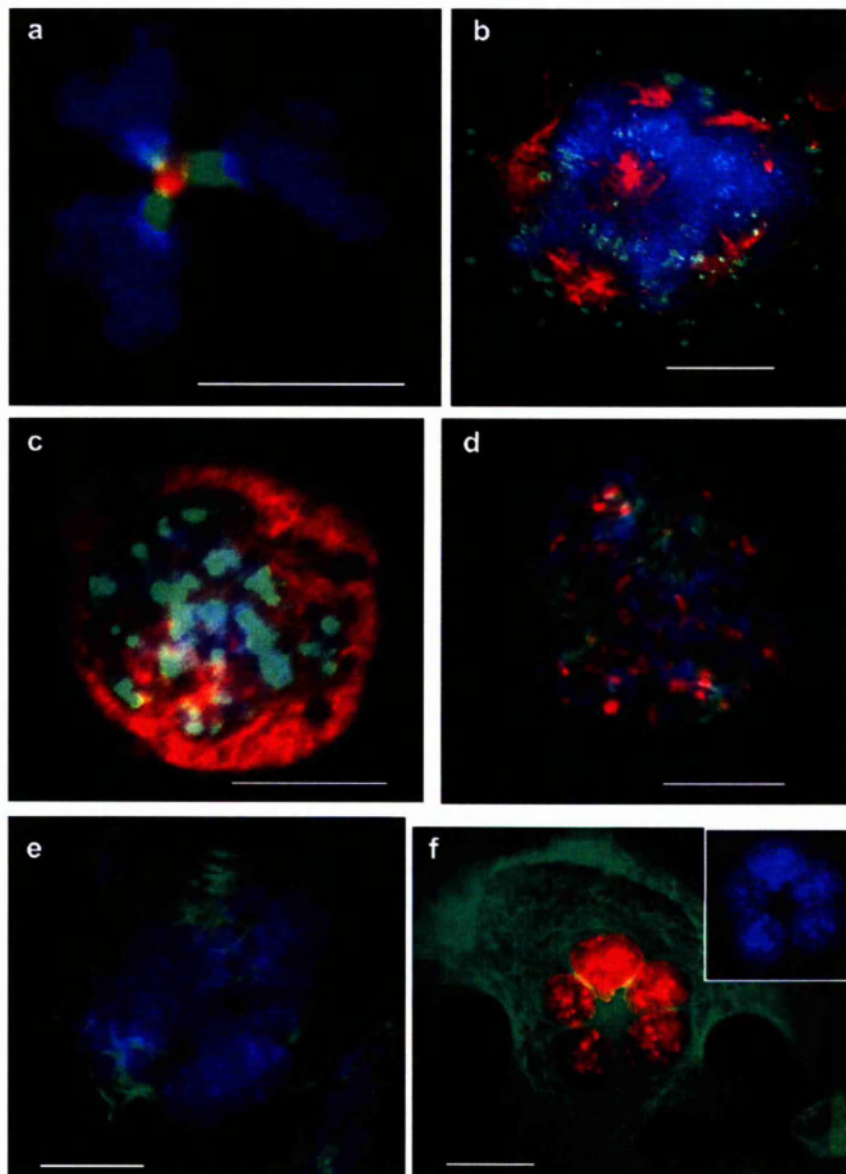


Fig. 8. Multi-polar mitoses in irradiated samples. (a) Clear central mid-body, Aurora-B (red) and α -tubulin (green) in a tri-twigged spindle. However, telophase nuclei (DAPI) possess very irregular contours. (b) Arrested multi-polar metaphase: α -tubulin revealing poles is red, Aurora-B (green) is poorly attached to chromosomes (blue), which are not sufficiently condensed and seem polytenised. (c) True endomitosis with condensed chromosomes (DAPI) and Aurora-B richly bound to them. Aurora-B (green), α -tubulin (red). (d, e) The cells were fixed 2 h after application of the calpain inhibitor. (d) A tripolar metaphase, chromosomes are well condensed and Aurora-B (red) is richly attached to them; α -tubulin of the poles is green. (e) Three spindles are seen decorated in their central part with the tandemly arranged Aurora-B-positive grains (green; tubulins were not stained), while DAPI reveals several anaphase figures. (f) Radial arrangement of the equal-sized Aurora-B-immunopositive (red) nuclei in the large adherent HeLa cell with active microtubular skeleton (green). Inset: the nuclei in DAPI channel. (a) 2, (b) 5, (c–e) 6, and (f) 8 days post-irradiation. Bars = 20 μ m.

of multi-polar (usually tri-polar) anaphase cells (Fig. 8e). Hence, after a series of mitoses aborted in metaphase at the earlier post-irradiation period, these cells attained the capacity to pass a spindle checkpoint and were found segregating their DNA and attempting to cleave cytoplasm into a number of discrete progeny. In most cases, full cytokinesis did not occur and mid-bodies did not form. However, in rarer cells, daughter sub-cells were released tearing (disjoining?) the chromosome bridges, as previously shown (Erenpreisa et al., 2005). The

non-segregated anaphases reverted in a circular or semi-circular arrangement of sub-nuclei at the periphery of giant cytoplasm (Fig. 8f). DNA image cytometry revealed circularly arranged post-mitotic sub-nuclei (Fig. 2h–j), ranging from 1C to 4C (Fig. 2h), often in odd numbers. However, ~60% of these sub-nuclei were para-2C. At later times (1–2 weeks post-irradiation) when regrowth of para-diploid mitotic fraction was renewed, post-mitotic giant cells underwent replicative senescence, as showed by positive staining for

monodansylcadaverine and Sa- β -galactosidase, absence of BrdU inclusion, and Aurora-B negativity (not shown). However, ~10% of late giant cells were Aurora-B positive (Fig. 8f) and also labelled for BrdU and cyclin B (not shown), indicating that they remained in an active cell cycle during at least 2 weeks of observation. These data demonstrate that active Aurora-B may contribute to the long-lasting reproductive capacity of endopolyploid cells.

The reproducible schedule of main reproductive activities of the two cell lines after genotoxic insult is summarised in Table 4. Although there are some differences, the main timing of events is similar in all of them.

4. Discussion

In developmental systems, endopolyploidy is usually a terminal point of cell differentiation (Nagl, 1978). In *Drosophila* metamorphosis salivary glands, the giant polytenic cells cycle only between G1 and S phase, with the down-regulated activity of mitotic cyclin kinase complex (Edgar and Orr-Weaver, 2001). However, in contrast to the absence of mitotic activity *Drosophila*, we have demonstrated that p53-deficient giant tumour cells formed by MC undergo ongoing mitosis. Firstly, we observed that endopolyploid giant cells are formed in irradiated p53 tumours as a result of aberrant mitotic activities in several ways, by: (1) division/fusion of daughter cells creating early MNGC; (2) asynchronous division/fusion of sub-nuclei of these multi-nucleated cells; (3) a series of polyploidising mitoses resetting replicative interphase from arrested metaphase and forming MONGC; (4) micronucleation of arrested metaphases; or (5) incomplete division in the multi-polar mitoses forming late MNGC. We also observed that these activities are able to albeit infrequently release para-diploid cells. Some of those descendants are likely to initiate a further round

of MC. All these events are displayed after genotoxic stress in a reproducible sequence extended for 1–2 weeks (summarised in Table 4). In brief, in the first period there are aberrant mitoses, mostly bridged, followed in the second phase (day 3–5) by the production of increasingly large polyploid cells, mostly due to metaphase arrest of polyploidising mitoses. This is followed in the third phase (day 5–6) by segregation by multi-polar anaphases, and in the fourth, from day 7, regrowth of paradiploid clones commences. Within our tumour model the events that occur between days 5 and 6 are a critical period, when the cells shift from the formation of increasingly large polyploid cells to the breakdown of these large polyploid cells and the start of an apoptotic crisis. Therefore it is worth noting that, preceding this trigger, endopolyploid Namalwa cells are undergoing the delayed wave of recombination repair of DNA double-strand breaks on days 4–5 which protects them from apoptosis (Ivanov et al., 2003). Only 10–20% of giant cells evade apoptosis (Hilidge et al., 2000; Ivanov et al., 2003), and as we have seen in this study, ~10% of those further overcome senescence arrest and continue cyclical mitotic activity. Hence the fraction of potential long-living survivors originating from endopolyploid cells may be 1–2% in this tumour, an estimation that corresponds with the counts obtained by live-imaging analysis in other systems (Prieur-Carrillo et al., 2003). We also found the same reproductive activities involving giant cells in the untreated tumour cell cultures during prolonged cell cultivation (10–20 days), although occurring slowly and to a much smaller proportion and extent.

Secondly, we have shown that 4 of the 5 mechanisms producing endopolyploid cells were marked by the presence of Aurora-B kinase, which localises at centromeres, the anaphase mid-zone, and the mid-body. Moreover, it was present in the interphase nuclei of giant cells, where immunoprobings for phosphor-H3 revealed that it was catalytically active

Table 4
Schedule of the tumour cell reproductive activities following 10 Gy insult

Days after irradiation	HeLa	Namalwa
1	Bridged mitoses/reunion of sister nuclei/cells	Arrest in G2
2	Bi-nucleation, bipolar mitoses of their sub-nuclei forming MNGC (about 70%); metaphase arrests of mono-nucleated cells	Aberrant mitoses, many of them are bridged
3	Bi-polar mitoses of sub-nuclei in bi- and MNGC	Metaphase arrests, emergence of MONGC (about 80%) and MNGC (about 20%)
4–5	<i>A new, smaller wave of bi-nucleation</i> Metaphase arrests of most polyploidy mitoses, increase of polyploidy to 32C; bi-polar mitoses of sub-nuclei in MNGC	Metaphase arrests of polyploidy mitoses, increase of polyploidy to 32C; bi-polar mitoses of sub-nuclei in MNGC
5–6	<i>A new, smaller wave of multi-nucleation^a</i> Major cessation of further polyploidisation, apoptotic crisis, true endomitosis, bi- and multi-polar cell divisions processing anaphase in surviving cells	Major cessation of further polyploidisation, apoptotic crisis, true endomitosis, bi- and multi-polar cell divisions processing anaphase in surviving cells
7–9	Beginning of clonogenic regrowth of small para-diploid cells; cessation of proliferative activities and appearance of senescence markers in the majority of giant cells; continuation of mitotic attempts in the minor fraction of giant cells	Beginning of clonogenic regrowth of small para-diploid cells; cessation of proliferative activities and appearance of senescence markers in the majority of giant cells; continuation of mitotic attempts in the minor fraction of giant cells

^a The second and possibly next waves of polyploidisation were noticed also in later terms.

(supposedly in the G2 state). This activity was particularly high in true endomitotic and giant mitotic cells. During de-polyploidisation stage, aurora-B shifted from centromeres to central spindles in cells starting multi-polar anaphases and occasionally was found as a mid-body in tripolar mitoses undergoing cytotomy. Similarly, association of overexpression of aurora-B with increased proliferative potential of megakaryocytes has been shown in transgenic mice (Zhang et al., 2004) and in polyploid cell formation through aborted mitoses in vascular smooth vessel cells (Nagata et al., 2005), suggesting common mechanisms.

Thus, in line with some previous reports (Baroja et al., 1998; Chu et al., 2004; Stewenius et al., 2005), we herein report that endopolyploid p53-deficient tumour cells are derived by active, yet aberrant mitotic events, and also that the process of ploidy reduction can occur by mitotic mechanisms, although mostly modified. The only exception to this observation are entirely micronucleated cells which lose the ability to enter mitosis (and apoptosis as well) and which in our models represented a minor fraction. There is some evidence and arguments in literature that chromosome bridges in colon cancer do not prevent clonogenic growth, while multi-polar mitoses likely may produce genomically less perspective cells (Stewenius et al., 2005; Gisselson, 2005). However, the interference of recombination and true endomitosis found by us between these events may account for more crucial effects on the genomes than only their simple segregation and needs further studies on different models.

The literature reports that deregulation of Aurora-B kinase, both by overexpression or knock-down, leads to polyploidy (Nguyen and Ravid, 2006). This paradox becomes more understandable in view of the present results showing the necessity of both mitosis and its failure or reverse for the formation of endopolyploid cells.

Overexpression of Aurora-B kinase is characteristic of many tumours correlating with genetic instability, endopolyploidy and aggressive behaviour (Adams et al., 2001; Giet et al., 2005). These characteristics are particularly prevalent in tumours lacking functional p53 or its target (Ditchfield et al., 2003; Hamada et al., 2003). Deregulated Aurora-kinase B is capable of transforming cells *in vitro*. Moreover, the *in vivo* anti-tumour activity of the inhibitors of aurora-kinases has been reported and the question of their use as anti-cancer targets is currently under investigation (Warner et al., 2003; Wilkinson et al., 2007).

5. Conclusions

We have shown that p53-deficient endopolyploid tumour cells are formed mostly as a result of abortive mitoses and that part of these cells retain a long-lasting reproductive potential, crucially supported by the activity of Aurora-B-kinase. These data suggest that endopolyploid cells and Aurora-B kinase may contribute to the formation of genotoxically resistant growth.

Acknowledgments

This work was supported by a grant from the Latvian Scientific Council 05.1634.1, by the scientific exchange grant

between USA and Latvia, and by the grant from the Royal Society allowing exchange visits between Brighton, Manchester and Riga. In Iowa, this work was partly funded by the National Institutes of Health grant 1R33CA94801 and by the Whitaker Foundation Special Opportunity Award. Work in SPW and TMI laboratories has been funded by Cancer Research UK. We acknowledge the work of the undergraduate student of the Latvian University Evgenia Kuznetsova, who assisted in interactive DNA cytometry, FISH staining, counts, and statistics funded by the Latvian Scientific Council. The advice of Prof. Dr M. Hausmann (Heidelberg) on FISH staining technique is also acknowledged.

Authors' contributions

J.E. designed experiments and carried them out cytologically and immunocytochemically in Riga, Iowa, Brighton, and Manchester, and drafted the paper; S.P.W. participated in experimental design, in establishing of some immunocytochemical methods, in microscopy, in the article drafting and editing; E.A.K. maintained in Iowa the HeLa cell culture, helped in the gamma-irradiation, worked at the LSDCAS imaging acquisition, analysed the LSDCAS images, and carried out DNA cytometry; F.I. and M.A.M. conceived the LSDCAS studies, participated in its design and coordination, and drafted the part of the paper related to the LSDCAS studies. F.I. also performed the gamma-irradiation at UI; A.P.A. contributed in the cytological analysis of HeLa irradiated and control samples; P.J.D. designed and wrote the event analysis software for LSDCAS and helped in the analysis of the LSDCAS images; G.P. carried out the irradiation experiments on HeLa in Riga and participated in the analysis of their results; A.I. carried out with J.E. the experiments on Namalwa in Manchester and participated in analysis of the results; T.M.I. participated in experimental design, analysis of results, drafting and editing of the manuscript.

References

- Adams RR, Eckley DM, Vagnarelli P, Wheatley SP, Gerloff DL, Mackay AM, et al. Human INCENP colocalizes with the Aurora-B/AIRK2 kinase on chromosomes and is overexpressed in tumour cells. *Chromosoma* 2001; 110:65–74.
- Andreassen PR, Lacroix FB, Lohez OD, Margolis RL. Neither p21WAF1 nor 14-3-3 sigma prevents G2 progression to mitotic catastrophe in human colon carcinoma cells after DNA damage, but p21WAF1 induces stable G1 arrest in resulting tetraploid cells. *Cancer Res* 2001;61:7660–8.
- Baroja A, de la Hoz C, Alvarez A, Ispizua A, Bilbao J, de Gandarias JM. Genesis and evolution of high-ploidy tumour cells evaluated by means of the proliferation markers p34(cdc2), cyclin B1, PCNA and 3[H]-thymidine. *Cell Prolif* 1996;29:89–100.
- Baroja A, de la Hoz C, Alvarez A, Vielba R, Sarat R, Aréchaga J, et al. Polyploidization and exit from cell cycle as mechanisms of cultured melanoma cell resistance to methotrexate. *Life Sci*. 1998;62:2275–82.
- Carmena M, Earnshaw WC. The cellular geography of aurora kinases. *Nat Rev Mol Cell Biol*. 2003;4:842–54.
- Castedo M, Perfettini JL, Roumier T, Andreau K, Medema R, Kroemer G. Cell death by mitotic catastrophe: a molecular definition. *Oncogene* 2004a;23: 2825–37.

- Castedo M, Perfettini J-L, Roumier T, Yakushijin K, Horne D, Medema R, et al. The cell cycle checkpoint kinase Chk2 is a negative regulator of mitotic catastrophe. *Oncogene* 2004b;23:4353–61.
- Chu K, Teele N, Dewey MW, Albright N, Dewey WC. Computerized video time lapse study of cell cycle delay and arrest, mitotic catastrophe, apoptosis and clonogenic survival in irradiated 14-3-3s and CDKN1A (p21) knockout cell lines. *Rad Res.* 2004;162:270–86.
- Come MG, Skladanowski A, Larsen AK, Laurent G. Dual mechanism of daunorubicin-induced cell death in both sensitive and MDR-resistant HL-6 cells. *Br J Cancer* 1999;79:1090–7.
- Davis PJ, Kosmacek EA, Sun Y, Ianzini F, Mackey MA. The large-scale digital cell analysis system: an open system for nonperturbing live cell imaging. *J Microsc.* 2007;228:296–308.
- de la Hoz C, Baroja A. Proliferative behaviour of high-ploidy cells in two murine tumour lines. *J Cell Sci.* 1993;104:31–6.
- Ditchfield C, Johnson VL, Tighe A, Ellston R, Haworth C, Johnson T, et al. Aurora-B couples chromosome alignment with anaphase by targeting BubR1, Mad2, and Cenp-E to kinetochores. *J Cell Biol.* 2003;161:267–80.
- Edgar BA, Orr-Weaver TL. Endoreplication cell cycles: more for less. *Cell* 2001;105:297–306.
- Erenpreisa JA, Cragg MS, Fringes B, Sharakhov I, Illidge TM. Release of mitotic descendants by giant cells from irradiated Burkitt's lymphoma cell line. *Cell Biol Int.* 2000;24:635–48.
- Erenpreisa J, Cragg MS. Mitotic death: A mechanism of survival? A review. *Cancer Cell Int.* 2001;1:1.
- Erenpreisa J, Cragg MS. Cancer: A matter of life-cycle? *Cell Biol Int.* 2007;31:1507–10.
- Erenpreisa J, Kalejs M, Ianzini F, Kosmacek EA, Mackey MA, Emzish D, et al. Segregation of genomes in polyploid tumour cells following mitotic catastrophe. *Cell Biol Int.* 2005;29:1005–11.
- Galluzzi L, Maiuri MC, Vitale I, Zischka H, Castedo M, Zitvogel L, et al. Cell death modalities: classification and pathophysiological implications. *Cell Death Differ* 2007;14:1237–43.
- Geitler L. Die Analyse des Kernbaus und der Kernteilung der Wasserläufer *Gerris lateralis* und *Gerris lacustris* (Hemiptera: Heteroptera) und die Somadifferenzierung. *Z. Zellforsch* 1937;26:641–72.
- Giet R, Petretti C, Prigent C. Aurora kinases, aneuploidy and cancer, a coincidence or a real link? *Trends Cell Biol.* 2005;15:241–50.
- Gisselson D. Mitotic instability in cancer: Is there method in the madness? *Cell Cycle* 2005;4:1007–10.
- Gromley A, Yeaman C, Rosa J, Redick S, Chen CT, Mirabelle S, et al. Centriolin anchoring of exocyst and SNARE complexes at the midbody is required for secretory-vesicle-mediated abscission. *Cell* 2005;123:75–87.
- Hamada M, Yakushijin Y, Ohtsuka M, Kakimoto M, Yasukawa M, Fujita S. Aurora2/BTAK/STK15 is involved in cell cycle checkpoint and cell survival of aggressive non-Hodgkin's lymphoma. *Br J Haematol.* 2003;121:439–47.
- Ianzini F, Mackey MA. Development of the large-scale digital cell analysis system. *Radiat Protect Dosim.* 2002;99:289–93.
- Illidge T, Cragg M, Fringe B, Olive P, Erenpreisa JE. Polyploid giant cells provide a survival mechanism for p53 mutant cells after DNA damage. *Cell Biol Int.* 2000;24:621–33.
- Ivanov A, Cragg MS, Erenpreisa J, Emzish D, Lukman H, Illidge TM. Endopolyploid cells produced after severe genotoxic damage have the potential to repair DNA double strand breaks. *J Cell Sci.* 2003;114:4095–106.
- Kroemer G, El-Deiry WS, Golstein P, Peter ME, Vaux D, Vandenabeele P, et al. Nomenclature Committee on Cell Death. Classification of cell death: recommendations of the Nomenclature Committee on Cell Death. *Cell Death Differ* 2005;(Suppl 2):1463–7.
- Macville M, Schröck E, Padilla-Nash H, Keck C, Ghadimi BM, Zimonjic D, et al. Comprehensive and definitive molecular cytogenetic characterization of HeLa cells by spectral karyotyping. *Cancer Res.* 1999;59:141–50.
- Nagata Y, Jones MR, Nguyen HG, McCrann DJ, St Hilaire C, Schreiber BM, et al. Vascular smooth muscle cell polyploidization involves changes in chromosome passenger proteins and an endomitotic cell cycle. *Exp Cell Res.* 2005;305:277–91.
- Nagl W. Endopolyploidy and polyteny in differentiation and evolution. Amsterdam: North-Holland/Elsevier; 1978.
- Nguyen HG, Ravid K. Tetraploidy/aneuploidy and stem cells in cancer promotion: The role of chromosome passenger proteins. Review. *J Cell Physiol.* 2006;208:12–22.
- Prieur-Carrillo G, Chu K, Lindqvist J, Dewey WC. Computerized video time-lapse (CVTL) analysis of the fate of giant cells produced by X-irradiating EJ30 human bladder carcinoma cells. *Radiat Res.* 2003;159:705–12.
- Rajaraman R, Guernsey DL, Rajaraman MM, Rajaraman SR. Stem cells, senescence, neosis and self-renewal in cancer. *Cancer Cell Int.* 2006;6:25.
- Stewenius Y, Gorunova L, Jonson T, Larsson N, Hoglund M, Mandahl N, Mertens F, Mitelman F, Gisselsson D. Structural and numerical chromosome changes in colon cancer develop through telomere-mediated anaphase bridges, not through mitotic multi-polarity. *Proc Natl Acad Sci USA* 2005;102:5541–6.
- Vagnarelli P, Earnshaw WC. Chromosomal passengers: the four dimensional regulation of mitotic events. *Chromosoma* 2004;113:211–22.
- Warner SL, Bearss DJ, Han H, Von Hoff DD. Targeting Aurora-2 kinase in cancer. *Mol Cancer Ther.* 2003;2:589–95.
- Wilkinson RW, Odedra R, Heaton SP, Wedge SR, Keen NJ, Crafter C, et al. AZD1152, a selective inhibitor of aurora-B kinase, inhibits human tumour xenograft growth by inducing apoptosis. *Clin Cancer Res.* 2007;13:3682–8.
- Zhang Y, Nagata Y, Yu G, Nguyen HG, Jones MR, Toselli P, et al. Aberrant quantity and localization of Aurora-B/AIM-1 and survivin during megakaryocyte polyploidization and the consequences of Aurora-B/AIM-1-deregulated expression. *Blood* 2004;103:3717–26.

Chapter 9

Mechanism of non-apoptotic cell death evoked by Type II anti-CD20 mAb (Tositumomab) and mAb to HLA-DR.

Ivanov A, Beers S, Walshe C, Cox K, Chan C, Glennie G, Illidge T, Cragg M.

Manuscript in preparation.

Title Page:

Mechanism of homotypic adhesion and lysosome-mediated non-apoptotic cell death evoked by anti-CD20 (Tositumomab) and HLA DR monoclonal antibodies.

Running Title: Antibody-induced cell death.

Andrei Ivanov¹, Stephen A Beers², Claire Walshe², Jamie Honeychurch¹, Waleed Alduaij¹, Kerry L Cox², Kathleen N Potter², Stephen Murray¹, Claude HT Chan², Jekaterina Erenpreisa³, Martin J Glennie², Tim M Illidge¹#, Mark S Cragg²*#

¹CRUK Paterson Institute for Cancer Research, School of Cancer and Imaging Sciences, School of Medicine, University of Manchester, UK. ²Cancer Sciences Division, Southampton University School of Medicine, General Hospital, Southampton, UK. ³ Biomedical Research and Study Centre, Riga, Latvia. # These authors should both be considered senior authors and contributed equally to the project. *Corresponding author

Address correspondence and reprint requests: Dr Mark Cragg, Tenovus Laboratory, Cancer Sciences Division, Southampton University School of Medicine, General Hospital, Southampton, SO16 6YD, UK. (FAX: +44 (0) 23 80704 061; e-mail: msc@soton.ac.uk)

Abstract

Monoclonal antibodies (mAb) are becoming increasingly utilized in the treatment of lymphoid disorders. Although Fc-Fc γ R interactions are thought to explain much of their therapeutic effect, this does not explain why certain mAb specificities are more potent than others. An additional effector mechanism available to mAb is the direct induction of cell death. Previously, we demonstrated that Type II anti-CD20 mAb were able to evoke a non-apoptotic mode of cell death that appeared linked with the induction of homotypic adhesion. Here, we reveal that peripheral re-localisation of actin is critical for the adhesion and cell death induced by both Type II anti-CD20 mAb and HLA DR Class II mAb in both lymphoma cell lines and primary CLL cells. Complex interactions between cells undergoing homotypic adhesion resulted in mutual exchange of plasma membrane components as well as the formation of transient cytoplasmic bridges between cells. Subsequent experiments involving FRAP and siRNA revealed that actin dynamics are rapidly altered after mAb stimulation and that the mode of cell death engaged is rapid, non-apoptotic, non-autophagic and dependent on both the integrity of plasma membrane cholesterol and activation of the V-type ATPase. The mode of cell death reflects V-ATPase-dependent cytoplasmic death involving lysosomes which swell and then disperse their contents into the cytoplasm. The resulting loss of plasma membrane integrity occurs in the absence of DNA fragmentation and is independent of caspase and Bcl-2 control. These experiments provide new insights into how clinically relevant mAb are able to bypass apoptotic regulation and provide a framework for developing anti-cancer antibodies against tumor cells refractory to apoptosis.

Introduction

Monoclonal antibodies (mAb) are becoming increasingly utilized in the treatment of lymphoid disorders (1, 2). In particular, mAb directed to cell surface antigens on malignant B cells have proven the most clinically effective with the anti-CD20 mAb, rituximab being the first mAb to be approved by the US FDA for the treatment of cancer. This mAb has substantially improved outcome for patients with many different types of Non Hodgkin lymphoma and it has now been administered to over 1 million patients in the decade since its approval. Given the success of rituximab, there is currently intense pre-clinical and clinical investigation of many other mAb directed to both CD20 and a host of other cell surface antigens (2). The current challenge in the development of novel anti-cancer mAb is to discover cell surface antigens that will lead to efficient tumor cell killing and to identify biological pathways that will augment the cytotoxic effects of these mAb. Central to this task is the need to identify the critical effector mechanisms involved in mAb therapy. Although Fc-FcγR interactions are thought to explain much of the therapeutic effect of mAb, this does not explain why certain mAb specificities are more potent than others. In addition to "classical" Fc-dependent effector mechanisms such as complement and antibody dependent cytotoxicity (CDC and ADCC, respectively) certain mAb are also able to trigger intracellular signaling in the target cell and directly induce programmed cell death (PCD) (reviewed in (3) and (4)). Whereas ADCC and CDC are dependent only upon the level of surface expression and degree of modulation of a target molecule, PCD is reliant upon the nature of the target molecule with its associated signal transduction cascade. An enhanced understanding of how different mAb evoke PCD is

clearly central to providing new insights regarding not only their mode of action, but also how they might function in vivo and how mAb efficacy might be augmented.

We previously defined anti-CD20 mAb as either Type I or II, based upon their ability to redistribute CD20 into plasma membrane lipid rafts and their potency in various assays measuring CDC, homotypic adhesion (HA) and PCD (5-7). These experiments indicated that Type II mAb (such as tositumomab/B1), with their greater tendency to promote PCD but not CDC, are more effective at depleting malignant B cells in xenograft models (6). We have recently confirmed that this superior efficacy also translates to syngeneic models of B cell depletion in human CD20 Tg mice (8). In both cases this enhanced activity was independent of the need for complement (6, 8) and no differences in ADCC (6) or macrophage uptake were apparent (8). Therefore, in the absence of other apparent effector mechanisms it is possible that the enhanced induction of PCD may account for the greater efficacy of Type II reagents. Previously, we demonstrated that the cell death induced by these Type II mAb was non-apoptotic, independent of caspase activity and correlated with HA (5).

The induction of physiological or cytotoxic responses by extracellular signals requires the spatial and temporal coordination of distinct signaling pathways. Actin cytoskeleton remodelling has been established as an integrating mechanism in lymphocyte activation and antigen presentation establishing immunological synapses and kinases (reviewed by Dustin (9)). Disruption of the actin cytoskeleton inhibits both HA and cell death induced by anti-HLA DR (10, 11) and anti CD99 antibodies (12, 13). Moreover, this form of cell

death is independent of caspase activation (12). LFA-1 dependent and independent HA has also been reported for B cells following the ligation of CD19, CD20, CD39, CD40 (10) and CD53 (14). Therefore, we hypothesized that cell signaling events leading to anti-CD20 mAb induced HA and death might be linked through actin signaling.

Here we show that actin redistribution towards the cell-to-cell contact area is critical for both the adhesion and cell death induced with Type II anti-CD20 mAb and HLA DR Class II mAb on a variety of cell-lines and primary chronic lymphocytic leukemia (CLL) samples. Furthermore, we demonstrate that actin dynamics are altered rapidly after mAb stimulation and that trogocytosis involving membrane swapping is stimulated. Actin redistribution is associated with a change in lysosomes which appear to swell and then disperse their contents into the cytoplasm, resulting in a loss of plasma membrane integrity, resulting in non-apoptotic cell death.

Results

Actin reorganization is involved in anti-CD20 and anti-HLA DR induced homotypic adhesion and cell death

Following our earlier observation that HA was correlated with cell death induced by anti-CD20 mAb (5), we performed experiments to investigate whether other mAb specificities were able to perform both of these functions. These experiments revealed that in addition to Type II anti-CD20 reagents, only mAb to HLA DR but not HLA-DQ, HLA-DP, CD37, CD38 or BCR were able to evoke both strong HA and cell death in Raji cells (Figure 1 A, B, D and data not shown). Death observed after 24h also correlated with a loss of clonogenic survival (~ 8-fold for tositumomab a Type II anti-CD20 mAb and ~ 80-fold for L243 anti-HLA DR) (data not shown). We concluded that the two processes of HA and cell death might be functionally linked for Type II anti-CD20 and HLA DR mAb. HA would require ultrastructural reorganization of the actin cytoskeleton and so we first investigated the effects of blocking this activity on HA and cell death. These experiments, using agents that stabilize (Jasplakinolide) or inhibit (cytochalasin D, Latrunculin B) actin polymerization, demonstrate a clear dependency of HA and cell death on actin reorganization (Figure 1 C, D). To confirm that these findings had relevance to primary tumor samples we next investigated a panel of seven chronic lymphocytic leukemia (CLL) samples in these assays with largely similar results (Figure 2). As such, both tositumomab and L243 mAb evoked HA (Figure 2A) and increased cell death (Figure 2B) in an actin dependent manner.

Cholesterol-rich plasma membrane rafts are important for antibody-induced homotypic adhesion and cell death.

In order to investigate the pattern of cell-to-cell contact in cells undergoing HA after treatment with mAb, we performed electron microscopy on Raji and SU-DHL4 cells. Ultrastructural studies of cells undergoing the early stages of HA revealed that the primary contact between cells was established by microvilli (Figure 3A). It has previously been reported that microvilli on B lymphocytes are enriched with detergent insoluble membrane rafts (15) containing CD20 (16) and are important for heterotypic adhesion during antigen presentation (15). We therefore assessed the impact of plasma membrane cholesterol on HA induced by mAb ligation of CD20 or HLA DR surface antigens. Treatment of cells with methyl- β -cyclodextrin (MCD) resulted in a prominent decrease in the amount of plasma membrane cholesterol as detected by flow cytometry of FITC-labeled cholera toxin B subunit (Figure 3B). No HA was observed in mAb-treated cells which were pre-treated with MCD whereas re-incubation of cells with MCD/cholesterol complex to replete plasma membrane cholesterol restored antibody-induced HA (Figure 3C). To test the effect of cholesterol depletion on the cell death response, Raji and SU-DHL4 cells were incubated in the presence or absence of MCD, with some samples replenished by incubation with MCD/cholesterol. The cells were further cultured in the presence of anti-CD20 (tositumomab) or anti-HLA DR (L243) mAb for 4h and then cell death was assessed. MCD pre-treatment attenuated cell death in both tositumomab and L243 mAb treated samples but not in those treated by staurosporine, which is well documented to induce apoptosis (17). MCD-treated samples that were cholesterol-replenished exhibited the same level of cell death as non-MCD

treated cells (Figure 3D). Importantly, the extraction of plasma membrane cholesterol did not alter the surface expression of CD20 or HLA DR (Supplemental Figure 1), although it was able to completely block the HA triggered by mAb to these antigens. Thus HA and cell death, induced by both of these mAb appear dependent upon membrane cholesterol most likely through the interaction of microvilli.

Peripheral relocalization and increased lateral mobility of actin during antibody-induced homotypic adhesion

After establishing the role of actin in cell death induced by anti-CD20 and HLA DR mAb we next investigated actin dynamics after ligation of CD20 or HLA DR. Using Alexa584-labelled phalloidin, we studied the distribution of F-actin in Raji cells before and after treatment with anti-CD20 (Figure 4A) and anti-HLA-DR mAb. These experiments revealed a clear cytoskeleton actin ring around nuclei in non-treated cells, while loss of its integrity accompanied by redistribution of F-actin to the areas of cell-cell contact was observed after treatment with both mAb. To allow us to assess the kinetics of actin relocalization we subsequently performed time-lapse microscopy of Raji cells transfected to express a GFP-actin fusion protein. The redistribution of actin towards cell-to-cell contact areas was also observed using this approach and started within 2-5 minutes, coinciding with the onset of HA, reaching completion/maximal adhesion in about 40 minutes (Figure 4B, Supplemental Video 1). Importantly, Western blotting analysis showed no increase in the total amount of actin during this period (Figure 4C), which is indicative of actin redistribution rather than additional de novo synthesis of G-actin. Furthermore, careful analysis of the actin staining pattern showed a decrease in the

fluorescence signal area (Figure 4D) suggestive that compartmentalization rather than de novo synthesis of cellular F-actin is responsible for the increased actin signal at the cell-cell contact area.

Next, we performed fluorescence recovery after photobleaching (FRAP) analysis to investigate the mobility of actin after treatment of cells with anti-CD20 and HLA DR mAb. The speed of fluorescence signal recovery was measured at several time points after addition of mAb (Figures 5A, B and Supplemental videos 2 – 4). These data indicate that the recovery of actin fluorescence is much faster in cells treated with tositumomab or L243 mAb than in control cells where no recovery could be observed within 100 seconds (Figure 5A, B and Supplemental videos 2 – 4). Moreover, the faster recovery of fluorescence was evident in both cytoplasmic and peripheral compartments in cells treated with tositumomab suggesting much faster overall turn-over of F-actin in mAb treated cells (data not shown). Importantly, all of the above measurements were performed in morphologically viable cells and no fluorescence recovery was detected in dead cells (data not shown). Furthermore, the recovery of the fluorescent actin signals returned to baseline levels or greater within the first 10 minutes after addition of mAb (data not shown). This suggests that the log phase of actin redistribution occurs within minutes of mAb treatment.

Video microscopy analysis also revealed that although cell aggregation occurred within five minutes following addition of mAb, it remained stable for at least 48 h (data not shown). Furthermore, close observation of the cell-cell interactions during HA revealed

the formation of small (~5 nm diameter) transient cytoplasmic bridges between cells which opened and closed with approximately 5 minute intervals (Figure 5C).

Interestingly, cells treated with tositumomab or L243 mAb also displayed peripheral relocation of enlarged mitochondria towards the cell-to-cell contact areas (Figure 5D and E). Electron microscopy shows well developed cristae in the juxtaposed mitochondria, suggesting that they are in an energy producing phase (Figure 5D). Furthermore JC1 staining for mitochondria revealed that only mitochondria maintaining high membrane potential, represented as J-aggregates of JC1 dye, were moving towards the cell-to-cell contact area (Figure 5E, arrows) and this process occurred within approximately three hours after addition of mAb (Figure 5F and Supplemental video 5). Furthermore, peripheral relocation of mitochondria could be inhibited with the actin polymerization inhibitor latrunculin B (Supplemental figure 2). These data indicate that adhesion of cells upon ligation of surface antigens may be an active process that requires energy from polarized mitochondria *in situ* that, in turn, are driven or immobilized by the actin cytoskeleton.

CD20 induced homotypic adhesion is accompanied by plasma membrane exchange and correlates with cell death

Having observed the apparent physical linkage between apposing cells participating in HA (Figure 5C), we hypothesized that mutual exchange of cellular components might occur between the cells undergoing HA. To address this hypothesis, we labeled Raji cells with the PKH26 cell membrane dye (red) and mixed them at a 1:1 ratio with Raji cells

expressing a GFP-Actin fusion protein (green). The cell mixture was treated with tositumomab or L243, and then the green and red fluorescence were assessed by fluorescence microscopy (Figure 6A) and flow cytometry (Figure 6B). Following control incubation in the absence of mAb stimulation for 24 h we observed that only a very low percentage ($< 1\%$) of cells became double-stained, indicating that spontaneous transfer of cellular material was a rare event. However, following stimulation with tositumomab or L243, PKH-26 labeled membrane was taken up by 8% and 15% of GFP-actin expressing cells, respectively (Figure 6B, left panels). Fluorescence microscopy indicated that actin patches were not detected in PKH-26 labeled cells, suggesting that cells undergoing HA exchange membranes but not actin cytoskeletal components (Figure 6A). Next we performed the same experiments mixing PKH-26 labeled cells with cells expressing YFP in the cytosol. Here, we observed a similar result to before, with up to 15% of cells dual stained (PKH-26 and YFP), after 24 h post L243 treatment (Figure 6B, right panels). Similar results were obtained when cells were incubated for shorter periods (2-4 h; data not shown). To expand these observations, we then tested a larger panel of mAb for their ability to induce inter-cell membrane exchange and investigated whether there was a relationship between mAb-induced membrane swap and cell death induction. Figure 6C clearly demonstrates that a correlation exists, as cells undergoing membrane exchange were more efficacious in evoking cell death. Interestingly, Fc:Fc γ R interactions did not appear to influence either of these properties as F(ab) $'_2$ fragments of tositumomab and L243 elicited the same amount of cell death and membrane exchange as did whole IgG (Figure 6C). Having established the dynamics and critical role of actin in the cell death

process engaged by both CD20 and HLA DR mAb, we next investigated more closely the nature of the cell death elicited by these mAb.

Antibody induced cell death has a distinctive morphology and is neither apoptotic nor autophagic

We previously demonstrated that cell death evoked by Type II CD20 mAb was not blocked by over-expression of Bcl-2 in Ramos-EHRB cells (5). Here, we performed similar experiments in Raji cells over-expressing Bcl-2. The data obtained 24 h after treatment with mAb confirm our previous observations and demonstrate that HLA DR mAb are also able to bypass the mitochondrial death pathway regulated by Bcl-2 (Figure 6A). Furthermore, inhibition of caspases using ZVAD-FMK or QVD-OPH had no effect on the cell death and furthermore the combination of caspase inhibition and Bcl-2 over-expression were also unable to block the cell death evoked by either mAb, confirming that this cell death was independent of typical apoptotic regulation (Figure 6A).

In the last five years, the number of non-apoptotic death pathways described in mammalian cells has steadily increased (18). Of those, perhaps the best characterized is that resulting from autophagy which involves the formation of autophagosomes which are governed through the tightly regulated interactions of Atg proteins. Therefore, given the absence of an apoptotic death program, we next investigated whether autophagy was elicited by CD20 and HLA DR mAb. First, we assessed the expression of several key Atg proteins, before and after mAb treatment. These experiments revealed that Atg5, Atg12 and Beclin-1 were unchanged over the 24h time course studied (Figure 7B and data not

shown). Moreover, two independent siRNA capable of reducing Beclin-1, one of the key proteins implicated in autophagic death, had no effect on either the level of HA (data not shown) or cell death evoked by tositumomab or L243 (Figure 7C). As a control in these experiments we also employed a non-functional siRNA targeted to Atg12 which had no effect on Beclin-1 or cell death. Previous workers have indicated that non-apoptotic, non-autophagic Type III death, such as evoked by CD47 ligation, results from activation of chymotrypsin-like serine proteases (19). To determine whether these enzymes were involved in the cell death evoked by tositumomab and L243 we examined the effects of previously characterized inhibitors of these enzymes in cell death assays. These experiments detailed in Figure 7D clearly demonstrate that cell death was not blocked by any of the inhibitors to chymotrypsin-like serine proteases (TPCK), or trypsin-like serine proteases (TLCK) indicating that death engaged by tositumomab and L243 mAb is independent of these enzymes.

Ultrastructural studies confirmed that neither classical apoptotic nor autophagic death was evoked with tositumomab or L243 mAb (Figure 8). First, there was no evidence of DNA condensation or apoptotic body formation typical of apoptosis. Instead, large cytoplasmic inclusions and vacuoles were observed in cells observed by Transmission Electron Microscopy (EM) (Figure 8A, B), that were distinct from control cells (Figure 8C) and cells undergoing classical apoptosis (Figure 8D). This pattern was coincident with cells displaying loss of microvilli (Figure 8E) and permeabilized plasma membranes (Figure 8F) whilst undergoing HA as assessed by Scanning EM (Figure 8 G, H). Again, this morphological pattern of cell death differed significantly from control cells (Figure

8I) and cells undergoing classical apoptosis (Figure 8J). Although vacuoles were evident, these were not autophagic in nature, as they lacked double membrane structure - the hallmark of autophagy. Rather, our findings are most in accordance with the morphological criteria described for cells said to be undergoing cytoplasmic cell death (20-22). In summary these data indicate that cell death arising after engagement of CD20 or HLA DR by mAb, is not evoked through conventional apoptotic or autophagic routes but instead appears to involve a "cytoplasmic" death pathway.

Involvement of lysosomes in cell death evoked by tositumomab or L243

It is well established that lysosomes play important roles in non-apoptotic cell death (23) and it has even been proposed that the lysosome is the primary organelle responsible for cell death triggered by engagement of the B cell receptor for antigen (24). Enlargement of the lysosomal compartment and subsequent lysosome membrane permeabilization are hallmarks of cytoplasmic cell death (25). Therefore, to characterize the involvement of lysosomes in the cell death induced by tositumomab or L243, we assessed these characteristics (25) in lysotracker-labeled (26) Raji and SU-DHL4 cells. These experiments revealed that the lysotracker fluorescence increased within 1 h after addition of mAb and reached its maximum within 4 h in cells treated with tositumomab or L243 mAb (Figure 9A), suggesting that the lysosomal compartment is indeed enlarged in these cells. The increase in lysotracker fluorescence was followed by the appearance of a lysotracker-low fraction in a proportion of cells after 4 h which suggests that the initial swelling of lysosomes is followed by the collapse of this compartment. Fluorescence

microscopy of lysotracker labeled cells also revealed its increased fluorescence in antibody treated cells undergoing HA (Figure 9A, right hand panels) as highly enlarged individual lysosomes were often observed in cells within cell aggregates (Figure 9A, insert).

The degree of lysosome membrane permeabilization (LMP) after treatment with tositumomab or L243 mAb was then assessed using a method modified from that used previously (27). Briefly, cells were first treated with acridine orange to label the lysosomes and then washed prior to addition of the mAb. Acridine orange at acidic pH (for example in lysosomes) fluoresces red, whereas its leakage from lysosomes into the more neutral pH of the cytosol results in green fluorescence, indicating an increase in LMP. Increased green fluorescence (FL1) was observed in ~30 % of cells 4 h after tositumomab treatment (Figure 9B). This increase was followed by a reduction in green fluorescence due to subsequent permeabilization of the plasma membrane and leakage of the cytoplasmic content. The latter was verified by fluorescence microscopy where cells with non-fluorescent/destained cytoplasm were observed after tositumomab or L243 mAb treatment (Figure 9C).

To confirm the involvement of lysosomes in this death process we utilized the well-characterized inhibitor of vacuolar ATPases (V-ATPases), concanamycin A. V-ATPases are proton pumps that serve to energize intracellular membranous vesicles such as lysosomes. As such, concanamycin A and the structurally related Bafilomycin A1, are able to inhibit the acidification of organelles, interfere with protein trafficking (28) and prevent cytotoxicity elicited through perforin and or Fas (29). Here, we examined

whether they could block cell death evoked by mAb engagement of CD20 or HLA DR. Low, sub-micromolar, concentrations of concanamycin A, which were non-toxic and thought to be specific for the V-ATPase, were able to markedly reduce the death of Raji cells following treatment with either tositumomab or L243, and in a dose dependent manner (Figure 10A). Similar results were generated with Bafilomycin A1, demonstrating a clear role for acidic vacuoles (likely lysosomes) in the death process (Figure 10B). In addition, we assessed the effect of concanamycin and Bafilomycin A1 on the lysosomal volume in cells treated with mAb. Figure 10C demonstrates that both concanamycin and Bafilomycin A1 reduce the increase in lysosomal volume triggered by tositumomab and L243 mAb.

Previously, we have demonstrated that Type I (but not Type II) anti-CD20 mAb such as rituximab transduce many of their intracellular signals by 'hijacking' the signaling capacity of the BCR (30). Therefore, given the similarity in cell death characteristics evoked by tositumomab and L243, we explored whether tositumomab might engage its cell death pathway by binding and interacting directly with HLA DR molecules. To explore this possibility we examined whether HLA DR expression was critical for tositumomab-induced cell death, making use of the HLA-negative Raji variant (RJ2.2.5). These cells were completely negative for HLA DR expression as expected but expressed equivalent levels of CD20 compared to wt Raji cells and remained sensitive to cell death evoked by tositumomab. These data indicate that despite eliciting a form of cell death kinetically, morphologically and mechanistically similar to that of anti-HLA DR tositumomab does not require HLA DR expression for the induction of cell death.

Discussion

The last decade has seen a considerable expansion in the number of mAb available for the treatment of malignant and autoimmune disease (2). Although the early enthusiasm in mAb therapy was dampened by disappointing results using mouse mAb, the advent of human/humanized mAb coupled with an increased understanding of the importance of antigen specificity has re-invigorated interest in development of this class of biologicals as effective therapeutics in the clinic (31). We have previously speculated that "signaling mAb" provide a selective advantage compared to other mAb specificities, potentially by eliciting direct cell death programs in the target cells (3). Here, we examined the effects of treating cells with mAb directed against two surface targets, namely CD20 and HLA DR that have been developed as anti-cancer therapeutics in the clinic.

In this study we have demonstrated that ligating CD20 and HLA DR (but not other B cell surface antigens e.g. CD37, CD38) on the surface of malignant B cells (including primary CLL samples) with certain mAb induced strong HA and subsequent cell death. Two important points arise from this observation, namely: 1) only certain cell surface targets are capable of evoking these types of responses and 2) the fine binding specificity of the mAb is critical. As such, only Type II anti-CD20 mAb evoke strong HA (and cell death) whilst only anti-HLA DR efficiently perform a similar function of those mAb targeting HLA molecules (mAb targeting HLA-DP, -DQ and pan-HLA do not). Establishing the link between the type/location of binding employed by the different mAb and their subsequent effects on HA and cell death is the subject of our ongoing research.

The engagement of HLA DR, CD38, CD40 and other B-cell surface antigens, including CD19, CD20, CD21, CD22, and CD23, has previously been shown to induce rapid HA of B cell lines (10). The HA was not the result of mAb-mediated aggregation and required cellular energy and an intact cytoskeleton, but not new mRNA or protein synthesis (10). Furthermore, anti-HLA DR and anti-CD20 mAb induced adhesion was LFA-1 independent (10) and was mediated by an as yet unidentified adhesion receptor. With respect to the HA it is particularly noteworthy that both CD20 and MHC class II antigens are localized to microvilli and constitutively associated with membrane rafts (15, 16) that, in turn, are required for the expression of microvilli on the cell surface. Therefore, we postulated that extraction of plasma membrane cholesterol would significantly impair the intercellular interaction induced by the mAb studied. Indeed, HA and cell death were inhibited if cells were pre-treated with MCD. In that context it is notable that cholesterol depletion prevented the association of hypercrosslinked CD20 with detergent-insoluble rafts, and attenuated both calcium mobilization and cell death induced by another anti-CD20 antibody, rituximab (32).

At the cell-to-cell contact areas we observed an enrichment of mitochondria in cells undergoing HA. Interestingly, this mitochondrial translocation occurred much later (hours after addition of mAb) than the cholesterol-dependant HA (minutes) and polarisation of cellular actin (tens of minutes). This temporal separation may suggest two stages of mAb triggered cellular aggregation when the initial microvilli and raft driven adhesion is followed by a stronger aggregation of cells mediated by relocalised actin supported by energy from grouping mitochondria. In that context junctional actin might

initially serve to maintain the cellular organelles within the intercellular contact site. In support of this hypothesis, emerging evidence indicates that while microtubules are important factors for mitochondrial transport, the actin cytoskeleton is required for immobilization of these organelles at the cell cortex (33, 34). The latter is in good agreement with our data showing that translocation of polarized mitochondria towards the cell-to-cell contact area was grossly impaired when cells were treated with the actin polymerization inhibitor latrunculin B. Although currently the function of cortical immobilization of mitochondria is not well understood, it is believed that these immobilization events are critical for localization of mitochondria at sites of high ATP utilization (35). In our system, only mitochondria having high membrane potential are relocated towards the intercellular contact area suggesting that these areas are the sites of high ATP use.

In addition to tight HA and formation of transient cytoplasmic bridges, we also observed clear evidence of membrane exchange between the interacting cells after treatment with both mAb. Previously, a number of reports have demonstrated that certain cell types, including pheochromocytoma (36), DCs (37-39), T cells (40), natural killer cells (41) and B cell lymphoma (42) have the capacity to transfer membrane and cellular components. In the case of B cell lymphomas, spontaneous membrane exchange is thought to be due to transfer of membrane components during direct cell contact (42), in processes that are enhanced by BCR cross-linking. Here we have revealed new evidence that strongly suggests there is a direct relationship between cell death induced by ligation of CD20 or HLA DR by mAb and exchange of plasma membrane components.

Following HA we observed the induction of non-apoptotic cell death with both tositumomab and L243 mAb. We previously reported that cell death triggered by tositumomab was not accompanied by DNA fragmentation and was independent of caspase activation, characteristic of classical apoptosis (5, 43). These observations were confirmed and extended here, with ultrastructural studies using transmission and scanning EM indicating that the mode of cell death evoked by both mAb specificities strongly resembles "cytoplasmic cell death" such as described previously (20-22). An equivalent mode of cell death was also evoked by L243 mAb, where both over-expression of Bcl-2 and pre-incubation with QVD-OPH did not have any impact on the extent of cell death.

The HLA DR molecule is an important component of the immune system, and its engagement on several cell types leads to various cellular events that modulate cell function. For example, signaling via this molecule can lead to rapid B cell death (44, 45) that is independent of caspase activation (45-47). In agreement with our data, this cell death involves the integrity of the cytoskeleton and is independent of the LFA-1 system.

It has previously been established that lysosomes control cell death at several levels. A limited release of lysosomal contents to the cytoplasm triggers apoptosis or apoptosis like cell death, whereas generalized lysosomal rupture results in rapid cellular necrosis (reviewed by Kroemer and Jaattela (23)). In response to endogenous or exogenous stress, lysosomal membrane permeabilisation (LMP) can occur, leading to the release of

catabolic hydrolases that can mediate caspase-independent cell death or necrosis following high levels of LMP. In accordance with this concept, we observed generalized swelling and rupture of the lysosomal compartment after ligation of CD20 and HLA DR with mAb, resulting in caspase and Bcl-2 independent cell death. In our system, both swelling of lysosomal compartment and cell death could be inhibited with V-type ATPase inhibitors concanamycin A and Bafilomycin A1. Interestingly, although bafilomycin A1 is a commonly used inhibitor of autophagy, its ability to inhibit anti-CD20 induced cell death was not dependent on the key regulator of autophagy: Beclin 1. This suggests the pleiotropic nature of vacuolar ATPase in non-apoptotic cell death modalities and that its pharmacological inhibition does not necessarily exclude forms of non-apoptotic death other than autophagy. Moreover, in our system, V-type ATPase appeared to be important for HA of cells, which, to our knowledge, has not been reported previously.

Both mAb evoked non-apoptotic cell death, as judged by the detailed ultrastructural analysis described above. Inhibition of apoptosis is considered an important factor in the treatment resistance of tumor cells. Therefore, the ability of tositumomab and HLA DR mAb such as L243 to bypass apoptotic regulation may be a critical factor in their mode of action. This independence from mitochondrial and death receptor signaling pathways potentially facilitates use of these reagents for treatment of tumors with impaired apoptotic machinery that have become resistant to conventional cytotoxic chemotherapy.

In summary, we have shown for the first time that HA and cell death induced by two clinically relevant mAb are inter-related. Treatment with tositumomab and L243 mAb accelerated the rate of membrane exchange between apposing cells in a process independent of Fc:FcγR interactions. Furthermore, adhesion and death were both dependent upon redistribution of actin filaments with the latter resulting from lysosomal enlargement and leakage. The loss of plasma membrane integrity was independent of Bcl-2 control, which coupled to the observed cell death pathway involved, indicates that these mAb are able to bypass the apoptotic machinery in tumor cells resistant to cytotoxic chemotherapy and radiotherapy induced apoptosis (43). In summary, this new data provides new insights into mAb induced death pathways that are potentially exploitable with novel therapeutics in the clinic.

Methods

Cell lines and reagents

Human cell lines (Raji and SU-DHL4) were obtained from the European Collection of Cell Cultures (ECACC, Salisbury, United Kingdom). RJ2.2.5 cells are a Raji variant which lack HLA expression (48) and were a kind gift from Dr Robert Accolla, Insubria, Italy. Cell-lines were maintained in antibiotic-free RPMI 1640 medium with fetal calf serum (Sigma, 10%) glutamine (2 mM, Gibco, Paisley, United Kingdom) and sodium pyruvate (1%) at 37°C, 5% CO₂. Jasplakinolide, cytochalasin D, latrunculin A, concanamycin A, LY294002 and Y27632 were purchased from Calbiochem (UK). Methyl-beta-cyclodextrin (MCD) and Bafalomysin A1 was purchased from Sigma.

Antibodies

Tositumomab (B1; GlaxoSmithKline, Uxbridge, UK), 1F5, WR17 (mouse anti-human CD37), L243 (anti-HLA DR) and OKT3 (anti-CD3) are all of the mIgG2a isotype and have been described previously (5). Rituximab (anti-CD20; Roche Welwyn Garden City, UK) and its murine IgG2a variant were provided by Dr Luke Nolan or produced in-house, respectively as detailed previously (8). M15/8 (anti-IgM), AT13/5 (CD38), F3.3 (pan HLA), A9-1 (pan HLA), B7-2.1 (HLA-DP), L2 (HLA-DQ), were all derived in-house, obtained from the ATCC or provided through the HLDA workshop VIII. IgG was produced from supernatant secreted by hybridomas in tissue culture and purified in-house

using protein A columns (GE Healthcare). F(ab')₂ fragments of antibodies were prepared by trypsin digestion as detailed previously (49).

Clinical Samples

Ethical approval for the use of clinical samples was obtained by the Southampton University Hospitals National Health Service (NHS) Trust from the Southampton and South West Hampshire Research Ethics Committee. Informed consent was provided in accordance with the Declaration of Helsinki. Blood was obtained from patients with typical CLL who attended the hematology outpatient clinics at the Royal Bournemouth Hospital, Hammersmith Hospital, Leicester Royal Infirmary, Portsmouth Hospital, Southampton General Hospital, and the Royal Wolverhampton Hospitals NHS Trust. Peripheral blood mononuclear cells (PBMCs) were isolated by Lymphoprep gradient centrifugation (Axis-Shield Diagnostics, Dundee, United Kingdom) washed, and cryopreserved in RPMI 1640 medium supplemented with 10% DMSO and 15% fetal calf serum. CLL samples were thawed in complete RPMI 1640 medium containing 10% fetal calf serum, 2 mM glutamine, and 1% sodium pyruvate. Cells were pelleted by centrifugation, resuspended in complete medium, and counted prior to use.

Western blotting

Cell lysates were prepared in PhoshoSafe lysis solution (MERCK biosciences Ltd, Nottingham, UK). Samples were then separated by SDS PAGE and proteins transferred immediately onto PVDF membrane (Hybond; Amersham Pharmacia Biotech, UK) using

a semi-dry transfer system (TE 22 system; Hoeffler, Amersham Pharmacia Biotech, UK). Membranes were blocked with 5% non-fat dried milk, then incubated with the appropriately diluted primary antibodies, washed and then incubated with horseradish peroxidase-conjugated anti-rabbit or anti-mouse IgG (Sigma-Aldrich, Gillingham, UK) and visualized by enhanced chemiluminescence (ECL; Amersham Pharmacia Biotech, United Kingdom) and exposure to light-sensitive film (Hyperfilm ECL, Amersham Pharmacia Biotech, UK).

Cholesterol modulation

For cholesterol depletion, cells were treated in RPMI containing 10 mM methyl- β -cyclodextrin (MCD; Sigma, Dorset, UK) for 30 minutes at 37°C. For cholesterol repletion, cholesterol-depleted cells were washed and treated in RPMI containing MCD/cholesterol complex (1.4 mM cholesterol in 10 mM MCD) (Sigma) for 30 minutes at 37°C, followed by washing.

Cholera Toxin B-Subunit staining

Control and MCD treated Raji cells were stained with FITC-conjugated Cholera Toxin B-Subunit (CTB-FITC; Sigma Chemicals) in PBS at 4°C for 30 min, washed and then fixed with 1% PFA at 4°C for 30 min. 10,000 cells were then analyzed by flow cytometry

(Becton-Dickinson) and WinMDI software (Version 2.8, Joseph Trotter, Scripps Research Institute, La Jolla, CA, USA).

Light microscopy for measuring homotypic adhesion

HA was assessed by adding mAb (5-10 $\mu\text{g/ml}$) to cells in flat bottomed plastic plates (Nunc, UK) and then examining them 4-24 h later. Cells were viewed with an Olympus CKX21 inverted microscope (Olympus, UK) using a 10x or 20x/0.25 PH lens. Images were acquired using a CCL2 digital cooled camera (Olympus) and were processed with Cell B (Olympus Soft imaging solutions) and Adobe Photoshop version CS2 software (Adobe, San Jose, CA).

Transmission electron microscopy (TEM)

Cells were washed and fixed in 3% glutaraldehyde (GA, Fluka Chemicals, Dorset, UK) before pelleting (1500rpm for 5 minutes) and fixing at 4°C over night. The fixative was removed and the pellets washed 3 times in PBS prior to pelleting again. Following removal of the supernatant, the cell pellets were post-fixed for 1 h in 1% osmium tetroxide (Agar Scientific Ltd, Stansted, UK) in PBS. Fixative was removed and the pellets washed a further 3 times. Cell pellets were dehydrated through a graded series of ethanol. The pellets were then placed in 100% Acetone (Merck Ltd, Lutterworth, UK), disaggregated, embedded with Agar 100 resin (Agar Scientific Ltd, Stansted,UK) and

placed into pre-labeled BEAM capsules (Agar Scientific Ltd, Stansted, UK) filled with fresh 100% Agar 100 and polymerized at 60°C for 48 h. The embedded pellets were sectioned (60 nm thick), collected on to copper TEM grids (Agar Scientific Ltd, Stansted, UK) post-stained with uranyl acetate and lead citrate prior to imaging in a JEOL1220 TEM at 120 kV (JEOL Ltd, Tokyo). Images were acquired digitally with a Gatan Orius side mount CCD camera and Digital Micrograph software (Gatan UK Ltd, Abingdon, UK).

Scanning electron microscopy (SEM)

Cells were washed and fixed overnight as detailed above. The cell suspension was spun (800 rpm for 5 minutes) and the pellet washed 3 times in PBS before mounting onto Polylysine (1 mg/ml) coated 5 mm silicon chips (Agar Scientific, Stansted, UK). The chips were removed and placed into 35 mm disposable Petri dishes containing 1 % osmium tetroxide in PBS and post fixed for 1 h. Chips were then washed in PBS, 5 minutes x 3 before being dehydrated through an ethanol series and then critical point dried in a Bal-Tec CPD030 (Bal-Tec AG, Lichtenstein) using CO₂ as the transition fluid. The chips were then coated with 8 nm of chromium in an Edwards Auto 308 Cryo sputter coater (BOCEdwards, Crawley, UK) and subsequently imaged in a lens DS130 FESEM (ABT, Tokyo) at 30 kV. Images were acquired digitally using an iScan image capture system (ISS-Group ltd, Manchester, UK).

Lysosomal Volume and Permeability Assessment.

To assess lysosomal volume, cells were labeled with 75 nM LysoTracker probe (Invitrogen) at different time points after treatment with mAb. FL2 fluorescence of LysoTracker labeled cells was assessed 1 h after labeling. Unlabeled cells have been used as a background control. For lysosome permeability measurements, cells were incubated with 5 μ M acridine orange (Molecular Probes) for 15 min at 37°C and washed twice with PBS before the indicated treatments or measurements. Acridine orange is a metachromatic fluorochrome and a weak base that exhibits red fluorescence when highly concentrated in acidic lysosomes and green fluorescence when outside lysosomes. Total lysosomal integrity was evaluated by assessing green fluorescence (FL1) by flow cytometry using a flow cytometer (Becton Dickinson) or fluorescence microscopy.

Fluorescence and time lapse microscopy

For immunofluorescence staining, harvested cells were cytopun onto clean poly-L-lysine-coated microscope slides. Samples were fixed in 2% paraformaldehyde for 15 minutes and rinsed briefly in ice-cold acetone. Slides were washed 3 times for 10 minutes, and then incubated with appropriate primary antibodies for 60 minutes at room temperature. The primary antibodies were diluted in TBS/0.1% BSA. Subsequently, slides were washed in TBS (3 x 10 minutes) and stained using anti-rabbit Alexafluor 488 or Alexafluor 594 SFX kit (Invitrogen Ltd. Paisley, UK) according to the manufacturer's protocol. After three washes in TBS/0.05% Tween 20, DNA was counterstained with 7-

aminoactinomycin D or DAPI before mounting in ProLong Gold antifade reagent (Invitrogen Ltd. Paisley, UK). For time lapse microscopy cells were put into thin glass bottom petri dish in humid atmosphere at 37°C and assessed using a Zeiss 7D time lapse microscope equipped with Coolsnap HQ camera and Metamorph software. Images were taken every 5 minutes.

Cell Transfection

Raji cells were transfected with pAcGFP-Actin (Clontech) using the Amaxa nucleofection device (Buffer T; Programme G16) according to manufacturer's instructions. Transfection efficiency was ~30% and cell death rate was ~5-10% above controls 24 h after transfection. 24 h later, cells were transferred to 96 well plates and selected in the presence of G418 (2mg/ml; Invitrogen Ltd. Paisley, UK). Two weeks later, wells were screened for GFP expression by flow cytometry, positive wells cloned and then expanded.

Fluorescence recovery after photobleaching (FRAP) analysis

Samples for FRAP experiments were prepared by placing a droplet of GFP-Actin labeled Raji cells into IWAKI glass-bottom Petri dishes. The optical plane was set to the middle of the sample. Before bleaching, a stack of 10 images was scanned using an Olympus BX71 microscope to record the pre-bleach situation. Bleaching was carried out with the Argon laser at a wavelength of 488 nm for 1 sec to the 1 μ m region of interest within the cytoplasm. The recovery of fluorescence was assessed every 2 seconds for 100 seconds overall.

Online supplemental material

Supplemental Figure 1 demonstrates that cholesterol extraction has no effect on surface expression of B cell antigens. Supplemental Figure 2 demonstrates the impact of inhibition of actin polymerization on peripheral relocalization of polarized mitochondria. Supplemental video 1 shows relocalisation of GFP-labelled actin towards the cell to cell contact area during homotypic adhesion. Supplemental video 2 shows FRAP of GFP-labeled actin in Raji cells treated with control antibody OKT3. Supplemental video 3 shows FRAP of GFP-labeled actin in Raji cells treated with anti-CD20 mAb tositumomab. Supplemental video 4 shows FRAP of GFP-labeled actin in Raji cells treated with anti-HLA DR mAb L243. Supplemental video 5 shows time-lapse video microscopy of the kinetics of polarized mitochondria in tositumomab-treated Raji cells.

Acknowledgments

We are grateful to Dr Robert Accolla, (Italy) for the kind gift of RJ2.2.5 cells. We are also grateful to Dr Ian Mockridge (Molecular Immunology Group, Southampton) and Isla Wheatley (ECMC, Southampton) for provision and assistance with clinical material. This work was supported by fellowships and grants from Leukaemia Research, UK, Cancer Research UK, Association of International Cancer Research, Tenovus and ECMC.

Author contributions

AI, TMI and MSC initiated the studies. AI, SAB, CAW, WA, KLC, SM, JH and JE performed experiments. KNP provided clinical samples and performed supplemental

assays and analysis. CHTC provided vital novel reagents. AI, MJG, TMI and MSC analyzed the data. AI, TMI and MSC wrote the paper. AI, SAB, MJG, TMI and MSC edited the paper. The authors have no competing financial interests.

Figure Legends

Figure 1. Actin dependent homotypic adhesion is involved in cell death evoked by mAb directed to CD20 or HLA DR. A) Raji cells were incubated with various mAb (10 $\mu\text{g/ml}$) for 4-6 hours, when homotypic adhesion was assessed by light microscopy. The number of +, indicate the strength/extent of adhesion as assessed semi quantitatively by microscopic visualisation. 20h later, samples were assessed for the extent of cell death following staining with AnV-FITC and PI and flow cytometry. Bars represent the mean cell death (AnV and PI positive cells) \pm SEM from three-seven independent experiments. Representative data are shown in B). A typical "apoptotic" plot is shown for reference following treatment of Raji cells with 4 Gy irradiation. C) Raji cells were treated with various actin inhibitors prior to the addition of anti-CD20 or HLA DR mAb and cell death assessed 6h later as previously described. D) Raji cells were treated with the actin inhibitor Latrunculin B (10 μM) prior to the addition of Tos or L243 and assessed for homotypic adhesion 4-6 h later. These data clearly demonstrate that adhesion and death evoked by both anti-CD20 and HLA DR mAb are dependent upon actin.

Figure 2. Actin dependent homotypic adhesion is involved in cell death evoked by CD20 and HLA DR mAb in CLL cells. A) CLL cells were treated or not with the actin inhibitor Latrunculin B (10 μM) for 45 minutes prior to the addition of various mAb (10 $\mu\text{g/ml}$) for 18 hours, when homotypic adhesion was assessed by light microscopy. A typical example of the results is demonstrated. B) The same samples were then assessed for the extent of cell death following staining with AnV-FITC and PI and flow cytometry.

Bars represent the mean cell death (AnV and PI positive cells) above cell death observed in the untreated samples \pm SEM from seven samples. These data clearly demonstrate that adhesion and death evoked by both anti-CD20 and HLA DR mAb in CLL samples are dependent upon actin.

Figure 3. Involvement of microvilli and plasma membrane cholesterol in mAb-induced homotypic adhesion. A) Raji cells were incubated with tositumomab or L243 antibodies for 1 hour. Then, samples were collected and processed for TEM as described in materials and methods. Left figure: the early stage of intercellular adhesion of Raji cells. Right figure: Involvement of microvilli in homotypic adhesion of Raji cells. B) Assessment of plasma membrane cholesterol in MCD pre-treated Raji cells. MCD treated cells were harvested and fixed with 1% paraformaldehyde and stained with FITC-labelled cholera toxin B and assessed by FACS. Prominent reduction of plasma membrane cholesterol was observed. C) Raji cells were pre-treated with 10 μ M MCD for 30 minutes, then washed and incubated with tositumomab or L243 antibodies for 4 hours. Then aggregation of cells was assessed under inverted phase contrast microscope. D) Involvement of plasma membrane cholesterol in anti-CD20 and anti-HLA DR induced cell death. Plasma membrane cholesterol was modulated as described and then cells were incubated with antibodies or staurosporin (STSP). Cell death was assessed 4 hours later and expressed as a percentage of death cells above control. Data represent the average of at least two independent experiments \pm S.E.M. * $p < 0.05$; ** $p < 0.006$.

Figure 4. Peripheral relocalisation of cellular actin in cells undergoing homotypic adhesion after treatment with tositumomab. A) Raji cells were incubated with anti-CD20 antibody tositumomab, washed and sedimented onto poly-L-lysine (PLL) coated microscope slides. After fixation with 1% paraformaldehyde in PBS, cells were stained with Alexa fluor 594-labelled phalloidin (red). DNA was counterstained with DAPI (blue). B) Time lapse microscopy of Raji cells expressing AcGFP-labelled actin. After addition of tositumomab, cell suspensions were put into a glass bottom Petri dish and assessed at 37°C under inverted time lapse microscope. Images were obtained every two minutes (see Supplemental video 1). The interval between images displayed is six minutes, except for the final two images (50 minutes). C) The total amount of cellular actin was assessed by Western blotting after measurement of total protein. Total amount of α -tubulin was assessed as a loading control. D) Image analysis of F-actin signal area. Cells were sedimented onto PLL coated slides, stained with phalloidin - Alexa fluor 594 and images were taken. Area of Alexa fluor positive signal was then measured using Image-Pro Plus software.

Figure 5. Lateral mobility of cellular actin, formation of syncytium and polarisation of mitochondria in cells undergoing homotypic adhesion. A) AcGFP-Actin expressing Raji cells were put into glass bottom Petri dish and actin fluorescence was quenched at a wavelength of 488 nm for 1s with the Argon laser. The recovery of fluorescence was assessed every 2 seconds for 100 seconds in overall. Upper panel: virtually no recovery was observed in control mAb treated cells. Lower panel: the recovery of junctional actin within the cell-to-cell-contact area was observed after approximately 80 seconds. B)

Typical fluorescence recovery pattern of AcGFP-Actin after photobleaching. No recovery within 100 seconds in control cell (left). Recovery of junctional actin fluorescence within about 80 seconds after photo-bleaching in cells treated with anti-CD20 (Tos) (centre) and anti HLA DR (right) antibodies. C) Transient cytoplasmic bridges between cells undergoing homotypic adhesion. Phase contrast time lapse microscopy of Raji cells treated with tositumomab. The interval between images is 5 min. D) and E) peripheral relocation of mitochondria towards cell-to-cell contact area as assessed by TEM (D) and JC1 (E). E) Cells were stained with JC1 according to manufacturer's instruction and treated with tositumomab. After that, images were captured detecting monomeric (green) and J-aggregate (red) forms of JC1. F) Time lapse videomicroscopy of the migration of J-aggregate form of JC1, representing mitochondria with high membrane potential, towards cell-to-cell contact area. Interval between images is 60 minutes.

Figure 6. CD20 induced homotypic adhesion is accompanied by plasma membrane exchange and correlates with cell death. A) Raji cells were labelled with PKH26 (red) and mixed with pGFP-Actin (green) expressing Raji cells, and treated with 10µg/ml tositumomab or L243 and examined by fluorescence microscopy after 24h. B) Flow cytometry profiles of membrane exchange using PKH26 labelled and YFP-expressing cells (right) and PKH26 labelled and GFP-Actin-expressing cells (left) at 24h after treatment with tositumomab or L243. C) Correlation between cell death and membrane exchange. The data clearly demonstrate that Type II and HLA DR mAb stimulate transfer of plasma membrane material between adhering cells whereas other mAb do not. This

property is independent of Fc-FcγR interactions and was correlated with the extent of cell death induced.

Figure 7. Cell death evoked by tositumomab and L243 is non-apoptotic and non-autophagic. A) Raji cells either WT or over-expressing Bcl-2 were treated with mAb (10μg/ml) in presence (black columns) or absence (white columns) of pan-caspase inhibitor QVD-OPH as indicated for 24 h and then assessed for cell death as before. B) Raji cells were treated for 24h (left panel) with various mAb or treated for 2h, 4h or 8h with various mAb (right panel) and then assessed by western blot for the expression of Beclin-1, ezrin or actin (the latter two as loading controls). C) Raji cells were nucleofected with siRNA to Atg12 or Beclin-1 and then incubated for 24 hours. Subsequently, cells were treated with mAb and assessed for cell death as previously described. The degree of knockdown was verified 48h after nucleofection by Western blot (inset). D) Raji cells were pre-incubated with TPCK, TLCK or Y27632 (20 μM) before being treated with tositumomab or L243 and cell death measured 24h later.

Figure 8. Morphological pattern of cell death induced by anti-CD20 mAb tositumomab. A) and B) Gross vacuolisation of cytoplasm (arrows) with relatively intact nuclei (N) is a typical TEM pattern of cell death in the presence of anti-CD20 (Tos) (A) and anti-HLA DR (L243) antibodies (B) . C) Morphology of control, non-treated cell and (D) – classical apoptosis. E-J) Scanning electron microscopy figures of tositumomab treated Raji cells. E) Loss of microvilli was a typical feature of tositumomab treated cell at 4h time point. F) Complete permeabilisation and decomposition of cytoplasm was

observed at 24 hours after treatment. G) homotypic adhesion of Raji cells following treatment with tositumomab. H) Fragment from (G). Non-apoptotic cell death of aggregated cell. I) Non-treated cell and J) morphological control of apoptosis after treatment with cycloheximide. Bars – 20 μ m.

Figure 9. Involvement of lysosomes in anti-CD20 and anti-MHC class II induced cell

death. A) Detection of total lysosomal volume in cells treated with mAbs. Cells were incubated with anti-CD20 mAb tositumomab or anti-MHC class II mAb L243 as described previously. After that cells were labelled with lysotracker red as described in methods. The volume of lysosomal compartment was measured by FACS and visualised using fluorescence microscopy. Insert: L243 treated cell displaying single large lysosome. B) Detection of lysosomal membrane permeabilisation followed by permeabilisation of cytoplasm. Cells were treated with mAbs as described previously and then stained with acridine orange (AO) as described in methods. Relative increase or decrease in FL1 fluorescence was assessed by FACS. C) Permeabilisation of plasma membrane as detected by destained cytoplasm (arrows) of tositumomab treated cells. Cells were stained with AO as described and then assessed under fluorescence microscope.

Figure 10. Lysosome-mediated cell death evoked by tositumomab and L243 is

blocked by inhibitors of vATPase. Raji cells were pre-incubated with concanamycin A (0.01-100 nM) (A) or Bafilomycin A1 (B) for 30 minutes before being treated with tositumomab or L243. Cell death (AnV/PI+ cells) (A and B) has been measured at 4 or 24 hours after treatment. C) The impact of vATPase inhibitors on the volume of cellular

lysosomal compartment. Cells were incubated with concanamycin A (1 nM) or Bafilomycin A1 (50nM) for 30 min and then antibodies were added. After that cells were labelled with lysotracker red for 1 h as described in methods. The volume of lysosomal compartment was measured by FACS as FL2 channel fluorescence. Fluorescence of control Raji cells not labelled with lysotracker (red histograms) was set as a background. Histograms represent FL2 fluorescence values of lysotracker-labelled control cells with (green histograms) or without (black histograms) vATPase inhibitors as well as antibody treated cells with (purple histograms) or without (blue histograms) vATPase inhibitors.

Supplemental Figure 1. No impact of cholesterol extraction on surface expression of B cell antigens. Raji cells were incubated with control antibody (OKT3) (solid red histogram) or antibody against the relevant B cell surface antigen with (blue histogram) or without MCD pre-treatment (black histogram). After two washing steps, cells were incubated with FITC-labeled anti-mouse antibody, washed and assessed by flow cytometry. As can be seen MCD had almost no impact on the expression of CD20 (A), HLA DR (B) or μ (IgM) surface antigen (C).

Supplemental Figure 2. The impact of inhibition of actin polymerization on peripheral relocation of polarized mitochondria. Raji cells were pre-incubated with 10 μ M latrunculin B and then JC1 dye was added at a final concentration of 10 μ g/ml. After that, cells were treated with either tositumomab or L243 mAb and live cells assessed six hours later at 37°C in a humidified chamber. Red channel shows J-

aggregates of JC1 dye obtained with excitation wavelength of 535 and emission 590 nm and representing polarized mitochondria. Bars 20 μ m.

Supplemental video 1. Time lapse microscopy of Raji cells expressing AcGFP-labeled actin. Peripheral relocalisation of cellular actin in cells undergoing HA after treatment with tositumomab. Images were captured every 2 minutes after addition of antibody and are presented at a speed of 2 frames per second.

Supplemental video 2. Fluorescence recovery after photo bleaching (FRAP) of GFP-labeled actin in Raji cells treated with control antibody OKT3. No recovery of actin signal was observed in 100 seconds. Images were captured every 2 seconds after photo bleaching and are presented at a speed of 2 frames per second.

Supplemental video 3. Fluorescence recovery after photo bleaching (FRAP) of GFP-labeled actin in Raji cells treated with anti-CD20 mAb tositumomab. Rapid recovery of actin within the cell-cell contact area suggests increased lateral mobility of cytoplasmic actin after treatment with tositumomab. Images were captured every 2 seconds after photo bleaching and are presented at a speed of 2 frames per second.

Supplemental video 4. Fluorescence recovery after photo bleaching (FRAP) of GFP-labeled actin in Raji cells treated with anti-HLA DR mAb L243. Rapid recovery of actin within the cell-cell contact area suggests increased lateral mobility of cytoplasmic

actin after treatment with anti-HLA DR antibody L243. Images were captured every 2 seconds after photo bleaching and are presented at a speed of 2 frames per second.

Supplemental video 5. Time-lapse video microscopy of the kinetics of polarized mitochondria in tositumomab-treated Raji cells. Cells were stained for J-aggregates with JC1 mitochondrial dye, treated with tositumomab and assessed under the time-lapse microscope for a period of 6 h (x100 original magnification) at 37°C in a humidified chamber, with excitation wavelength of 535 and emission 590 nm. The dichroic filter has been set to 570 nm. Images were captured every 5 minutes and are presented at a speed of 2 frames per second.

References

1. Glennie, M.J., and Johnson, P.W. 2000. Clinical trials of antibody therapy. *Immunol Today* 21:403-410.
2. Glennie, M.J., and van de Winkel, J.G. 2003. Renaissance of cancer therapeutic antibodies. *Drug Discov Today* 8:503-510.
3. Cragg, M.S., French, R.R., and Glennie, M.J. 1999. Signaling antibodies in cancer therapy. *Curr Opin Immunol* 11:541-547.
4. Glennie, M.J., French, R.R., Cragg, M.S., and Taylor, R.P. 2007. Mechanisms of killing by anti-CD20 monoclonal antibodies. *Mol Immunol* 44:3823-3837.
5. Chan, H.T., Hughes, D., French, R.R., Tutt, A.L., Walshe, C.A., Teeling, J.L., Glennie, M.J., and Cragg, M.S. 2003. CD20-induced lymphoma cell death is independent of both caspases and its redistribution into triton X-100 insoluble membrane rafts. *Cancer Res* 63:5480-5489.
6. Cragg, M.S., and Glennie, M.J. 2004. Antibody specificity controls in vivo effector mechanisms of anti-CD20 reagents. *Blood* 103:2738-2743.
7. Cragg, M.S., Morgan, S.M., Chan, H.T., Morgan, B.P., Filatov, A.V., Johnson, P.W., French, R.R., and Glennie, M.J. 2003. Complement-mediated lysis by anti-CD20 mAb correlates with segregation into lipid rafts. *Blood* 101:1045-1052.
8. Beers, S.A., Chan, C.H., James, S., French, R.R., Attfield, K.E., Brennan, C.M., Ahuja, A., Shlomchik, M.J., Cragg, M.S., and Glennie, M.J. 2008. Type II (tositumomab) anti-CD20 monoclonal antibody out performs Type I (rituximab-like) reagents in B-cell depletion regardless of complement activation. *Blood*.
9. Dustin, M.L. 2007. Cell adhesion molecules and actin cytoskeleton at immune synapses and kinapses. *Curr Opin Cell Biol* 19:529-533.
10. Kansas, G.S., and Tedder, T.F. 1991. Transmembrane signals generated through MHC class II, CD19, CD20, CD39, and CD40 antigens induce LFA-1-dependent and independent adhesion in human B cells through a tyrosine kinase-dependent pathway. *J Immunol* 147:4094-4102.
11. Leverkus, M., McLellan, A.D., Heldmann, M., Eggert, A.O., Brocker, E.B., Koch, N., and Kampgen, E. 2003. MHC class II-mediated apoptosis in dendritic cells: a role for membrane-associated and mitochondrial signaling pathways. *Int Immunol* 15:993-1006.
12. Cerisano, V., Aalto, Y., Perdichizzi, S., Bernard, G., Manara, M.C., Benini, S., Cenacchi, G., Preda, P., Lattanzi, G., Nagy, B., et al. 2004. Molecular mechanisms of CD99-induced caspase-independent cell death and cell-cell adhesion in Ewing's sarcoma cells: actin and zyxin as key intracellular mediators. *Oncogene* 23:5664-5674.
13. Kasinrerk, W., Tokrasinwit, N., Moonsom, S., and Stockinger, H. 2000. CD99 monoclonal antibody induce homotypic adhesion of Jurkat cells through protein tyrosine kinase and protein kinase C-dependent pathway. *Immunol Lett* 71:33-41.
14. Cao, L., Yoshino, T., Kawasaki, N., Sakuma, I., Takahashi, K., and Akagi, T. 1997. Anti-CD53 monoclonal antibody induced LFA-1/ICAM-1-dependent and -independent lymphocyte homotypic cell aggregation. *Immunobiology* 197:70-81.

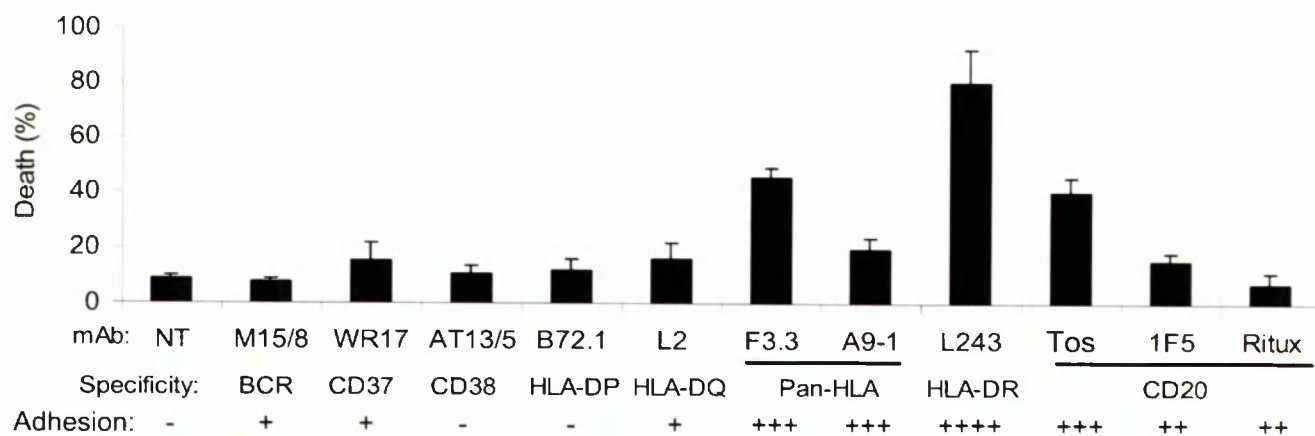
15. Greicius, G., Westerberg, L., Davey, E.J., Buentke, E., Scheynius, A., Thyberg, J., and Severinson, E. 2004. Microvilli structures on B lymphocytes: inducible functional domains? *Int Immunol* 16:353-364.
16. Li, H., Ayer, L.M., Polyak, M.J., Mutch, C.M., Petrie, R.J., Gauthier, L., Shariat, N., Hendzel, M.J., Shaw, A.R., Patel, K.D., et al. 2004. The CD20 calcium channel is localized to microvilli and constitutively associated with membrane rafts: antibody binding increases the affinity of the association through an epitope-dependent cross-linking-independent mechanism. *J Biol Chem* 279:19893-19901.
17. Stepczynska, A., Lauber, K., Engels, I.H., Janssen, O., Kabelitz, D., Wesselborg, S., and Schulze-Osthoff, K. 2001. Staurosporine and conventional anticancer drugs induce overlapping, yet distinct pathways of apoptosis and caspase activation. *Oncogene* 20:1193-1202.
18. Melino, G., Knight, R.A., and Nicotera, P. 2005. How many ways to die? How many different models of cell death? *Cell Death Differ* 12 Suppl 2:1457-1462.
19. Bras, M., Yuste, V.J., Roue, G., Barbier, S., Sancho, P., Virely, C., Rubio, M., Baudet, S., Esquerda, J.E., Merle-Beral, H., et al. 2007. Drp1 mediates caspase-independent type III cell death in normal and leukemic cells. *Mol Cell Biol* 27:7073-7088.
20. Sperandio, S., de Belle, I., and Bredesen, D.E. 2000. An alternative, nonapoptotic form of programmed cell death. *Proc Natl Acad Sci U S A* 97:14376-14381.
21. Wang, Y., Li, X., Wang, L., Ding, P., Zhang, Y., Han, W., and Ma, D. 2004. An alternative form of paraptosis-like cell death, triggered by TAJ/TROY and enhanced by PDCD5 overexpression. *J Cell Sci* 117:1525-1532.
22. Zhang, C., Xu, Y., Gu, J., and Schlossman, S.F. 1998. A cell surface receptor defined by a mAb mediates a unique type of cell death similar to oncosis. *Proc Natl Acad Sci U S A* 95:6290-6295.
23. Kroemer, G., and Jaattela, M. 2005. Lysosomes and autophagy in cell death control. *Nat Rev Cancer* 5:886-897.
24. He, J., Tohyama, Y., Yamamoto, K., Kobayashi, M., Shi, Y., Takano, T., Noda, C., Tohyama, K., and Yamamura, H. 2005. Lysosome is a primary organelle in B cell receptor-mediated apoptosis: an indispensable role of Syk in lysosomal function. *Genes Cells* 10:23-35.
25. Groth-Pedersen, L., Ostensfeld, M.S., Hoyer-Hansen, M., Nylandsted, J., and Jaattela, M. 2007. Vincristine induces dramatic lysosomal changes and sensitizes cancer cells to lysosome-destabilizing siramesine. *Cancer Res* 67:2217-2225.
26. Ono, K., Kim, S.O., and Han, J. 2003. Susceptibility of lysosomes to rupture is a determinant for plasma membrane disruption in tumor necrosis factor alpha-induced cell death. *Mol Cell Biol* 23:665-676.
27. Nylandsted, J., Gyrd-Hansen, M., Danielewicz, A., Fehrenbacher, N., Lademann, U., Hoyer-Hansen, M., Weber, E., Multhoff, G., Rohde, M., and Jaattela, M. 2004. Heat shock protein 70 promotes cell survival by inhibiting lysosomal membrane permeabilization. *J Exp Med* 200:425-435.
28. Muroi, M., Shiragami, N., Nagao, K., Yamasaki, M., and Takatsuki, A. 1993. Folimycin (concanamycin A), a specific inhibitor of V-ATPase, blocks

- intracellular translocation of the glycoprotein of vesicular stomatitis virus before arrival to the Golgi apparatus. *Cell Struct Funct* 18:139-149.
29. Kataoka, T., Shinohara, N., Takayama, H., Takaku, K., Kondo, S., Yonehara, S., and Nagai, K. 1996. Concanamycin A, a powerful tool for characterization and estimation of contribution of perforin- and Fas-based lytic pathways in cell-mediated cytotoxicity. *J Immunol* 156:3678-3686.
 30. Walshe, C.A., Beers, S.A., French, R.R., Chan, C.H., Johnson, P.W., Packham, G.K., Glennie, M.J., and Cragg, M.S. 2008. Induction of cytosolic calcium flux by CD20 is dependent upon B Cell antigen receptor signaling. *J Biol Chem* 283:16971-16984.
 31. Houshmand, P., and Zlotnik, A. 2003. Targeting tumor cells. *Curr Opin Cell Biol* 15:640-644.
 32. Unruh, T.L., Li, H., Mutch, C.M., Shariat, N., Grigoriou, L., Sanyal, R., Brown, C.B., and Deans, J.P. 2005. Cholesterol depletion inhibits src family kinase-dependent calcium mobilization and apoptosis induced by rituximab crosslinking. *Immunology* 116:223-232.
 33. Yang, H.C., Palazzo, A., Swayne, T.C., and Pon, L.A. 1999. A retention mechanism for distribution of mitochondria during cell division in budding yeast. *Curr Biol* 9:1111-1114.
 34. Van Gestel, K., Kohler, R.H., and Verbelen, J.P. 2002. Plant mitochondria move on F-actin, but their positioning in the cortical cytoplasm depends on both F-actin and microtubules. *J Exp Bot* 53:659-667.
 35. Hollenbeck, P.J., and Saxton, W.M. 2005. The axonal transport of mitochondria. *J Cell Sci* 118:5411-5419.
 36. Rustom, A., Saffrich, R., Markovic, I., Walther, P., and Gerdes, H.H. 2004. Nanotubular highways for intercellular organelle transport. *Science* 303:1007-1010.
 37. Watkins, S.C., and Salter, R.D. 2005. Functional connectivity between immune cells mediated by tunneling nanotubes. *Immunity* 23:309-318.
 38. Valdez, Y., Mah, W., Winslow, M.M., Xu, L., Ling, P., and Townsend, S.E. 2002. Major histocompatibility complex class II presentation of cell-associated antigen is mediated by CD8alpha+ dendritic cells in vivo. *J Exp Med* 195:683-694.
 39. Harshyne, L.A., Watkins, S.C., Gambotto, A., and Barratt-Boyes, S.M. 2001. Dendritic cells acquire antigens from live cells for cross-presentation to CTL. *J Immunol* 166:3717-3723.
 40. Nolte-'t Hoen, E.N., Wagenaar-Hilbers, J.P., Peters, P.J., Gadella, B.M., van Eden, W., and Wauben, M.H. 2004. Uptake of membrane molecules from T cells endows antigen-presenting cells with novel functional properties. *Eur J Immunol* 34:3115-3125.
 41. Onfelt, B., Nedvetzki, S., Yanagi, K., and Davis, D.M. 2004. Cutting edge: Membrane nanotubes connect immune cells. *J Immunol* 173:1511-1513.
 42. Poupot, M., and Fournie, J.J. 2003. Spontaneous membrane transfer through homotypic synapses between lymphoma cells. *J Immunol* 171:2517-2523.
 43. Ivanov, A., Krysov, S., Cragg, M.S., and Illidge, T. 2008. Radiation therapy with tositumomab (B1) anti-CD20 monoclonal antibody initiates extracellular signal-

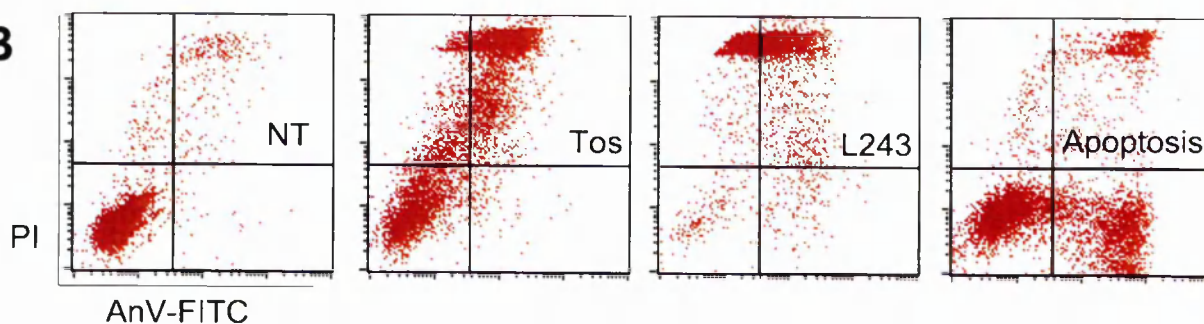
- regulated kinase/mitogen-activated protein kinase-dependent cell death that overcomes resistance to apoptosis. *Clin Cancer Res* 14:4925-4934.
44. Leveille, C., Zekki, H., Al-Daccak, R., and Mourad, W. 1999. CD40- and HLA-DR-mediated cell death pathways share a lot of similarities but differ in their use of ADP-ribosyltransferase activities. *Int Immunol* 11:719-730.
 45. Zhang, N., Khawli, L.A., Hu, P., and Epstein, A.L. 2007. Lym-1-induced apoptosis of non-Hodgkin's lymphomas produces regression of transplanted tumors. *Cancer Biother Radiopharm* 22:342-356.
 46. Bains, S.K., Mone, A., Yun Tso, J., Lucas, D., Byrd, J.C., Weiner, G.J., and Green, J.M. 2003. Mitochondria control of cell death induced by anti-HLA-DR antibodies. *Leukemia* 17:1357-1365.
 47. Carmagnat, M., Drenou, B., Chahal, H., Lord, J.M., Charron, D., Estaquier, J., and Mooney, N.A. 2006. Dissociation of caspase-mediated events and programmed cell death induced via HLA-DR in follicular lymphoma. *Oncogene* 25:1914-1921.
 48. Accolla, R.S. 1983. Human B cell variants immunoselected against a single Ia antigen subset have lost expression of several Ia antigen subsets. *J Exp Med* 157:1053-1058.
 49. Glennie, M.J., McBride, H.M., Worth, A.T., and Stevenson, G.T. 1987. Preparation and performance of bispecific F(ab' gamma)2 antibody containing thioether-linked Fab' gamma fragments. *J Immunol* 139:2367-2375.

Figure 1

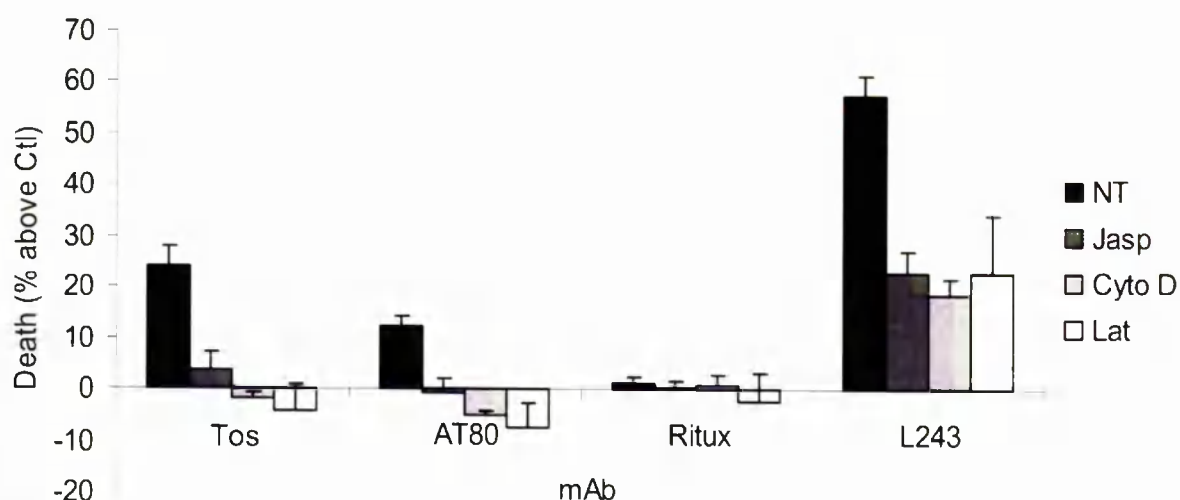
A



B



C



D

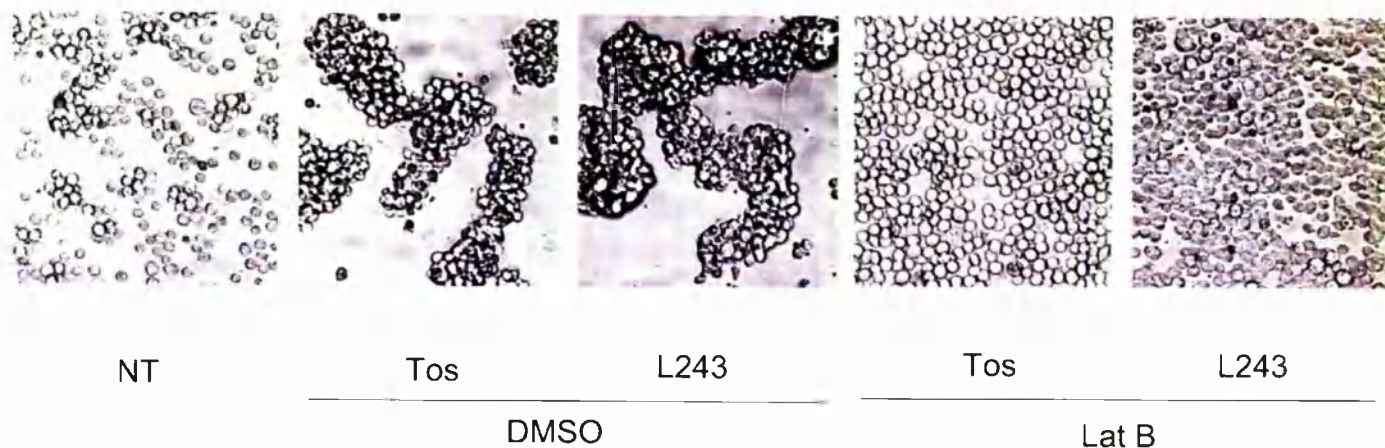


Figure 2

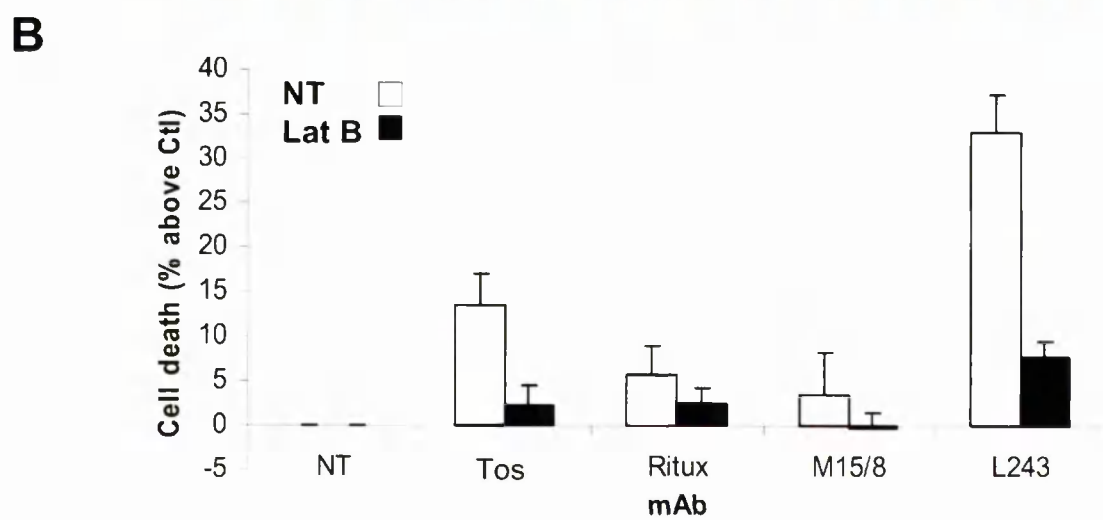
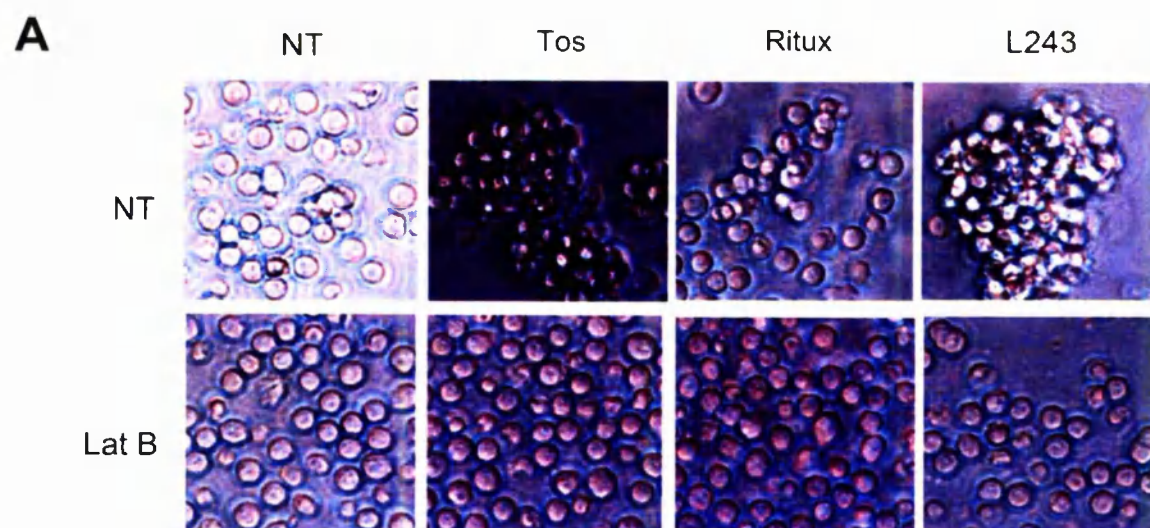
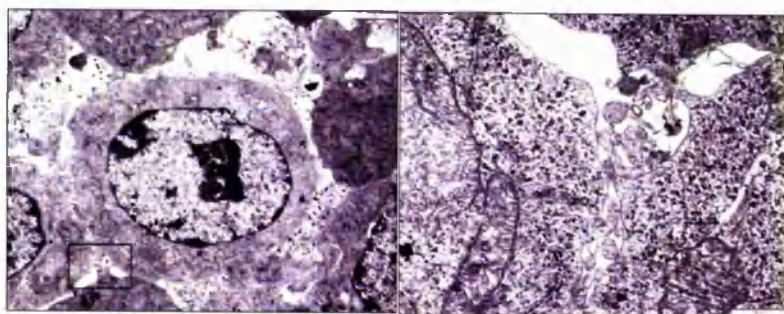
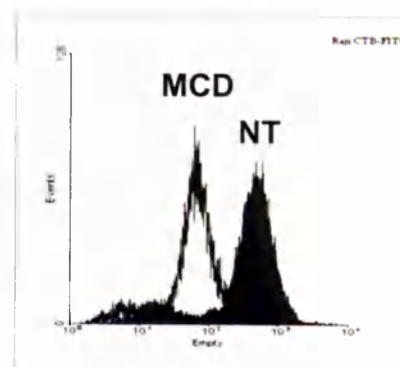


Figure 3

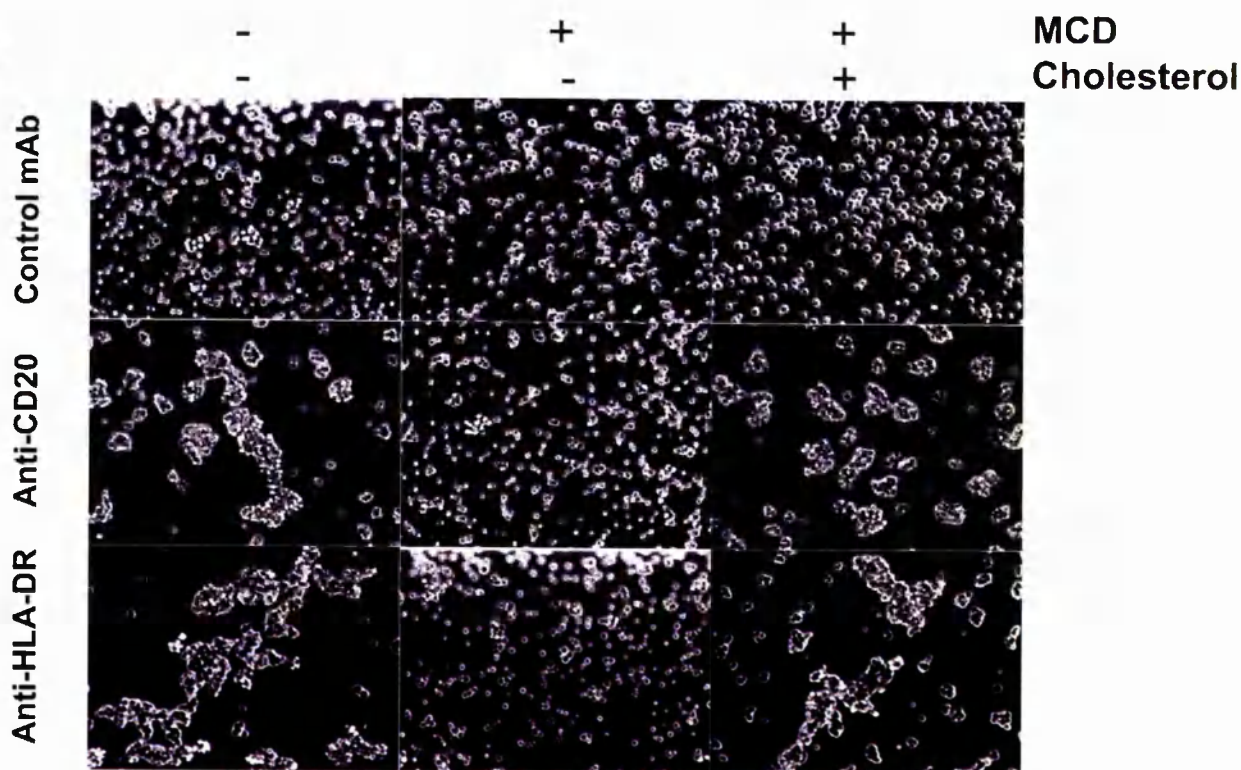
A



B



C



D

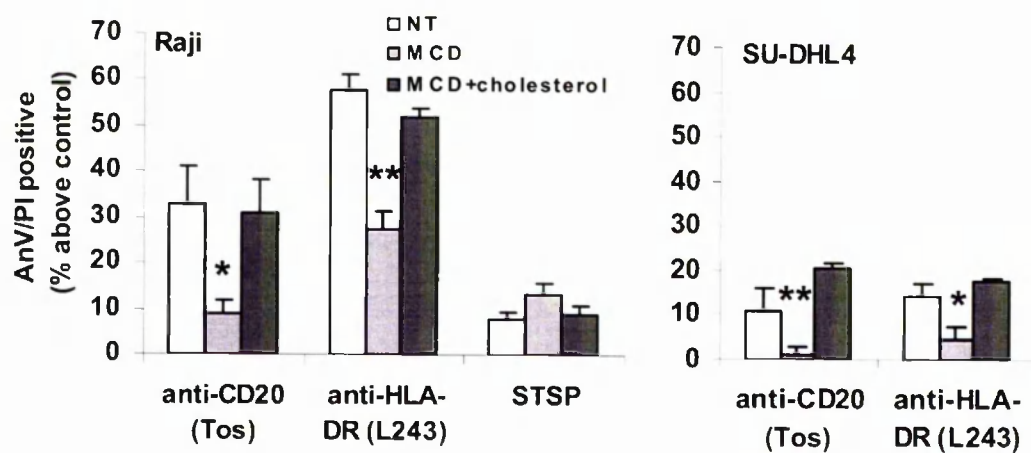


Figure 4

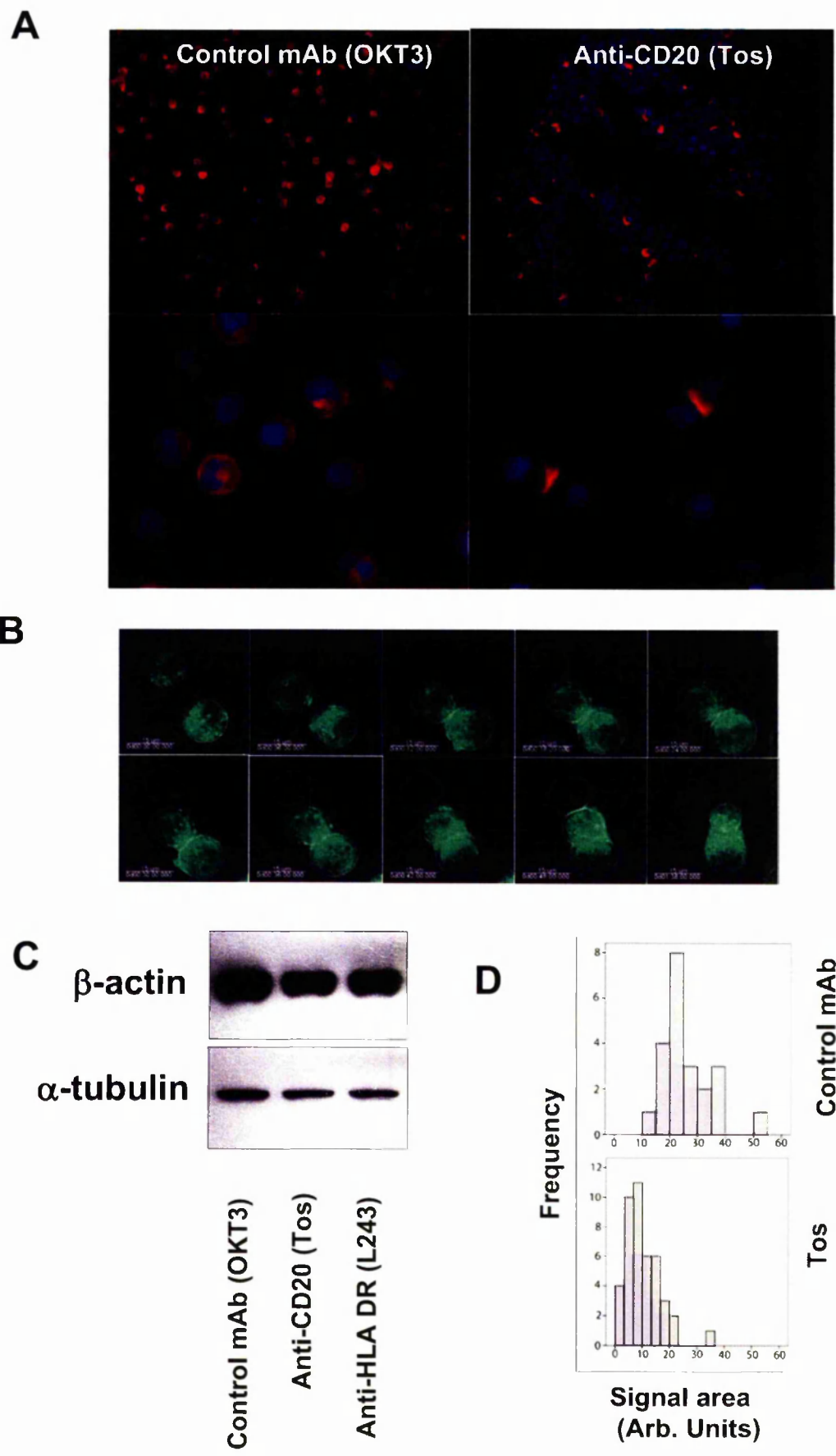


Figure 5

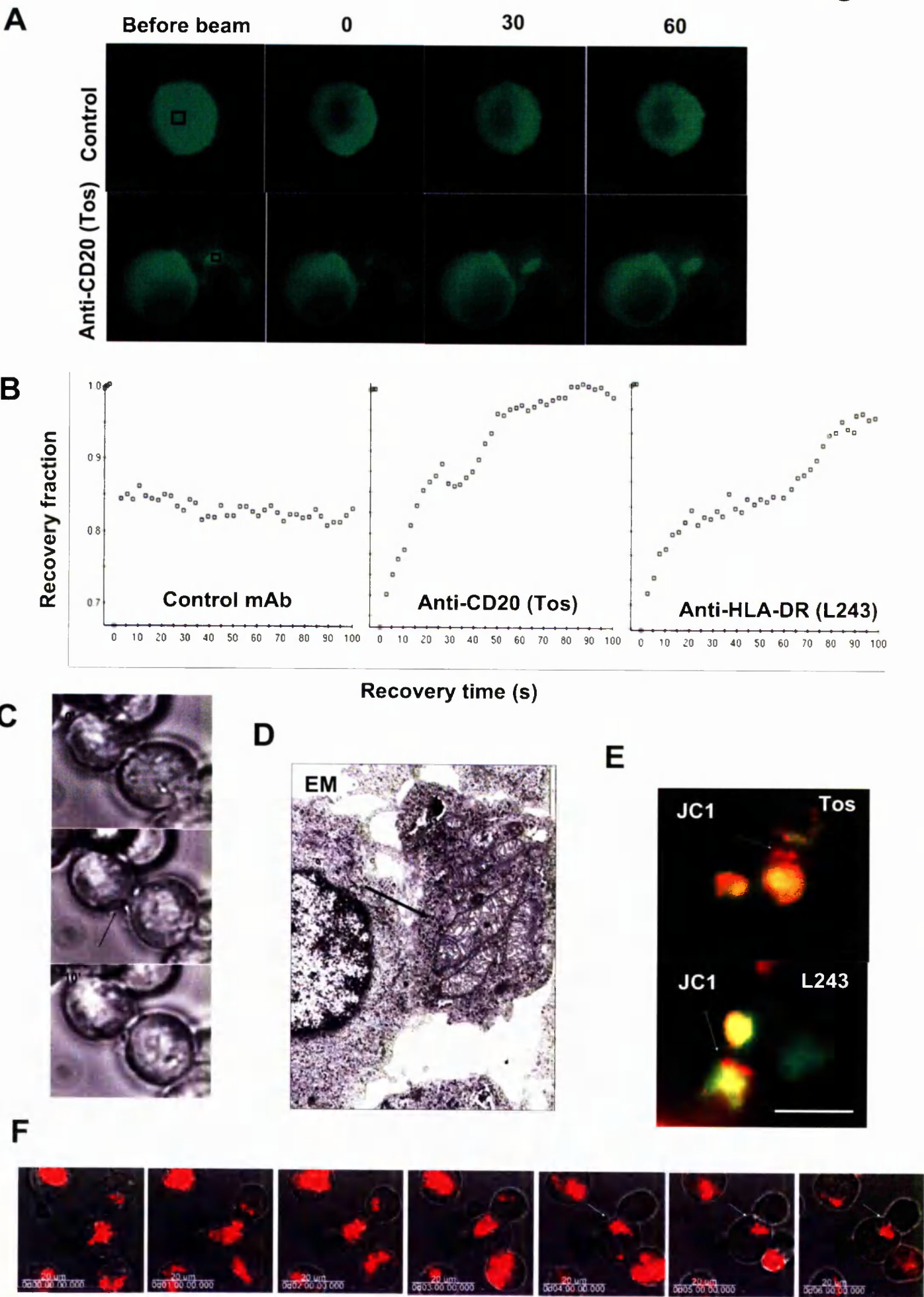
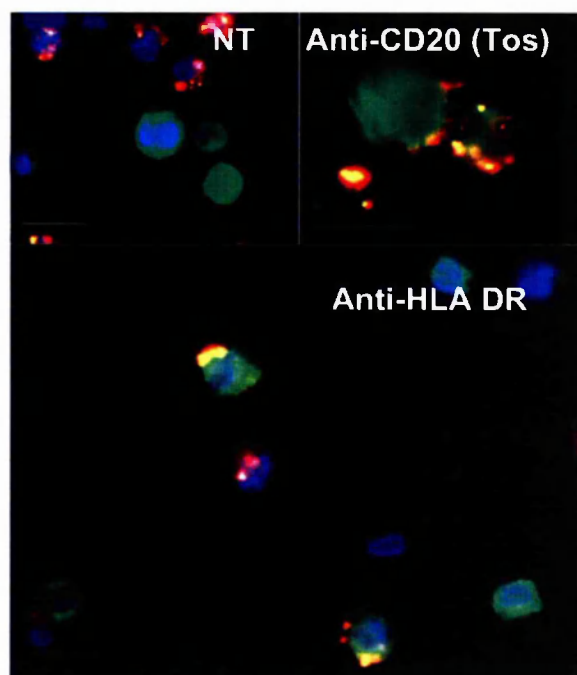
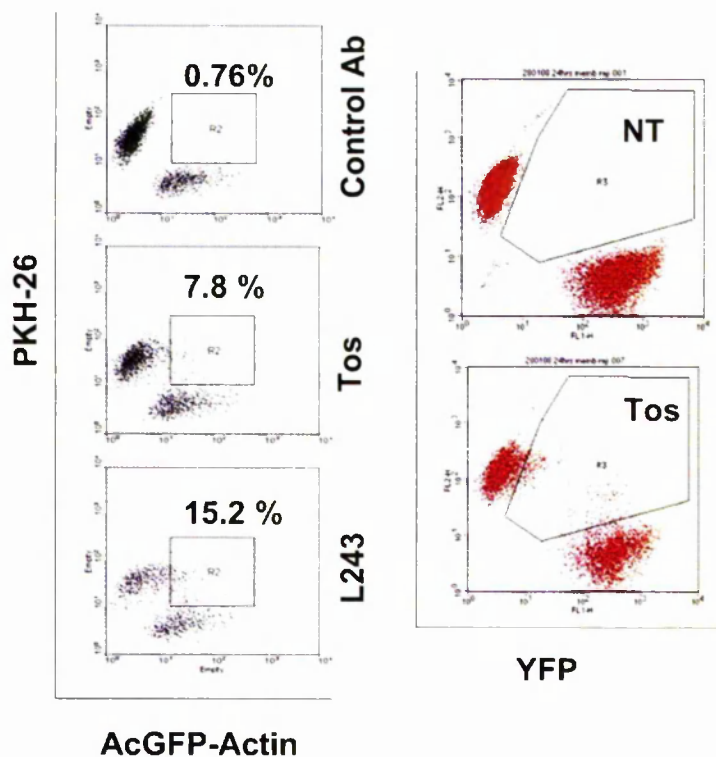


Figure 6

A



B



C

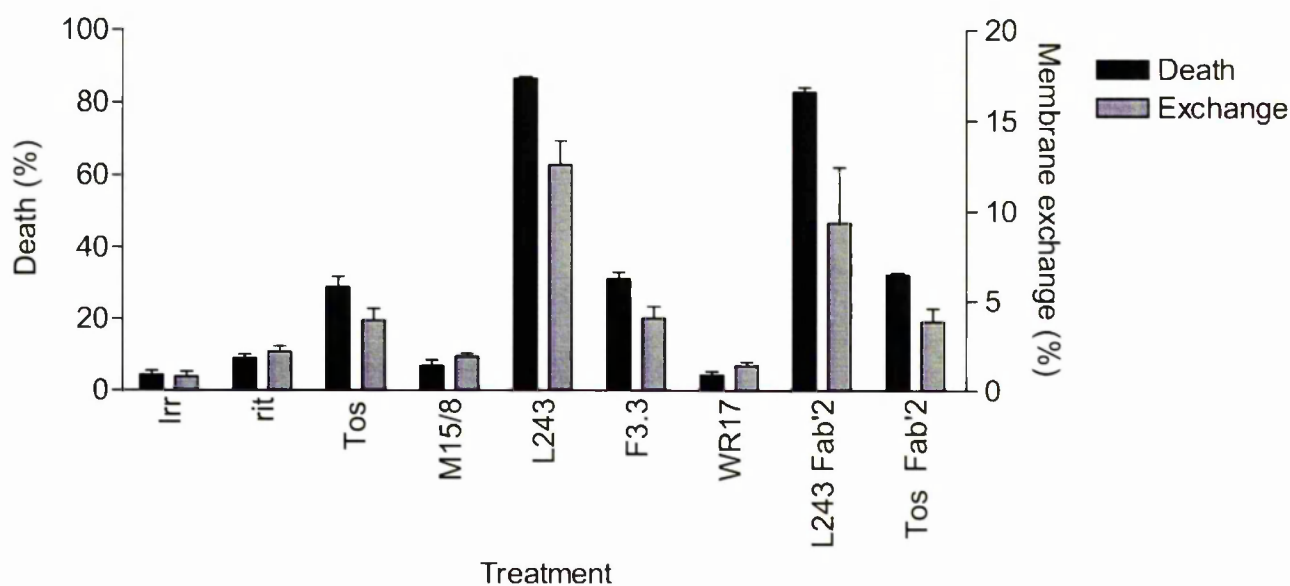


Figure 7

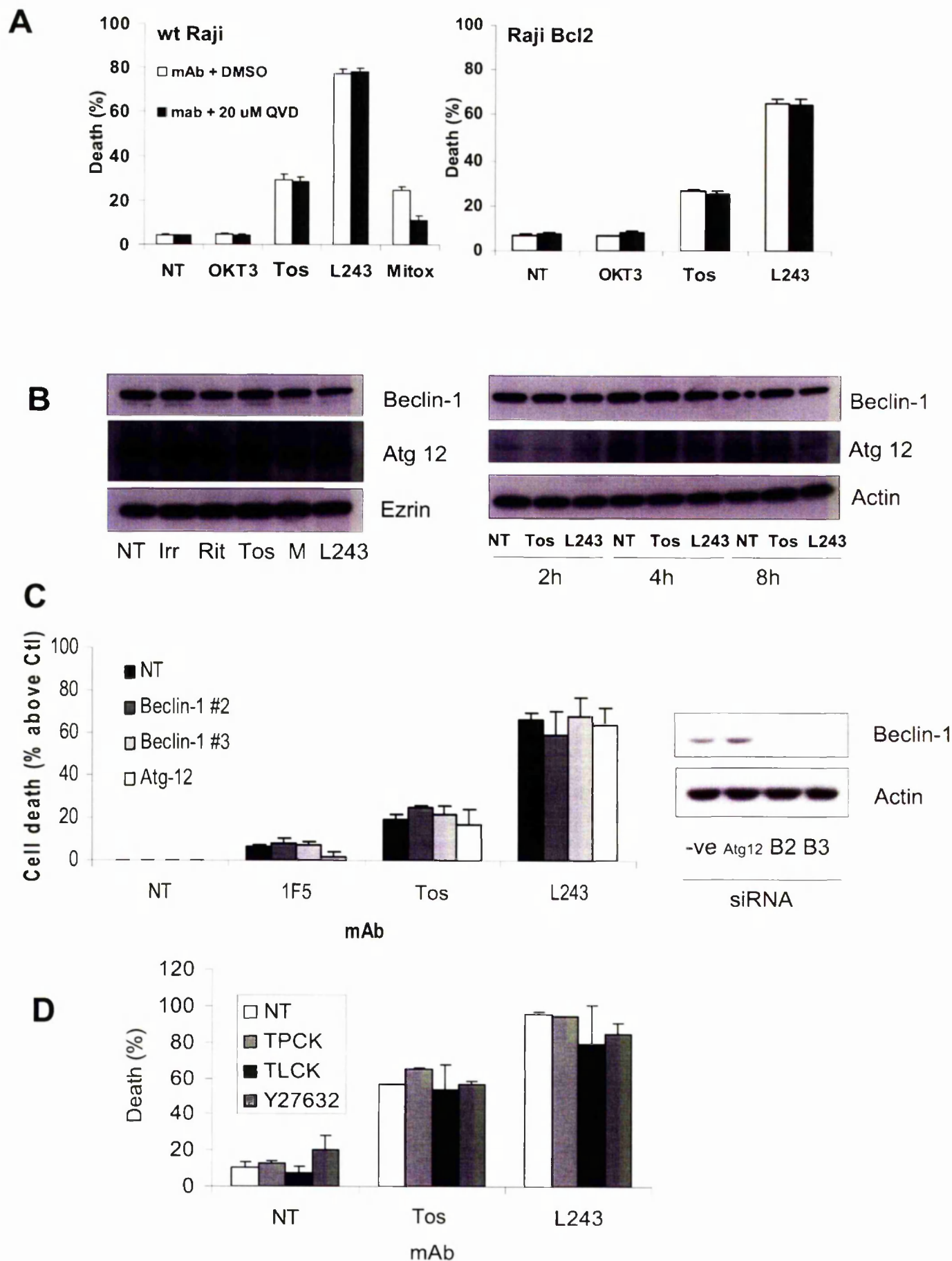


Figure 8

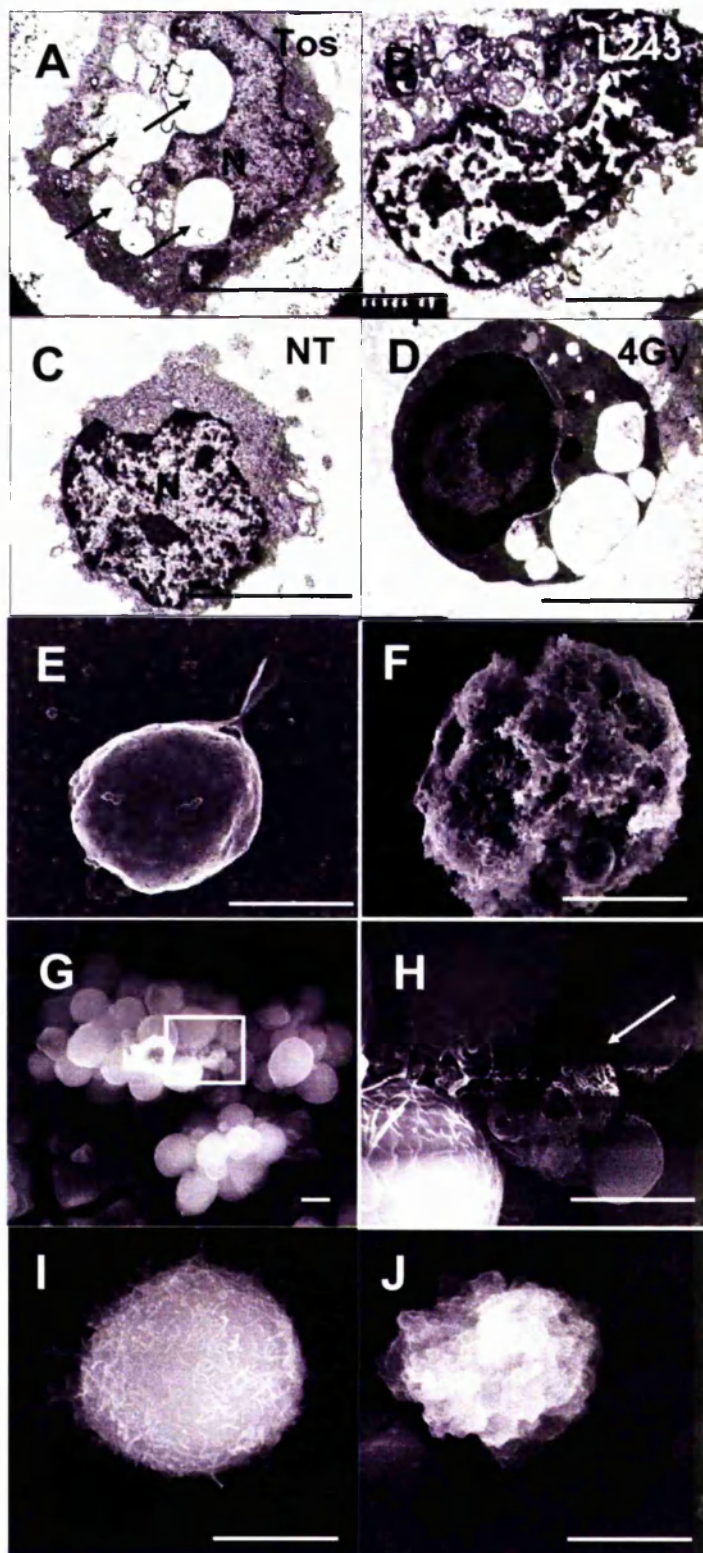
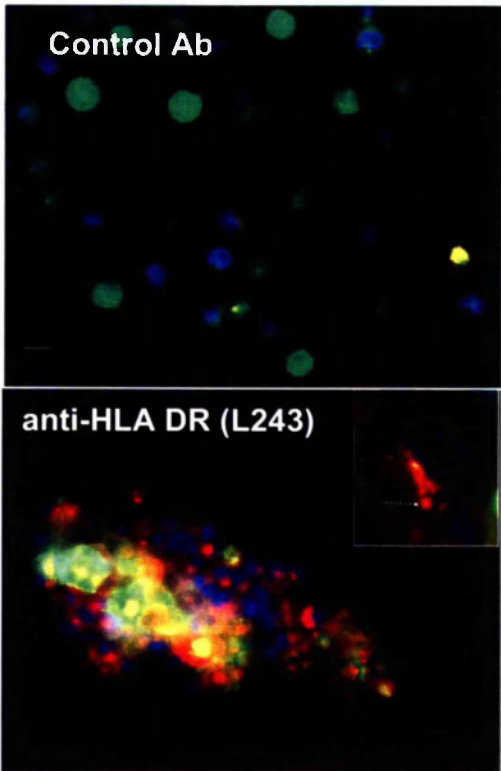
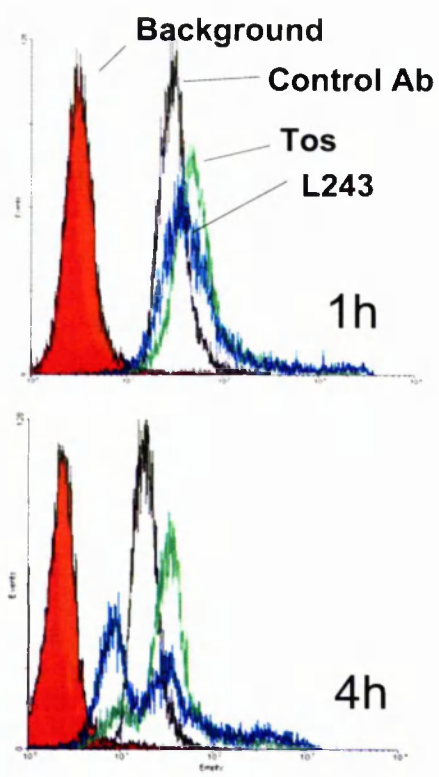
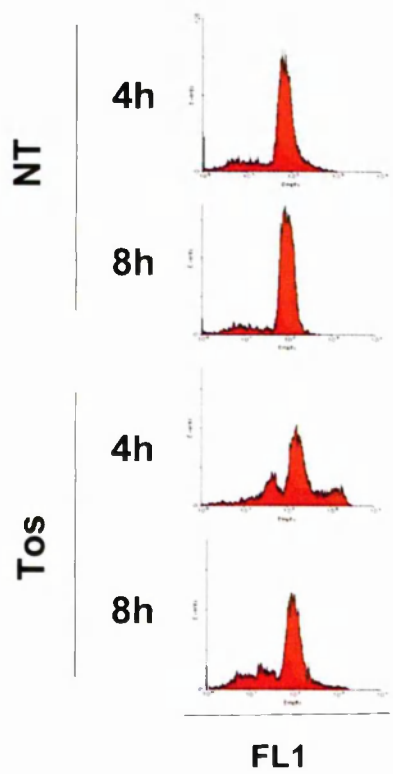


Figure 9

A



B



C

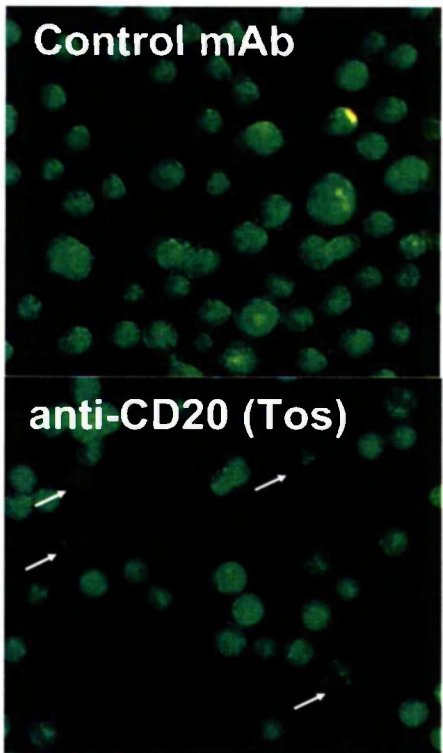
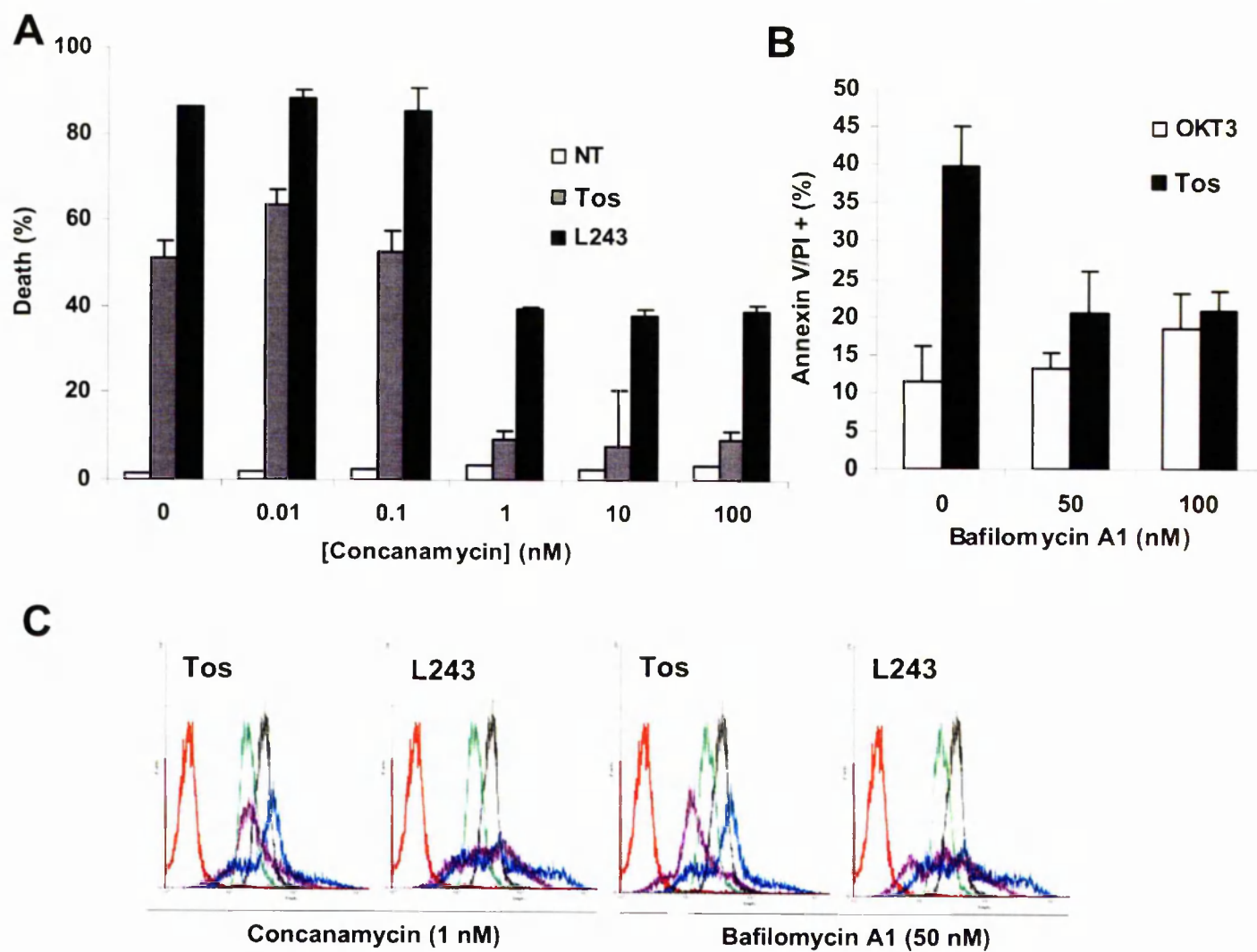
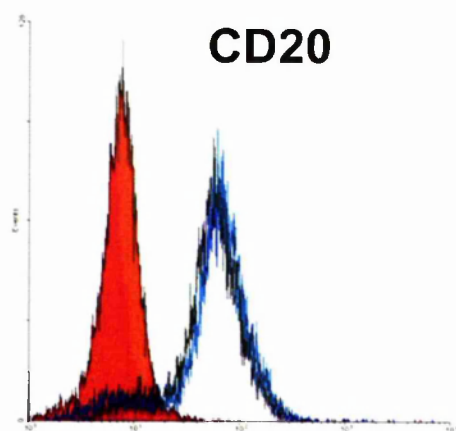


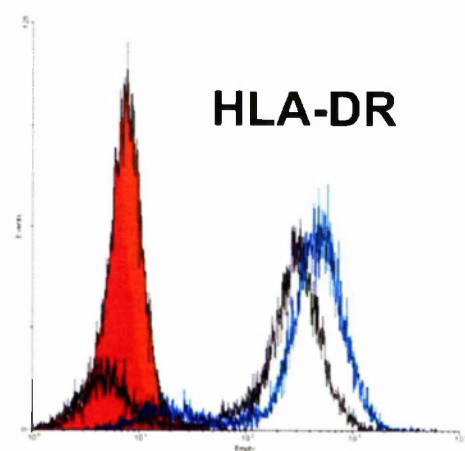
Figure 10



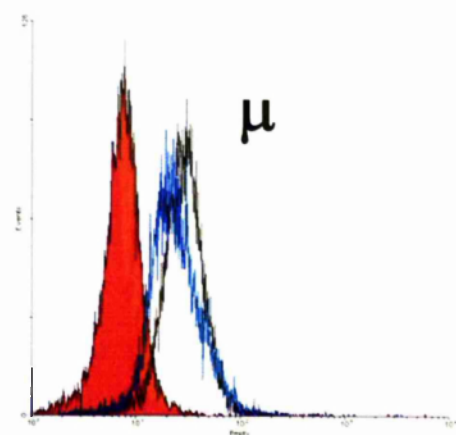
A

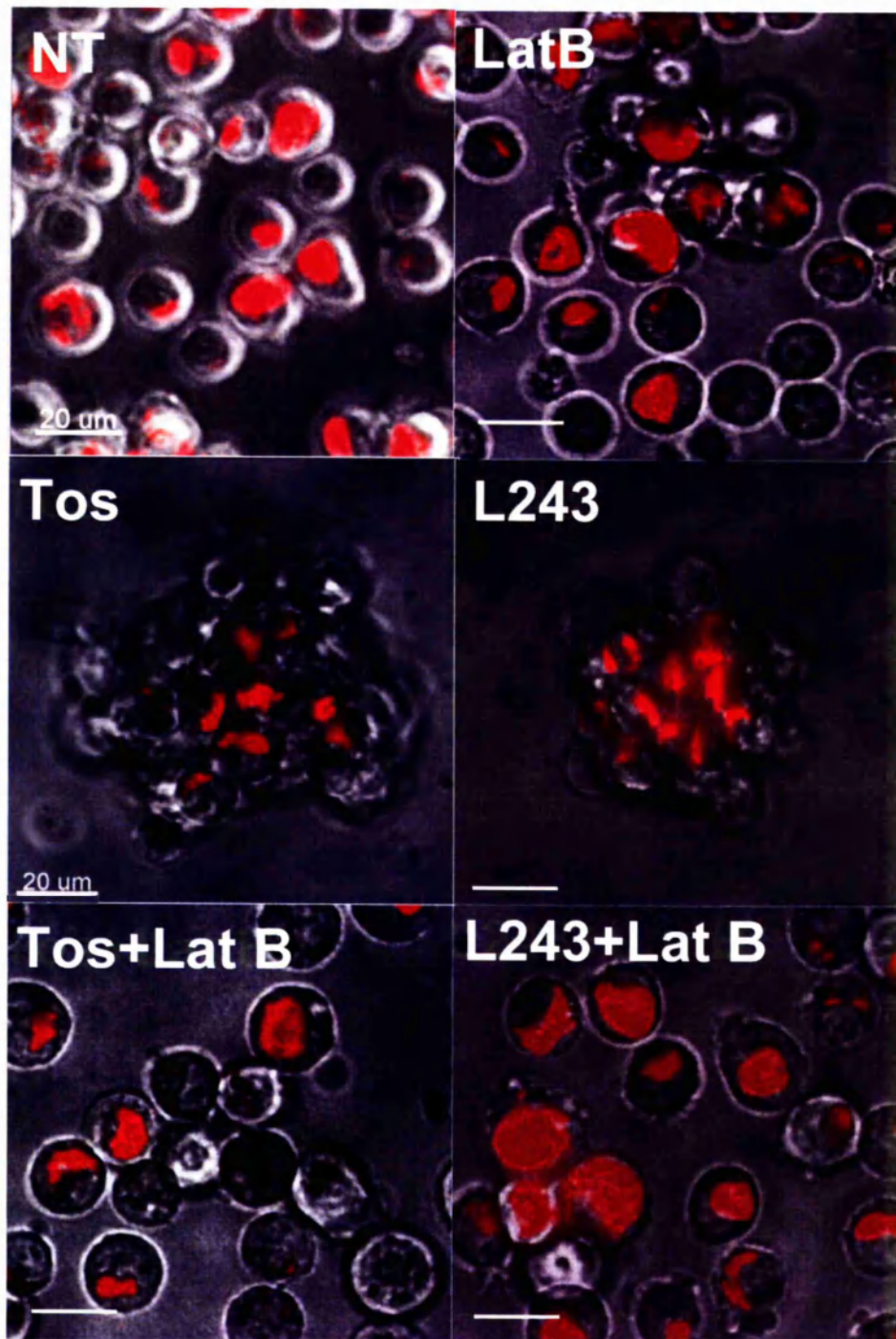


B



C





Chapter 10

Radiation therapy with Tositumomab (B1) anti-CD20 mAb initiates ERK/MAPK dependent cell death that overcomes resistance to apoptosis.

Ivanov A, Krysov S, Cragg M, Illidge T. Clin Cancer Res. 2008

Radiation Therapy with Tositumomab (B1) Anti-CD20 Monoclonal Antibody Initiates Extracellular Signal-Regulated Kinase/Mitogen-Activated Protein Kinase – Dependent Cell Death that Overcomes Resistance to Apoptosis

Andrey Ivanov,¹ Sergei Krysov,² Mark S. Cragg,² and Tim Illidge¹

Abstract Purpose: The use of targeted radiation therapy (RT) in conjunction with anti-CD20 monoclonal antibodies (mAb) delivers high clinical response rates in B-cell lymphomas as part of radioimmunotherapy. The mechanisms underlying these impressive responses, particularly in patients whose lymphomas have become refractory to chemotherapy, are poorly understood.

Experimental Design: In this study, we have investigated the signaling pathways and mode of cell death induced in B-cell lymphoma cells after the combination of RT and either type I (rituximab) or type II (tositumomab/B1) anti-CD20 mAb.

Results: Increased tumor cell death was observed when RT was combined with tositumomab, but not rituximab. This additive cell death was found to be mitogen-activated protein kinase/extracellular signal-regulated kinase (ERK) – dependent and could be reversed with mitogen-activated protein/extracellular signal-regulated kinase kinase (MEK) inhibitors, as well as small interfering RNA targeting MEK1/2. Furthermore, we found that this increased death was associated with ERK1/2 nuclear accumulation after tositumomab treatment, which was enhanced in combination with RT. Importantly, although Bcl-2 overexpression resulted in resistance to RT-induced apoptosis, it had no effect on the tumor cell death induced by tositumomab plus RT, indicating a nonapoptotic form of cell death.

Conclusions: These findings indicate that RT and type II anti-CD20 mAb combine to stimulate a prodeath function of the MEK-ERK1/2 pathway, which is able to overcome apoptotic resistance potentially explaining the efficacy of this modality in treating patients with chemoresistant disease.

Although most non-Hodgkin's lymphomas initially respond well to conventional treatment, the majority of patients with advanced disease will still relapse (1). Therefore, more effective treatments are being sought, and the introduction of the anti-CD20 monoclonal antibody (mAb) rituximab has significantly improved patient outcome in non-Hodgkin's lymphomas. As a single agent, rituximab results in a 46% response rate in

patients with relapsed low-grade lymphomas with complete responses occurring in around 6% (2). However, when rituximab is combined with chemotherapy, greatly enhanced response rates, durations of remissions, and improvements in survival are observed (3). An alternative approach to chemimmunotherapy is radioimmunotherapy, wherein radioisotopes have been conjugated to mAb. Radioimmunotherapy using anti-CD20 mAb radioimmunoconjugates has also led to impressive clinical results in relapsed indolent B-cell malignancies with high overall (80-97%) and complete (30-75%) response rates (4-6). To date, two distinct anti-CD20 radioimmunotherapy approaches have been approved by the U.S. Food and Drug Administration for the treatment of relapsed indolent B-cell malignancies, namely ⁹⁰Y ibritumomab tiuxetan (Zevalin) and ¹³¹I tositumomab (Bexxar). Despite these clinical successes, the underlying cellular mechanisms behind these impressive clinical responses are poorly understood and commonly attributed simply to efficient targeting of systemic radiation by the mAb (7).

Previous studies have suggested that several mechanisms might be involved in the therapeutic action of anti-CD20 mAb, including antibody-dependent cellular cytotoxicity, complement-dependent cytotoxicity, and the induction of growth arrest or cell death (reviewed in ref. 8). How anti-CD20 mAb and radiation treatment (RT) might combine to increase

Authors' Affiliations: ¹School of Cancer and Imaging Sciences, CRUK Paterson Institute for Cancer Research, University of Manchester, United Kingdom and ²Tenovus Laboratory, Cancer Sciences Division, University of Southampton, Southampton, United Kingdom

Received 12/5/07; revised 3/7/08; accepted 3/11/08.

Grant support: Cancer Research UK, American Institute for Cancer Research, and Tenovus.

The costs of publication of this article were defrayed in part by the payment of page charges. This article must therefore be hereby marked *advertisement* in accordance with 18 U.S.C. Section 1734 solely to indicate this fact.

Note: M.S. Cragg and T. Illidge should both be considered senior authors and contributed equally to the project.

Requests for reprints: Tim Illidge, School of Cancer Imaging Sciences, School of Medicine, University of Manchester, Manchester, M20 4BX, United Kingdom. Phone: 00-44-161-918-7024; Fax: 00-44-161-446-3109; E-mail: tmi@manchester.ac.uk.

© 2008 American Association for Cancer Research.

doi:10.1158/1078-0432.CCR-07-5072

therapeutic efficacy are poorly understood. Furthermore, it is now emerging that fine specificity differences exist in the epitope binding site of different anti-CD20 mAb, which may determine their biological activity (9).

Our group has previously shown that anti-CD20 mAb may be subdivided as either rituximab-like (type I) or tositumomab-like (type II) according to their linked activity in a number of *in vitro* assays. For example, rituximab and other type I mAb redistribute CD20 into Triton X-100 insoluble membrane rafts, correlating with their ability to engage complement effectively and cause complement-dependent cytotoxicity (10). In contrast, type II mAb, such as tositumomab, do not redistribute CD20 into Triton X-100 rafts but are more potent at inducing homotypic adhesion and cell death of target cells (11). Importantly, these differences seem to translate to the *in vivo* mechanisms used by these mAb, at least in xenograft tumor models (12).

Binding of anti-CD20 mAb to lymphoma cells *in vitro* has been shown to induce modest levels of cell death, presumably via signaling through the CD20 molecule (13). A range of signaling events may be induced after ligation of CD20 (reviewed in ref. 8), including activation of the mitogen-activated protein kinase (MAPK) cascade (14). The Ras-Raf-mitogen-activated protein/extracellular signal-regulated kinase (ERK) kinase (MEK)-ERK1/2 pathway is an evolutionary conserved pathway that is involved in the control of many fundamental cellular processes, including cell proliferation, survival, differentiation, cell death, motility, and metabolism (reviewed by ref. 15). Although commonly thought of as a component of proliferation and survival pathways, ERK1/2 signaling has also been associated with apoptotic signaling in immature B-cell lymphoma (16) and diffuse large B-cell lymphoma cells (17). Similarly, it has been suggested that the overall balance of MAPK activity may determine B-cell fate depending on the kinetics of activation and maturation state of the cell (18, 19).

Intriguingly, the MAPK cascade is also triggered by RT and other DNA-damaging agents (20, 21) where it may be involved in signaling for DNA double-strand break repair by homologous recombination (22). Given that both anti-CD20 mAb and RT have been shown to trigger MAPK activation and that MAPK activation can result in diverse biological outcomes, we have therefore investigated the effect of combining RT with anti-CD20 mAb on this cell signaling pathway. Specifically, we have attempted to investigate the anti-CD20 mAb used in the U.S. Food and Drug Administration-approved radioimmunotherapy modalities, ^{90}Y ibritumomab tiuxetan (zevalin) and ^{131}I tositumomab (Bexxar), by combining rituximab and its murine parent mAb (ibritumomab), as well as tositumomab with RT.

Here, we report that when tositumomab is combined with RT an additive increased level of cell death that is not seen with either rituximab or ibritumomab in combination with RT is observed. We show that MEK/ERK1/2 activity seems critical for this additive cell death. Furthermore, although Bcl-2 overexpression mediated protection of cells against RT alone, it had no effect on the additive tumor cell death seen with tositumomab plus RT. This study provides potentially new clinically relevant insights into the involvement of MEK/ERK1/2 signaling in cell death induced by type II anti-CD20 mAb and RT that seems to bypass the apoptotic machinery.

Materials and Methods

Cell lines and materials. Human cell lines were obtained from the European Collection of Animal Cell Cultures and maintained in antibiotic-free RPMI 1640 with FCS (Sigma; 10%), glutamine (2 mmol/L; Life Technologies) at 37°C, 5% CO₂. The following therapeutic antibodies were used at 5 µg/mL: tositumomab (anti-CD20; GlaxoSmithKline), rituximab (anti-CD20; Roche), ibritumomab (anti-CD20; IDEC Pharmaceuticals), L243 (anti-IL1A DR; American Type Tissue Collection), OKT3 (anti-CD3). F(ab')₂ fragments of antibodies were kindly prepared by Dr. S.A. Beers and Dr. A. Tutt (Tenovus Laboratory). Diagnostic antibodies used in this study were as follows: MEK1 and MEK2 (Labvision/Neomarkers), phosphorylated ERK1/2 (pERK1/2) and total ERK1/2 (New England Biolabs (UK) Ltd.), Bcl-2-FTIC (Dako UK Ltd.), goat anti-rabbit horseradish peroxidase (Sigma), rabbit anti-mouse horseradish peroxidase (Sigma-Aldrich). Inhibitors used in the study were as follows: MEK1/2 inhibitors U0126 (10 µmol/L; Promega), PD98059 (10 µmol/L), or general caspase inhibitor QVD (20 µmol/L; both Calbiochem, Merck Chemicals Ltd.). For experiments involving pharmacologic inhibition of cellular signaling cascades, cells were preincubated in the presence of the relevant inhibitor for 30 min.

Irradiation of cells. Cell lines were irradiated using a Gulmay D3 225 X-ray source using a dose rate of 0.77 Gy/min. Low-dose rate irradiations were carried out using a ^{60}Co γ-ray source, as described previously (23).

Transfection of Raji and BL60 cells. Transfection of Raji and BL60 cells with pEF plasmid encoding Bcl-2 vector, kindly donated by Dr. Andreas Strasser and Dr. David Huang, was achieved via electroporation using standard electroporation techniques. Selection with geneticin (1-2 mg/mL) or puromycin (1 µg/mL) was applied 24 to 48 h later. Bcl-2 expression levels were determined by flow cytometric intracellular staining methods using an anti-Bcl-2 antibody (BD Pharmingen) according to the manufacturer's instructions.

Silencing of MEK1 and MEK2 with small interfering RNA. Silencer validated small interfering RNA (siRNA) against MEK1 and MEK2 (or scrambled control siRNA) were obtained from Ambion (Europe Ltd.) and used at 100 nmol/L. siRNA was delivered to cells using the Amaxa nucleofection device, nucleofection, kit T, and program G016. The nucleofection efficiency was assessed using the pmaxGFP control vector (supplied with nucleofection kit) and was 86% to 93% for Raji and 55% to 60% for SU-DHL4 cells at the 24-h time point.

Western blotting. Cell lysates were prepared in PhoshoSafe lysis solution (MERCK Biosciences Ltd.) containing protease inhibitors. Protein samples were separated by SDS/PAGE and then electroblotted onto a polyvinylidene difluoride membrane (Hybond; Amersham Pharmacia Biotech). Antibodies were added for either 1 h at room temperature or at 4°C overnight as indicated by the manufacturers. Detection was done with horseradish peroxidase-conjugated secondary antibodies (specific to mouse or rabbit IgG) and enhanced chemiluminescence (Amersham Biosciences).

Detection of cell surface phosphatidylserine exposure: Annexin V/propidium iodide assay. Cells (1×10^5) were washed and resuspended in binding buffer [10 mmol/L HEPES (pH 7.4), 140 mmol/L NaCl, and 2.5 mmol/L CaCl₂], containing 1 µg/mL FITC-Annexin V (BD Biosciences). Propidium iodide (PI; 10 µg/mL) was added to the samples to distinguish between early cell death and secondary necrosis. Subsequently, cells were assessed by flow cytometry on a FACScan (BD Biosciences).

Measurement of DNA fragmentation: fluorescence in situ end labeling. The fluorescence variant of terminal dUTP N-end labeling has been done essentially as described previously (24). The reaction mix (100 µL) contained 1 µL (25 units) terminal transferase (Promega), 20 µL 5 × cacodylate buffer (supplied with the enzyme), 1 µL 0.5 mmol/L biotin-16-dUTP (Roche), 3 µL 0.5 mmol/L dTTP, and 75 µL H₂O. Preparations were incubated at 37°C for 1 h with this reaction

mix, and the reaction was terminated by washing. The incorporated biotin-dUTP was detected with FITC-conjugated avidin (Vector Laboratories). The proportion of fluorescence *in situ* end labeling (FISEL)-positive cells was determined using a fluorescence microscope (Zeiss AxioScope). At least 300 cells in at least five viewing fields were observed.

Clonogenic survival assay. To measure clonogenic survival, a serial dilution assay was done using a method similar to that published previously (25). Briefly, each sample was treated with a range of doses of irradiation and seeded into individual wells of a 96-well plate over a range of cell densities (12 wells per cell density, eight cell densities per dose) in 20% conditioned medium. After 14 d, the fraction of wells containing no surviving cells was determined using a light microscope. The cell number that resulted in 30% empty wells was calculated and used to generate a clonogenic survival curve that was normalized according to plating efficiency.

2,3-Bis[2-methoxy-4-nitro-5-sulphophenyl]-2H-tetrazolium-5-carboxanilide inner salt cell viability assay. Colorimetric 2,3-bis[2-methoxy-4-nitro-5-sulphophenyl]-2H-tetrazolium-5-carboxanilide inner salt (XTT; Roche Diagnostics Ltd.) according to the manufacturer's instructions. Briefly, cells were treated in 96-well plates, and 72 h later, XTT reagent was added. After 4 h of incubation, absorbance was measured with the GENios Multi-Detection Microplate Reader (Pecan UK Ltd.) using 485 nm detection and 680 nm reference filters.

Fluorescence microscopy and image analysis. For immunofluorescent staining, harvested cells were cytospun onto clean poly-L-lysine-coated microscope slides. Samples were fixed in absolute methanol at -20°C for 30 min and rinsed in ice-cold acetone for a few seconds. Slides were washed thrice for 10 min and then incubated with primary antibodies for 60 min at room temperature. Subsequently, slides were washed in TBS (3 × 10 min) and stained using anti-rabbit Alexa fluor 488 SFX kit (Invitrogen Ltd.) according to the manufacturer's protocol. After three washes in TBS/0.05% Tween 20, DNA was counterstained with 7-aminoactinomycin D before mounting in ProLong Gold antifade reagent (Invitrogen Ltd.). Images were obtained using an epifluorescence microscope (Olympus BX51), equipped with a ColorView 12 camera. The amount of pERK1/2 colocalized with DNA was determined using the colocalization module in Image-Pro Plus 6.0 software (MediaCybernetics) using algorithms (26) to generate colocalization coefficients (Cgr). Cgr represents the fraction of green pixels that have a red component and is determined by the equation, $Cgr = \sum G_i (\text{coloc}) / \sum G_i$, wherein G_i is green intensity. At least 50 cells in at least three viewing fields were analyzed per sample.

Statistical analysis. To compare differences between the experimental groups, a two-tailed *t* test was done using Microsoft Excel or SPSS 13 software (SPSS, Inc.).

Results

Tositumomab in combination with RT induces additive tumor cell death, which is MEK/ERK1/2 dependent. To investigate the potential effect of ERK1/2 on cell death induced by anti-CD20 mAb with and without RT, we assessed the amount of cell death induced in Raji and SUDHL-4 tumor cells by measuring the number of Annexin V/PI-positive cells 24 hours after treatment. Figure 1 shows that treatment with the anti-CD20 mAb tositumomab in combination with 4 Gy RT results in a greater induction of cell death than after tositumomab or RT alone. However, this increased additive tumor cell death was inhibited with the specific MEK1/2 inhibitors U0126 and PD98059 (Fig. 1A-C), but no such inhibition was seen with U0124, a structural analogue of U0126, that lacks MEK-inhibiting properties (Fig. 1C). In contrast, the other anti-CD20 mAb used rituximab and ibritumomab (the murine parent mAb of

rituximab), both failed to cause the significant increases in cell death observed in combination with tositumomab and RT (Fig. 1A-D).

Similar results were obtained with BL60 tumor cells; tositumomab and 4 Gy RT alone induced ~40% death, whereas the combination of the two treatments increased the percentage of Annexin V-positive cells to ~80%. This additive cell death was again inhibited by preincubation of cells with U0126, which reduced cell death to ~50%. The decrease in tumor cell death resulted in a highly significant difference between combination of tositumomab plus RT in the presence and absence of the MEK1/2 inhibitor ($P < 0.006$).

We previously showed that Fc-lacking tositumomab F(ab')₂ fragments are as efficient at triggering cell death as whole IgG molecules (reviewed in ref. 8). However, Fc-FcγR interactions are also known to be able to influence signaling pathways and in a manner dependent upon mAb isotype. Tositumomab displays a mouse IgG2a Fc region, whereas rituximab and ibritumomab, which share identical variable regions, have human IgG1 and mouse IgG1 Fc regions, respectively. Therefore, to verify that the differing Fc domains were not accounting for the varying potency of these anti-CD20 mAb and to establish whether the effects of tositumomab on cell death were Fc-independent, we did a series of experiments comparing whole IgG and F(ab')₂ fragments of rituximab or tositumomab and examined their effects with or without RT. These experiments revealed that a similar amount of cell death was induced in Raji cells given either the whole IgG or F(ab')₂ fragments of tositumomab or rituximab in either the presence or absence of RT and/or U0126 (Fig. 1D). The amount of cell death induced by ibritumomab and rituximab in these different conditions was almost identical. Taken together, these data indicate that the Fc region of these mAb is not important for inducing direct cell killing and that differences in the F(ab') binding sites account for the different effects of rituximab and tositumomab alone and when examined in combination with RT.

To address whether tositumomab had a similar effect in combination with low-dose rate radiation, we compared the proportion of dead cells induced after irradiating cells at 150 Gy/h (as before) or 0.3 Gy/h with or without anti-CD20 mAb. We observed an enhanced level of cell death in the samples treated with tositumomab plus RT, irrespective of the dose rate applied (Fig. 1E). In fact, these results suggested that lower dose rate was more effective at inducing cell death both alone and in combination with tositumomab.

MEK inhibition reverses the loss of clonogenic survival induced by tositumomab plus RT. Next, we investigated the importance of ERK1/2 signaling on the clonogenic survival of Raji, SUDHL4, and BL60 cells treated with tositumomab with and without RT. In all three cell lines, tositumomab decreased clonogenic survival by 50% to 80% in the absence of RT. Loss of clonogenic survival was, however, much more prominent when tositumomab was combined with RT (Fig. 2A; data not shown). Addition of U0126 improved the clonogenic survival for cells treated with tositumomab plus RT to that seen with RT alone. No significant differences in clonogenic survival were seen between cells treated with rituximab, RT, or both (Fig. 2A). These data were also confirmed using a 72-hour XTT growth inhibition assay (Fig. 2B). Taken together with the Annexin V assay data, these results indicate that there are fundamental differences in the cell death pathways evoked by

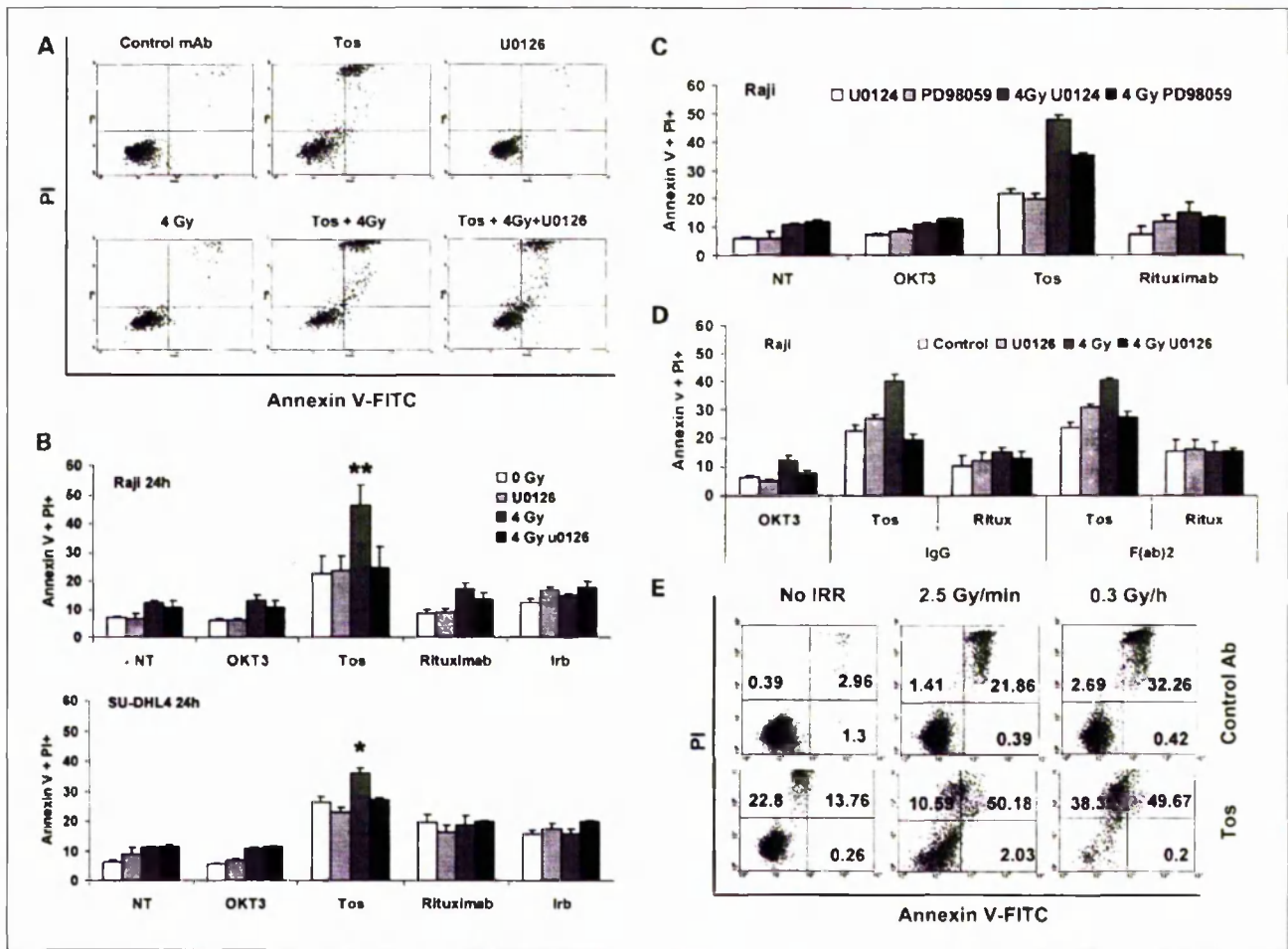


Fig. 1. Effect of U0126 on tositumomab and radiation-induced additive cell death. **A**, Raji cells were incubated with tositumomab (5 µg/mL) with or without MEK1/2 inhibitor U0126 (10 µmol/L). RT (4 Gy) was then delivered to a selection of the samples 30 min after addition of mAb. Cell death was assessed 24 h later as the proportion of cells binding FITC-labeled Annexin V and staining positively with PI. **B-D**, graphical representation of the proportion of Annexin V/PI – positive Raji (*top*) and SU-DHL4 cells (*bottom*) 24 h after treatment with various mAb and RT (4 Gy). Columns, average values of at least two independent experiments; bars, SE. *, $P < 0.05$; **, $P < 0.006$. **E**, effect of different dose rates on tositumomab and radiation-induced synergistic cell death in Raji cells. Cells were treated with tositumomab and then irradiated with 4 Gy at different dose rates. For control purposes, tositumomab or control mAb-treated cells were incubated in a water tank for the amount of time equal to irradiation time. The proportion of Annexin V/PI – positive cells was assessed by flow cytometry 24 h after irradiation was completed.

these two different types of anti-CD20 mAb when combined with RT.

As DNA damage is known to disrupt the cell cycle, we also assessed the cell cycle distribution of Raji cells 24 hours after 4-Gy irradiation in the presence or absence of anti-CD20 mAb. As expected, a clear arrest in the G₂-M phase was observed after irradiation. However, coincubation with anti-CD20 antibodies did not have any additional effect on the proportion of cells in G₂-M phase (data not shown).

Effect of anti-CD20 mAb and RT on ERK1/2 phosphorylation. To examine the activation status of the MAPK cascade after ligation of CD20 and/or RT, we did Western blot analysis to detect dually phosphorylated pERK1/2 in cells treated with tositumomab or rituximab plus RT over a range of radiation doses and time points. Elevated levels of pERK1/2 were observed 10 min after treatment with rituximab or tositumomab in SU-DHL4 cells. For cells treated with rituximab, levels

of pERK1/2 peaked 1 hour after treatment and then subsequently decreased. In contrast, stable and prolonged phosphorylation of ERK1/2 was observed in cells treated with tositumomab, although levels of pERK1/2 never reached those seen after rituximab treatment at 1 hour. The amount of pERK1/2 induced by RT alone was minimal and diminished to background levels after 1 hour. When RT was combined with mAb, the pERK responses were similar but enhanced compared with when either mAb was used alone. Rituximab combined with RT resulted in a maximal pERK1/2 signal 1 hour after treatment and then decreased (Fig. 3A). In contrast, there was a slower but more prolonged level of pERK1/2 when cells were treated with both tositumomab and RT, with the pERK1/2 signal lasting for at least 24 hours. These data indicate that both rituximab and tositumomab are able to stimulate the MAPK cascade, resulting in ERK1/2 activation, but with marked differences in the kinetics of activation. High but transient

levels of pERK are observed after rituximab treatment, whereas slower but extremely prolonged levels of pERK are seen in tositumomab-treated cells. Furthermore, this pERK activation is more prominent when anti-CD20 mAb are combined with RT.

Recent data have suggested that the trafficking of activated (phosphorylated) ERK1/2 between the cytoplasm and nucleus, rather than phosphorylation per se, determines its biological activity (27–29). Therefore, we next investigated the spatial distribution of pERK1/2 in cells after the various treatments detailed above, using immunocytochemical techniques and image analysis. Rituximab-induced and tositumomab-induced phosphorylation of ERK1/2 was assessed at 8-hour and 24-hour time points in SU-DHL4 (Fig. 3B) and Raji cells (not shown). After treatment with tositumomab, pERK1/2 signals were observed in the center of individual cells and colocalized with 7-aminoactinomycin D, confirming the translocation of pERK1/2 into the nucleus (Fig. 3B). In contrast, although rituximab was able to trigger the phosphorylation of ERK1/2, it remained cytoplasmic and pERK1/2 was not observed in the nucleus (Fig. 3B). To quantify the degree of colocalization of pERK1/2 and 7-aminoactinomycin D, we did image analysis according to a previously published protocol (28). In brief, we determined the proportion of green pixels (representing pERK1/2) that contained a red component (nucleus). This

analysis confirmed our earlier observation that tositumomab, but not rituximab, induced nuclear translocation of pERK (Fig. 3C). RT further enhanced the proportion of pERK1/2 signals colocalized with the nucleus compared with the mAb alone, in particular with tositumomab. Thus, the proportion of colocalized nuclear signals was slightly enhanced in the rituximab plus RT-treated cells compared with either treatment alone but the degree of colocalized nuclear signals was much greater after the tositumomab plus RT combination than after tositumomab or RT alone.

Cell death evoked by tositumomab combined with RT is nonapoptotic. We next investigated the mode of cell death induced with tositumomab with or without RT and began by looking for DNA fragmentation, a classic feature of apoptosis. Initially, we did a fluorescent variant of the terminal dUTP N-end labeling assay (FISEL) on Raji and SU-DHL4 cells to establish whether the cell death induced after tositumomab plus RT involves DNA fragmentation. The proportion of FISEL-positive cells in tositumomab and rituximab-treated samples did not significantly differ from nontreated controls (Fig. 4) in keeping with our previously published data (11). This proportion increased to 10% to 12% 24 hours after RT, in accordance with the suggestion that apoptosis is induced after this treatment. However, we found no difference in the

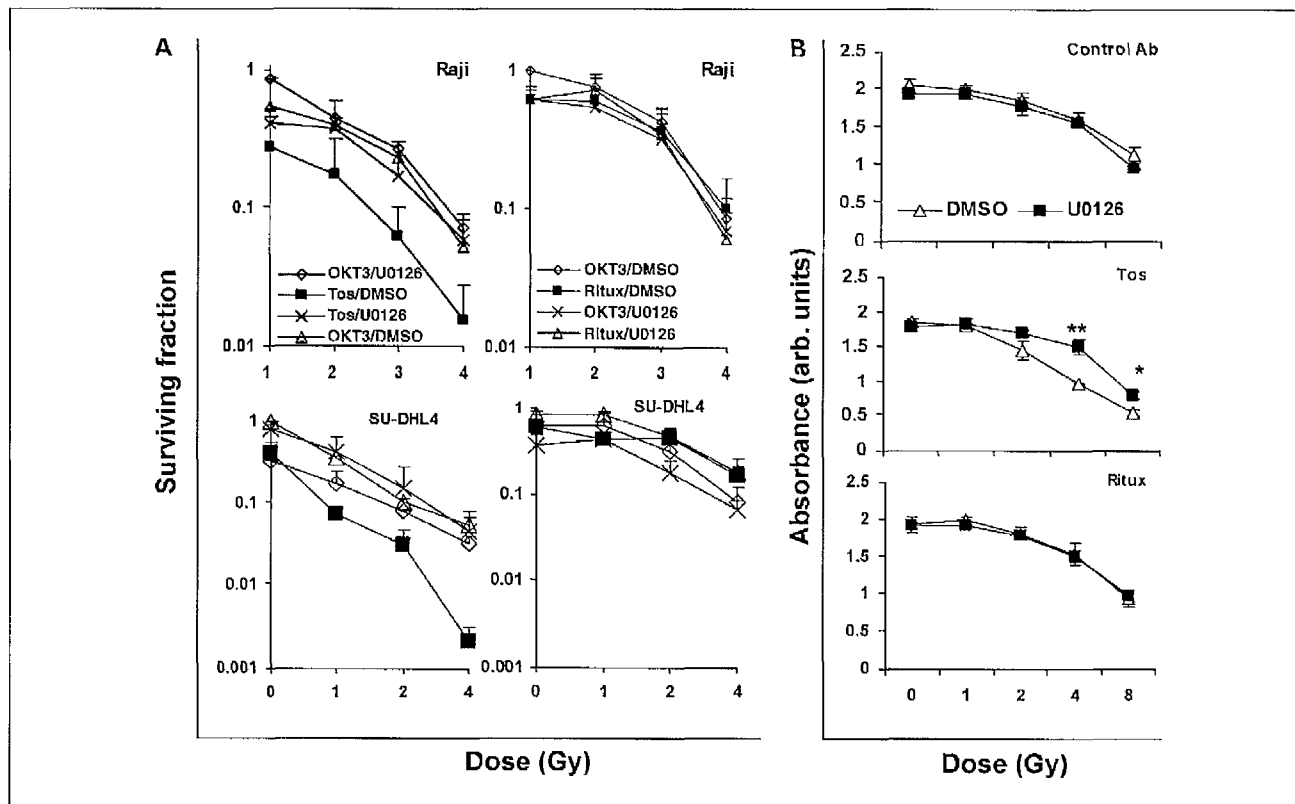


Fig. 2. Clonogenic survival of Raji and SU-DHL4 cells after treatment with tositumomab or rituximab and RT. **A**, different concentrations of cells were plated into 96-well plates and incubated with control mAb OKT3 in the presence (\diamond) or absence of U0126 (Δ) or with one of two anti-CD20 mAb (tositumomab, *left* and rituximab, *right*) in combination with U0126 (\times) or without inhibitor (\blacksquare). Plates were then irradiated with various doses of RT. After 14 d, the fraction of wells containing no surviving cells was determined. The cell number that resulted in 30% empty wells was calculated and used to generate a clonogenic survival curve that was normalized according to plating efficiency. Average results of three independent experiments are shown in logarithmic scale \pm SE. **B**, effect of tositumomab and radiation on growth of Raji cells assessed by XTT assay. Raji cells were incubated with or without MEK1/2 inhibitor U0126 (10 μ M/L) before the addition of tositumomab. RT (4 Gy) was then delivered 30 min after addition of mAb. Inhibition of cell growth was assessed 72 h later using an XTT assay as detailed in Materials and Methods. Points, average; bars, SE. *, $P < 0.05$.

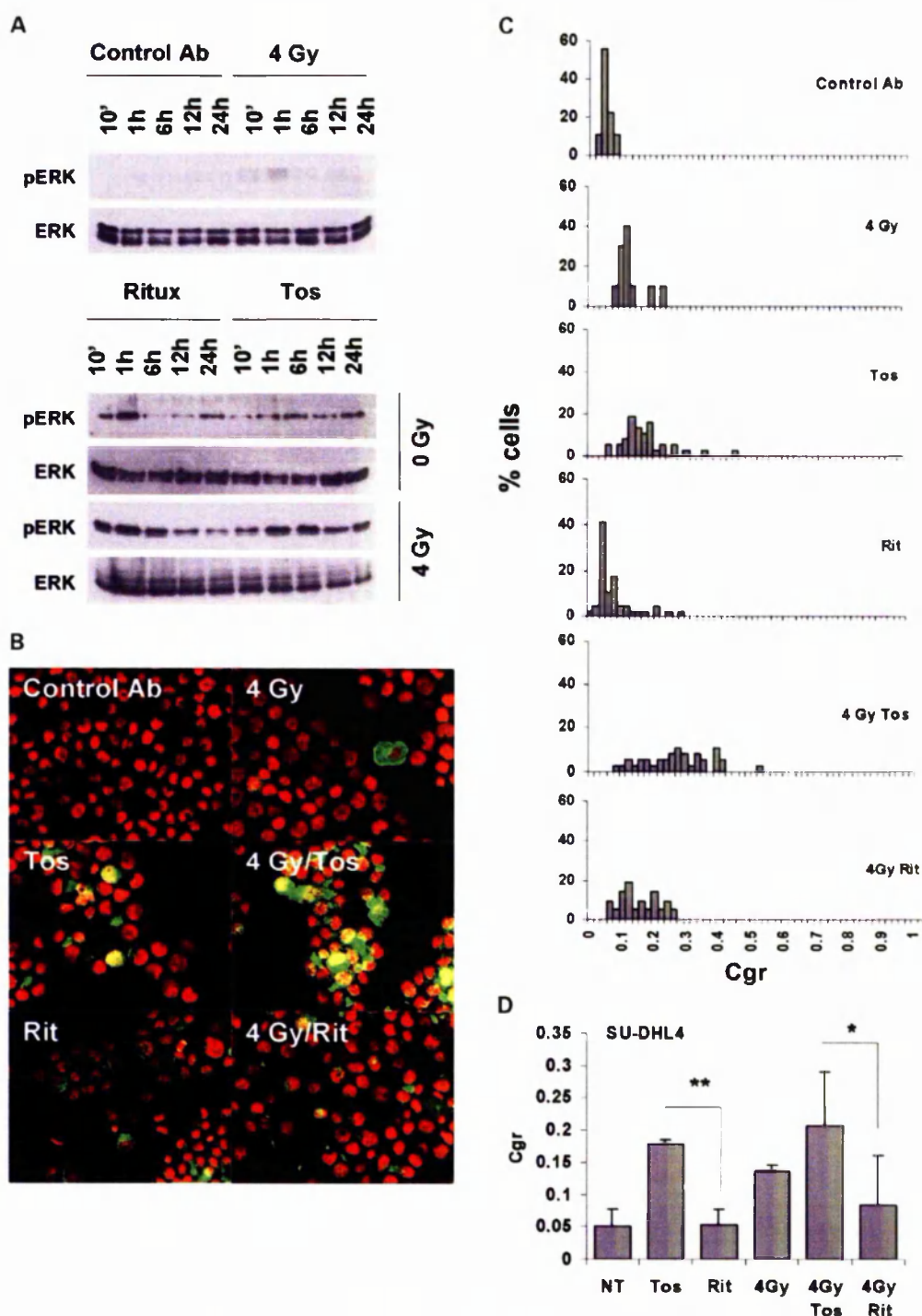


Fig. 3. ERK1/2 activation after treatment with anti-CD20 mAb and radiation. **A**, kinetics of ERK1/2 activation at various time points within 24 h posttreatment in SU-DHL4 cells. Cells were treated as indicated, then lysed, and assessed by Western blot using reagents specific for pERK or total ERK. **B**, the effect of different anti-CD20 mAb on the intracellular localization of activated ERK1/2 at the 24-h time point. SU-DHL4 cells were treated with anti-CD20 mAb (5 μ g/mL) in the presence or absence of RT (4 Gy). Cells were then harvested 24 h after treatment, carefully sedimented onto PLL-coated microscope slides, and stained for pERK (green) and DNA (7-aminoactinomycin D, red) as described in Materials and Methods. **C**, quantification of pERK1/2 localization in the nucleus. When cells were treated with anti-CD20 mAb, the colocalization of pERK1/2 and 7-aminoactinomycin D was assessed using digital pixel colocalization studies. Results represent the typical distribution of Cgr values representing the proportion of green pixels that have a red component. **D**, comparison of the average Cgr values of SU-DHL4 cells treated with various stimuli. Columns, average values of at least two independent experiments; bars, SE. *, $P = 0.02$; **, $P = 0.008$ (Student's t test).

percentage of FISEL-positive cells in samples treated with RT or RT combined with either tositumomab or rituximab. These data indicate that apoptotic DNA degradation does not seem to contribute to tositumomab plus RT-induced cell death, and therefore, classic apoptosis is unlikely to be responsible for the increased cell death observed.

Cell death induced by tositumomab plus RT is not blocked by Bcl-2 overexpression. To further investigate whether the mechanism of cell death induced by tositumomab plus RT involved the mitochondrial cell death machinery, we transfected Raji cells with the antiapoptotic, prosurvival molecule Bcl-2. These cells overexpressed Bcl-2 as shown in Fig. 5A and were, as

expected, more resistant to cell death induced by RT alone (Fig. 5B). In contrast, tositumomab was able to evoke similar levels of cell death in both wild-type and Bcl-2-overexpressing cells in agreement with our earlier published data (11). A similar result was observed when tositumomab was combined with RT. Taken together, these data indicate that, although Bcl-2 is capable of blocking apoptosis in these cells, tositumomab in the presence or absence of RT triggers a mode of cell death that is independent of Bcl-2 controlled mitochondrial regulation. Importantly, this independence was not simply due to down-regulation of Bcl-2, as there was an increase in the amount of intracellular Bcl-2 protein after treatment with tositumomab or tositumomab plus RT in both wild-type and Bcl-2-overexpressing Raji cells (Fig. 5A).

Cell death induced by tositumomab is not dependent on caspase activation. Next, we investigated the effect of caspases on cell death triggered by tositumomab and RT by preincubating cells with the pan-caspase inhibitor QVD-OPH and examining cell death over a 24-hour period. In the presence of control antibody OKT3, RT caused a modest level of cell death that was partially blocked by QVD-OPH (Fig. 5C). QVD-OPH treatment had no effect on cell death triggered by tositumomab alone. However, there was a partial reduction in the proportion of dying cells after preincubation with QVD-OPH and treatment with tositumomab plus RT. This inhibition was first apparent after 12 hours but was unable to fully suppress the cell death induced even when QVD-OPH concentrations were increased to 100 $\mu\text{mol/L}$ (data not shown), indicating a high degree of caspase independency (Fig. 5C). In contrast, there was no significant effect of QVD-OPH on rituximab-treated cells with or without RT.

siRNA targeting MEK1 and MEK2 abolishes tositumomab plus RT additive cell death. Finally, to further confirm that the MEK/ERK1/2 pathway is critical for the enhanced cell death observed when tositumomab and RT are combined, we investigated the effect of down-regulating MEK1 or MEK2 using siRNA. Importantly, siRNA to MEK1 or MEK2 were able to down-regulate the expression of their respective targets efficiently for up to 96 hours and with good specificity (MEK1 siRNA did not down-regulate MEK2 and vice versa; Fig. 6A). Furthermore, the reduction in expression of either MEK1 or MEK2 correlated with a reduction in the degree of cell death observed when tositumomab was combined with RT. As with the pharmacologic studies done earlier, the extent of cell death after treatment with RT or tositumomab alone was unchanged.

Discussion

In this study, we have shown that RT and the type II anti-CD20 mAb tositumomab combine to evoke enhanced levels of cell death compared with either treatment alone and that the MAPK signaling pathway downstream of ERK1/2 is important for this effect. The additive cell death and loss of clonogenic survival seen with tositumomab and RT were reversed with specific MEK inhibitors U0126 and PD98059, as well as with siRNA targeting MEK1 or MEK2. This effect seemed to be specific for tositumomab, as rituximab was unable to trigger prominent cell death either alone or in combination with RT and no significant reduction in clonogenic survival was seen with rituximab.

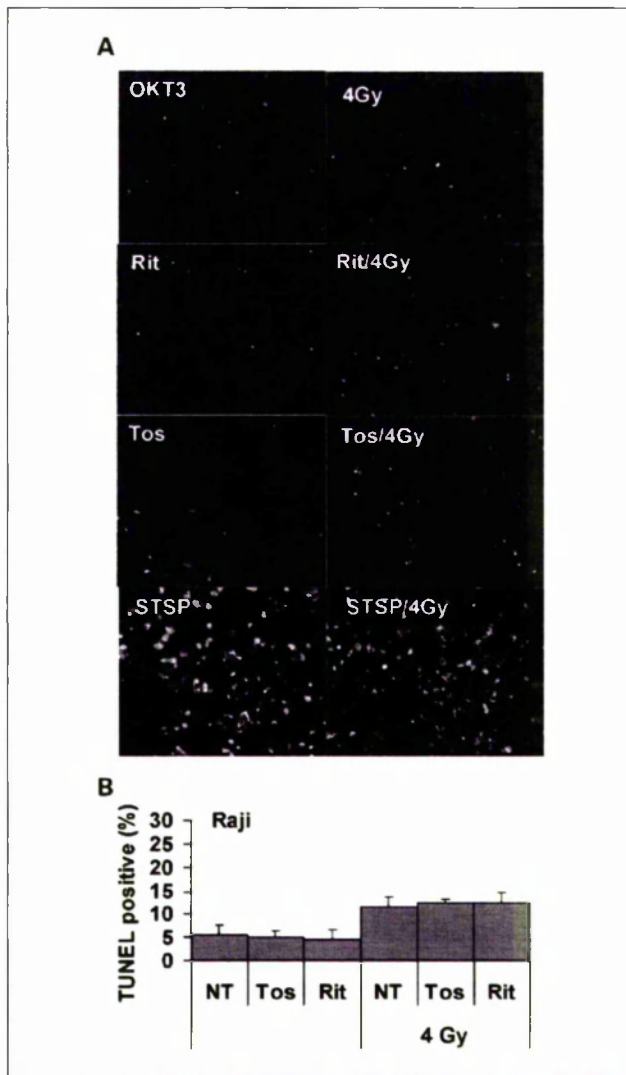


Fig. 4. Tumor cell death triggered by the combination of anti-CD20 mAb and RT does not involve DNA fragmentation. **A**, left, FISEL assay done on Raji cells 24 h after treatment with control mAb OKT3, tositumomab, rituximab (all 5 $\mu\text{g/mL}$), or staurosporine (STSP, 2 $\mu\text{mol/L}$) as a positive control. Right, combination of the treatments mentioned above with 4 Gy RT. Bar, 200 μm . **B**, the proportion of terminal dUTP N-end labeling – positive cells after treatment with tositumomab or rituximab with or without 4 Gy RT. At least 300 cells in at least four viewing fields were counted in a blind manner using a 40 \times objective. Columns, results from at least three experiments; bars, SE.

The cell death triggered by tositumomab was not accompanied by the DNA fragmentation characteristic of classic apoptosis. Furthermore, although overexpression of Bcl-2 mediated resistance to RT-induced apoptosis, it had little or no effect on the death induced by tositumomab alone or with the combination of tositumomab plus RT. Moreover, the increase in intracellular Bcl-2 observed after treatment with tositumomab with or without RT gives further evidence that the cell death evoked by the combination of tositumomab and RT is independent of Bcl-2 controlled mitochondrial regulation.

A number of recent reports have suggested that the activation of the ERK1/2 MAPK cascade may promote nonapoptotic, cytoplasmic forms of cell death (30, 31). Prodeath signaling through the MAPK/ERK1/2 pathway has been previously reported for immature B-cell lymphoma (19) and thymocytes (32). It has also been shown that prolonged ERK1/2 activation promotes reactive oxygen species-induced nonapoptotic cell death (reviewed in ref. 33), whereas transient activation of ERK1/2 protects cells from death (34). In our model system, prolonged activation (at least 24 hours) of ERK1/2 was evident

after treatment with tositumomab, coincident with elevated cell death. In contrast, rituximab evoked a more rapid, transient activation of ERK1/2 without any accompanying cell death. Therefore, our data provide further evidence to support the hypothesis that sustained ERK1/2 activation is required for cell death induction through MAPK signaling.

In the present study, the extent of cell death induced after ligation of CD20 seemed to directly correlate with the translocation of active pERK1/2 into the nucleus, which was enhanced by RT. Under physiologic conditions, pERK1/2 is thought to translocate into the nucleus where it is dephosphorylated by MAPK phosphatases, such as the ERK1/2 selective MAPK phosphatase-3 (35). Under oxidative conditions, sustained nuclear accumulation of pERK1/2 can occur (36, 37) and is a major contributor to oxidative toxicity in neurons (38). RT is known to induce the formation of reactive oxygen species and membrane peroxidation that can last for several hours after initial administration (38), thereby providing a potential explanation for its ability to prolong and enhance ERK1/2 phosphorylation and nuclear translocation. In

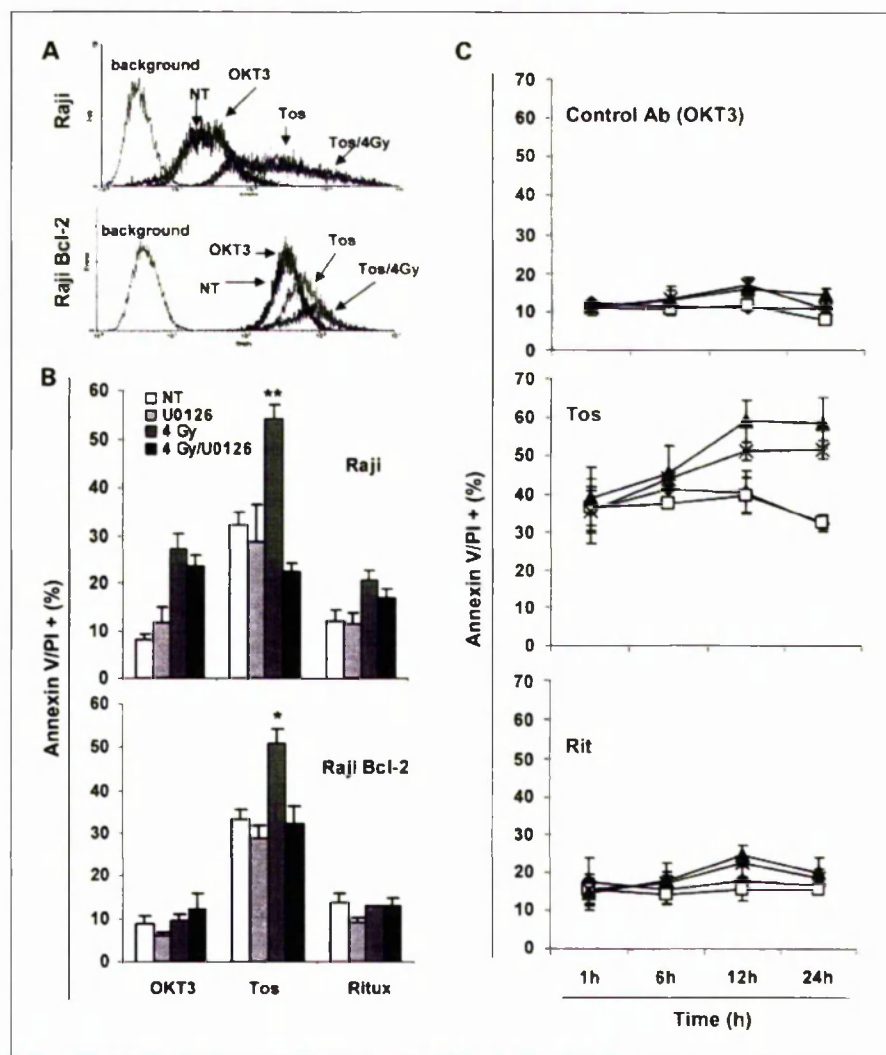


Fig. 5. The effect of Bcl-2 overexpression and caspase inhibition on anti-CD20 mAb and radiation-induced cell death. **A**, Raji cells treated with nothing (NT), OKT3, tositumomab (both at 5 μ g/mL), or a combination of RT (4 Gy) and tositumomab were fixed, permeabilized, and then incubated with FITC-labeled anti-Bcl-2 antibody (or an irrelevant control to set the background) and then assessed by intracellular flow cytometry. Identically prepared Raji cells transfected to overexpress Bcl-2 (Raji bcl-2) were also assessed (**bottom**). **B**, WT and Bcl-2 overexpressing Raji cells were treated with tositumomab or rituximab with or without U0126 and/or irradiation (4 Gy) and then the percentage of Annexin V/PI-positive cells was assessed by flow cytometry 48 h after treatment. Columns, results from three independent experiments; bars, SE. *, $P < 0.05$; **, $P < 0.01$. **C**, Raji cells were preincubated with QVD-OPH (20 μ mol/L) for 30 min before treatment with control mAb OKT3, tositumomab or rituximab with or without (□) 4 Gy RT. In parallel, mAb-treated and RT (▲) or non-RT (◆) samples not treated with QVD-OPH were analyzed. The percentage of Annexin V/PI-positive cells was assessed by flow cytometry at different time points after treatment. Data represent the results from three independent experiments \pm SE.

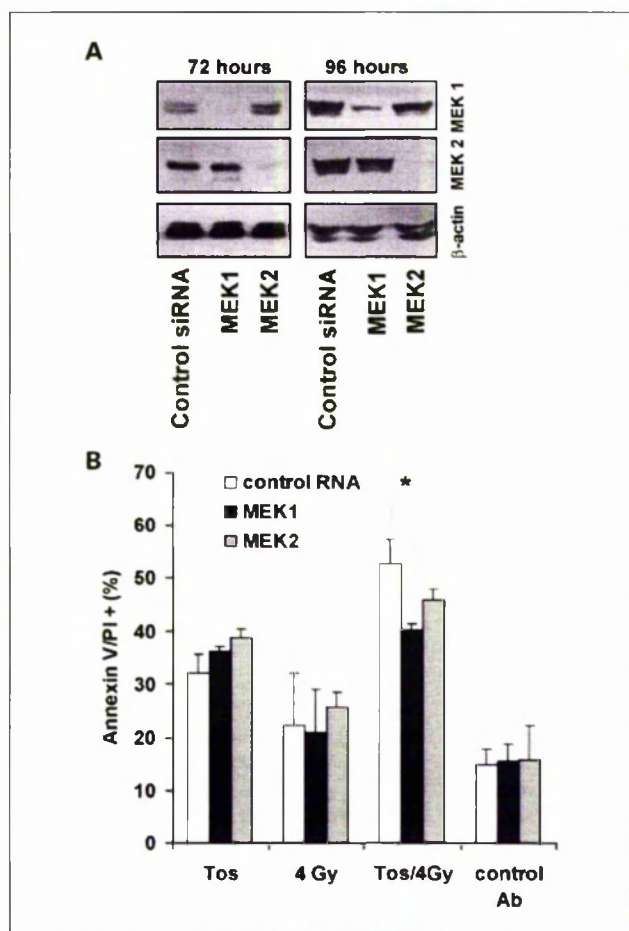


Fig. 6. The effect of MEK1 and MEK2 siRNA on tositumomab and radiation-induced synergistic cell death. **A.** Raji cells were transfected with siRNAs against MEK1 or MEK2, and their expression levels were assessed by Western blot 3 or 4 d after transfection in comparison with a loading control (β -actin). **B.** 3 d posttransfection, the cells were either treated with a control mAb (OKT3), tositumomab (both 5 μ g/mL), a 4-Gy dose of RT or tositumomab plus RT. The proportion of Annexin V/PI – positive cells was assessed by flow cytometry 24 h after treatment. Columns, results from three independent experiments; bars, SE. *, $P = 0.006$.

support of this suggestion, radiation-induced free radicals are thought to play a major role in the activation of the ERK1/2 pathway in carcinoma cell lines (20).

The distinct properties of tositumomab and other type II mAb have been reported by us previously (8, 10). Unlike other anti-CD20 mAb, they fail to redistribute CD20 into Triton X-100 insoluble lipid rafts and do not induce potent complement-dependent cytotoxicity of target cells. Instead, tositumomab and other type II mAb are more able to induce cell death (10, 13, 39).

Moreover, this cell death was previously found by us and others to occur in the absence of DNA fragmentation and independently of the mitochondrial apoptosis pathway (11, 13, 40). Our current results are in agreement with these previous reports and provide new insights into the existing literature by demonstrating that even small DNA nicking, as detected by FISEL, does not occur during tositumomab-induced cell death. Moreover, we have extended these observations by demonstrating that the increased cell death triggered by the combination of tositumomab with RT is also independent of mitochondrial regulation and DNA fragmentation.

We believe that these data may provide some potentially important mechanistic insights into the impressive results observed in the clinic with targeted radiation combined with tositumomab, albeit that the type and quality of radiation is different from high dose rate external RT. The efficacy of tositumomab has been shown to be greatly enhanced by its conjugation to the radionuclide ^{131}I resulting in highly significant improvements in complete response rates and relapse-free survival (6). Our data indicate that the increased therapeutic efficacy seen with targeted radiation may relate to the MEK-dependent enhanced cell death induced with the combination of tositumomab plus RT. We have also shown that the combination of tositumomab plus RT is able to produce an increased tumor cell death that is independent of Bcl-2 regulation. Overexpression of Bcl-2 is a frequent and defining feature of follicular lymphoma and is known to inhibit apoptotic cell death. Inhibition of apoptosis by Bcl-2 and other antiapoptotic Bcl-2 family members is considered to be an important factor in making this lymphoma refractory to treatment with conventional chemotherapy (41). In relation to the potential clinical implications of these findings, it is interesting to note that high response rates have been seen with ^{131}I tositumomab in patients with follicular lymphoma who are refractory to both chemotherapy and rituximab (42). While we have not directly investigated the effects of the radioisotopes ^{131}I or ^{90}Y used in Bexxar and Zevalin, respectively, we have found that low-dose rate external beam RT, more equivalent to that produced during radioimmunotherapy, also increased tumor cell kill in combination with tositumomab. In conclusion, we believe our data may provide new molecular insights into the clinical efficacy of targeted radiation and tositumomab in chemorefractory patients.

Disclosure of Potential Conflicts of Interest

No potential conflicts of interest were disclosed.

Acknowledgments

We thank Waleed Alduaij for his technical assistance.

References

- Armitage JO. Treatment of non-Hodgkin's lymphoma. *N Engl J Med* 1993;328:1023–30.
- Maloney DG, Grillo-López AJ, White CA, et al. IDEC-C2B8 (rituximab) anti-CD20 monoclonal antibody therapy in patients with relapsed low-grade non-Hodgkin's lymphoma. *Blood* 1997;90:2188–95.
- Kneba M, Dreyling M, Schmitz N, et al. Frontline therapy with rituximab added to the combination of cyclophosphamide, doxorubicin, vincristine, and prednisone (CHOP) significantly improves the outcome for patients with advanced-stage follicular lymphoma compared with therapy with CHOP alone: results of a prospective randomized study of the German Low-Grade Lymphoma Study Group. *Blood* 2005;106:3725–32.
- Fisher RI, Kaminski MS, Wahl RL, et al. Tositumomab and iodine-131 tositumomab produces durable complete remissions in a subset of heavily pretreated patients with low-grade and transformed non-Hodgkin's lymphomas. *J Clin Oncol* 2005;23:7565–73.
- Knox SJ, Goris ML, Trisler K, et al. Yttrium-90-labeled anti-CD20 monoclonal antibody therapy of recurrent B-cell lymphoma. *Clin Cancer Res* 1996;2:457–70.

6. Kaminski MS, Tuck M, Estes J, et al. ¹³¹I-tositumomab therapy as initial treatment for follicular lymphoma. *N Engl J Med* 2005;352:441-9.
7. DeNardo GL, O'Donnell RT, Oldham RK, DeNardo SJ. A revolution in the treatment of non-Hodgkin's lymphoma. *Cancer Biother Radiopharm* 1998;13:213-23.
8. Cragg MS, Walshe CA, Ivanov AO, Glennie MJ. The biology of CD20 and its potential as a target for mAb therapy. *Curr Dir Autoimmun* 2005;8:140-74.
9. Teeling JL, Mackus WJ, Wiegman LJ, et al. The biological activity of human CD20 monoclonal antibodies is linked to unique epitopes on CD20. *J Immunol* 2006;177:362-71.
10. Cragg MS, Morgan SM, Chan HT, et al. Complement-mediated lysis by anti-CD20 mAb correlates with segregation into lipid rafts. *Blood* 2003;101:1045-52.
11. Chan HT, Hughes D, French RR, et al. CD20-induced lymphoma cell death is independent of both caspases and its redistribution into triton X-100 insoluble membrane rafts. *Cancer Res* 2003;63:5480-9.
12. Cragg MS, Glennie MJ. Antibody specificity controls *in vivo* effector mechanisms of anti-CD20 reagents. *Blood* 2004;103:2738-43.
13. Shan D, Ledbetter JA, Press OW. Apoptosis of malignant human B cells by ligation of CD20 with monoclonal antibodies. *Blood* 1998;91:1644-52.
14. Mathas S, Rickers A, Bommert K, Dörken B, Mapara MY. Anti-CD20- and B-cell receptor-mediated apoptosis: evidence for shared intracellular signaling pathways. *Cancer Res* 2000;60:7170-6.
15. Kolch W. Coordinating ERK/MAPK signaling through scaffolds and inhibitors. *Nat Rev Mol Cell Biol* 2005;6:827-37.
16. Lee JR, Koretzky GA. Extracellular signal-regulated kinase-2, but not c-Jun NH2-terminal kinase, activation correlates with surface IgM-mediated apoptosis in the WEHI 231 B cell line. *J Immunol* 1998;161:1637-44.
17. Hollmann CA, Owens T, Nalbantoglu J, Hudson TJ, Sladek R. Constitutive activation of extracellular signal-regulated kinase predisposes diffuse large B-cell lymphoma cell lines to CD40-mediated cell death. *Cancer Res* 2006;66:3550-7.
18. Sutherland CL, Heath AW, Pelech SL, Young PR, Gold MR. Differential activation of the ERK, JNK, and p38 mitogen-activated protein kinases by CD40 and the B cell antigen receptor. *J Immunol* 1996;157:3381-90.
19. Gauld SB, Blair D, Moss CA, Reid SD, Harnett MM. Differential roles for extracellularly regulated kinase-mitogen-activated protein kinase in B cell antigen receptor-induced apoptosis and CD40-mediated rescue of WEHI-231 immature B cells. *J Immunol* 2002;168:3855-64.
20. Hagan M, Wang L, Hanley JR, Park JS, Dent P. Ionizing radiation-induced mitogen-activated protein (MAP) kinase activation in DU145 prostate carcinoma cells: MAP kinase inhibition enhances radiation-induced cell killing and G2/M-phase arrest. *Radiat Res* 2000;153:371-83.
21. Lyng FM, Maguire P, McClean B, Seymour C, Mothersill C. The involvement of calcium and MAP kinase signaling pathways in the production of radiation-induced bystander effects. *Radiat Res* 2006;165:400-9.
22. Golding SE, Rosenberg E, Neill S, Dent P, Povirk LF, Valerie K. Extracellular signal-related kinase positively regulates ataxia telangiectasia mutated, homologous recombination repair, and the DNA damage response. *Cancer Res* 2007;67:1046-53.
23. Mitchell CR, Folkard M, Joiner MC. Effects of exposure to low-dose-rate (80)co γ rays on human tumor cells *in vitro*. *Radiat Res* 2002;158:311-8.
24. Raderschall E, Golub EI, Haaf T. Nuclear foci of mammalian recombination proteins are located at single-stranded DNA regions formed after DNA damage. *Proc Natl Acad Sci U S A* 1999;96:1921-6.
25. Olive PL, Banath JP, Durand RE. Development of apoptosis and polyploidy in human lymphoblast cells as a function of position in the cell cycle at the time of irradiation. *Radiat Res* 1996;146:595-602.
26. Manders EEM, Verbaek FJ, Aten JA. Measurement of co-localisation of objects in dual-colour images. *J Microsc* 1993;169:375-82.
27. Costa M, Marchi M, Cardarelli F, et al. Dynamic regulation of ERK2 nuclear translocation and mobility in living cells. *J Cell Sci* 2006;119:4952-63.
28. Koistinaho M, Lin S, Wu X, et al. Apolipoprotein E promotes astrocyte colocalization and degradation of deposited amyloid-β peptides. *Nat Med* 2004;10:719-26.
29. Sperandio S, de Belle I, Bredesen DE. An alternative, nonapoptotic form of programmed cell death. *Proc Natl Acad Sci U S A* 2000;97:14376-81.
30. Subramaniam S, Unicker K. Extracellular signal-regulated kinase as an inducer of non-apoptotic neuronal death. *Neuroscience* 2006;138:1055-65.
31. Sperandio S, Poksay K, de Belle I, et al. Paraptosis: mediation by MAP kinases and inhibition by AIP-1/Alix. *Cell Death Differ* 2004;11:1066-75.
32. Mariathasan S, Ho SS, Zakarian A, Ohashi PS. Degree of ERK activation influences both positive and negative thymocyte selection. *Eur J Immunol* 2000;30:1060-8.
33. Zhuang S, Schnellmann RG. A death-promoting role for extracellular signal-regulated kinase. *J Pharmacol Exp Ther* 2006;319:991-7.
34. di Mari JF, Davis R, Safirstein RL. MAPK activation determines renal epithelial cell survival during oxidative injury. *Am J Physiol* 1999;277:195-203.
35. Groom LA, Sneddon AA, Alessi DR, Dowd S, Keyse SM. Differential regulation of the MAPK/SAP and RK/p38 kinases by Pyst1, a novel cytosolic dual-specificity phosphatase. *EMBO J* 1996;15:3621-32.
36. Shinozaki Y, Koizumi S, Ohno Y, et al. Extracellular ATP counteracts the ERK1/2-mediated death-promoting signaling cascades in astrocytes. *Glia* 2006;54:606-18.
37. Levinthal DJ, Defranco DB. Reversible oxidation of ERK-directed protein phosphatases drives oxidative toxicity in neurons. *J Biol Chem* 2005;280:5875-83.
38. Rugo RE, Schiestl RH. Increases in oxidative stress in the progeny of X-irradiated cells. *Radiat Res* 2004;162:416-25.
39. Cardarelli PM, Quinn M, Buckman D, et al. Binding to CD20 by anti-B1 antibody or F(ab')₂ (2) is sufficient for induction of apoptosis in B-cell lines. *Cancer Immunol Immunother* 2002;51:15-24.
40. van der Kolk LE, Evers LM, Omene C, et al. CD20-induced B cell death can bypass mitochondria and caspase activation. *Leukemia* 2002;16:1735-44.
41. Gandhi MK, Marcus RE. Follicular lymphoma: time for a re-think? *Blood Rev* 2005;19:165-78.
42. Horning SJ, Younes A, Jain V, et al. Efficacy and safety of tositumomab and iodine-131 tositumomab (Bexxar) in B-cell lymphoma, progressive after rituximab. *J Clin Oncol* 2005;23:712-9.

Chapter 11

General discussion

The introduction of passive immunotherapy with the anti-CD20 mAb rituximab has revolutionised the treatment of NHL and brought about highly significant improvements in survival for the first time in 3 decades in the common B cell lymphomas. Despite these improvements little is known about the underlying mechanisms of action of effective treatment. Furthermore the outcome is poor for many patients who still succumb to these malignancies. Therefore, there is an urgent need to identify alternative treatment approaches as well as to dissect the molecular pathways that underlie the current treatment approaches used successfully in the clinic.

Over the past several years the idea that cells can commit suicide by mechanisms other than apoptosis has been gaining momentum. Basic and clinical studies have clearly established that most anti-cancer agents induce apoptosis and that inhibition of apoptotic programmes can reduce the sensitivity of tumour cells to anti-cancer treatment. However, sensitivity of isolated tumour cells to apoptosis does not always correlate with sensitivity of the whole tumour to anti-cancer treatment. Inhibition of the programme of apoptosis has been reported to have little effect on clonogenic survival in several tumours (reviewed by Roninson et al., 2001). A decrease in apoptosis is compensated in such cell lines by an arrest in the fractions of cells that undergo permanent growth arrest with phenotypic features of cell senescence or mitotic catastrophe. Mitotic catastrophe can be induced by several classes of cytotoxic agents, but the pathways of abnormal mitosis differ depending on the mechanism of action of the drug and the point within the

cell cycle when the tumour cells are exposed to the cytotoxic treatment. Furthermore mitotic catastrophe can develop as a consequence of aberrant re-entry of tumour cells into cell cycle after prolonged growth arrest. Elucidation of the factors that regulate different aspects of treatment-induced mitotic catastrophe as well as the kinetics with which cells transit the different cell cycle phase during this process should assist in improving efficacy and decreasing side-effects of cancer therapy.

In this work we have shown that after severe genotoxic damage with irradiation, p53 mutated Burkitt lymphoma cells undergo mitotic catastrophe that is accompanied by complex changes in cell cycle redistribution as well as new patterns of gene expression. We have shown for the first time that endopolyploid cells produced as a result of mitotic arrest induced by genotoxic stress have the capacity to repair DNA DSB, which may provide a survival advantage for cells that undergo mitotic catastrophe in response to severe genotoxic treatment.

From the context of cell cycle progression after severe genotoxic insult, it is notable that p39^{mos} found to be translated in our system after irradiation, is an oncogene that acts as an upstream regulator of the MAPK cascade that, in turn might act as a drive to bypass G2/M and DNA repair (see Chapter 3 appendix). Thus, it is reasonable to suggest that activation of MAPK cascade by cytotoxic treatment, driven by oncogene expression (e.g. Ras, Raf, Mos, epidermal growth factor receptor (EGFR), platelet-derived growth factor receptor (PDGFR), vascular endothelial growth factor receptor (VEGFR), HER2/neu etc), might be the universal mechanism of adaptation of cell cycle checkpoints after genotoxic treatment before adequate DNA repair takes place. DNA lesions in these cells are subsequently being detected by a spindle checkpoint that serves as a “final bastion” of DNA integrity. If it fails and cells progress through mitosis,

primary DNA DSB are converted into chromosome aberrations that are not compatible with cell survival. However, if mitosis is reversed without proceeding into anaphase, one or more endoreduplication rounds drive cells into the endocycle, giving rise to the polyploid cells. In this thesis we have shown for the first time the complex nature of this pathway and that the fraction of polyploid cells comprises an extra cell cycle compartment that confers on the tumour cell a further opportunity for DNA DSB repair and survival.

Furthermore, the work contained in this thesis implies that several parallels exist between radiation-induced mitotic catastrophe, induction of polyploidy and the evolutionarily conserved endoreduplication pathways. Although the induction of polyploidy was deemed a reproductive dead-end, this work and more recently that of others in this field (Puig et al., 2008; Sundaram et al., 2004; Rajaraman et al., 2006), have indicated that this might not always be the case. Through a series of defined complex nuclear rearrangements the endopolyploid tumour cells can switch from the endocycle back to mitosis, through a process of somatic reduction.

In an attempt to discover the molecular regulators of the somatic reduction which occurs in these endopolyploid tumour cells, we took note of the fact that features reminiscent of mitotic catastrophe are also observed during normal development. This observation suggests that mitotic catastrophe might not be simply a deregulated deviation from the mitotic cycle caused by DNA damage but rather a programmed event. Indeed, both during ontogenetical development and in p53 mutated tumour cells after DNA damage, this response is linked to a specific form of the endocycle, endomitosis. Endomitosis was originally defined as 'meiosis without karyogamy' and is also observed in numerous phylogenetic and ontogenetic studies. Importantly, in the life cycles of several protozoa

it is seen as a prerequisite of asexual meiosis enabling somatic reduction of polyploid nuclei. We therefore propose that in our model endomitosis facilitates a similar function in endopolyploid tumour cells. Although the currently accepted paradigm suggests that the endocycle is simply a mitotic cycle with suppressed mitosis-engine machinery, the appearance of condensed chromosomes in the endomitotic cells does not fit with this paradigm. Instead it indicates that an additional molecular pathway is likely to be in operation and we suggest that key meiotic regulator $p39^{mos}$ is involved in the induction of mitotic catastrophe and subsequent endomitosis in our model. Furthermore, we suggest that meiotic regulators may also provide the molecular basis for somatic reduction and the return to mitosis of endopolyploid tumour cells.

Another feature of the activated MAPK cascade we observed was the ability to induce non-apoptotic cytoplasmic cell death when radiation was combined with the anti-CD20 antibody tositumomab. The cell death triggered by tositumomab was not accompanied by the DNA fragmentation characteristic of classical apoptosis. Furthermore, although over-expression of Bcl-2 mediated resistance to radiation-induced apoptosis, it had little or no impact on the death induced by tositumomab alone or with the combination of tositumomab plus radiation. Furthermore, cell death triggered by tositumomab was independent of caspases as the pan-caspase inhibitor QVD failed to inhibit the death.

Classically, the ERK/MAPK pathway has been described as a pro-survival pathway triggering cell proliferation and activation. Based on its central role in regulating the growth and survival of cells from a broad spectrum of human tumours, this cascade has long been viewed as an attractive pathway for anti-cancer therapies with several emerging ERK/MAPK cascade inhibitors producing significant therapeutic advances against a broad range of human cancers (reviewed by Sebolt-Leopold and English,

2007). Contrary, but not contradictory to this paradigm, in this thesis, we have found that both mitotic catastrophe and cytoplasmic cell death involve the ERK/MAPK pathway as a central player triggering cell death and loss of clonogenic survival in the model systems we have explored (Figure 11-1).

This dependence of cytoplasmic cell death on normally pro-survival signalling pathways and its independence from natural inhibitors of apoptosis might be an important paradigm for refining cancer treatment for the following reasons:

1. The ERK/MAPK cascade is a target for every oncogene involving a G protein-coupled receptor pathway. Activation of this pathway often results in failure to trigger canonical apoptosis by anti-tumour therapy, leading to formation of refractory or relapsed tumours. A cell death mechanism that would positively involve this over-activated G protein/MAPK axis might trigger preferential cell death in highly advanced and relapsed tumours when all other treatment options have been exhausted.
2. The independence of non-apoptotic cell death from mitochondrial (Bcl-2) and death receptor (caspases) signalling pathways provides a potential explanation for the clinical efficacy of anti-CD20 antibodies in the treatment of follicular and other lymphomas. Most cases of follicular lymphomas have a t(14;18) gene translocation resulting in a rearranged and constitutively over-expressed BCL-2 gene. As these tumours develop larger numbers of mutations they increasingly become refractory to apoptosis and become resistant to chemotherapy. The independence of cytoplasmic cell death from anti-apoptotic effects of overexpressed BCL-2 may provide an explanation as to why combining

radiation with anti-CD20 in radioimmunotherapy is so effective in the clinic and works in patients who are both refractory to chemotherapy and rituximab.

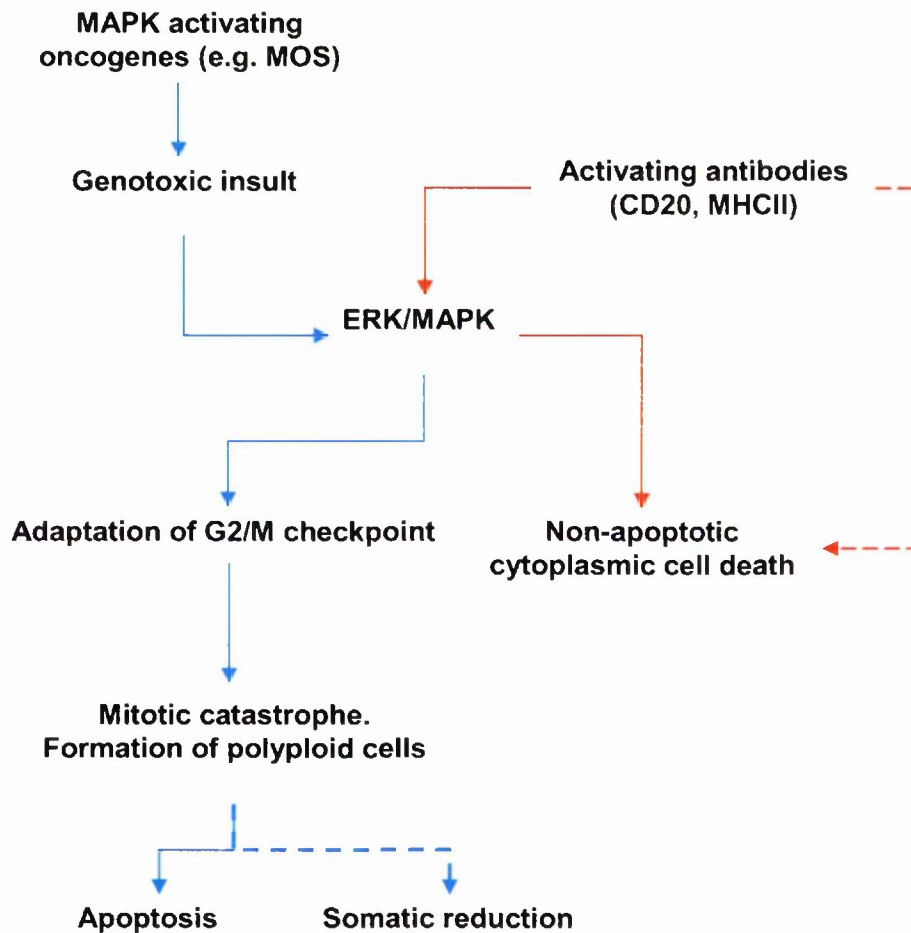


Figure 11- 1. Hypothetical scheme of the involvement of ERK/MAPK cascade in radiation-induced mitotic catastrophe and antibody-induced non-apoptotic cell death. Both mitotic catastrophe and cytoplasmic cell death comprise two parallel cell death pathways with MAPK being a shared chain. The possibility of cross-talk between these pathways requires further investigation.

In our further experiments, we have extended the aforementioned observations and, using a variety of techniques, revealed that actin redistribution is critical for both homotypic adhesion and cell death induced by both Type II anti-CD20 mAb and HLA DR Class II mAb. Subsequent experiments revealed that actin dynamics is altered rapidly after mAb stimulation and that the mode of cell death engaged is rapid, non-

apoptotic, non-autophagic but instead reflect cytoplasmic death involving lysosomes which swell and then disperse their contents into the cytoplasm. This results in loss of plasma membrane viability and decomposition of cytoplasm in the absence of DNA fragmentation. We also show here for the first time that malignant B cells, undergoing homotypic adhesion, actively communicate via ~ 5 nm wide temporary inter-cytoplasmic bridges. The formation of these channels is accompanied by the exchange of plasma membrane components. Moreover, the extent of plasma membrane swapping correlates with the extent of cell death induced by both anti-CD20 and anti-HLA DR antibodies. The precise mechanisms of this are still to be investigated. To our knowledge there are no known precedents for these phenomena recorded for any of the cell types.

In conclusion, in this thesis we have presented clear evidence that apoptosis is not the only way of eliciting the death of lymphoma cells. In fact, although apoptosis is a component of the cell death repertoire of the lymphoma cells we have studied, non-apoptotic death modalities are at least as frequently observed. Several novel principles of cell death regulation have been discovered that we hope will be useful in designing further refinements to current cancer therapies.

References

Puig PE, Guilly MN, Bouchot A, Droin N, Cathelin D, Bouyer F, Favier L, Ghiringhelli F, Kroemer G, Solary E, Martin F, Chauffert B. Tumor cells can escape DNA-damaging cisplatin through DNA endoreduplication and reversible polyploidy. *Cell Biol Int* 2008 May 2. [Epub ahead of print].

Rajaraman R, Guernsey DL, Rajaraman MM, Rajaraman SR. Stem cells, senescence, neosis and self-renewal in cancer. *Cancer Cell Int* 2006 6:25.

Roninson IB, Broude EV, Chang BD. If not apoptosis, then what? Treatment-induced senescence and mitotic catastrophe in tumour cells. *Drug Resist Updat* 2001 4:303-13.

Sebolt-Leopold JS, English JM. Mechanisms of drug inhibition of signalling molecules. *Nature* 2006 441:457-462.

Sundaram M, Guernsey DL, Rajaraman MM, Rajaraman R. Neosis: a novel type of cell division in cancer. *Cancer Biol Ther* 2004 3:207-218.

Appendix 1

The biology of CD20 and its potential as a target for mAb therapy.

Reprinted from: Cragg MS, Walshe CA, Ivanov AO, Glennie MJ. Curr Dir Autoimmun. 2005;8:140-74

.....

The Biology of CD20 and Its Potential as a Target for mAb Therapy

Mark S. Cragg, Claire A. Walshe, Andrey O. Ivanov, Martin J. Glennie

Tenovus Research Laboratory, Cancer Sciences Division, Southampton University,
Southampton General Hospital, Southampton, UK

Abstract

CD20 is a 33–37 kDa, non-glycosylated phosphoprotein expressed on the surface of almost all normal and malignant B cells. It is also the target for rituximab, the most effective anti-cancer monoclonal antibody developed to date. Rituximab has now been given to over 300,000 lymphoma patients in the last decade and interestingly is now being explored for use in other disorders, such as autoimmune conditions including rheumatoid arthritis and systemic lupus erythematosus. Despite the success in immunotherapy, knowledge about the biology of CD20 is still relatively scarce, partly because it has no known natural ligand and CD20 knockout mice display an almost normal phenotype. However, interesting insight has come from work showing that CD20 is resident in lipid raft domains of the plasma membrane where it probably functions as a store-operated calcium channel following ligation of the B cell receptor for antigen. In the current review, these and data relating to its activity as a therapeutic target will be discussed in depth. It is clear that a greater understanding of CD20 biology and the effector mechanisms, such as antibody-dependent cellular cytotoxicity, complement-dependent cytotoxicity and growth regulation, which operate with anti-CD20 mAb *in vivo* will allow more efficient exploitation of CD20 as a therapeutic target.

Copyright © 2005 S. Karger AG, Basel

CD20 Gene and Protein Structure

The gene for human CD20 consists of 8 exons, is 16 kbp long and was completely cloned in 1988 [1–9]. It is located on chromosome 11q12–q13.1, in close proximity to genes encoding FcεRIβ chain and HTm4 proteins. On a basis of haemopoietic cell expression, limited (20%) homology and similar gene structures in mouse, human and rat, these three genes were originally grouped into a

small family. However, Tedder et al. [10, 11] have recently identified several new family members, describing the enlarged group as the MS4A gene family containing 21 distinct human and mouse proteins. Six out of 8 human MS4A members map to the same chromosomal location as CD20 and a number of these display features which indicate that they arose from a common precursor gene and may share a similar function.

The CD20 gene lacks a classical TATA box and instead appears to have several minor initiation sites, such that transcription starts at several different points in exon 1 and 2 resulting in different mRNA lengths from 2.6 to 3.4 kb [7]. However, despite the difference in mRNA length, the translated region is found at exon 3, resulting in a single form of the protein.

Initial predictive analysis of the cDNA sequence suggested that CD20 was a tetraspan protein (fig. 1), with cytoplasmic carboxyl- and amino-termini and a single extracellular loop of approximately 44 amino acids residing between the third and fourth transmembrane regions [reviewed in 12]. This suggestion has been confirmed by proteolytic cleavage experiments [13], although a second, much smaller extracellular loop is also predicted from the structure. However, it is not clear if this second loop is exposed at the surface of the plasma membrane. Interestingly, the homology between the MS4A genes is focussed in the first three transmembrane regions, with little or no conservation of sequence observed in the extracellular loop. This characteristic indicates that the transmembrane regions play a critical role in the function of these proteins, with the extracellular loop maintaining a divergent or non-vital function.

Regulation of CD20 Expression

CD20 is an archetypal B cell antigen whose expression appears to be regulated by a number of transcription factors. Positive and negative regulatory *cis* elements were initially defined [14] followed by the identification of a BAT box at -225 to -201 which was found to contain an octamer binding site for the B cell-specific transcription factor Oct-2 and the ubiquitously expressed Oct-1 [15, 16]. However, mutation of the BAT box does not fully ablate CD20 transcription indicating that other regions are of more critical importance in the regulation of CD20 expression [16].

Human CD20 expression commences at the early pre-B cell stage just before the expression of the cytoplasmic μ H chain and is lost during terminal plasma cell differentiation [reviewed in 12]. This tight control of CD20 expression coincides with important stages of B cell development and may be due to PU.1/Pip binding to the proximal end of the CD20 promoter at position -160 [17]. PU.1 and Pip are members of the Ets family and are important regulators

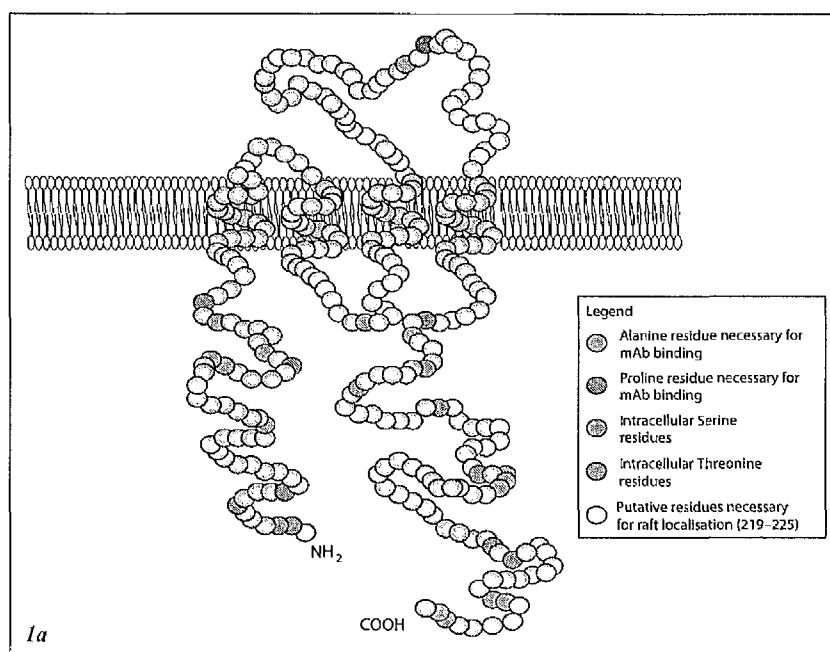
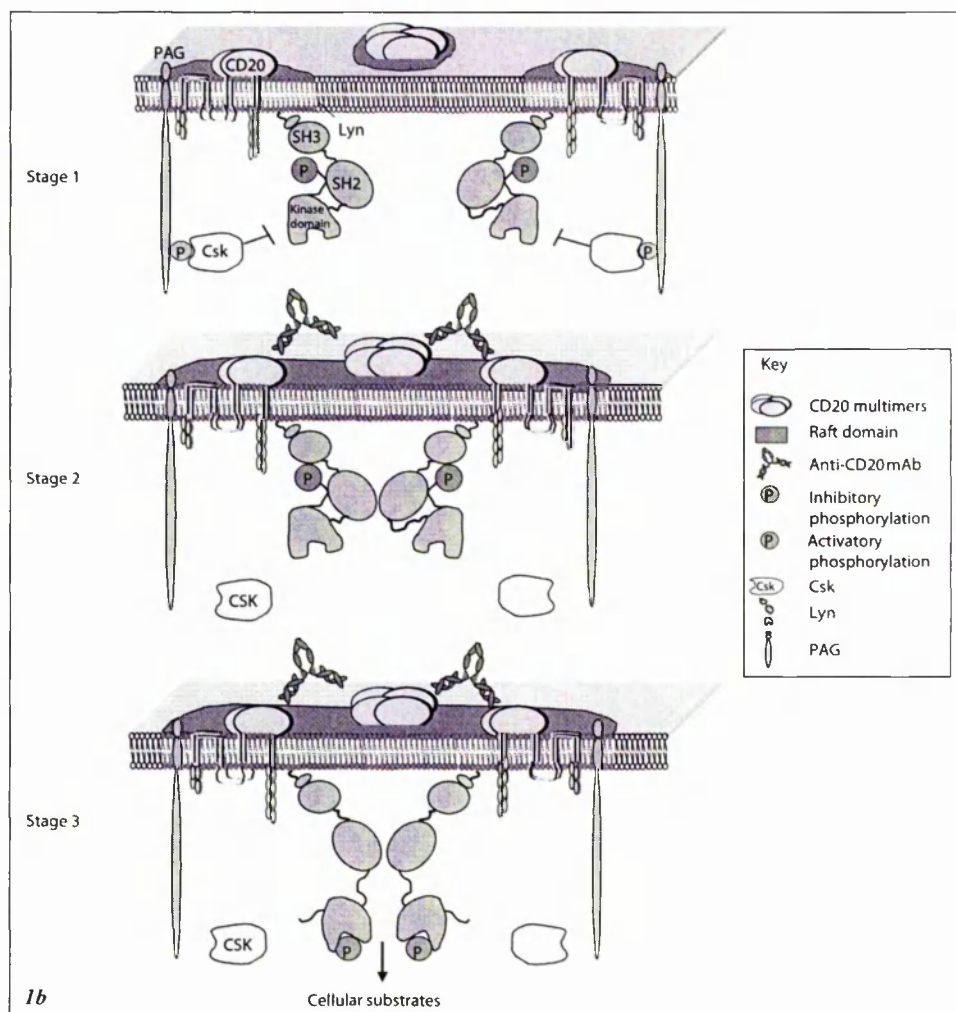


Fig. 1. a Schematic diagram of the structure of CD20. CD20 spans the membrane 4 times and possesses intracellular C- and N-termini. Two regions of CD20 are extracellular, forming a small and large loop, although only the large loop which contains an Ala \times Pro motif appears vital for mAb binding. Also shown are the potential sites for Ser/Thr phosphorylation and region of human CD20 thought to be important for localisation to membrane rafts. **b** Proposed signaling mechanism of anti-CD20 mAb: In resting cells, (stage 1) CD20 multimers (probably at least tetramers) are found in small pre-formed mini-raft domains associated with PAG. PAG is constitutively phosphorylated, resulting in its association with Csk via a phosphotyrosine at residue 317. Csk inhibits Src kinases such as Lyn through phosphorylation of an inhibitory tyrosine in the C-terminus. Together, these three proteins establish a steady state of kinase activity. When anti-CD20 mAb bind, they cause clustering of CD20 multimers (stage 2). This may cause a change in the steady-state interaction of Lyn, Csk and PAG, possibly resulting in a reduction in the phosphorylation of PAG at residue 317, leading to the release of Csk. Once Lyn is released from Csk-mediated inhibition (stage 3), it will become dephosphorylated on the C-terminal inhibitory tyrosine and adopt a more open conformation with a corresponding increase in kinase activity. Potentially, Lyn will then phosphorylate the stimulatory tyrosine residue present in the active site of an adjoining Lyn molecule, causing a further increase in protein tyrosine kinase activity, resulting in the phosphorylation of other cellular substrates.



of other B cell-specific genes such as the Ig light chain and CD72. Interestingly, these regulators are absent in non-B cell lines, CD20-negative pre-B cell lines and are down-regulated during plasma cell differentiation [17, 18]. In addition to the PU.1/Pip binding site, a binding site for basic helix-loop-helix-zipper (bHLHZ) family proteins is present at position -45 [17]. This site binds

μ E3-specific transcription factors such as TFE3 and USF that are found expressed in most cell types. Intriguingly, co-transfection experiments with mouse fibroblast cells demonstrated that even though the μ E3 proteins are not B cell specific, they are the most potent at inducing CD20 expression, causing a 9-fold increase in expression compared to a 2-fold increase with the presence of either Oct-2 or PU.1/Pip complexes [17]. However, the lack of apparent potency of the B cell-specific transcription factors may be due to the lack of other proteins in the mouse fibroblast cells as previous experiments have shown that members of the Ets family are poor transcriptional activators and often function as part of a multiprotein complex [19].

Another regulatory region in the CD20 promoter contains a binding site for the B cell-specific activator protein (BSAP). This protein is encoded by the Pax5 gene which itself is highly regulated and required for B cell commitment [20]. BSAP is involved in the regulation of CD19 and Blk amongst other B cell-specific genes. How or what BSAP interacts with to induce CD20 expression is not fully understood although it has been demonstrated that BSAP and members of the Ets family can interact to induce translation of CD79a/Ig α [21], the signaling element of the BCR.

In summary, the major site of promoter activity of the CD20 gene is believed to be in the region of -40 to -450. At least four regulatory regions have been identified within these 400 bases. How these transcription factors interact either in complexes or individually to control CD20 expression is still unclear. However, it is evident that CD20 is regulated both by transcription factors that are involved in B cell-specific differentiation and also by ubiquitously expressed proteins which are not dependent on the stage of B cell development. A similar developmental profile has recently been described for murine CD20, with CD20 expression being initiated at the time of immunoglobulin heavy chain expression late during pre-B cell maturation [4].

Although generally highly regulated and confined to normal and malignant B cells, aberrant CD20 expression is occasionally observed on malignant T cells and has been reported in rare cases of T cell acute lymphoblastic leukemia (T-ALL), non-Hodgkin's lymphoma (T-NHL) and chronic lymphocytic leukemia (T-CLL) as well as on the normal CD8+ T cells of multiple myeloma [22-26].

Subcellular Location of CD20

Once expressed, evidence suggests that both human and mouse CD20 reside in the cell membrane as multimers [27, 28]. Immunoprecipitation experiments following lysis in weak detergents or after cell surface cross-linking

yielded products 33, 70 and 140 kDa suggesting that CD20 exists as dimers and tetramers. In addition, CD20 has been reported to localise with CD40 and MHC class II [29, 30] as well as the B cell receptor for antigen (BCR) prior to antigenic stimulation [31]. Although little is known regarding how CD20 interacts with and influences these molecules, it is interesting to note that all of them play vital roles in controlling B cell development and function. Recently, Li et al. [32] have shown using confocal and electron microscopy of the Burkitt's lymphoma B cell line, Ramos, that approximately 90% of membrane CD20 appears to be localized to particular membrane protrusions known as microvilli. Interestingly, another molecule that targets to microvilli is the BCR, consistent with the reported association of CD20 and BCR [31] and in line with the suggestion that CD20 cooperates with the BCR to detect and signal the detection of antigen, perhaps hinting at the true biological function of CD20.

Biological Function of CD20

The function of CD20 has remained obscure. This probably in part reflects the lack of suitable murine reagents, as although antibodies to human CD20 have existed for over 20 years, reagents specific to murine CD20 have remained elusive until very recently [4]. In addition, although the first CD20 knockout mouse strain was derived several years ago, its phenotype was surprisingly normal [5]. Therefore, much of our understanding has been based upon experiments using mAb to ligate CD20 on human B cells and B cell lines. Engagement of CD20 with mAb results in several measurable biologic events such as enhanced survival [33], activation and proliferation [34, 35], adhesion [29, 36] as well as growth inhibition [37] and death [37–43]. Molecular consequences include elevated Ser/Thr and Tyr phosphorylation of numerous targets (including CD20 itself), up-regulation of CD18, CD58, CD95 and MHC class II molecules, increased levels of *c-myc* and *b-myb*, and phosphorylation of phospholipase C- γ (PLC- γ) [13, 34–36, 44–50]. However, even these experiments have been confusing, as different mAb directed to CD20 have caused opposing effects.

Effects of Anti-CD20 mAb

The first anti-human CD20 mAb, B1, was characterised over 20 years ago and since then a considerable panel of anti-CD20 mAb have been generated. As detailed above, it has long been known that the biologic response observed after ligation is dependent on the mAb itself, as depicted in table 1. This phenomenon

Table 1. Characteristics of selected anti-CD20 mAb

mAb	Type	Isotype	Ao	CDC	ADCC	Adhesion	Tx-100-insoluble
LT20	I	mIgG1	+	++	+	—	+++
AT80	I	mIgG	++	+	+	++	+++
IF5	I	mIgG2a	—	+++	++	—	++
2H7	I	mIgG2b	—	++	+	—	+++
Rituximab	I	chIgG1	+	+++	+++	+	+++
7D8	I	HuIgG1	—	++++	+++	—	+++
2F2	I	HuIgG1	—	++++	+++	—	+++
B1	II	mIgG2a	+++	—	++	+++	—
11B8	II	HuIgG1	++	—	+++	++	—

Summary of the effects of anti-CD20 mAb on Burkitt's lymphoma cell lines. The mAb shown were assessed for their ability to induce apoptosis (Ao), CDC, ADCC, homotypic adhesion and insolubility in 0.5–1% Tx-100. Information is taken from data shown in references 13, 28, 42, 43, 50, 53, 54 and references mentioned therein. The number of plus signs indicates the potency in the assay.

is perhaps best illustrated when considering the actions of B1 and IF5 on B cells. In pioneering experiments, Clark and Tedder showed that these two mAb, which carry the same murine IgG2a isotype, cause either enhanced transit of resting B cells in the cell cycle from G0 into G1 [51], or blocked progression from G1 into S/G2+M [37]. Based on early blocking experiments it was thought that the extracellular loop of CD20 only contained two distinct epitopes, one recognised by the vast majority of anti-CD20 mAb and the second recognised by IF5 [reviewed in 12]. In fact, all anti-CD20 mAb block binding of other CD20 mAb and interestingly, appear dependent upon two critical residues (Ala at position 170 and a proline at position 172) in the extracellular loop for their binding. Using an incremental mouse-human mutation strategy, Polyak and colleagues [28] were able to show that the extracellular loop offers a more diverse binding platform than at first thought whereby 16 mAb can be categorised into four groups depending on their ability to bind this A-x-P motif, and induce various cellular effects such as homotypic aggregation. Our group has extended this work to show that anti-CD20 mAb can be classified according to two functional subgroups [42, 43, 52]. Whilst both types of mAb appear to induce antibody-dependent cellular cytotoxicity (ADCC) mechanisms equivalently, type I mAb, typified by rituximab and IF5, induce translocation of CD20 into Triton X-100 (Tx-100)-insoluble lipid rafts and potent complement-dependent cytotoxicity

(CDC). In contrast, type II mAb do not cause redistribution of CD20 or mediate CDC [43], but are inclined to induce more homotypic aggregation and apoptosis as exemplified by the B1 mAb [53]. These distinctions will be discussed in more detail later. Importantly, this functional distinction appears to be borne out in vivo, such that rituxinab and 1F5 but not B1 are dependent upon complement activity for most of their therapeutic activity [52].

The various effects of anti-CD20 mAb have been discussed comprehensively in excellent reviews elsewhere [12, 54] and will not be considered extensively here. Instead, this review will concentrate (a) on the recent findings concerning three of the best known properties of CD20 – its role as an ion channel, its association with membrane rafts, and its modulation, and (b) on its potential as a target antigen in immunotherapy.

CD20 as Calcium Channel

The reported oligomeric structure of CD20 along with its tetraspan structure soon led to suggestions that CD20 may form a membrane channel and play a role in the regulation of ion flux. This suggestion was supported by the fact that CD20 shares close homology with FcεRIβ, which has long been associated with calcium conductance. More definitive evidence came from Bubien and colleagues [27] who demonstrated that transfection of CD20 into a variety of CD20 cell lines resulted in an increase in the basal level of cytosolic Ca^{2+} . Perhaps most revealing were experiments on Daudi B cells, where anti-CD20 mAb were shown to induce a range of different calcium flux responses according to the mAb used; with B1 inducing a slow, steady increase of cytoplasmic Ca^{2+} , measurable at 24 h, and 1F5 inducing an acute calcium flux within 1 min with basal levels evident at 24 h [27]. Intriguingly, these and other authors had already demonstrated that CD20 ligation with different mAb has different effects on cell cycle progression as detailed above (B1 and 1F5 inhibiting or enhancing proliferation, respectively [37, 51]). Therefore, it is likely that the different functional effects of anti-CD20 mAb relate in part to the differences in calcium flux they induce.

The studies reported above relate to the ability of anti-CD20 mAb to induce calcium flux directly upon engagement of CD20. However, as CD20 has no known ligand, this may not reflect a true biological function of CD20. Instead, CD20 is likely to be involved in the generation and regulation of calcium flux transduced by other receptors. One direct example of this was shown in 3T3 fibroblast cells transfected with CD20 where CD20 expression in these cells not only served to raise the basal concentration of cytosolic calcium in the presence of extracellular calcium but it also enhanced the progression of cells through the

G1 phase of the cell cycle after stimulation with IGF-1 [55]. Although this underlines the ability of CD20 to induce cell cycle effects transduced through other receptors, clearly CD20 expression in fibroblasts is non-physiologic. Of much greater significance in terms of the true function of CD20 is the recent work by Tedder and colleagues showing that the calcium flux observed upon BCR or CD19 stimulation is reduced in CD20 knockout mice [4]. Given the earlier evidence that CD20 plays a role as a calcium channel, this recent data was much anticipated. However, earlier studies by O'Keefe et al. [5] assessing BCR-induced Ca^{2+} flux did not reveal such striking differences between CD20 wild-type and knockout mice. One possible explanation relates to the fact that the CD20^{-/-} cells reported by Tedder et al. displayed reduced surface expression of IgM, potentially accounting for a decreased calcium flux through the BCR. Conceivably, as CD19 functions as an associated co-receptor of the BCR, decreased IgM expression could also affect the degree of signaling after CD19 ligation also. However, alternatively it is possible that other calcium regulators may compensate its absence in the knockout animals, masking the expected phenotype. Interestingly, Li et al. [56] have recently presented convincing data indicating that human CD20 is involved in the calcium flux that is generated during BCR signaling. It is known that full B cell activation requires sustained elevation of cytoplasmic free calcium, achieved through a combination of its release from intracellular stores and influx of extracellular calcium via membrane channels. In their work, Li et al. indicate that CD20 plays a role in the latter component and operates as a store- or capacitance-operated channel. These channels are not directly opened upon ligation but instead rely on a prior release of Ca^{2+} from the cells intracellular stores. Such stores are generally derived from the endoplasmic reticulum (ER), and their depletion in some way activates certain channels in the plasma membrane to open, facilitating extracellular calcium influx and subsequent repletion of the intracellular stores [reviewed in 57]. The mechanism involved in this activation is not understood, although several scenarios have been proposed such as the involvement of secondary messengers, transporting of ion channels to the surface via vesicles and actual physical docking of the ER with the plasma membrane [reviewed in 57]. The available data indicate that CD20 is a central component of a non-voltage-gated capacitance calcium channel in B cells [56]. This conclusion is based upon the fact that CD20, when expressed in CHO cells, dramatically enhances capacitance entry following intracellular store depletion. Furthermore, in B cells, reduction of CD20 expression with siRNA caused a corresponding reduction in BCR-stimulated calcium entry. Although it is possible that CD20 facilitates this capacitance calcium flux via an indirect pathway, there is strong evidence to indicate that CD20 itself forms the ion channel. First, it has been shown that the resting state intracellular Ca^{2+} concentration is proportional to the CD20 expression level [27]. Second,

CD20 has a structure reminiscent of other known calcium channel components, in that it is a tetraspan phosphoprotein with cytoplasmic N- and C-termini that have no intrinsic enzymatic activity [8, 9, 12]. Third, CD20 can exist in an oligomeric state on the cell surface, which would facilitate the formation of an ion channel [27, 28]. Fourth, capacitance entry correlates with the level of CD20 expression and is sensitive to mutation of a short 219–225 amino acid stretch in the C terminal tail [56]. Fifth, in whole cell patch-clamp analysis where transmembrane Ca^{2+} current is measured, most conventional secondary messengers such as diacylglycerol (DAG), inositol trisphosphate (IP_3), cAMP and GTP are removed by dialysis. Sixth, studies in hairy cell leukaemia reveal that CD20 phosphorylation correlates with an elevated level of cytosolic calcium [58, 59] and that treatment with IFN- α causes a tandem reduction in intracellular calcium and CD20 phosphorylation. Although it is not clear whether the hyperphosphorylation or the elevated Ca^{2+} comes first, phosphorylation is known to play an important role in the regulation of other ion channels, it again supports the direct involvement of CD20 as the channel.

In contrast, only weak evidence indicates that CD20 Ca^{2+} flux may occur through a signaling cascade. For example, incubation of Ramos B cells with PP2 (a Lyn tyrosine kinase inhibitor) is shown to result in abrogation of the calcium flux observed after hyper-cross-linking anti-CD20 mAb 2H7. In this signaling pathway, Lyn kinases would become activated after CD20 ligation, potentially resulting in PLC γ 2 phosphorylation (a known result of CD20 ligation [45]). PLC γ 2 cleaves membrane-bound phosphatidylinositol 4,5-bisphosphate (PIP_2) into IP_3 and DAG. IP_3 can diffuse to the ER and stimulate release of calcium from intracellular stores and so provides a direct route for a CD20-dependent signaling cascade resulting in Ca^{2+} release. However, it should be noted that the level of PLC γ 2 phosphorylation and IP_3 release is probably not sufficient to cause store depletion and the resulting capacitance entry, known to be facilitated by CD20 [44]. Furthermore, as CD20 has no known ligand, these signaling pathways resulting from ligation with anti-CD20 mAb may well be entirely non-physiologic. The current evidence suggests that the most important function of CD20 relates to its involvement in BCR activation and signaling. BCR signaling produces extensive Syk and PLC γ 2 activation, resulting in IP_3 and DAG generation, release of Ca^{2+} from intracellular stores and the capacitance signal required to open membrane channels, such as CD20. Once extracellular Ca^{2+} has been allowed entry, the intracellular stores will then begin to re-fill and presumably the capacitance signal diminishes, resulting in channel closure. Interestingly, the second cleavage product of PIP_2 , DAG, is a substrate for protein kinase C (PKC) and PKC has a binding site on the intracellular domain of CD20. PKC activation has been shown to enhance CD20 phosphorylation [60, 61] and also the Ca^{2+} flux associated with CD20 stimulation. Therefore,

PKC generation triggered through BCR ligation may serve to provide a negative feedback pathway of calcium flux through CD20.

Although all of this data is persuasive, it should not be forgotten that the phenotype of the CD20 knockout mouse is extremely mild. Therefore, although there is evidence to support the suggestion that CD20 operates as a capacitance channel during BCR ligation, it is presumably not the only one. Certainly, other calcium channels expressed on B cells have been identified and recently, channels that demonstrate L-type voltage-gated characteristics have been associated with BCR-mediated calcium flux [62]. In addition, TRP1 (transient receptor potential 1), which is a member of the TRP family expressed in B cells, is believed to form part of a calcium channel [63]. Alternatively, the mild phenotype of the CD20 knockout mouse may be due to redundancy as discussed above or may reflect the fact that CD20 does not perform the same function in the mouse, as it has been noted that the motif that affords human CD20 the ability to associate with lipid rafts (see below) is not present in mouse CD20 [56].

CD20 and Lipid Rafts

One of the proximal effects induced following ligation of CD20 with type I mAb is its redistribution in the plasma membrane (table 1) [28, 43, 53, 64]. This is characterised by CD20 becoming insoluble to Tx-100 detergent at low temperatures, indicative of its redistribution into lipid rafts (fig. 2). Lipid rafts are highly ordered membrane domains rich in glycosphingolipids and cholesterol, as well as vital signaling proteins such as Src kinases. As such, these domains are believed to function as signal transduction platforms and have been shown to be involved in cellular adhesion, transmembrane signaling and virus budding. The propensity for CD20 to translocate into these membrane domains upon ligation is relatively rare as Filatov and colleagues [65] found that only CD5, CD20 and sIgM out of 24 surface antigens studied were able to redistribute into Tx-100-insoluble fractions after incubation with mAb. In fact, most raft-enriched proteins are either GPI-linked, such as CD55 and CD59, or are intracellular molecules with substantially modified fatty acid chains attached, such as the Src-like PTK lyn, fyn and lck, which are all dually acylated with myristate and palmitate. CD20 is not GPI-linked or otherwise modified and no evidence has yet been presented to show this occurs after mAb ligation. Indeed, mutation of the two potential palmitoylation sites in CD20 at Cys 110 and 220 causes no difference in raft association [13]. We have shown that redistribution into Tx-100-insoluble rafts does not require involvement of the actin cytoskeleton using inhibition with cytochalasin D, Latrunculin and Jasplakinolide (fig. 2). Similarly, Deans et al. [32] have shown no effect of

kinase inhibition, ATP depletion and cytoskeletal disruption on mAb-induced redistribution of CD20 to Tx-100 rafts. We and others have shown that the redistribution of CD20 into Tx-100 rafts is mAb-dependent and only marginally effected by hyper-cross-linking [43]. Therefore, it is not clear what facilitates the raft localisation of CD20, although amino acids 216–226 in the C-terminus appear to play an important role in this activity [13, 53]. Using highly purified Fab' fragments, Li et al. [32] have recently shown that bivalent cross-linking is not required for increasing insolubility in Tx-100 with the 2H7 mAb. In our own work, we have noted that even after extensive hyper-cross-linking type II mAb, such as B1 and 11B8, only partially render CD20 Tx-100 insoluble [43]. Although some of these data require validation with other anti-CD20 mAb, together, collectively they indicate that cross-linking may not be essential for the redistribution of CD20 to Tx-100 rafts and that it is instead an epitope-dependent phenomenon.

Furthermore, the significance of this translocation to Tx-100-insoluble domains is itself uncertain, as recently this definition of lipid rafts has been questioned. In fact, the work of Deans' group [32] and our own work [S. Morgan, unpubl. observations (cf. fig. 2b)] suggest that CD20 may already exist in smaller raft units that are soluble in Tx-100. In support of this suggestion, Li et al. have recently shown that CD20 is insoluble and raft associated in a range of other detergents such as 1% solutions of CHAPS, Thesit, BRIJ35, BRIJ58 and even low (0.05%) concentrations of Tx-100. This observation coupled to other microscopic evidence has led Li et al., to conclude that CD20 is constitutively raft-associated but with lower affinity than other raft-resident molecules. Therefore it is envisaged that Tx-100-insoluble CD20 rafts may reflect either larger aggregates of these constitutive raft units, brought about by the binding properties of the mAb or a higher affinity interaction of CD20 for the same rafts.

In support of the suggestion that CD20 is constitutively associated with rafts, some anti-CD20 mAb such as FMC7 appear to bind a conformation of CD20 that depends on lipid rafts for its conformation. Polyak et al. [66] recently showed that the perturbation of lipid rafts using the cholesterol-depleting agent MCD completely destroyed the binding site for FMC7 whilst retaining at least 60% of binding activity for another anti-CD20 mAb, B1. In our own work, we have found a similar phenomenon, but find it to be crucially dependent upon the cell line used. We found that cell lines could be loosely categorized into three groups of low, moderate and high sensitivity to cholesterol depletion as is demonstrated in figure 3. It should be noted that both of these studies involve the use of methyl- β -cyclodextrin (MCD) to remove cholesterol and it has been suggested that this treatment can result in a significant loss of protein from the surface, for example Fc ϵ RI [67]. However, our data

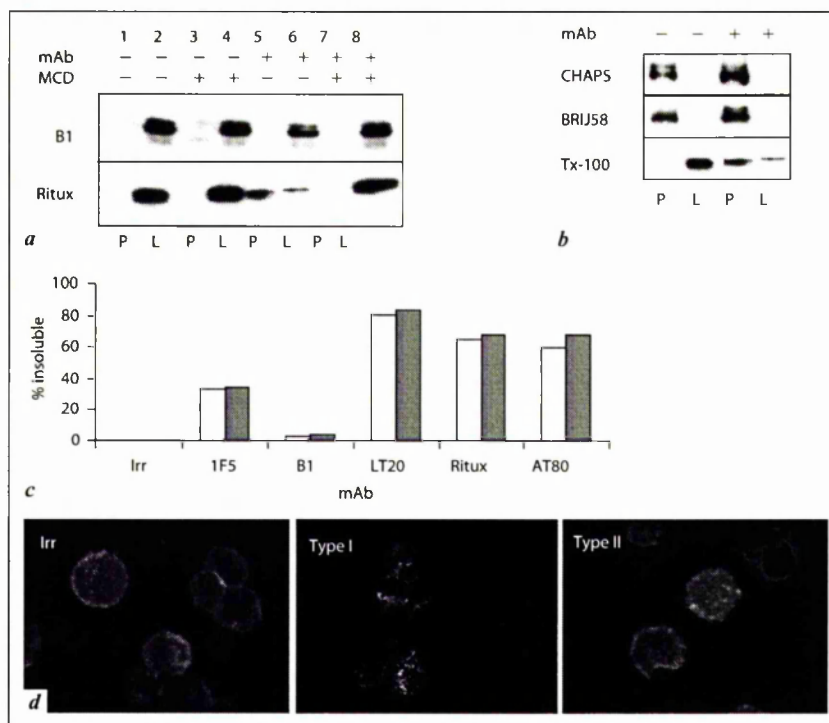


Fig. 2. Distribution of CD20 in the plasma membrane before and after mAb cross-linking. *a* Daudi B cells were treated or not with MCD, stimulated with anti-CD20 mAb for 15 min at 37°C, before lysis in 1% Tx-100. Lysates and insoluble pellets were assessed by SDS-PAGE and Western blotting for CD20. This figure clearly demonstrates that CD20 is soluble to 1% Tx-100 prior to mAb engagement as shown by the lack of CD20 in the insoluble pellet (P) and abundance in the detergent cell lysate (L) (lanes 1 and 2, panel *a*). Removal of cholesterol with 10 mM MCD does not effect this distribution (lanes 3/4). Binding of rituximab and other type I mAb, but not B1 and other type II mAb, causes efficient redistribution of CD20 from the soluble (L) to insoluble (P) fraction (lanes 5/6), which is inhibited by the pre-treatment of the cells with MCD (lanes 7/8). NB: Equal numbers of cell equivalents were loaded in each lane to allow direct comparison between L and P fractions. *b* Untreated cells and cells stimulated with rituximab were lysed in 'weaker' detergents such as 1% CHAPS or BRIJ58, and compared with lysis in Tx-100. CD20 is shown to be present in the insoluble fraction of the cell membrane prior to mAb ligation with the weaker detergents. This insolubility is not affected by ligation with rituximab. NB: In general the amount of CD20 recovered seems less when these weaker detergents are used. *c* The redistribution of CD20 into TX-100-insoluble membrane domains can also be assessed using a simple flow cytometry assay, shown here for various mAb in Ramos-EHRB cells. The data (open bars) confirm that type I but not type II mAb (B1) confer insolubility on CD20. Furthermore, the data shown

suggest that MCD treatment does not have such a detrimental effect on CD20, wherein Western blot analysis using a mAb specific for an intracellular domain of CD20 demonstrated that even though CD20 was lost from the raft fraction, the total amount of CD20 detected in blots was similar (fig. 2). Therefore it appears likely that the difference in mAb binding pre- and post-cholesterol depletion is indicative of an epitope loss/change rather than a loss of surface expression per se. In the initial study, Polyak et al. [66] focused on FMC7 and its dependency on cholesterol for binding. However, our data reveals that even though FMC7 is the most sensitive mAb, most anti-CD20 mAb have a reduced binding level after MCD treatment. Therefore, it should be noted that in experiments such as these, where it is known that CD20 redistribution and mAb binding is cholesterol-dependent, differences in the cholesterol content of the plasma membrane may severely influence the results. In addition to cholesterol depletion, we also investigated the effect on mAb binding when cells were loaded with cholesterol (fig. 3) and asked whether other surface antigens were susceptible to cholesterol depletion and repletion. From this work it is evident that CD20 appears more sensitive than other surface antigens – regardless of whether they constitutively reside in lipid rafts like CD55, are tetra-span molecules like CD37 or can be induced to translocate into rafts like the BCR.

Recent work by Li and colleagues has demonstrated that CD20 must be resident in membrane rafts to facilitate Ca^{2+} entry induced after BCR ligation. Using a variety of approaches including mutant CD20 molecules that do not reside in rafts, these authors elegantly showed a marked reduction of Ca^{2+} influx when CD20 is not present in rafts. This result was mirrored by the treatment of cells with MCD. Importantly, these data are in accordance with data showing that the initial calcium flux provided from intracellular stores in B cells is independent of rafts (and CD20) and actually elevated upon MCD treatment [68], providing further evidence that raft-associated CD20 is not important in initial intracellular store depletion but instead

indicate that pre-treatment of the cells with inhibitors of actin polymerisation (shaded bars) such as cytochalasin D ($1\ \mu\text{M}$), does not affect this property. Similar results were obtained with other inhibitors of actin physiology such as Latrunculin A and Jasplakinolide (data not shown). *d* Distribution of CD20 in the membrane of living cells. Using CD20-YFP transfected mouse 3B3 cells, it is possible to assess the distribution of CD20 in the plasma membrane both before and after mAb ligation. Here we show the pattern of CD20 distribution in cells after ligation for 20 min with an irrelevant mAb (Irr), with a type I mAb (AT80) and with a type II mAb (B1). Note the lack of CD20 clustering prior to treatment and following addition of B1, but the dense clustering after treatment with AT80.

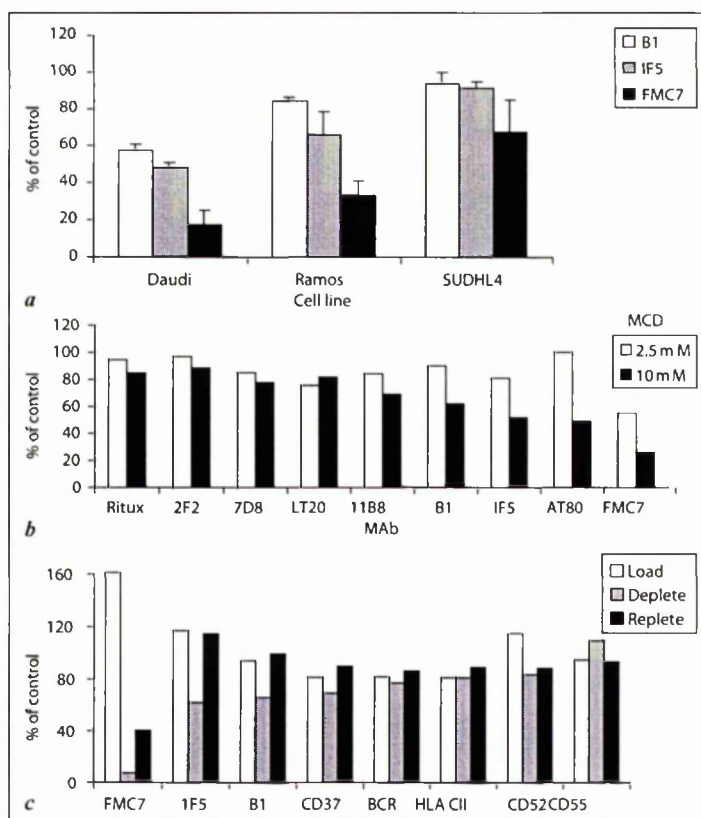


Fig. 3. Importance of cholesterol in CD20 mAb binding. *a* The level of anti-CD20 mAb binding lost after prior incubation for 15 min at 37°C with 10 mM MCD was assessed and shown to be both mAb- and cell-line-dependent. As such, FMC7 was most sensitive to the effects of MCD, followed by IF5 and then B1, and anti-CD20 mAb binding to SUDHL4 cells was relatively refractory to MCD treatment, binding to Ramos cells was moderately sensitive and Daudi cells strongly affected. *b* The level of binding retained after MCD treatment (2.5 or 10 mM) for Daudi cells is clearly dependent upon the specific mAb with rituximab and LT20 relatively unaffected by cholesterol depletion but FMC7 binding severely reduced. There is no clear segregation into type I and II mAb. *c* To assess if increasing the level of cholesterol in the membrane could enhance binding of anti-CD20 mAb, we also loaded cells with cholesterol prior to mAb binding (open bars). To address if other specificities of mAb are also effected by cholesterol depletion, we treated cells with MCD and assessed the binding properties of a range of different mAb to CD37, CD52, CD55, the B cell receptor for antigen and HLA DR. mAb to these antigens appear less susceptible to cholesterol depletion. With the exception of FMC7, repletion of the cholesterol depleted cells with 50 µg/ml soluble cholesterol for 1 h, was able to fully restore mAb binding levels, demonstrating the cholesterol dependence of these effects.

forms an important component of the capacitance entry seen during BCR signaling.

Perhaps the most important interaction of CD20 with the lipid rafts derives from the association of CD20 with members of the Src-family PTK *lyn*, *fyn* and *lck* [46]. However, this interaction is not direct and requires the involvement of an adaptor protein, PAG, which is acylated, and hence raft-enriched [46, 69]. PAG in turn binds Csk, a kinase which targets a specific residue within the Src-family PTK, inhibiting their activity. Current models therefore suggest that Src-family kinases are linked to CD20 via PAG and that PAG-bound Csk regulates the Src-like PTKs within the raft, maintaining them in a resting-inactive state. This theory is supported by the observations that CD20-associated kinase activity is regulated by the expression level of PAG, and that only a low level of kinase activity is associated with CD20 prior to activation with mAb [69]. Upon ligation of CD20, PLC γ and other unidentified substrates become tyrosine phosphorylated, presumably through the interaction of PAG, Csk and the Src kinases. A speculative schema of this interaction is proposed in figure 1.

One important question that is still unresolved is whether the signaling events that proceed after ligation of CD20 with type I mAb simply reflects a ligation of rafts, as opposed to any specific characteristic of CD20. The evidence for this suggestion comes from the observation that cross-linking other raft-resident proteins such as CD59 and other GPI-linked molecules, causes similar signaling effects to those reported for CD20 such as calcium flux and tyrosine phosphorylation [70]. In addition, it is still not clear whether CD20 forms its own homogenous rafts or whether it localises in heterogenous rafts along with other raft proteins and furthermore if these rafts are selective in their components. Intriguingly, Deans et al. [32] have proposed that CD20 and other trans-membrane proteins with relatively weak affinity for rafts might preferentially occupy a subgroup of microvillar rafts. However, they also suggest that the strongly associated raft marker CD59 co-localises with CD20 prior to ligation in a relatively high proportion of rafts. In our own work using FRET and confocal microscopy, we have found that CD20 does not heavily co-localise with CD59 or other raft markers on most B cell lines before or after ligation [Walshe et al., unpubl. results, 2003]. Therefore, this question still requires resolution.

Finally, it is important to mention that the existence of lipid rafts themselves has recently been seriously challenged. The major thrust of this challenge relates to the experimental methods used to infer lipid raft involvement in biological processes, such as detergent insolubility and cholesterol dependence, as these techniques have the potential to introduce significant artefacts [for review, see 71]. Currently, various other techniques, including FRET, are being used to investigate the lipid structure of membranes in their native environment

in intact cells [72–74] but clearly, the nature of lipid rafts and their involvement in cellular signaling requires further study.

Modulation of CD20

One aspect of CD20 biology that has recently been revisited concerns its modulation. Although numerous reports have demonstrated the lack of CD20 modulation *in vitro* and *in vivo* [75–78], two recent papers on CLL cells have suggested that CD20 may in fact become modulated [79, 80]. Perhaps the most surprising result in the first report was the observation that culturing CLL or Raji B cells with rituximab *in vitro* caused an apparent almost complete (100%) modulation of CD20 within 2 h but that this only occurred in the presence of plasma [79]. In contrast, the second report on CLL cells documented an extremely modest modulation of CD20 *in vitro* (approximately 14% within 7 h in the presence of 50% serum) [80]. Our own work detecting bound rituximab with a highly specific anti-Id reagent [81] supports this latter suggestion, such that we observe only very minor CD20 modulation *in vitro* [82]. Therefore, the current data support the historical observation that CD20 does not extensively modulate *in vitro*, irrespective of the B cell type or presence of plasma. However, perhaps more important is the suggestion that CD20 modulates *in vivo*, a finding also reported by Pickartz et al. [83]. Particularly persuasive are experiments where the intracellular domain of CD20 is detected using the L26 antibody, as these mAb are not subject to the blocking/masking problems of extracellular mAb [84, 85]. If we accept that CD20 is indeed modulated in CLL cells after treatment with rituximab, next we must consider the potential mechanisms. Jilani et al. [79] propose a combined mechanism whereby CD20 is both internalised and mRNA down-regulated upon co-incubation with rituximab and plasma. Conversely, Kennedy et al. [80] suggest that CD20 expression is 'modulated', not in the conventional sense, but through removal of CD20:rituximab:C3b complexes via their interactions with phagocytes. This complex mechanism probably occurs in the liver where Kupffer cells pluck the complexes from the opsonised CLL cells during circulation. Subsequent work will be necessary to dissect fully the mechanism of CD20 modulation *in vivo* and to determine several important aspects with respect to treatment with anti-CD20 mAb. For example, is this process specific to CLL cells alone or all CD20 expressing cells? Is complement and/or FcR binding necessary and required for this activity? Does this mean that non-complement-activating, type II mAb may be more suited for immunotherapy of CLL? Clearly this work has important consequences for all aspects of anti-CD20 therapy.

Other recent work has shown that CD20 can be down-regulated on normal B cells after CD40 activation [86]. This effect required the extensive CD40 cross-linking activity provided by CD40L as anti-CD40 mAb were ineffective. This down-regulation was shown to occur through parallel internalisation of CD40 and CD20 in lipid raft domains and was thought to involve cytoplasmic vesicles in a process inhibitable by cytochalasin D and PKC antagonists. Paradoxically, this down-regulation was shown to enhance calcium signaling after CD20 cross-linking. However, it should be noted that these latter experiments were performed using hyper-cross-linking conditions and so conclusions based on these experiments may not truly reflect CD20 phenomenon as opposed to raft phenomenon as discussed earlier. In addition, it is important to note that CD40L-transfected fibroblasts rather than activated T cells were used to induce the down-regulation in this study. Although the number of transfectant cells required to cause the modulation of CD20 was titrated in the study, the amount of CD40L expressed per cell was not. Therefore, it is possible that the levels of CD40L expressed on these cells may well exceed that seen on activated T cells and so the physiological significance of these observations is not clear.

A range of other reagents have also been shown to modulate the expression of CD20 including IL-4, PKC and IFN- α although at least some of these are due to changes in epitope presentation rather than protein expression [60, 87–89]. The biological significance of these effects is not currently clear.

CD20 as a Target Antigen for Cancer Immunotherapy

The efficacy of the chimeric anti-CD20 mAb, rituximab, in treating B cell disorders such as cancer and more recently autoimmunity has been remarkable, particularly when used in combination with chemotherapy [2]. This success has focused attention on the precise mechanisms that make anti-CD20 mAb therapeutically effective. Four potential mechanisms for mAb immunotherapy exist, involving either complement, ADCC through effector cells, direct induction of growth inhibition and/or cell death, or stimulation of host-adaptive immunity [90]. Large amounts of experimental data support all three of the former mechanisms in anti-CD20 mAb immunotherapy, although good evidence for the latter is currently lacking. In particular, several lines of evidence indicate that rituximab operates through conventional effector mechanisms involving complement and effector cells [91]. Perhaps the most conclusive early evidence comes from primate experiments where an IgG4 variant of rituximab was shown to be unable to deplete normal B cells [92]. Recently, we have provided similar data showing that type I mAb such as rituximab and 1F5 require their Fc domains for therapeutic activity in xenograft models [52].

Effector Cell Mechanisms for CD20 Immunotherapy

Taking the complement and effector cell mechanisms separately, a direct role for FcR-bearing effector cells has been implicated in animal models [93] and also from clinical data where high-affinity antibody binding FcR allotypes have been shown to correlate with improved response rates in follicular lymphoma (FL) patients [94]. This data is now well accepted along with similar data relating to systemic lupus erythematosus [95] and so will not be discussed further. However, intriguingly, recent data from Weng et al. indicate that in addition to the well-characterised 158 FF vs. VV allotype in Fc γ RIIIa, an allelotypic difference in Fc γ RIIa96 also provides better responses to rituximab, although the mechanism involved is unclear given that IgG2 rather than IgG1 binding is known to be enhanced by this polymorphism [97]. In addition, it is now clear that the previously described FcR γ IIIa allotype is not predictive of the response to rituximab in all tumors, as it does not predict the response to rituximab in B-CLL [96]. This is extremely intriguing and suggests that control of different tumour types may require different antibody effector mechanisms.

Complement Mechanisms for CD20 Immunotherapy

Support for complement-dependent mechanisms as an important effector function in rituximab treatment comes from several sources. Firstly, complement is consumed during rituximab treatment [98], demonstrating that it is activated after mAb administration. Second, in some cases cells remaining after treatment have increased CD59 expression [99], consistent with the idea that the targeted cells were subject to immunological selective pressure from complement. Third, the resistance of different lymphoma cells to rituximab *in vivo* appears related to their sensitivity to CDC *in vitro*, again indicating that sensitivity to complement lysis dictates therapeutic response [100]. In this regard, it is intriguing that exogenous addition of the complement component C2 boosts the cytotoxicity of rituximab *ex vivo*, indicating that consumption of C2 *in vivo* in the presence of high tumour load may limit cell lysis [80]. Finally, direct evidence for the role of complement has been provided in two animal models [52, 101]. In these, complement activity was removed either by performing the experiments in C1q-deficient mice or by utilising cobra venom factor. An additional mechanism whereby complement may be playing a role in rituximab therapy is in stimulating opsonisation as opposed to direct cell lysis. Similarly, rituximab generation of C3a/C5a may promote enhanced activation of effector cells. This could help explain why FcR and complement are required to work cooperatively. Unfortunately, both of the experimental models detailed above

block early stage complement activation and do not discriminate between potential roles for complement activation in opsonisation, enhanced activation of effector cells, or direct target cell lysis. These possible mechanisms are currently being explored in our laboratory.

One of the main arguments against complement being a major effector is that the therapeutic activity of rituximab does not always correlate with the expression levels of the complement defence molecules, CD55 or CD59 [102]. However, these studies consider ADCC and CDC as separate processes and thus exclude any possible cooperative activity, such as discussed above where complement opsonisation might be important for phagocytosis and regulation of immune responses. It is also unknown whether complement products such as C3b and the membrane attack complex (MAC) could have important signaling functions via complement receptors on the tumour cells that might potentiate or modulate signaling activity provided by anti-CD20 mAb.

Given that CD20 is an extremely potent target protein for focussing complement mechanisms, it is worth examining why this may be the case. First, CD20 is highly expressed. However, although CD20 expression level is known to correlate with tumour cell lysis in CDC, it should be noted that other more highly expressed antigens such as MHCII are not as potent [43]. Second, as discussed, CD20 does not appear to modulate *in vitro* after mAb ligation [75–77], allowing complement activation to proceed without down-regulation of the initiating stimulus. Third, the only available binding surface of CD20 is a surface proximal loop region, meaning the mAb is bound very close to the plasma membrane, a property shared by other potent CDC antigens such as CD52 [103]. Such close binding presumably enhances the deposition of complement products onto the cell surface, facilitating lysis. However, clearly this property is not sufficient as CD37 is also membrane proximal but is a much less effective target antigen [43]. Therefore, although all of these former properties afford the potential for CD20 to recruit and activate complement efficiently at the cell surface, other factors must also play a role. One important property appears to relate to the lateral mobility of Ab:Ag complexes in the plasma membrane. As such, type I anti-CD20 mAb that cause redistribution into Tx-100-insoluble areas of the plasma membrane, but not type II mAb, are extremely potent at activating lytic complement [43]. This property is not due to inherent deficiencies of type II mAb to activate complement *per se* as C1s and C3 deposition by B1 is equivalent to the isotype matched 1F5 in solid-phase ELISA experiments (fig. 4). Why translocation of Ab:Ag complexes into lipid rafts should influence the ability of mAb to activate complement so markedly is not fully resolved but certainly involves the ability of different mAb to bind the first component of complement C1. As such, C1q is shown to bind readily to type I but not type II mAb on the surface of B cells after CD20

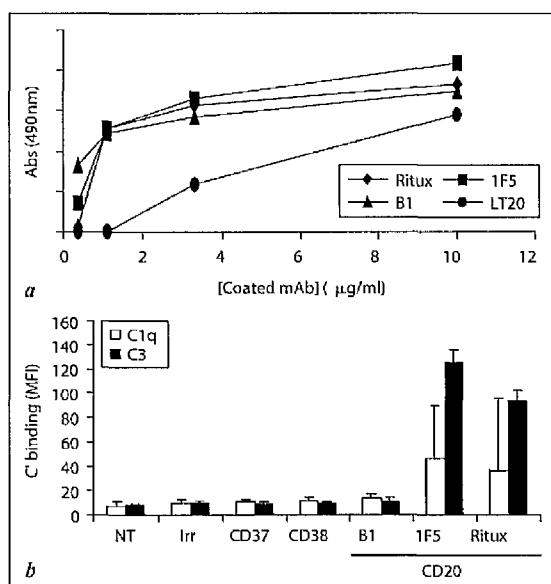


Fig. 4. Complement activation by anti-CD20 mAb: type I but not type II mAb bind C1 at the cell surface and cause deposition of C3. *a* To demonstrate the inherent similarity of the different anti-CD20 mAb in binding C1, a solid-phase ELISA was performed. Following coating of different anti-CD20 mAb to the plate at a range of concentrations, the plate was incubated with normal human serum, washed and incubated with anti-C1 mAb before washing and detection with an HRP-conjugated mAb. These data clearly show that C1 binds equivalently to 1F5, rituximab and B1 when they are adhered in the same manner to the surface of a plastic plate. NB: The binding of C1 to LT20 is lower as expected for a mouse IgG1 isotype. *b* The binding of C1q and C3 to the surface of EHRB cells was explored, following binding of Irr, CD37, CD38 and different CD20 mAb. With the exception of rituximab, all of these were of the same IgG2a isotype. The data represent the mean and SD of three separate experiments and illustrate that only type I anti-CD20 mAb bind C1q and C3, when bound to the surface of B cells.

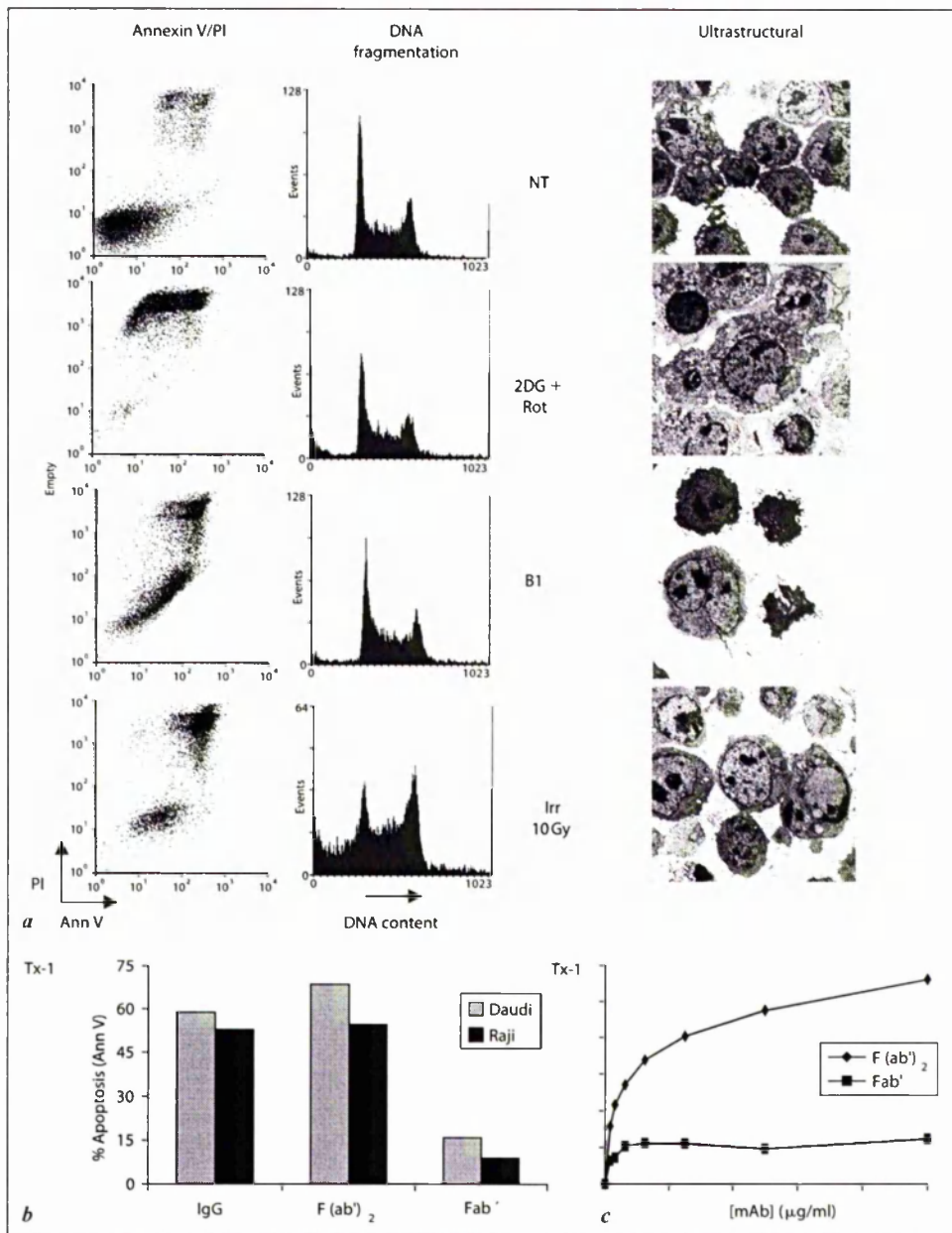
redistribution [52] (fig. 4). Because of the requirement for multiheaded binding to engage and activate C1q, the most straightforward explanation is that concentrating mAb into a defined, clustered area of the plasma membrane provides a high local density of juxtaposed Fc regions for engaging the globular heads of C1q, thereby triggering the classical complement pathway. However, a second possibility is that the membrane environment provided by lipid rafts is particularly advantageous for complement activation and/or deposition. This may be through enhanced deposition of C3 in membrane rafts or by providing a

region of the membrane that is more susceptible to penetration by MAC, perhaps because the lipid is more rigid or because the MAC is less likely to be removed from the plasma membrane by internalisation or shedding. Previous work with red blood cells supports the hypothesis that rafts may be favourable sites for complement lysis wherein susceptibility to lysis increases with increasing cholesterol content [104]. In this respect, it is interesting that most complement-defence molecules, being GPI-linked, are constitutively associated with rafts and consequently ideally placed to protect cells from any damage focused on the rafts. Hopefully, in the near future it will be interesting to learn whether ligated CD20 is surrounded by complement control proteins in membrane rafts or protected from them.

Signaling for Cell Death

Anti-CD20 mAb can also transmit signals which evoke cell cycle arrest and or cell death, at least in some B cell lines [38–43, 91]. This ability appears to be a desirable trait in anti-cancer mAb and may distinguish those mAb which are successful in the clinic from those which are not [reviewed in 105]. Indeed, Byrd et al. [106] have recently shown in rituximab-treated B-CLL patients, that a better clinical response and more extensive depletion of CD20-positive cells correlates with apoptosis, as detected by caspase-3 and -9 processing, although it should be noted that some of these readouts may be due to complement-dependent lysis as discussed elsewhere [53]. Using mAb fragments, we and others have shown that the Fc region of certain anti-CD20 mAb is unimportant, with F(ab')₂ fragments inducing similar levels of cell death as whole IgG [41, 53]. However, clearly bivalency is the minimum requirement as Fab' fragments are unable to induce substantial levels of cell death (fig. 5). Therefore, at least a degree of CD20 cross-linking is required for apoptotic induction.

It has recently been suggested that membrane rafts may be important in propagating cell death induced through anti-CD20 mAb based on the finding that rituximab can redistribute CD20 to the TX-100-insoluble lipid membrane compartment of the cell, where many important signaling enzymes and mediators are located [54]. This notion seems reasonable as lipid rafts are generally considered to be the main signaling platforms of the cell, and their coalescence into synapses provides a rationale for how transmembrane signaling is organised within the membrane. Furthermore, several lines of evidence indicate that Src-like tyrosine kinases, which are enriched in lipid rafts, may be important in CD20-induced apoptosis [39]. The most straightforward model of anti-CD20 mAb-induced cell death is that CD20, through its ability to redistribute into rafts, associates with PAG, causing a change in the regulation of



Csk and hence the kinase activity of Src kinases, which then signal for cell death. This model requires that the association of CD20 with lipid rafts is crucial to the cell death pathway. In support of this suggestion, the Src inhibitor PP2 is able to inhibit cell death transduced after hyper-cross-linking rituximab [39]. However, several lines of evidence indicate that CD20-induced cell death does not require lipid raft redistribution, similar to the situation for BCR apoptosis in immature B cells [107]. First, the B1 mAb, which is generally the most potent in cell death assays, does not cause redistribution of CD20 to Tx-100-insoluble rafts as mentioned earlier [43, 50]. Second, mutant molecules of CD20 that do not redistribute into lipid rafts appear equally capable of inducing cell death as the wild-type counterparts [53]. Third, although cell death induction requires at least bivalent engagement of mAb, it appears that redistribution of CD20 to Tx-100-insoluble rafts does not [32]. The explanation for at least some of these conflicting data is that CD20 signaling may occur through small raft platforms which are soluble in Tx-100 and that large CD20 surface aggregates are not important. However, recent evidence from Deans et al. [32, 56] indicate that mutations similar to those used by us (219–225) also remove CD20 from BRIJ58-insoluble smaller rafts, indicating that even these smaller rafts are unimportant for apoptotic signaling through CD20. An alternative suggestion is that CD20 in its resting state forms small oligomeric complexes, perhaps along with various other surface proteins (such as MHCII, CD40, etc.) in association with a small lipid raft shell containing the requisite

Fig. 5. Nature of cell death induced by anti-CD20 mAb. a Daudi cells were treated with anti-CD20 mAb (B1) and the type of cell death compared with that induced by 2-deoxyglucose + rotenone, or γ -irradiation (10 Gy) treatment. Cell death was assessed by annexin V:PI staining, DNA fragmentation and electron microscopy. The 2DG+Rot treatment induces extensive cell death in the absence of elevated levels of DNA fragmentation. This treatment appears to cause necrotic death as indicated by the electron microscopy analysis whereby cell swelling and loss of membrane integrity is apparent. By contrast, γ -irradiation of these cells gives rise to extensive cell death via classical apoptosis with the ensuing DNA fragmentation and hallmark chromatin condensation. By contrast, although anti-CD20 mAb treatment causes phosphatidylserine (PS) flipping and PI permeability, no obvious nuclear change is apparent and neither classical apoptosis nor necrosis is induced. *b* As shown, the cell death induced by anti-CD20 mAb is independent of the Fc region but requires bivalent ligation where Daudi and Raji cells were treated with saturating concentrations (10 μ g/ml) of IgG, F(ab')₂ or Fab' fragments of B1 for 24 h prior to harvesting and analysis with the annexin V PI assay. These data illustrate the equivalent activity of IgG and F(ab')₂ fragments, but greatly diminished potency of the univalent Fab'. Similar results were seen with fragments of rituximab and AT80 (data not shown). *c* The concentration dependence of these different fragments are compared, demonstrating that the F(ab')₂ fragments are much more potent than the Fab'.

PAG and Src kinases and that bivalent ligation of these is sufficient for cell death signaling. A second possibility is that the Src-dependent cell death detailed previously reflects the hyper-cross-linking methods used and actually merely reflects cell death that is induced by aggregating lipid raft domains as opposed to CD20 specifically as discussed earlier. In agreement with this suggestion it is known that cross-linking raft-resident proteins such as CD52, CD55, CD59 and lipids such as GM1, results in similar levels of Src kinase activation and cell death [108–110].

Several reports have also implied that Ca^{2+} influx may be important in CD20-induced apoptosis. These experiments have used intracellular (BAPTA) and extracellular (EGTA) Ca^{2+} chelators to inhibit apoptosis transduced after hyper-cross-linking rituximab [38, 39, 111]. Although recent experiments convincingly support a role for CD20 in BCR-induced Ca^{2+} signaling, with the exception of the work of Bubien et al. [27], direct evidence that CD20 ligation causes opening of a Ca^{2+} channel in B cells is lacking with observable Ca^{2+} flux only apparent after hyper-cross-linking [39, 44, 45, 112]. Therefore, although it is known that Ca^{2+} flux can result in apoptosis, whether the low level (it is generally unmeasurable) Ca^{2+} flux generated after addition of non-hyper-cross-linked anti-CD20 mAb, can cause apoptosis is uncertain. Clearly, further work is required to delineate the role of calcium in CD20 apoptosis and whether type I and II mAb have the same requirements. The mechanics of the cell death evoked will be discussed in a latter section.

Another interesting aspect of CD20-induced cell death relates to the fact that all type II mAb bind at a half-maximal level compared with type I mAb. Presumably then, their efficacy is related to how or in what conformation they bind CD20. Interestingly, these properties of half-maximal binding and cell death also appear to correlate with the degree of homotypic adhesion such that type II mAb which bind at 50% of the level of type I mAb, are more inclined to promote homotypic adhesion. This in turn may indicate that an enhanced level of signaling is evoked when anti-CD20 mAb bind in this conformation. The nature of the signals transduced after different (type I and II) mAb and how cell death is affected, forms the basis of our ongoing studies.

Concerning the mechanics of death induced, several authors have reported that cell death induced by anti-CD20 mAb requires extensive cross-linking and involves the activation of caspases with the resulting cleavage of PARP [38–40, 54, 111, 113, 114]. However, in some instances these conclusions are compromised by the high concentrations of inhibitors and inappropriate measures of cell death used. In addition, the effects of anti-CD20 mAb are often only studied in one cell line with rituximab, following hyper-cross-linking, which may reflect an unnaturally high level of cross-linking compared to that achieved in vivo. Interestingly, such hyper-cross-linking has been shown to convert BCR

apoptosis from a caspase-independent to caspase-dependent process [115] and similar conversion may occur with CD20. Furthermore, additional cross-linking produces variable effects in relation to both the mAb and the cells used. For example, the level of cell death induced by B1 is not affected by hyper-cross-linking and when anti-CD20 mAb such as AT80 are coated to plates or hyper-cross-linked with polyclonal antibody, the level of apoptosis induced is actually less than when the mAb is not further cross-linked. For these reasons we have studied anti-CD20 mAb-induced cell death in the absence of additional cross-linking. Under these conditions we observe that the type of cell death induced by anti-CD20 mAb is not classical apoptosis, wherein DNA fragmentation is not apparent, and the nucleus does not condense. Furthermore, we have shown that caspases, although possibly cleaved, are unimportant for transmitting the death signal [53] (fig. 5). Similar findings were made by others [116, 117]. Furthermore, we have also observed that overexpression of Bcl₂ is only partially able to block the apoptotic effects of anti-CD20 mAb [53]. This was demonstrated in three separate cell lines and agrees with work by others [117]. Therefore, ligated but non-hyper-cross-linked CD20 appears to engage a novel, caspase-independent cell death pathway that is also partly independent of the usually strict mitochondrial controls.

Immune Response

A fourth potential effector mechanism of anti-CD20 mAb relates to generating/potentiating an immune response against the target cell. The direct evidence that anti-CD20 mAb induce immune responses in cancer patients is scarce and appears restricted to a single study of 12 rituximab-treated FL patients wherein 17% of the patients had evidence of CTL activity following rituximab treatment [118]. In addition to this study, one group has shown that rituximab can opsonise target Daudi B cells and facilitate their uptake into DC for cross-priming to CTL in vitro [119, 120]. However, no evidence has been presented to date to demonstrate that this occurs in vivo. Therefore, although possible, good evidence that anti-CD20 mAb provide therapeutically relevant immune responses in vivo is currently lacking.

CD20 – The Ideal Target Antigen?

In summary, several factors make CD20 an ideal target antigen. First, it is tightly restricted to the B cell lineage with no known ligand. It is expressed on the majority of B cell malignancies but not on pro-B, plasma or hematopoietic

stem cells, which allows for good tumour specificity, maintenance of serum IgG levels and recovery from pro-B and stem cell pools post-treatment. Second, CD20 is not shed from the cell surface after mAb binding, and in most studies is not modulated, which makes it an attractive immunotherapeutic target for CDC and ADCC mechanisms. Third, CD20 is highly expressed (at approximately 100–200,000 copies on most B cell lines). This also is of benefit when targeting CDC and ADCC mechanisms. Fourth, treatment very rarely results in the outgrowth of antigen-negative variants, making repeat use of anti-CD20 mAb a tenable proposition. Fifth, anti-CD20 mAb have the potential to deliver anti-proliferative death signals to the target cells. Last, although still unproven, it is possible that anti-CD20 mAb can provide a means for cross-priming and development of T cell responses.

Given all of these beneficial factors, it is perhaps not surprising that CD20 is currently being investigated for a wide range of therapeutic applications. For example, it is being assessed as an inducible suicide gene. Using a lentiviral transduction system, Serafini et al. [121, 122] have shown that CD20 can be expressed in various target cells such as primary T lymphocytes. These targets have been shown to be sensitive to subsequent rituximab-induced CDC, providing a means for the target cell deletion. This approach is currently being considered for use in the treatment of graft-versus-host disease.

An additional therapeutic approach currently being assessed in mice but potentially also in humans, involves generating immune reactivity to CD20 [123–125]. The mouse approach involves immunising with CD20 peptides in a variety of formats (coupled to either human IgG Fc [125] or KLH [124]) and in the presence of a range of adjuvants. These experiments have shown that vaccination with the CD20 peptides resulted in a 25–40% decrease in CD19+ splenic B cells relative to controls and demonstrate that an active, specific immune response to CD20 can be elicited in mice vaccinated in this way. However, in this approach it is not clear (a) why the depletion is not more pronounced, (b) if this low level reduction would be sufficient to provide a therapeutic response, and (c) how the normal B cell population would be effected long term after such treatment. In humans, this ability to generate reactivity to CD20 is being explored using ex vivo T cells pulsed with CD20 peptides, and recent work by Grube et al. [123] has suggested that it is possible to generate CTL reactivity towards two separate peptides present in CD20. Importantly, these authors demonstrated that CTL activity could be generated using NHL and CLL patient T cells and in fact the frequency of activity was higher in the CLL cases. However, it should be noted that the T cells generated were of a low potency, only responding to high (50 µg/ml) concentrations of peptide. Therefore, it is not clear whether they would be sufficiently active against cell bound CD20 to

achieve therapeutic effects or how the T cells would be regulated with respect to the normal B cell population.

One recently suggested barrier to anti-CD20 therapy is the presence of circulating CD20 (cCD20). Although not yet confirmed by other groups, Albitar and colleagues [126, 127] have shown that CD20 (and CD52) is present in the blood of healthy and diseased patients in some kind of soluble form. Of particular note are the observations that the concentration of cCD20 (and cCD52) are increased in CLL and that this cCD20 can block rituximab binding to target cells. However, strangely, significant blocking was only seen in the presence of 500 μ l of plasma. Given that 1 μ l of plasma contains enough cCD20 to be detected in Western blot analysis, with an intensity equivalent to that seen in cell lysates, it is not clear why such high levels of plasma are required for blocking. Furthermore, with rituximab remaining at μ g/ml levels during treatment for long periods of time, the physiological implications of these findings remain to be fully elucidated. However, irrespective of these concerns, cCD20 levels appear to have important prognostic significance in CLL, correlating with patient survival as well as the proportion of CD38-positive tumour cells and the stage of disease. Interestingly, both cCD20 and cCD52 are increased in NHL, but decreased in Hodgkin's disease. Therefore, the function of these circulating proteins in disease, the mechanism through which they are generated and the form they take remain to be elucidated.

The Optimal Anti-CD20 mAb – Type I or II?

Clearly, CD20 is an excellent target antigen for mAb immunotherapy. However, what is not yet fully resolved is whether the optimal antibody has been generated and whether different types of mAb might suit different types of disease. For example, given that the extent of CD20-mediated cell death induced by rituximab treatment is quite small [53, 128, 129], whilst the CDC activity is extremely and unusually high [43, 52], one may conclude that the central effector mechanism of rituximab *in vivo* involves complement. Therefore, in situations where complement mechanisms are expected to provide the main therapeutic component, such as when the target cell is predominantly blood borne, facilitating good complement access, type I mAb would be the mAb of choice. Conversely, type II mAb, such as B1, which are more inclined to function through direct induction of cell death and in the absence of the complement effector arm, might fare better in situations where cells are sensitive to apoptosis and/or are resistant to complement or where inflammation is to be avoided such as in the treatment of certain autoimmune conditions. We are currently exploring these suggestions.

Conclusions and New Avenues of Research

The CD20 surface antigen has proven to be an extremely potent target in the treatment of B cell malignancies. Further investigation into the nature of the cell death pathway signalled through CD20 ligation will be of clear benefit. In particular, understanding the importance of the interaction of CD20 with the PAG binding protein, and the exact role of calcium in the death pathway will be of great interest as will understanding whether type I and type II mAb inherently differ in their means of signaling for death. Other research may reveal the importance of the membrane location of CD20, what it is associated with and if these associations are important for its biological and mAb-signalled functions. Concerning the true biological function of CD20, it may be informative to develop conditional CD20 knockout mice. In addition, it will be interesting to understand how the new CD20 gene family members interact together and what physiological role they may play.

Acknowledgements

The authors would like to thank all of the members of Tenovus Research Laboratory and in particular members of the CD20 team. We are also indebted to our colleagues in the Cancer Sciences Division, in the School of Medicine, in particular Peter Johnson. Finally, we acknowledge our ongoing collaboration with the CD20 team at Genmab, Utrecht, and their work with the human CD20 mAb. We apologise to those authors whose work has not been cited in this review due to space limitations.

Funding is provided from the CRUK; AICR, LRF, Tenovus, Cardiff; and BBSRC.

References

- 1 Boye J, Elter T, Engert A: An overview of the current clinical use of the anti-CD20 monoclonal antibody rituximab. *Ann Oncol* 2003;14:520–535.
- 2 Coiffier B: Monoclonal antibodies combined to chemotherapy for the treatment of patients with lymphoma. *Blood Rev* 2003;17:25–31.
- 3 Dillman RO: Treatment of low-grade B-cell lymphoma with the monoclonal antibody rituximab. *Semin Oncol* 2003;30:434–447.
- 4 Uchida J, Lee Y, Hasegawa M, Liang Y, Bradney A, Oliver JA, Boven K, Steeber DA, Haas KM, Poe JC, Tedder TF: Mouse CD20 expression and function. *Int Immunol* 2004;16:119–129.
- 5 O'Keefe TL, Williams GT, Davies SL, Neuberger MS: Mice carrying a CD20 gene disruption. *Immunogenetics* 1998;48:125–132.
- 6 Tedder TF, Klejman G, Disteché CM, Adler DA, Schlossman SF, Saito H: Cloning of a complementary DNA encoding a new mouse B lymphocyte differentiation antigen, homologous to the human B1 (CD20) antigen, and localization of the gene to chromosome 19. *J Immunol* 1988;141:4388–4394.
- 7 Tedder TF, Streuli M, Schlossman SF, Saito H: Isolation and structure of a cDNA encoding the B1 (CD20) cell-surface antigen of human B lymphocytes. *Proc Natl Acad Sci USA* 1988;85:208–212.

- 8 Stamenkovic I, Seed B: Analysis of two cDNA clones encoding the B lymphocyte antigen CD20 (B1, Bp35), a type III integral membrane protein. *J Exp Med* 1988;167:1975-1980.
- 9 Einfeld DA, Brown JP, Valentine MA, Clark EA, Ledbetter JA: Molecular cloning of the human B cell CD20 receptor predicts a hydrophobic protein with multiple transmembrane domains. *EMBO J* 1988;7:711-717.
- 10 Liang Y, Buckley TR, Tu L, Langdon SD, Tedder TF: Structural organization of the human MS4A gene cluster on chromosome 11q12. *Immunogenetics* 2001;53:357-368.
- 11 Liang Y, Tedder TF: Identification of a CD20-, FcεRIβ-, and HTm4-related gene family: Sixteen new MS4A family members expressed in human and mouse. *Genomics* 2001;72:119-127.
- 12 Tedder TF, Engel P: CD20: A regulator of cell-cycle progression of B lymphocytes. *Immunol Today* 1994;15:450-454.
- 13 Polyak MJ, Tailor SH, Deans JP: Identification of a cytoplasmic region of CD20 required for its redistribution to a detergent-insoluble membrane compartment. *J Immunol* 1998;161:3242-3248.
- 14 Rieckmann P, Wilson GL, Thevenin C, Hong JX, Kehrl JH: Analysis of cis-acting elements present in the CD20/B1 antigen promoter. *J Immunol* 1991;147:3994-3999.
- 15 Thevenin C, Rieckmann P, Kozlow EJ, Kehrl JH: Identification of a diverged octamer binding site important in the B cell-specific expression of the CD20 gene. *Trans Assoc Am Physicians* 1992;105:15-24.
- 16 Thevenin C, Lucas BP, Kozlow EJ, Kehrl JH: Cell type- and stage-specific expression of the CD20/B1 antigen correlates with the activity of a diverged octamer DNA motif present in its promoter. *J Biol Chem* 1993;268:5949-5956.
- 17 Himmelmann A, Riva A, Wilson GL, Lucas BP, Thevenin C, Kehrl JH: PU.1/Pip and basic helix loop helix zipper transcription factors interact with binding sites in the CD20 promoter to help confer lineage- and stage-specific expression of CD20 in B lymphocytes. *Blood* 1997; 90:3984-3995.
- 18 Nagy M, Chapuis B, Matthes T: Expression of transcription factors Pu.1, Spi-B, Blimp-1, BSAP and oct-2 in normal human plasma cells and in multiple myeloma cells. *Br J Haematol* 2002;116:429-435.
- 19 Crepieux P, Coll J, Stehelin D: The Ets family of proteins: Weak modulators of gene expression in quest for transcriptional partners. *Crit Rev Oncog* 1994;5:615-638.
- 20 Nutt SL, Eberhard D, Horcher M, Rolink AG, Busslinger M: Pax5 determines the identity of B-cells from the beginning to the end of B-lymphopoiesis. *Int Rev Immunol* 2001;20:65-82.
- 21 Fitzsimmons D, Hodsdon W, Wheat W, Maira SM, Wasyluk B, Hagman J: Pax-5 (BSAP) recruits Ets proto-oncogene family proteins to form functional ternary complexes on a B-cell-specific promoter. *Genes Dev* 1996;10:2198-2211.
- 22 Blakolmer K, Vesely M, Kummer JA, Jurecka W, Mannhalter C, Chott A: Immunoreactivity of B cell markers (CD79a, L26) in rare cases of extranodal cytotoxic peripheral T- (NK/T-) cell lymphomas. *Mod Pathol* 2000;13:766-772.
- 23 Quintanilla-Martinez L, Preßler F, Rubin D, Ferry JA, Harris NL: CD20+ T-cell lymphoma. Neoplastic transformation of a normal T-cell subset. *Am J Clin Pathol* 1994;102:483-489.
- 24 Yokose N, Ogata K, Sugisaki Y, Mori S, Yamada T, An E, Dan K: CD20-positive T cell leukemia/lymphoma: Case report and review of the literature. *Ann Hematol* 2001;80:372-375.
- 25 Yao X, Teruya-Feldstein J, Raffeld M, Sorbara L, Jaffe ES: Peripheral T cell lymphoma with aberrant expression of CD79a and CD20: A diagnostic pitfall. *Mod Pathol* 2001;14:105-110.
- 26 Katopodis O, Liossis SN, Viglis V, Pouli A, Dimopoulos MA, Sfrikakis PP: Expansion of CD8+ T cells that express low levels of the B cell-specific molecule CD20 in patients with multiple myeloma. *Br J Haematol* 2003;120:478-481.
- 27 Bubien JK, Zhou LJ, Bell PD, Frizzell RA, Tedder TF: Transfection of the CD20 cell surface molecule into ectopic cell types generates a Ca²⁺ conductance found constitutively in B lymphocytes. *J Cell Biol* 1993;121:1121-1132.
- 28 Polyak MJ, Deans JP: Alanine-170 and proline-172 are critical determinants for extracellular CD20 epitopes; heterogeneity in the fine specificity of CD20 monoclonal antibodies is defined by additional requirements imposed by both amino acid sequence and quaternary structure. *Blood* 2002;99:3256-3262.

- 29 Leveille C, Al-Daccak R, Mourad W: CD20 is physically and functionally coupled to MHC class II and CD40 on human B cell lines. *Eur J Immunol* 1999;29:65-74.
- 30 Szollosi J, Horejsi V, Bene L, Angelisova P, Damjanovich S: Supramolecular complexes of MHC class I, MHC class II, CD20, and tetraspan molecules (CD53, CD81, and CD82) at the surface of a B cell line JY. *J Immunol* 1996;157:2939-2946.
- 31 Petrie RJ, Deans JP: Colocalization of the B cell receptor and CD20 followed by activation-dependent dissociation in distinct lipid rafts. *J Immunol* 2002;169:2886-2891.
- 32 Li H, Ayer LM, Polyak MJ, Mutch CM, Petrie RJ, Gauthier L, Shariat N, Hendzel MJ, Shaw AR, Patel KD, Deans JP: The CD20 calcium channel is localized to microvilli and constitutively associated with membrane rafts; antibody binding increases the affinity of the association through an epitope-dependent cross-linking independent mechanism. *J Biol Chem* 2004;279:19893-19901.
- 33 Holder M, Grafton G, MacDonald I, Finney M, Gordon J: Engagement of CD20 suppresses apoptosis in germinal center B cells. *Eur J Immunol* 1995;25:3160-3164.
- 34 Smeland EB, Beiske K, Ek B, Watt R, Pfeifer-Ohlsson S, Blomhoff HK, Godal T, Ohlsson R: Regulation of c-myc transcription and protein expression during activation of normal human B cells. *Exp Cell Res* 1987;172:101-109.
- 35 Clark EA, Shu G: Activation of human B cell proliferation through surface Bp35 (CD20) polypeptides or immunoglobulin receptors. *J Immunol* 1987;138:720-725.
- 36 Kansas GS, Tedder TF: Transmembrane signals generated through MHC class II, CD19, CD20, CD39, and CD40 antigens induce LFA-1-dependent and independent adhesion in human B cells through a tyrosine kinase-dependent pathway. *J Immunol* 1991;147:4094-4102.
- 37 Tedder TF, Forsgren A, Boyd AW, Nadler LM, Schlossman SF: Antibodies reactive with the B1 molecule inhibit cell cycle progression but not activation of human B lymphocytes. *Eur J Immunol* 1986;16:881-887.
- 38 Shan D, Ledbetter JA, Press OW: Signaling events involved in anti-CD20-induced apoptosis of malignant human B cells. *Cancer Immunol Immunother* 2000;48:673-683.
- 39 Hofmeister JK, Cooney D, Coggeshall KM: Clustered CD20-induced apoptosis: Src-family kinase, the proximal regulator of tyrosine phosphorylation, calcium influx, and caspase 3-dependent apoptosis. *Blood Cells Mol Dis* 2000;26:133-143.
- 40 Pedersen IM, Buhl AM, Klausen P, Geisler CH, Jurlander J: The chimeric anti-CD20 antibody rituximab induces apoptosis in B-cell chronic lymphocytic leukemia cells through a p38 mitogen-activated protein-kinase-dependent mechanism. *Blood* 2002;99:1314-1319.
- 41 Cardarelli PM, Quinn M, Buckman D, Fang Y, Colcher D, King DJ, Bebbington C, Yarranton G: Binding to CD20 by anti-B1 antibody or F(ab')₂ is sufficient for induction of apoptosis in B-cell lines. *Cancer Immunol Immunother* 2002;51:15-24.
- 42 Cragg MS, Asadipour A, O'Brien L, Tutt A, Chan HTC, Anderson VA, Glennie MJ: Opposing Properties of CD20 mAb. *Leukocyte Typing VII*. Oxford, Oxford University Press, 2002, pp 95-97.
- 43 Cragg MS, Morgan SM, Chan HT, Morgan BP, Filatov AV, Johnson PW, French RR, Glennie MJ: Complement-mediated lysis by anti-CD20 mAb correlates with segregation into lipid rafts. *Blood* 2003;101:1045-1052.
- 44 White MW, McConnell F, Shu GL, Morris DR, Clark EA: Activation of dense human tonsillar B cells. Induction of c-myc gene expression via two distinct signal transduction pathways. *J Immunol* 1991;146:846-853.
- 45 Deans JP, Schieven GL, Shu GL, Valentine MA, Gilliland LA, Aruffo A, Clark EA, Ledbetter JA: Association of tyrosine and serine kinases with the B cell surface antigen CD20. Induction via CD20 of tyrosine phosphorylation and activation of phospholipase C- γ 1 and PLC phospholipase C- γ 2. *J Immunol* 1993;151:4494-4504.
- 46 Deans JP, Kalt L, Ledbetter JA, Schieven GL, Bolen JB, Johnson P: Association of 75/80-kDa phosphoproteins and the tyrosine kinases Lyn, Fyn, and Lck with the B cell molecule CD20. Evidence against involvement of the cytoplasmic regions of CD20. *J Biol Chem* 1995; 270: 22632-22638.
- 47 Popoff II, Savage JA, Blake J, Johnson P, Deans JP: The association between CD20 and Src-family tyrosine kinases requires an additional factor. *Mol Immunol* 1998;35:207-214.
- 48 Wagner N, Engel P, Tedder TF: Regulation of the tyrosine kinase-dependent adhesion pathway in human lymphocytes through CD45. *J Immunol* 1993;150:4887-4899.

- 49 Tedder TF, Schlossman SF: Phosphorylation of the B1 (CD20) molecule by normal and malignant human B lymphocytes. *J Biol Chem* 1988;263:10009–10015.
- 50 Deans JP, Robbins SM, Polyak MJ, Savage JA: Rapid redistribution of CD20 to a low-density detergent-insoluble membrane compartment. *J Biol Chem* 1998;273:344–348.
- 51 Golay JT, Clark EA, Beverley PC: The CD20 (Bp35) antigen is involved in activation of B cells from the G0 to the G1 phase of the cell cycle. *J Immunol* 1985;135:3795–3801.
- 52 Cragg MS, Glennie MJ: Antibody specificity controls in vivo effector mechanisms of anti-CD20 reagents. *Blood* 2004;103:2738–2743.
- 53 Chan HT, Hughes D, French RR, Tutt AL, Walshe CA, Teeling JL, Glennie MJ, Cragg MS: CD20-induced lymphoma cell death is independent of both caspases and its redistribution into Triton X-100-insoluble membrane rafts. *Cancer Res* 2003;63:5480–5489.
- 54 Deans JP, Li H, Polyak MJ: CD20-mediated apoptosis: Signaling through lipid rafts. *Immunology* 2002;107:176–182.
- 55 Kanzaki M, Shibata H, Mogami H, Kojima I: Expression of calcium-permeable cation channel CD20 accelerates progression through the G1 phase in Balb/c 3T3 cells. *J Biol Chem* 1995;270:13099–13104.
- 56 Li H, Ayer LM, Lytton J, Deans JP: Store-operated cation entry mediated by CD20 in membrane rafts. *J Biol Chem* 2003;278:42427–42434.
- 57 Parekh AB: Store-operated Ca^{2+} entry: Dynamic interplay between endoplasmic reticulum, mitochondria and plasma membrane. *J Physiol* 2003;547:333–348.
- 58 Genot E, Valentine MA, Degos L, Sigaux F, Kolb JP: Hyperphosphorylation of CD20 in hairy cells. Alteration by low molecular weight B cell growth factor and IFN- α . *J Immunol* 1991;146:870–878.
- 59 Genot EM, Meier KE, Licciardi KA, Ahn NG, Uittenbogaart CH, Wietzerbin J, Clark EA, Valentine MA: Phosphorylation of CD20 in cells from a hairy cell leukemia cell line. Evidence for involvement of calcium/calmodulin-dependent protein kinase II. *J Immunol* 1993;151:71–82.
- 60 Valentine MA, Cotner T, Gaur L, Torres R, Clark EA: Expression of the human B-cell surface protein CD20: Alteration by phorbol 12-myristate 13-acetate. *Proc Natl Acad Sci USA* 1987;84:8085–8089.
- 61 Valentine MA, Meier KE, Rossie S, Clark EA: Phosphorylation of the CD20 phosphoprotein in resting B lymphocytes. Regulation by protein kinase C. *J Biol Chem* 1989;264:11282–11287.
- 62 Grafton G, Stokes L, Toellner KM, Gordon J: A non-voltage-gated calcium channel with L-type characteristics activated by B cell receptor ligation. *Biochem Pharmacol* 2003;66:2001–2009.
- 63 Mori Y, Wakamori M, Miyakawa T, Herinosura M, Hara Y, Nishida M, Hirose K, Mizushima A, Kurosaki M, Mori E, Gotoh K, Okada T, Fleig A, Penner R, Iino M, Kurosaki T: Transient receptor potential 1 regulates capacitative Ca^{2+} entry and Ca^{2+} release from endoplasmic reticulum in B lymphocytes. *J Exp Med* 2002;195:673–681.
- 64 Deans JP, Robbins SM, Polyak MJ, Savage JA: Rapid redistribution of CD20 to a low-density detergent-insoluble membrane compartment. *J Biol Chem* 1998;273:344–348.
- 65 Filatov AV, Shmigol IB, Kuzin II, Sharonov GV, Feofanov AV: Resistance of cellular membrane antigens to solubilization with Triton X-100 as a marker of their association with lipid rafts – Analysis by flow cytometry. *J Immunol Methods* 2003;278:211–219.
- 66 Polyak MJ, Ayer LM, Szczepek AJ, Deans JP: A cholesterol-dependent CD20 epitope detected by the FMC7 antibody. *Leukemia* 2003;17:1384–1389.
- 67 Sheets ED, Holowka D, Baird B: Critical role for cholesterol in Lyn-mediated tyrosine phosphorylation of Fc ϵ R1 and their association with detergent-resistant membranes. *J Cell Biol* 1999;145:877–887.
- 68 Awasthi-Kalia M, Schnetkamp PP, Deans JP: Differential effects of filipin and methyl- β -cyclodextrin on B cell receptor signaling. *Biochem Biophys Res Commun* 2001;287:77–82.
- 69 Semac I, Palomba C, Kulangara K, Klages N, van Echten-Deckert G, Borisch B, Hoessli DC: Anti-CD20 therapeutic antibody rituximab modifies the functional organization of rafts/microdomains of B lymphoma cells. *Cancer Res* 2003;63:534–540.
- 70 Morgan BP, van den Berg CW, Davies EV, Hallett MB, Horejsi V: Cross-linking of CD59 and of other glycosyl phosphatidylinositol-anchored molecules on neutrophils triggers cell activation via tyrosine kinase. *Eur J Immunol* 1993;23:2841–2850.
- 71 Munro S: Lipid rafts: Elusive or illusive? *Cell* 2003;115:377–388.

- 72 Nichols BJ: GM1-containing lipid rafts are depleted within clathrin-coated pits. *Curr Biol* 2003;13:686–690.
- 73 Glebov OO, Nichols BJ: Lipid raft proteins have a random distribution during localized activation of the T-cell receptor. *Nat Cell Biol* 2004;6:238–243.
- 74 Sharma P, Varma R, Sarasij RC, Ira, Gousset K, Krishnamoorthy G, Rao M, Mayor S: Nanoscale organization of multiple GPI-anchored proteins in living cell membranes. *Cell* 2004;116:577–589.
- 75 Press OW, Howell-Clark J, Anderson S, Bernstein I: Retention of B-cell-specific monoclonal antibodies by human lymphoma cells. *Blood* 1994;83:1390–1397.
- 76 Press OW, Farr AG, Borroz KI, Anderson SK, Martin PJ: Endocytosis and degradation of monoclonal antibodies targeting human B-cell malignancies. *Cancer Res* 1989;49:4906–4912.
- 77 Vervoorde donk SF, Merle PA, van Leeuwen EF, von dem Borne AE, Slaper-Cortenbach IC: Preclinical studies with radiolabeled monoclonal antibodies for treatment of patients with B-cell malignancies. *Cancer* 1994;73:1006–1011.
- 78 Press OW, Appelbaum F, Ledbetter JA, Martin PJ, Zarling J, Kidd P, Thomas ED: Monoclonal antibody 1F5 (anti-CD20) serotherapy of human B cell lymphomas. *Blood* 1987;69:584–591.
- 79 Jilani I, O'Brien S, Manshuri T, Thomas DA, Thomazy VA, Imam M, Naeem S, Verstovsek S, Kantarjian H, Giles F, Keating M, Albitar M: Transient down-modulation of CD20 by rituximab in patients with chronic lymphocytic leukemia. *Blood* 2003;102:3514–3520.
- 80 Kennedy AD, Beum PV, Solga MD, DiLillo DJ, Lindorfer MA, Hess CE, Densmore JJ, Williams ME, Taylor RP: Rituximab infusion promotes rapid complement depletion and acute CD20 loss in chronic lymphocytic leukemia. *J Immunol* 2004;172:3280–3288.
- 81 Cragg MS, Bayne MC, French R, Tutt A, Glennie MJ, Illidge TM: A new anti-idiotypic antibody capable of binding rituximab on the surface of lymphoma cells. *Blood* 2004, submitted.
- 82 Cragg MS, Bayne MC, Illidge TM, Valerius T, Johnson PW, Glennie MJ: Apparent modulation of CD20 by rituximab: An alternative explanation. *Blood* 2003;102:3514–3520.
- 83 Pickartz T, Ringel F, Wedde M, Renz H, Klein A, von Neuhoff N, Dreger P, Kreuzer KA, Schmidt CA, Srock S, Schoeler D, Schriever F: Selection of B-cell chronic lymphocytic leukemia cell variants by therapy with anti-CD20 monoclonal antibody rituximab. *Exp Hematol* 2001;29:1410–1416.
- 84 Grillo-Lopez AJ, Kunkel L: Correspondence re: Davis T, et al: Therapy of B-cell lymphoma with anti-CD20 antibodies can result in loss of CD20 antigen expression. *Clin Cancer Res* 1999;5: 611–615. *Clin Cancer Res* 2000;6:317–318.
- 85 Davis TA, Czervinski DK, Levy R: Therapy of B-cell lymphoma with anti-CD20 antibodies can result in the loss of CD20 antigen expression. *Clin Cancer Res* 1999;5:611–615.
- 86 Anolik J, Looney RJ, Bottaro A, Sanz J, Young F: Down-regulation of CD20 on B cells upon CD40 activation. *Eur J Immunol* 2003;33:2398–2409.
- 87 Dancescu M, Wu C, Rubio M, Delespesse G, Sarfati M: IL-4 induces conformational change of CD20 antigen via a protein kinase C-independent pathway. Antagonistic effect of anti-CD40 monoclonal antibody. *J Immunol* 1992;148:2411–2416.
- 88 Venugopal P, Sivaraman S, Huang XK, Nayini J, Gregory SA, Preisler HD: Effects of cytokines on CD20 antigen expression on tumor cells from patients with chronic lymphocytic leukemia. *Leuk Res* 2000;24:411–415.
- 89 Genot E, Wietzerbin J: Investigating hairy cell leukemia dysregulations. Looking for interferon α site of action in hairy cells. *Leuk Lymphoma* 1994;14(suppl 1):23–26.
- 90 Cragg MS, Glennie MJ: Complexity of the anti-tumor mechanisms of anti-CD20 antibodies. *Cancer Conference Highlights* 2004, in press.
- 91 Johnson P, Glennie MJ: The mechanisms of action of rituximab in the elimination of tumor cells. *Semin Oncol* 2003;30:3–8.
- 92 Anderson DR, Grillo-Lopez A, Varns C, Chambers KS, Hanna N: Targeted anti-cancer therapy using rituximab, a chimeric anti-CD20 antibody (IDEC-C2B8) in the treatment of non-Hodgkin's B-cell lymphoma. *Biochem Soc Trans* 1997;25:705–708.
- 93 Clynes RA, Towers TL, Presta LG, Ravetch JV: Inhibitory Fc receptors modulate in vivo cytotoxicity against tumor targets. *Nat Med* 2000;6:443–446.
- 94 Cartron G, Dacheux L, Salles G, Solal-Celigny P, Bardos P, Colombat P, Watier H: Therapeutic activity of humanized anti-CD20 monoclonal antibody and polymorphism in IgG Fc receptor Fc γ RIIIa gene. *Blood* 2002;99:754–758.

- 95 Anolik JH, Campbell D, Felgar RE, Young F, Sanz I, Rosenblatt J, Looney RJ: The relationship of Fc γ RIIIa genotype to degree of B cell depletion by rituximab in the treatment of systemic lupus erythematosus. *Arthritis Rheum* 2003;48:455–459.
- 96 Weng WK, Levy R: Two immunoglobulin G Fc receptor polymorphisms independently predict response to rituximab in patients with follicular lymphoma. *J Clin Oncol* 2003;21:3940–3947.
- 97 Parren PW, Warmerdam PA, Boeijs LC, Arts J, Westerdal NA, Vlug A, Capel PJ, Aarden LA, van de Winkel JG: On the interaction of IgG subclasses with the low affinity Fc γ RIIa (CD32) on human monocytes, neutrophils, and platelets. Analysis of a functional polymorphism to human IgG2. *J Clin Invest* 1992;90:1537–1546.
- 98 Van der Kolk LE, Grillo-Lopez AJ, Baars JW, Hack CE, van Oers MH: Complement activation plays a key role in the side-effects of rituximab treatment. *Br J Haematol* 2001;115:807–811.
- 99 Treon SP, Mitsiades C, Mitsiades N, Young G, Doss D, Schlossman R, Anderson KC: Tumor cell expression of CD59 is associated with resistance to CD20 serotherapy in patients with B-cell malignancies. *J Immunother* 2001;24:263–271.
- 100 Manches O, Lui G, Chaperot L, Gressin R, Molens JP, Jacob MC, Sotto JJ, Leroux D, Bensa JC, Plumas J: In vitro mechanisms of action of rituximab on primary non-Hodgkin lymphomas. *Blood* 2003;101:949–954.
- 101 Di Gaetano N, Cittera E, Nota R, Vecchi A, Grieco V, Scanziani E, Botto M, Introna M, Golay J: Complement activation determines the therapeutic activity of rituximab in vivo. *J Immunol* 2003;171:1581–1587.
- 102 Weng WK, Levy R: Expression of complement inhibitors CD46, CD55, and CD59 on tumor cells does not predict clinical outcome after rituximab treatment in follicular non-Hodgkin lymphoma. *Blood* 2001;98:1352–1357.
- 103 Xia MQ, Hale G, Waldmann H: Efficient complement-mediated lysis of cells containing the CAMPATH-1 (CDw52) antigen. *Mol Immunol* 1993;30:1089–1096.
- 104 Cohen AM, Shinitzky M: Modulation of complement lysis of human erythrocytes by the membrane lipid viscosity. *Vox Sang* 1982;43:23–27.
- 105 Cragg MS, French RR, Glennie MJ: Signaling antibodies in cancer therapy. *Curr Opin Immunol* 1999;11:541–547.
- 106 Byrd JC, Kitada S, Flinn IW, Aron JL, Pearson M, Lucas D, Reed JC: The mechanism of tumor cell clearance by rituximab in vivo in patients with B-cell chronic lymphocytic leukemia: Evidence of caspase activation and apoptosis induction. *Blood* 2002;99:1038–1043.
- 107 Sproul TW, Malapati S, Kim J, Pierce SK: Cutting edge: B cell antigen receptor signaling occurs outside lipid rafts in immature B cells. *J Immunol* 2000;165:6020–6023.
- 108 Nashar TO, Williams NA, Hirst TR, Nahar TO: Cross-linking of cell surface ganglioside GM1 induces the selective apoptosis of mature CD8+ T lymphocytes. *Int Immunol* 1996;8:731–736.
- 109 Rowan W, Tite J, Topley P, Brett SJ: Cross-linking of the CAMPATH-1 antigen (CD52) mediates growth inhibition in human B- and T-lymphoma cell lines, and subsequent emergence of CD52-deficient cells. *Immunology* 1998;95:427–436.
- 110 Shenoy-Scaria AM, Kwong J, Fujita T, Olszowy MW, Shaw AS, Lublin DM: Signal transduction through decay-accelerating factor: Interaction of glycosylphosphatidylinositol anchor and protein tyrosine kinases p56lck and p59fyn 1. *J Immunol* 1992;149:3535–3541.
- 111 Shan D, Ledbetter JA, Press OW: Apoptosis of malignant human B cells by ligation of CD20 with monoclonal antibodies. *Blood* 1998;91:1644–1652.
- 112 Clark EA, Shu GL, Luscher B, Draves KE, Banchemreau J, Ledbetter JA, Valentine MA: Activation of human B cells. Comparison of the signal transduced by IL-4 to four different competence signals. *J Immunol* 1989;143:3873–3880.
- 113 Mathas S, Rickers A, Bommert K, Dorken B, Mapara MY: Anti-CD20- and B-cell receptor-mediated apoptosis: Evidence for shared intracellular signaling pathways. *Cancer Res* 2000;60:7170–7176.
- 114 Ghetie MA, Bright H, Vitetta ES: Homodimers but not monomers of Rituxan (chimeric anti-CD20) induce apoptosis in human B-lymphoma cells and synergize with a chemotherapeutic agent and an immunotoxin. *Blood* 2001;97:1392–1398.
- 115 Besnault L, Schrantz N, Auffredou MT, Leca G, Bourgeade MF, Vazquez A: B cell receptor cross-linking triggers a caspase-8-dependent apoptotic pathway that is independent of the death effector domain of Fas-associated death domain protein. *J Immunol* 2001;167:733–740.

- 116 Rose AL, Smith BE, Maloney DG: Glucocorticoids and rituximab in vitro: Synergistic direct antiproliferative and apoptotic effects. *Blood* 2002;100:1765–1773.
- 117 Van der Kolk LE, Evers LM, Omene C, Lens SM, Lederman S, van Lier RA, van Oers MH, Eldering E: CD20-induced B cell death can bypass mitochondria and caspase activation. *Leukemia* 2002;16:1735–1744.
- 118 Weng WK, Levy R: Analysis of tumor-specific T cell immune response in follicular non-Hodgkin's lymphoma patients treated with Rituximab. *ASH* 2003.
- 119 Selenko N, Maidic O, Draxier S, Berer A, Jager U, Knapp W, Stockl J: CD20 antibody (C2B8)-induced apoptosis of lymphoma cells promotes phagocytosis by dendritic cells and cross-priming of CD8+ cytotoxic T cells. *Leukemia* 2001;15:1619–1626.
- 120 Selenko N, Majdic O, Jager U, Sillaber C, Stockl J, Knapp W: Crosspriming of cytotoxic T cells promoted by apoptosis-inducing tumor cell reactive antibodies? *J Clin Immunol* 2002;22:124–130.
- 121 Serafini M, Manganini M, Borleri G, Bonamino M, Imberti L, Biondi A, Golay J, Rambaldi A, Introna M: Characterization of CD20-transduced T lymphocytes as an alternative suicide gene therapy approach for the treatment of graft-versus-host disease. *Hum Gene Ther* 2004;15:63–76.
- 122 Serafini M, Bonamino M, Golay J, Introna M: Elongation factor 1 (EF1 α) promoter in a lentiviral backbone improves expression of the CD20 suicide gene in primary T lymphocytes allowing efficient rituximab-mediated lysis. *Haematologica* 2004;89:86–95.
- 123 Grube M, Rezvani K, Wiestner A, Fujiwara H, Sconocchia G, Melenhorst JJ, Hensel N, Marti GE, Kwak LW, Wilson W, Barrett JA: Autoreactive, cytotoxic T lymphocytes specific for peptides derived from normal B-cell differentiation antigens in healthy individuals and patients with B-cell malignancies. *Clin Cancer Res* 2004;10:1047–1056.
- 124 Roberts WK, Livingston PO, Agus DB, Pinilla-Ibarz J, Zelenetz A, Scheinberg DA: Vaccination with CD20 peptides induces a biologically active, specific immune response in mice. *Blood* 2002;99:3748–3755.
- 125 Huang J, Sheu JJ, Wu SC, Chang TW: Down-regulation of B cells by immunization with a fusion protein of a self CD20 peptide and a foreign IgG.Fc fragment. *Immunol Lett* 2002;81:49–58.
- 126 Giles FJ, Vose JM, Do KA, Johnson MM, Manshouri T, Bociek G, Bierman PJ, O'Brien SM, Keating MJ, Kantarjian HM, Armitage JO, Albitar M: Circulating CD20 and CD52 in patients with non-Hodgkin's lymphoma or Hodgkin's disease. *Br J Haematol* 2003;123:850–857.
- 127 Manshouri T, Do KA, Wang X, Giles FJ, O'Brien SM, Saffer H, Thomas D, Jilani I, Kantarjian HM, Keating MJ, Albitar M: Circulating CD20 is detectable in the plasma of patients with chronic lymphocytic leukemia and is of prognostic significance. *Blood* 2003;101:2507–2513.
- 128 Voso MT, Pantel G, Rutella S, Weis M, D'Alo F, Urbano R, Leone G, Haas R, Hohaus S: Rituximab reduces the number of peripheral blood B-cells in vitro mainly by effector cell-mediated mechanisms. *Haematologica* 2002;87:918–925.
- 129 Manches O, Lui G, Chaperot L, Gressin R, Molens JP, Jacob MC, Sotto JJ, Leroux D, Bensa JC, Plumas J: In vitro mechanisms of action of rituximab on primary non-Hodgkin lymphomas. *Blood* 2003;101:949–954.

Mark S. Cragg, BSc, PhD
 Tenovus Research Laboratory
 Cancer Sciences Division, Southampton University
 Southampton General Hospital, Southampton SO16 6YD (UK)
 Tel. +44 23 8079 6910, Fax +44 23 8070 4061, E-Mail mig@soton.ac.uk or msc@soton.ac.uk

Appendix 2

New insights into mechanisms of action of radioimmunotherapy.

Reprinted from: Ivanov A, Swann R, Illidge. J Pharm Pharmacol. In press. 2008

New insights into the mechanisms of action of radioimmunotherapy in lymphoma

Andrei Ivanov, Ruth Swann and Tim Illidge

Abstract

The exquisite sensitivity of haematological malignancies to targeted radiation alongside the impressive results achieved by the pioneers in this field suggests that radioimmunotherapy is likely to be a productive area for future clinical research. Recent experimental work has demonstrated that the combination of targeted radiation and antibody effector mechanisms are critical to long-term clearance of tumour. This review provides the background of clinical and biological insights into the mechanisms of action of radioimmunotherapy.

Introduction—The principles of radioimmunotherapy

The use of monoclonal antibodies (mAbs) in routine clinical practice is now well established and has led to impressive improvements in outcome for patients with a range of human cancers (Robak 2004; Adams & Weiner 2005). Although the single-agent activity of most mAbs has been modest, when used in combination with both chemotherapy and radiotherapy highly impressive increases in clinical responses and improvement in survival have been seen (Coiffier et al 2002, 2003; Robak 2004). Radioimmunotherapy (RIT) is, in contrast, the administration of mAb or mAb-derived constructs, which are chemically conjugated to therapeutic radioisotopes targeted to tumour. In this context, mAbs were initially regarded simply as direct carriers for the radioisotope, which deliver systemically targeted cytotoxic radiation to areas of disease, with relative sparing of normal tissue. It is, however, becoming clearer that the mAb effector mechanisms may also play an important additional role in killing lymphoma cells. The nature of RIT determines that its efficacy depends on a number of factors, including the properties of the targeted antigen (specificity, density, availability, shedding and heterogeneity of expression), the tumour (degree of vascularization, blood flow and permeability), the mAb (specificity, immunoreactivity, stability and affinity) and the properties of the chosen radioisotope (emission characteristics, half-life and bioavailability) (Knox & Meredith 2000).

A wide variety of different mAbs, delivery schedules, radioisotopes and doses of radioactivity have been used in RIT and have resulted in impressive durable partial and complete responses in the treatment of non-Hodgkin's lymphoma (NHL) (Park & Press 2007). In this review the principles of radioimmunotherapy will be discussed along with some recent data that provide new insights into the mechanism of action of RIT. Finally, the clinical data that led to the two radioimmunconjugates, ^{131}I -tositumomab and ^{90}Y -ibritumomab, being approved by the US FDA (US Food and Drug Administration) and ^{90}Y -ibritumomab tiuxetan within the EU, will be discussed.

Antigen targeting

The use of radiotherapy in the treatment of haematological malignancies is well established and for localized disease it is a highly effective treatment modality, given the exquisite sensitivity of lymphomas and leukaemias to radiation-induced cell death. The systemic nature of the majority of lymphomas and leukaemias, however, makes localized irradiation inappropriate for most patients. Therefore the systemic delivery of targeted radiation in the form of RIT is a logical strategy given for disseminated tumours, especially those known to be so radiosensitive. The effective delivery of RIT requires the selection of a suitable tumour antigen target.

School of Cancer and Imaging Sciences, Paterson Institute for Cancer Research, University of Manchester, Manchester, UK

Andrei Ivanov, Ruth Swann, Tim Illidge

Correspondence: T. Illidge, School of Cancer and Imaging Sciences, Paterson Institute for Cancer Research, University of Manchester, Manchester, UK. E-mail: tmi@manchester.ac.uk

Table 1 Summary of characteristics considered ideal in an antigen target for RIT

Tumour cell specific
Highly expressed on tumour cells
No tendency to mutation
Not secreted or shed
Not rapidly modulated on antibody binding
Critical for target cell survival
Not expressed on critical or non-renewable host cells

Tumour specific antigens would be the ideal targets for RIT, but such a degree of specificity is unusual. In practice tumour-associated antigens expressed abundantly on tumour cells as well as some normal tissues represent the majority of potential targets. As most NHLs are of B-cell origin the pan-B-cell antigens, such as human leukocyte antigen DR (HLA-DR), CD19, CD20, CD22, CD37, CD52 and MHC II have been extensively evaluated as targets for RIT (Press et al 1989; DeNardo et al 1998; Illidge et al 1999; Kaminski et al 2001; Robak 2004; Adams & Weiner 2005). Table 1 shows the antigen characteristics that are considered ideal for RIT.

From these initial investigations, the CD20 antigen emerged as having many of the characteristics thought to be important for a good tumour target. Targeting this antigen has thus dominated clinical RIT of lymphoma (Grossbard et al 1992). The CD20 antigen is a transmembrane phosphoprotein that is expressed on mature B cells and at a higher density on pre-B cells. The antigen is also expressed on greater than 90% of B-cell NHLs. The CD20 complex does not internalize or shed from the cell surface and initiates signal transduction that triggers cell death through a caspase-independent pathway (Chan et al 2003). CD20 is highly expressed on the majority of B-cell lymphomas but is not expressed on stem cells or plasma cells. Following radiolabelled anti-CD20 mAb RIT, the B-cell pool of both malignant and normal B cells is substantially depleted, with the normal B cells recovering within 6 months (Witzig et al 2002b). Other B-cell antigens that are currently being investigated include the CD22 antigen (Sharkey et al 1997).

Radioisotopes used in RIT

The physical characteristics considered important for a radioisotope in RIT include half-life, type of radioactive emissions (α -, β - or γ -) and ionization path length. Particle energy and mean path length in tissue are also important determinants of therapeutic efficacy. The emission profile of the radioisotope not only determines its suitability for therapy, but also the toxicological profile of the radiopharmaceutical.

The majority of clinical trials to date have used either iodine-131 or yttrium-90 because of their favourable emission characteristics, widespread availability and well-documented radiochemistry that permit reliable and stable attachment to mAbs. Iodine-131 has the advantage of a long history of successful use in the management of thyroid cancer and a well-documented safety profile. It is readily available,

inexpensive, easily conjugated and emits both β -particles with a path length of 0.8 mm and penetrating γ -emissions. The γ -photons enable uncomplicated imaging using a gamma camera for dosimetry purposes, but also result in a significant non-targeted normal tissue radiation dose, as well as radiation protection issues for visitors and medical/nursing staff.

Yttrium-90 offers a number of theoretical advantages over iodine-131, although the radioisotopes have not been directly compared by labelling the same mAb and performing a comparative study. Yttrium-90 is a pure β -emitter that produces higher energy radiation (2.3 MeV vs 0.6 MeV) at a longer path length than iodine-131 (5.3 mm vs 0.8 mm). Radiolysis induces cellular damage in both the targeted lymphoma cells and neighbouring cells. The increased path length would be expected to enhance the 'cross fire' effect and could therefore be potentially advantageous in treating bulky, poorly vascularized tumours with heterogeneous antigen expression (Knox & Meredith 2000). This longer path length is likely, however, to increase the normal tissue dose when targeting microscopic disease for which the shorter β -particle path length of iodine-131 may be preferable. The physical half-life of yttrium-90 is 64 h and it decays to a stable (non-radioactive) form of zirconium (^{90}Zr). The physical half-life of 64 h approximates to the biological half-life of murine mAbs and the absence of penetrating γ -emissions enables delivery as an outpatient (Press & Rasey 2000). Additionally, if a cell internalizes yttrium-90, it is likely to be retained within the cell (Sharkey et al 1997). In contrast, once iodine-131 conjugates are internalized by a cell there is rapid dehalogenation of the free iodide and subsequent excretion of the iodinated products out of the cell, reducing the desired tumour absorbed radiation dose as well as increasing normal tissue radiation exposure (Press et al 1996). The major disadvantages of yttrium-90 relate to its greater expense, relatively limited availability and requirement for chelation radiochemistry making radiolabelling a more complex procedure. Yttrium-90 does not emit γ -photons and therefore indium-111 is used as a surrogate to obtain images for biodistribution studies. Rhenium-186 and copper-67 are both β -emitters and have physical and chemical properties that make them attractive alternatives to either iodine-131 or yttrium-90. Nevertheless, their current limited availability has meant that these radioisotopes have received limited clinical use (DeNardo et al 1999).

α -Emitters produce a helium nucleus particle of very high energy but with a very short path length. The high Linear Energy Transfer (LET) radiation of α -emitters may be lethal to cells with a single collision, although the very short path length means that the isotope must be adjacent to, or internalized by, the cell to be effective and is likely to have little or no 'cross fire' effect. The suitability of α -emitters therefore appears limited to readily accessible tumours such as leukaemia cells confined to the blood or bone marrow. The short half-life of α -emitters (e.g. ^{211}At 7 h or ^{213}Bi 45 min) complicates the radiopharmaceutical preparation, meaning that such radioisotopes are likely to require generation on the same site as delivery in the clinic. Despite this logistical hurdle, early clinical data in the treatment of leukaemia appear extremely promising (McDevitt et al 1998; Jurcic et al 2002).

In practice, the choice of the optimal radioisotope for RIT remains controversial, with proponents advocating the relative merits of iodine-131, yttrium-90, rhenium-186, copper-67, and α -emitters such as astatine-211 (Press & Rasey 2000). Comparative studies are difficult to conduct and scientifically robust randomized human trials have not been performed. The ideal properties of a radioisotope for RIT remain unclear and it is likely that the optimal radioisotope for a particular situation will depend upon the bulk and type of tumour being targeted. An important area of potential future research will be to define the optimal radioisotope, or potentially a cocktail of different radioisotopes used in combination that may have separate benefits for tumour of varying sizes.

Factors affecting the therapeutic efficacy of radioimmunotherapy in lymphomas

Although RIT has emerged as a highly effective treatment for NHL, the mechanisms underlying the high response rates and in particular the interaction of tumour irradiation and mAb signalling in RIT are still poorly understood (Illidge & Johnson 2000; Press & Rasey 2000). A number of important translation research questions remain to be answered and to optimize RIT delivery, including: the optimal pre-dose of cold mAb; the relative contribution of targeted radiation and mAb effector mechanisms to the high response rates and the mechanisms involved in the durable responses seen in some patients; defining whether a tumour radiation dose-response exists in RIT for lymphomas and leukaemias.

Pre-dosing of mAb in radioimmunotherapy

There are several factors that may theoretically limit lymphoma targeting of radiolabelled pan-B-cell mAbs in RIT. These include the complex formation of administered mAb with free circulating target antigen, the cross-reactivity with antigen-positive circulating lymphoma cells, normal B-cells in the blood or spleen or non-lymphoid tissues and finally the non-antigenic binding of mAb, via the Fc region of a mAb. Poor tumour targeting of a radioimmunoconjugate leads to lower tumour-to-normal-tissue radiation dose ratios resulting in potentially reduced therapeutic efficacy.

To improve the biodistribution of radiolabelled mAb in RIT, it has become the established practice to give a pre-dose of 'cold' or unlabelled anti-CD20 mAb before the therapeutic dose of the anti-CD20 radioimmunoconjugate (Wahl 2003). The pre-dose is considered to prolong the circulating half-life of the radiolabelled mAb, block 'non-specific' binding sites (e.g. circulating and splenic B cells) and result in increased tumour retention of the labelled mAb. Buchsbaum et al (1992) investigated whether a pre-dose of anti-B1 improved the delivery of a subsequent radiolabelled mAb to tumour using in-vivo pre-clinical human xenograft models. The anti-B1 (anti-CD20) pan-B-cell mAb, reactive with human B-cell lymphomas but not with host mouse B cells, was used. A pre-dose of unlabelled anti-B1 was found to significantly increase the tumour uptake of the subsequent radiolabelled anti-B1 by blocking the B1-specific Fc receptor sites, although this improvement

in tumour targeting appeared to plateau at the highest pre-doses of unlabelled anti-B1.

Relative contribution of antibody effector mechanisms and targeted radiation to therapy

Although RIT has emerged as an effective treatment for lymphoma, the relative contributions of antibody effector mechanisms and targeted radiation to tumour cell death remain poorly understood. By using different syngeneic murine B-cell lymphoma models the relative contributions of mAb and targeted radiation to the clearance of tumour in-vivo have been investigated (Du et al 2004). There is now substantial evidence that mAbs can form an active component of RIT and that mAb effector mechanisms may be important in the clearance of tumour in-vivo.

With regard to mAb-induced tumour cell killing, four potential mechanisms are thought to play a role: complement-dependent cytotoxicity (CDC); antibody-dependent cellular cytotoxicity (ADCC) via the recruitment of immune effector cells; direct induction of growth inhibition or cell death; and stimulation of host-adaptive immunity (Cragg et al 2005). Large amounts of experimental data support the first three of the aforementioned mechanisms in anti-CD20 mAb immunotherapy, although robust evidence for the fourth is currently lacking. In particular, several lines of evidence indicate that rituximab operates through conventional effector mechanisms involving complement and immune effector cells (Johnson & Glennie 2003). The most conclusive initial evidence for the role of immune effector cell recruitment by antibody Fc receptors comes from primate experiments where an IgG4 variant of rituximab was shown to be unable to deplete normal B cells (Anderson et al 1997). More recently, data has emerged demonstrating that type I anti-CD20 mAbs, such as rituximab and IF5, require the presence of their Fc domains for optimal therapeutic activity in human lymphoma xenograft models (Cragg & Glennie 2004).

Despite impressive clinical effectiveness, however, the biological function of CD20 has remained obscure. This is at least in part due to the lack, until recently, of murine anti-CD20 mAb (Uchida et al 2004) to probe in-vivo the mechanisms of anti-CD20 mAb. Furthermore the enigma of the precise role of CD20 was compounded by the discovery that the CD20 knockout mouse surprisingly had a normal phenotype (O'Keefe et al 1998). Therefore, much of our understanding has been based upon experiments using mAb to ligate CD20 on human B cells and B-cell lymphoma cell lines. Engagement of CD20 with mAbs results in several measurable biologic events, such as enhanced survival (Holder et al 1995), activation and proliferation (Clark & Shu 1987; Smeland et al 1987) and adhesion (Kansas & Tedder 1991; Leveille et al 1999) as well as growth inhibition (Tedder et al 1986) and death (Shan et al 1998; Hofmeiseter et al 2000; Chan et al 2003). The exact in-vivo mechanisms of tumour killing by anti-CD20 mAb remain incompletely understood. Pre-clinical data have suggested that the action of rituximab may include mAb-dependent cellular cytotoxicity (ADCC), complement-dependent cytotoxicity (CDC) and the direct induction of caspase-independent cell death through cell-surface-mediated downstream signal transduction (Cragg et al 2005). Cragg et al (2005) have previously shown that

anti-CD20 mAbs may be sub-divided as either rituximab-like (type I) or B1-like (type II) according to their linked activity in a number of in-vitro assays. For example, rituximab and other type I mAbs redistribute CD20 into Triton X-100 insoluble membrane rafts, correlating with their ability to engage complement effectively and cause target cell lysis (Cragg et al 2005). In contrast type II mAbs such as B1 do not redistribute CD20 membrane rafts, but are generally potent at inducing cell death in target cells (Chan et al 2003). Importantly, these differences appear to translate to the in-vivo mechanisms employed by these mAbs, at least in xenograft tumour models (Cragg & Glennie 2004).

Binding of anti-CD20 mAb to lymphoma cells in-vitro has been shown to induce modest levels of cell death presumably via signalling through the CD20 molecule (Shan et al 1998). A range of signalling events may be induced following ligation of CD20 (reviewed by Cragg et al 2005), including activation of the mitogen-activated protein kinase (MAPK) cascade (Mathas et al 2000). The Ras-Raf-MEK-ERK1/2 pathway is an evolutionarily conserved pathway that is involved in the control of many fundamental cellular processes that include cell proliferation, survival, differentiation, cell death, motility and metabolism (reviewed by Kolch et al 2005). Although commonly thought of as a component of proliferation and survival pathways, ERK1/2 signalling has been associated with apoptotic signalling in immature B-cell lymphoma (Lee & Koretzky 1998) and diffuse large B-cell lymphoma cells (Hollmann et al 2006). Similarly, it has been suggested that the overall balance of MAPK activity may determine B-cell fate depending on the kinetics of activation and maturation state of the cell (Sutherland et al 1996; Gauld et al 2002).

Intriguingly, the MAPK cascade is also triggered by radiation and other DNA-damaging agents (Hagan et al 2000; Lyng et al 2006) where it may be necessary for DNA double-strand break repair by homologous recombination (Golding et al 2007). Given the observation that both anti-CD20 mAb and radiation can trigger MAPK activation and that MAPK activation can result in diverse biological outcomes, we have therefore investigated the impact of combining radiation and anti-CD20 mAb on this signalling pathway in an attempt to further elucidate the potential underlying mechanisms of cell death seen when anti-CD20 mAbs are combined with radiation in RIT. Specifically, we have attempted to investigate the two RIT modalities currently approved by the US FDA, ^{90}Y -ibritumomab tiuxetan (Zevalin) and ^{131}I -tositumomab (Bexxar) by combining rituximab (derived from ibritumomab) and tositumomab with irradiation (IRR).

We have specifically investigated the mechanisms underlying cell death in B-cell lymphoma cells treated with irradiation (IRR) and either type I (rituximab) or type II (B1/tositumomab) anti-CD20 mAb. Increased cell death was observed with B1 mAb combined with IRR but not with rituximab. This additive cell death was found to be MAPK/ERK kinase signalling dependent and could be reversed with pharmacological MEK inhibitors as well as siRNA targeting MEK1/2. Furthermore we found that this increased death was associated with ERK1/2 nuclear accumulation following B1 mAb treatment, which was greatly enhanced in combination

with IRR (Figure 1). Importantly, although Bcl-2 overexpression resulted in resistance to IRR-induced apoptosis, it had no impact on the cell death induced by B1 plus IRR, suggesting a non-apoptotic cytoplasmic form of cell death that was confirmed by ultrastructural and TUNEL analysis. Taken together our data provide new clinically relevant insights into how radioimmunotherapy with B1 mAb causes additive cell death that can overcome apoptosis resistance (Ivanov et al 2008).

The relative importance of mAb effector mechanisms and targeted radiation is difficult to quantify and it is not possible to dissect the action of the two components, using in-vitro assays, as an intact host immune system to augment the antibody effector functions. It is also challenging to answer this type of question in the clinic. We have therefore turned to pre-clinical studies using well-defined syngeneic animal models to further clarify the relative contributions of mAb effector mechanisms and targeted radiation. Du et al (2004) investigated the relative contributions of antibody and targeted radiation to the clearance of tumour in-vivo using two different syngeneic murine B-cell lymphoma models. We used the highly expressed non-modulating major histocompatibility complex class II (MHCII) as a target antigen. This target was initially pioneered in the clinic by DeNardo et al (1998), see

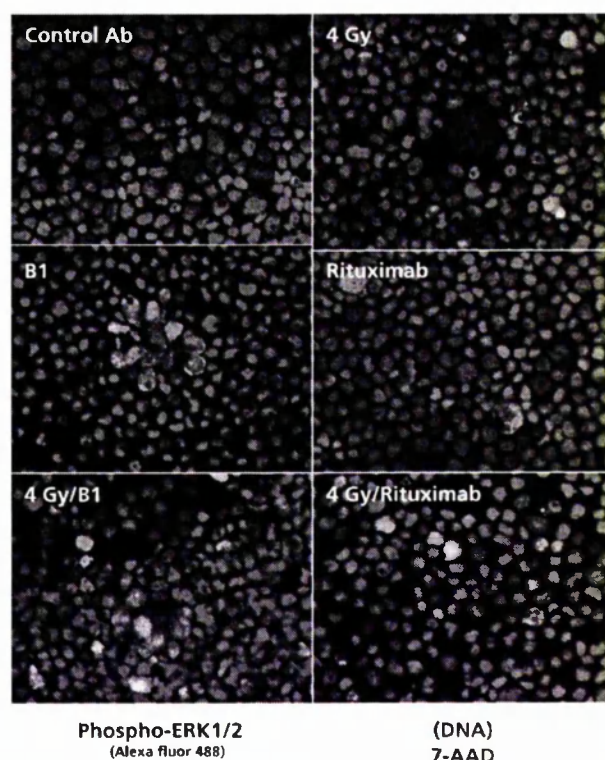


Figure 1 ERK1/2 activation following treatment with anti-CD20 antibodies and radiation. The effect of different anti-CD20 antibodies on the intracellular localization of activated ERK1/2 at the 24-h time point. SU-DHL4 cells were treated with anti-CD20 mAb ($5 \mu\text{g mL}^{-1}$) in the presence or absence of IRR (4 Gy). Cells were then harvested 24 h after treatment, carefully sedimented onto PLL-coated microscope slides and stained for phosphorylated ERK (green) and DNA (7-AAD, red).

below. We had previously shown that this target was the best of a number of different antigen targets in delivering the highest dose of radiation to the tumour (Illidge et al 1999). Although RIT with ^{131}I -anti-MHCII was effective in targeting radiation to tumour, no improvement in survival was seen by escalating the radiation dose alone and there were no long-term survivors (Du et al 2004). In contrast, using the combination of ^{131}I -anti-MHCII in the presence of unlabelled anti-idiotypic (Id) 100% prolonged disease free survival was seen in both B-cell lymphoma models at the higher radiation dose. Using in-vivo tracking we showed that treatment with radiation plus anti-Id mAb results in a substantially greater reduction of splenic tumour cells than with either treatment alone. Prolonged survival could also be achieved using ^{131}I -anti-MHCII plus the signalling anti-CD19 mAb. Furthermore, the ability of some anti-B-cell mAbs to improve survival with targeted radiotherapy appeared to correlate with their ability to initiate intracellular signal transduction. Together these data illustrate that using one mAb to target radiation to tumour and a second to induce cell signalling may be an effective new treatment strategy in RIT.

We next went on to investigate how the microdistribution of the targeted radiation component of this combination impacts on the long-term clearance of lymphoma. ^{131}I -labelled mAbs targeting CD45 and MHCII antigens were found to deliver similar doses of radiation to tumour-bearing organ using conventional dosimetry (approximately 1.0 Gy per MBq when ^{131}I was labelled to 500 μg mAb and given intravenously per mouse), but when used as radiation vectors in combination therapy only ^{131}I -anti-MHCII plus anti-Id produced long-term survival. The profound differences in therapy did not appear to be dependent on levels of ^{131}I -mAb tumour binding or antibody-dependent cytotoxicity. Instead the microscopic intratumoural dosimetry appeared to be critical with the ^{131}I -anti-MHCII delivering more concentrated and therefore substantially higher radiation dose to tumour cells. When the administered activity of ^{131}I -anti-CD45 was increased, a radiation dose response was demonstrated in the presence of anti-Id and long-term survival seen. We believe that these new insights should influence the selection of new antigen targets and the design of dosimetric methods in RIT of lymphoma.

Defining whether a tumour radiation dose response exists in radioimmunotherapy

There is currently little preclinical data that demonstrates whether a radiation dose response exists. Du et al (2004) have demonstrated that there does appear to be a radiation dose response in syngeneic B-cell murine lymphoma models and that this radiation dose response becomes more significant in the presence of an additional 'cold' antibody that provides cell death signalling (Du et al 2004).

To date, despite the high response rates seen in lymphoma RIT, clinical dosimetry studies have thus far failed to show a consistent dose-response relationship (Knox & Meredith 2000). More recently, the Michigan group has concluded that there could be a radiation dose response at least for ^{131}I -tositumomab (Koral et al 2003a,b; Wahl 2003), although their conclusions differ to others (Postema 2004; Goldenberg & Sharkey 2005). Postema (2004) argues that none of the RIT

dosing methods use tumour dosimetry to determine the dose administered to patients because the myelotoxicity of radiolabelled mAb will limit the increments of radioactivity dose, but not the tumour-absorbed dose. More recently, Goldenberg and colleagues commented that because RIT has two potentially therapeutic arms, namely radiation and mAb mechanisms, poor radiation targeting does not exclude a good therapeutic response from the mAb (Goldenberg & Sharkey 2005).

Clinical non-myeloablative radioimmunotherapy in lymphomas

Clinical RIT trials in NHL differ in terms of eligibility criteria, mAb and radioisotope used, dose, number of treatments, dose of unlabelled mAb pre-infused or co-infused and the biodistribution or dosimetry estimation required for administration of a therapeutic dose of radiolabelled mAb. Nevertheless, virtually all clinical studies performed to date have shown high response rates for RIT in NHL and have been well reviewed (Wilder et al 1996; Knox & Meredith 2000; Davis et al 2004; Kaminski et al 2005; Sharkey & Goldenberg 2005; Park & Press 2007).

DeNardo et al (1998) initially pioneered RIT for NHL with ^{131}I -anti-HLA-DR mAb (Lym-1). The efficacy of escalating fractionated doses of ^{131}I -Lym-1 in the range 1480–3700 MBq m^{-2} (40–100 mCi m^{-2}) resulted in an overall response rate of 52% in 21 treatment courses administered to 20 patients, with seven patients (33%) achieving complete response and four patients (19%) achieving partial response (DeNardo et al 1998). Goldenberg et al (1991) used an ^{131}I -LL2 (anti-CD22) mAb to treat a variety of B-cell lymphomas. In one of their trials, 4 out of 17 patients achieved objective remission, including one complete response. In another trial, ^{90}Y -LL2 was administered to seven patients with B-cell lymphomas, two of whom achieved partial response (Goldenberg et al 1991). Table 2 summarizes the results of randomized controlled trial of Zevalin versus rituximab in refractory low-grade, or transformed follicular B-cell lymphoma.

Impressive responses have been observed in all of the clinical trials using ^{90}Y -ibritumomab tiuxetan and ^{131}I -tositumomab in relapsed B-cell lymphomas. Although both ^{131}I -tositumomab and ^{90}Y -ibritumomab tiuxetan bind to the same CD20 antigen, tositumomab binds to a unique epitope of CD20 (Tedder & Engel 1994). The radioisotopes also have important differences in their emission characteristics. Table 3 compares the main characteristics of ^{131}I -tositumomab and ^{90}Y -ibritumomab tiuxetan.

^{90}Y -ibritumomab tiuxetan consists of a monoclonal IgG1 kappa light chain anti-CD20 mAb, the murine parent immunoglobulin of rituximab, covalently attached to a metal chelator molecule (tiuxetan; an isothiocyanatobenzyl derivative of the polyaminocarboxylic acid DTPA), which stabilizes the mAb-isotope complex for delivery to the lymphoma site (Grillo-Lopez 2002). The biological elimination half-life of ^{90}Y -ibritumomab tiuxetan is 30 h. More than 90% of the β -radiation is absorbed within a 5-mm proximity (corresponding to a diameter of 100–200 cells) of the radiation source. This facilitates highly targeted delivery of radiation without the need for patient isolation or shielding (Press & Rasey 2000).

Table 2 Updated duration of response data in two phase II and the single phase III 'pivotal' trials of ^{90}Y -ibritumomab tiuxetan versus rituximab in relapsed or refractory low-grade or transformed follicular B-cell NHL

	Phase I/II (n=51) (Gordon et al 2004)	Phase II (n=30) (Witzig et al 2002a)	Phase III (n=73) (Witzig et al 2002b)
Overall response (%)	73	83	80
Median DR (months)	11.7	11.5	13.9
CR, CRu (%)	29*	47	34
Median DR (months)	28*	23	23
Ongoing CR, CRu (%)	19	14	32
Median DR (months)	62.1	41.2	42.2
Range	60+ to 66+	40+ to 42+	33+ to 48+

DR, duration of response; CR, complete response; CRu, unconfirmed complete response.

*Patients with CR only.

Table 3 Characteristics of ^{131}I -tositumomab (Bexxar) and ^{90}Y -ibritumomab tiuxetan (Zevalin)

	^{131}I -tositumomab	^{90}Y -ibritumomab tiuxetan
US Trade name	Bexxar	Zevalin
Monoclonal antibody	Tositumomab (anti-B1)-murine	Ibritumomab (2B8)-murine
Chelation	Simple	More complex
Isotope	^{131}I	^{90}Y
Isotope emissions	γ and β	β only
β -energy	0.606 MeV	2.293 MeV
β -particle path length	0.8 mm	5.3 mm
Isotope half-life	8 days	2.6 days
γ -energy	0.364 MeV	None
Radiation protection measures	4–6 day inpatient stay in shielded room. Outpatient in USA	Outpatient
Isotope excretion	Renal (variable)	Limited
Normal tissue uptake	Bone marrow. Thyroid (pre-blocked with KI)	Bone
Pre-dose (unlabelled mAb)	Tositumomab (450 mg/patient)	Rituximab (250 mg m^{-2}) \times 2
Dose	75 cGy whole body dose Dosimetric dose obligatory Dose reduction for thrombocytopenia	14.8 MBq kg^{-1} (0.4 mCi kg^{-1}) Dosimetric dose not required Dose reduction for thrombocytopenia

The tiuxetan chelator molecule provides a stable link between the mAb and the radioisotope, and therefore free isotope clearance rates are minimal and predictable with $7.3 \pm 3.2\%$ of the radiolabelled activity being excreted in the urine over 7 days (Witzig et al 1999). Consequently ^{90}Y -ibritumomab tiuxetan may be administered on an outpatient basis. Figure 2 outlines the ^{90}Y -ibritumomab tiuxetan therapeutic regimen.

Four clinical trials, including three phase I/II and one randomized study, formed the basis of the FDA submission for ^{90}Y -ibritumomab tiuxetan. The initial phase I/II study demonstrated that the dose-limiting factor was myelotoxicity (Witzig et al 1999). The maximum tolerated dose was identified as 14.8 MBq kg^{-1} (0.4 mCi kg^{-1}) to a maximum of 1184 MBq (32 mCi) for patients with a baseline platelet count of $\geq 150 \times 10^9 \text{ L}^{-1}$ and 11.1 MBq kg^{-1} (0.3 mCi kg^{-1}) for patients with baseline platelet counts of $< 150 \times 10^9 \text{ L}^{-1}$ but $\geq 100 \times 10^9 \text{ L}^{-1}$. In this study a high overall response rate for the intent-to-treat population (n=51) was seen at 67% (26% complete response; 41% partial response); for low-grade disease (n=34), 82% (26% complete response; 56% partial response); for intermediate-grade disease (n=14), 43%.

A phase II study of patients with mild thrombocytopenia (baseline platelet count of $100 \times 10^9 \text{ L}^{-1}$ to $150 \times 10^9 \text{ L}^{-1}$) was conducted using the reduced dose of 11.1 MBq kg^{-1} (0.3 mCi kg^{-1}). The overall response rate was 83% (37% complete response, 6.7% complete response unconfirmed, and 40% partial response). Kaplan–Meier estimated median time to progression (TTP) was 9.4 months (range, 1.7–24.6). In responders, Kaplan–Meier estimated median TTP was 12.6 months (range, 4.9–24.6). Toxicity was primarily haematological, transient and reversible. The incidence of grade 4 neutropenia, thrombocytopenia and anaemia was 33%, 13% and 3%, respectively. The conclusion from this study was that reduced-dose ibritumomab tiuxetan is safe and well tolerated and has significant clinical activity in this patient population (Wiseman et al 2002).

A further single-arm phase II study of ^{90}Y -ibritumomab tiuxetan was undertaken to examine the efficacy of ^{90}Y -ibritumomab tiuxetan in a group with rituximab-refractory disease (Witzig et al 2002a). Fifty-four heavily pre-treated patients with follicular lymphoma were recruited who were refractory to, or progressed after, rituximab. The trial showed an overall response rate of 74% and a complete response rate

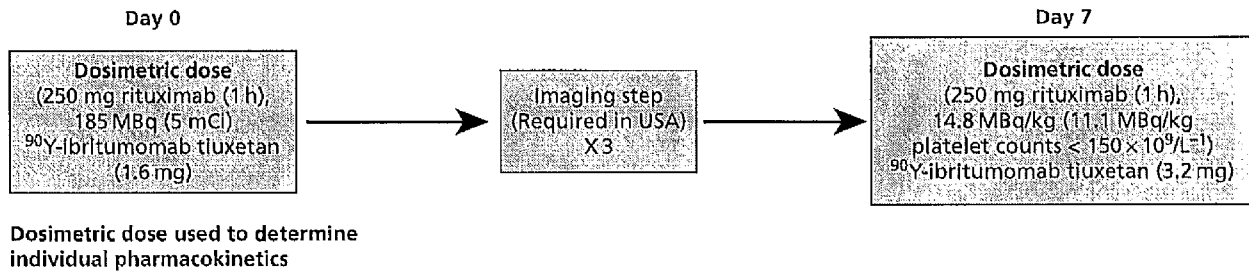


Figure 2 Treatment regimen for ⁹⁰Y-ibritumomab tiuxetan.

of 15%, despite a median of 4 previous therapies and 73% of patients having bulky disease (≥ 5 cm diameter). Kaplan–Meier-estimated duration of response was 6.4 months, with a time to progression of 6.8 months in all patients and 8.7 months in responders. The randomized controlled trial has been described earlier and compared ⁹⁰Y-ibritumomab tiuxetan with rituximab in relapsed or refractory low-grade B-cell NHL. This confirmed that ⁹⁰Y-ibritumomab tiuxetan results in superior overall and complete response rates to those seen with the ‘naked’ mAb, rituximab.

A randomized phase III trial including 143 patients with relapsed or refractory low-grade, follicular or transformed NHL compared the efficacy of a single dose of 14.8 MBq kg⁻¹ (0.4 mCi kg⁻¹) ⁹⁰Y-ibritumomab tiuxetan with rituximab (375 mg m⁻² once weekly for 4 weeks) (Witzig et al 2002b). Response rates were significantly higher in the ⁹⁰Y-ibritumomab tiuxetan arm with an overall response rate of 80% vs 56% ($P=0.002$) and a complete response rate of 30% vs 16% ($P=0.004$). Subgroup analysis revealed a superior benefit for patients with follicular histology with an overall response rate of 86% vs 55% ($P<0.001$) and a significantly increased ($P<0.04$) time to treatment progression for this subgroup. The overall time to progression was, however, no different between both treatment groups, but patients treated with ⁹⁰Y-ibritumomab tiuxetan showed a trend towards longer median duration of response (14.2 months vs 12.1 months) and more often achieved responses lasting longer than 6 months (64% vs 47%).

A recent retrospective analysis suggests that treatment with ⁹⁰Y-ibritumomab tiuxetan is associated with higher response rates and longer duration of response when used earlier in the therapy schedule (Gordon et al 2004). An integrated analysis of 211 patients treated in clinical trials compared efficacy and safety of ⁹⁰Y-ibritumomab tiuxetan in patients who had received one previous therapy ($n=63$) with patients who received two or more previous therapies ($n=148$). Patients receiving ⁹⁰Y-ibritumomab tiuxetan as second-line therapy had a greater overall response rate (86% vs 72%; $P=0.051$) and confirmed or unconfirmed complete response rate (CR/CRu; 49% vs 28%; $P=0.004$) and a significantly longer median time to disease progression (TTP) (12.6 months vs 7.9 months; $P=0.038$). In CR/CRu patients, the median TTP (23.9 months vs 15.6 months; $P=0.0442$) and median duration of response (22.8 months vs 14.6 months; $P=0.0429$) were both significantly increased in patients with only one previous therapy ($n=53$).

The results from a large phase III randomized European and Canadian intergroup study ($n=414$) in previously untreated follicular NHL were presented at the American Society of Hematology (ASH) in 2007 (Hagenbeek et al 2007). This study included patients with follicular (grade 1 or 2) lymphoma, advanced stage (III or IV) at time of diagnosis. The initial chemotherapy used was left to the discretion of the individual clinician between single-agent oral chlorambucil and anthracycline-based combination chemotherapy. For patients who responded to first-line chemotherapy (i.e. partial response or CR/CRu), ⁹⁰Y-ibritumomab tiuxetan (Zevalin) was administered 6–12 weeks after the last doses of chemotherapy. For all patients the complete response rate in the control group was 53.3% compared with 87.4% in those that received ⁹⁰Y-ibritumomab tiuxetan (Zevalin). This high complete response rate was almost identical in all subgroups of pre-treatment chemotherapy despite the difference in complete response rate between the initial regimens, such as single-agent chlorambucil (complete response rate 31%) and CHOP (complete response rate 56%). In summary it appears that ⁹⁰Y-ibritumomab tiuxetan (Zevalin) was the ‘equaliser’ for less active chemotherapy and as a consolidation therapy improved the response quality in 77% from partial response to CR/CRu in all patients, regardless of the type of initial chemotherapy given. ⁹⁰Y-ibritumomab tiuxetan (Zevalin) consolidation significantly ($P<0.0001$) prolonged the median progression-free survival by 2 years compared with no further treatment in patients responsive to first-line induction treatment. For the patients receiving Zevalin the median progression-free survival was 37 months compared with 13.5 months in the control group (Hagenbeek et al 2007).

Interestingly a 2-year improvement in progression-free survival was seen in patients with CR/CRu after first-line treatment, which suggests that ⁹⁰Y-ibritumomab tiuxetan benefits those with minimal residual disease and the median progression-free survival was increased to 54.6 months compared with 29.9 months for the control patients ($P=0.01$). For patients who only achieved a partial response after initial induction chemotherapy, ⁹⁰Y-ibritumomab tiuxetan improved the progression-free survival from 6.3 months (control) to 29.7 months ($P<0.0001$). The improvement in response quality with conversion from partial response to CR/CRu in 77% of patients after ⁹⁰Y-ibritumomab tiuxetan (Zevalin) is impressive, and ⁹⁰Y-ibritumomab tiuxetan consolidation was well tolerated with no unexpected toxicity and a low incidence of infectious events despite a high proportion of patients with grade 3/4 neutropenia (66%).

In summary, there is now good evidence to demonstrate that RIT is extremely effective at improving the quality of the response, from partial to complete in follicular lymphoma after primary chemotherapy, and an overall complete response rate of over 87% makes this a highly active approach that leads to a large improvement in progression-free survival. Using RIT in patients that fail to achieve a complete response after initial induction therapy may therefore be a useful strategy. A definitive role for RIT in the rituximab-chemotherapy (R-Chemo) era has not, however, been conclusively demonstrated and this question forms the basis of a European inter-group study whereby patients receive R-Chemo induction regimens and are then randomized to receive ^{90}Y -ibritumomab plus maintenance rituximab or maintenance rituximab alone.

Clinical responses have also been observed for transformed follicular and relapsed diffuse large B-cell lymphoma (DLBCL) when treated with ^{90}Y -ibritumomab tiuxetan. An initial phase I/II study reported a response rate of 58% with a 33% complete response rate in a group of just 12 patients that had relapsed following 2 previous chemotherapy regimens that included CHOP (Witzig et al 2002b). A prospective, single-arm, open-label, non-randomized, multi-centre phase II trial was therefore undertaken to evaluate the efficacy and safety of ^{90}Y -ibritumomab tiuxetan in patients over 60 years of age with relapsed or primary refractory DLBCL not suitable for autologous stem cell transplantation (ASCT). Patients were divided into two groups—those previously treated with chemotherapy alone (Group A, $n=76$) and those previously treated with chemotherapy and rituximab but who had a short duration of response (Group B, $n=28$) (Morschhauser et al 2007). All patients received a single dose of 14.8 MBq kg^{-1} (0.4 mCi kg^{-1}) of ^{90}Y -ibritumomab tiuxetan up to a maximum dose of 1184 MBq kg^{-1} (32 mCi). In total, 103 patients were able to be evaluated for treatment efficacy, and 104 for safety. An overall response rate of 44% was observed in the entire study population. In Group A, the overall response rate was >50%. In Group B, where 37% of patients were refractory to rituximab-CHOP, the overall response rate was 19%. Adverse events, with the exception of haematological side-effects, were generally mild (grade 1/2) and the incidence of severe infection was low, with only 7% of patients hospitalized for infection during the study. The results of this study

were encouraging and clinical trials are now underway in the US, or at an advanced stage of development in the EU, to integrate ^{90}Y -ibritumomab tiuxetan into a front-line treatment for DLBCL alongside R-chemo schedules.

Tositumomab was the first mAb to be produced against a B-cell antigen (Nadler et al 1981). The ^{131}I -tositumomab regimen is completed within 1–2 weeks and consists of a tracer dose of the radioimmunoconjugate followed by the therapeutic dose 7–14 days later. Each infusion of ^{131}I -tositumomab is preceded by an infusion of a pre-dose of 450 mg 'cold' or unlabelled tositumomab and the therapeutic regimen is outlined in Figure 3. Whole-body gamma camera imaging is performed three times over the week following the trace-labelled infusion to calculate the whole-body half-time and the dose required for the therapeutic infusion to deliver a 65–75 cGy whole-body dose (WBD) (usually 3700–5550 MBq (100–150 mCi). Dose adjustments to 65 cGy were made for a baseline platelet count of $100\,000 \text{ mm}^{-3}$ to $<150\,000 \text{ mm}^{-3}$ and for obesity.

Kaminski and colleagues initially conducted a series of trials at the University of Michigan using ^{131}I -tositumomab, for the treatment of relapsed follicular lymphoma (Kaminski et al 1993, 1996). In a pivotal study, 60 extensively pre-treated patients were given a single administration of ^{131}I -tositumomab (Kaminski et al 2001). Disease responses were compared with the patients' previous responses to chemotherapy for follicular or transformed follicular NHL. A partial or complete response was observed in 39 patients (65%) after iodine ^{131}I -tositumomab, compared with 17 patients (28%) after their last qualifying chemotherapy ($P<0.001$). ^{131}I -tositumomab therapy was shown to provide greatly superior relapse-free survival compared with the last qualifying chemotherapy. Gregory et al (2005) have demonstrated, in an analysis of large numbers of patients (>1100), that superior outcomes were associated with earlier use of the drug and, conversely, that lower overall and complete response rates were observed in patients that were more extensively pre-treated.

Since 1990, well over 1000 patients with 'low-grade' and transformed lymphoma have been treated with ^{131}I -tositumomab. Long-term follow-up data were published by Fisher et al (2005) who performed an integrated efficacy analysis of five clinical trials of ^{131}I -tositumomab in 250 patients with

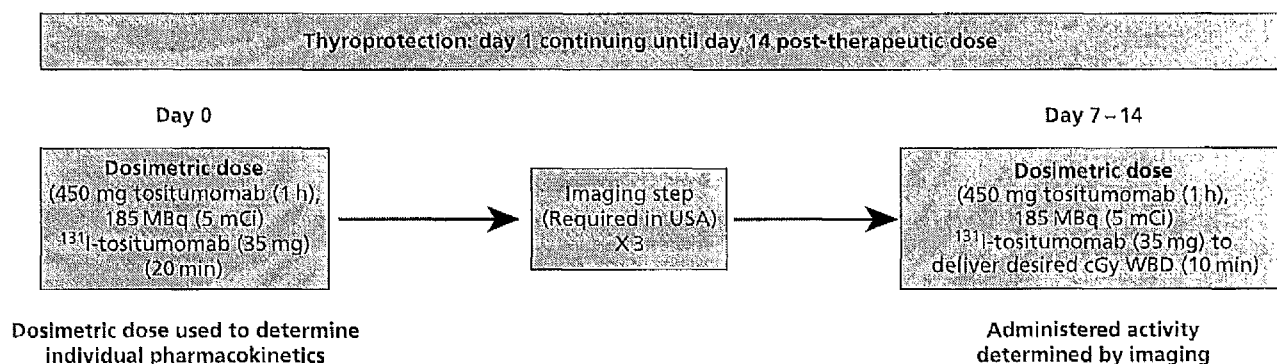


Figure 3 Treatment regimen for ^{131}I -tositumomab.

relapsed or refractory follicular or transformed follicular NHL, and the durability of these responses are discussed below.

Impressive response rates have also been seen in patients that were refractory to rituximab who were subsequently treated with ^{131}I -tositumomab. Horning et al (2005) used ^{131}I -tositumomab to treat 40 patients with low-grade NHL, 72% of whom had received four or more previous lines of therapy and 60% of whom had failed to respond to rituximab. An overall response rate of 68%, with a complete response rate of 30%, was noted and a median duration of response of 14.7 months was reported. Of the 12 complete responders, 9 remained in complete response at the time of presentation with a range of 12–26 months.

Kaminski and colleagues have shown highly promising results in the front-line treatment of previously untreated low-grade follicular lymphoma using ^{131}I -tositumomab (Kaminski et al 2005; Kaminski 2007). An encouraging overall response rate of 95% was seen, with 75% achieving complete response. PCR (polymerase chain reaction) was used to detect rearrangement of the *BCL2* gene, which revealed molecular responses in 80% of assessable patients who had a clinical complete response. The most recent update included 76 patients with a median follow-up of 5.1 years. The actuarial 5-year progression-free survival for all patients was 59%, with a median progression-free survival of 6.1 years. Haematological toxicity was moderate, with no patient requiring transfusion or G-CSF (granulocyte colony stimulating factor) (Kaminski et al 2005), though 48 out of 76 (63%) patients developed detectable HAMA (human anti-mouse antibody) responses after a single-course of treatment with ^{131}I -tositumomab.

Contribution of targeted radiation to clinical response

The contribution of targeted radiation to the overall response seen in RIT has been addressed with two randomized studies comparing the radioimmunoconjugates ^{90}Y -ibritumomab tiuxetan and ^{131}I -tositumomab with the unlabelled mAbs (Witzig et al 2002b; Davis et al 2004). Both studies have shown greatly superior clinical responses of RIT over the unlabelled mAb. The study of ^{90}Y -ibritumomab tiuxetan versus rituximab is described above and the second study, comparing treatment outcomes for unlabelled tositumomab (pre-dose) and ^{131}I -tositumomab with those for an equivalent total dose of unlabelled tositumomab, involved 78 patients with refractory or relapsed low-grade NHL (Davis et al 2004). The investigators reported an overall response rate of 55% versus 19% ($P=0.002$) with a complete response rate of 33% versus 8% ($P=0.012$) in ^{131}I -tositumomab versus unlabelled tositumomab groups, respectively. The median duration of the overall response was not reached for ^{131}I -tositumomab and was 28.1 months for unlabelled tositumomab. The median duration of complete response was not reached in either arm and the median time to progression was 6.3 versus 5.5 months ($P=0.031$), respectively. Although haematological toxicity was more severe and non-haematological side-effects were more frequent after ^{131}I -tositumomab than after tositumomab alone, there were no serious infectious or bleeding complications. The frequency of developing HAMA was similar in the two

arms at 27% (^{131}I -tositumomab group) versus 19% (tositumomab alone group). This study demonstrated that although unlabelled tositumomab showed single-agent activity, the conjugation of iodine-131 to tositumomab significantly enhanced the therapeutic efficacy and improved responses were observed in the cross-over part of the study whereby patients who had failed to respond to unlabelled tositumomab subsequently responded to ^{131}I -tositumomab (Davis et al 2004).

Radioimmunotherapy induces durable remissions

Perhaps the most impressive finding to emerge from these maturing data using RIT in follicular lymphoma is the remarkable duration of response enjoyed by some patients. Fisher et al (2005) performed an analysis of the long-term follow-up of patients treated with ^{131}I -tositumomab. The overall response rate was 47–68%, with complete response rates of 20–38%. At a median follow-up of 5.3 years, 5-year progression-free survival was 17% and 81 of 250 patients (32%) had a time-to-progression of ≥ 1 year. These patients were termed the durable response population. For the durable response population, 44% had not progressed at ≥ 2.5 to ≥ 9.5 years, with a median duration of response of 45.8 months and, impressively, the median duration of those patients who had achieved a complete response had not been reached. Interestingly many of the patients who enjoyed these long durable responses had many poor prognostic characteristics, including bone-marrow involvement (41%), bulky disease ≥ 5 cm (49%) and transformed histology (23%). Forty-three percent of the patients had been treated with more than four previous therapies and 36% had not responded to their most recent therapy. The durability of the responses seen with RIT has also been observed with ^{90}Y -ibritumomab tiuxetan (Gordon et al 2004). In all of the RIT studies, around 70% of those patients who achieved a complete response remained in remission for years (Witzig 2003; Gordon et al 2004). Further, some patients treated in the early studies have now been in remission for more than 5 years afterwards and have a median follow-up of almost 4 years (Table 2). An analysis of long-term responders underscores the potential of ^{90}Y -ibritumomab tiuxetan to achieve durable remissions with an observed median duration of response approaching 2 years and responses greater than 6 years being observed in some patients (Gordon et al 2004).

An analysis of prognostic factors has confirmed that this remarkable durability of response is unlikely to be accounted for by patient selection as most of these durable remissions have been achieved in heavily chemotherapy pre-treated and chemo-refractory patients with validated poor prognostic factors, such as extensive previous therapy (1–9 regimens), chemo-refractory disease, high lactate dehydrogenase level and extra-nodal disease. The only clinical factor that was found to correlate to clinical response to RIT was the maximum dimension of the largest tumour. Patients with tumours that had a maximum dimension of <5 cm had an overall response rate of 90% ($P<0.001$), whereas patients that had tumours more bulky than this were less likely to respond (Witzig et al 2003).

Integration into treatment algorithms for NHL

The high response rates and durable remissions achieved with either ^{90}Y -ibritumomab or ^{131}I -tositumomab make single-agent RIT an attractive treatment option for many patients with relapsed follicular lymphoma. Furthermore, the impressive duration of response seen after achieving a complete response is achieved with a treatment that is completed within a week; the treatment is very well tolerated, has minimal non-myelotoxic toxicity and easily manageable myelotoxicity.

The introduction of RIT has some parallels with the introduction of rituximab into clinical practice in the late 1990s. There is no doubt that RIT drugs are highly active but considerable uncertainty remains as to when and how best to integrate RIT into clinical practice, even within the licensed indication of relapsed low-grade (in the US) or relapsed rituximab failure or refractory follicular lymphoma (within the EU). The treatment is well tolerated by older patients and RIT makes this approach a strong recommendation for relapsed follicular NHL.

In the education session on follicular NHL at the American Society of Hematologists (2004), an algorithm was suggested for follicular lymphoma, where RIT was recommended upon the first relapse after a rituximab-chemotherapy combination (Figure 4) (Winter et al 2004). Currently this seems a reasonable treatment approach to follicular lymphoma as it does not exclude transplantation options at a later date especially if, as recommended, progenitor stem cell collection is performed at the time of the initial remission. Although data is emerging to suggest RIT can be given after transplantation (see above) this is inevitably at lower doses. Further clinical trials are needed to further define the role of RIT in the treatment of other NHL, although the recent randomized data from the FIT trial suggest that RIT may play a useful part in consolidating response from partial to complete and thereby potentially increasing the progression-free survival

and perhaps even overall survival, although this remains unproven.

Conclusion

In summary, the exquisite sensitivity of haematological malignancies to targeted radiation, alongside the impressive results achieved by the pioneers in this field, suggests that radioimmunotherapy is likely to be a productive area for future clinical research. Despite these clinical advances there remains much to discover about the mechanisms of action in successful radioimmunotherapy. Recent experimental work has demonstrated that the combination of targeted radiation and antibody effector mechanisms are critical to long-term clearance of tumour. Further work is required to enhance our understanding and determine whether a prolonged host immune response is induced by RIT and whether this underlies the long durable remissions over many years that some patients enjoy. The huge progress made over the last decade with the development of RIT in the treatment of haematological malignancies leads to distinct optimism that further development of RIT over the next five years will lead to significant improvement in clinical outcome for patients.

References

- Adams, G. P., Weiner, L. M. (2005) Monoclonal antibody therapy of cancer. *Nat. Biotechnol.* **23**: 1147–1157
- Anderson, D. R., Grillo-López, A., Varns, C., Chambers, K. S., Hanna, N. (1997) Targeted anti-cancer therapy using rituximab, a chimeric anti-CD20 antibody (IDEC-C2B8) in the treatment of non-Hodgkin's B-cell lymphoma. *Biochem. Soc. Trans.* **25**: 705–708
- Buchsbaum, D. J., Wahl, R. L., Glenn, S. D., Normolle, D. P., Kaminski, M. S. (1992) Improved delivery of radiolabeled anti-B1 monoclonal antibody to Raji lymphoma xenografts by predosing with unlabeled anti-B1 monoclonal antibody. *Cancer Res.* **52**: 637–642
- Chan, H. T., Hughes, D., French, R. R., Tutt, A. L., Walshe, C. A., Teeling, J. L., Glennie, M. J., Cragg, M. S. (2003) CD20-induced lymphoma cell death is independent of both caspases and its redistribution into triton X-100 insoluble membrane rafts. *Cancer Res.* **63**: 5480–5489
- Clark, E. A., Shu, G. (1987) Activation of human B cell proliferation through surface Bp35 (CD20) polypeptides or immunoglobulin receptors. *J. Immunol.* **138**: 720–725
- Coiffier B. (2003) Monoclonal antibodies combined to chemotherapy for the treatment of patients with lymphoma. *Blood Rev.* **17**: 25–31
- Coiffier, B., Lepage, E., Briere, J., Herbrecht, R., Tilly, H., Bouabdallah, R., Morel, P., Van Den Neste, E., Salles, G., Gaulard, P., Reyes, F., Lederlin, P., Gisselbrecht, C. (2002) CHOP chemotherapy plus rituximab compared with CHOP alone in elderly patients with diffuse large-B-cell lymphoma. *N. Engl. J. Med.* **346**: 235–242
- Cragg, M. S., Glennie, M. J. (2004) Antibody specificity controls in vivo effector mechanisms of anti-CD20 reagents. *Blood* **103**: 2738–2743
- Cragg, M. S., Walshe, C. A., Ivanov, A. O., Glennie, M. J. (2005) The biology of CD20 and its potential as a target for mAb therapy. *Curr. Dir. Autoimmun.* **8**: 140–174
- Davis, T. A., Kaminski, M. S., Leonard, J. P., Hsu, F. J., Wilkinson, M., Zelenetz, A., Wahl, R. L., Kroll, S., Coleman, M., Goris, M.

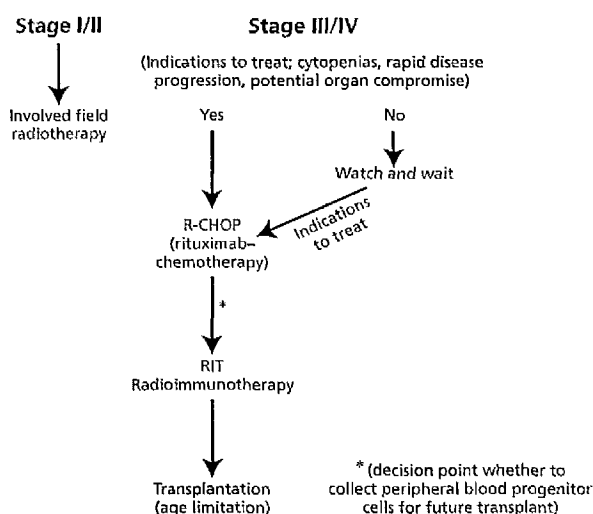


Figure 4 A proposed treatment algorithm for follicular lymphoma patients after first relapse following a rituximab-chemotherapy combination (Winter et al 2004).

- Levy, R., Knox, S. J. (2004) The radioisotope contributes significantly to the activity of radioimmunotherapy. *Clin. Cancer Res.* 10: 7792-7798
- DeNardo, G. L., DeNardo, S. J., Goldstein, D. S., Kroger, L. A., Lamborn, K. R., Levy, N. B., McGahan, J. P., Salako, Q., Shen, S., Lewis, J. P. (1998) Maximum-tolerated dose, toxicity, and efficacy of (131)I-Lym-1 antibody for fractionated radioimmunotherapy of non-Hodgkin's lymphoma. *J. Clin. Oncol.* 16: 3246-3256
- DeNardo, G. L., Kukis, D. L., Shen, S., DeNardo, D. A., Meares, C. F., DeNardo, S. J. (1999) 67Cu-versus 131I-labeled Lym-1 antibody: comparative pharmacokinetics and dosimetry in patients with non-Hodgkin's lymphoma. *Clin. Cancer Res.* 5: 533-541
- Du, Y., Honeychurch, J., Cragg, M. S., Baync, M., Glennie, M. J., Johnson, P. W., Illidge, T. M. (2004) Antibody-induced intracellular signaling works in combination with radiation to eradicate lymphoma in radioimmunotherapy. *Blood* 103:1485-1494
- Fisher, R. I., Kaminski, M. S., Wahl, R. L., Knox, S. J., Zelenetz, A. D., Vose, J. M., Leonard, J. P., Kroll, S., Goldsmith, S. J., Coleman, M. (2005) Tositumomab and iodine-131 tositumomab produces durable complete remissions in a subset of heavily pretreated patients with low-grade and transformed non-Hodgkin's lymphomas. *J. Clin. Oncol.* 23:7565-7573
- Gauld, S. B., Blair, D., Moss, C. A., Reid, S. D., Harnett, M. M. (2002) Differential roles for extracellularly regulated kinase-mitogen-activated protein kinase in B cell antigen receptor-induced apoptosis and CD40-mediated rescue of WEHI-231 immature B cells. *J. Immunol.* 168: 3855-3864
- Goldenberg, D. M., Sharkey, R. M. (2005) Radioimmunotherapy of non-Hodgkin's lymphoma revisited. *J. Nucl. Med.* 46: 383-384.
- Goldenberg, D. M., Horowitz, J. A., Sharkey, R. M., Hall, T. C., Murthy, S., Goldenberg, H., Lee, R. E., Stein, R., Siegel, J. A., Izon, D. O. (1991) Targeting, dosimetry, and radioimmunotherapy of B-cell lymphomas with iodine-131-labeled LL2 monoclonal antibody. *J. Clin. Oncol.* 9: 548-564
- Golding, S. E., Rosenberg, E., Neill, S., Dent, P., Povirk, L. F., Valerie, K. (2007) Extracellular signal-related kinase positively regulates ataxia telangiectasia mutated, homologous recombination repair, and the DNA damage response. *Cancer Res.* 67: 1046-1053
- Gordon, L. I., Molina, A., Witzig, T., Emmanouilides, C., Raubitschek, A., Darif, M., Schilder, R. J., Wiseman, G., White, C. A. (2004) Durable responses after ibritumomab tiuxetan radioimmunotherapy for CD20+ B-cell lymphoma: long-term follow-up of a phase 1/2 study. *Blood* 103: 4429-4431
- Gregory, S. A., Leonard, J. P., Vose, J. M., Zelenetz, A. D., Horning, S. J., Knox, S. J., Lister, T. A., Radford, J. A., Press, O. W., Kaminski, M. S. (2005) Superior outcomes associated with earlier use: experience with tositumomab and iodine 131 tositumomab in 1,177 patients (pts) with low-grade, follicular, and transformed non-Hodgkin's lymphoma (NHL). *J. Clin. Oncol.* ASCO Annual Meeting Proceedings. Vol 23, No. 16S, Part 1 of 11 (June 1 Supplement): 6561
- Grillo-Lopez, A. J. (2002) Zevalin: the first radioimmunotherapy approved for the treatment of lymphoma. *Expert Rev. Anticancer Ther.* 2: 485-493
- Grossbard, M. L., Press, O. W., Appelbaum, F. R., Bernstein, I. D., Nadler, L. M. (1992) Monoclonal antibody-based therapies of leukemia and lymphoma. *Blood* 80: 863-878
- Hagan, M., Wang, L., Hanley, J. R., Park, J. S., Dent, P. (2000) Ionizing radiation-induced mitogen-activated protein (MAP) kinase activation in DU145 prostate carcinoma cells: MAP kinase inhibition enhances radiation-induced cell killing and G2/M-phase arrest. *Radiat. Res.* 153: 371-383
- Hagenbeek, A., Bischof-Delaloye, A., Radford, J. A., Rohatiner, A., Salles, G., Van Hoof, A., Putz, B., Kunz, M., Morschhauser, F. (2007) ⁹⁰Y-ibritumomab tiuxetan (Zevalin) consolidation of first remission in advanced stage follicular non-Hodgkin's lymphoma: first results of the international randomized phase 3 First-line Indolent Trial (FIT) in 414 patients *Blood* 110: 198a, Abstract 643
- Hofmeister, J. K., Cooney, D., Coggeshall, K. M. (2000) Clustered CD20-induced apoptosis: Src-family kinase, the proximal regulator of tyrosine phosphorylation, calcium influx, and caspase 3-dependent apoptosis. *Blood Cells Mol. Dis.* 26: 133-143
- Holder, M., Grafton, G., MacDonald, I., Finney, M., Gordon, J. (1995) Engagement of CD20 suppresses apoptosis in germinal center B cells. *Eur. J. Immunol.* 25: 3160-3164
- Hollmann, C. A., Owens, T., Nalbantoglu, J., Hudson, T. J., Sladek, R. (2006) Constitutive activation of extracellular signal-regulated kinase predisposes diffuse large B-cell lymphoma cell lines to CD40-mediated cell death. *Cancer Res.* 66: 3550-3557
- Horning, S. J., Younes, A., Jain, V., Kroll, S., Lucas, J., Podaloff, D., Goris, M. (2005) Efficacy and safety of tositumomab and iodine-131 tositumomab (Bexxar) in B-cell lymphoma, progressive after rituximab. *J. Clin. Oncol.* 23: 712-719
- Illidge, T. M., Johnson, P. W. (2000) The emerging role of radioimmunotherapy in haematological malignancies. *Br. J. Haematol.* 108: 679-688
- Illidge, T. M., Cragg, M. S., McBride, H. M., French, R. R., Glennie, M. J. (1999) The importance of antibody-specificity in determining successful radioimmunotherapy of B-cell lymphoma. *Blood* 94: 233-243
- Ivanov, A., Krysov, S., Cragg, M. S., Illidge, T. M. (2008) Radiation therapy combined with anti-CD20 antibody tositumomab initiates ERK/MAPK dependent cell death. *Clin. Cancer Res.* In press
- Johnson, P., Glennie, M. (2003) The mechanisms of action of rituximab in the elimination of tumor cells. *Semin Oncol.* 30: 3-8
- Jurcic, J. G., Larson, S. M., Sgouros, G., McDevitt, M. R., Finn, R. D., Divgi, C. R., Ballangrud, A. M., Hamacher, K. A., Ma, D., Humm, J. L., Brechbiel, M. W., Molinet, R., Scheinberg, D. A. (2002) Targeted alpha particle immunotherapy for myeloid leukemia. *Blood* 100: 1233-1239
- Kaminski, M. (2007) T131-tositumomab monotherapy as frontline treatment for follicular lymphoma: Updated results after a median follow-up of 8 years. *J. Clin. Oncol.* ASCO Annual Meeting Proceedings Part 1. Vol 25, No. 18S (June 20 Supplement), 2007: 8033
- Kaminski, M. S., Zasadny, K. R., Francis, I. R., Milik, A. W., Ross, C. W., Moon, S. D., Crawford, S. M., Burgess, J. M., Petry, N. A., Butchko, G. M., Glenn, S. D., Wahl, R. L. (1993) Radioimmunotherapy of B-cell lymphoma with [131I]anti-B1 (anti-CD20) antibody. *N. Engl. J. Med.* 329: 459-465
- Kaminski, M. S., Zasadny, K. R., Francis, I. R., Fenner, M. C., Ross, C. W., Milik, A. W., Estes, J., Tuck, M., Regan, D., Fisher, S., Glenn, S. D., Wahl, R. L. (1996) Iodine-131-anti-B1 radioimmunotherapy for B-cell lymphoma. *J. Clin. Oncol.* 14: 1974-1981
- Kaminski, M. S., Zelenetz, A. D., Press, O. W., Saleh, M., Leonard, J., Fehrenbacher, L., Lister, T. A., Stagg, R. J., Tidmarsh, G. F., Kroll, S., Wahl, R. L., Knox, S. J., Vose, J. M. (2001) Pivotal study of iodine 131 tositumomab for chemotherapeutic-refractory low-grade or transformed low-grade B-cell non-Hodgkin's lymphomas. *J. Clin. Oncol.* 19: 3918-3928
- Kaminski, M. S., Tuck, M., Estes, J., Kolstad, A., Ross, C. W., Zasadny, K., Regan, D., Kison, P., Fisher, S., Kroll, S., Wahl, R. L. (2005) ¹³¹I-tositumomab therapy as initial treatment for follicular lymphoma. *N. Engl. J. Med.* 352: 441-449
- Kansas, G. S., Tedder, T. F. (1991) Transmembrane signals generated through MHC class II, CD19, CD20, CD39, and CD40 antigens induce LFA-1-dependent and independent adhesion in human B cells through a tyrosine kinase-dependent pathway. *J. Immunol.* 147: 4094-4102
- Knox, S. J., Meredith, R. F. (2000) Clinical radioimmunotherapy. *Semin. Radiat. Oncol.* 10: 73-93

- Kolch, W. (2005) Coordinating ERK/MAPK signaling through scaffolds and inhibitors. *Nat. Rev. Mol. Cell Biol.* **6**: 827-837
- Koral, K. F., Dewaraja, Y., Li, J., Barrett, C. L., Regan, D. D., Zasady, K. R., Rommelfanger, S. G., Francis, I. R., Kaminski, M. S., Wahl, R. L. (2003a) Update on hybrid conjugate-view SPECT tumor dosimetry and response in ¹³¹I-tositumomab therapy of previously untreated lymphoma patients. *J. Nucl. Med.* **44**: 457-464
- Koral, K. F., Kaminski, M. S., Wahl, R. L. (2003b) Correlation of tumor radiation-absorbed dose with response is easier to find in previously untreated patients. *J. Nucl. Med.* **44**: 1541-1543
- Lee, J. R., Koretzky, G. A. (1998) Extracellular signal-regulated kinase-2, but not c-Jun NH2-terminal kinase, activation correlates with surface IgM-mediated apoptosis in the WEHI 231 B cell line. *J. Immunol.* **161**: 1637-1644
- Leveille, C., Al-Daccak, R., Mourad, W. (1999) CD20 is physically and functionally coupled to MHC class II and CD40 on human B cell lines. *Eur. J. Immunol.* **29**: 65-74
- Link, B., Kaminski, M. S., Coleman, M. (2004) Phase II study of CVP followed by tositumomab and iodine I ¹³¹ tositumomab (Bexxar therapeutic regimen) in patients with untreated follicular non-Hodgkin lymphoma. *Proc. ASCO* **23**: Abstract No. 6520
- Lying, F. M., Maguire, P., McClean, B., Seymour, C., Mothersill, C. (2006) The involvement of calcium and MAP kinase signaling pathways in the production of radiation-induced bystander effects. *Radiat. Res.* **165**: 400-409
- Mathas, S., Rickers, A., Bommert, K., Dörken, B., Mapara, M. Y. (2000) Anti-CD20- and B-cell receptor-mediated apoptosis: evidence for shared intracellular signaling pathways. *Cancer Res.* **60**: 7170-7176
- McDevitt, M. R., Sgouros, G., Finn, R. D., Humm, J. L., Jurcic, J. G., Larson, S. M., Scheinberg, D. A. (1998) Radioimmunotherapy with alpha-emitting nuclides. *Eur. J. Nucl. Med.* **25**: 1341-1351
- Morschhauser, F., Illidge, T., Huglo, D., Martinelli, G., Paganelli, G., Zinzani, P. L., Rule, S., Liberati, A. M., Milpied, N., Hess, G., Stein, H., Kalmus, J., Marcus, R. (2007) Efficacy and safety of yttrium-90 ibritumomab tiuxetan in patients with relapsed or refractory diffuse large B-cell lymphoma not appropriate for autologous stem-cell transplantation. *Blood* **110**: 54-58
- Nadler, L. M., Ritz, J., Hardy, R., Pesando, J. M., Schlossman, S. F., Stashenko, P. (1981) A unique cell surface antigen identifying lymphoid malignancies of B cell origin. *J. Clin. Invest.* **67**: 134-140
- O'Keefe, T. L., Williams, G. T., Davies, S. L., Neuberger, M. S. (1998) Mice carrying a CD20 gene disruption. *Immunogenetics* **48**: 125-132
- Park, S. I., Press, O. W. (2007) Radioimmunotherapy for treatment of B-cell lymphomas and other hematologic malignancies. *Curr. Opin. Hematol.* **14**: 632-638
- Postema, E. J. (2004) Dosimetry and radioimmunotherapy of non-Hodgkin's lymphoma. *J. Nucl. Med.* **45**: 2126-2127
- Press, O. W., Rasey, J. (2000) Principles of radioimmunotherapy for hematologists and oncologists. *Semin Oncol.* **27**: 62-73
- Press, O. W., Farr, A. G., Borroz, K. I., Anderson, S. K., Martin, P. J. (1989) Endocytosis and degradation of monoclonal antibodies targeting human B-cell malignancies. *Cancer Res.* **49**: 4906-4912
- Press, O. W., Shan, D., Howell-Clark, J., Eary, J., Appelbaum, F. R., Matthews, D., King, D. J., Haines, A. M., Hamann, P., Hinman, L., Shochat, D., Bernstein, I. D. (1996) Comparative metabolism and retention of iodine-125, yttrium-90, and indium-111 radioimmunoconjugates by cancer cells. *Cancer Res.* **56**: 2123-2129
- Robak, T. (2004) Monoclonal antibodies in the treatment of chronic lymphoid leukemias. *Leuk. Lymphoma* **45**: 205-219
- Shan, D., Ledbetter, J. A., Press, O. W. (1998) Apoptosis of malignant human B cells by ligation of CD20 with monoclonal antibodies. *Blood* **91**: 1644-1652
- Sharkey, R. M., Goldenberg, D. M. (2005) Perspectives on cancer therapy with radiolabeled monoclonal antibodies. *J. Nucl. Med.* **46**: 1155-1275
- Sharkey, R. M., Behr, T. M., Mattes, M. J., Stein, R., Griffiths, G. L., Shih, L. B., Hansen, H. J., Blumenthal, R. D., Dunn, R. M., Juweid, M. E., Goldenberg, D. M. (1997) Advantage of residualizing radiolabels for an internalizing antibody against the B-cell lymphoma antigen, CD22. *Cancer Immunol Immunother.* **44**: 179-188
- Smeland, E. B., Beiske, K., Ek, B., Watt, R., Pfeifer-Ohlsson, S., Blomhoff, H. K., Godal, T., Ohlsson, R. (1987) Regulation of c-myc transcription and protein expression during activation of normal human B cells. *Exp. Cell Res.* **172**: 101-109
- Sutherland, C. L., Heath, A. W., Pelech, S. L., Young, P. R., Gold, M. R. (1996) Differential activation of the ERK, JNK, and p38 mitogen-activated protein kinases by CD40 and the B cell antigen receptor. *J. Immunol.* **157**: 3381-3390
- Tedder, T. F., Engel, P. (1994) CD20: a regulator of cell-cycle progression of B lymphocytes. *Immunol. Today* **15**: 450-454
- Tedder, T. F., Forsgren, A., Boyd, A. W., Nadler, L. M., Schlossman, S. F. (1986) Antibodies reactive with the B1 molecule inhibit cell cycle progression but not activation of human B lymphocytes. *Eur. J. Immunol.* **16**: 881-887
- Uchida, J., Lee, Y., Hasegawa, M., Liang, Y., Bradney, A., Oliver, J. A., Bowen, K., Steeber, D. A., Haas, K. M., Poe, J. C., Tedder, T. F. (2004) Mouse CD20 expression and function. *Int. Immunol.* **16**: 119-129
- Wahl, R. L. (2003) The clinical importance of dosimetry in radioimmunotherapy with tositumomab and iodine I ¹³¹ tositumomab. *Semin. Oncol.* **30**: 31-38
- Wilder, R. B., DeNardo, G. L., DeNardo, S. J. (1996) Radioimmunotherapy: recent results and future directions. *J. Clin. Oncol.* **14**: 1383-1400
- Winter, J. N., Gascoyne, R. D., Van Besien, K. (2004) Low-grade lymphoma. *Hematology (Am Soc Hematol Educ Program)*, 2004: pp 203-220
- Wiseman, G. A., Gordon, L. I., Multani, P. S., Witzig, T. E., Spies, S., Bartlett, N. L., Schilder, R. J., Murray, J. L., Saleh, M., Allen, R. S., Grillo-López, A. J., White, C. A. (2002) Ibritumomab tiuxetan radioimmunotherapy for patients with relapsed or refractory non-Hodgkin lymphoma and mild thrombocytopenia: a phase II multicenter trial. *Blood* **99**: 4336-4342
- Witzig, T. E., White, C. A., Wiseman, G. A., Gordon, L. I., Emmanouilides, C., Raubitschek, A., Janakiraman, N., Gutheil, J., Schilder, R. J., Spies, S., Silverman, D. H., Parker, E., Grillo-López, A. J. (1999) Phase I/II trial of IDEC-Y2B8 radioimmunotherapy for treatment of relapsed or refractory CD20 (+) B-cell non-Hodgkin's lymphoma. *J. Clin. Oncol.* **17**: 3793-3803
- Witzig, T. E., Flinn, I. W., Gordon, L. I., Emmanouilides, C., Czuczman, M. S., Saleh, M. N., Cripe, L., Wiseman, G., Olejnik, T., Multani, P. S., White, C. A. (2002a) Treatment with ibritumomab tiuxetan radioimmunotherapy in patients with rituximab-refractory follicular non-Hodgkin's lymphoma. *J. Clin. Oncol.* **20**: 3262-3269
- Witzig, T. E., Gordon, L. I., Cabanillas, F., Czuczman, M. S., Emmanouilides, C., Joyce, R., Pohlman, B. L., Bartlett, N. L., Wiseman, G. A., Padre, N., Grillo-López, A. J., Multani, P., White, C. A. (2002b) Randomized controlled trial of yttrium-90-labeled ibritumomab tiuxetan radioimmunotherapy versus rituximab immunotherapy for patients with relapsed or refractory low-grade, follicular, or transformed B-cell non-Hodgkin's lymphoma. *J. Clin. Oncol.* **20**: 2453-2463
- Witzig, T. E., White, C. A., Gordon, L. I., Wiseman, G. A., Emmanouilides, C., Murray, J. L., Lister, J., Multani, P. S. (2003) Safety of yttrium-90 ibritumomab tiuxetan radioimmunotherapy for relapsed low-grade, follicular, or transformed non-Hodgkin's lymphoma. *J. Clin. Oncol.* **21**: 1263-1270

Appendix 3



Curriculum Vitae

Andrejs Ivanovs

MBChB (Hons)

Cancer Research UK

Paterson Institute for Cancer Research

Professional Experience

Position	Details of experience	Period	Place
Postdoctoral Scientist	Epigenetics of cellular and organismal senescence	May 2009 -	Beatson Institute. University of Glasgow.
Postdoctoral Scientist	Cancer Research	Sept 2008 – Apr 2009	Paterson Institute for Cancer Research, Manchester, UK
Cancer Research UK PhD student	Cancer Research	4th January 2004 – July 2008	Paterson Institute for Cancer Research, Manchester, UK
Visiting Postgraduate Student	Cancer Research. Performing specific experiments on low-dose-rate irradiation. Integral part of PhD project.	Feb 2004-Apr 2004 and August 2004-Sept 2004	Gray Cancer Institute, Northwood, London
Visiting Research Fellow	Cancer Research	November 2002 – November 2003	Cancer Sciences Division, University of Southampton
Research Assistant	Cancer Research	July 2002 November 2002	Biomedical Research And Study Centre, Riga, Latvia

Research Interests

- Cell Death, especially non apoptotic cell death
- Signal transduction pathways
- Radiation-induced cell death
- Cancer Immunotherapy

Procedures

I am proficient in a wide range of biomedical procedures such as:

- Flow cytometry (including cell sorting),
- Tissue culture
- Advanced cell imaging (including FRET and FRAP analysis; confocal and widefield fluorescence microscopy; time-lapse microscopy).
- Immunohistochemistry and immunocytochemistry.
- Molecular cloning.
- Cell irradiation (including low-dose-rate irradiation).
- Tumour modelling *in-vivo*

Aims and Career objectives

The ultimate career objective is to set up my own research group that would contribute significantly to our understanding of the mechanisms of cell death, cell proliferation and senescence and their roles in biology and disease (e.g. cancer, autoimmunity, diabetes).

Courses and Training

Name of course	Details
Biotechnology Young Entrepreneurs Scheme 2007	Extensive training in entrepreneurship and commercial awareness for young bioscientists in a competition format provided by <u>Biotechnology and Biological Sciences Research Council (BBSRC)</u> and the <u>University of Nottingham Institute for Enterprise and Innovation (UNIEI)</u> .
Academic Writing in English	University of Manchester. 3-6 Sept. 2007
Publish or perish: how to survive the review process	University of Manchester.
Personal Home Office license under the Animals (Scientific Procedures) Act.	AstraZeneca. Alderley Park. 2006

Publications

Full peer-reviewed original articles

Ivanov A, Krysov S., Cragg MS, Illidge TM. Radiation Therapy with Tositumomab (B1) Anti-CD20 Monoclonal Antibody Initiates Extracellular Signal-Regulated Kinase/Mitogen-Activated Protein Kinase Dependent Cell Death that Overcomes Resistance to Apoptosis. *Clin Cancer Res*, 2008 Aug 1;14(15):4925-34.

Erenpreisa J, Ivanov A, Wheatley SP, Kosmacek EA, Ianzini F, Anisimov AP, Mackey M, Davis P, Plakhins G, Illidge TM. Endopolyploid cells resulting from irradiated p53 deficient tumours display long-lasting mitotic potential and active Aurora B- kinase. *Cell Biol. Int.* 2008 Sep;32(9):1044-56.

Kalejs M, Ivanov A, Plakhins G, Cragg MS, Emzinsh D, Illidge TM, Erenpreisa J. Upregulation of meiosis-specific genes in lymphoma cell lines following genotoxic insult and induction of mitotic catastrophe. *BMC Cancer*. 2006 Jan 9;6:6.

Erenpreisa J, Kalejs M, Ianzini F, Kosmacek EA, Mackey MA, Emzinsh D, Cragg MS, Ivanov A, Illidge TM. Segregation of genomes in polyploid tumour cells following mitotic catastrophe. *Cell Biol Int.* 2005 Dec;29(12):1005-11.

Erenpreisa J, Erenpreiss J, Freivalds T, Slaidina M, Krampe R, Butikova J, Ivanov A, Pjanova D. Toluidine blue test for sperm DNA integrity and elaboration of image cytometry algorithm. *Cytometry A*. 2003 Mar;52(1):19-27.

Ivanov A, Cragg MS, Erenpreisa J, Emzinsh D, Lukman H, Illidge TM. Endopolyploid cells produced after severe genotoxic damage have the potential to repair DNA double strand breaks. *J Cell Sci.* 2003 Oct 15;116 (Pt 20):4095-106.

Erenpreisa J, Ivanov A, Cragg M, Selivanova G, Illidge T. Nuclear envelope-limited chromatin sheets are part of mitotic death. *Histochem Cell Biol.* 2002 Mar;117(3):243-55.

Erenpreisa JE, Ivanov A, Dekena G, Vitina A, Krampe R, Freivalds T, Selivanova G, Roach HI. Arrest in metaphase and anatomy of mitotic catastrophe: mild heat shock in two human osteosarcoma cell lines. *Cell Biol Int.* 2000;24(2):61-70.

Review articles:

Ivanov A., Swann R., Illidge T. Novel aspects of radioimmunotherapy of lymphoma. *J Pharm Pharmacol.* 2008, Aug;60(8):987-98. Review

Cragg MS, Walshe CA, Ivanov AO, Glennie MJ. The biology of CD20 and its potential as a target for mAb therapy. Review. *Curr Dir Autoimmun.* 2005;8:140-74.

National and international conferences attended:

- **European Association for Cancer Research 20th conference.** Lyon, France. 5-8 July 2008
- **National Cancer Research Institute conference.** Birmingham ICC. 1-3 October 2007. Abstract shortlisted for British Oncological Association Young Investigator Award.
- **Association for Radiation Research Meeting.** Manchester. 18-20th March 2008.
- **Association for Radiation Research Meeting.** Belfast. 3rd-5th April 2007. Oral presentation of Nic McNally award receiving work.
- **National Cancer Research Institute conference.** Birmingham ICC. 8-11 October 2006
- **Joint CRUK and MRC postgraduate student conference.** Oxford. April 2006. Oral presentation. Only 20 abstracts have been selected for oral presentation among more than 200 CRUK PhD students.
- **Riga Meeting on Comprehensive Cell Biology.** June 2-4 2005. Riga. Latvia.
- **British Cancer Research Meeting 2003.** Bournemouth.
- **The 15th International Congress on Electron Microscopy.** Durban, South Africa. September 1-6, 2002. Here I was the official representative of the Latvian Society for Microscopy. Oral presentation.
- **13th European student conference.** Berlin, *Charite*. 3-8 October 2002. Oral presentation
- **British Cancer Research Meeting 2000.** 9-12 July. Brighton.

Honours and Awards

- **Nic McNally Memorial Prize for Cancer Research 2006.** Established by the British Institute of Radiology in memory of Dr. Nic McNally, a long serving Editor of British Journal of Radiology and the President Elect of the BIR before his untimely death in 1991. The

prize is awarded to a young scientist aged 35 or under for original work in cancer biology or radiation biology.

- **Scholarship. International Federation of Societies for Microscopy** 2002
- **Latvian Medical Student *Research Conference*** 1st prize 2002
- **Latvian Medical Student *Research Conference*** 2nd prize 2001

Member of the following organizations:

- **British Association for Cancer Research**
- **European Association for Cancer Research**
- **British Institute of Radiology**
- **Association for Radiation Research**

Languages

Latvian – native
Russian – native
English - excellent
German – reading

Computer skills

Microsoft Office; WinLab; WinMDI; Opera, Outlook Express and The Bat. Adobe Photoshop, ACDSee 5.0 image editor and similar graphical software. CellQuest^{PRO}, Paint-a-Gate, WinMDI, FCS Express, FlowJo, Summit and other Flow Cytometry software. SigmaPlot 8.0, Statistica 6.0 and similar software for statistics and data analysis.

Interests

Music (I play clarinet, guitar and piano)

Poetry (I write songs and poems)

Sport (Fitness, Swimming)

Referees

Professor Timothy Illidge

Professor of Targeted Therapy and Oncology
Paterson Institute for Cancer Research
Cancer Sciences Division
University of Manchester
Wilmslow Road
M20 4BX
United Kingdom

Dr Mark Cragg

Senior Lecturer and Group Leader
Cancer Sciences Division
University of Southampton
Southampton, SO16 6YD
United Kingdom

Dr. Geoff Margison

Group leader
Paterson Institute for Cancer Research
Cancer Sciences Division
University of Manchester
Wilmslow Road
M20 4BX
United Kingdom

116